

1. Report No. DOT-RSPA-DMA-50/83/3	2. Government Accession No.	3. Recipient's Catalog No.	
4. Title and Subtitle Theoretical and Experimental Study of Fracture in Pipelines Containing Circumferential Flaws		5. Report Date August 1982	
		6. Performing Organization Code	
7. Author(s) F. Erdogan		8. Performing Organization Report No.	
9. Performing Organization Name and Address Lehigh University Department of Mechanical Engineering and Mechanics Bethlehem, PA 18015		10. Work Unit No. (TRAIS)	
		11. Contract or Grant No. DOT-RC-82007	
12. Sponsoring Agency Name and Address Office of University Research Research and Special Programs Administration U.S. Department of Transportation Washington, DC 20590		13. Type of Report and Period Covered Final Report September 1978-August 1982	
		14. Sponsoring Agency Code DMA-50	
15. Supplementary Notes Technical Monitor: Oscar Orringer			
16. Abstract This report presents the theoretical and experimental results of a four year research program on the fatigue crack propagation and ductile fracture in pipelines and relatively thin-walled cylindrical containers. The objectives of the program were (a) to identify the possible modes of fracture failure in pipelines and pressurized cylinders containing a circumferential flaw, (b) to review the field and to develop the appropriate theoretical models for various phases of the fatigue and fracture in pipelines, and to carry out the necessary analytical investigations in order to develop the tools needed for the application of these models, and (c) to design and perform an experimental research program in order to test the validity and limitations of the theoretical models. The theoretical part of the program deals with the development of analytical techniques for an accurate calculation of stress intensity factors in pipes and flat plates containing a through or a part-through crack, and with the development of an elastic-plastic model for studying ductile fracture in pipelines. The experimental study was carried out on single edge notched and surface cracked X70 steel plate specimens and on circumferentially cracked standard X60 pipes. Baseline fatigue crack propagation data was collected from single edge notched specimens. The fatigue crack propagation rates in surface cracked plates and pipes were obtained by using the periodic crack front marking technique. After the fatigue tests, all three types of specimens were subjected to ductile fracture by gradually increasing the applied load. The results show that correctly calculated stress intensity factors could be highly effective as a predictive tool in fatigue crack propagation studies. Also, the pipe experiments generally confirm the validity of the theoretical ductile fracture instability model.			
17. Key Words Pipelines, Brittle Fracture, Ductile Fracture, Circumferential Crack, Crack Opening Displacement, Stress Intensity Factor, Fatigue Crack Propagation, Part-through Crack.		18. Distribution Statement This document is available to the U.S. public through the National Technical Information Service, Springfield, Virginia 22161.	
19. Security Classif. (of this report) Unclassified	20. Security Classif. (of this page) Unclassified	21. No. of Pages	22. Price

of fatigue crack propagation and fracture in single edge notched specimens under tension and bending. The material used in these experiments was 5/8 in. thick X70 pipeline steel. The purpose of these experiments was to collect baseline data on the fatigue crack propagation rates in pipeline steels, to gain some insight about the ductile fracture behavior of the material, and to test the validity of the ductile fracture instability model developed in the theoretical part. The second study on the plates involved the fatigue crack propagation and ductile fracture in an X70 steel plate containing a surface crack. This is a limiting case of the pipe problem when the diameter becomes infinitely large. Since it has a great variety of practical applications, the problem is also important in its own right. The experimental investigations on the pipes were carried out by using 20 in. diameter (OD) 0.344 in. thick standard X60 line pipes as test specimens. Approximately 18 ft. long sections were tested under four point bending. After introducing a circumferential initial cut, the pipes were subjected to fatigue by means of hydraulic jacks. The loads were then gradually increased until the pipe "failed" due to ductile fracture or inelastic buckling. The results are then analyzed by using the theoretical model developed earlier.

Following are some of the findings and conclusions:

The fatigue crack propagation rate in pipes containing a surface crack can be predicted from the baseline data obtained for simple standard specimens of the same material provided a reliable estimate of the stress intensity factor is available.

For this purpose an analytical technique was developed for an accurate calculation of stress intensity factors in pipes and relatively thin walled cylinders containing an axial or a circumferential part-through or through crack. Extensive calculated results are given for certain standard line pipes and for various practical crack geometries.

A ductile fracture model for pipes containing a through or a part-through crack is developed. The model is based on a shell theory and elastic plastic analysis. It may be used in estimating the fracture instability load in pipes or in flat plates. It may also be used, in conjunction with the critical crack tip opening displacement concept, to obtain a conservative estimate of the ductile fracture initiation load.

TABLE OF CONTENTS

PART I		<u>page</u>
THEORETICAL INVESTIGATION OF PLATES AND SHELLS CONTAINING A PART-THROUGH CRACK		1
1.	INTRODUCTION	1
1.1	Fracture Mechanics Approach	2
1.2	Brief Survey of the Field	3
1.3	Circumferential Flaws	4
2.	FRACTURE FAILURE IN PIPES	5
2.1	Types of Fracture Failure	6
2.2	Formation of a Through Crack in Plates or Cylinders	13
2.3	Ductile Fracture of Cylinders with an Axial Crack: An Example	17
3.	CIRCUMFERENTIAL CRACK IN A PIPE: ELASTIC SOLUTIONS	27
3.1	The Through Crack Problem: Transverse Shear Effects	28
3.2	Results for the Cylinder with a Circumferential Through Crack	31
3.3	Comparison with Other Crack Geometries	43
3.4	The Part-Through Crack Problem in Pipes	47
3.5	Exact Bounds for the Part-Through Crack Results	54
3.6	Stresses Due to Radial Weld Shrinkage	57
3.7	Stresses in a Pipe under "Four-Point" Bending	60
4.	DUCTILE FRACTURE MODEL: ELASTIC-PLASTIC SOLUTIONS	67
4.1	The Plane Problem for an Edge-Notched Plate	69
4.2	A Long Part-Through Crack in a Plate with Fully- Yielded Net Ligament	76
4.3	Circumferential Part-Through Crack in a Cylinder	79
PART II		
EXPERIMENTAL INVESTIGATION OF PLATES AND PIPES CONTAINING A PART-THROUGH CRACK		103
1.	INTRODUCTION	103
2.	FATIGUE AND FRACTURE OF SINGLE EDGE NOTCHED SPECIMENS	
2.1	Fatigue Crack Growth Experiments	
2.2	Fracture Tests	

- 3. PLATES CONTAINING A SURFACE CRACK
 - 3.1 Fatigue Crack Growth Experiments
 - 3.2 Fracture Tests
- 4. THE PIPE EXPERIMENTS
 - 4.1 Mechanical Properties of the Material
 - 4.2 The Fatigue Experiments
 - 4.3 Fracture Tests
 - 4.4 Examination of Fracture Surfaces

CONCLUSIONS

REFERENCES

PART III

APPENDICES

APPENDIX A.	CYLINDRICAL SHELL WITH A CIRCUMFERENTIAL THROUGH CRACK	A-1
APPENDIX B.	THE PART-THROUGH CRACK PROBLEM IN PIPES	B-1
APPENDIX C.	STRESS INTENSITY FACTORS FOR STANDARD LINE PIPES CONTAINING A PART-THROUGH SURFACE CRACK	C-1
APPENDIX D.	CIRCUMFERENTIALLY CRACKED CYLINDERS UNDER EXTENSION OR BENDING	D-1
APPENDIX E.	STRESS INTENSITY FACTORS IN A HOLLOW CYLINDER CONTAINING A RADIAL CRACK	E-1
APPENDIX F.	AN EDGE-CRACKED PLATE OR BEAM WITH TENSILE OR COMPRESSIVE YIELD ZONES	F-1
APPENDIX G.	ELASTIC-PLASTIC PROBLEM FOR A PLATE WITH A PART-THROUGH CRACK UNDER EXTENSION AND BENDING	G-1
APPENDIX H.	CALCULATED COD VS. σ_0/σ_F FOR SOME STANDARD PIPES	H-1

1.2 Brief Survey of the Field

For the purpose of a brief review one may consider the research efforts regarding pipeline fracture analysis in the following categories:

(i) theoretical work aimed at the calculation of quantities such as stress intensity factor, crack opening displacement, or J-integral which may be used in an appropriate fracture or fatigue theory as the representative of the external loads and flaw geometry, (ii) the theoretical and experimental work aimed at the development of proper "models," "criteria," or "theories" for fatigue crack propagation, corrosion fatigue, stress corrosion cracking, and fracture in pipeline materials, (iii) experimental work aimed at the verification or demonstration of the related theories in pipes, including crack morphology studies, (iv) dynamics of crack propagation in pipelines. The technical literature in the field is quite extensive (see, for example, [1] for an extensive list of references and a critical review). Most of the theoretical work in category (i) which is relevant to pipeline studies has been on the elastic solutions for part-through cracks in plates and for through cracks in shells. Some of the significant solutions and results regarding the part-through cracks in plates may be found in [2]. Reference [3] reviews most of the recent results and gives perhaps the most accurate solution of the part-through crack problem to date. The problem of a through crack in cylindrical and spherical shells has been discussed in a recent review article [4] where, in addition to a nearly complete list of references, a summary of the existing results has been included. The plasticity effects in cylindrical shells with an axial crack have been considered in [5-7]. References [8] and [9] summarize some of the recent approximate and finite element results on the thick-walled cylinders with a part-through crack.

The phenomena of brittle and quasi-brittle fracture, and the sub-critical crack propagation due to fatigue, corrosion fatigue, and stress corrosion cracking appear to be, at least from an empirical viewpoint, well-understood and the models dealing with such phenomena have been adequately standardized (see, for example, [10-13]). The stress intensity factor is almost universally accepted and used as the primary correlation parameter in all these models. However, in the presence of relatively large scale plastic deformations the effects of specimen and crack geometry, elastic-plastic stress-strain behavior of the material, and the nature of the external loads on the fracture initiation and propagation is much too great to permit the treatment of the phenomenon by

means of a single parameter (such as K_{IC} , G_{IC} , or J_{IC}). Thus, the relatively successful ductile fracture models contain more than one material constant. For example, the crack extension resistance curve (R or K_R - curve) [14] is a continuously distributed parameter model and Newman's criterion [15,16] is a two-parameter model. A discussion of these and other ductile fracture models and related references may be found in a recent review article [17]. References [18] and [19] contain applications of some of these fracture theories to welded bridge structures and pipes. A good deal of work on pipeline fracture has been done at Battelle-Columbus Laboratories. A partial summary of the results and the techniques used in these studies may be found in [20]. Fracture instability of type 304 stainless steel pipes containing a circumferential through crack was investigated in [21] under load controlled conditions. An extensive review of fracture mechanics approaches dealing with girth weld discontinuities is given in [22]. Reference [23] describes the results of a study dealing with the tensile failure of girth weld repair grooves in pipes. The results of other studies dealing with the application of fracture mechanics to girth weld failures in pipelines may be found in [24-27].

Studies of the factors dealing with the specification of tolerable defect sizes in pipelines are described in [28] and [29]. A summary-review of analytical methods and related experimental data dealing with the rupture of light water reactor piping is given in [30].

The importance of dynamic problems lies in the fact that in natural gas pipelines once the axial through crack appears in the pipe wall it rapidly grows and reaches a velocity which is generally greater than the decompression wave velocity of the gas in the pipe. Hence, the crack is subjected to a constant driving force and, unless it is arrested by some obstacle or is diverted in the hoop direction, it may run rather long distances causing considerable damage to the surroundings. The papers in Reference [31] provide a good sampling of the recent work in this area (see also [32] for more recent work and references, and [33] for work in finite volume containers).

1.3 Circumferential Flaws

Despite some interest recently shown to circumferential flaws in pipes, most of the existing studies on the fatigue and fracture of pipelines and pressurized cylinders in the past have dealt with the longitudinal flaws in the

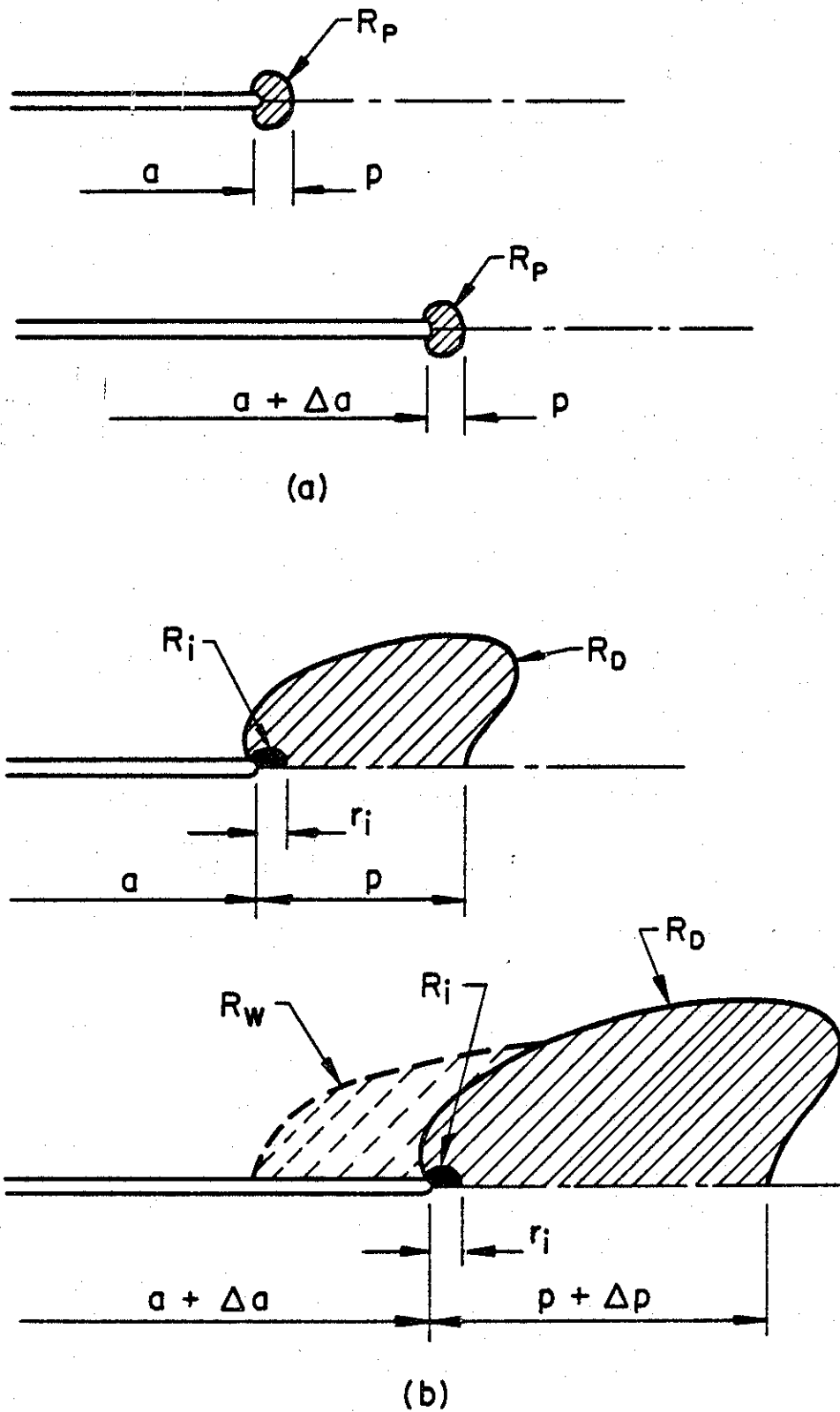


Figure 1. The types of fracture: (a) Brittle fracture, R_p ; fracture process zone, (b) ductile fracture, R_D : energy dissipation zone, R_i : fracture initiation zone, R_W : the wake region of residual stresses.

critically dependent on the details of the inelastic stress and deformation states in R_p . The important consequence of this observation is that, for the purpose of calculating the energy available for fracture $\Delta(U-V)$, one may assume that the stress state in the fracture process zone R_p is also elastic. The energy $\Delta(U-V)$ can then be calculated quite simply by using the elastic crack solution. Thus, if the solid is linearly elastic and is under Mode I loading and if K_I is the stress intensity factor, using the concept of crack closure energy it can easily be shown that for a unit length along the crack front (Figure 1a)

$$\frac{d}{da} (U-V) = \frac{K_I^2}{E_I} \quad (2)$$

where $E_I = E$ for plane stress and $E_I = E/(1-\nu^2)$ for plane strain, E and ν being the elastic constants. Combined with the notion that the fracture resistance is independent of the crack size, i.e.,

$$\frac{dD}{dA} = G_{IC} \quad (3)$$

is a material constant, from (1-3) it follows that

$$\frac{K_I^2}{E_I} \geq G_{IC} \text{ or } K_I \geq K_{IC} = \sqrt{G_{IC} E_I} \quad (4)$$

The simple form of the energy balance criterion as expressed by (4) shows that the low energy or brittle fracture can be characterized by a single parameter, the fracture toughness G_{IC} or its equivalent the critical stress intensity factor K_{IC} being the related fracture resistance parameter.

On the other hand in high energy or ductile fracture the energy exchange process during fracture propagation is much more complex. The most important characteristic features of the process are that (a) the characteristic size p of the energy dissipation zone R_D around the crack front is of the same order as (or greater than) the characteristic crack length a , and (b) as the crack propagates (i.e., as a increases), generally the dissipation zone size p also increases (Figure 1b). The physical consequence of these observations is that generally the fracture resistance of the solid increases with the increasing crack length and it is not possible to characterize the fracture process by a single parameter. On closer examination of the phenomenon one may distinguish three regions around the crack front which may be involved in the energy

exchange process during crack propagation. One is the main dissipation zone R_D where the material is plastically deformed (Figure 1b). The second is the wake region R_W of the residual stresses which develops behind the plastic zone as the crack propagates. Finally one may conjecture the existence of a very small fracture initiation zone R_i at the crack tip where the actual rupture separation takes place. For a progressively propagating crack under in-plane loading conditions even though the actual size and shape of the regions R_D and R_W may be very heavily dependent on the part-crack geometry and on the loading conditions, it is reasonable to assume that the conditions regarding the stresses and deformations in R_i would remain unchanged. It can therefore be argued that for a crack to propagate two conditions must be satisfied. One is the necessary condition regarding the fracture initiation at the crack tip and requires that a certain local strength parameter representing the intensity of the applied loads and the crack geometry reach and remain at a critical value. For a given type of in-plane crack propagation one may assume that this critical strength parameter is a material constant. The second condition is the fundamental global energy balance condition expressed by (1) where the dissipation energy D is a function of the crack length. The condition simply states that to create a new fracture surface ΔA the input energy $\Delta(U-V)$ must be equal to or greater than the dissipation energy ΔD . If a is a length parameter characterizing the fracture area A , then the stability condition for a propagating crack may be expressed as

$$\frac{d^2}{da^2} (U-V-D) \begin{cases} < 0, & \text{stable crack propagation,} \\ = 0, & \text{equilibrium crack,} \\ > 0, & \text{unstable crack propagation.} \end{cases} \quad (4)$$

In ductile fracture initially there is always a slow stable crack growth and the magnitude of the external loads needs to be increased in order to keep the crack growing. However, at a certain critical value of the load the third condition in (4) is satisfied and the crack growth becomes unstable.

The "high energy" fracture is generally geometry-dependent and is a highly complicated phenomenon to model. Therefore, it is often discussed in three different categories, namely the elastic-plastic fracture, post-yield or ductile fracture, and net section collapse or rupture. It is true that beyond brittle fracture the microstructural mechanisms leading to the fracture of the component may be the same in all three types of fracture. The basic mechanism here is

known to be the formation, growth, and coalescence of "holes" in the high strain region ahead of the crack tip, invariably at the inclusions or inclusion boundaries. Hence, from the metallurgical viewpoint, the distinction seems to be rather minor. On the other hand, in attempting to calculate the load bearing capacity of a certain component with a known flaw geometry, the materials considerations alone do not seem to be sufficient, the mechanics of the problem must also be taken into account. For example, for relatively high constraints and small crack sizes, the plastic or energy dissipation zone R_D (Figure 1) may be confined to some limited region around the crack front. In this case, the related fracture process is sometimes characterized as "elastic-plastic" fracture and may be dealt with either by a plasticity correction in the standard fracture toughness type analysis or by the plastic intensity factor calculated from the (small deformation) nonlinear analysis. The other extreme may be the gross yielding of the entire net section of the component in which case the existence of the crack would play no significant role in calculating the rupture load. The large class of problems falling between the elastic-plastic fracture and the gross yielding of the component is generally called post-yield or ductile fracture problems. The characteristic feature of ductile fracture is that the plastic zone size around the crack front is relatively large and increases noticeably with increasing crack size, and the fracture takes place in the form of progressive tearing.

Generally, in a well-defined two-dimensional crack geometry (for example, in a plate or shell component containing a through crack), even though the "ductile fracture" process cannot be characterized in terms of a single strength parameter, an analysis based on a crack extension resistance curve may be used quite effectively to predict the fracture instability load. This is basically the application of the general energy balance concept. The resistance curve (R-curve) itself is dD/da vs. the crack extension Δa where D is the total dissipated energy during crack propagation. The standard R-curve concept of determining the instability load (σ_{cr}) is shown in Figure 2. The concept applies to fracture problems in which the total fracture area can be represented by a single length parameter a (i.e., mostly two-dimensional crack geometries). In the diagram given in Figure 2, the load factor representing the intensity of the applied load and the severity of the crack geometry is assumed to be G , the strain energy release rate, and the corresponding resistance parameter of the material G_R is assumed to be a known (i.e., experimentally determined) function

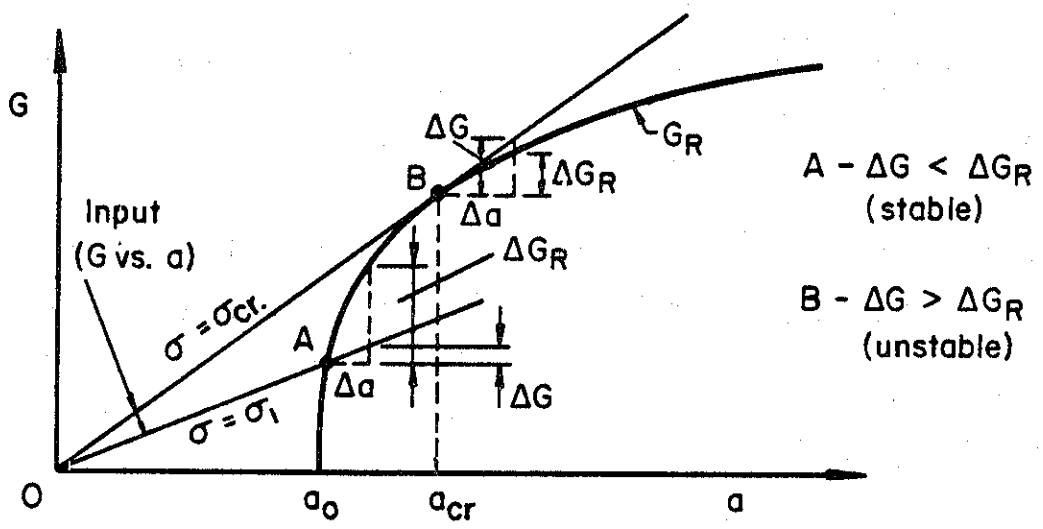
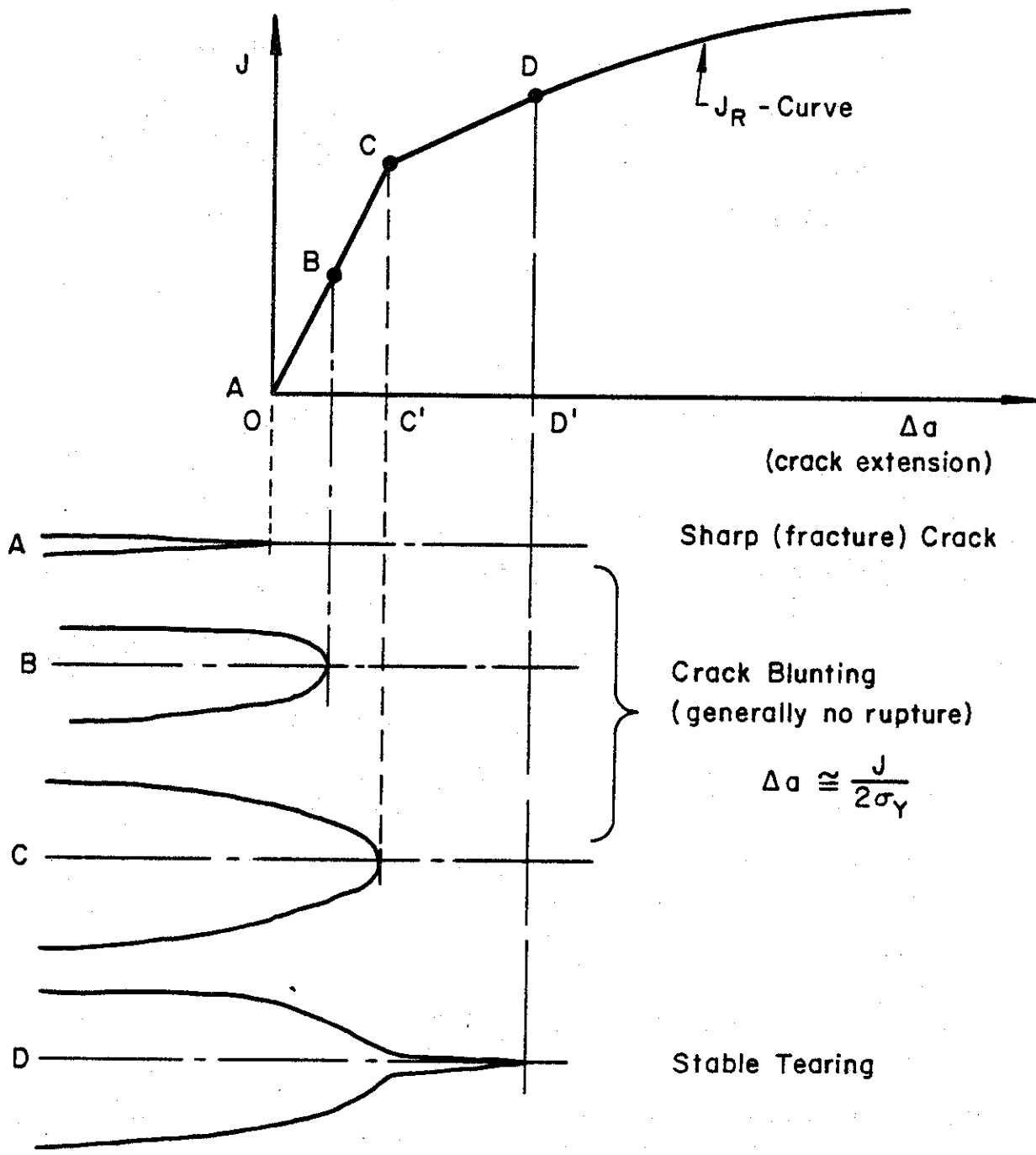


Figure 2. Typical crack extension resistance curve.



AC' - Crack Extension Due to Blunting
 C'D' - Crack Extension Due to Tearing

Figure 3. Resistance curve based on J-integral.

of a. In the terminology of the energy balance concept mentioned earlier (Eqs. 1-4) G is $d(U-V)/da$, G_R is dD/da , and Figure 2 clearly show the stability condition expressed by (4). It is seen that as applied in the manner shown in Figure 2 R-curve represents a continuous parameter characterization of the fracture propagation process.

Most of the practical early applications of the R-curve concept were based on the stress intensity factor K and K_R (with or without plasticity correction) for analytical simplicity. In recent years, the tendency is toward using a parameter which is more representative of the state of plastic deformations around the crack front such as crack opening displacement, or particularly J-integral. Figure 3 shows the crack extension resistance curve based on J-integral. Initially, the material may behave in a somewhat nonlinear elastic manner and there may be some crack extension without rupture due to blunting. After tearing or fracture starts (at C), typically the fracture resistance of the material increases with the increasing crack size. This is primarily due to the increased plastic zone size for larger cracks. One may observe that even though the application of the technique to a given problem may not be very easy or convenient (largely because of the fact that J_R , the resistance parameter is generally geometry-dependent), the concept is sound. However, one may also note that it is mostly restricted to two-dimensional crack geometries.

2.2 Formation of a Through Crack in Plates or Cylinders

Pipelines and pressurized containers are relatively thin-walled structures with a constant wall thickness. In such structures generally a fracture failure may evolve as follows: (i) as a first step a fatigue or corrosion fatigue crack may be initiated around the imbedded or the surface flaw having the worst possible combination of geometry and loading conditions. (ii) Next this dominant flaw may grow subcritically into a part-through surface flaw rupturing the weaker net ligament if the initial flaw is an imbedded defect. Gradually the surface flaw may take roughly a semi-elliptic shape growing both in length and thickness direction (see Figure 4a). At the initial stages of the subcritical crack propagation the cylinder wall would be mostly elastic and the plastic deformations would be confined to a region along the crack border only (Figure 4b). (iii) As a result of increased crack depth the net ligament through the cylinder wall becomes fully plastic and the rate of subcritical

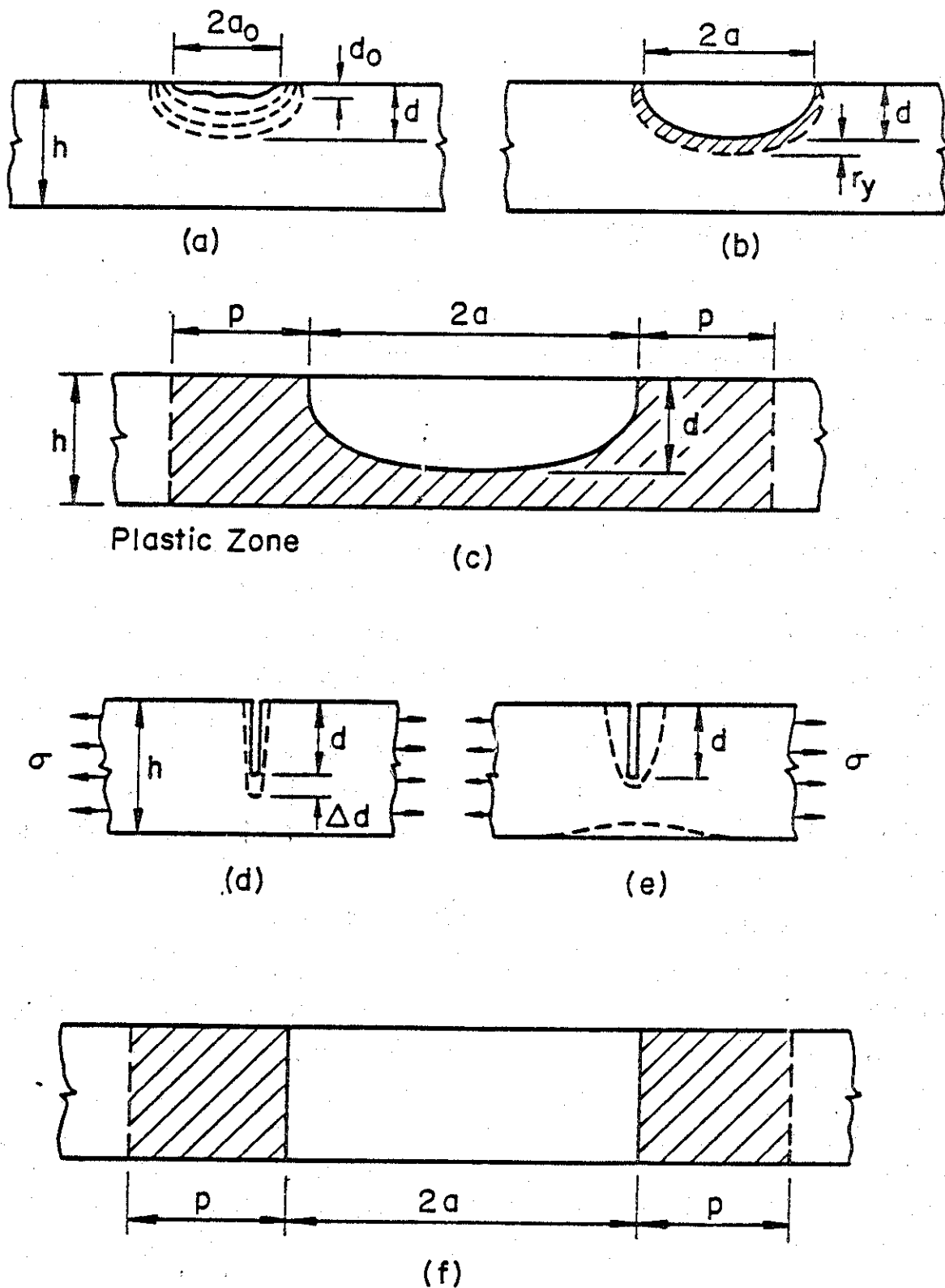


Figure 4. Evolution of a through crack. (A) initial flaw and sub-critical crack propagation, (b) part-through crack with confined plastic zone and largely elastic net ligament, (c) part-through crack with fully yielded net ligament, (d) progressive growth of part-through crack, (e) plastic necking of the net ligament, (f) through crack with relatively large plastic zones.

crack growth would increase very markedly (Figure 4c). (iv) Finally, under the peak load the net ligament would become unstable and rupture (Figure 4f). Depending on a combination of factors which consists mainly of relative magnitudes of the fracture resistance of the material and the crack driving force, the resulting through crack would either be arrested or would continue to grow in an unstable fashion. These phenomena are respectively known as the "leak" or the "break".

In fracture safety analysis it is usually assumed that an unfavorable flaw always exists and the time needed for its transformation into a dominant fatigue crack is insignificant in comparison with the expected life of the structure. For phase (ii), namely the subcritical crack propagation, phenomenologically the process is well understood and there are highly effective and reliable analytical models to estimate the crack propagation rate. The primary correlation parameter used in these models is the stress intensity factor. For example, if the process is a fatigue crack growth the surface crack would assume a shape for which the Mode I stress intensity factor along the crack border is approximately constant and the crack propagation rate may be expressed as (see, for example, [12,34])

$$\frac{dc}{dn} = F(\Delta K, C_1, \dots, C_k) \quad (5)$$

where c represents the crack size at an arbitrary location along the crack border, n is the number of load cycles, ΔK is the stress intensity amplitude, and the constants C_1, \dots, C_k represent the secondary factors such as the average and the threshold stress intensity factors, and the fracture toughness. At this stage while the net ligament is still mostly elastic (Figure 4b), if for some reason the maximum stress intensity factor exceeds K_{IC} , then the cylinder wall would rupture in a brittle manner. However, this possibility can be prevented by a proper fracture analysis, design, and material selection. Up to this point the fracture analysis is based on essentially the stress intensity factor which can be calculated by solving the related linear elastic problem for the part-through crack.

For a given load level when the crack depth d reaches a certain value the yield zone spreads through the entire net ligament and part of the cylinder wall as seen in Figure 4c. In this case the important problem is the development of a realistic model for the analysis of the net ligament rupture and the ensuing phenomenon of leak or break. Physical observations of the fracture of deeply

edge-notched plate specimens indicate that there are actually two different mechanisms which may be active in the fracture of the net ligament. One is the progressive crack growth shown in Figure 4d. The second mechanism is the plastic necking of the net ligament shown in Figure 4e. In the latter case the plastic deformations and the stretch in the net ligament is extensive and the final rupture takes place as a result of plastic necking instability. Under static loading in high toughness materials the final stage of the rupture process may always be the net ligament plastic instability. However, under cyclic loads of relatively low magnitude (and for relatively low toughness materials under static loads) the mechanism of progressive crack growth may be active for the entire fracture process.

Because of the large scale plastic deformations, linear elastic fracture mechanics is generally not a suitable approach to analyze the net ligament fracture problem. In particular, the stress intensity factor will not be a proper correlation parameter to develop an analytical model for the process. A realistic model will have to be based on a parameter which is a reasonably accurate representative of the intensity of the local plastic deformations around the crack tip. There are only two such parameters currently used in fracture mechanics to model various aspects of ductile fracture, namely the J-integral and the crack opening stretch, δ . From an application viewpoint J-integral is still a two-dimensional concept and almost always requires extensive numerical calculations based invariably on the finite element method. Hence, at this point its direct use in the cylinder problems does not seem to be very practical or even possible. Therefore, partly because of the absence of any other suitable plasticity related fracture parameter and partly because of analytical expediency with regard to its evaluation in cylinder problems, in this study the crack opening stretch will be used to model the ductile fracture problem.

There is some experimental evidence indicating that for a given material and thickness the value of the crack opening stretch at the crack initiation is approximately constant [35,36]. Referring to Figure 1b and to the general discussion given in the previous section, this implies that one can use the critical crack opening stretch as the necessary local condition for fracture initiation. Whether the ductile fracture occurs as a result of progressive crack growth or net ligament plastic necking instability would depend primarily

on the relative crack depth d/h , the yield behavior and toughness of the material, and the nature of the external loads. The following section gives some results showing the application of the crack opening stretch concept to the ductile fracture problem in cylinders with an axial crack.

2.3 Ductile Fracture of Cylinders with an Axial Crack: An Example

Let a relatively thin-walled pressurized cylinder contain a surface crack which is sufficiently deep and long so that under the given pressure the net ligament and the cylinder wall around the crack are plastically deformed. Using a plastic strip model and the bending theory of shells one can calculate the crack opening stretch along the leading edge of the crack [5,7]. Figures 4c and 4f show the geometries of the part-through and the through crack, respectively. A sample result for the crack opening stretch δ calculated at the tips of a through crack on the mid-surface of the cylinder is shown in Figure 5 where $N_0 = p_0 R$ is the membrane resultant in hoop direction, σ_Y is the flow stress representing the yield behavior of the material, and the shell parameter λ and the normalization factor d_1 are given by

$$\lambda = [12(1-\nu^2)]^{1/2} a/\sqrt{Rh}, \quad d_1 = 4a\sigma_Y/E \quad (6)$$

R , h , and $2a$ being the mean shell radius, the wall thickness, and the crack length, respectively. The curve $\lambda=0$ corresponds to the flat plate results.

One can use such results in three different ways. First, if one assumes that the critical crack opening stretch can be used as the local crack initiation criterion, then based on Figure 5 and on similar results obtained from a part-through crack solution a set of design curves may be prepared which would give the load carrying capacity of the cylinder against crack initiation. These curves are shown in Figure 6 where the varying parameter δ/d_1 correspond to the prescribed critical crack opening stretch ratio (which is a property of the material). Note that the results are general and may be used for any material for which the critical stretch falls between $0.4 d_1$ and $12 d_1$. Some sample results for a part-through crack are shown in Figure 7. Here δ_c is the maximum crack opening stretch which is at the deepest penetration point (or the mid-point) of the crack. The dots on the right hand side of the figure correspond to the load carrying capacity of the cylinder having a through crack of the same

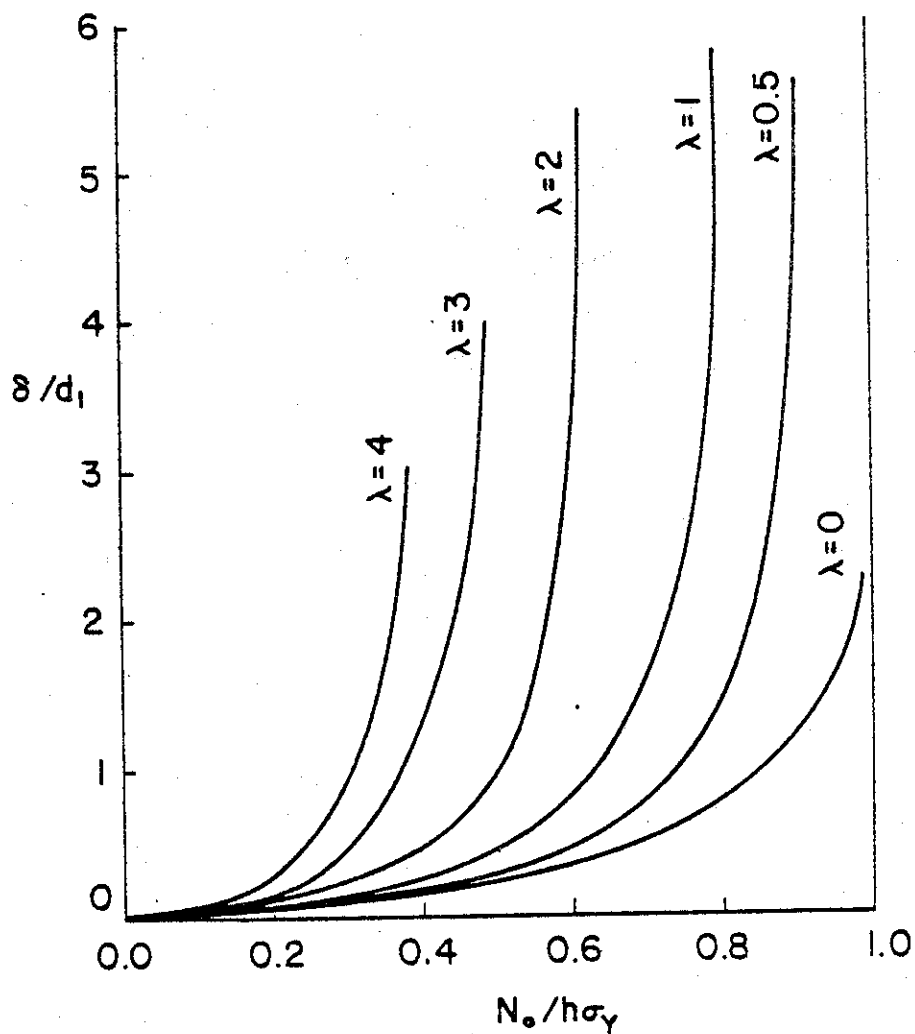


Figure 5. Crack opening stretch at the crack tip and on the mid-surface of a cylindrical shell with an axial through crack.

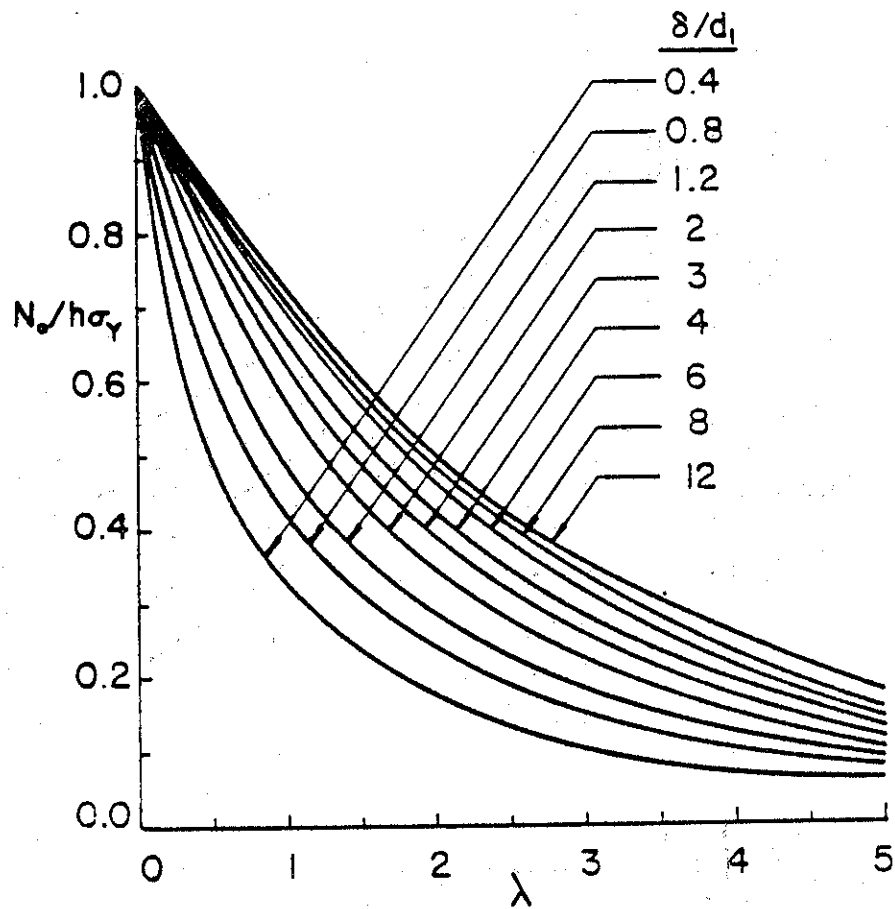


Figure 6. Load carrying capacity of a cylindrical shell with an axial through crack against crack initiation.

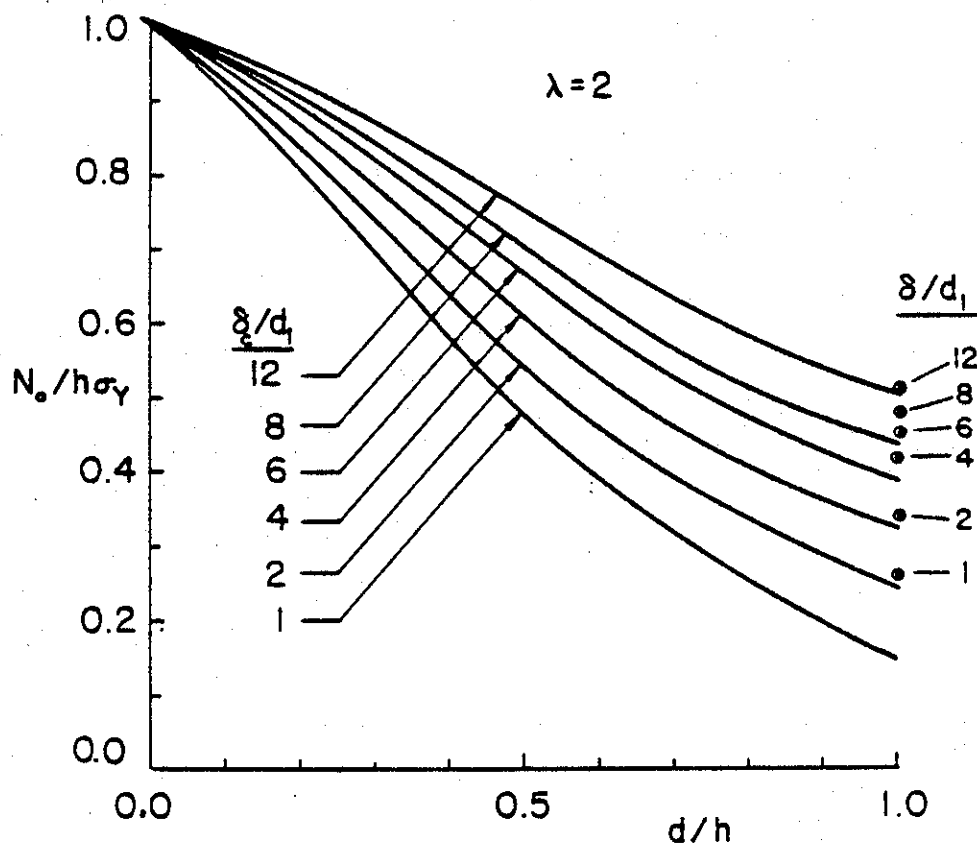


Figure 7. Load carrying capacity of a pressurized cylinder with a part-through axial crack, δ_c is the stretch at the deepest penetration point (i.e. at the midpoint) of the crack.

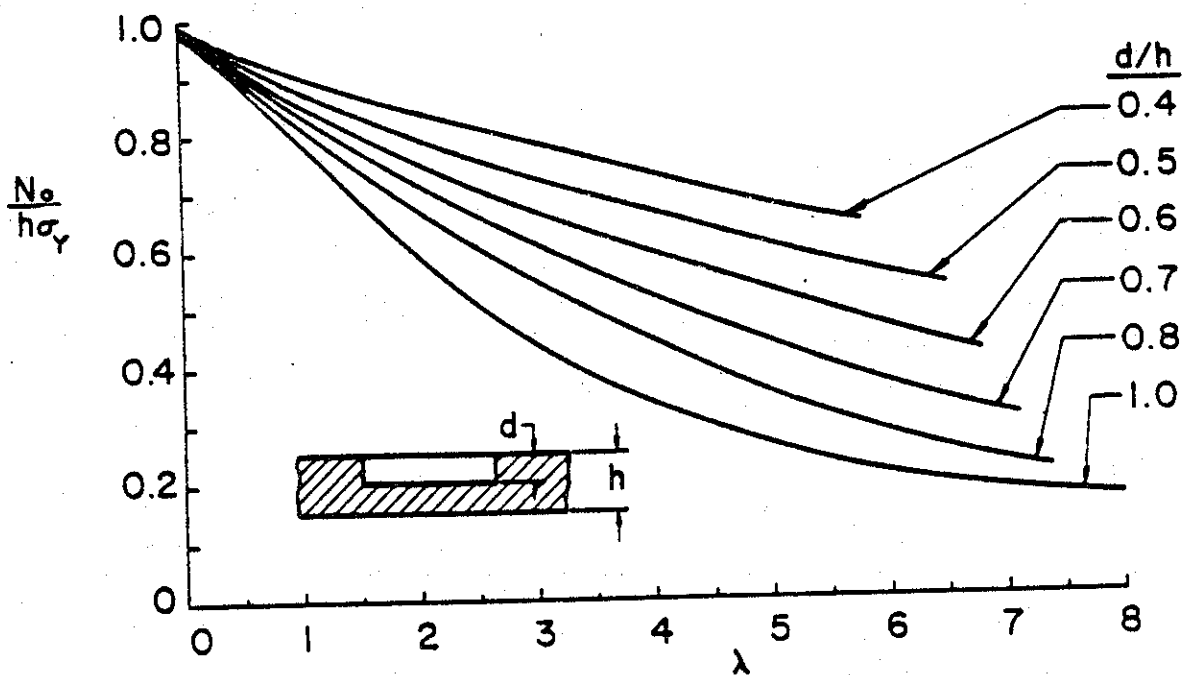


Figure 8. The instability load $N_0 = p_0 R$ for a pressurized cylinder with a progressively growing part-through ($d/h < 1$) or through ($d/h = 1$) crack.

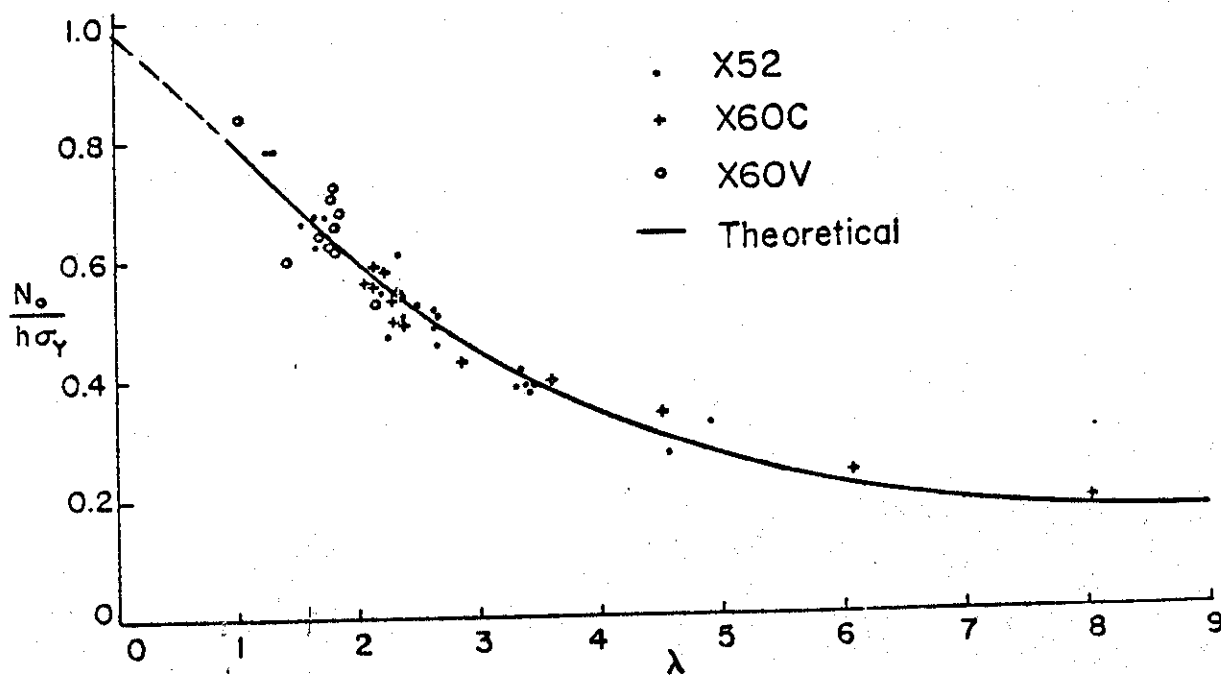


Figure 9. Comparison of the calculated (Figure 6) and experimental [20] instability loads in pipelines with an axial through crack.

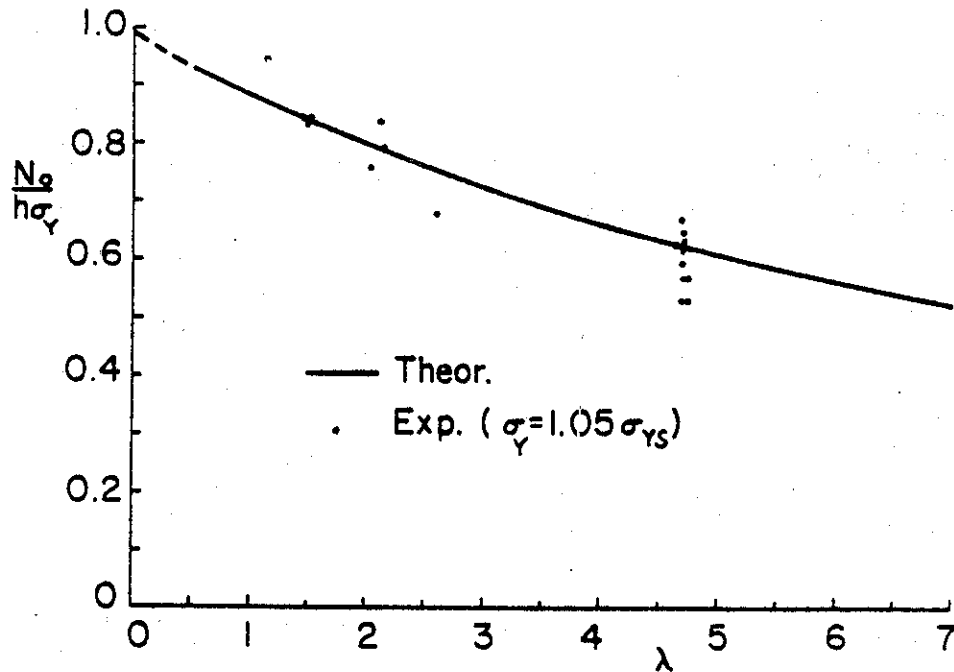


Figure 10. Comparison of the calculated (Figure 6) and experimental [20] instability loads in pipelines with an axial part-through crack.

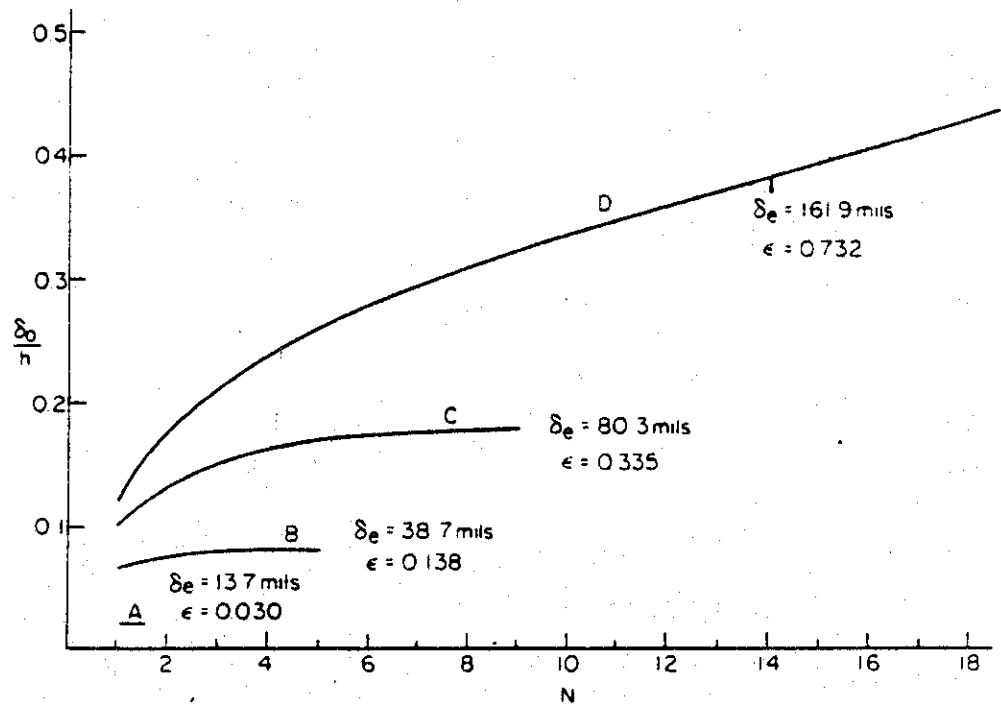


Figure 11. Results of the successive approximation calculations to determine the burst pressure (N is the number of iterations).

level, is a constant) and let δ_z be the average net ligament stretch (i.e., total elongation over the yielded gage length) calculated at the midpoint of the net ligament, then the nominal value of the average tensile strain in the net ligament may be expressed as

$$\epsilon_z \cong \delta_z / C(h-d) . \quad (7)$$

For the development of plastic necking in pipeline steels it is estimated that $\epsilon_z \geq 0.1$. In [20] near conditions of failure ϵ_z was found to be above 0.15. We now note that the instantaneous net ligament thickness may be expressed as

$$t_n = (1 + \epsilon_y) (h - d_0) . \quad (8)$$

Also note that (the current value of) the effective crack depth is approximately given by

$$d = h - t_n . \quad (9)$$

Thus, from $\epsilon_y = -\epsilon_z$ and (7)-(9) it follows that

$$d = d_0 + \frac{h - d_0}{Ct_n} \delta_z . \quad (10)$$

The constant C is related to the current value of the average strain ϵ_z . The net ligament thickness t_n too may be considered as a function of ϵ_z . Therefore, for any strain ϵ_z greater than 0.1 the effective crack depth d may be expressed as

$$d = d_0 + \alpha(\epsilon_z) \delta_z \quad (11)$$

where $\alpha(\epsilon_z)$, except for certain limiting trends, is not known. For large values of ϵ_z , $d \sim d_0 + |\delta_y|$ and $|\delta_y| \sim \delta_z$, hence $\alpha(\epsilon_z)$ would approach unity, where δ_y is the total contraction in y (or thickness) direction. Therefore, if one assumes that $\alpha(\epsilon_z)$ is a given function, by observing that for given dimensions R, h, a and d_0 and pressure p_0 , δ_z is a function of the crack depth d which can be calculated (by using the elastic-plastic shell theory) and by taking (7) into consideration, in principle d can be calculated from (11). Since (11) is a highly nonlinear equation, this can only be done numerically, for example, by setting up the following successive approximation scheme:

$$d(0) = d_0, \delta_z(0) = \delta_z \Big|_{d=d_0, p=p_0}, \epsilon_z(0) = \epsilon_z \Big|_{d=d_0, p=p_0}$$

$$d(N+1) = d_0 + \alpha(\epsilon_z(N))\delta_z(N), N = 0, 1, 2, \dots \quad (12)$$

Now, if d has an equilibrium value it can be obtained from (12) as the limit for $N \rightarrow \infty$. Clearly for the given pressure if the successive approximation formulated by (12) is convergent giving a finite value which is less than the thickness h , then there would be a load redistribution around the crack accommodating a stable net ligament thickness. On the other hand the divergence of the successive approximation technique (as defined by d exceeding h) would mean the fracture due to net ligament plastic necking instability.

As an illustration of the technique to estimate the failure pressure in cylinders we consider the tests carried out on full scale line pipes at Battelle [20]. Following is the relevant information regarding the tests.

Dimensions: $R = 18$ in, $h = 0.403$ in, $d_0 = 0.201$ in,
 $2a = 3.8$ in, $\sigma_{YS} = 64.6$ ksi;

Test Pressure p_0 (ksi):	1.0	1.2	1.25	1.29
δ_e (mills):	29	60	80	Failure

Here δ_e is the measured crack opening displacement on the outside surface of the cylinder and at the center section of the crack corresponding to the pressure levels shown. In applying the technique it was assumed that

$$\sigma_Y = \sigma_{YS} + 2 \text{ ksi}, \alpha(\epsilon_z) = 0.46 + 0.54 \left(1 - \frac{0.1}{\epsilon_z}\right). \quad (13)$$

The calculation was carried out for the pressures 1.0, 1.2, 1.25, and 1.267 ksi. The result is shown in Figure 11. The ordinate in the figure is the crack opening displacement δ_0 on the middle surface of the cylinder and at the center section of the crack. Which one of the quantities δ_0 , δ_e and d is used as an ordinate in the figure is, of course, immaterial. It is seen that the calculations for the first three pressures are convergent meaning that these pressures are below the instability or failure value. For $p_0 = 1.267$ ksi the calculations diverge, implying that this pressure is equal to or greater

than the failure value. The figure also shows, for each pressure, calculated values of the average net ligament strain ϵ_z and δ_e . Note that the iteration technique predicts the failure pressure quite accurately. However, particularly at smaller pressures, the predictions for δ_e are not good. This is somewhat understandable, as the model is based on large scale yielding and large plastic strains which may not in fact exist at lower pressures.

3. CIRCUMFERENTIAL CRACK IN A PIPE: ELASTIC SOLUTIONS

The types of problems one may encounter in a complete fracture analysis of pipelines and pressurized cylinders were described in the previous section. Again, Figure 4 may be used as a rough guide for this purpose. From the figure it is seen that one needs reliable analytical tools for modeling of such diverse phenomena as fatigue crack propagation of a part-through or a through crack in the cylinder wall, elastic-plastic fracture, post-yield fracture, and net ligament plastic necking instability of the cylinder wall containing a part-through surface crack, and static or dynamic ductile tear of the cylinder wall with a through crack. Analytically, the corresponding three-dimensional crack problems appear to be intractable. Most of the existing solutions are therefore based on some type of a numerical technique. The two widely used methods along these lines have been the finite element method (see, for example, [38] and [39]) and the boundary integral equation method [40]. Related solutions for a flat plate containing a semielliptic surface crack may be found, for example, in [41-45]. The finite element method is used in [41-43], and the successive approximations or the alternating method is used in [44] and [45].

The main objective of this study is the fracture analysis of pipelines and pressurized cylindrical containers. The radius-to-thickness ratio in these structures varies generally from 40 to 50 in pipelines to approximately 100 in tank cars. It is therefore clear that one could treat the cylinders as "shallow shells" and try to take advantage of certain simplifications offered by the shell theory in solving the crack problems.

In this section we first develop the elastic solutions for a cylinder containing a part-through surface crack or a through crack. These solutions are essential for estimating the subcritical crack growth rate and, if necessary, the residual strength of the cylinder against a possible quasi-brittle

fracture. The solutions are also needed for the application of the plastic line spring model to study the ductile fracture problems in pipelines and pressure cylinders.

3.1 Through Crack Problem: The Transverse Shear Effect

Chronologically, even though the through crack solution corresponds to the last stage of the fracture process, it will be treated first for the following reasons: a) the problem can be treated analytically and very accurate results can be obtained without costly numerical analysis, b) the solution is needed for introducing the curvature effect into the development of approximate techniques to calculate the stress intensity factors for the part-through cracks in shells, and c) it is the starting point for the elastic-plastic analysis of the part-through crack problem.

Because of the complexity of the problem the early studies of the cracked shells were based on the relatively simpler classical shell theory (see, for example, the review article [4]). The classical shell theory is an eighth order theory which can analytically accommodate only four conditions on the boundary. On the other hand, referring to the shell element given in Figure 12, it may be seen that there are five physical conditions on the boundary. For example, along a part of the boundary described by $X_1 = \text{constant}$ the membrane resultants N_{11} , N_{12} , the moment resultants M_{11} , M_{12} and the transverse shear resultant V_1 would have to be prescribed as the stress boundary conditions. Thus, to make the number of the boundary conditions compatible with the order of differential equations, in the classical shell theory the conditions regarding the transverse shear and the twisting moment are combined into a single boundary condition as the Kirchhoff's effective transverse shear resultant. For example along $X_1 = \text{constant}$ the four conditions would then be in terms of

$$N_{11}, N_{12}, M_{11}, Q_1 = V_1 + \frac{\partial}{\partial X_2} M_{12}. \quad (14)$$

The consequence of the Kirchhoff assumption is that in a narrow layer along the boundary generally the solution is not sufficiently accurate. In crack problems since the crack tip is in the boundary layer the discrepancy can be significant. For example in a symmetrically-loaded cylindrical or spherical shell having a through crack along the X_2 axis (Figures 12,13) the

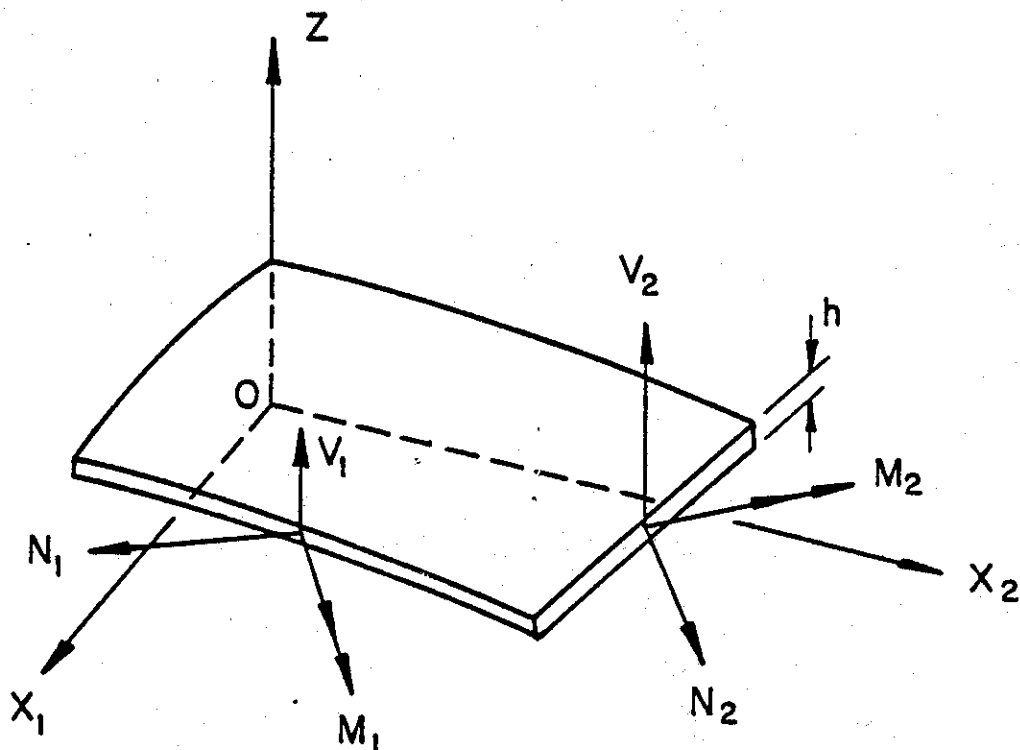


Figure 12. Notation for the stress and moment resultants in a shallow shell.

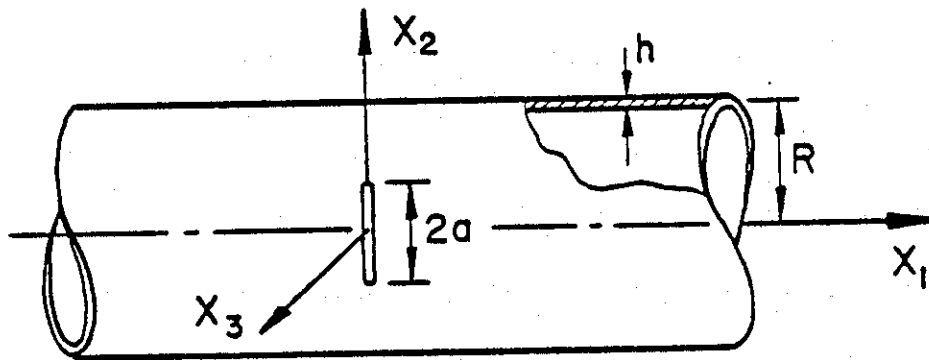


Figure 13. The cylinder with a circumferential through crack.

classical theory would give the following asymptotic results for the stress distribution around the crack tip [4]:

$$\sigma_{11}^m(r, \theta) \sim \frac{k_m}{4\sqrt{2r}} (5 \cos \frac{\theta}{2} - \cos \frac{5\theta}{2}) ,$$

.....

$$\sigma_{11}^b(r, \theta, X_3) \sim \frac{k_b}{\sqrt{2r}} \frac{X_3}{2h} [-5(1-\nu)^2 \cos \frac{\theta}{2} + (1-\nu)^2 \cos \frac{5\theta}{2}] ,$$

.....

$$Q_1 \sim \frac{1}{r^{3/2}} , \tag{15}$$

where σ_{ij}^m and σ_{ij}^b ($i, j = 1, 2$) are respectively membrane and bending components of the stresses, k_m and k_b are the membrane and the bending stress intensity factors and r and θ are the local polar coordinates in X_1X_2 plane. The physics of the problem would indicate that the discrepancy between the angular distributions of membrane stresses and bending stresses and the power of singularity of the effective transverse shear Q_1 are unacceptable. Also, because of the difference between the angular distributions, it is difficult to interpret and combine the stress intensity factors k_m and k_b in any fracture analysis.

To eliminate these undesirable features of the solution given by the classical theory it is clear that a higher order theory compatible with the number of physical boundary conditions must be used. Such a theory for specially orthotropic shallow shells has been described in Appendix A which for symmetric loading conditions gives the following asymptotic stress distribution around the crack tip:

$$\sigma_{11}(r, \theta, X_3) \sim \frac{k_m + k_b}{4\sqrt{2r}} \frac{2X_3/h}{2h} (5 \cos \frac{\theta}{2} - \cos \frac{5\theta}{2}) ,$$

$$\sigma_{22}(r, \theta, X_3) \sim \frac{k_m + k_b}{4\sqrt{2r}} \frac{2X_3/h}{2h} (3 \cos \frac{\theta}{2} + \cos \frac{5\theta}{2}) ,$$

$$\sigma_{12}(r, \theta, X_3) \sim \frac{k_m + k_b}{4\sqrt{2r}} \frac{2X_3/h}{2h} (-\sin \frac{\theta}{2} + \sin \frac{5\theta}{2}) ,$$

$$V_1(r, \theta) \sim k_t \sqrt{r} \sin \theta \cos \frac{\theta}{2} , \tag{16 a-d}$$

where again k_m and k_b are the membrane and bending stress intensity factors. Equations (16 a-c) indicate that, as expected the membrane and bending stress components have the same angular distribution. Equation (16d) simply gives the expected result, namely under symmetric loading the transverse shear resultant has no singularity. One may also note that the angular distribution of the stress state around the crack tip given by (16 a-c) and obtained from the higher order shell theory is identical to the results obtained from the two-dimensional elastic crack solution.

Another important difference between the results given by the classical and the higher order shell theories is that whereas in the classical theory the standard shell parameter $\lambda_2 = [12(1-\nu^2)]^{1/4} a/\sqrt{Rh}$ is the only dimensionless geometric variable entering the analysis and affecting the results, the higher order theory contains, in addition to λ_2 , a/h as a separate geometric variable, where $2a$, R , and h are, respectively, the crack length, the mean radius of the cylinder, and the thickness. In both theories, the Poisson's ratio ν enters the analysis separately as well as through λ_2 . In the specially orthotropic materials ν is replaced by $\sqrt{\nu_1\nu_2}$ and the ratio E_1/E_2 appears in the analysis as an additional material constant.

3.2 The Results for the Cylinder with a Circumferential Through Crack

The detailed analysis of the problem for a cylindrical shell containing a circumferential through crack and subjected to arbitrary symmetric external loads is given in Appendix A. Figures 12 and 13 show the basic notation for the stress and moment resultants and for the crack geometry. The stress intensity factors for an isotropic cylinder obtained from the solution under uniform membrane loading and uniform bending moment (on the crack surfaces) are given by Figures 14-17 and by table 1 of Appendix A. Note that in the shell problem the membrane and bending results are coupled and the stress intensity factors are linear functions of the distance X_3 from the neutral surface. Thus, referring to Figure 13, the Mode I stress intensity factor for the symmetric shell problem may be defined as

$$k_1(X_3) = \lim_{X_2 \rightarrow a} \sqrt{2(X_2 - a)} \sigma_{11}(0, X_2, X_3) . \quad (17)$$

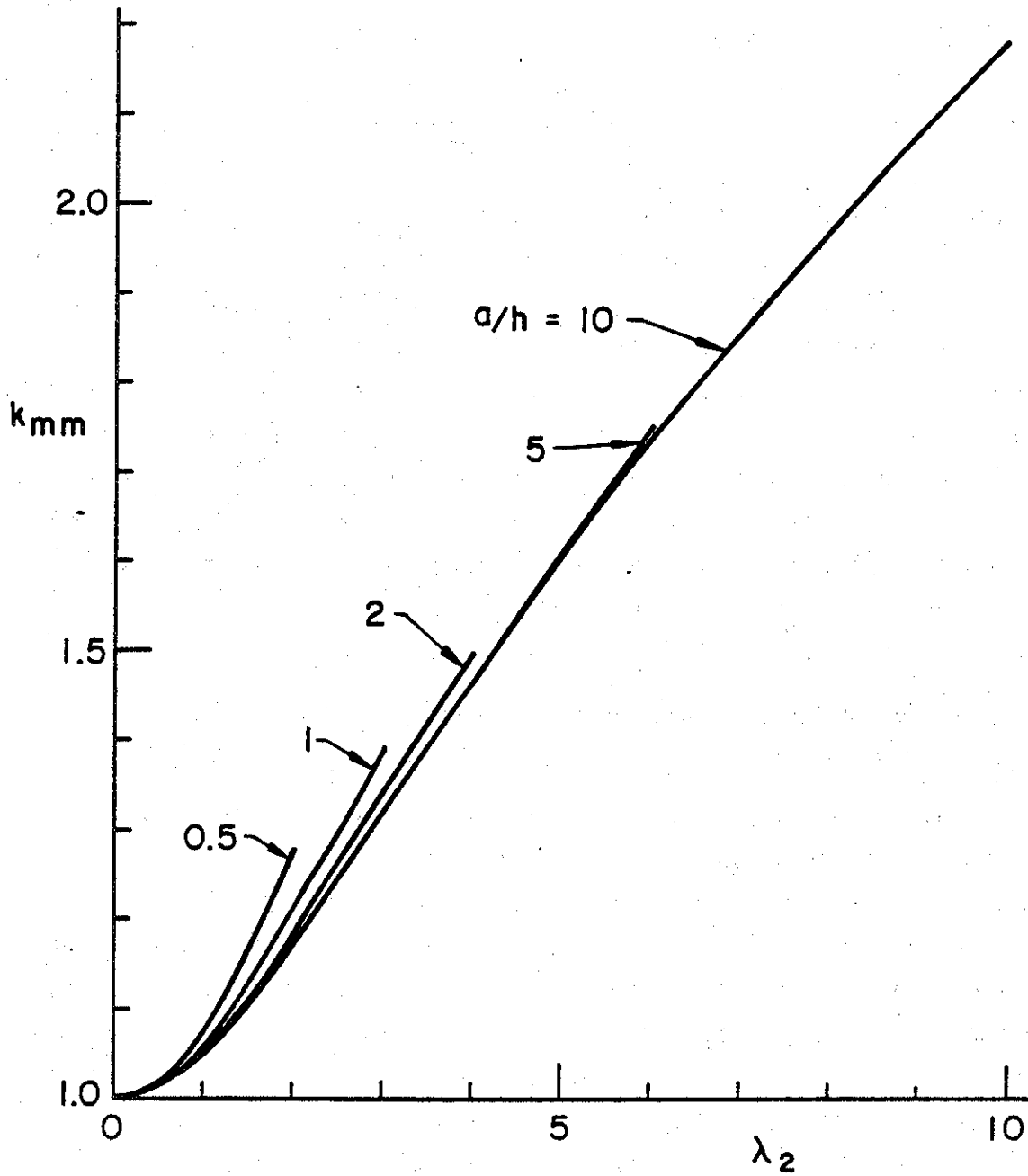


Figure 14. Membrane component of the stress intensity ratio for a circumferentially cracked cylinder under uniform membrane loading ($N_{11} \neq 0, M_{11} = 0$).

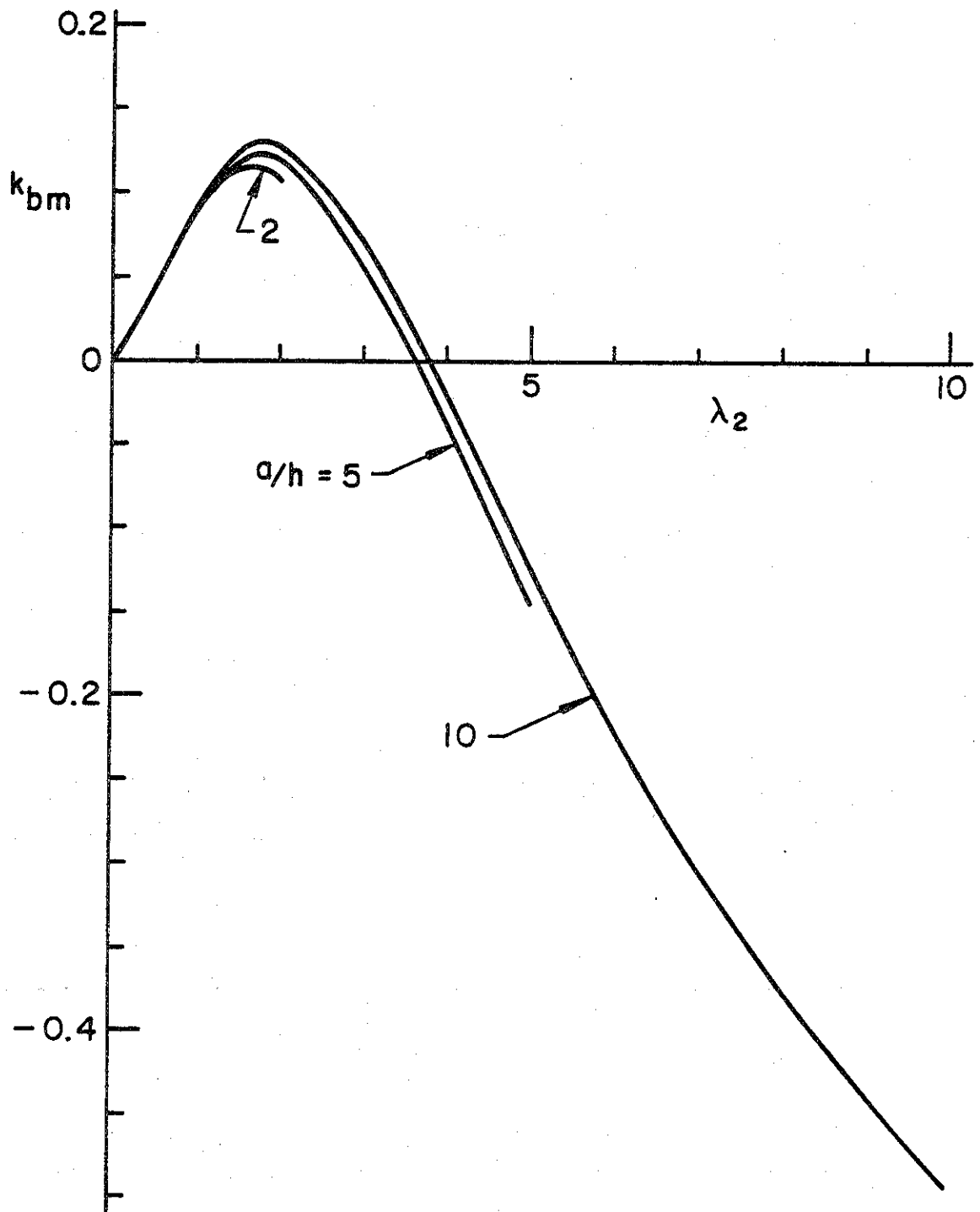


Figure 15. Bending component of the stress intensity ratio for a circumferentially cracked cylinder under uniform membrane loading ($N_{11} \neq 0$, $M_{11} = 0$).

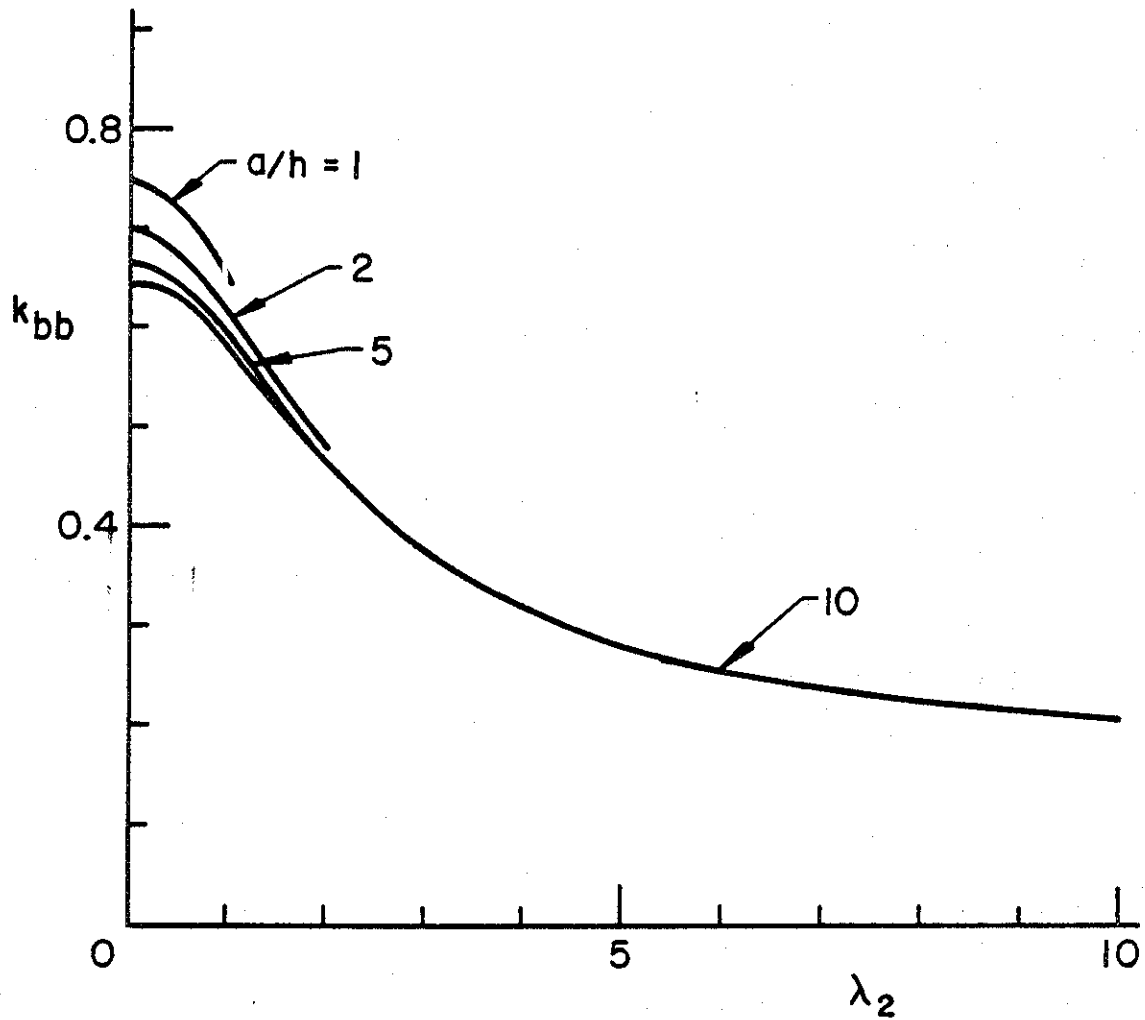


Figure 16. Bending component of the stress intensity ratio for a circumferentially cracked cylinder under uniform crack surface bending moment ($N_{11} = 0, M_{11} \neq 0$).

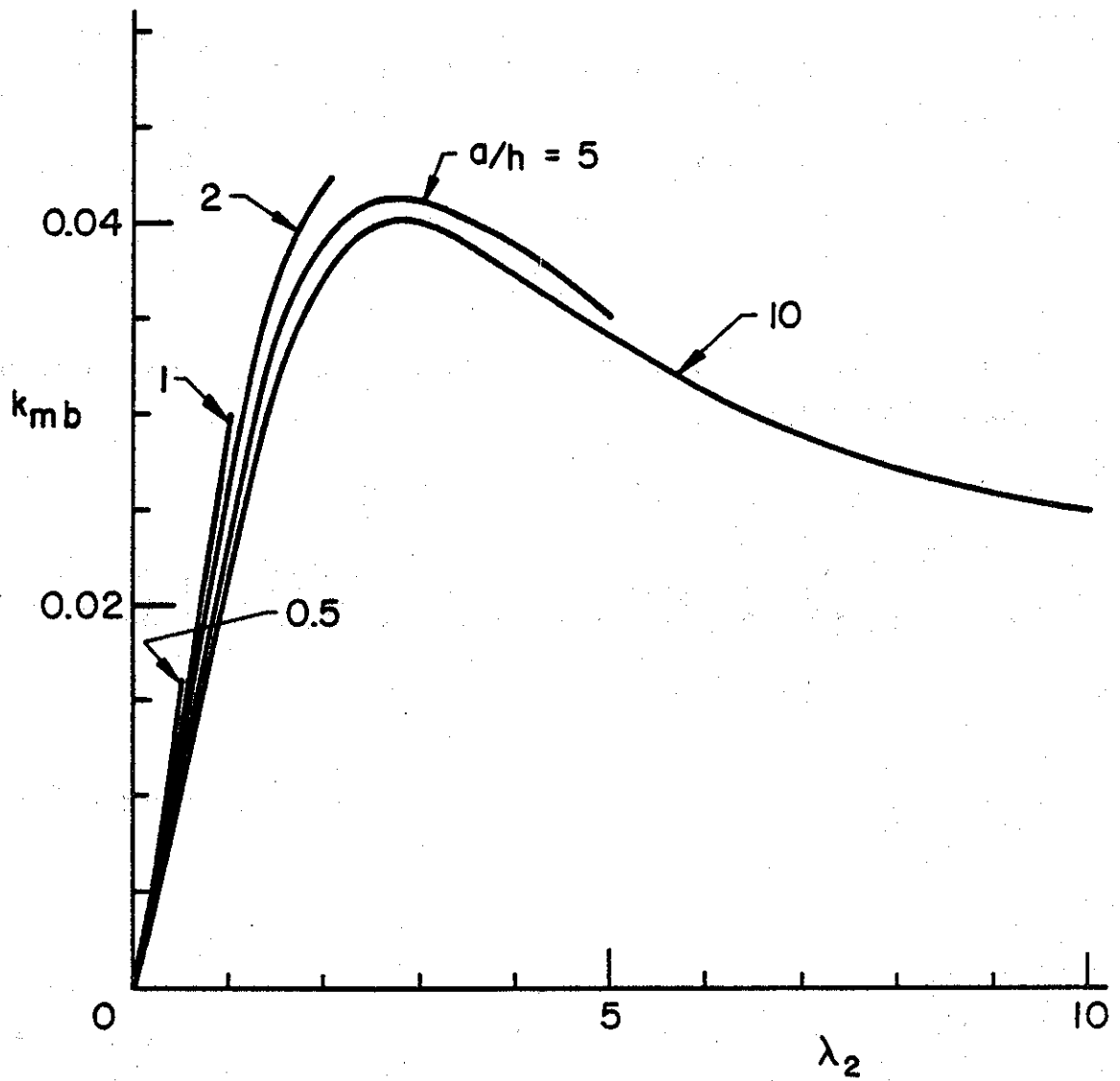


Figure 17. Membrane component of the stress intensity ratio for a circumferentially cracked cylinder under uniform crack surface bending moment ($N_{11} = 0$, $M_{11} \neq 0$).

or

$$k_1(X_3) = k_m + k_b X_3 / (h/2)$$

$$k_m = k_1(0) , k_b = k_1(h/2) - k_1(0) , \quad (18 \text{ a-c})$$

where k_m and k_b are the membrane and bending components of the stress intensity factor.

The figures show the stress intensity factors normalized with respect to a corresponding flat plate value. For example, in the cylinder under only uniform loading in X_1 (axial) direction (i.e., for $N_{11} \neq 0$, $M_{11} = 0$) the corresponding flat plate stress intensity factor is

$$k_p = \sigma_m \sqrt{a} , \sigma_m = N_{11} / h , \quad (19)$$

and the normalized stress intensity factors k_{mm} and k_{bm} shown in Figures 12 and 13 are defined by

$$k_{mm} = k_m / \sigma_m \sqrt{a} , k_{bm} = k_b / \sigma_m \sqrt{a} . \quad (20)$$

Also, if the cylinder is subjected only to pure bending M_{11} on the crack surface (i.e., $N_{11} = 0$), then the normalizing stress intensity factor is

$$k_p = \sigma_b \sqrt{a} , \sigma_b = \frac{6M_{11}}{h^2} , \quad (21)$$

and the stress intensity factor ratios shown in Figures 16 and 17 are defined by

$$k_{bb} = \frac{k_b}{\sigma_b \sqrt{a}} , k_{mb} = \frac{k_m}{\sigma_b \sqrt{a}} . \quad (22)$$

In the isotropic shells since the Poisson's ratio ν enters the analysis explicitly as well as through λ_2 , a value for ν had to be selected in the numerical calculations. The results given in Figures 14-17 are based on $\nu = 1/3$. The effect of ν on the stress intensity factors is separately studied for a specific geometry. The results obtained for $\lambda_2 = 3$ and $a/h = 5$ are shown in Table 2 of Appendix A. The effect of the Poisson's ratio on the two primary stress intensity ratios k_{mm} and k_{bb} does not seem to be significant.

Therefore, the results obtained for $\nu = 1/3$ can be used for nearly all structural materials in which ν varies between 0.2 and 0.4.

In Figures 14-17 the stress intensity ratios are given as functions of the shell parameter λ_2 with the second dimensionless variable a/h as a discrete parameter. For given a and h as $R \rightarrow \infty$ the shell becomes a flat plate, hence the shell results should approach the corresponding stress intensity factors in flat plates. The figures, in fact, show that as $R \rightarrow \infty$ λ_2 approaches zero, $k_{mm} \rightarrow 1$ (or $k_m \rightarrow k_p$), and k_{bb} approaches the values obtained for a flat plate. Also, for flat plates since the membrane and bending problems are uncoupled, as $\lambda_2 \rightarrow 0$ the coupling components of the stress intensity factors (k_{bm} and k_{mb}) approach zero.

Comparing the shell results given in this report with those obtained from the classical theory as, for example, given by [34] the following observations may be made: the stress intensity ratios k_{mm} obtained from the two theories become identical as $a/h \rightarrow \infty$. In fact the result given in Figure 14 for $a/h = 10$ is indistinguishable from that obtained in [34]. However, for values of a/h smaller than 5 the thickness effect on k_{mm} becomes noticeable and for small values of a/h it may be significant. One may add that the thickness effect on k_{mm} is on the nonconservative side. On the other hand the convergence of the results of a higher order shell theory to that of the classical theory for $a/h \rightarrow \infty$ (or for $h \rightarrow 0$) appears to be valid only for k_{mm} . The behavior of the remaining three stress intensity factors with respect to varying h/a ratio indicate no such trend. Also, the results obtained from the two theories for k_{bm} , k_{bb} , and k_{mb} are generally quite different.

Sample results showing the bulging of the shell around the crack region are given in Figures 18 and 19. The figures show the displacement component perpendicular to the shell surface along the crack line, $W(0, X_2, 0)$ in a circumferentially cracked cylinder under uniform membrane loading and pure bending. It should be emphasized that the technique of superposition is used to solve the crack problem described in Appendix A. This means that in the perturbation problem considered the crack surface membrane stress is compressive and the bending moment is applied in such a way that the outer layer of the shell on the crack surface is again compressive. As may be seen from Figures 18 and 19, under these loads the crack surface displacement W is in outward direction.

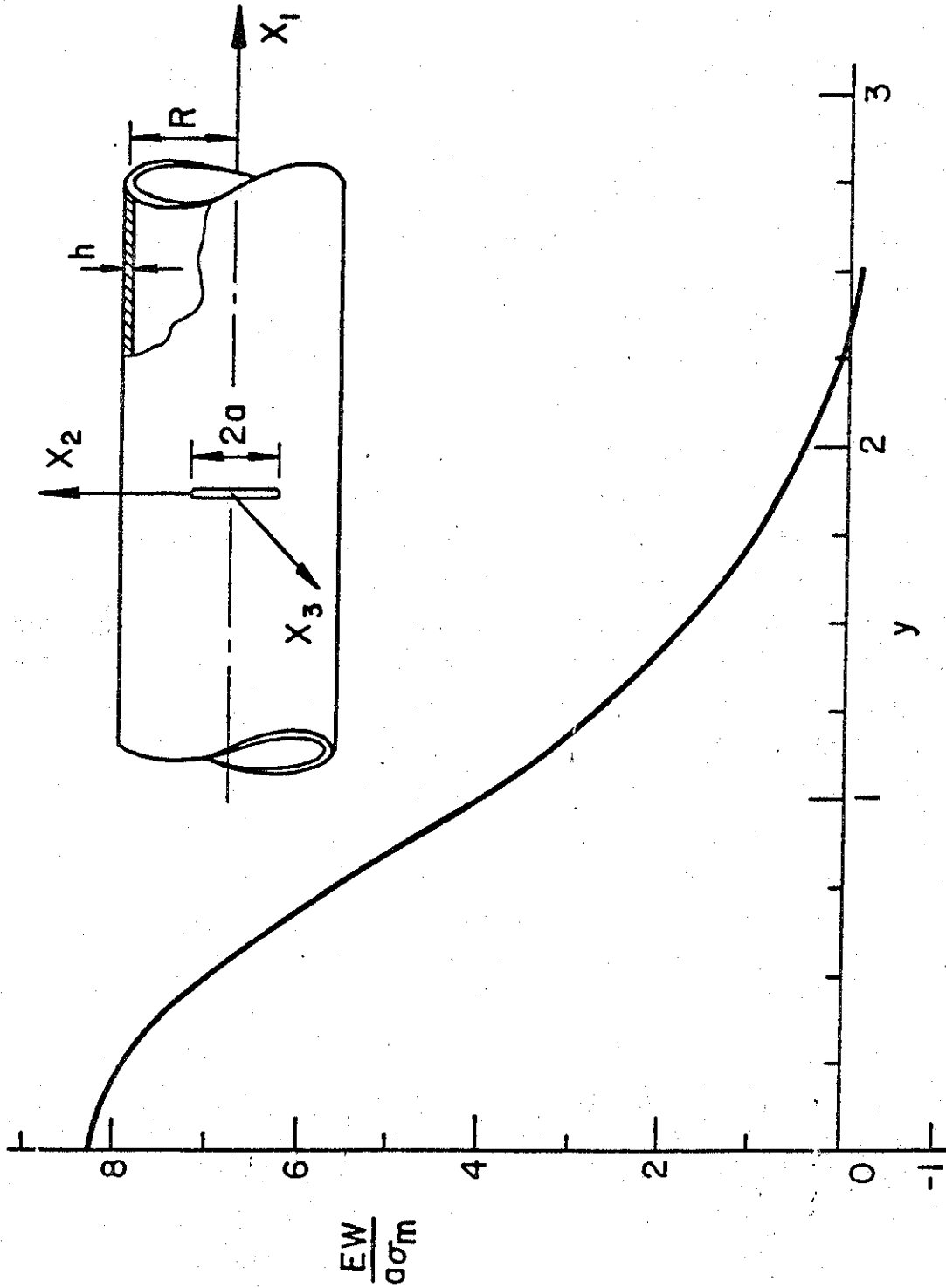


Figure 18. A sample result showing the crack surface displacement W perpendicular to the shell surface (i.e., in X_3 -direction) for $N_{11} = h$, $\sigma_m \neq 0$, $M_{11} = 0$, $a/h = 5$, $\lambda_2 = 3$, and $\nu = 1/3$.

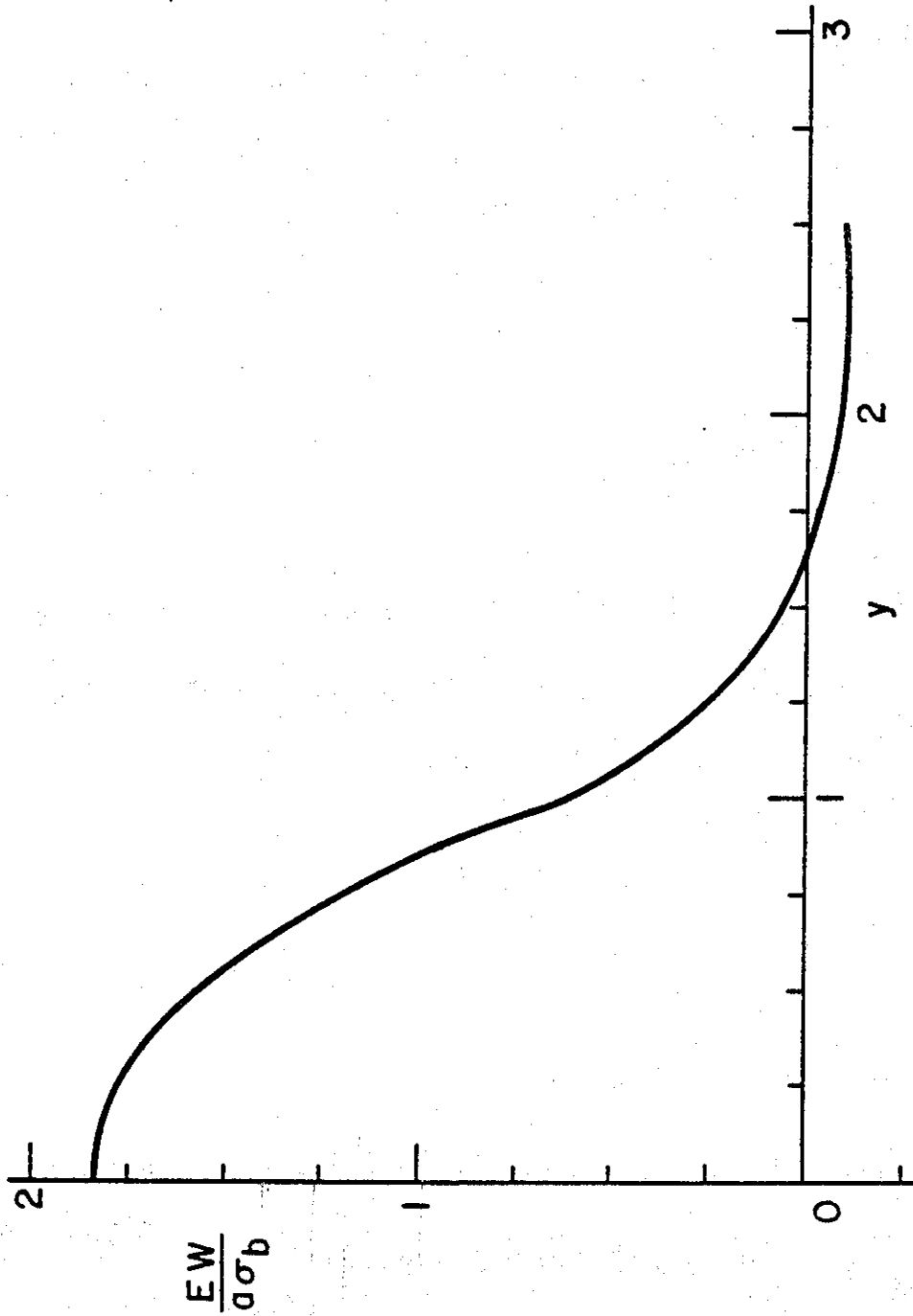


Figure 19. The crack surface displacement perpendicular to the shell surface for $M_{11} = 0$, $M_{11} = h^2 \sigma_b / 6 \neq 0$, $a/h = 5$, $\lambda_2 = 3$, $\nu = 1/3$.

Two most common loading conditions in pipelines and in relatively long pressure cylinders giving axial stresses are the uniform axial loading caused by internal pressure or axial constraints and the gross bending. The stress intensity factors corresponding to these loading conditions are given in Appendix A, Tables A1 and A4.

The quantity which is a great deal of interest in fracture studies is the strain energy release rate G . In Mode I plane problems G is related to the stress intensity factor k_I by

$$G = \frac{\pi k_I^2}{E_0} \quad (23)$$

where $E_0 = E$ for plane stress and $E_0 = E/(1-\nu^2)$ for plane strain. Here G is the energy released per unit crack extension and per unit thickness. In the symmetric shell problems, the Mode I stress intensity factor k_I consists of membrane and bending components, i.e., k_I is a function of the thickness coordinate z . Thus in a small neighborhood of the crack tip $x=0, y=a$ the cleavage stress and the crack opening displacement may be given in terms of the following asymptotic expressions:

$$\sigma_{11}(0, X_2, X_3) = \frac{k_I(X_3)}{\sqrt{2(X_2-a)}} \quad (24)$$

$$u_1(0, X_2, X_3) = u_1(0, X_2, 0) + X_3 \beta_1 = \frac{2k_I(X_3)}{E} \sqrt{2(a-X_2)} \quad (25)$$

$$k_I(X_3) = k_m + k_b X_3/(h/2) \quad (26)$$

where k_m and k_b are, respectively, the membrane and the bending component of the Mode I stress intensity factor. The strain energy release rate (at one crack tip, per unit crack extension and per unit thickness) may then be obtained from

$$G = - \frac{dV}{dA} \quad , \quad dA = h \, da,$$

$$dV = -2 \int_{-h/2}^{h/2} \int_0^{da} \frac{1}{2} \sigma_{11}(0, X_2, X_3) u_1(0, X_2-da, X_3) \, dX_2 \, dX_3 \quad (27)$$

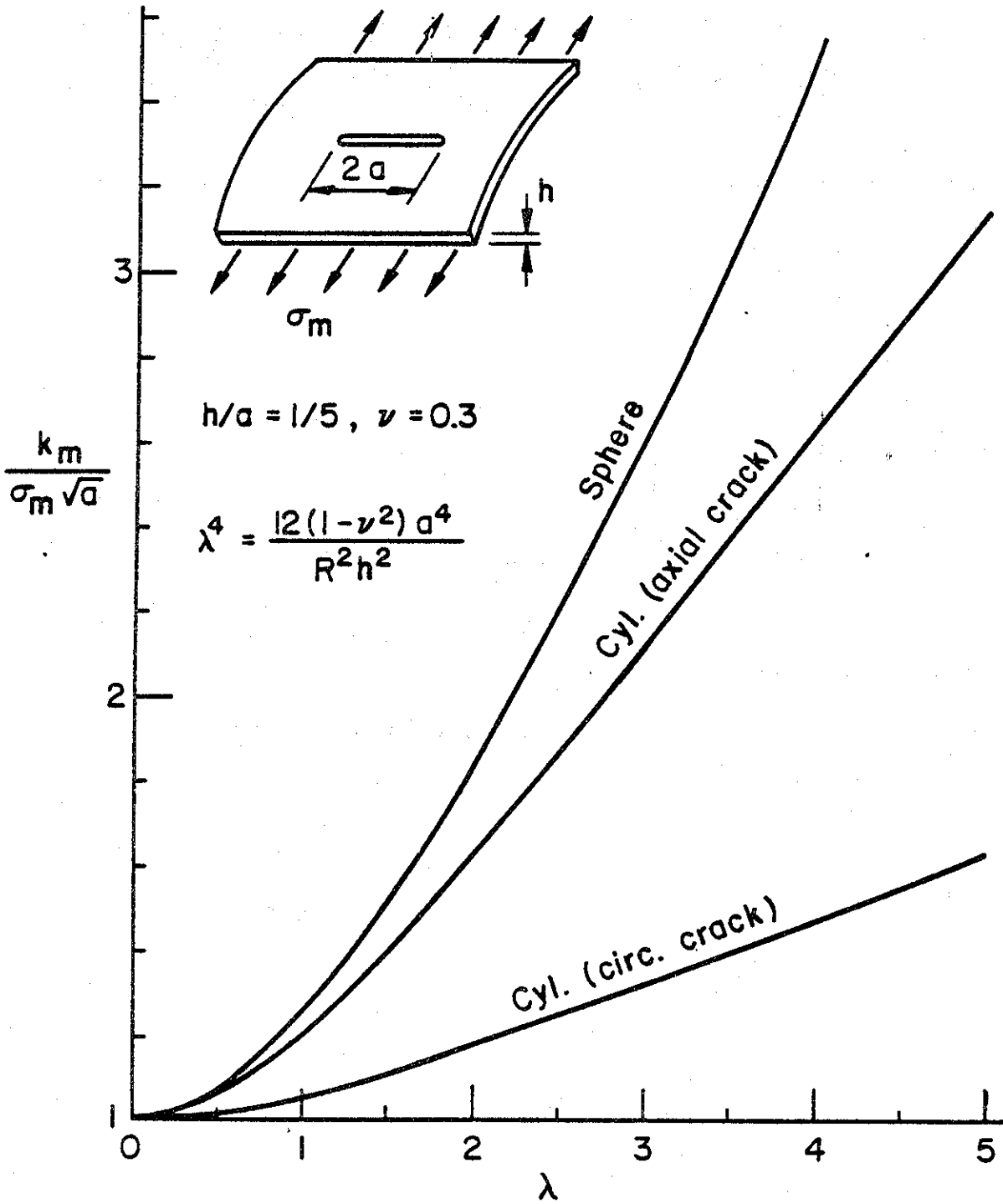


Figure 20. Comparison of the Mode I stress intensity factors in a cylindrical and a spherical shell under uniform membrane loading.

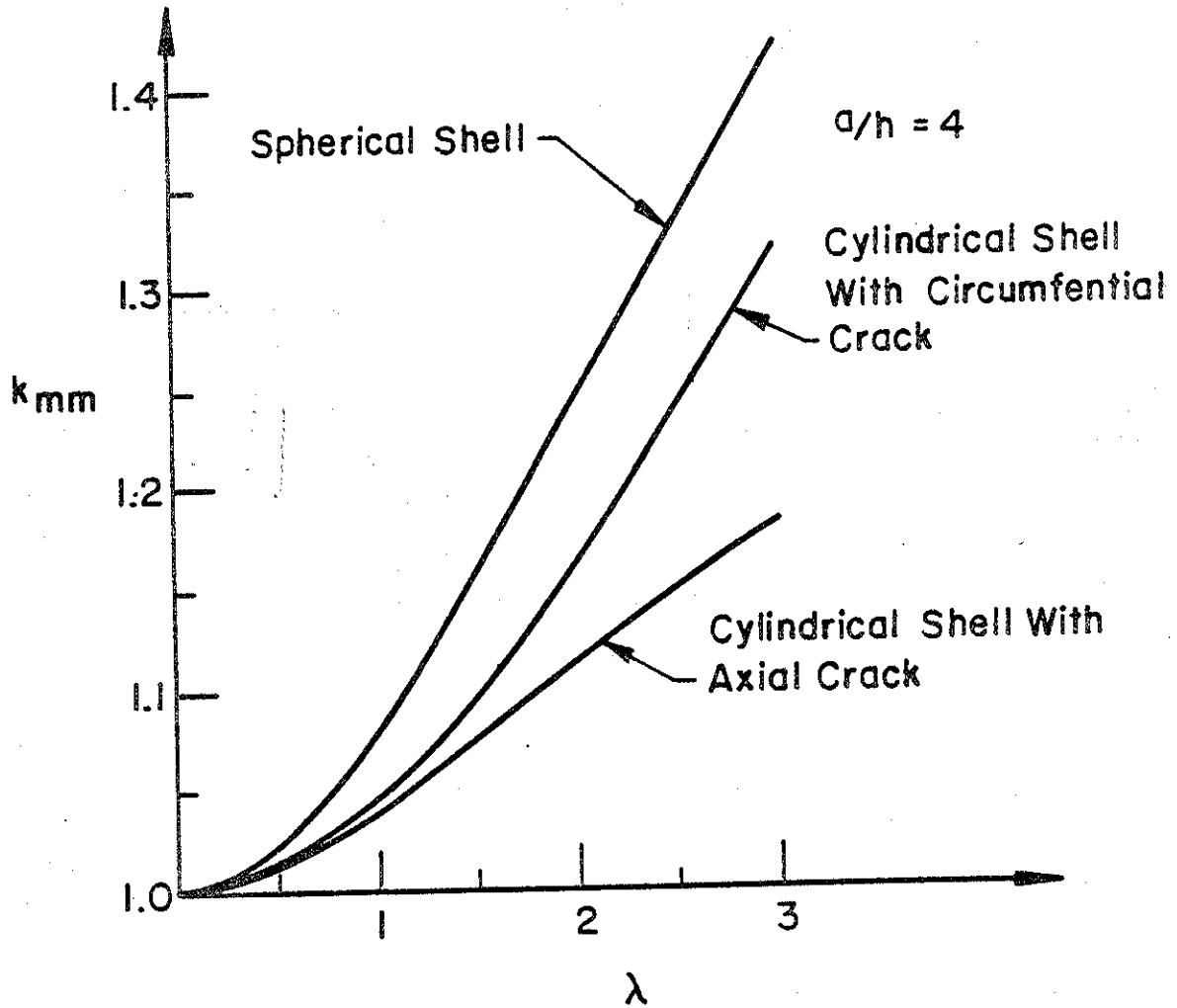


Figure 21. Comparison of the Mode II stress intensity factors in a cylindrical and a spherical shell under torsion.

where V is the strain energy. Substituting from (24-26) into (27) we find

$$G = \frac{\pi}{E} (k_m^2 + k_b^2/3) . \quad (28)$$

The importance of (28) lies in the means it provides to deal with problems of fatigue crack propagation and fracture in plate and shell structures in which the bending component of the stress intensity factor is not zero.

3.3 Comparison with Other Crack Geometries

The results given in this section show that the shell curvature may have a very significant adverse influence on the strength of pipes and cylinders containing a through crack. Needless to say, the stress intensity factors are dependent on the orientation of the crack in the cylinder as well as on the crack and shell dimensions. To compare the severity of a circumferential crack in a cylinder with that of an axial crack in a cylinder and of a meridional crack in a spherical shell, some sample results are shown in Figures 20 and 21. Figure 20 shows the membrane component k_m of the stress intensity factor in the shells subjected to uniform membrane loading (e.g., internal pressure). Similar results for the shells under torsion (i.e., uniform in-plane shear) are shown in Figure 21. Note that for the same dimensional constants the stress intensity factor is highest in spheres. Also note that in cylinders the stress intensity factor for an axial crack is greater for membrane loading and less for torsion than the corresponding values for a circumferential crack.

To give an idea about the possible influence of material orthotropy (which may result, for example, from rolling), some limited results for an axially cracked cylindrical shell are shown in Figures 22-24. The modulus ratios $E_1/E_2 = 26.67$ and 1.38 correspond respectively to a highly orthotropic (e.g., a fiber-reinforced composite) and to a mildly orthotropic (e.g., a rolled metallic sheet) material. Similar results for an axially cracked cylinder under torsion are shown in Figure 24.

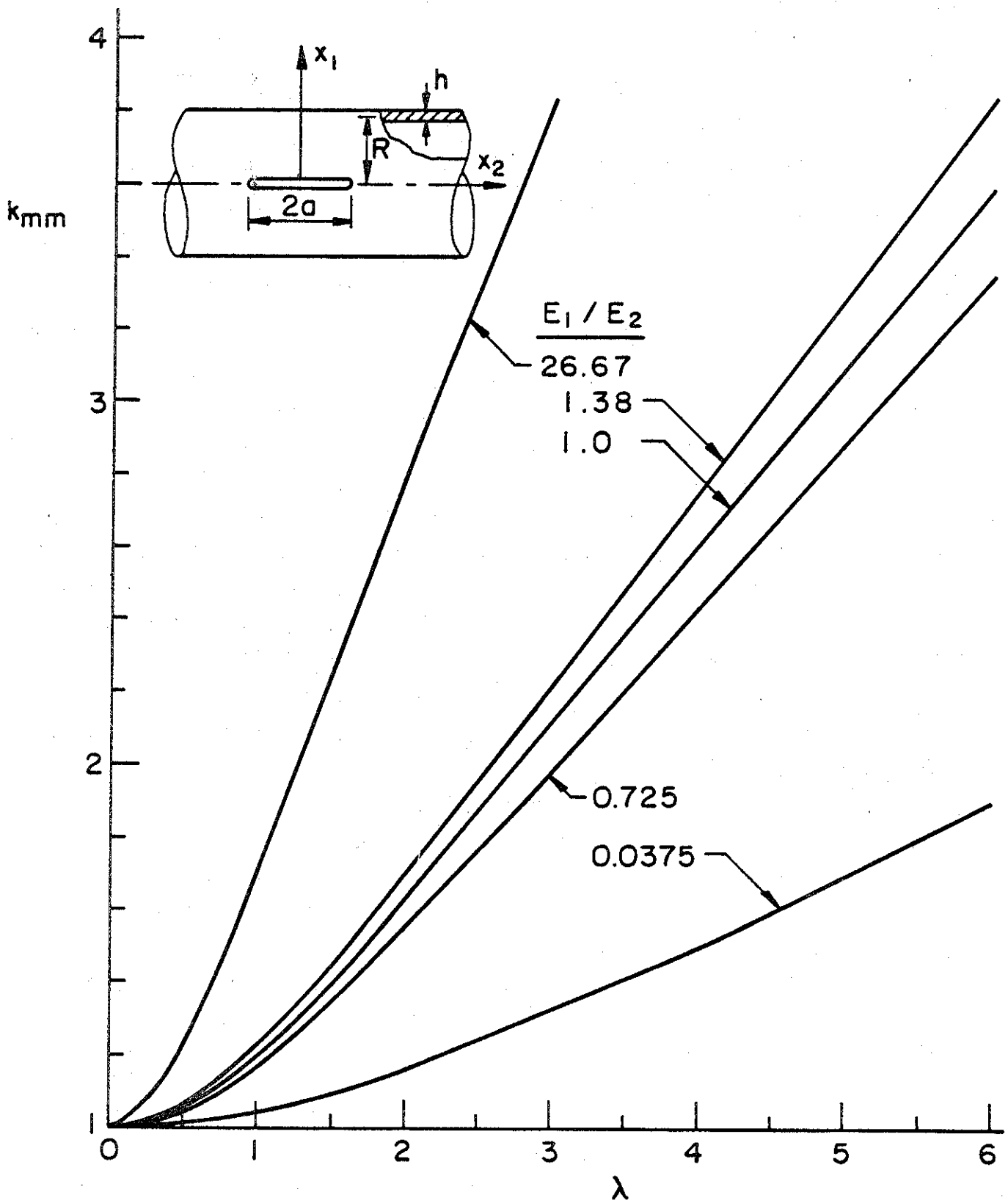


Figure 22. The effect of material orthotropy on the Mode I stress intensity factor in an axially cracked cylindrical shell under uniform membrane loading ($a/h = 10$, $\nu = 0.3$).

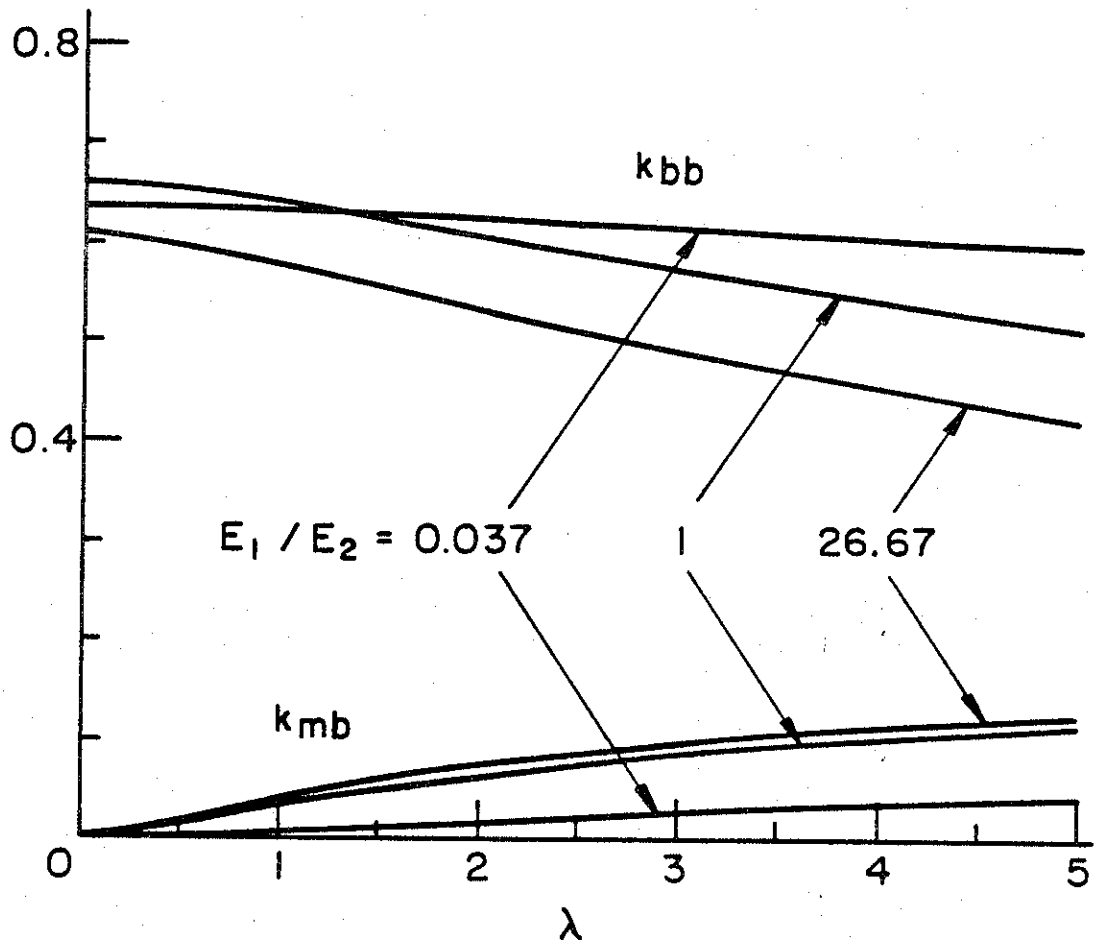


Figure 23. The effect of material orthotropy on the membrane and bending components of the stress intensity factor in an axially cracked cylindrical shell under uniform (local) bending ($a/h = 5$, $\nu = 0.3$).

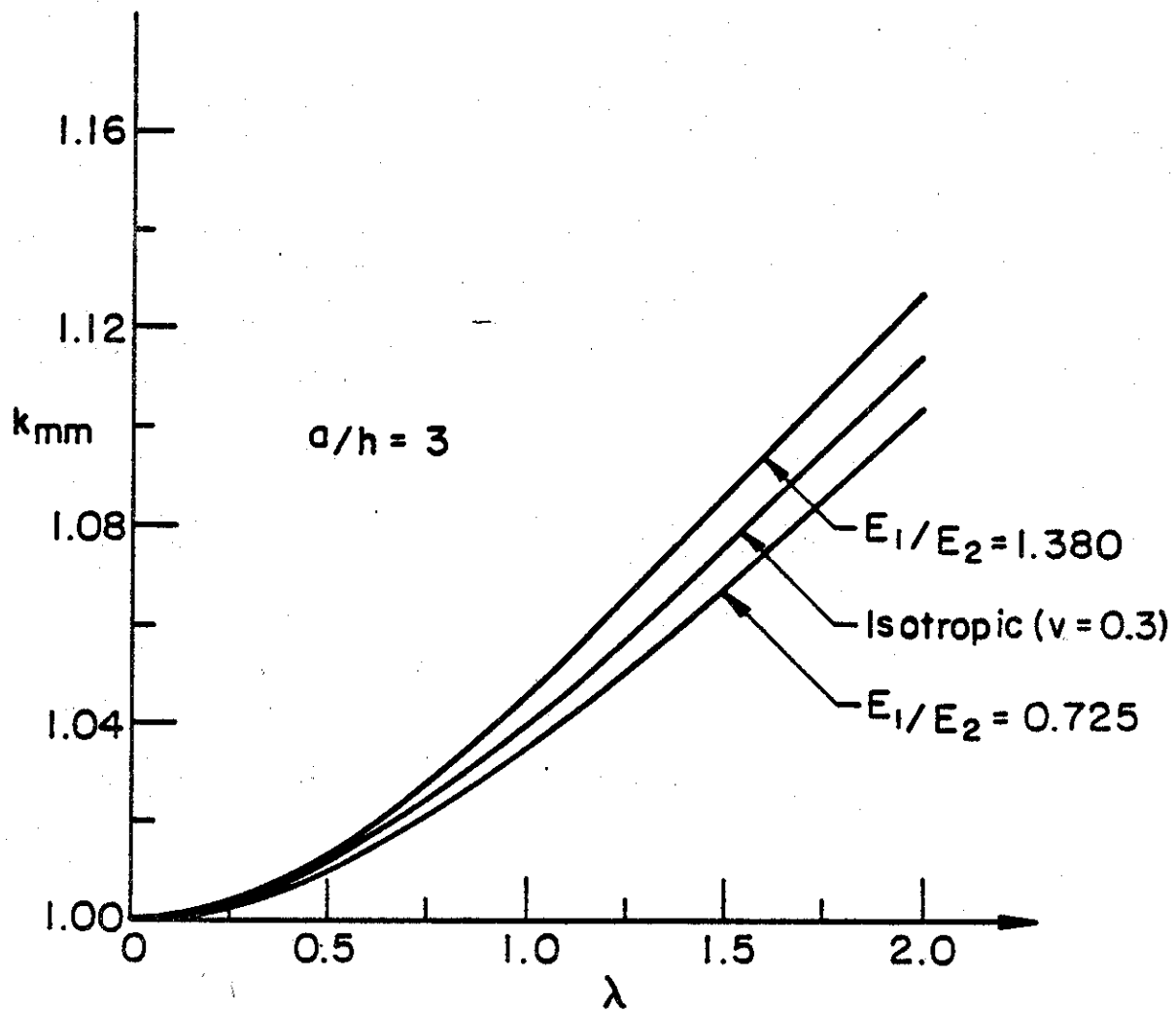


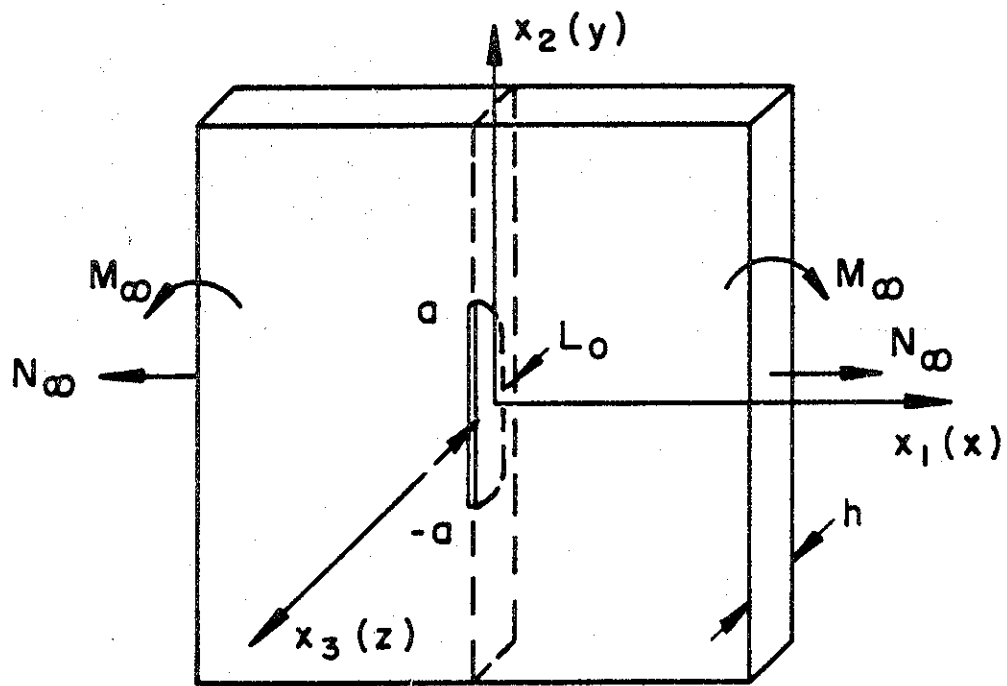
Figure 24. The effect of the material orthotropy in an axially cracked cylindrical shell under torsion ($a/h = 3$, $\nu = 0.3$).

3.4 The Part-Through Crack Problem in Pipes

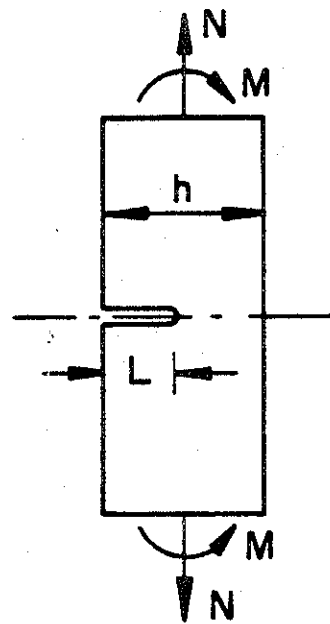
The initial stage of a fracture failure in pipes and cylinders usually is the formation and propagation of a fatigue crack from a surface flaw (such as a scratch or an arc burn). For a number of reasons it is essential that one ought to have a good estimate of the subcritical fatigue or corrosion fatigue crack growth rate in the structure under the given loading conditions. Since the stress intensity factor is used almost universally to correlate the subcritical crack propagation rate, this in turn requires carrying out the elastic solution of a shell which contains a part-through surface crack. Ideally, the problem is a three-dimensional elasticity problem and is analytically intractable. The existing finite element type numerical solutions are expensive and do not lend themselves to simple parametrization. In this research program therefore the simpler line-spring model [46] is used to solve the problem. The details of the analysis as well as some general results are given in Appendix B. The Appendix also shows the comparison of the results obtained from the line spring model and from the three-dimensional elasticity solution given by the finite element method [38]. The agreement appears to be quite satisfactory.

The problem has also been solved for a flat plate containing a surface crack [47], where again the calculated results have been compared with those obtained from the finite element solution. In addition to its relative simplicity, an advantage of the technique described in Appendix B is that the profile of the surface crack can be prescribed numerically or analytically in an arbitrary manner. The plate problem is described in Figure 25 and the stress intensity factor at the deepest penetration point of a semi-elliptic surface crack in a plate under tension and under bending is given in Figures 26 and 27, respectively. The results for a crack with a rectangular profile (i.e., with constant depth $L=L_0$) are given in Figures 28 and 29. The normalization factor K_∞ used in these figures is the corresponding stress intensity factor in an edge-cracked strip under plane strain conditions subjected to uniform tension N_∞ or bending M_∞ of the same magnitude and having the same crack depth ratio L_0/h (Figure 1b) as the plate with the semi-elliptic surface crack. The factor K_∞ for tension and bending is given by

$$K_\infty^t = \frac{N_\infty}{h} \sqrt{h} g_t(L_0/h) , \quad K_\infty^b = \frac{6M_\infty}{h^2} \sqrt{h} g_b(L_0/h) \quad (29)$$



(a)



(b)

Figure 25. Geometry of the plate with a part-through crack.

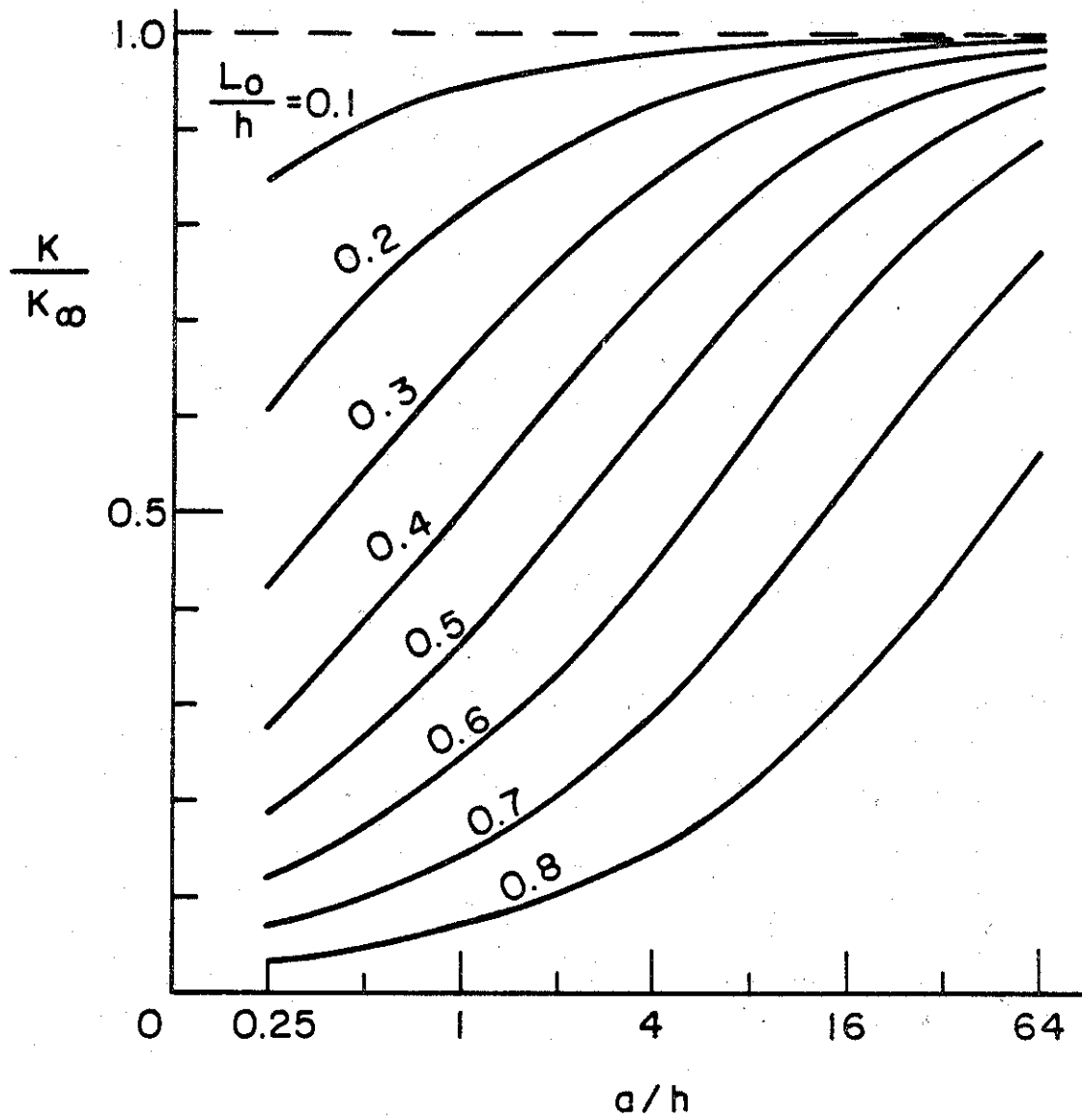


Figure 26. The stress intensity factor at the maximum penetration point of a semi-elliptic surface crack in an infinite plate under uniform tension ($\nu = 0.3$).

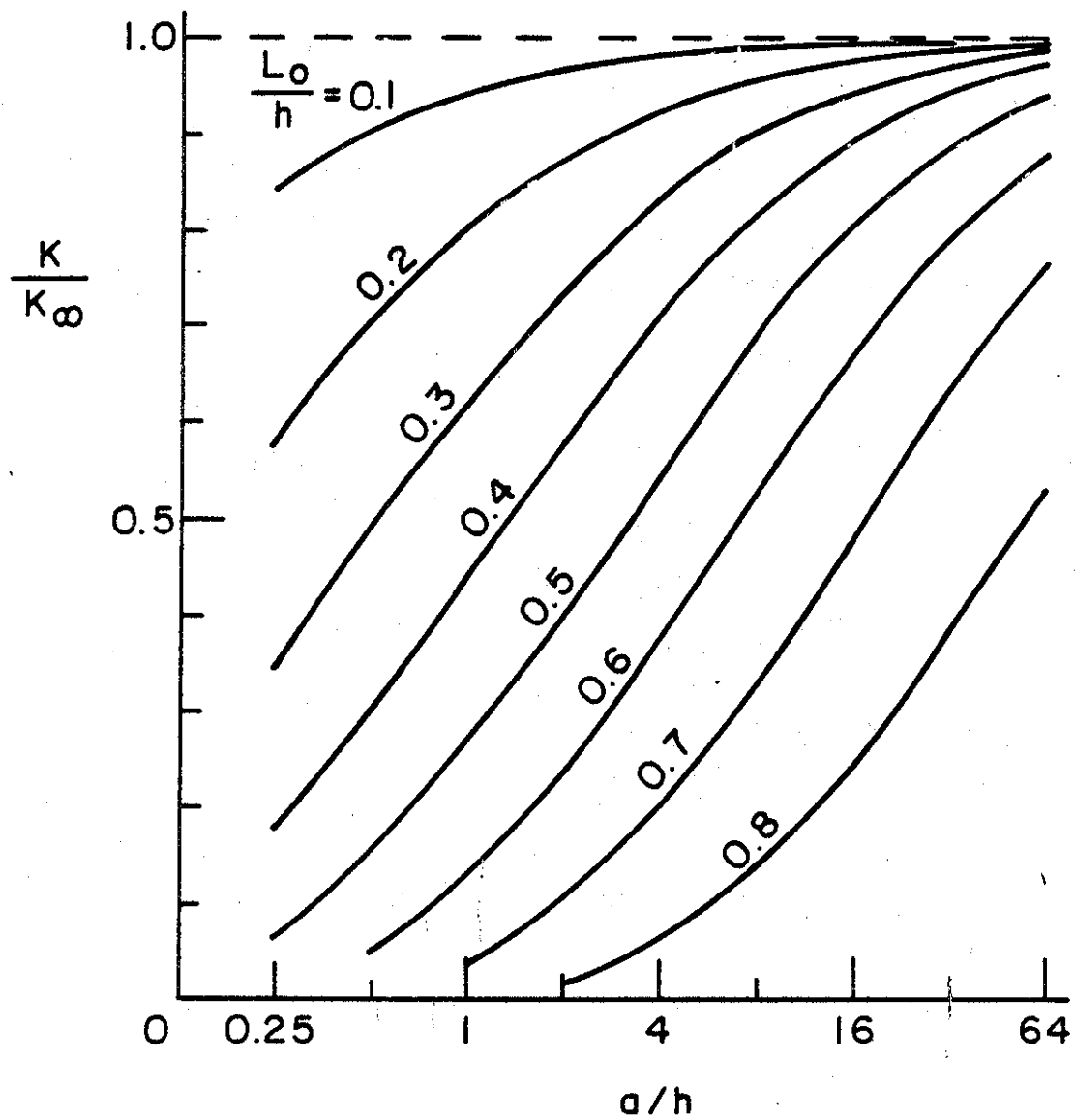


Figure 27. The stress intensity factor at the maximum penetration point of a semi-elliptic surface crack in an infinite plate under pure bending ($\nu = 0.3$).

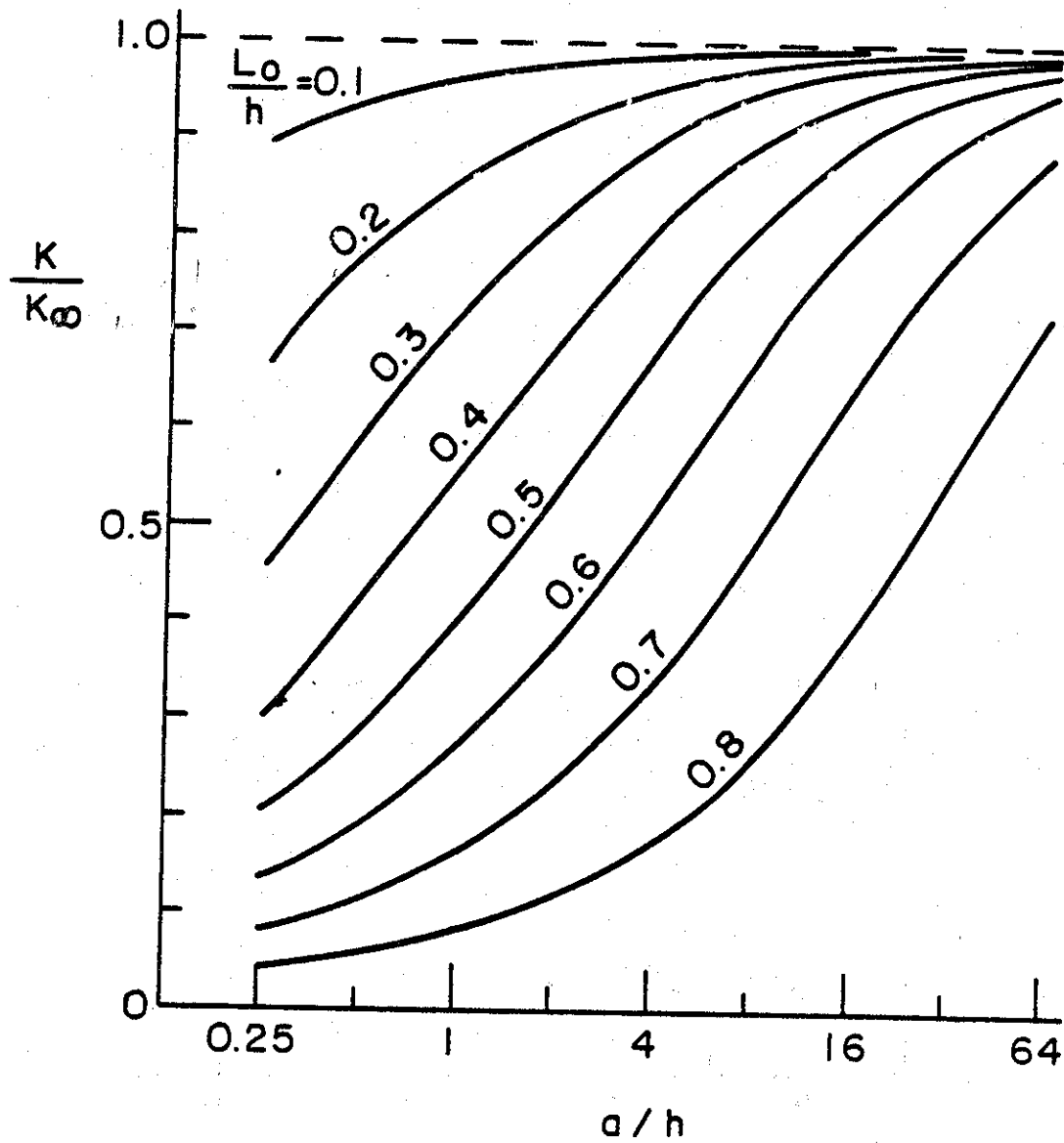


Figure 28. The stress intensity factor at the midpoint of a rectangular surface crack in an infinite plate under uniform tension ($\nu = 0.3$).

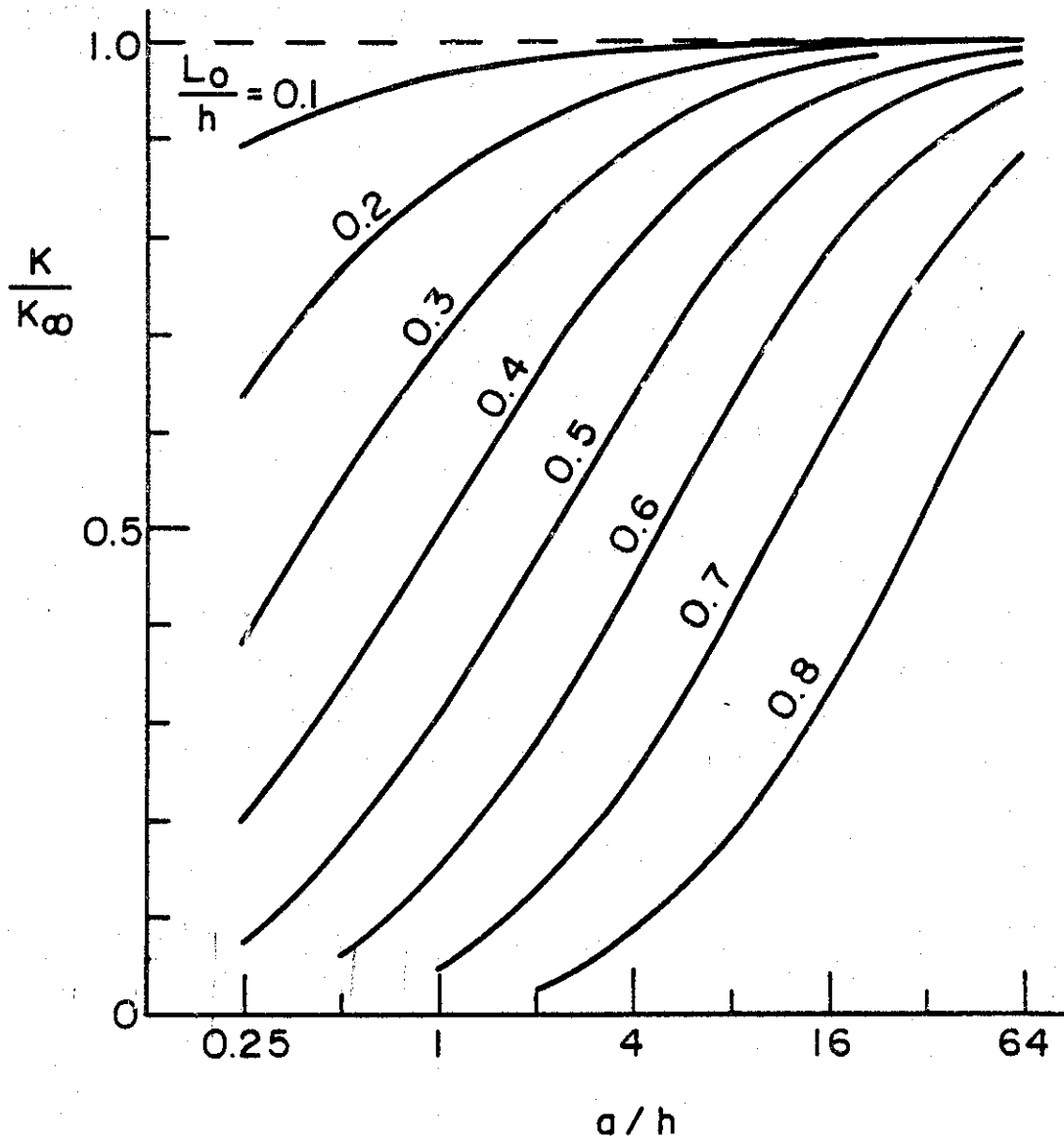


Figure 29. The stress intensity factor at the midpoint of a rectangular surface crack in an infinite plate under pure bending ($\nu = 0.3$).

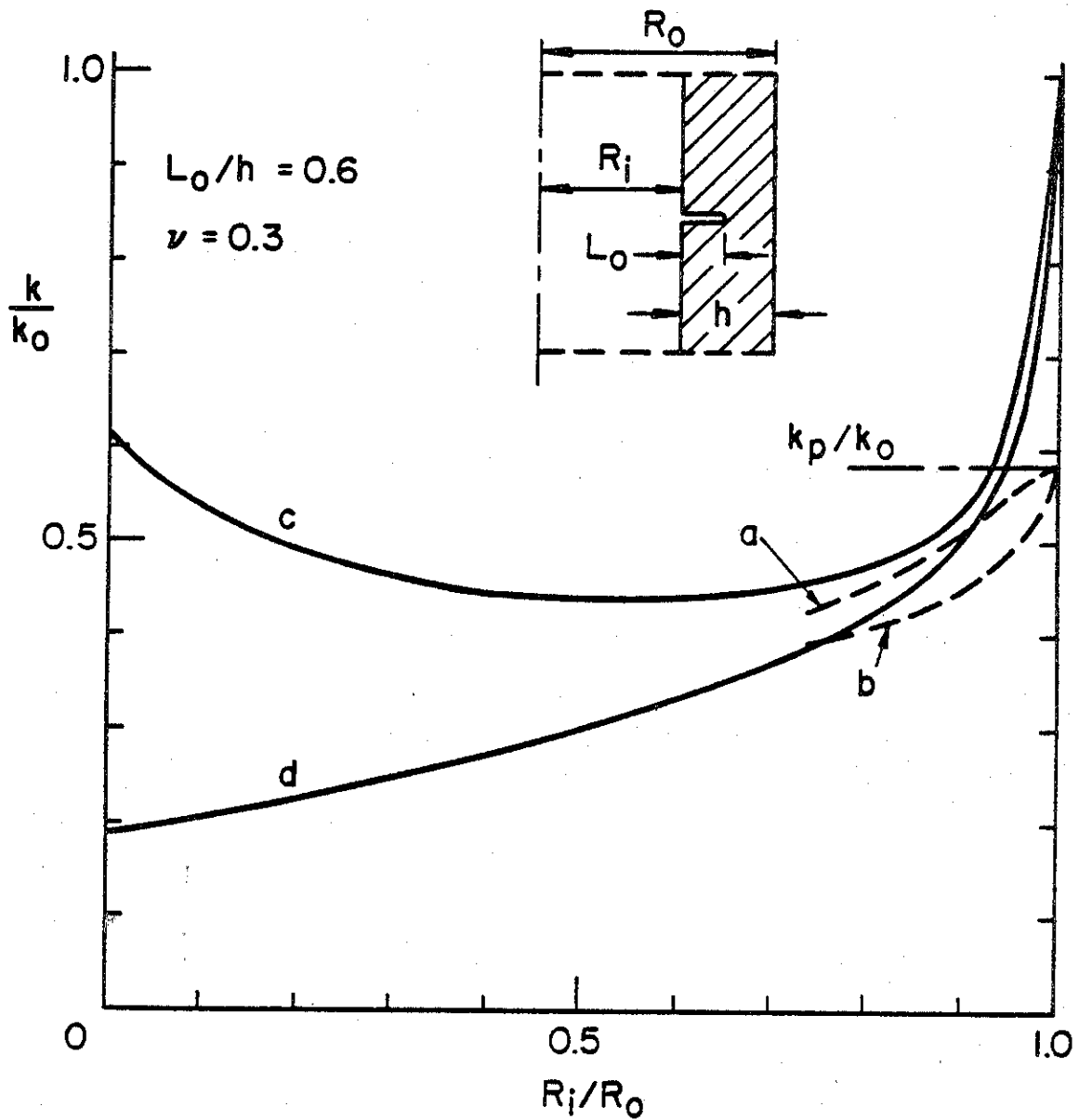


Figure 30. Comparison of the Mode I stress intensity factors obtained from the line-spring shell model and the axisymmetric elasticity solution. (a) External semi-elliptic surface crack, (b) internal surface crack, (c) elasticity result for the external axisymmetric crack, (d) internal axisymmetric crack. ($k_0 = 4.035\sigma_0\sqrt{L_0}$, $k_p = 0.582k_0$, $a/h = 8$, σ_0 : uniform axial stress)

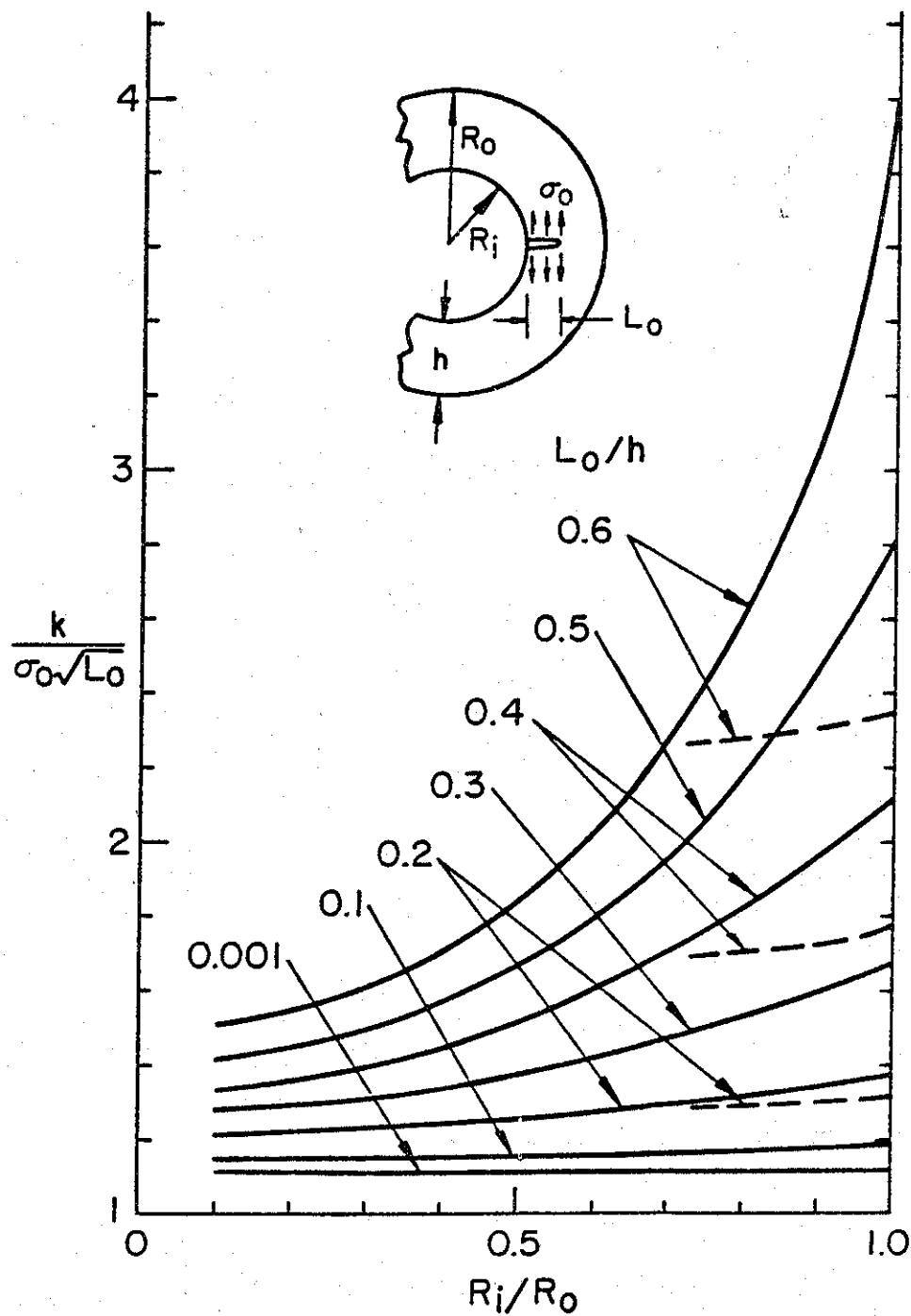


Figure 31. Comparison of the line-spring shell stress intensity factor at the deepest point of an internal axial surface crack (dashed lines) with the corresponding plane strain cylinder result (full lines), $a/h = 8$.

axisymmetric edge cracks in a thick-walled cylinder under uniform axial tension obtained from the elasticity solution. As $R_i/R_o \rightarrow 1$ the stress intensity factors approach that for an edge crack in a flat plate under plane strain conditions. The dashed lines are the stress intensity factors at the deepest penetration point of a semi-elliptic surface crack which are obtained from the line-spring model (Appendix B). The discrepancy between the axisymmetric crack and the semi-elliptic surface crack results is highest for $R_i/R_o = 1$ (i.e., for the flat plate). For the plate the maximum stress intensity factor in a semi-elliptic surface crack (Figure 26, $a/h = 0.8$, $L_o/h = 0.6$) is only 58.2% of the plane strain value. This is, of course, due to the fact that in the uniformly loaded plate containing the semi-elliptic crack the section containing the crack carries less than the average load per unit plate width. One may note that because of the use of the shell theory, the surface crack results given for $R_i/R_o < 0.9$ would be highly approximate.

Appendix D also gives the stress intensity factors in a thick-walled cylinder containing an axisymmetric inner or outer edge crack due to thermal and residual stresses.

Similarly, exact bounds for the axial surface crack problem may be obtained by assuming that the part-through crack in the axial direction is "infinitely" long. Consequently, the problem may be assumed to be a plane strain problem for a thick-walled cylinder which contains a part-through radial crack. The related elasticity problem is considered in Appendix E where the general solution and some extensive results are given. The partial results reproduced in Figure 31 are qualitatively quite similar to those given for the circumferential crack problem (see Figure 30). As expected, for relatively long and shallow cracks the plane strain and semi-elliptic surface crack results are much closer to each other than the deep crack results. Other results given in Appendix E include that of the imbedded radial crack and the rotating cylinder.

3.6 Stresses Due to Radial Weld Shrinkage

In solving the crack problems the general practice is first to perform the stress analysis of the structure separately by ignoring the crack, and to calculate the normal and shear stresses in the plane of the crack. Then

a "perturbation" problem is solved for the cracked structure in which the equal and opposite of the stresses calculated from the first solution applied to the crack surface are the only nonzero external loads. In relatively thin-walled structures such as pipes and pressurized cylinders these local stresses are usually a combination of membrane, bending, and transverse shear resultants. Many of the solutions for pipes and cylinders obtained by using the shell theory may be found in published literature or may be obtained by some elementary method. Two problems of special interest in this study are the stresses in a cylindrical shell caused by the radial shrinkage of girth welds and those in a pipe under four point bending.

If the pipe is not properly preheated before circumferential welding or if the heating does not match the weld shrinkage, then upon cooling the pipe may undergo "waisting" which results in gross residual stresses in the neighborhood of the girth weld. It should be pointed out that in addition to this gross residual stresses which may be obtained by using a shell theory, in and around the weld seams there would be statically self-equilibrating residual stresses the determination of which would require a three-dimensional elastic-plastic analysis. A useful solution for the gross residual stresses may be obtained by approximating the weld by a ring and by treating the problem as a statically indeterminate ring-shell problem.

To do this, let us define the following quantities:

- a,b: inner and outer radii of the cylinder,
- $R = (a+b)/2$: mean radius,
- $h = b-a$: wall thickness,
- ΔT : the mismatch temperature,
- α : coefficient of thermal expansion of the weld,
- t: the average weld width,
- E_w : modulus of elasticity of the weld metal,
- E_c : modulus of elasticity of the cylinder (base metal).

The total displacement mismatch in radial direction may be expressed as

$$\Delta w = R\alpha\Delta T = w_c + w_w \quad (31)$$

where w_c and w_w are the displacements of the cylinder and the weld, respectively. Let Q_0 be the (radial) resultant shear force acting along the

ring-shell interfaces. In terms of Q_0 the radial displacement of the weld may be expressed as

$$w_w = \frac{Q_0 R^2}{htE_w} \quad (32)$$

For a cylindrical shell acted upon by axisymmetric transverse shear force Q_0 the maximum radial displacement is found to be [48]

$$w_c = \frac{Q_0 R^2}{2hE_c} \frac{[3(1-\nu^2)]^{3/4}}{\sqrt{Rh}} \quad (33)$$

From (31-33) Q_0 may be obtained as

$$Q_0 = \frac{2thE_c E_w \sqrt{Rh}}{R\{2E_c \sqrt{Rh} + tE_w [3(1-\nu^2)]^{3/4}\}} \alpha \Delta T \quad (34)$$

Once ΔT is estimated and Q_0 is evaluated, the maximum bending moment (which is also under the load) may be obtained as [48]

$$(M_z)_{\max} = \frac{Q_0 \sqrt{Rh}}{4[3(1-\nu^2)]^{3/4}} \quad (35)$$

giving the stress distribution

$$\sigma_{zz}(r,0) = \sigma_{\max} \frac{2R}{h} \left(1 - \frac{r}{R}\right) \quad (36)$$

where

$$\sigma_{\max} = \frac{6Q_0 \sqrt{Rh}}{4h [3(1-\nu^2)]^{3/4}} \quad (37)$$

For example, if the shell contains a circumferential crack, then to determine the solution due to the gross residual stresses, the related integral equations in Appendix B or Appendix D must be solved by substituting the crack surface traction $-\sigma_{zz}$ from (36).

3.7 Stresses in a Pipe under "Four-Point" Bending

In solving the crack problems in pipes it was indicated that for a given loading condition the stresses in the pipe without the crack are known. The crack problem was then solved under self-equilibrating loads applied to the crack surfaces only. A problem of particular interest in this research program is a pipe under "four-point" bending (Figure 32). Generally in such problems it is assumed that the pipe is subjected to gross bending and the stresses may be obtained by treating the pipe as a "beam". However, in most cases, it is necessary to verify the results given by the beam theory by carrying out a somewhat more realistic stress analysis of the pipe and by considering the details of the loading fixtures.

At the four points shown in Figure 32 the loads were applied to the pipe by 6 in. wide semicircular saddles. To prevent a possible collapse of the pipe wooden blocks of 4 in. x 4 in. cross-section were inserted into the pipe at the load locations (Figure 33). Other relevant dimensions are shown in Figure 32.

A shell theory was used to calculate the stresses in the pipe^(*). This is a numerical technique in which all field quantities including the external loads are expanded into Fourier series in θ and a segmental integration is used in the axial direction. The shell equations are expressed in terms of a system of first order differential equations. The resulting "two-point boundary value problem" is then solved by reducing it to an initial value type problem.

In order to avoid a highly complicated contact problem, the form of the "contact" stresses at the locations of the loads was assumed beforehand (see Figure 33). Following were the main assumptions: (a) the contact at all locations is frictionless, (b) the pressure distribution under the saddles is independent of the axial coordinate and has a cosine distribution in θ , and (c) the pressure distribution between the wooden blocks and the shell is uniform. Thus, the transverse load $N(\theta)$ applied to the pipe would be of the

(*) KSHEL developed by Professor A. Kalnins at Lehigh University.

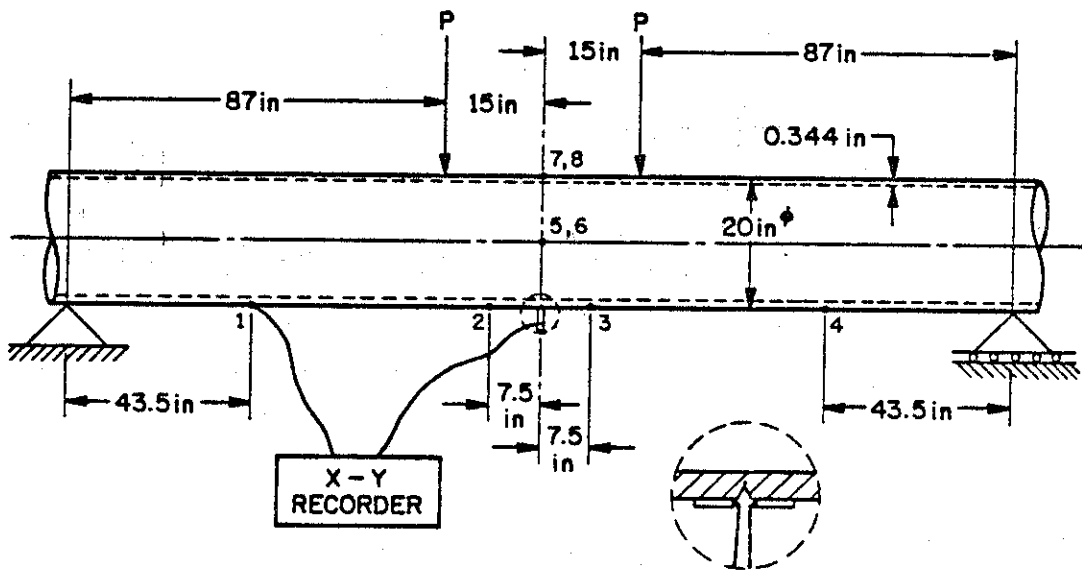


Figure 32. The geometry and dimensions of the pipe specimens.

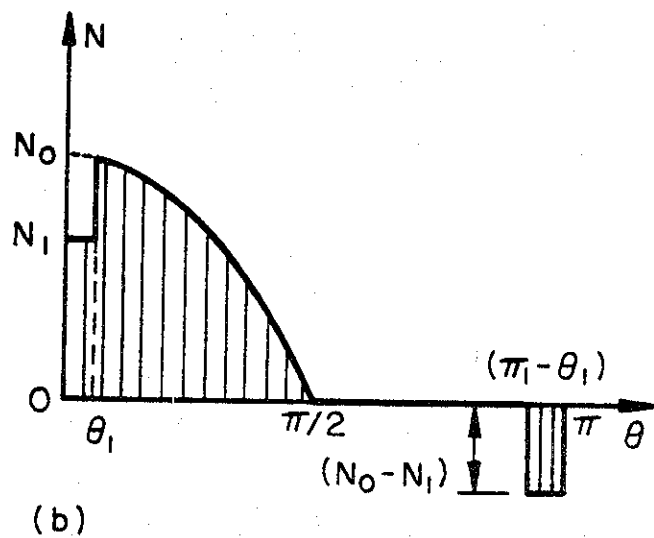
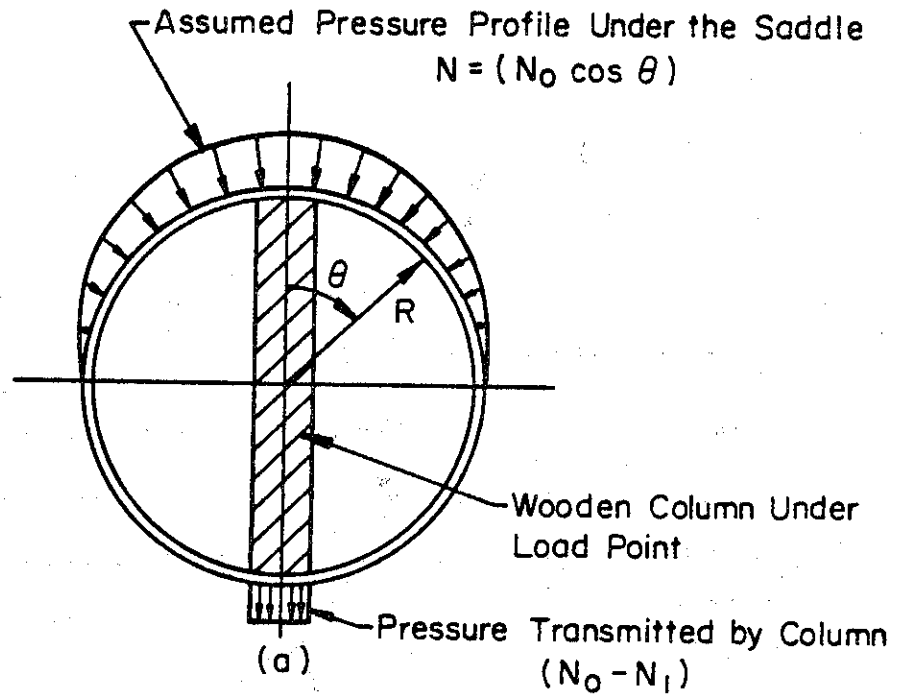


Figure 33. Assumed distribution of the applied load through the saddles and the wooden blocks in the pipe specimens.

form shown in Figure 33, where

$$N(\theta) = N_0 \cos\theta \quad , \quad (38)$$

N_1 is unknown, and $\theta_1 = c/2R \cong 0.2$ rad., $c = 4$ in. being the width of the wooden block. From the equilibrium condition N_0 is found to be

$$\int_{-\pi/2}^{\pi/2} N(\theta) \cos\theta R d\theta = P \quad , \quad N_0 = 2P/\pi R \quad . \quad (39)$$

The load N_1 is determined from the following displacement compatibility conditions:

$$W(0) + W(\pi) = \frac{\sigma_w \ell_w}{E_w} \quad , \quad (40)$$

where $W(\theta)$ is the radial displacement in the shell (positive if outward), σ_w is the stress in and ℓ_w and E_w are the length and the Young's modulus of the wooden block.

In the analysis the loading condition shown in Figure 33 is used only in the interior load locations $x = \mp 15$ in. (Figure 32). For simplicity the pipe ends were assumed to be "simply-supported", that is, at $x = \mp 102$ in. it was assumed that

$$(N_{\phi\phi}, M_{\phi\phi}, N_{\phi\theta}, W) = 0 \quad , \quad (41)$$

where ϕ and θ are respectively the axial and the circumferential coordinates and N_{ij} and M_{ij} ($i, j = \phi, \theta$) are the membrane and bending resultants.

Some calculated results for the dimensions shown in Figure 32 are given in Figures 34-36. Figure 34 shows the θ -distribution of the circumferential stress $\sigma_{\theta\theta}$ and the axial stresses σ_{xi} and σ_{x0} in the pipe at the plane of symmetry $x=0$ where the subscripts o and i stand for points on the "outer" and the "inner" surface of the shell, respectively. $\sigma_{x0} \neq \sigma_{xi}$ implies local bending of the shell wall; that is,

$$(\sigma_{x0} + \sigma_{xi})/2 = N_{\phi\phi}/h, \quad (\sigma_{x0} - \sigma_{xi})/2 = 6M_{\phi\phi}/h^2 \quad . \quad (42)$$

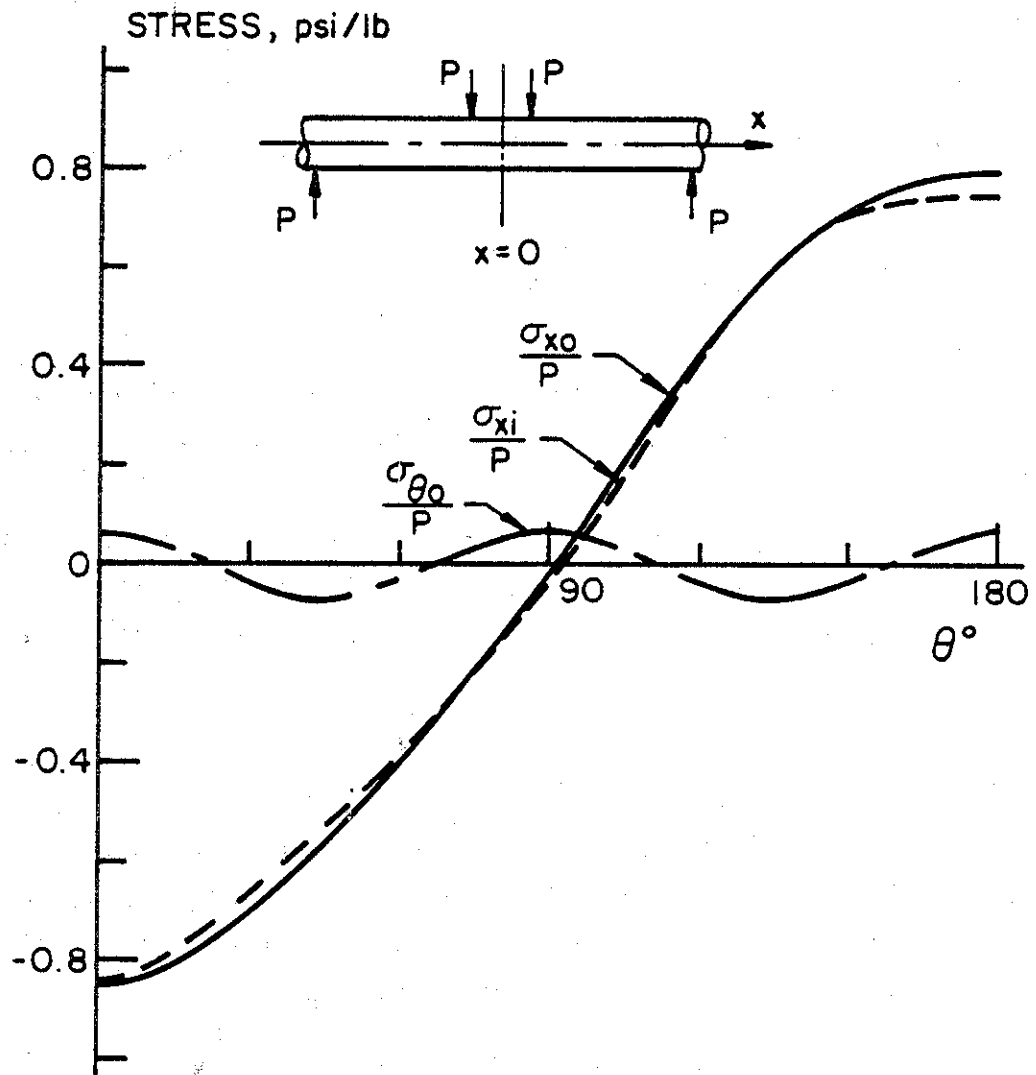


Figure 34. Circumferential variation of the hoop ($\sigma_{\theta\theta}$) and the axial stresses (σ_{xi}, σ_{xo}) at $x=0$ plane in the pipe under "four-point-bending".

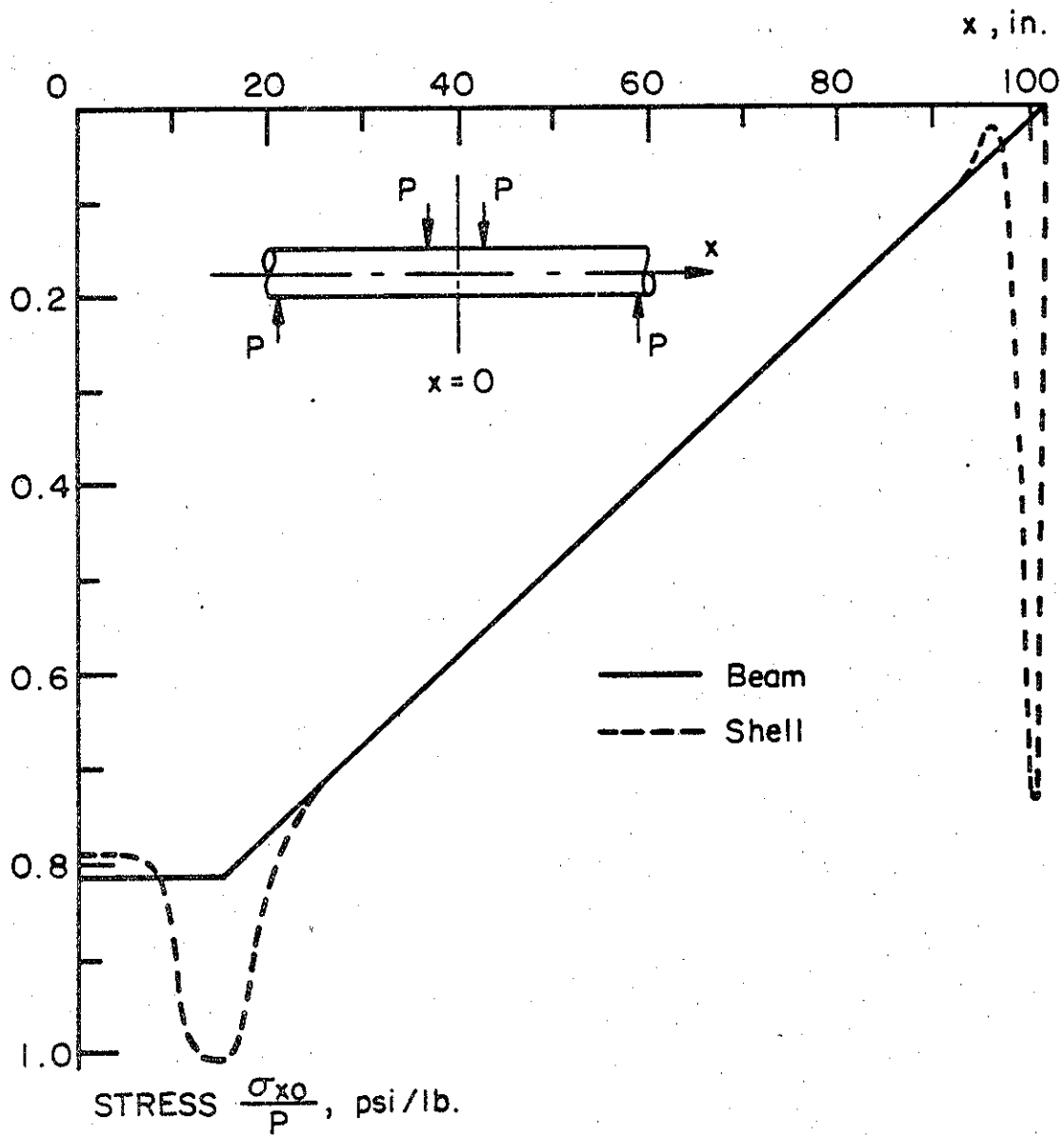


Figure 35. Variation of the maximum axial stress (σ_{x0} at $\theta=\pi$) along the pipe.

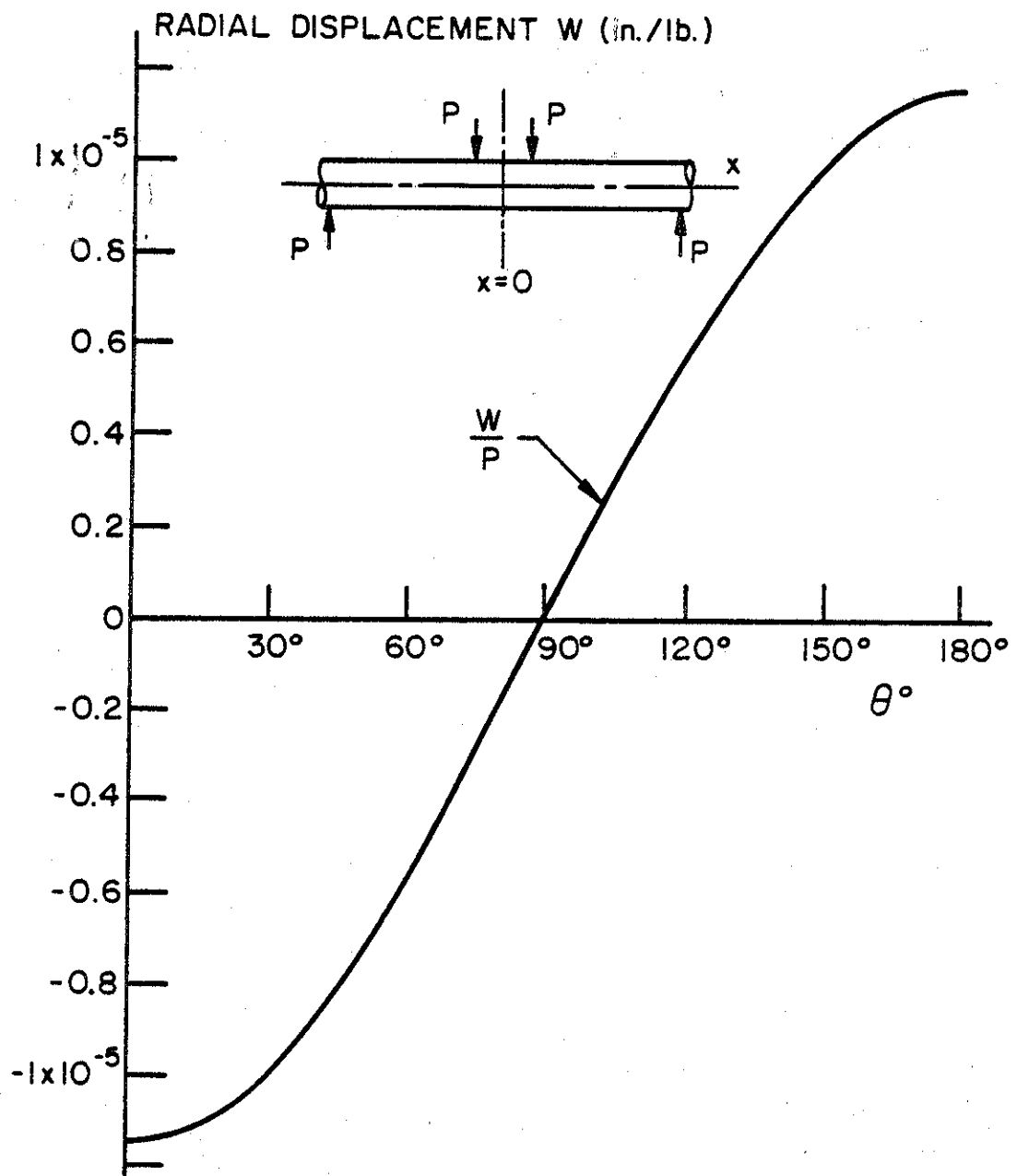


Figure 36. The circumferential variation of the radial displacement W at $x=0$ plane.

Figure 35 shows the distribution of the axial stress σ_{x0} at $\theta = \pi$ as a function of x . The figure also shows the same stress component obtained from the beam theory. From Figures 34 it may be observed that the local bending due to the variation of the membrane stress σ_x in thickness direction at the location of the crack (i.e., $x=0$, $\theta=\pi$) is not very significant (the maximum bending stress $\sigma_b = 6M_{\phi\phi}/h^2$ is approximately 3.7% of the membrane stress $\sigma_m = N_{\phi\phi}/h$). Similarly, the difference between the stresses at the crack location obtained from the shell and the beam theories is approximately 3.1% of the nominal value (Figure 35). Therefore, in this study using the beam theory to calculate the stresses would involve no substantial error.

Figure 36 gives some idea about the ovalization of the pipe at $x=0$ plane. In this figure $W(\theta)$ is the radial component of the displacement (positive if outward). It should be emphasized that the problem was solved for $P=1$ by using the actual dimensions of the pipe given in Figure 32. Thus all quantities shown in Figures 34-36 are per unit applied load and are not dimensionless.

4. DUCTILE FRACTURE MODEL: ELASTIC-PLASTIC SOLUTIONS

As pointed out in Section 2, if the part-through crack in the plate or the shell is relatively deep and long, the net ligament rupture would seldom be preceded by a K or J-controlled progressive self-similar crack growth. In such situations a more likely mode of fracture would be either an unstable growth of a shear crack or plastic necking instability. In either case the related fracture process is very complex and is highly dependent on the global mechanics (i.e., on the structure-crack geometry and the nature of the external loads) of the problem. Therefore, even if one assumes that the fracture is basically "ductile" and some such mechanism as hole formation, growth, and coalescence is responsible for further cracking, for plates and shells the development of a realistic one-parameter quantitative failure criterion does not seem to be feasible. Tearing modulus, J_{IC} , COD, Charpy energy and other similar parameters associated with the ductile fracture strength of the material are extremely useful for fracture characterization and comparative classification of the structural materials. However, because of the mechanics of the surface crack problem in plates and shells, they cannot

be used directly in a fracture criterion governing the related ductile fracture process. On the other hand, for the purpose of correlating and studying the experimental results, it is clearly advantageous to select a single parameter.

Because of the complexity of the related mechanics problem, in pipes it would be preferable to select a parameter which may be considered as a measure of the intensity of local strains and at the same time the theoretical evaluation of which would be relatively insensitive to the accuracy of the continuum modeling of the elastic-plastic stress-strain relations in the crack region. The rationale here is that whatever the actual mechanism of the fracture process, the intensity of the local plastic strains may be looked upon as an acceptable measure of the material resistance as well as the intensity of the applied load. The parameter selected for this purpose in this study is the crack opening displacement (COD). COD can be measured accurately and is certainly a realistic measure of the intensity of plastic deformations. Also the crack mouth opening displacement is a "global" quantity in the sense that it reflects the integrated effects of the plastic deformations in the crack region. Hence, it is reasonable to assume that its calculated value would not be as sensitive as some other parameters to the details of the elastic-plastic modeling of the part-through crack problem. It should again be strongly emphasized that here we are not proposing a specific fracture criterion which is based on COD and particularly is dependent on a "critical COD." We are rather proposing to use COD as a correlation parameter in analyzing certain types of ductile fracture problems in the sense that the stress intensity factor range ΔK is used to analyze and correlate the subcritical crack propagation results.

In this section the theoretical model for the evaluation of the crack opening displacement is developed. The basic problem is the elastic-plastic edge crack problem in a part with finite thickness. There are three problems which are of interest in studying the fracture of plates and shells. In the order of increasing complexity they are the plane problem of a single edge notched specimen under tension and bending, the problem of a flat plate with a surface crack, and the cylindrical shell with a circumferential or axial part-through crack. The main objective of this section is to describe the analytical techniques dealing with the elastic-plastic crack problems for these three geometries.

4.1 The Plane Problem for an Edge-Notched Plate

If the part-through crack in a plate or shell is long relative to the thickness, then in the middle portion of the crack one may assume that the plane strain conditions are valid (Figure 37). In this case an idealized model representing the states of deformation and stress in this region would be the single edge-notched plate under plane strain conditions (Figure 37a). However, it should be emphasized that such a model would be qualitative and would be useful in investigating the related ductile fracture mechanisms only. As pointed out in Section 3 (see Figures 26, 28, 30 and 31), quantitatively the results would be highly approximate. Again in this case too the load carrying capacity obtained from the elastic-plastic plane strain solution would provide an upper bound for the plate with a part-through surface crack.

The primary purpose of solving this problem is to obtain an accurate estimate of the crack opening stretch at the leading edge of the crack. This quantity plays an important role in the evaluation of crack growth initiation and instability loads in plate and shell structures with a part-through crack. The problem is described by Figure 37. Physically it is clear that for certain combinations of applied loads and the crack length because of the nonsymmetric nature of the plate geometry, the longitudinal stress σ_{xx} near and at the surface opposite to the crack (i.e., in the neighborhood of the point $x = 0, y = h$) may be compressive. Also, for high magnitudes of the load this stress may exceed the compressive yield strength of the material. The yielding on the compressive side of the plate would then have to be taken into consideration for a realistic modeling of the problem. The previous studies of this problem have been either purely elastic or have considered only the tensile yield zone around the crack tip. In this study we consider the plane strain problem shown in Figure 37 first by assuming that the magnitude of the maximum compressive stress is not much higher than the flow stress in compression and hence by ignoring the yielding on the compression side of the plate (Problem 1). The numerical results show that this is a fairly good assumption for a plate under uniform tension ($\sigma_{xx} = \sigma_0$). Next, the problem is considered with compressive as well as tensile yield zones (Problem 2). For an edge-notched plate under bending

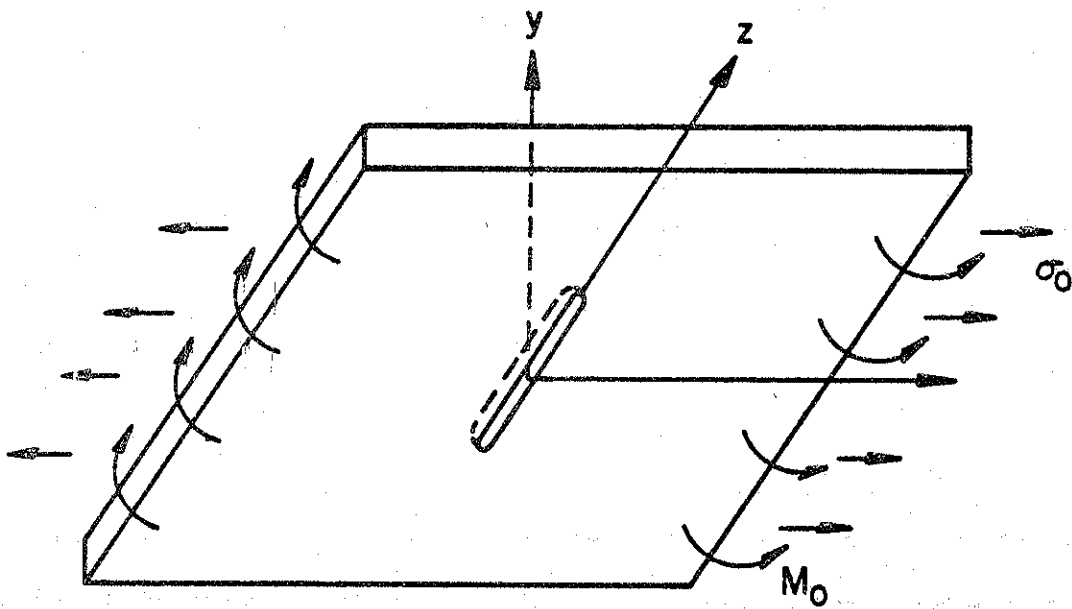
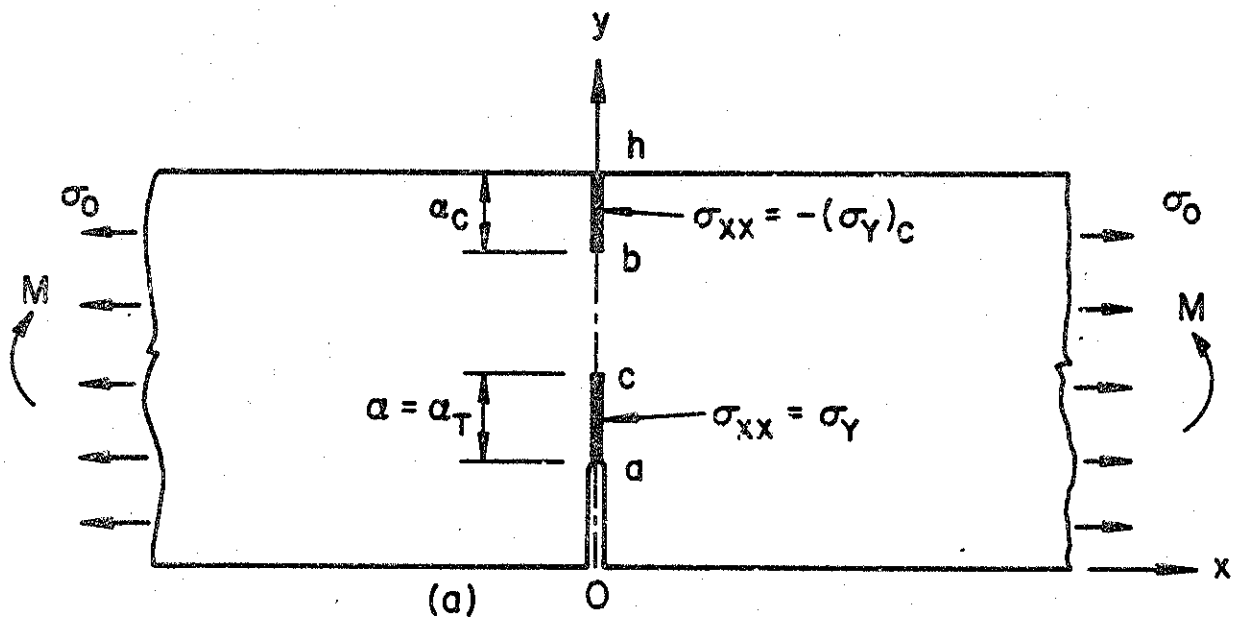


Figure 37. Notation for the plane strain problem for a plate with an edge crack.

consideration of compressive yielding appears to be unavoidable. Finally, the effect of strain hardening in the yield zone is investigated (Problem 3).

The analysis of the problem is described in Appendix F where the problems 1, 2, and 3 are discussed separately. Referring to Figure 37(a), in solving this problem, first it is assumed that the yielding takes place only in the tensile zone adjacent to the crack, $\alpha = c-a = \alpha_T$ being the size of the unknown yield zone. Table F1 shows that in the plate under uniform tension in the backside of the plate ($x=0, y=h$) the compressive stress may easily reach the yield point for moderately deep cracks and high load ratios σ_0/σ_Y . However, trial calculations also showed that in this case the introduction of a compressive yield zone in ($x=0, b<y<h$) did not significantly change the crack opening displacements $\delta(0)$ and $\delta(a)$. The results given in Table F1 are, therefore, based on the assumption that the yielding is restricted to the tensile region only. Figure 38 shows a sample result giving the crack tip opening displacement (CTOD) $\delta(a)$ and the crack mouth opening displacement (COD) $\delta(0)$ for a plate under uniform tension. The figure shows that when the external load σ_0 reaches a certain level, any small increase in the load may cause relatively a very large increase in COD or CTOD. Mechanically, this may be interpreted as an indication of a crack instability or plastic collapse in the net section. From the results given for the strain hardening materials in Appendix F one may also observe that the strain hardening model gives calculated values for $\delta(0)$ and $\delta(a)$ which are slightly lower than those given by the elastic-perfectly plastic model. In practice, however, this is compensated for by using a flow stress σ_F in place of the yield strength σ_Y . Since $\sigma_F > \sigma_Y$, the COD values based on σ_F would be somewhat lower than that obtained from σ_Y .

If the plate is under pure bending, then as seen from Table F2 even for relatively shallow cracks the yielding on the compression side of the plate must be taken into consideration. A sample result for this case showing the variation of COD on the plate surface, $\delta(a)$ at the crack tip and the tensile (α_T) and compressive (α_C) plastic zone sizes with the load ratio σ_B/σ_Y is given in Figure 39 ($\sigma_B = Mh/2I$). This figure shows much more distinctly the signs of a possible crack instability or plastic collapse mechanism in the neighborhood of a certain load ratio (in this case approximately $\sigma_B/\sigma_Y = 0.375$).

As indicated in Appendix F, if needed the stress distribution in the net ligament may easily be calculated. Some sample results for a plate having an

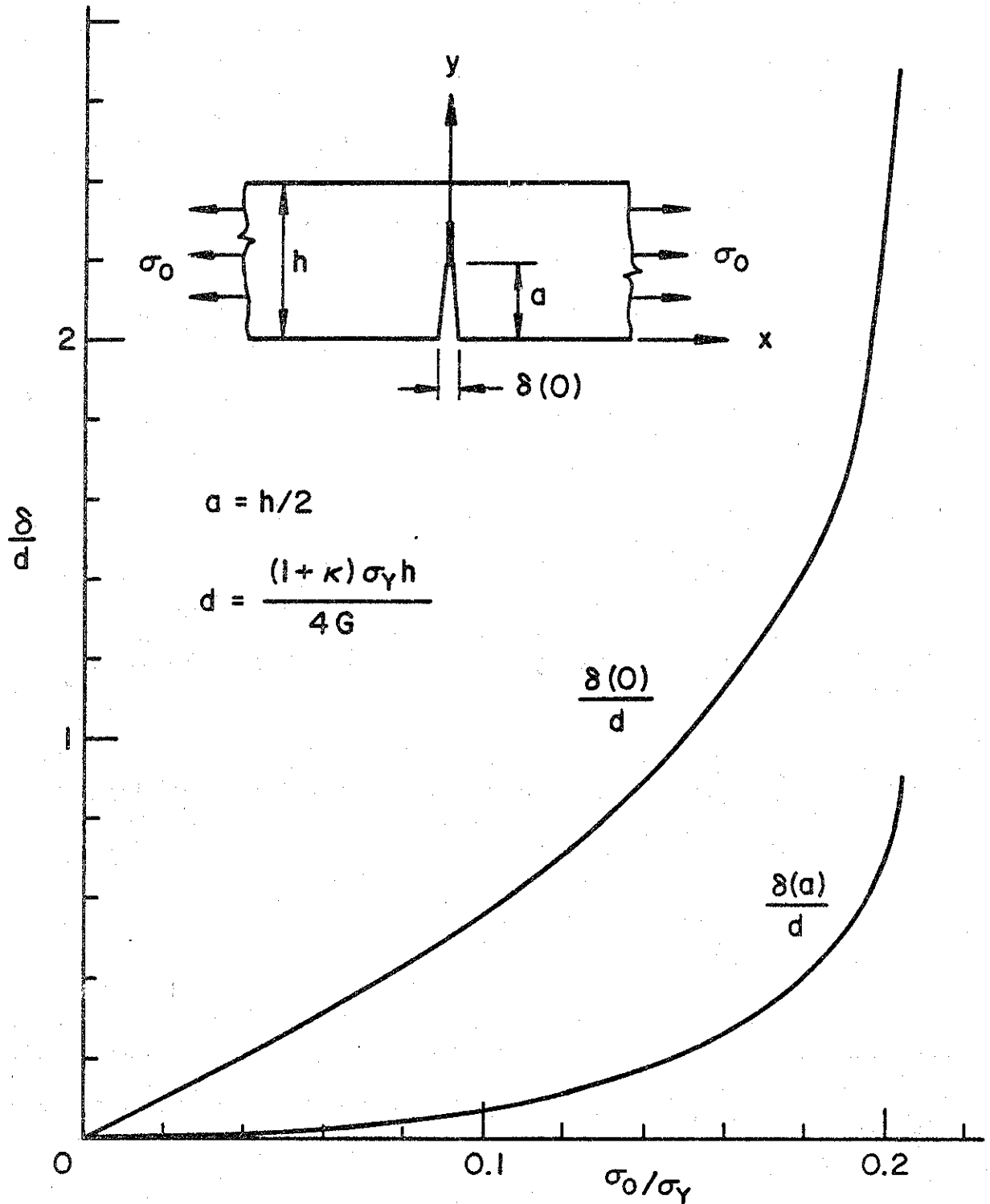


Figure 38. Crack opening stretch $\delta(a)$ at the leading edge of the crack and COD on the surface of a plate under uniform tension (yielding in tension only, σ_Y : the flow stress in tension).

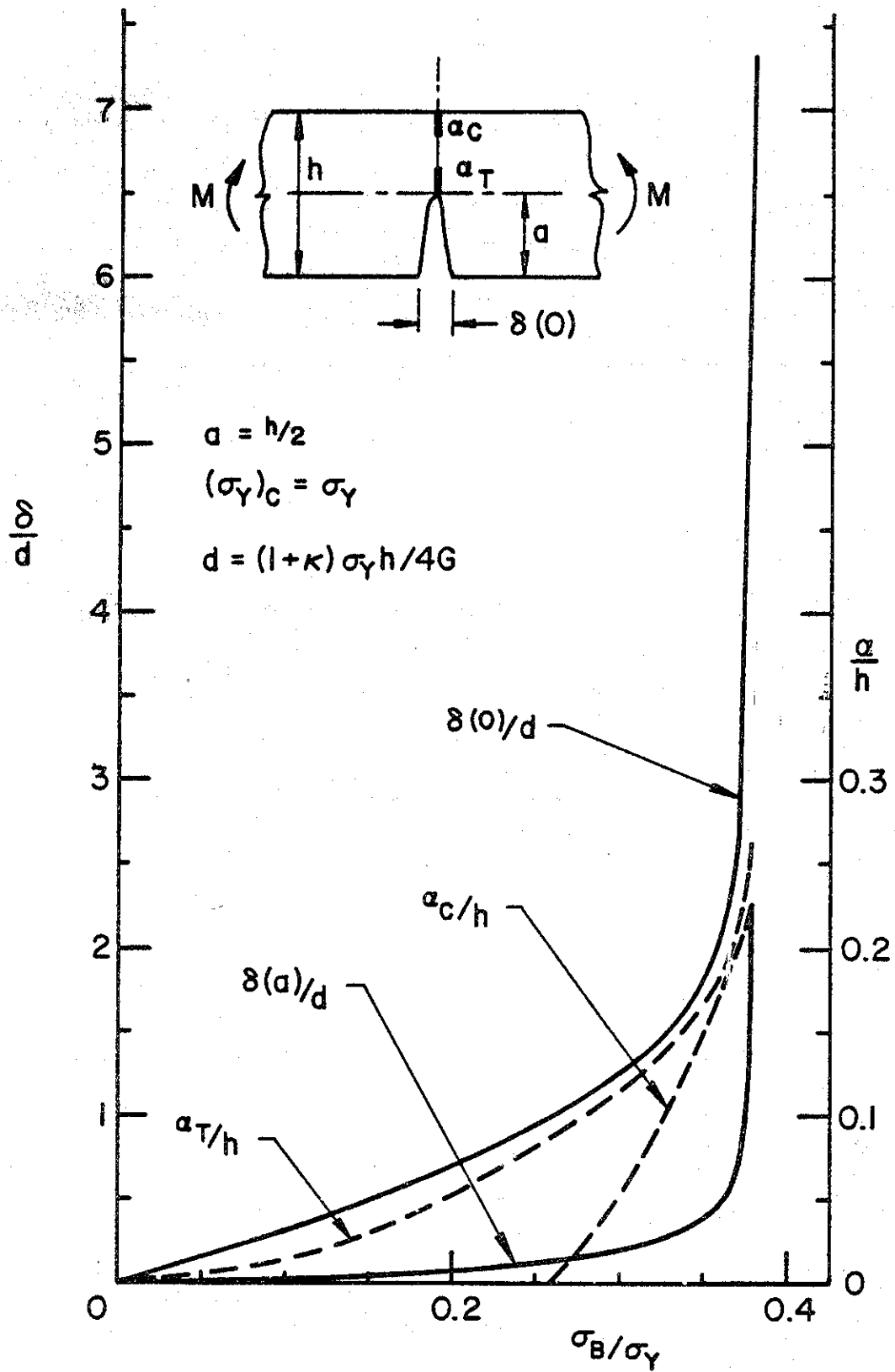


Figure 39. Crack opening stretch $\delta(a)$ at the crack tip and COD on the surface of a plate under pure bending (yielding in tension and in compression, σ_Y : the flow stress in tension, $(\sigma_Y)_C$: the flow stress in compression, α_T : tensile plastic zone size, α_C : compressive plastic zone size).

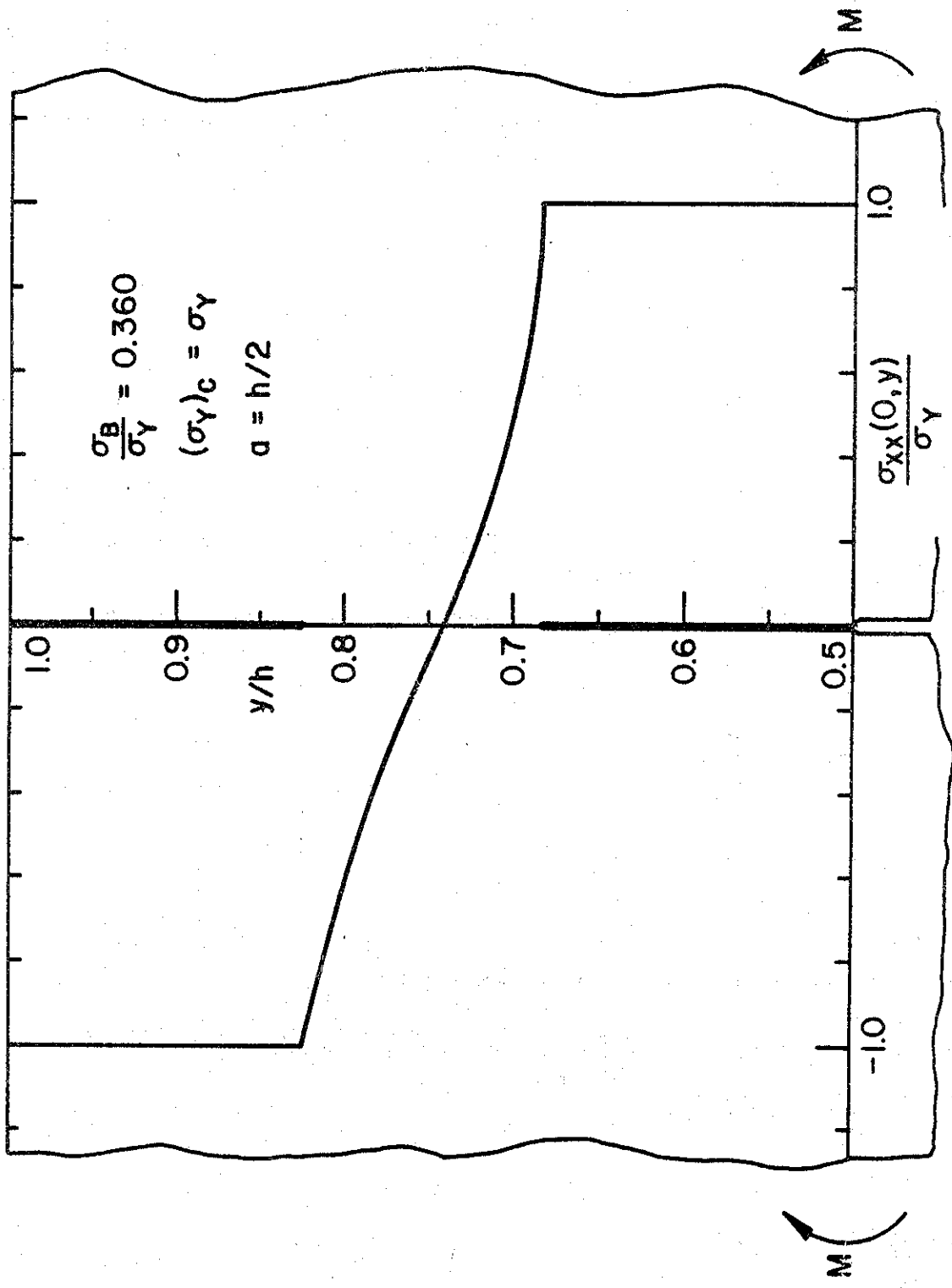


Figure 40. Stress distribution in the net ligament of a plate with an edge crack subjected to pure bending. (The case of equal flow stresses in tension and in compression.)

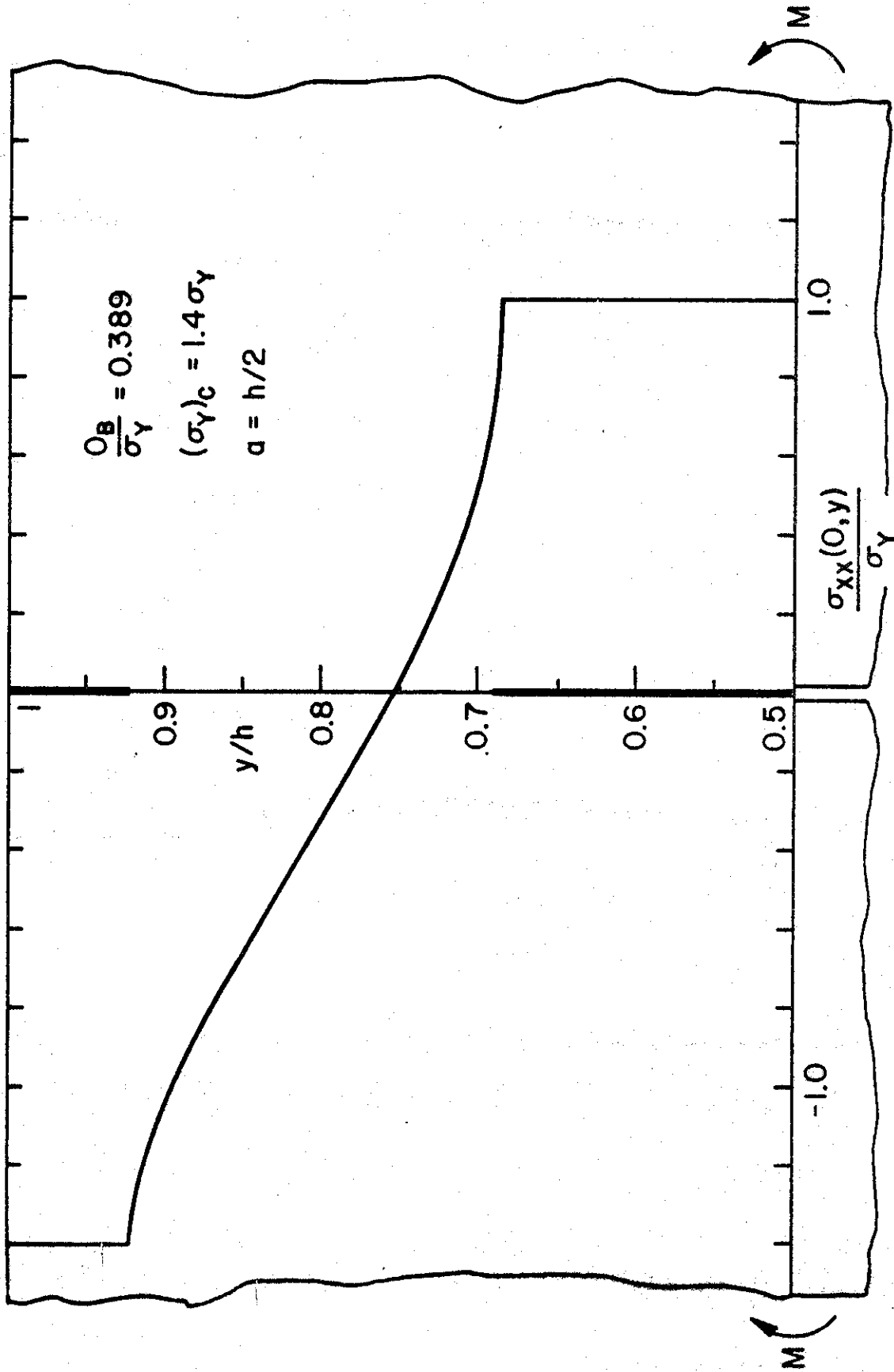


Figure 41. Same as Figure 40. (The case for which the flow stress in compression is greater than that in tension.)

edge crack and subjected to pure bending are shown in Figures 40 and 41. For the example given in Figure 40 the tensile and compressive flow stresses are assumed to be equal. Figure 41 shows an example for which $(\sigma_Y)_C = 1.4 \sigma_Y$.

4.2 A Long Part-Through Crack in a Plate with Fully-Yielded Net Ligament

The second elastic-plastic problem which is considered analytically is an infinite plate containing a relatively long and deep part-through surface crack. The problem is described in Figure 42. If the plate is subjected to uniform membrane loading as shown in the figure, because of the nonsymmetric nature of the stress distribution in thickness direction in the plane of the crack $x_2=0$, around the crack region one would expect a certain amount of bulging of the plate. The bulging, in turn, would affect the plastic deformations around the crack. In particular, if one is interested in calculating the crack opening displacement on the surface of the plate (for the purpose of, for example, using it in compliance-type analysis) or the crack opening stretch along the leading edge of the crack (for the purpose of using it in ductile fracture initiation and in a net ligament instability analysis), then it may be necessary to estimate the effect of bulging on these quantities and to take it into consideration if it proves to be significant. Because of its practical importance in recent past the problem has attracted some attention (see, for example, [49-52]). However, in none of the previous studies has the bulging effect been evaluated or taken into consideration.

In the present study the problem described in Figure 42 is considered. It is assumed that plastic deformations take place in a certain portion of the plate around the crack tips as well as in the entire net ligament. The problem is the limiting case of a cylindrical or a spherical shell for $R \rightarrow \infty$. A fully-plastic version of the line-spring model is used to account for the plastic deformations. The details of the solution and extensive results are given in Appendix G. COD (or CTOD) in the plate has been calculated and tabulated at eight different locations (Table G3). In order to avoid an iteration in the numerical analysis the table lists the calculated results for fixed values of $a_p = a + p$ and d (a , p and d being the half crack length, the plastic zone size, and the crack depth).

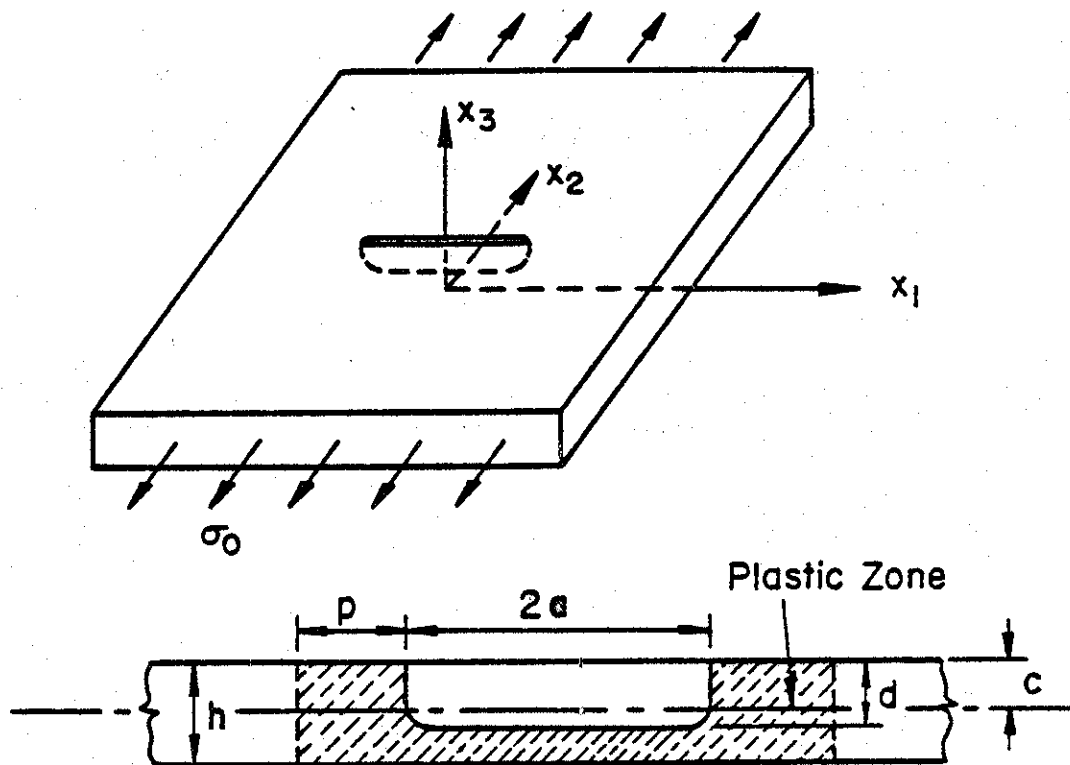


Figure 42. Notation for a flat plate containing a long part-through surface crack with fully-yielded net ligament.

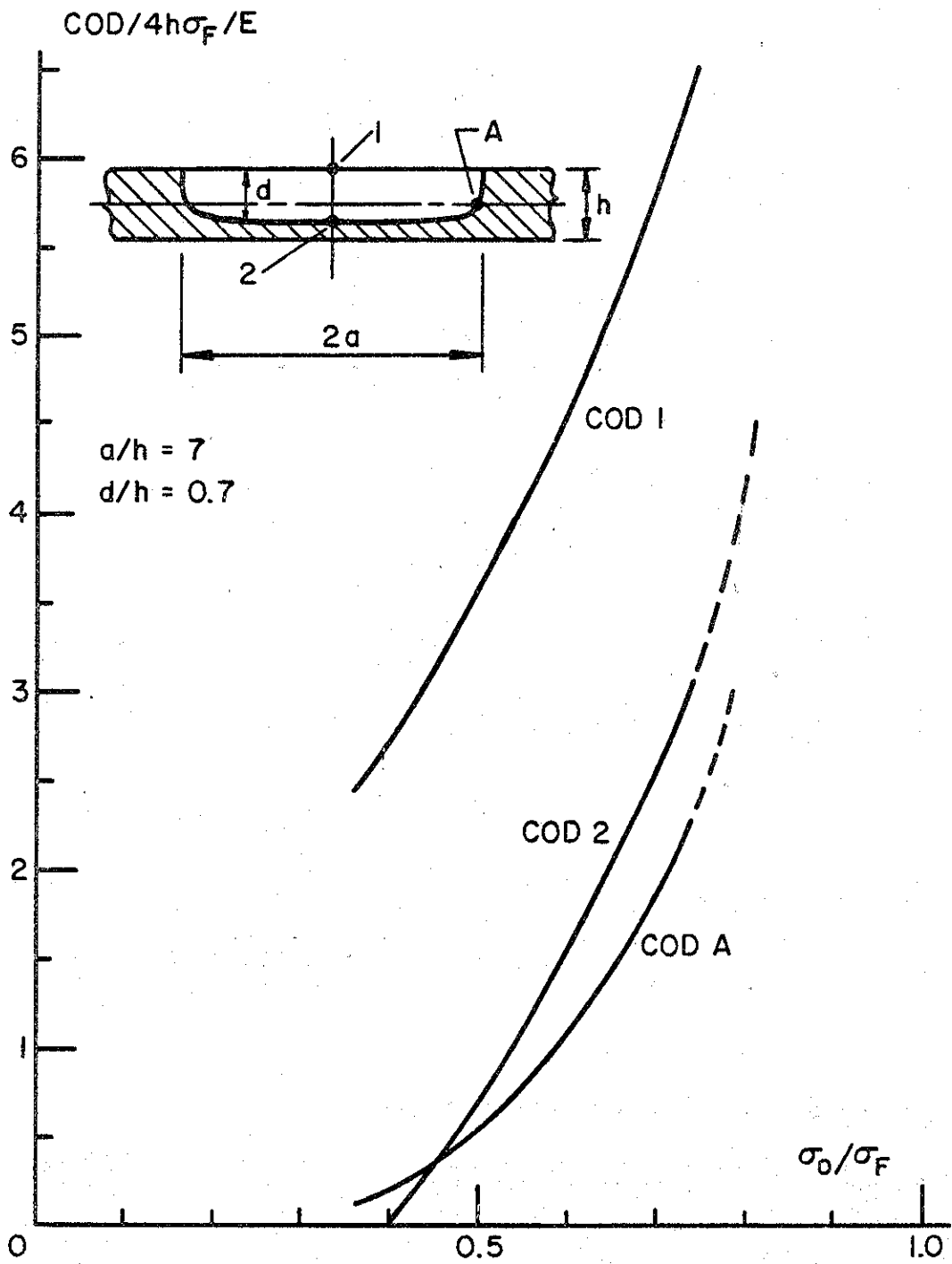


Figure 43. Crack opening displacements in a flat plate containing a part-through crack with a fully-yielded net ligament.

A sample result for a "long and deep" surface crack is also shown in Figure 43 where COD1, COD2 and CODA, respectively, correspond to the crack opening displacement on the plate surface, crack tip opening displacement at the midsection of the plate, and the crack tip opening displacement at the ends of the crack and in the neutral plane, $x_3 = 0$ (see Figure 42). From Figure 43, too, it may be observed that in the neighborhood of a certain value of the external load σ_0 a small change in σ_0 may cause relatively large changes in COD or CTOD. This again indicates that at this particular load level net ligament may undergo some kind of mechanical instability.

4.3 Circumferential Part-Through Crack in a Cylinder

The third elastic-plastic problem considered in this study is that of a pipe or cylindrical container with a part-through circumferential crack. Again, if the related ductile fracture process involves progressive stable crack growth, it is generally agreed that the size of the energy dissipation zone around the crack front is an increasing function of the crack length. Thus, in a structural component undergoing slow progressive ductile fracture the fracture resistance of the material increases with increasing crack length, hence, the concept of "crack extension resistance curve" or the R-curve. There is some experimental evidence to the effect that during such a fracturing process the "crack opening angle" or the "crack opening stretch" at the tip of a growing crack remains constant. Even though this notion has not been fully documented, it may still be used to support the conjecture that for the initiation of ductile fracture growth some local strength parameter must reach a critical value at the crack tip and, in the absence of a more suitable load factor, the crack opening stretch may be used as the measure of this parameter. This is a necessary condition for fracture propagation and is related to the formation, growth and coalescence of holes in the small fracture initiation or "fracture process zone" at the crack front (Figure 1b). On the other hand continuous (stable) growth and instability of fracture require that the condition of global energy balance be satisfied. The latter constitutes essentially the sufficient condition for fracture propagation.

The type of ductile fracture resulting from progressively growing cracks would occur usually in structural components having a through crack or having

a part-through crack with a relatively small crack depth to wall thickness ratio (Figure 4d and f). However, for some crack-structure geometry and material combinations the crack opening stretch may reach and far exceed the local critical value and yet the condition of global energy balance may not be satisfied. Some plate and shell structures of high toughness materials having a relatively long and deep surface cracks may fall into this category. In this case the net ligament would generally undergo plastic "necking", and the net ligament rupture may result from a "necking instability" under increased membrane loads (Figure 4e). As shown in [7] the solutions of crack problems in shells properly accounting for plastic deformations may be used as the basis of both types of ductile fracture mentioned above. It should perhaps be pointed out that the concept of "tearing modulus" recently introduced by Paris appears to be a very effective way of characterizing and classifying structural materials with respect to their ductile fracture resistance. However, the concept is confined to certain types of J-controlled progressive fracture and is not applicable to net ligament plastic necking instability.

For the evaluation of the crack opening stretch along the crack front the elastic-plastic solution of the problem of a cylindrical shell containing a relatively long and deep part-through circumferential crack is needed. The problem by using a modified version perfectly plastic strip model to account for the plastic deformations in the crack region is considered in this section.

The analytical solution of the elastic-plastic problem for a cylindrical shell containing a part-through or a through crack does not seem to be feasible. In this study the plastic deformations in the crack region will be accounted for by assuming a perfectly plastic strip model similar to a conventional Dugdale Model used in plane problems. The model has been used before in conjunction with the classical shell theory to study the plasticity problem in cylindrical shells containing an axial crack [5] (see, also [19] for applications). Briefly, in using this approximation it is assumed that the plastic deformations in the shell is confined to a "thin layer" in the plane of the crack which becomes fully plastic upon loading the shell. The size of the plastic zone is unknown and is determined from the magnitude of the external loads. Thus, the problem is treated basically as an elasticity problem subject to the conditions that the stress state in the plastic layer satisfy an appropriate yield condition and that the stresses everywhere in the shell be bounded.

The problem in the circumferentially cracked shell is described in Figure 44 where the shaded area shows the fully plastic layer. In the part-through crack case (Figure 44 a,b) it is assumed that the fully-yielded net ligament under the crack may carry only a constant flow stress σ_F and in the plastic zones of length p at the ends of the crack the membrane and bending stress resultants are such that the stress state in the crack region is non-singular. The flow stress σ_F depends on the yield behavior of the material. Even though there is no definite way of selecting σ_F , it may be expressed as $\sigma_F = \sigma_{ys} + \gamma(\sigma_u - \sigma_{ys})$ where σ_{ys} is the yield and σ_u is the ultimate strength of the material and the factor γ is a constant ($0 < \gamma < 1$, usually $\gamma = 1/2$). Thus, in addition to the usual field quantities appearing in the elasticity solution of the shell, the symmetric elastic-plastic crack problem has three unknowns, namely the size of the plastic zone p and the membrane and bending stress resultants N and M in the plastic zone. The problem is solved by assuming that the shell has a through crack of length $2(a+p)$ (Figure 44) and by using the stresses in the plastic layer as crack surface tractions. The three additional conditions to account for the three unknowns p , N , and M may then be expressed as

$$k_m(a+p) = 0 \quad , \quad (43)$$

$$k_b(a+p) = 0 \quad , \quad (44)$$

$$\frac{N}{h\sigma_F} + \frac{2|M|}{h^2\sigma_F} = 1 \quad . \quad (45)$$

Conditions (43) and (44) state that the membrane and bending stress intensity factors at the fictitious crack tip $(a+p)$ are zero thereby insuring nonsingular stress state in the shell and (45) expresses the yield condition. It should be noted that the conventional yield condition in plates and shells is stated by

$$\left(\frac{N}{h\sigma_F}\right)^2 + \frac{M}{\sigma_F(h/2)^2} = 1 \quad . \quad (46)$$

In practice, generally the condition (46) is linearized by approximating the parabola by straight lines going through the intercepts on N and M axes.

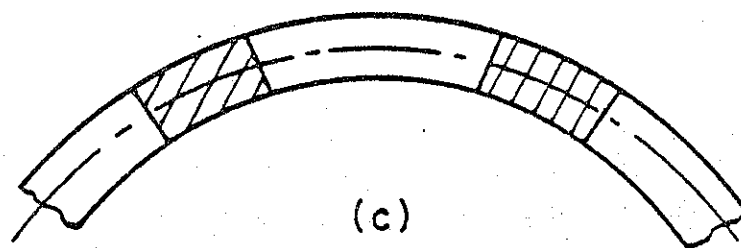
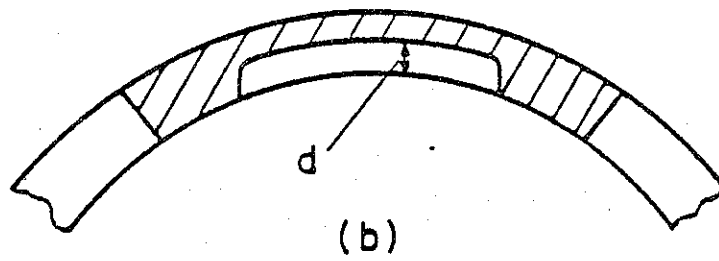
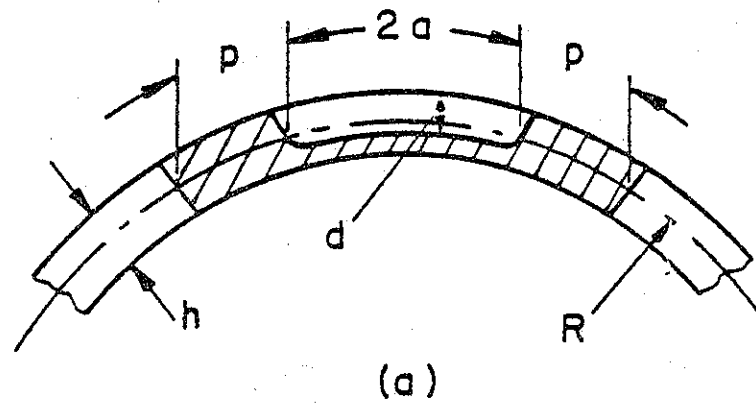


Figure 44. The crack geometry.

However, in shell problems of practical interest, generally the membrane stress resultant N is dominant and therefore a more realistic linearization of (46) may be obtained by approximating the parabola by its tangent at the point $N = h\sigma_F$, $M = 0$ as given by (45).

In Appendix A it was shown that in a cylindrical shell containing a circumferential through crack of length $2b$ under symmetric loading conditions the problem may be formulated as a pair of singular integral equations of the following form

$$\sum_{j=1}^2 \int_{-b}^b k_{ij}(y,t)G_j(t)dt = F_i(y), \quad -b < y < b, \quad i = 1,2, \quad (47)$$

$$\int_{-b}^b G_i(t)dt = 0, \quad i = 1,2 \quad (48)$$

where y is the coordinate along the crack in the tangent plane to the neutral surface, x is parallel to the axis of the cylinder, z is perpendicular to the shell surface, the kernels k_{ij} are given in Appendix A and the unknown and input functions G_i and F_i , ($i=1,2$) are defined by

$$G_1(y) = \frac{\partial}{\partial y} u(+0,y), \quad G_2(y) = \frac{\partial}{\partial y} \beta_x(+0,y), \quad (49)$$

$$F_1(y) = N_{xx}(0,y), \quad F_2(y) = M_{xx}(0,y), \quad -b < y < b, \quad (50)$$

$u(x,y)$ and $\beta_x(x,y)$ being the x components of displacement and rotation, respectively. The elastic-plastic results in a cylinder subjected to a uniform axial membrane load $N_{xx} = N_0$ in the crack region may be obtained by solving the integral equations (47) under the following two sets of crack surface tractions and by adding the results

$$F_1^1(y) = -N_0, \quad F_2^1(y) = 0, \quad -b < y < b, \quad b = a+p, \quad (51)$$

$$\left. \begin{aligned}
 F_1^2(y) &= \left\{ \begin{array}{l} N, \quad a < |y| < a+p, \\ h\sigma_F(1-\frac{d}{h}), \quad -a < y < a, \end{array} \right. \\
 F_2^2(y) &= \left\{ \begin{array}{l} M, \quad a < |y| < a+p, \\ -\frac{h^2\sigma_F}{2} \left[\left(1-\frac{c-d}{h-2h}\right)\left(\frac{c+d}{h+2h}\right) - \left(1-\frac{c+d}{h+2h}\right)\left(\frac{c-d}{h-2h}\right) \right], \\ -a < y < a \end{array} \right.
 \end{aligned} \right\} \quad (52)$$

where the crack, located at $x=0$ plane, has a length $2a$ in y direction and depth d in z direction, and its position in z direction is determined by the distance c of its center line from the outer surface of the shell, $z = h/2$. Thus, the crack occupies the domain ($x=0, -a < y < a, \frac{h}{2}-c-\frac{d}{2} < z < \frac{h}{2}-c+\frac{d}{2}$). Under the loading conditions (51) and (52) the stress intensity factors k_m^i and k_b^i , ($i=1,2$) obtained from the solution would be linear in N_0 , N , and M and nonlinear in p . Noting that N_0 is known and

$$k_m = k_m^1 + k_m^2, \quad k_b = k_b^1 + k_b^2, \quad (53)$$

equations (51-53) would then give N , M , and p . For example, Figures 45 and 46 show some sample results for the plastic zone size p . Figure 45 provides the information to obtain p in a shell with a through crack of length $2a$ for $a/h = 1$, $\nu = 0.3$ and for various values of the second dimensionless length parameter λ_2 , which is defined by

$$\lambda_2 = [12(1-\nu^2)]^{\frac{1}{4}} a/\sqrt{Rh}. \quad (54)$$

The curve for $\lambda_2 = 0$ corresponds to the flat plate solution which is known to be

$$\frac{a}{a+p} = \cos \left(\frac{\pi N_0}{2h\sigma_F} \right). \quad (55)$$

Figure 46 shows indirectly the effect of a/h on p for a fixed value of $\lambda_2=2$. It may be seen that this effect is rather insignificant.

Once the unknown constants p , N , and M and the functions G_1 and G_2 are obtained, then any desired field quantity in the shell, in particular, the crack opening stretch (COS) at any point on the crack border and the crack opening displacement (COD) at any point on the crack surface, may easily be evaluated^(*). On the crack surface and along the crack border the COD and COS are given by the relative displacement $\delta(y,z)$ calculated from

$$\delta(y,z) = u(+0,y,z) - u(-0,y,z). \quad (56)$$

Three particular quantities used in fracture analysis are

$\delta_0 = \delta(0,0)$: COD on the neutral surface at the midsection of the crack.

$\delta_a = \delta(a,0)$: COS on the neutral surface at the crack tips.

δ_c : COS on the border of a part-through surface crack at the midsection $y=0$.

The quantity δ_0 is related to the clip-gage type measurements and δ_a and δ_c are the crack opening stretches of critical interest in the through and part-through cracks, respectively. From (49) and (56) it is seen that

$$\delta_0 = -2 \int_0^{a+p} G_1(t) dt, \quad (57)$$

$$\delta_a = -2 \int_a^{a+p} G_1(t) dt, \quad (58)$$

$$\delta_c = \delta_0 + z_0 [\beta_x(+0,0) - \beta_x(-0,0)] \quad (59)$$

(*) In this report the term "crack opening stretch" COS or "crack tip opening displacement" CTOD is used for the relative displacement along the actual crack border which is assumed to be a measure of the strains or the stretch. The term "crack opening displacement" COD is used for the physically measurable relative crack surface displacement.

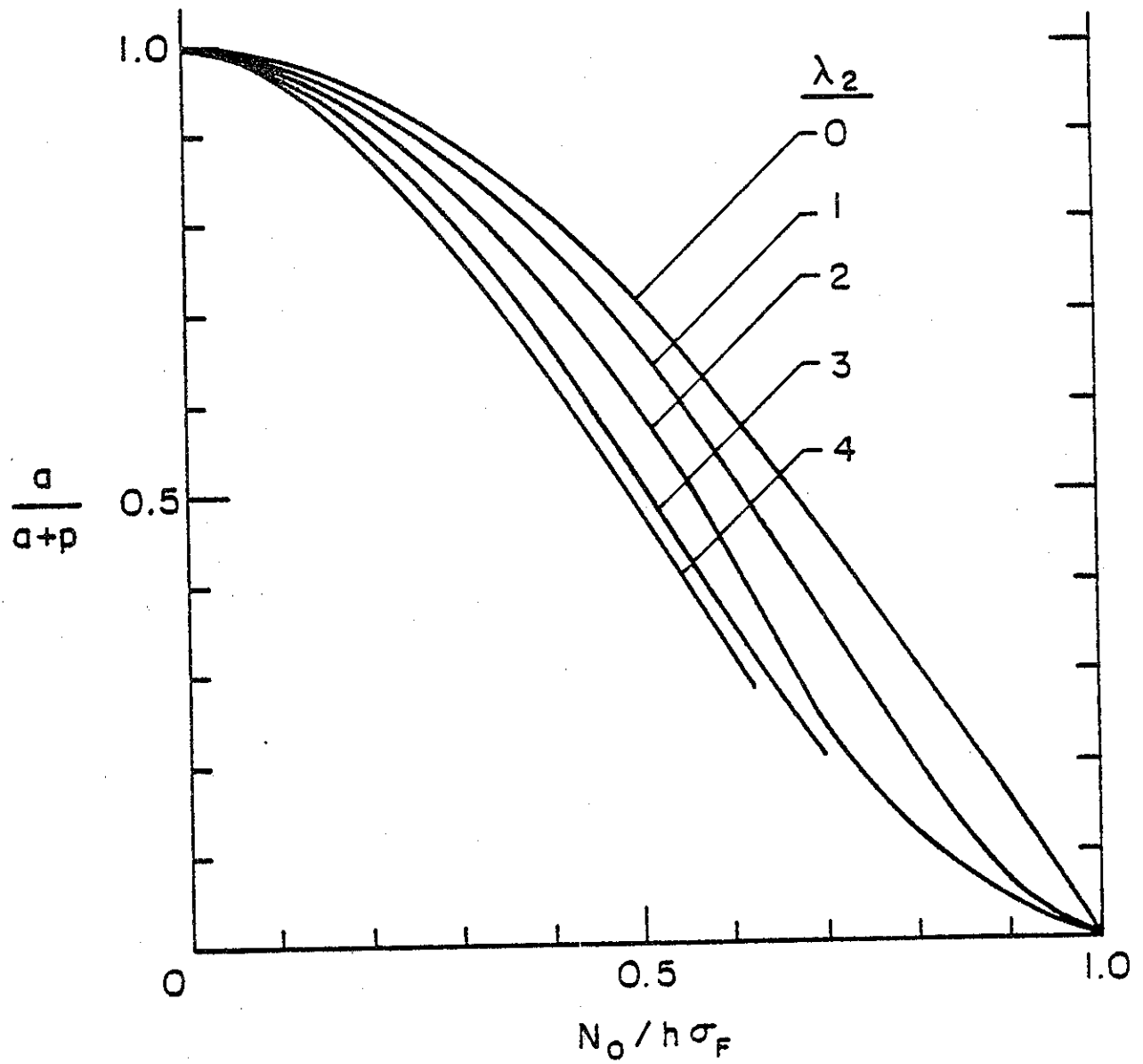


Figure 45. Curves giving the plastic zone size p for a circumferential through crack in a cylinder under uniform axial membrane loading, $a/h = 1$, $\nu = 1/3$.

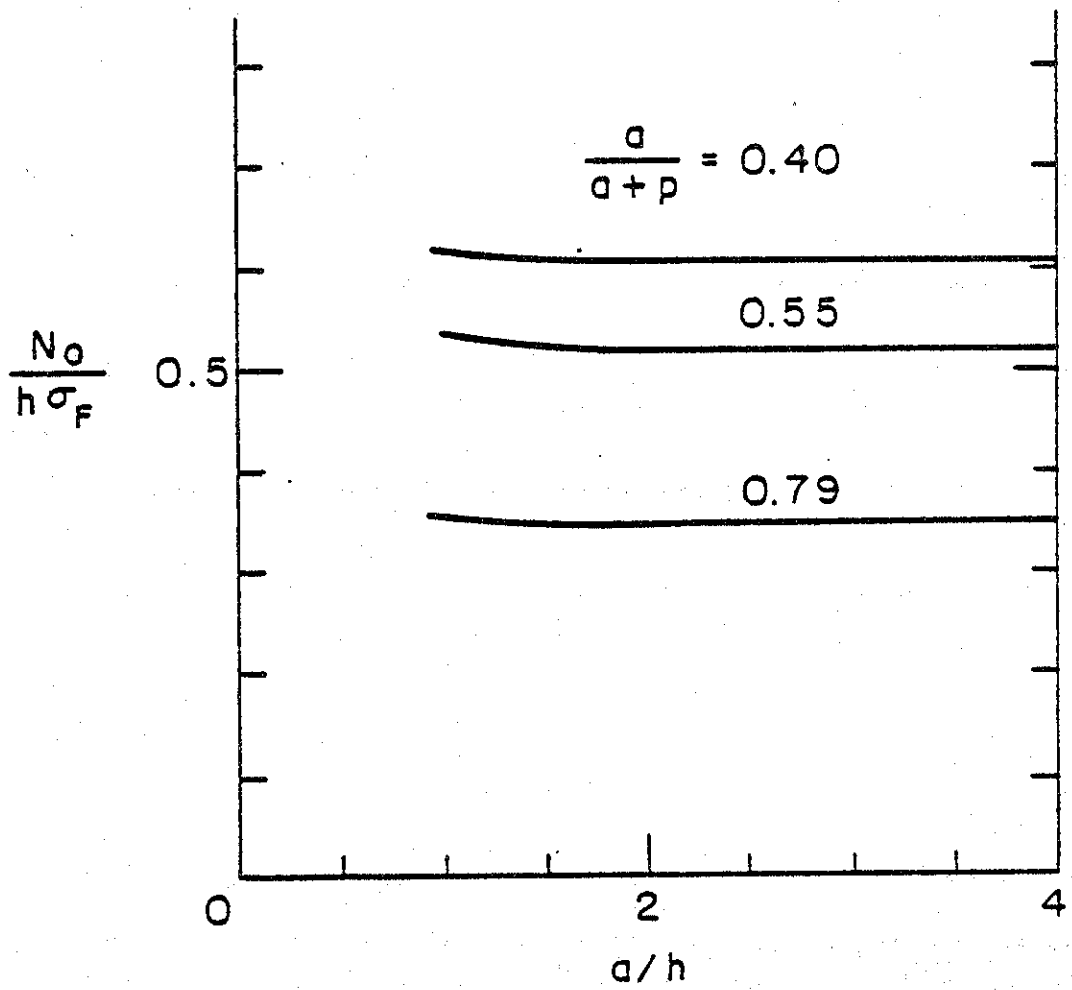


Figure 46. The effect of a/h on the plastic zone size.

where $z_0 = (h/2) - d$ for the external surface crack (i.e., $c=d/2$), $z_0 = d-(h/2)$ for the internal surface crack (i.e., $c=h-d/2$), and $\beta_x(+0,0)$ and $\beta_x(-0,0)$ are the crack surface rotations at $y=0$. In the special case of flat plate the solution for the through crack problem is known in closed form and the limiting values of δ_0 and δ_a for $\lambda_2 = 0$ may be expressed as

$$\frac{\delta_0}{\sigma_F a/E} = \frac{8}{\pi} \log [(1 + \sin\alpha)/\cos\alpha],$$

$$\frac{\delta_a}{\sigma_F a/E} = -\frac{8}{\pi} \log (\cos\alpha), \quad \alpha = \frac{\pi N_0}{2h\sigma_F}. \quad (60)$$

Further results for the membrane solution of the part-through crack problem in flat plates may be found in [49].

Typical results for COD and COS in a cylindrical shell containing a circumferential through crack or a part-through crack with a fully-yielded net ligament obtained by using Reissner's shell theory and the perfectly plastic layer model are given in Figures 47-54. In addition to the magnitude of the external loads N_0 and the dimensionless length parameters a/h and λ_2 , the part-through crack problem has two more length parameters, namely d/h and c/h representing depth and position of the crack. Thus, the complete solution of the problem requires that five independent constants be varied in some systematic fashion requiring quite extensive calculations. In this respect the aim of this paper is somewhat limited and is restricted to obtaining results which are sufficient to give some demonstrative examples regarding the applications. The primary restriction in the results shown in Figures 47-54 concerns the length parameter a/h which is fixed at 2. Figure 46 shows the COD δ_0 for a through crack. The corresponding COS δ_a calculated as a function of the axial membrane load N_0 for various values of λ_2 is shown in Figure 48. In these figures the results shown for $\lambda_2=0$ correspond to the flat plate case and are given by (60).

Figures 49-51 show the crack opening stretch δ_c in a cylinder with a part-through external surface crack calculated for $a/h=2$ and $d/h=0.7, 0.8, 0.9$, N_0 and λ_2 again being the variable and the constant parameter. Similar results for $d/h = 0.7$ are shown in Figure 52 for the cylinder with an internal surface crack. Figures 53 and 54 show the crack opening stretch δ_a at the

crack tips and on the neutral surface for a cylinder containing surface cracks. Comparison of the results given in Figures 53, 54 and 49, 52 shows that for the same crack geometry and load magnitude $\delta_c > \delta_a$ indicating that in the case of relatively long and deep part-through cracks, as expected, the critical location for crack initiation is the leading edge of the crack in the midsection.

As pointed out earlier in this report for progressively growing ductile fracture a local strength parameter in the fracture process zone must reach a critical value and the condition of the global energy balance must be satisfied. If one assumes that the local strength parameter remains constant during the stable fracture propagation and the crack opening stretch may be used as a measure of this parameter, then by using the type of results given in this section one can obtain the load carrying capacity of the structure against the crack growth initiation. To demonstrate the concept consider a cylindrical shell containing a circumferential through crack and subjected to uniform axial membrane loading in the crack region. At the crack growth initiation and during the stable crack growth, δ_a must be equal to some constant, the critical COS for the material, $(\delta_a)_{cr}$. Referring now to results such as those given by Figure 48, for the given parameters a/h and λ_2 the critical value of the load N_0 may be obtained by taking $\delta_a = (\delta_a)_{cr}$. For $a/h=2$ the results are shown in Figure 55. Note that for fixed a/h , λ_2 is proportional to $\sqrt{h/R}$ and for fixed a and h the figure directly shows the effect of the curvature $1/R$ on the load carrying capacity. Also, from Figure 48 one may observe that for $(\delta_a)_{cr} > 7$ the curve giving $(N_0)_{cr}$ and shown in Figure 55 would not be significantly different from that corresponding to $(\delta_a)_{cr} = 7$. As the material becomes more brittle $(\delta_a)_{cr}$ would be expected to be smaller. In this case the fracture process is governed by the concept of fracture toughness and the curvature effect on the fracture load is reflected by the change in the stress intensity factor with the curvature. For example, for $a/h = 2$, $\lambda_2 = 2$ the ratio of the membrane stress intensity factor in the shell to that in the plate is $k_{mm} = 1.179$ (Table AI, Appendix A), (indicating that the plate may carry 18% higher membrane stress) whereas from Figure 55 it may be seen that the ratio of $(N_0)_{cr}$ for the plate to that for the shell is 1.15 for $(\delta_c)_{cr} = 0.5$, 1.20 for $(\delta_c)_{cr} = 1$ and greater than 1.20 for $(\delta_c)_{cr} > 1$. Clearly, similar curves may be obtained

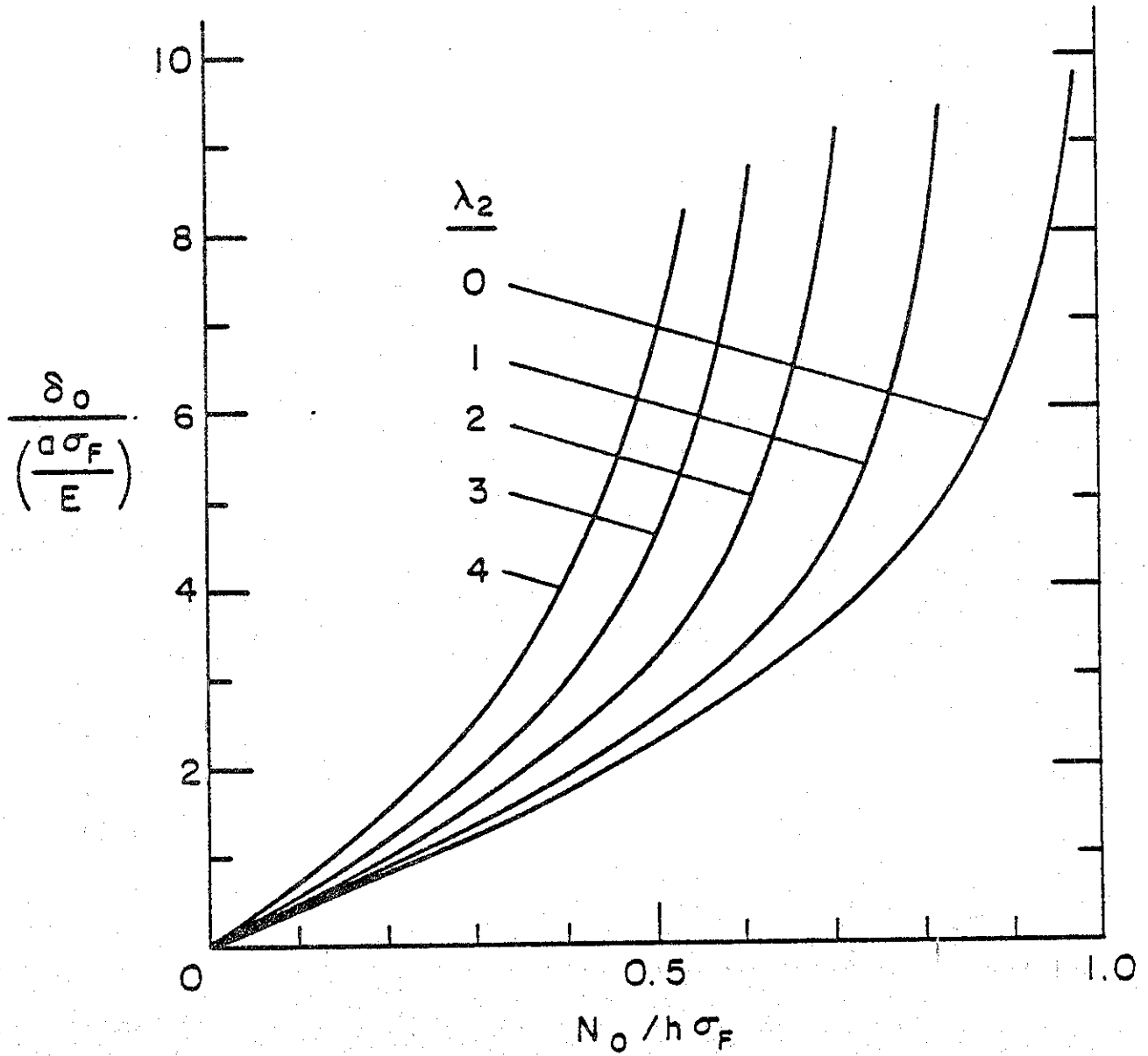


Figure 47. Crack opening displacement at the center of the crack and on the neutral surface in a cylinder with a circumferential through crack under uniform axial load, $a/h = 2$, $\nu = 1/3$.

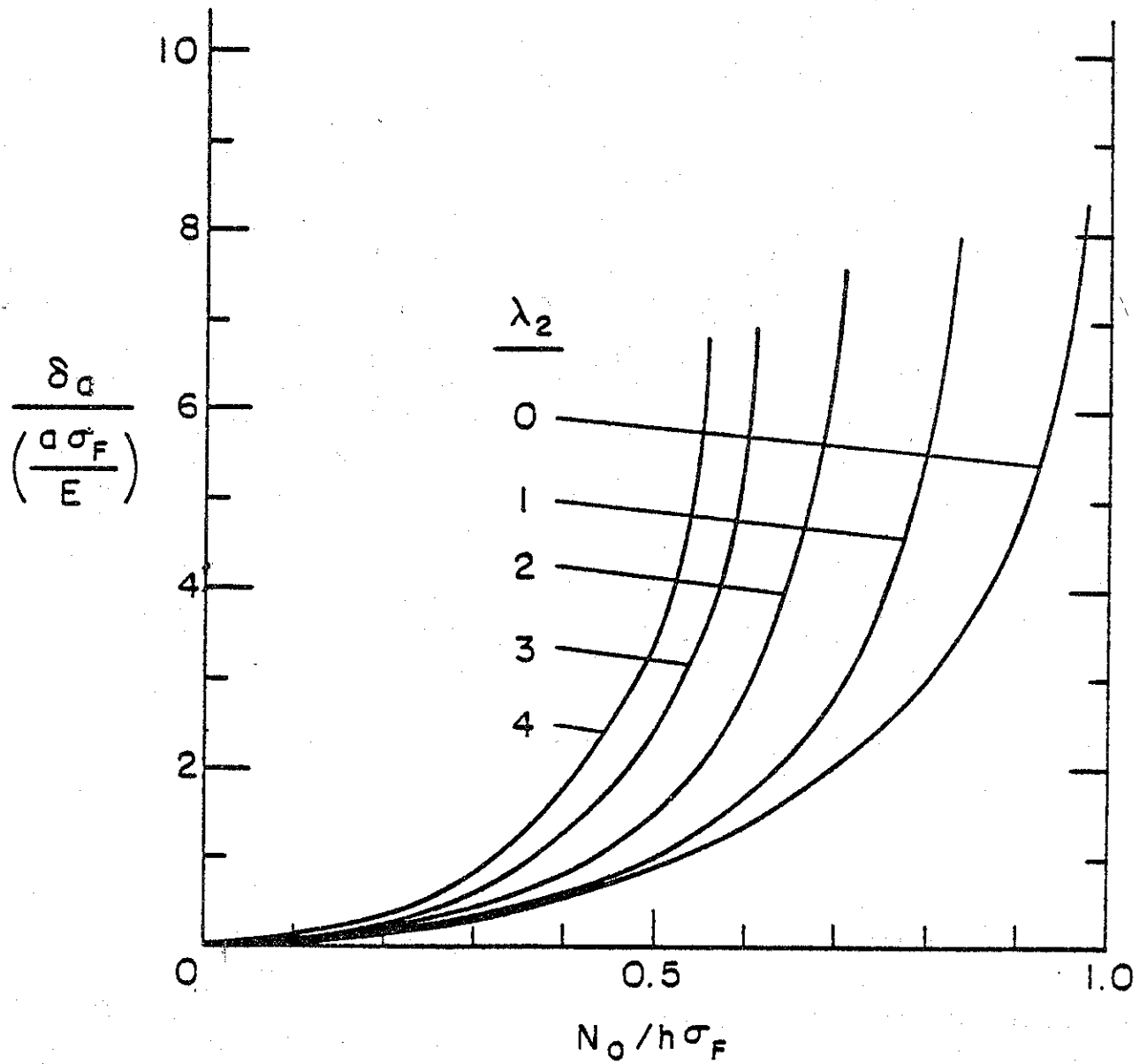


Figure 48. Crack opening stretch at the crack tip and on the neutral surface in a cylinder with a through crack, $a/h = 2$, $\nu = 1/3$.

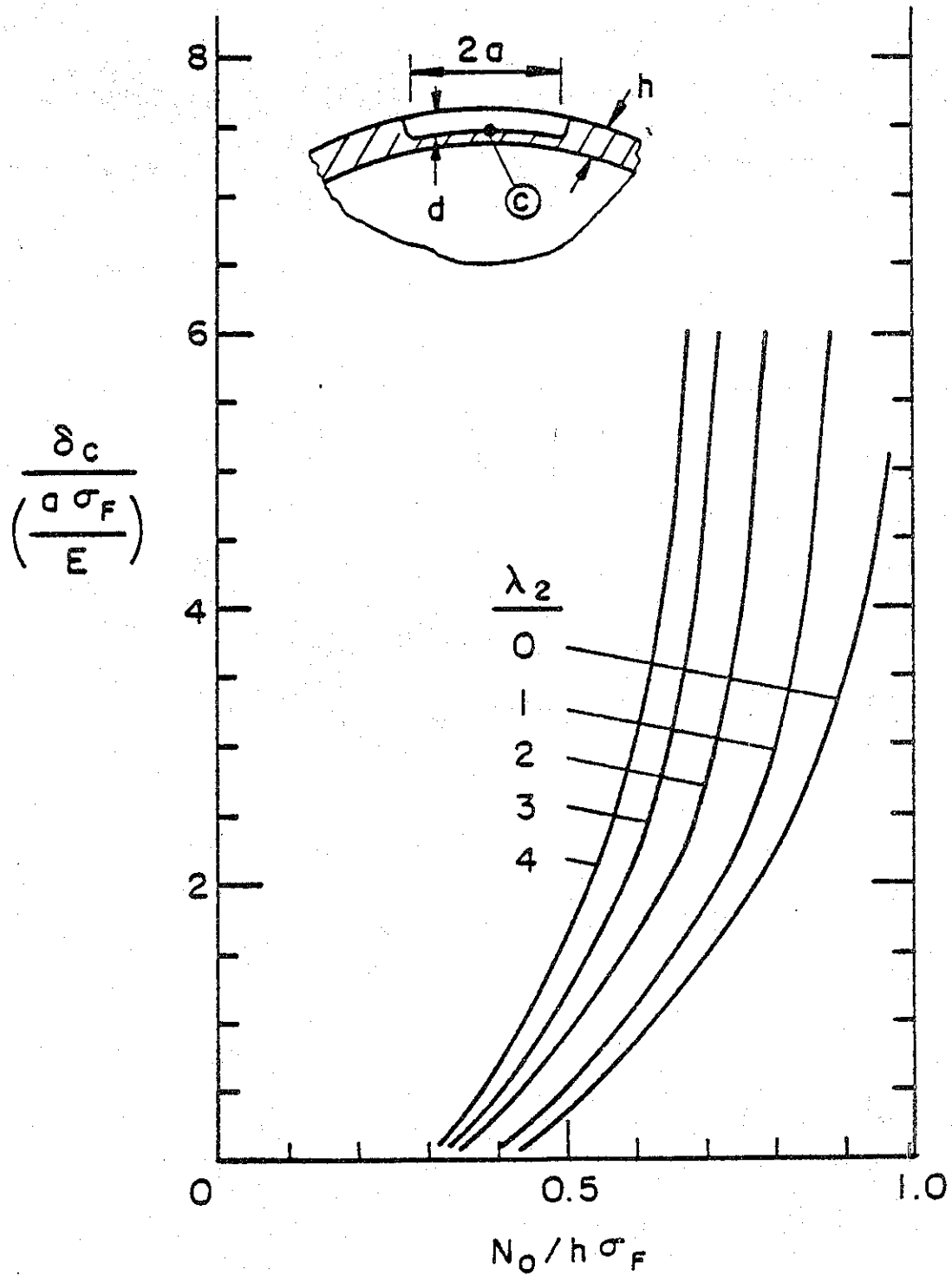


Figure 49. $\text{COS } \delta_c$ at the leading edge and midsection of the crack in a cylinder with an external part-through crack, $a/h = 2$, $d/h = 0.7$, $\nu = 1/3$.

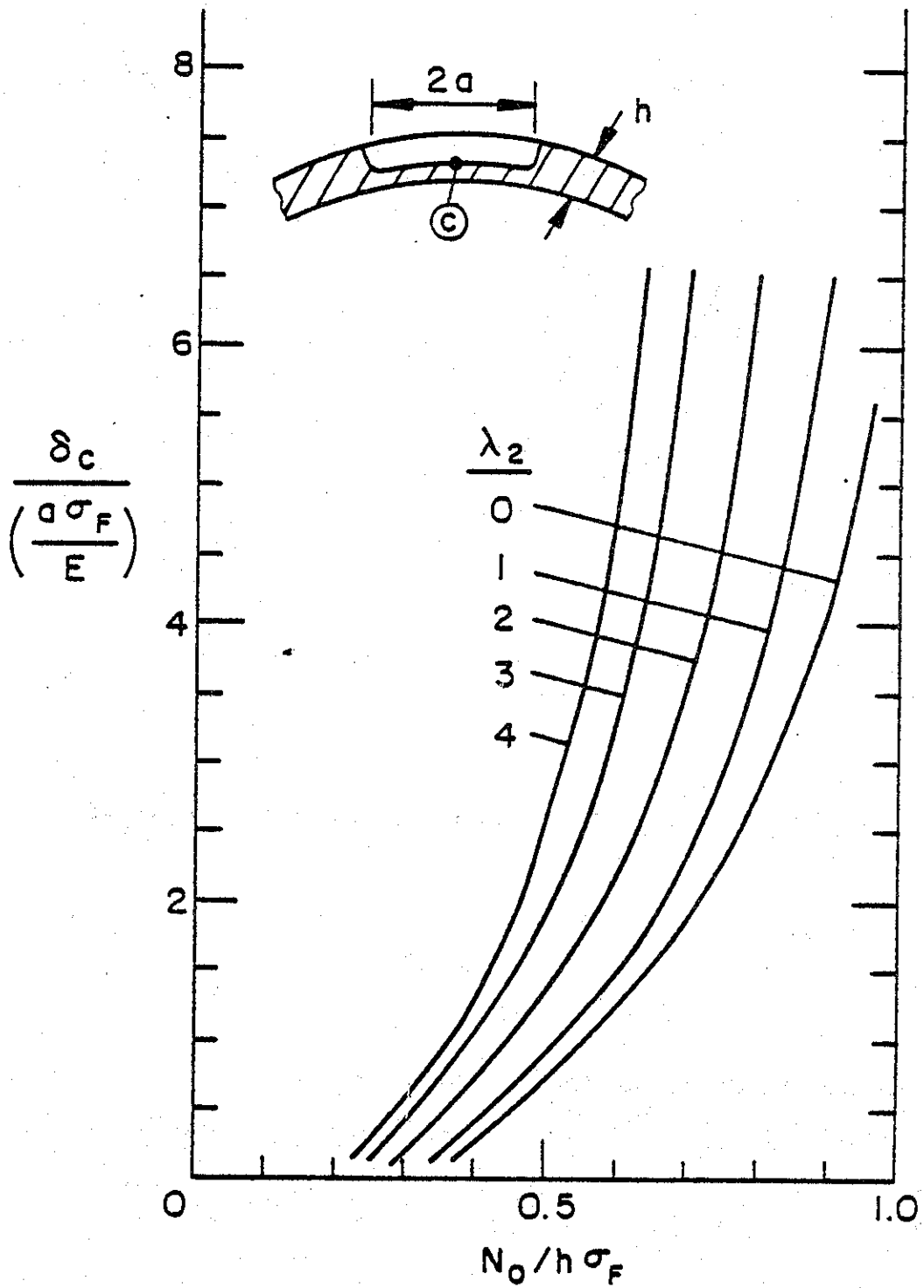


Figure 50. Same as Figure 49, $a/h = 2$, $d/h = 0.8$, $\nu = 1/3$.

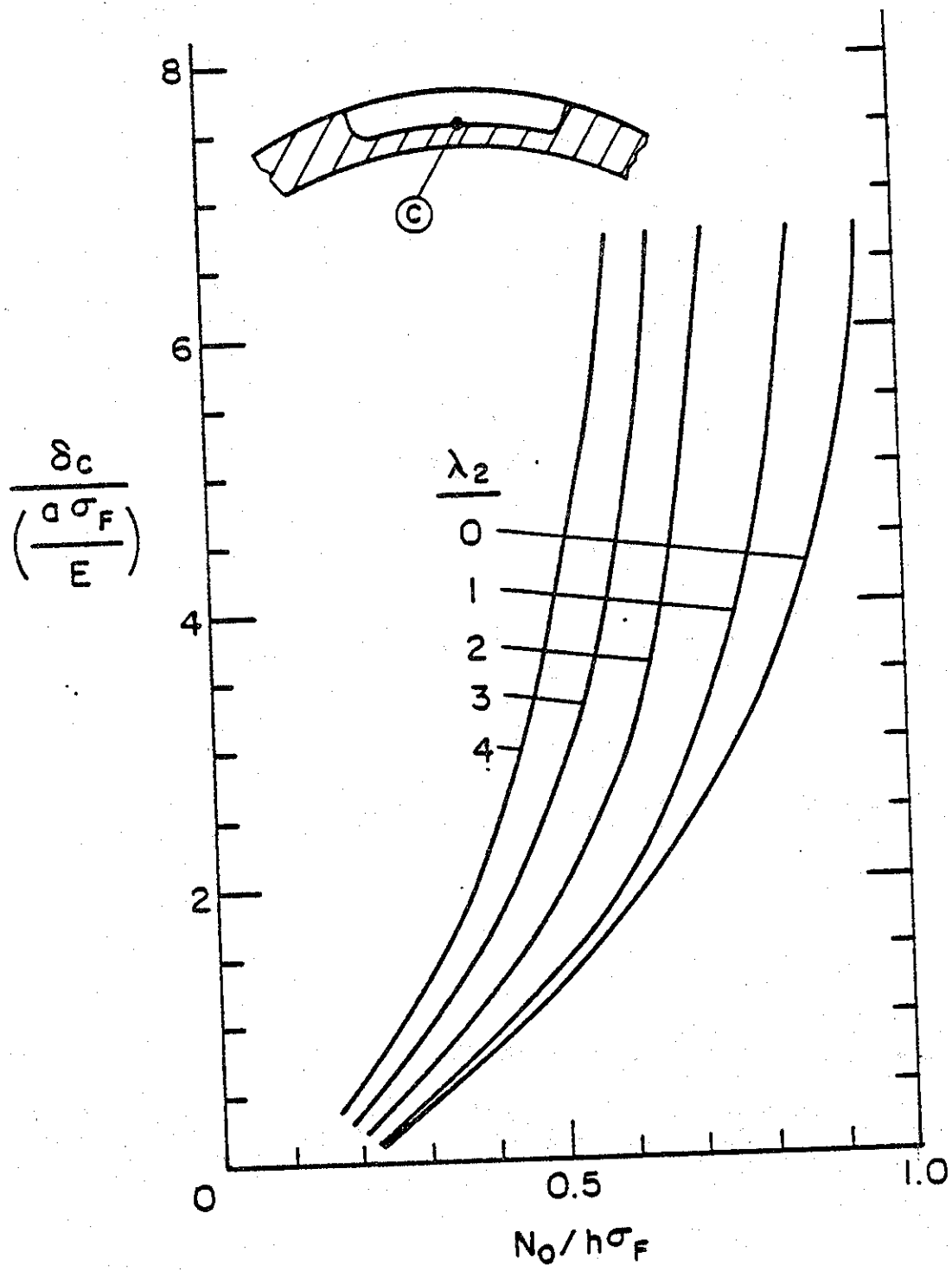


Figure 51. Same as Figure 49, $a/h = 2$, $d/h = 0.9$, $\nu = 1/3$.

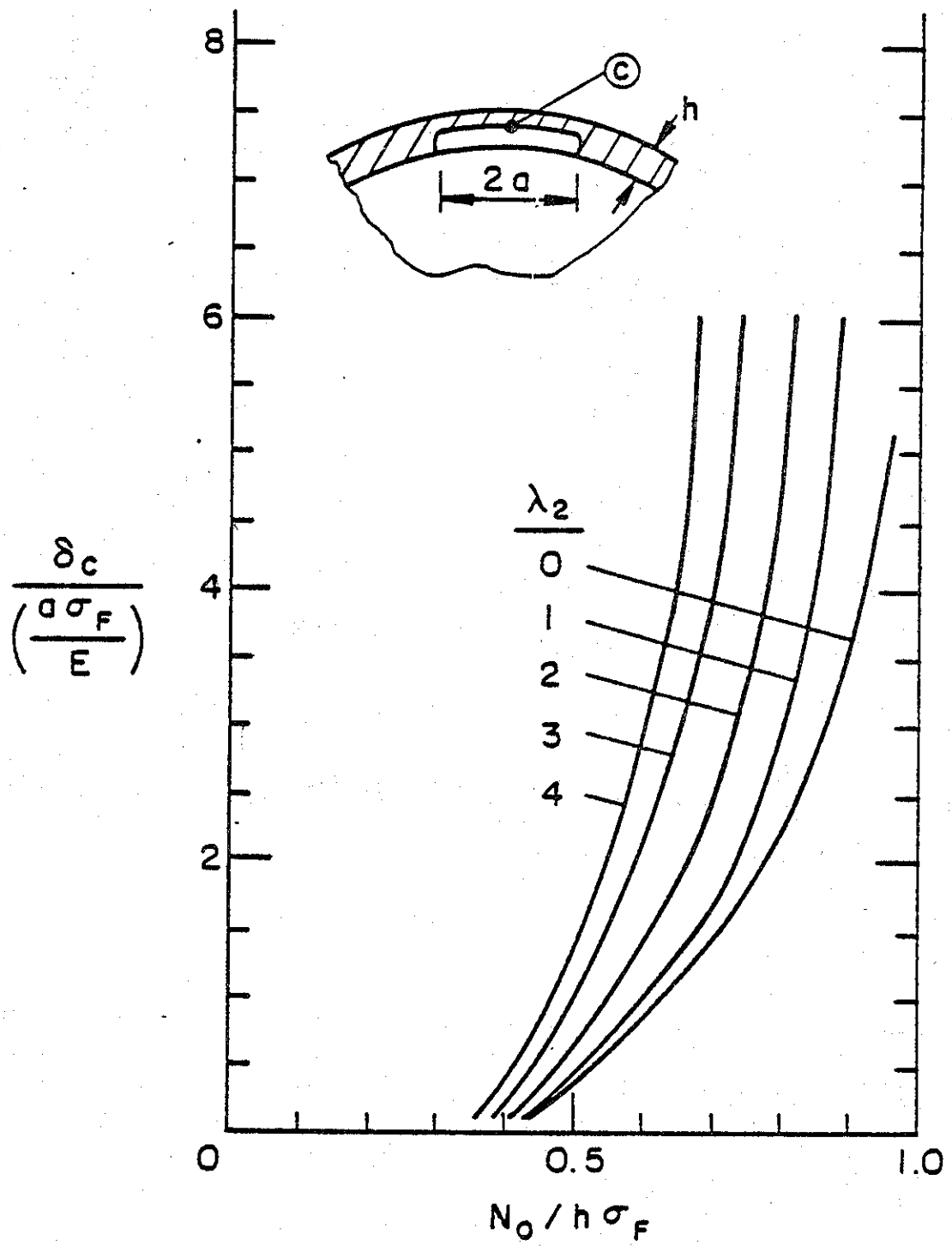


Figure 52. δ_c in a cylinder with an internal part-through crack, $a/h = 2$, $d/h = 0.7$, $\nu = 1/3$.

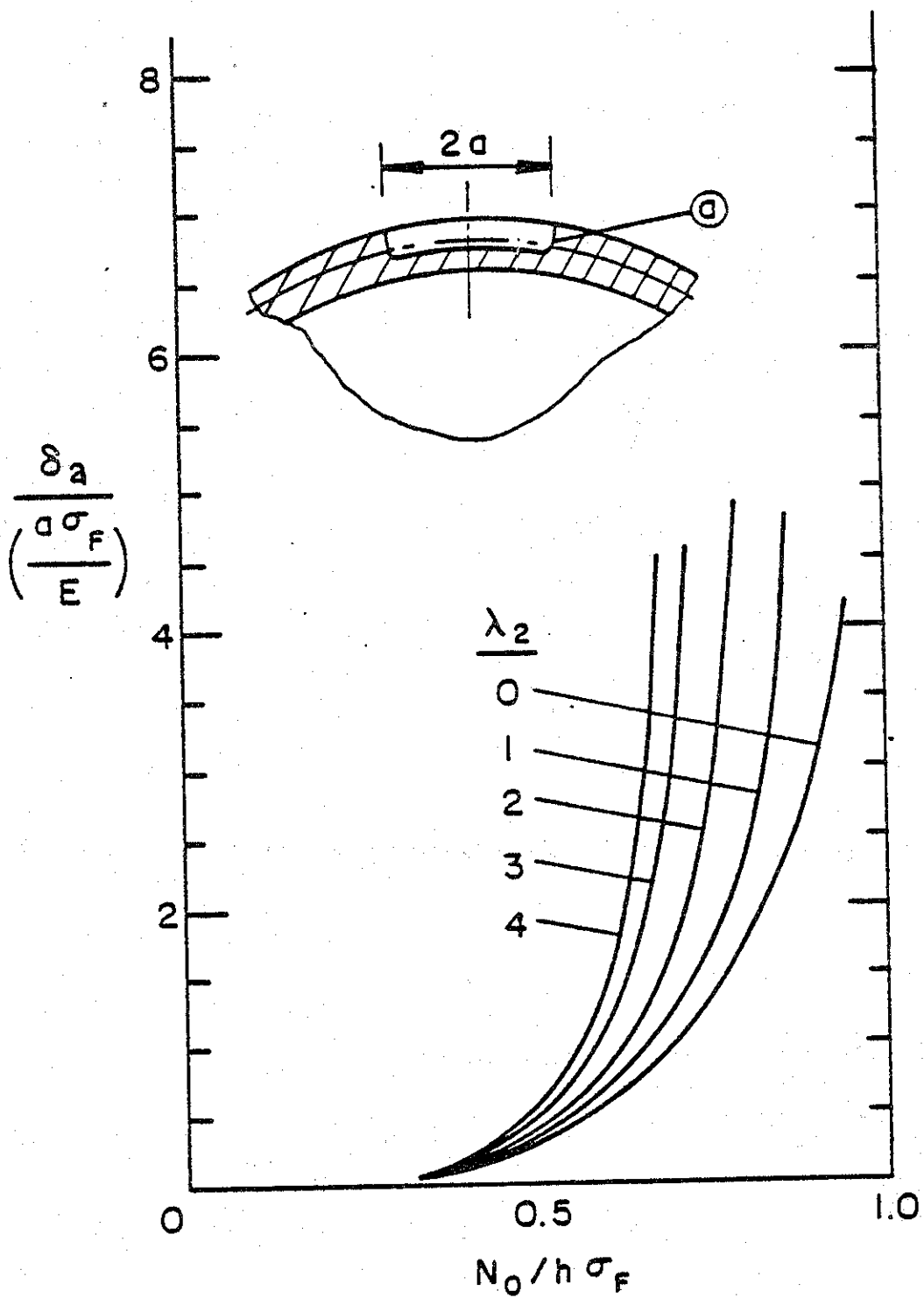


Figure 53. δ_a in a cylinder with an external part-through crack, $a/h = 2$, $d/h = 0.7$, $\nu = 1/3$.

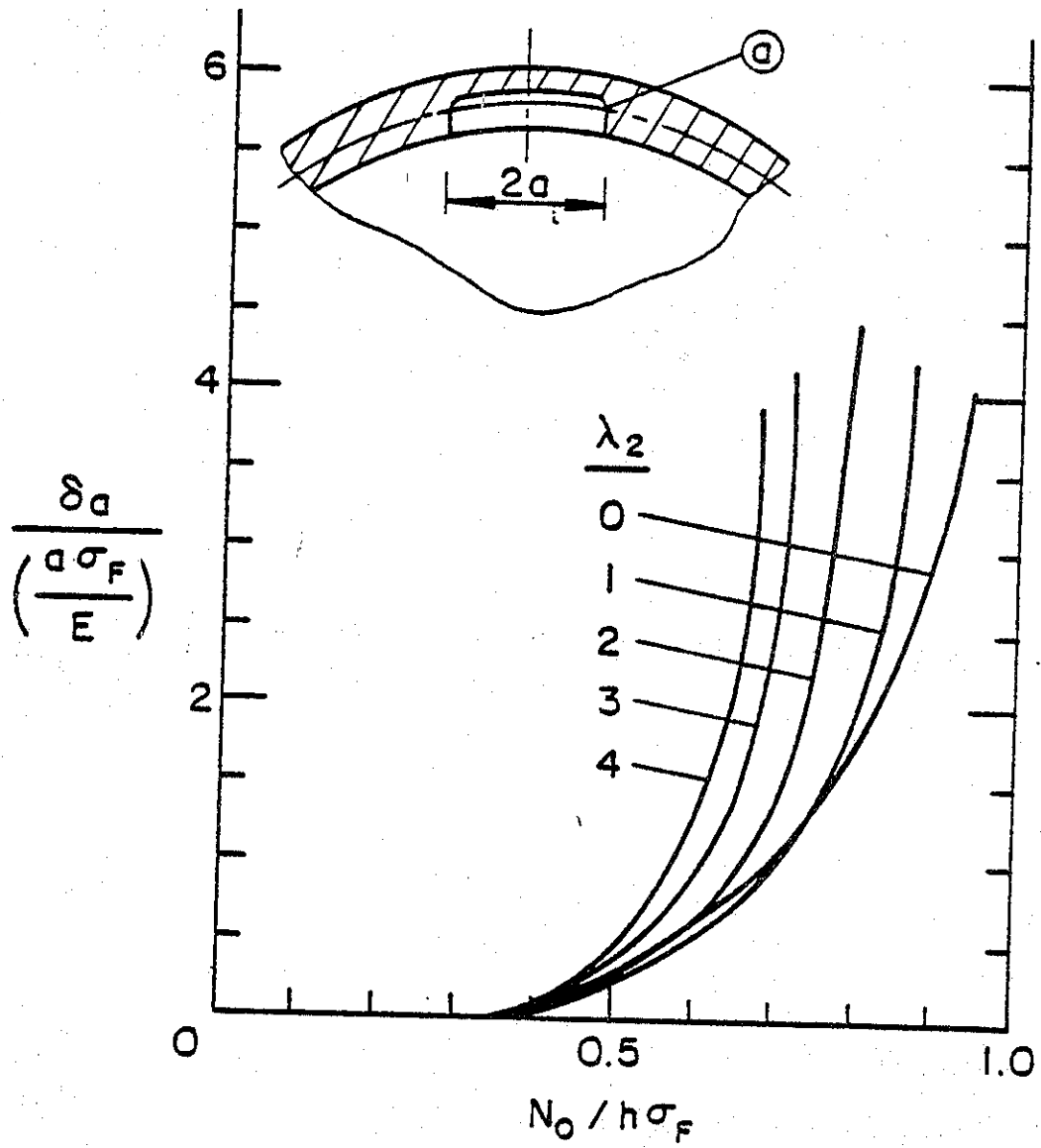


Figure 54. δ_a in a cylinder with an internal part-through crack, $a/h = 2$, $d/h = 0.7$, $\nu = 1/3$.

for the load carrying capacity of cylinders containing a part-through crack by using the results such as those given in Figures 49-52. It should again be emphasized that the membrane loads such as those given by Figure 55 are the crack growth initiation loads and are expected to be far below the fracture instability loads.

If the cylinder contains a through crack with large scale plastic deformations, for progressive crack growth and unstable fracture, in addition to the local condition in the fracture initiation or process zone, at each level of the external load the condition of the global energy balance must be satisfied. As in flat plates, in this case, too, the fracture process will be governed by the R-curve concept. Even though the problem is very complicated, if the resistance curve of the material is known, an approximate estimate of the fracture stability load may be obtained by using a plasticity-corrected stress intensity as the input. Thus, with $K_R(a)$ known noting that $K(a) = f(a)(N_0/h)\sqrt{a}$ (Table A1, Appendix A), $(N_0)_{cr}$ and a_{cr} may be obtained from

$$K(a_{cr}) = K_R(a_{cr}), \quad \frac{d}{da} K(a_{cr}) = \frac{d}{da} K_R(a_{cr}). \quad (61)$$

Note that since the shell correction factor $f(a)$ is a monotonically increasing function of a and is always greater than one, the values of $(N_0)_{cr}$ and a_{cr} for the shell would always be smaller than the corresponding flat plate values.

In the case of part-through crack, if, in addition to the local crack initiation condition, the global energy balance condition per local crack advance is satisfied, then it is possible to have progressive crack propagation and resulting fracture instability. In this problem since the crack front would not remain self-similar as it advances, it cannot be simplified and treated as a one-dimensional crack growth problem. However, a very simple technique to find a rough estimate of the fracture instability load for the cylinder with a relatively long and deep part-through crack or a through crack may be developed from the COS curves such as those given by Figures 48-52. From these figures it may be observed that for a given shell-crack geometry (i.e., for given a/h , d/h , and λ_2), in the neighborhood of a certain value of N_0 a small increase in N_0 would cause relatively a very large increase in δ_c or δ_a . Physically this may be interpreted as a tendency to the onset

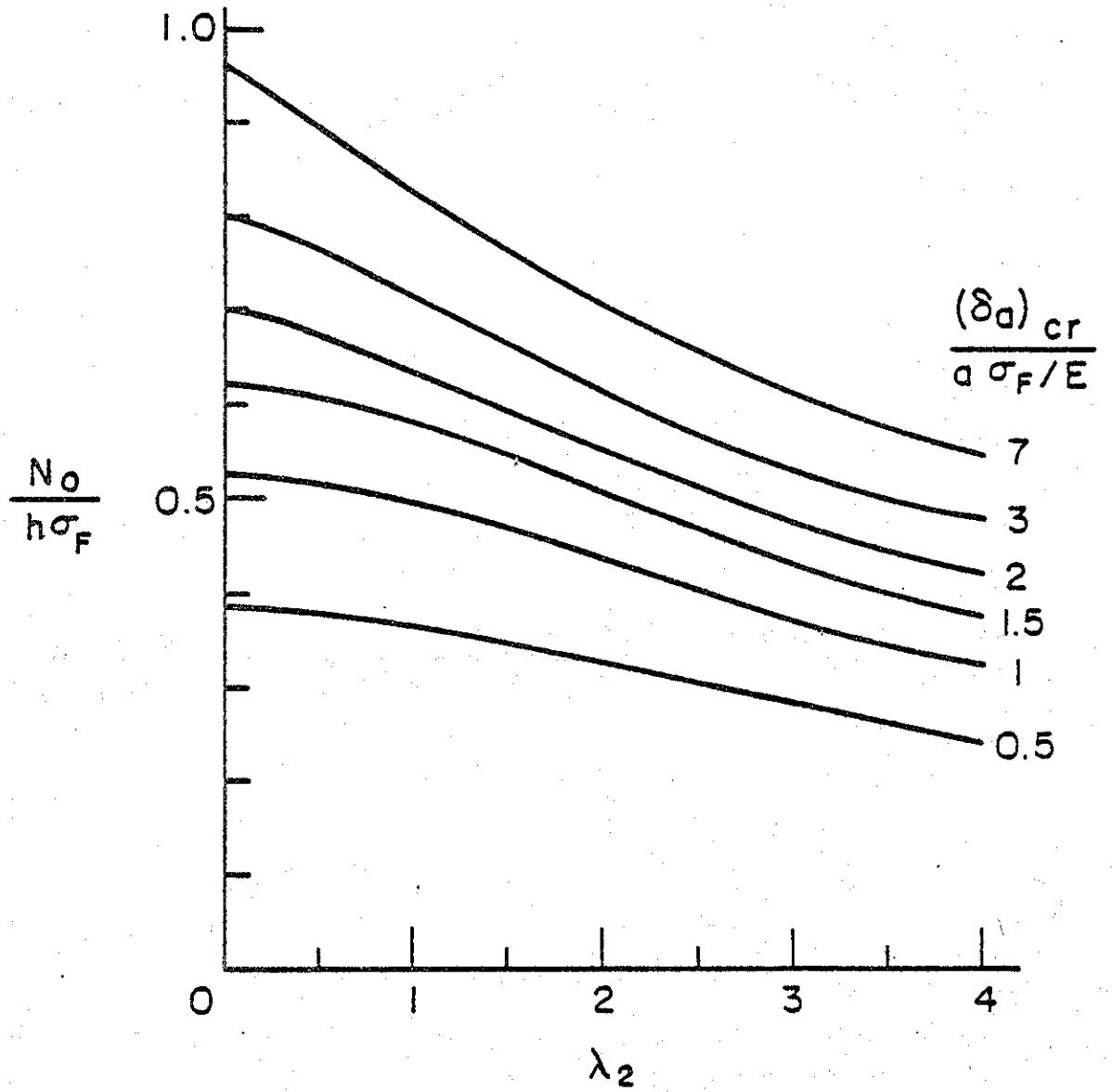


Figure 55. Load carrying capacity of a cylinder with a circumferential through crack corresponding to crack growth initiation with $(\delta a)_{cr}$ as the local crack initiation parameter, $a/h = 2$.

of an instability process. Thus, one may consider the value of the membrane load N_0 corresponding to the point on the COS vs. N_0 curve with an arbitrarily high slope as a rough estimate of the fracture instability load. An example is shown in Figure 15 which is obtained from Figures 48, 49 and 52 by assuming the value of the slope to be 40/1 (for the nondimensionalizing units shown in the figures). Qualitatively the results shown in Figure 56 have the expected trends, namely that the shell with an inner surface crack has the highest and that with a through crack the lowest load carrying capacity.

As mentioned earlier in this report, for certain crack geometry-material combinations the crack opening stretch along part of the crack front may reach and far exceed the critical crack initiation value before overall energy balance condition is satisfied. This means that in spite of very large values of COS the crack may not propagate and instead the net ligament would undergo plastic necking. For this mode of fracture the net ligament plastic necking instability load may be obtained by using the technique described in [7].

Finally, it should be pointed out that the stability of the through crack upon rupturing the net ligament (or the leak vs. the break) would depend on the net ligament thickness, or more precisely, on the part-through crack geometry at the instant of the onset of unstable fracture of the net ligament. Even if the dynamic effects are excluded, for a relatively shallow part-through crack the net ligament fracture instability load would be too high to be sustained by the resulting through crack. On the other hand if the crack becomes very deep as a consequence of substantial subcritical growth, then it is possible that the load magnitude necessary to rupture the net ligament would be smaller than that necessary to propagate the resulting through crack, hence the net ligament rupture would be followed by "leak" rather than "break". A qualitative demonstration of this argument may be observed from Figures 48, 49, and 51. Using the COS as the basis of comparison, from Figures 48 and 49 it is seen that corresponding to the same (critical) values of COS the load levels N_0 for the part-through crack with $d/h = 0.7$ are consistently greater than the load levels for the through crack. On the other hand, comparing Figures 48 and 51 it may be observed that corresponding, for example, to $\delta_c / (a\sigma_F/E) = 2$ the load level for the part-through crack with $d/h = 0.9$ is smaller than the load level for the through crack.

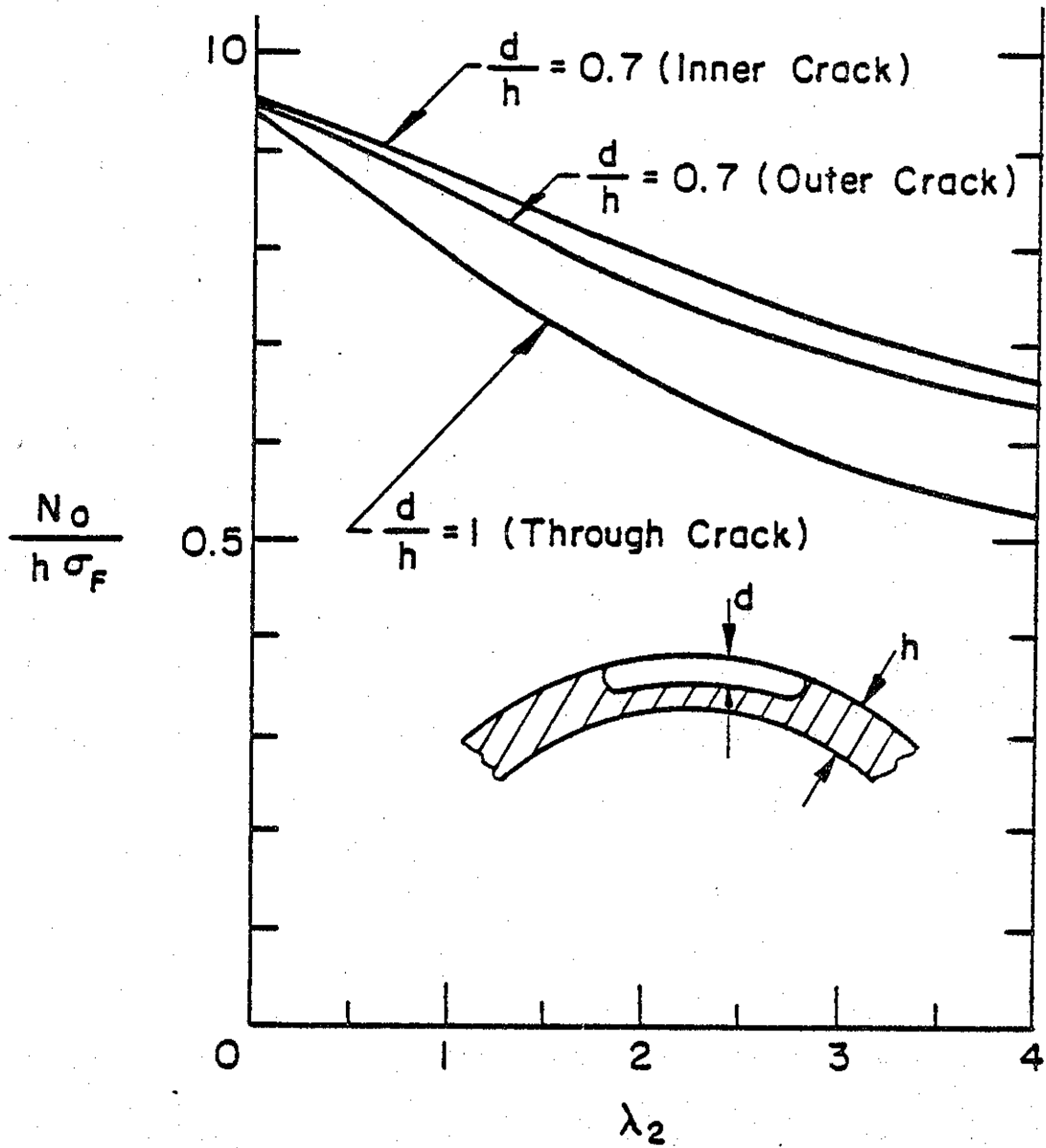


Figure 56. Approximate values of the load carrying capacity of a cylinder with a circumferential part-through or through crack corresponding to fracture instability of progressively growing crack, $a/h = 2$.

The technique developed and the results given in this section refer to a general cylindrical shell containing a part-through circumferential crack. In applications the practical measurable quantity is the COD on the outside surface of the shell and in the mid-section of the crack. The useful information is, therefore, plots of COD vs. σ_0 for a specific shell and crack geometry, where σ_0 is the axial stress in the cylinder. For standard pipe diameters (OD) of 24, 30, 36, and 48 inches and for various values crack dimensions a/h and ^(*) $d/h = L_0/h$ the calculated COD vs. σ_0/σ_F graphs are given in Appendix H. Qualitatively the results are quite similar to those given in this section. The results for a 20 in. diameter pipe which was used in the experiments are described in the following sections with the experimental program, where the technique of applying such analytical results as those given in the Appendix H is also discussed.

^(*) In Appendix H the maximum crack depth is indicated by L_0 in order to be consistent with the elasticity solution given in Appendices B and C.

THEORETICAL AND EXPERIMENTAL STUDY
OF FRACTURE IN PIPELINES CONTAINING
CIRCUMFERENTIAL FLAWS

PART II

EXPERIMENTAL INVESTIGATION OF PLATES AND PIPES
CONTAINING A PART-THROUGH CRACK

1. INTRODUCTION

The primary objectives of the current study were (a) to develop a methodology which may be used in analyzing fatigue crack propagation and fracture problems in pipelines containing circumferential surface flaws, and (b) to carry out an appropriate experimental program in order to verify the theoretical findings and to determine their limitations. From a viewpoint of fracture failure due to circumferential defects two major problems in pipelines are known to be the propagation of fatigue or corrosion fatigue cracks initiating from existing surface flaws, and the problem of "leak" or "break" following the fatigue phase. The first problem which relates to a subcritical crack propagation is empirically well-understood in the sense that knowing the stress intensity factor and the load-time profile, and having access to the baseline laboratory fatigue data for the given material and the environment, it is possible to perform a reliable analysis to predict the crack propagation rate in the pipe wall. In this regard the main problem is the calculation of the stress intensity factors for a circumferential surface crack in pipes. This research is described in Part I of the report. Related experimental studies on plates and pipes containing a circumferential part-through crack will be discussed in this part.

The question of ductile fracture leading to a leak or break in the pipe is, on the other hand, far from being understood. Microstructurally, the basic mechanism of ductile fracture appears to be first formation and growth of "holes" or "voids" as a result of the fracture of inclusions or inclusion boundaries, or fracture taking place at other localized sites of high stress

concentrations and constraints, followed by the "necking" of ligaments formed by the holes, and finally rupture of the ligaments leading to the coalescence of holes and to the formation or extension of cracks. Various kinds of ductile fracture were discussed in Part I. However, it should again be emphasized that the ductile fracture propagation is very highly dependent on the geometry of the structural component and of the crack. Therefore, in modeling and analyzing it the mechanics of the problem is expected to play a major role.

The experimental program was undertaken for three different crack geometries, namely the plane single edge notched specimen of X70 pipeline steel, a flat plate with a part-through surface crack again of X70 steel, and 20 in. OD X60 line pipe having a circumferential part-through crack. In this study the pipe problem is the one which is of primary practical interest and is related to fatigue and fracture of pipelines containing a circumferential flaw (such as, for example, a weld defect) and subjected to secondary loads giving largely time-dependent axial stresses. The first two problems in plates were considered as idealized special cases, mostly to check the validity of the ductile fracture model.

2. FATIGUE AND FRACTURE OF SINGLE EDGE NOTCHED SPECIMENS

2.1 Fatigue Crack Growth Experiments

The specimen used in these experiments was a 12 in. long 2 in. wide and 5/8 in. thick edge-notched plate shown in Figure 57. Twenty specimens were cut from a 4x12 ft. X70 line pipe steel (U.S.S.). The plate was rolled from a slab which has the following chemical analysis (in percent):

												<u>ppm</u>	
<u>C</u>	<u>Mn</u>	<u>P</u>	<u>S</u>	<u>Si</u>	<u>Cu</u>	<u>Ni</u>	<u>Cr</u>	<u>Mo</u>	<u>Cb</u>	<u>Al</u>	<u>N</u>	<u>O₂</u>	<u>C_a</u>
.06	.34	.008	.004	.22	.33	.10	.10	.31	.04	.027	.009	40	19

Figure 58 shows the stress-strain curve and some relevant mechanical properties of the material. All specimens were cut parallel to the rolling direction with the crack perpendicular to it largely because of the fact that the main interest in the study is in the growth of circumferential flaws in pipelines (where the crack would also be perpendicular to the rolling direction).

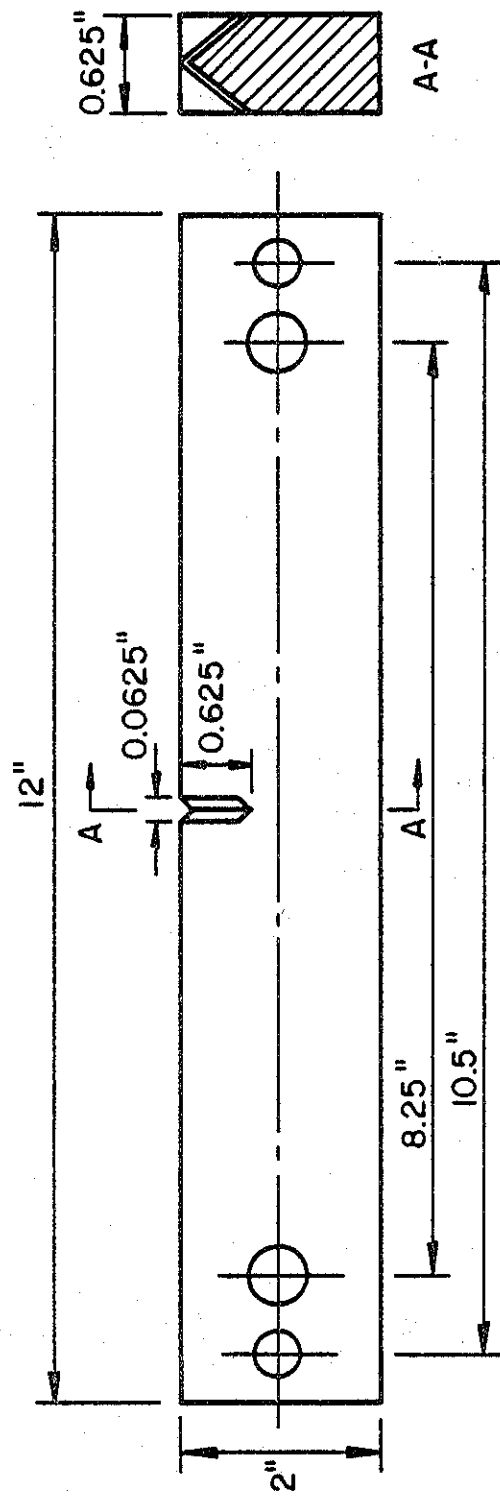


Figure 57. Geometry of the single edge notched specimen.

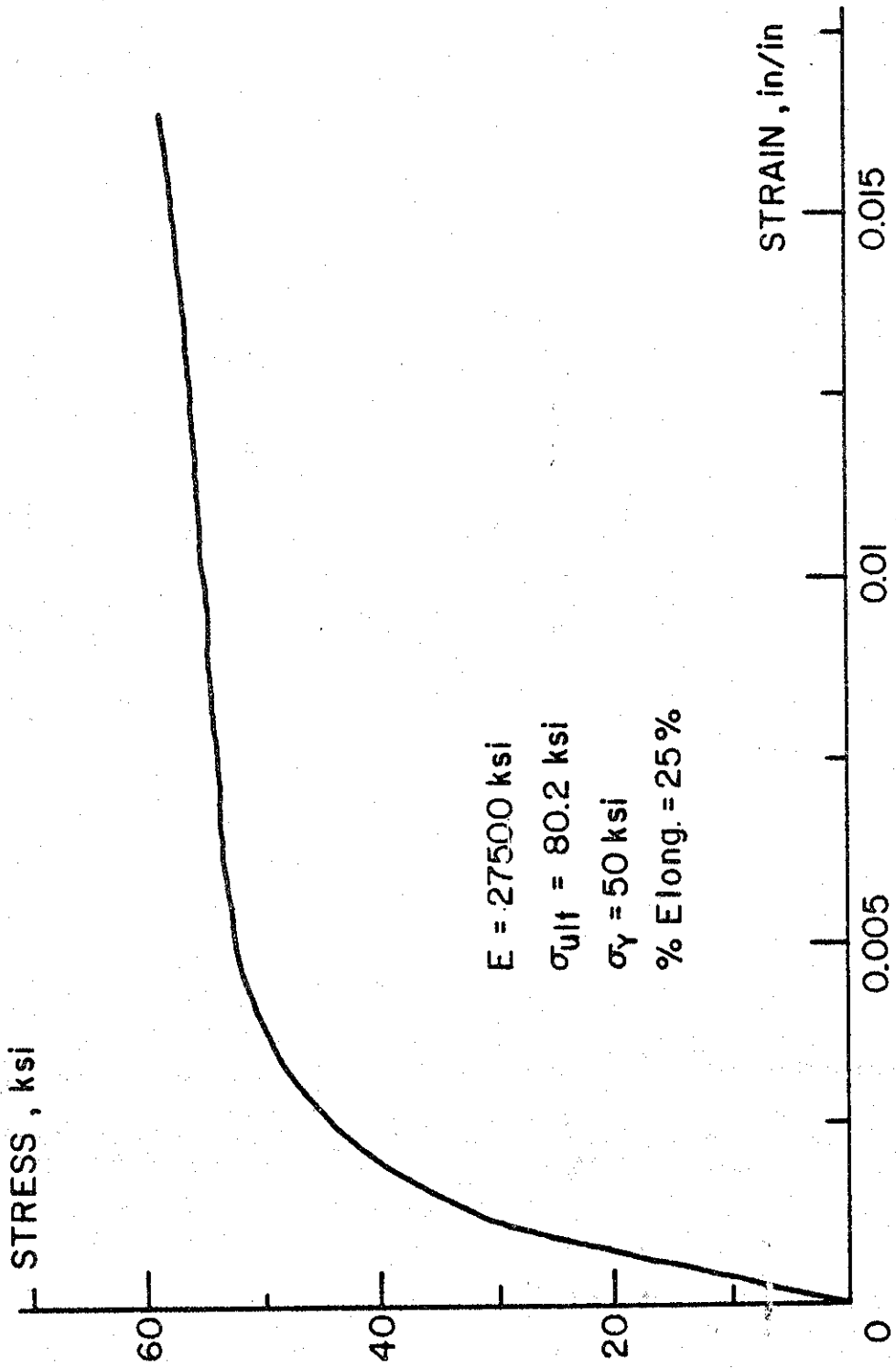


Figure 58. Mechanical properties of the X70 plate material obtained from a tensile specimen cut parallel to the rolling direction.

All twenty specimens were precracked in an Amsler Vibrophore at room temperature. The specimens were loaded in three-point bending and precracked under low amplitude and high frequency loading. The specimens were divided into five groups of four. In the first group, the precracking was stopped as soon as the natural crack was visible ahead of the machined chevron notch. This group was used in the fatigue crack growth characterization of the material. In the remaining four groups the crack was allowed to grow to four different crack-to-specimen width ratios, namely $a/h \approx 0.4, 0.5, 0.6, 0.7$. These specimens were used in the static fracture tests. Throughout the precracking phase and in all five groups, the load amplitude was held sufficiently low in order to avoid any permanent plastic deformations.

The fatigue crack growth characterization tests were conducted at room temperature on a 20-Kips Instron machine using a full sine load wave. The frequency and load ratio $R (P_{\min}/P_{\max})$ for all four specimens were 10 Hz. and 0.05, respectively. The specimens were pinloaded and the crack growth was monitored by a travelling microscope which required that the surface of the specimen be adequately cleaned and polished. The growth rates were calculated from subsequent crack length measurements and the stress intensity factor amplitude ΔK was computed as follows:

$$\Delta K = \Delta\sigma\sqrt{h} g_t(\xi), \quad \xi = \frac{a}{h} \quad (62)$$

where $\Delta\sigma = \Delta P/ht$ is the stress amplitude, ΔP the load amplitude, h the specimen width, t the specimen thickness, a the crack length and g_t is given by (see Appendix B)

$$g_t(\xi) = \sqrt{\pi\xi} (1.1216 + 6.52\xi^2 - 12.3877\xi^4 + 89.0554\xi^6 - 188.608\xi^8 + 207.387\xi^{10} - 32.0524\xi^{12}) \quad (63)$$

The fatigue crack propagation results are shown in Figure 59. The figure also shows the results obtained from surface crack experiments in plates and pipes. The solid line in Figure 59 represents the approximate fit to the air data obtained by Vosikovsky [53]. The specimens used in [53] were also pinloaded edge-notched X70 steel strips with the same crack orientation with respect to the rolling direction as the edge-notched specimens, plates, and pipes shown in Figure 59 and used in this study, that is in all cases the

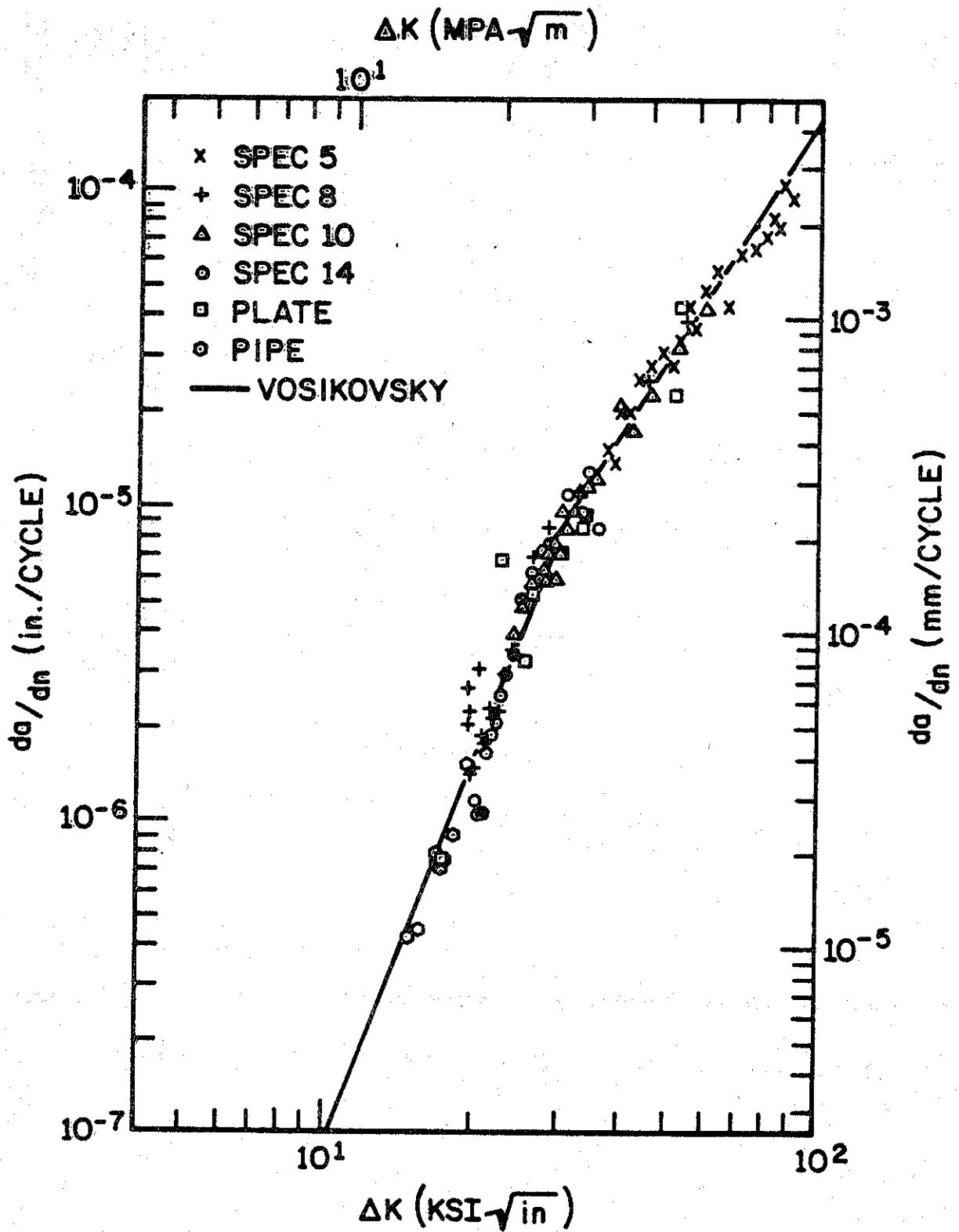


Figure 59. Fatigue crack propagation in X70 single edge notched and surface cracked plates, and in circumferentially cracked X60 pipes.

crack was perpendicular to the rolling direction. Generally, there seems to be a good agreement among the fatigue data obtained from various sources and crack geometries.

2.2 Fracture Tests

After precracking to various crack length-to-plate width (a/h) ratios, the single edge notched specimens were tested to fracture. The original intention was to perform the fracture tests under tension (through pin loads) and under three point bending. However, the toughness of the material proved to be too high to obtain rupture separation in bend tests. Under bending the shear cracks developed and propagated at an angle near and at the surfaces of the specimen, and the specimen essentially tended to "fold" as the displacement of the loading ram is increased. Therefore, all fracture experiments were performed under tension.

The primary reliable output of the experiments was the clip-gage displacement measured at the specimen surface (or at the crack mouth). Measurement of the entire crack opening profile by the replication technique through injecting a fast-setting plastic into the crack proved to be very tedious and unreliable. Hence, no quantitative results were obtained by this technique. A continuous recording of the pin-load P vs. the crack mouth opening displacement COD was obtained by feeding the outputs from the load cell of the testing machine and the clip gage into an x-y recorder. The information was also stored on a disk as a back-up. The results obtained for the same a/h (crack length-to-specimen width) ratio were found to be quite reproducible. Figures 60-63 show some sample results for each a/h ratio tested. The results are also plotted in normalized form in Figures 64-67. For the a/h ratios tested (i.e., for $a/h = 0.415, 0.499, 0.610, 0.725$) typical fracture surfaces are shown in Figure 68.

As may be partially observed from Figure 68 that in the fracture tests there was no evidence of (brittle or quasi-brittle) "pop-in". As the load was increased, there was severe yielding and a narrow stretch zone developed away from the surfaces, followed by dimple fracture in a "thumb-nail" zone in the mid-portion of the plate. The thumb-nail zone was approximately symmetric with respect to the mid-plane of the plate. In the mid plane where

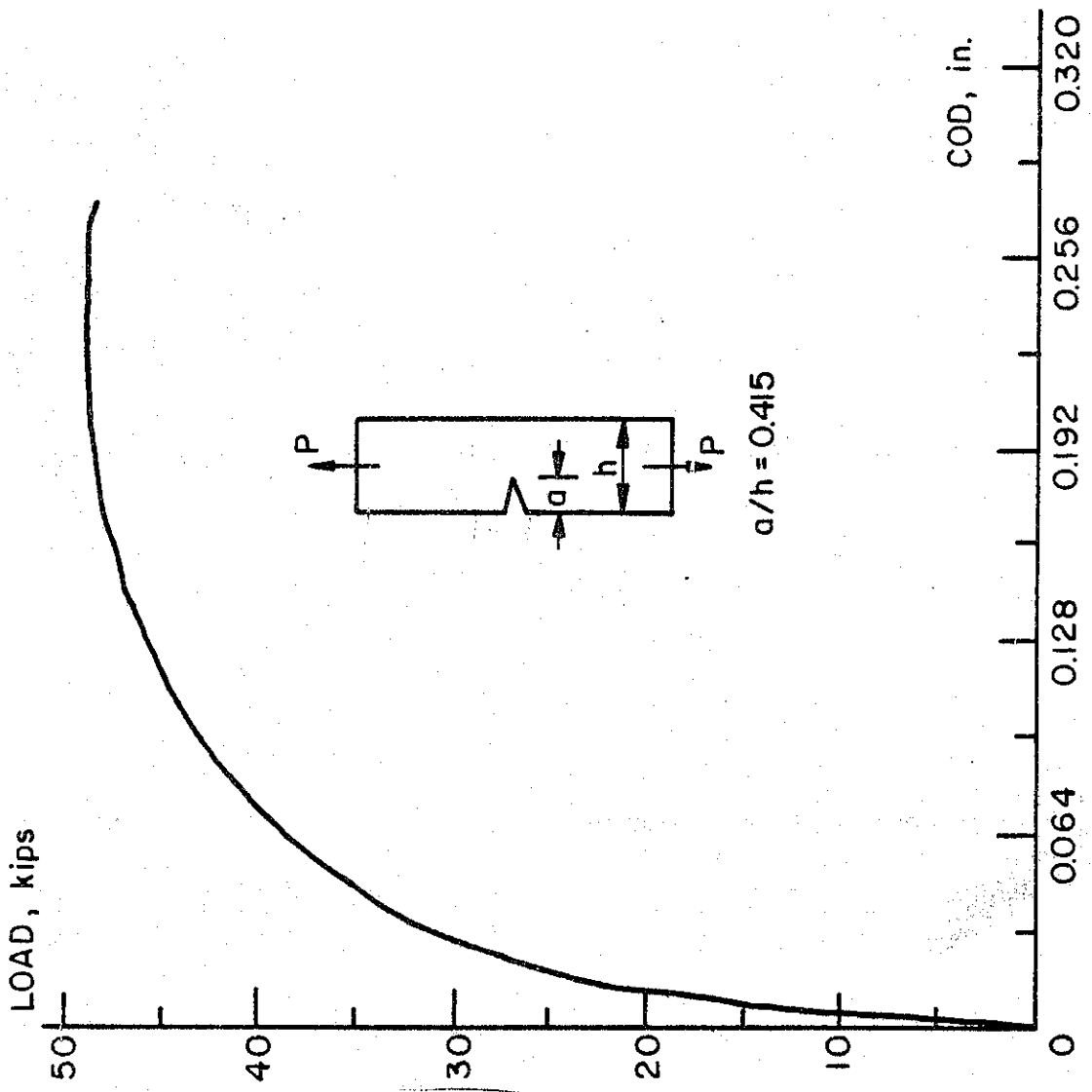


Figure 60. Load P vs. COD for the single edge notched (SEN) specimen, $a/h = 0.415$.

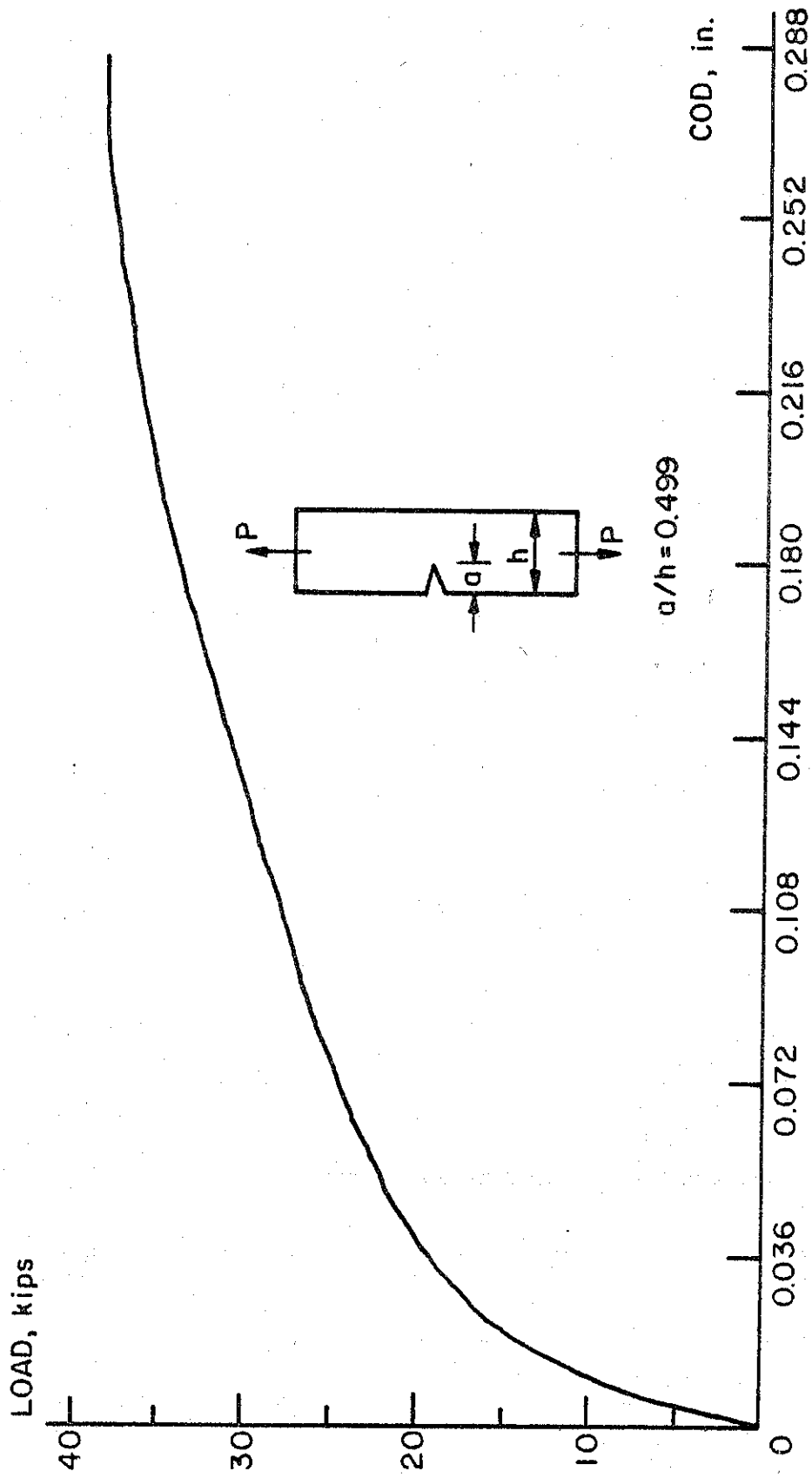


Figure 61. P vs. COD for the SEN specimen, $a/h = 0.499$.

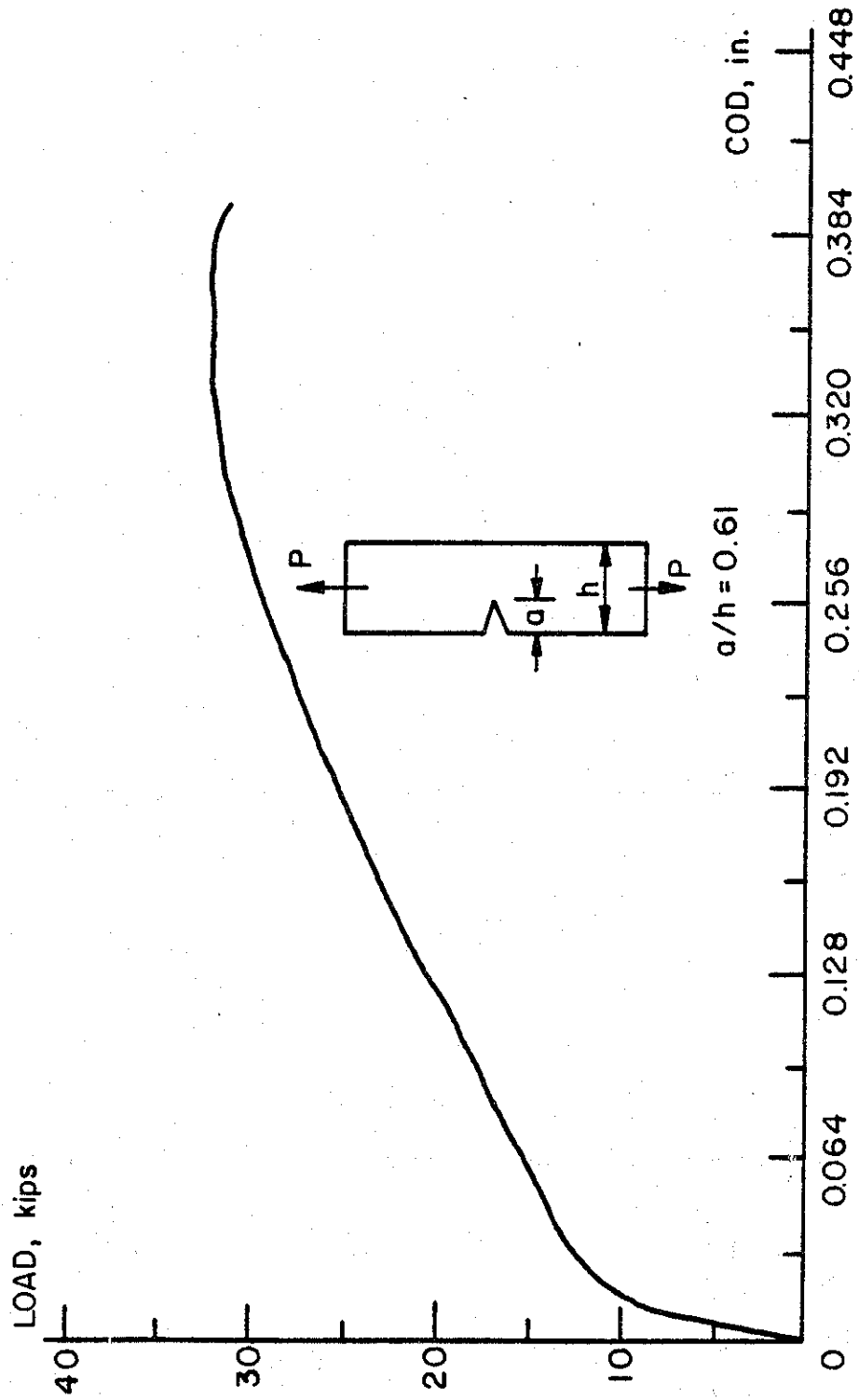


Figure 62. P vs. COD for the SEN specimen, $a/h = 0.61$.

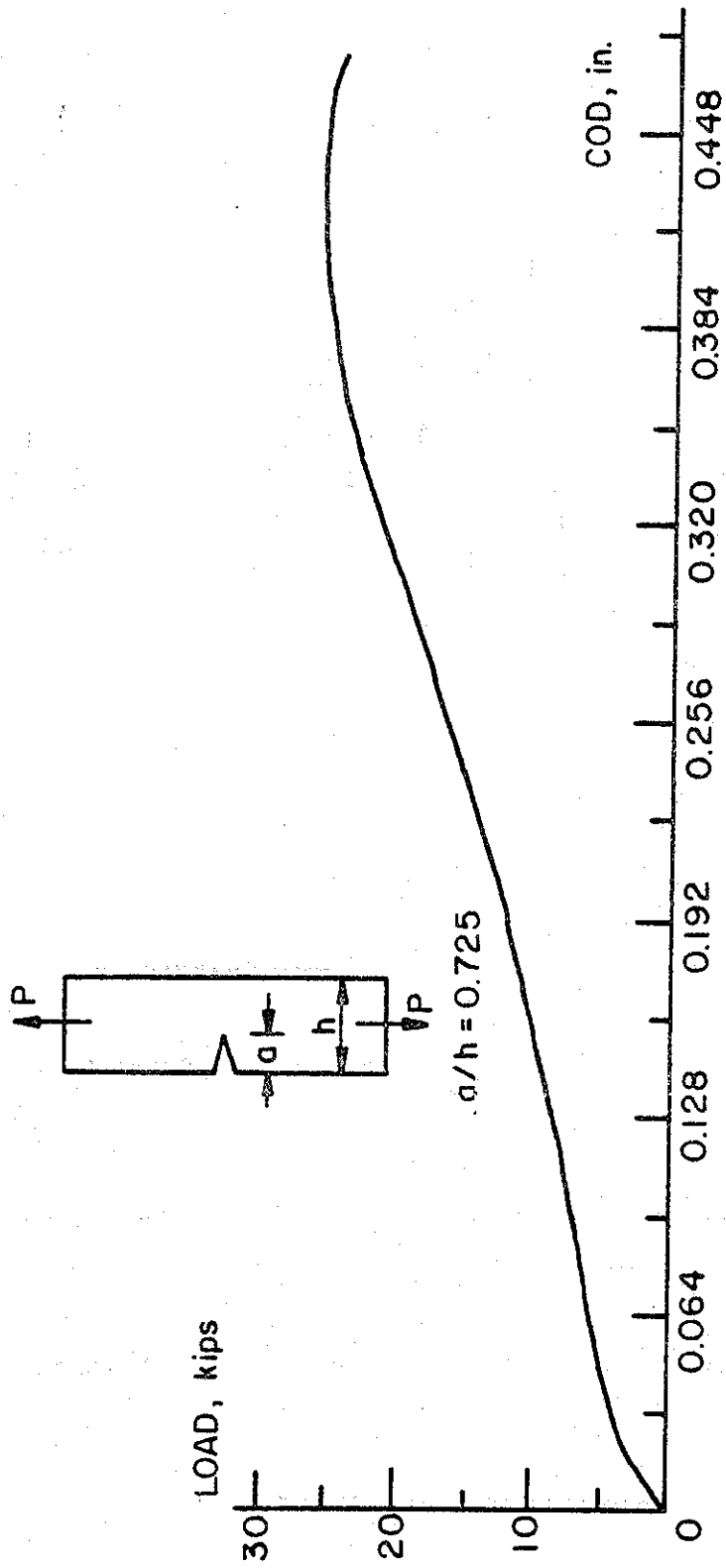


Figure 63. P vs. COD for the SEN specimen, $a/h = 0.725$.

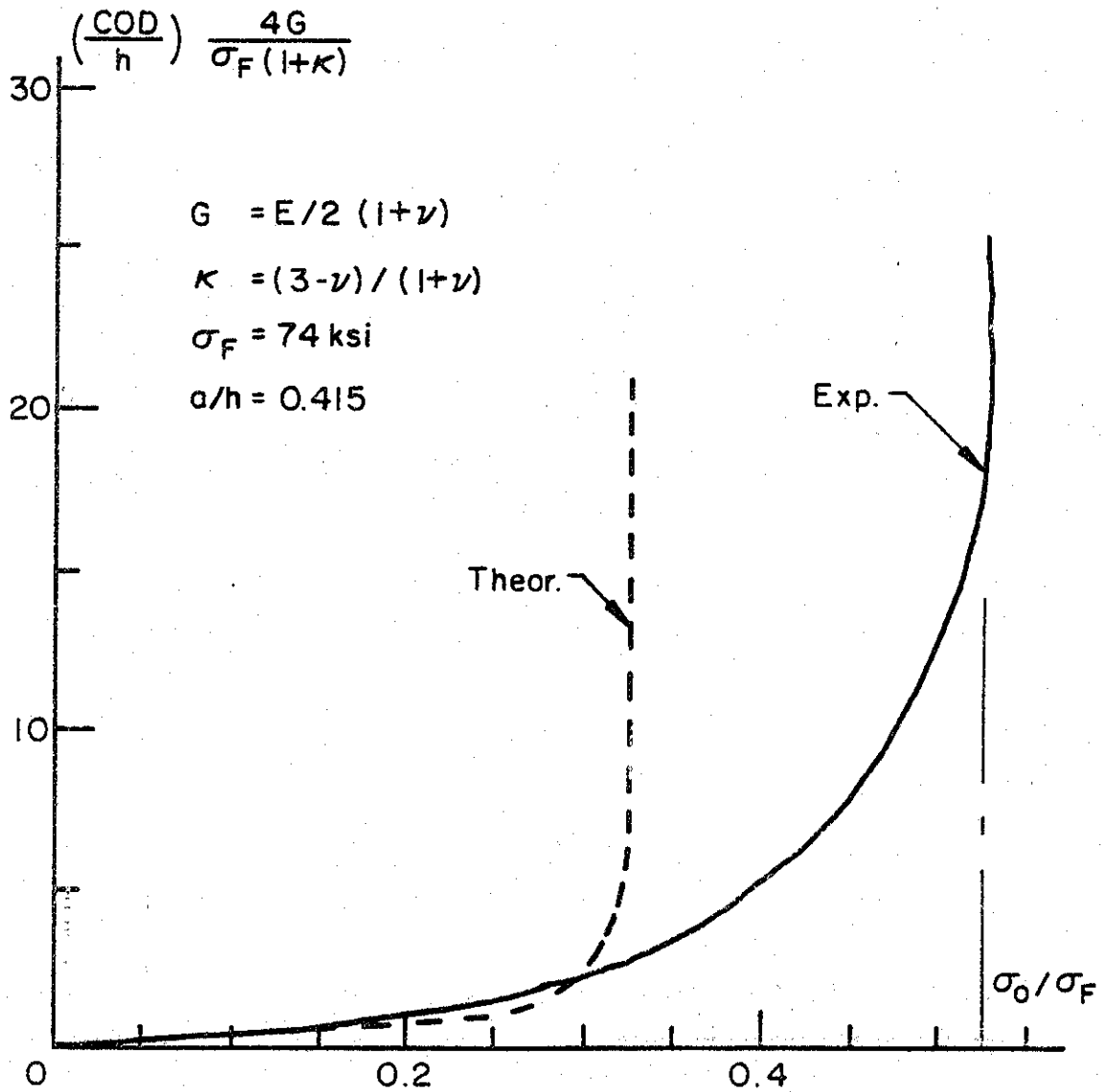


Figure 64. Normalized COD vs. stress ratio for the SEN specimen, $a/h = 0.415$.

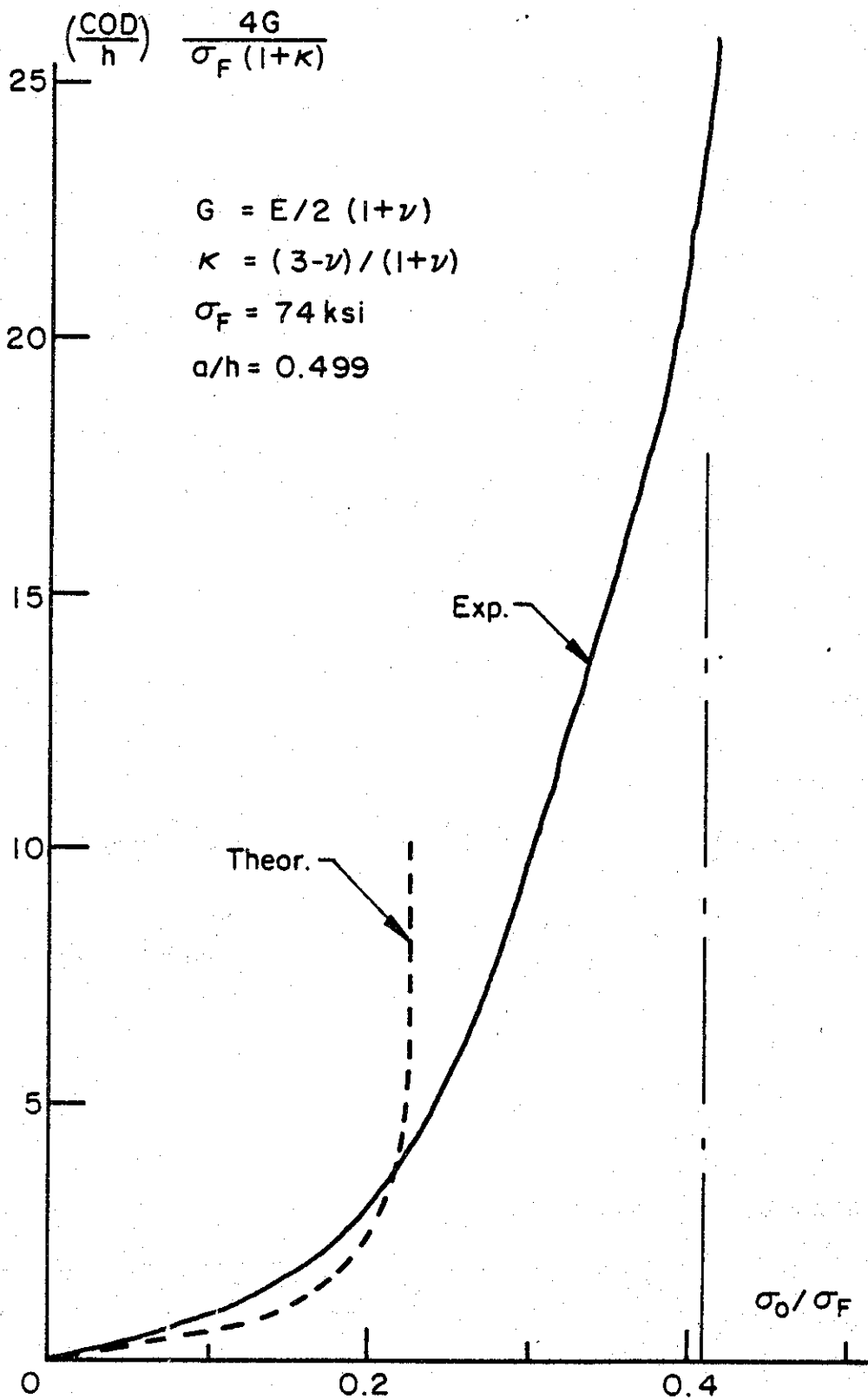


Figure 65. Normalized COD vs. stress ratio for the SEN specimen, $a/h = 0.499$.

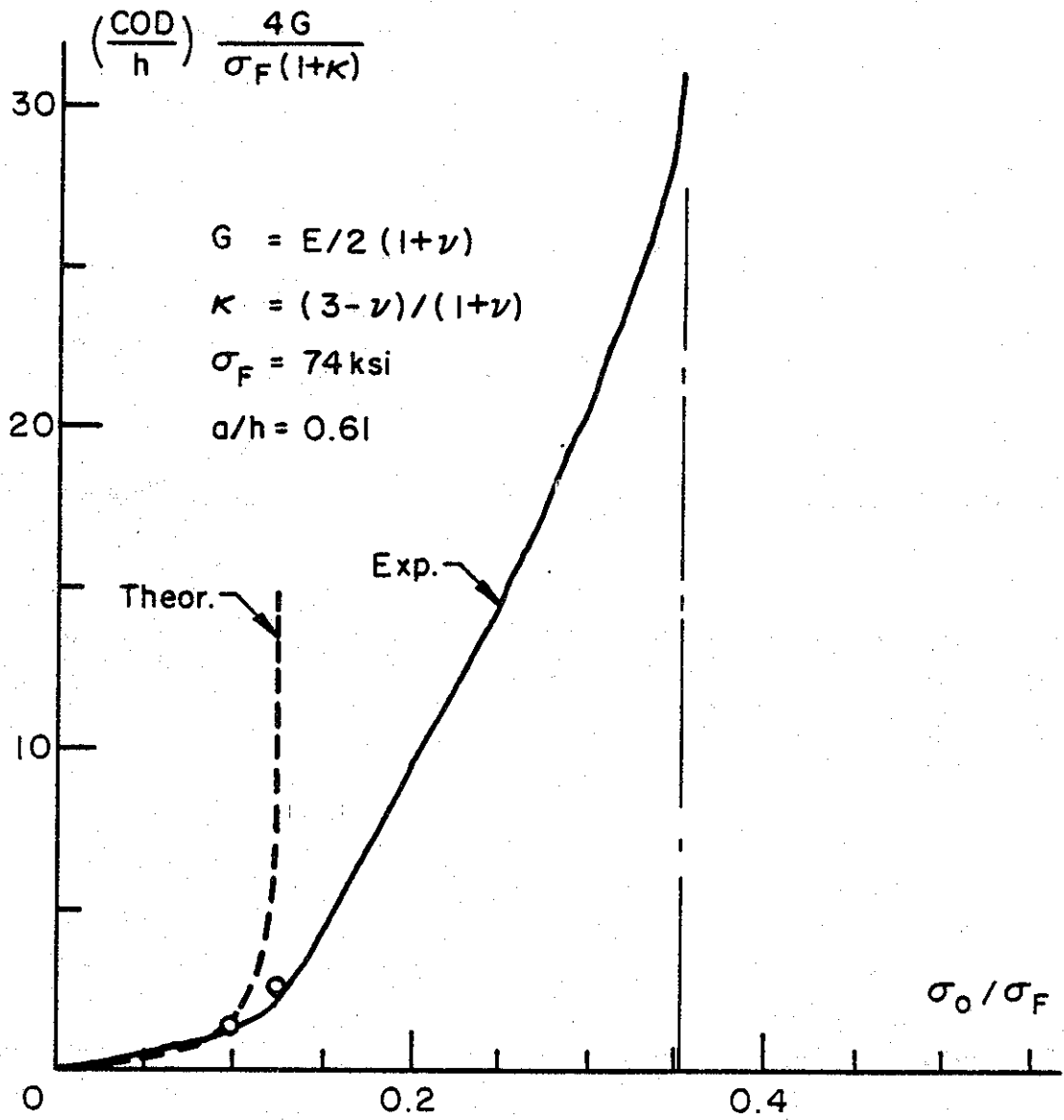


Figure 66. Normalized COD vs. stress ratio for the SEN specimen, $a/h = 0.61$.

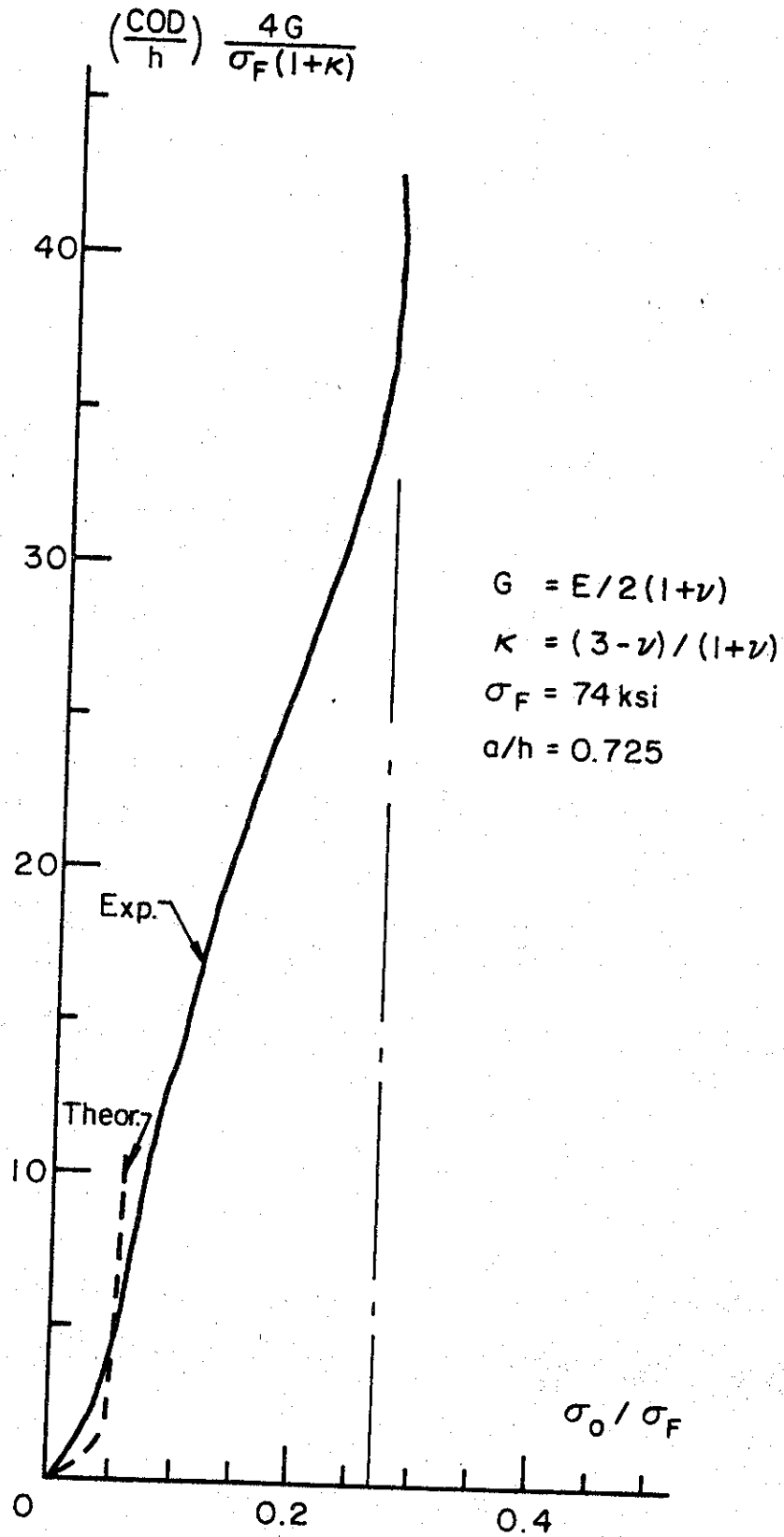


Figure 67. Normalized COD vs. stress ratio for the SEN specimen, $a/h = 0.725$.

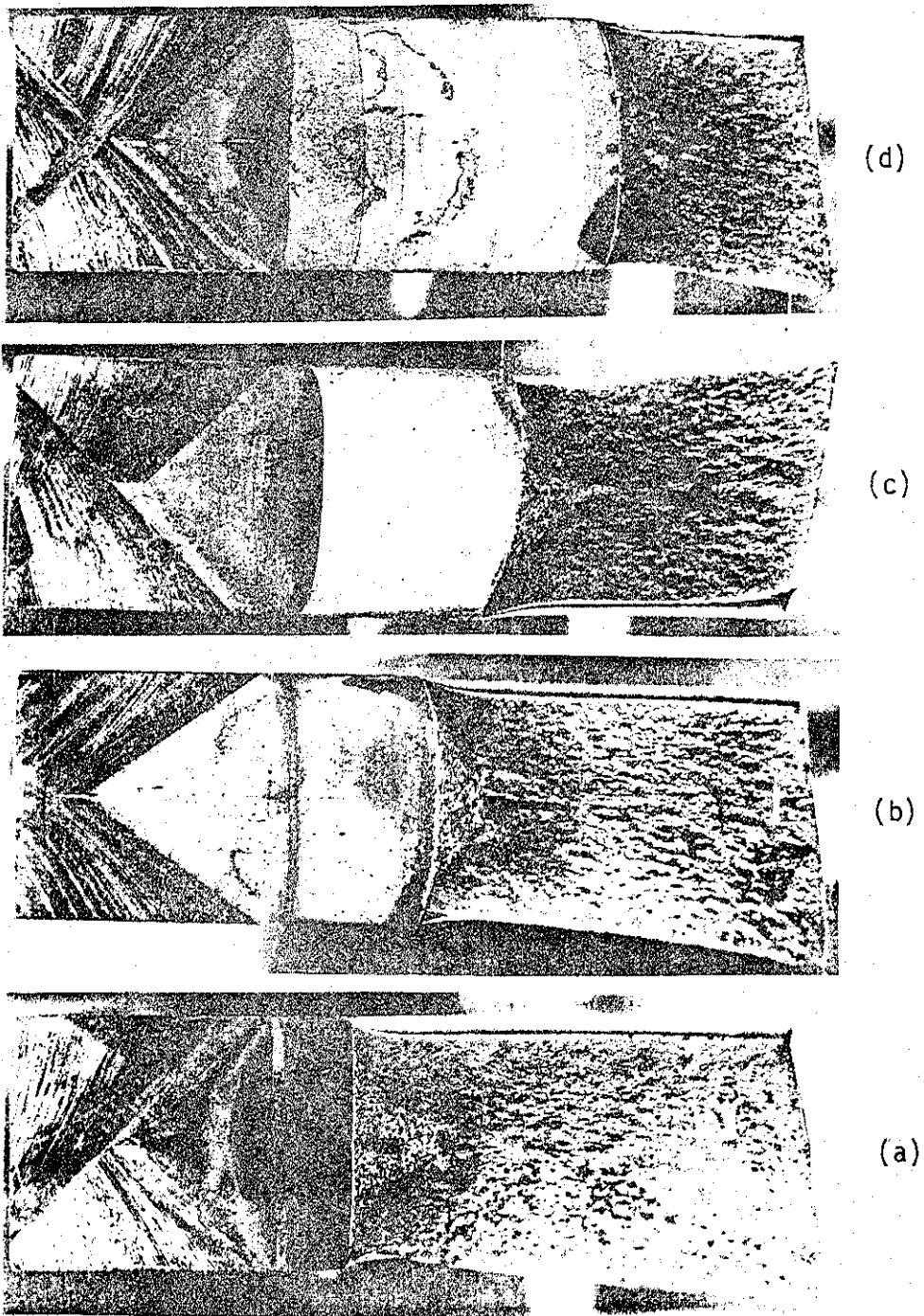


Figure 68. Fracture surface of SEN specimens, (a) $a/h = 0.415$, (b) $a/h = 0.499$, (c) $a/h = 0.61$, (d) $a/h = 0.725$.

the ductile fracture results obtained from these experiments cannot be directly linked with the plate and the pipe results regarding the net ligament rupture which is the main focus of the ductile fracture studies in this report. Even for the deepest crack (for which the net ligament width $h-a = 0.55$ in. was less than the specimen thickness 0.625 in.) the fracture was a 45° slant fracture (Figure 68d). However, as expected the fracture mode of the through cracks in plate, pipe, and the SEN specimens were all alike.

3. PLATES CONTAINING A SURFACE CRACK

3.1 Fatigue Crack Growth Experiments

The geometry of the surface cracked plate specimens is shown in Figure 69. Again, the specimens were cut in rolling direction from a 5/8 in. thick X70 steel plate. The thickness in the test section of the specimens was reduced to 0.425 in. largely because of the capacity of the testing machine used in the fracture experiments. In three of the five specimens tested the initial surface notch was cut by a vertical milling machine, and in the remaining two by an electric discharge process. From the viewpoint of reducing the precracking time, obtaining the desired notch profile, and notch root acuity, the latter was by far the better technique. However, after initiation, the subsequent fatigue crack propagation process was not affected by the geometry of the initial notch.

The fatigue experiments were conducted in an Amsler machine at 250 cycles per minute and a load ratio P_{\min}/P_{\max} of approximately 0.3. The fatigue crack propagation was monitored by fatigue crack front markings which were obtained by reducing rather than increasing the load amplitude. Increased load amplitude has the advantage of being faster (i.e., requires relatively small number of cycles) and perhaps of giving somewhat sharper markings. However, it also has the disadvantage of causing some uncertainty in the crack growth rate analysis because of the delay effect resulting from the overloads. In the present problem in using the technique of overloads there was also the danger of premature net ligament rupture for very deep cracks.

Figure 70 shows a typical fatigue crack surface on which the markings are visible. The figure shows that regardless of the initial notch geometry

the fatigue crack assumes approximately a semi-elliptic shape and maintains it as it grows.

In analyzing the fatigue crack growth results the stress intensity factor at the deepest penetration point of the crack was calculated by using the expression developed in [42] for a semi-elliptic surface crack in a plate having a finite width:

$$K = \sigma(\pi a/Q)^{1/2} F \quad , \quad (66)$$

$$Q \approx 1 + 4.64(a/c)^{1.65} \quad , \quad (a < c) \quad , \quad (67)$$

$$F = \{M_1 + [(\frac{Qc}{a})^{1/2} - M_1](\frac{a}{t})^{\sqrt{\pi}} + (\frac{Qc}{a})^{1/2}(M_2-1)(\frac{a}{t})^{2\sqrt{\pi}}\} f_w \quad , \quad (68)$$

$$M_1 = 1.13 - 0.1(\frac{a}{c}) \quad , \quad (0.03 \leq \frac{a}{c} < 1) \quad , \quad (69)$$

$$M_2 = (\pi/4)^{1/2} \quad , \quad a \leq c, \quad (70)$$

$$f_w = [\cos(\frac{\pi c}{W} \sqrt{a/t})]^{-1/2} \quad , \quad (71)$$

where $2c$ is the crack length on the surface, a is the maximum crack depth, t is the plate thickness, W is the plate width and σ is the uniform tensile stress away from the crack region.

The crack growth rates obtained from the plate experiments are shown in Figure 59 with the remaining X70 results. These results simply confirm the contention that the fatigue crack growth rates in plates with a surface crack may be predicted from the baseline data provided a reliable estimate of the stress intensity factor is available.

3.2 Fracture Tests

After fatigue cracking the plates to various crack depths, the plates were fractured under static tension (see Figure 71). Again, COD measured on the plate surface in the center of the crack was found to be the only reliable output in the experiment. The outputs from the crack opening gage and

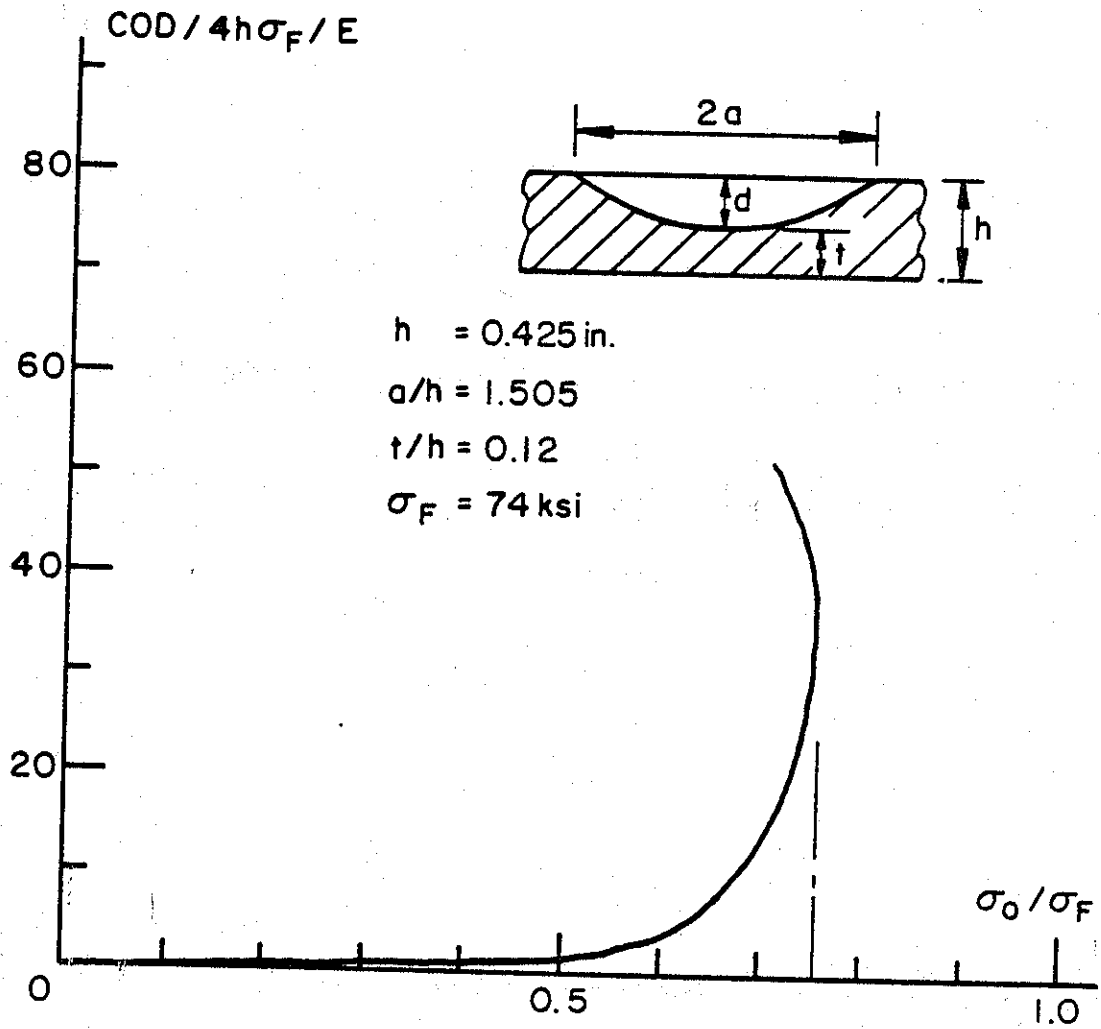


Figure 73. Normalized COD vs. stress ratio for the plate with a surface crack, $t/h = 0.12$.

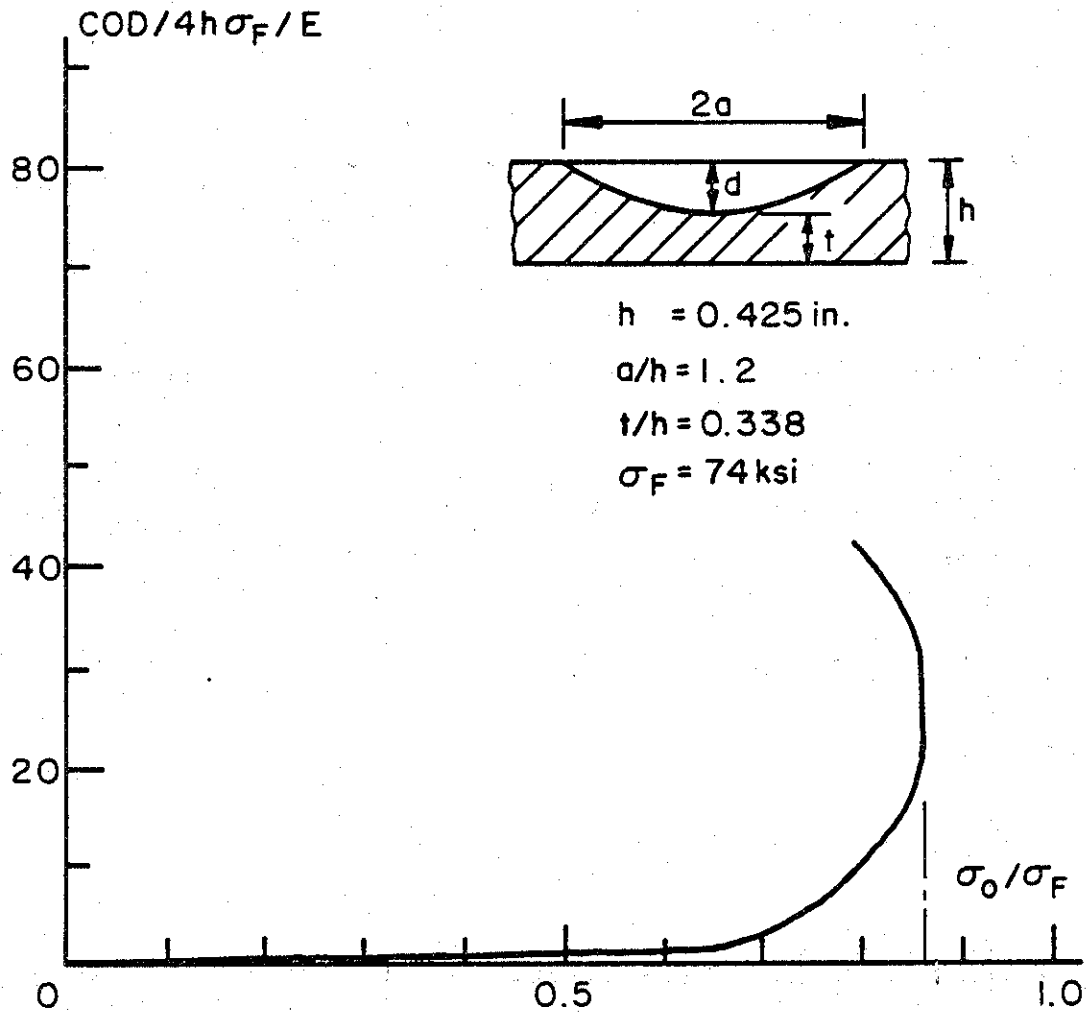


Figure 74. Normalized COD vs. stress ratio for the plate with a surface crack, $t/h = 0.338$.

4. THE PIPE EXPERIMENTS

The main part of the experimental program was the fatigue and fracture tests on a "full-scale" line pipe in order to test the validity of some of the ideas and models developed in the theoretical part of this study, and to investigate the mechanical nature of the net ligament rupture. Despite our initial preference for X70 pipes, availability of standard pipes within the capability of the testing equipment in the laboratory was the main factor in selecting 20 in. diameter X60 line pipes. The pipes had the standard dimensions (20 in. OD and 0.344 in. thick) in accordance with the American Petroleum Institute Specification 5LX. Again, after an initial cut, the pipe was subjected to fatigue under a "four-point" bending. The same load frame as that used in the fatigue tests was also used for static fracture tests. The geometry of the specimens and the loading frame are shown in Figures 76 and 77.

4.1 Mechanical Properties of the Material

Before testing the pipes, specimens were cut from the pipe in the longitudinal direction to obtain simple mechanical properties of the material. A sample result of the tensile tests is shown in Figure 78. Even though the material was nominally designated as being X60 the yield and ultimate strengths were found to be $\sigma_{YS} \cong 68$ ksi, $\sigma_{UL} \cong 82.9$ ksi. Various views of the ruptured tensile specimen are shown in Figure 79. The most striking feature of the fracture surfaces was the severe delamination of the material parallel to the pipe surfaces. There was also severe necking in both thickness and circumferential directions before fracture.

Specimens were also cut from the pipe in the longitudinal direction for Charpy V-notch experiments. In these specimens the notch was cut in the circumferential (or θ) direction (that is, the loads were applied in θ -z plane, see Figure 79). The test results are shown in Figure 80 where the solid line represents an approximate fit to the data. The results are characteristic of pipeline steels, namely they indicate relatively high toughness, and no distinct shelf values.

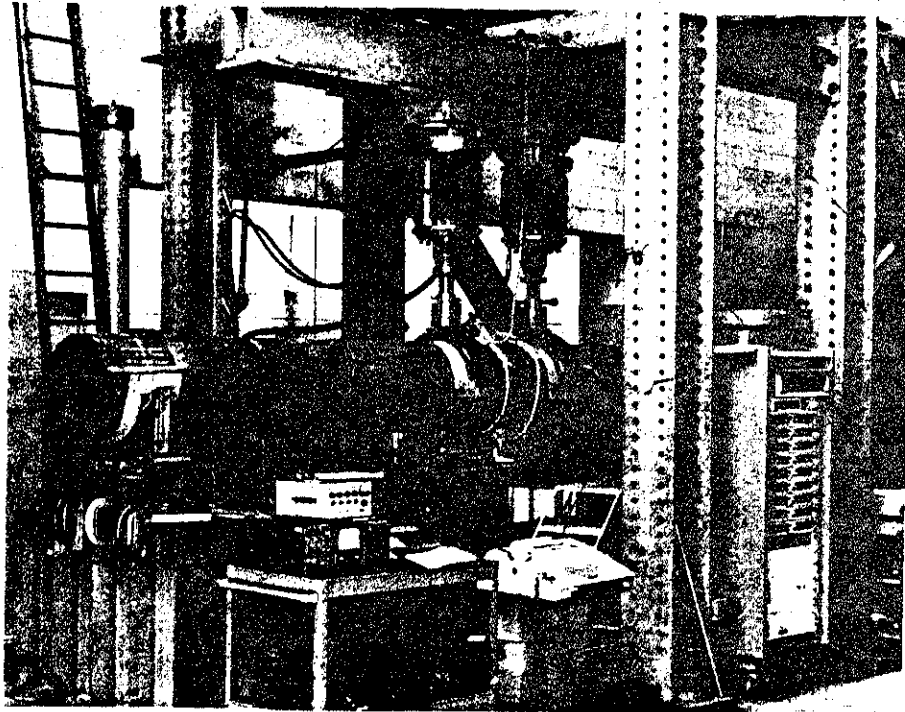


Figure 77. Loading frame for the pipe under "four point bending".

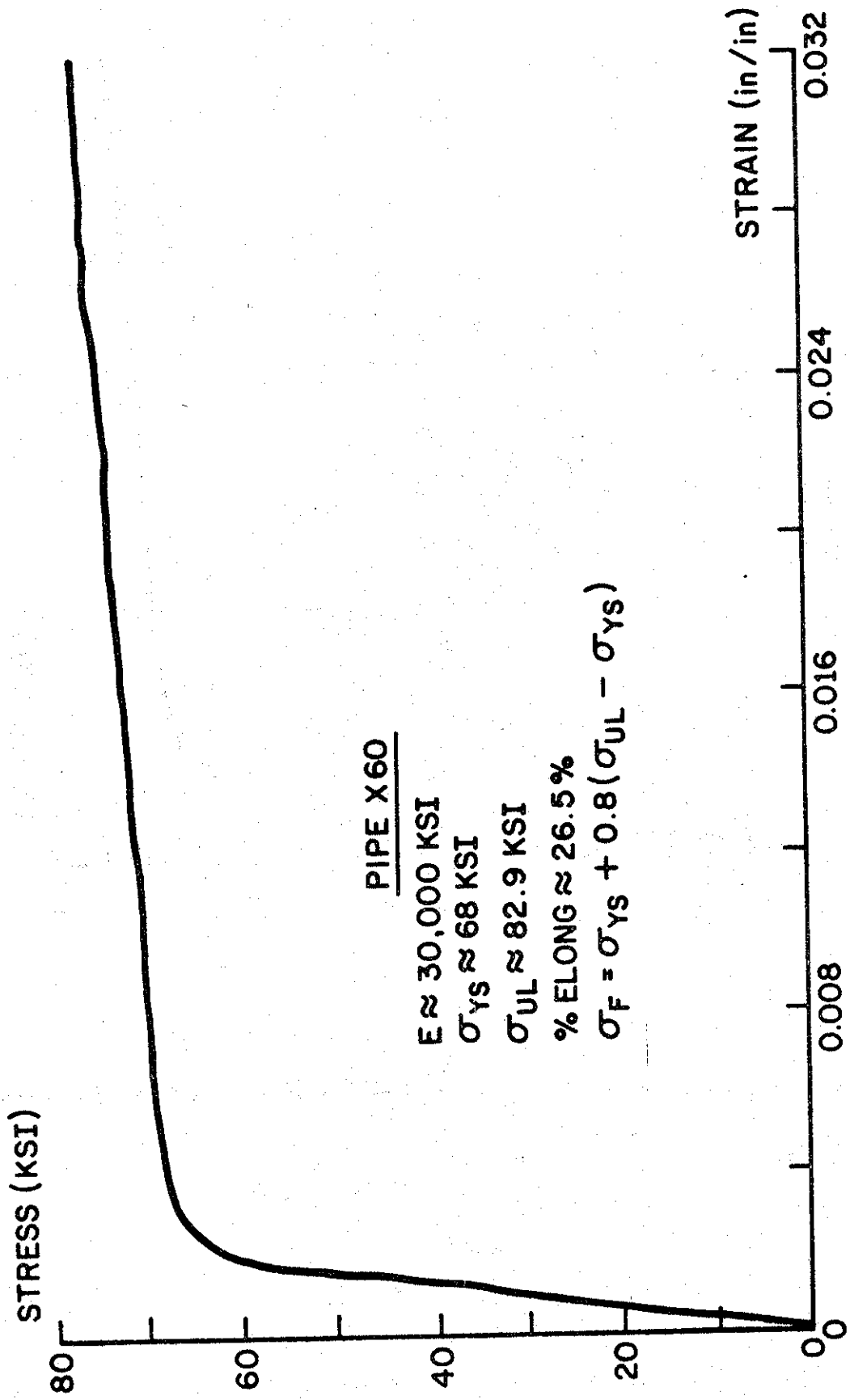
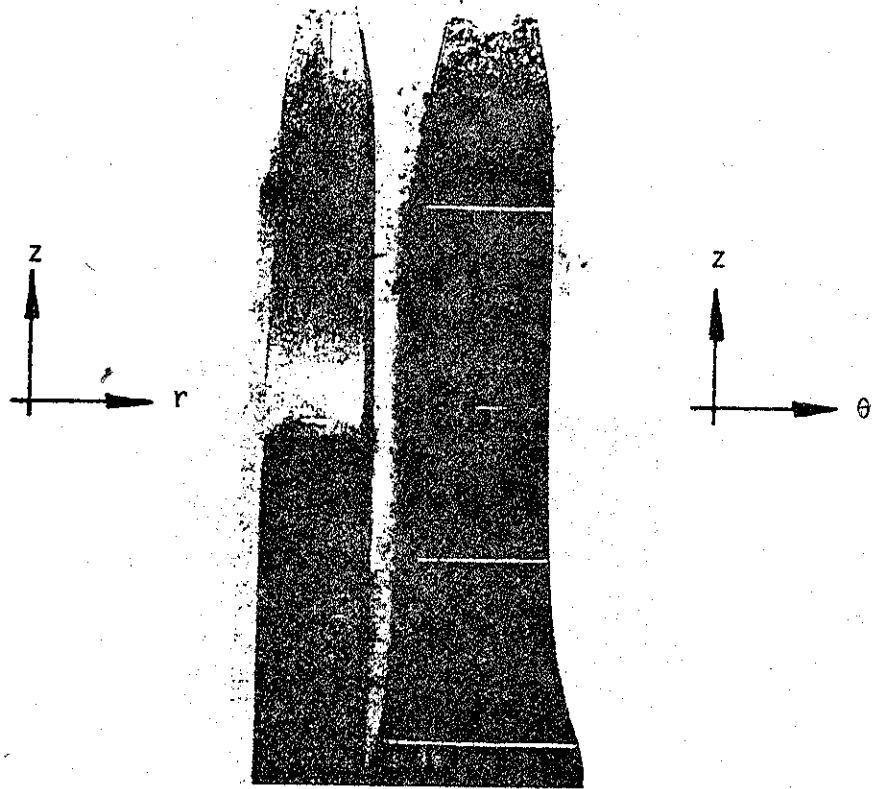
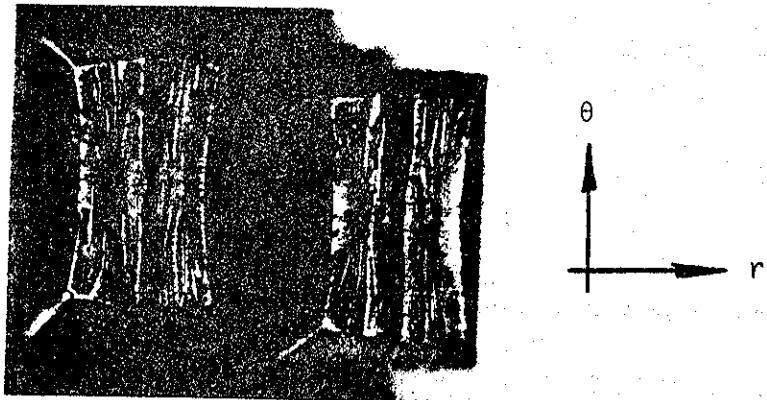


Figure 78. Mechanical properties of the pipe material, nominally designated as X60, obtained from a tensile specimen cut parallel to the axis of the pipe (i.e. the rolling direction).



(a)



(b)

Figure 79. Various views of the X60 tensile specimen cut from the pipe; r , θ , and z refer to the radial, circumferential, and axial directions, respectively.

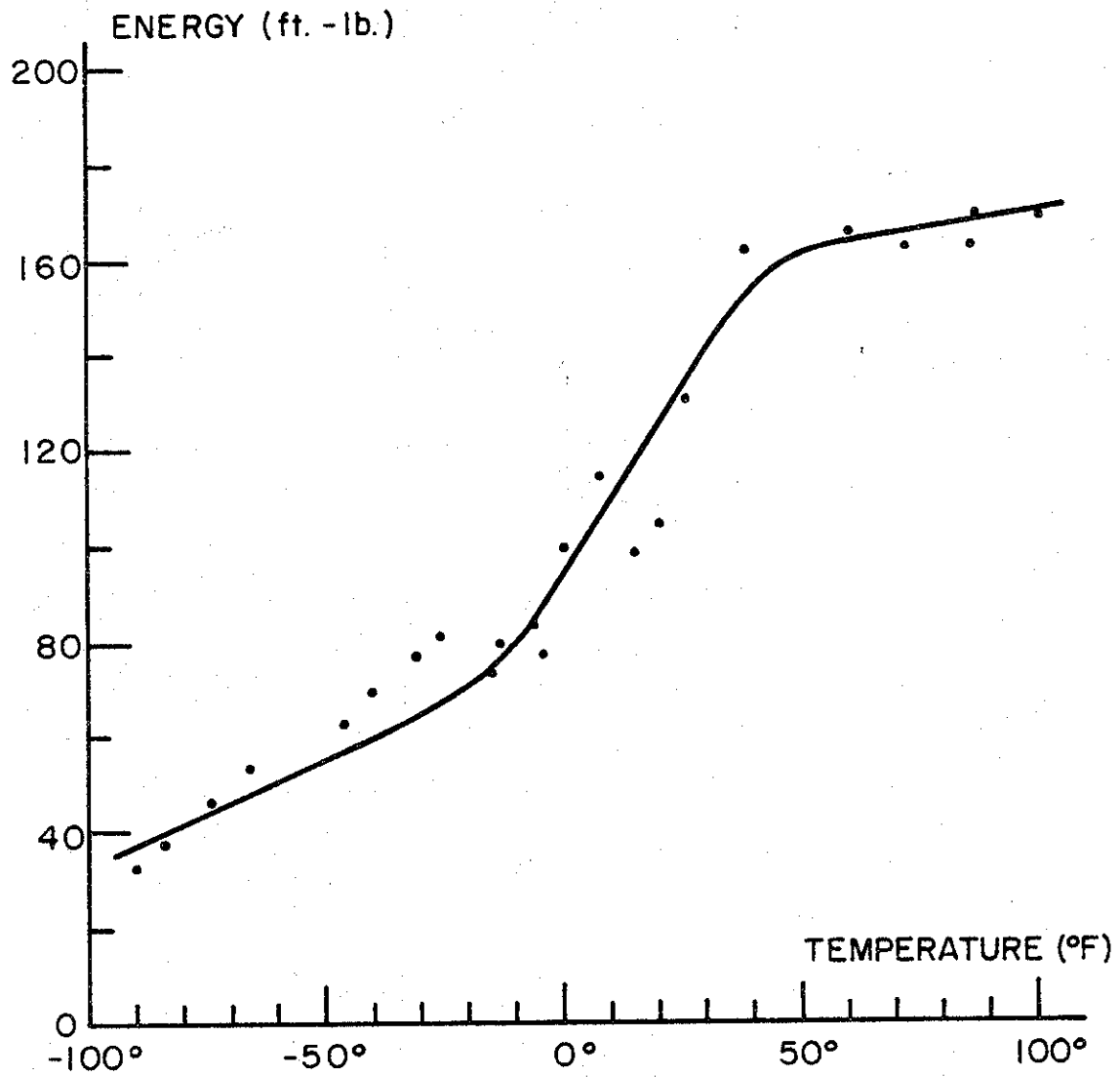


Figure 80. Results of the Charpy tests for the X60 pipe material.

4.2 The Fatigue Experiments

The length and load point locations of the pipe specimens shown in Figure 76 were determined largely to accommodate the capacity of the Amsler hydraulic jacks used for loading the specimens. The machine capacity had to be sufficient to produce a bending moment in the unnotched pipe near the full yield or "hinge" value of the moment. Another consideration was the buckling of the pipe on the compression side. Since premature elastic instability could spoil the entire program, some elementary buckling calculations had to be made. First, the following empirical formula developed for the elastic buckling of thin shells under bending was used to calculate an equivalent critical stress [55]:

$$\sigma_{cr} = \frac{Eh}{R\sqrt{3(1-\nu^2)}} [1 - 0.731 (1-e^{-\phi})], \quad \phi = \frac{1}{16} \sqrt{R/h}, \quad (72)$$

where σ_{cr} is the critical stress for elastic buckling initiation, R the mean radius, h the thickness, and E , ν are the elastic constants. For the 20 in. diameter steel pipe under consideration (72) gives $\sigma_{cr} \cong 500$ ksi indicating no danger of buckling according to (72).

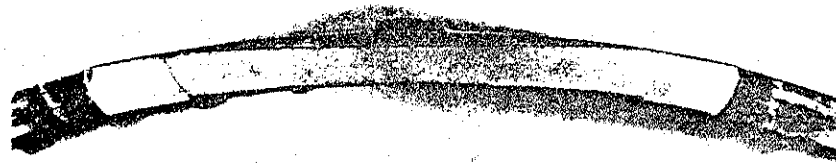
A second calculation was made by assuming that the pipe is under axial compression. Following [56], the critical stress for this case is given by

$$\sigma_{cr} = \frac{E \left(\frac{0.6h}{R} - 10^{-7} \frac{R}{h} \right)}{1 + 0.004 \frac{E}{\sigma_{PL}}} \quad (73)$$

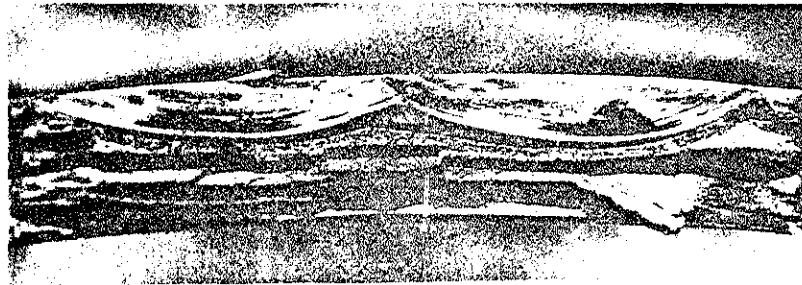
where σ_{PL} is the proportionality limit of the material. Equation (73) takes into account initial imperfections (i.e., deviations of the shell surface from an ideal circular cylinder) and assumes that the deflections may not be small. Taking $\sigma_{PL} = 58$ ksi, (73) gives $\sigma_{cr} \cong 205$ ksi.

It then appears that the elastic buckling should not pose a problem in the pipe tests.

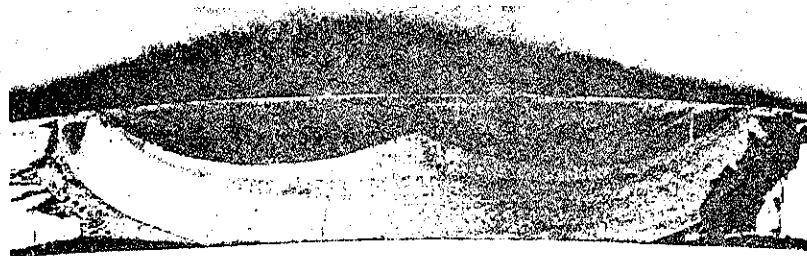
The first pipe contained a circumferential starter notch introduced by a straight saw and was subjected to cyclic loading until the crack became a through crack and grew over four inches long (Figure 81a). This was a pilot test to obtain some information on the number of cycles required for crack



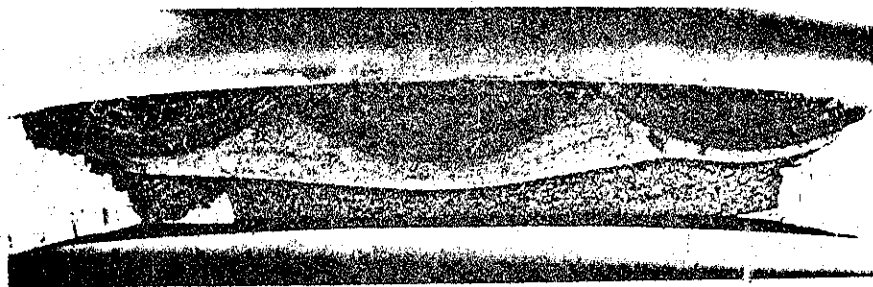
(a)



(b)

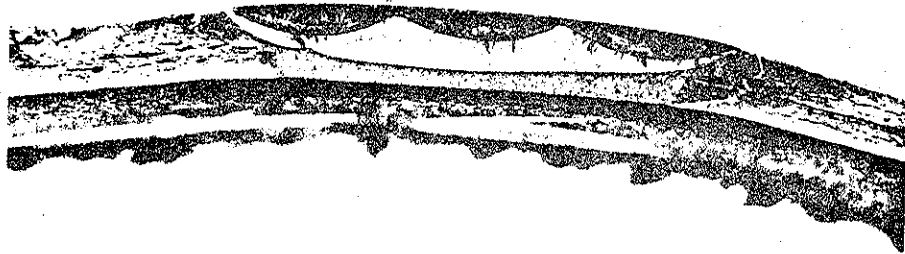


(c)



(d)

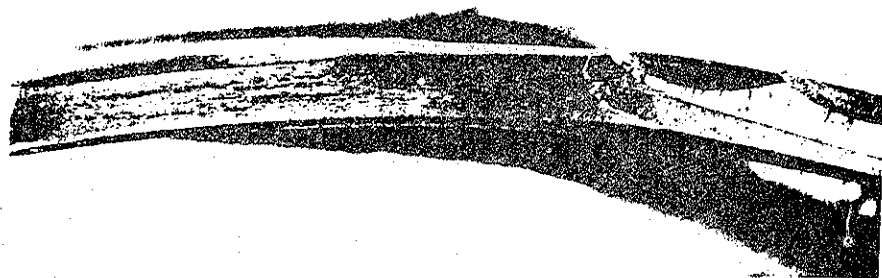
Figure 81. Fracture surfaces of the pipes. The dimensions after fatigue cracking: (a) $L_0 = h$, $2a = 4.28$ in. (through crack), (b) $L_0 = 0.545h$, $2a = 1.688$ in., (c) $L_0 = h$, $2a = 1.77$ in. (through crack), (d) $L_0 = 0.773h$, $2a = 2.063$ in.



(a)



(b)



(c)

Figure 82. Various views of the fracture surface of the pipe #6,
 $L_0 = 0.68$ in., $2a = 1.97$ in.

initiation and on the crack propagation rate. The straight cut proved to be highly unsatisfactory mostly because of the very large number of cycles required for crack initiation. For the remaining pipes the starter notch was introduced by a 1 in. diameter 0.025 in. thick abrasive disk. Two or three overlapping initial cuts were made to have the desired initial flaw size and particularly to create a "chevron" effect to shorten the crack initiation time (Figure 81, b-d). The pipe was then placed in the test frame with the crack on the compression side and the notch was subjected to a precompression stress of approximately 75% of the yield strength of the material. The reason for this was to further speed up the crack initiation process. With this technique the problem of excessively delayed crack initiation was entirely eliminated.

The objective of the fatigue tests was twofold. The first was to introduce a natural crack to the pipe wall prior to the fracture tests. The second was to try to collect some fatigue crack propagation data in shells in order to verify the general fatigue model. To collect fatigue crack growth data we had to again rely on program loading and crack front marking technique (Figures 81 and 82). The markings were obtained by reducing the amplitude of the cyclic load to approximately one-fifth of its maximum. This was a precaution against a premature net ligament rupture. The limited data points which were obtained by this technique are shown in Figure 59 superimposed on the results obtained from plates and single edge notched specimens. The fatigue tests were performed at a frequency of 250 cycles/min, and at the load ratio P_{\min}/P_{\max} of approximately 0.6. The stress intensity factors used in analyzing the data was calculated by using the technique described in Appendix B and the actual pipe and crack dimensions. Assuming that the materials X70 and X60 have similar fatigue crack growth characteristics, Figure 59 shows that the fatigue crack propagation rate in a pipe with a part-through crack can be predicted from the data obtained by using simpler specimens provided the stress intensity factor for the pipes is available.

4.3 Fracture Tests

Following each fatigue experiment the transverse loads P were slowly increased in order to observe the development of ductile fracture in the pipe

(Figures 76 and 77). The fracture tests were carried out by using the same hydraulic jacks and the same load frame as used in the fatigue experiments. Strain gages were mounted at various locations on the specimen to monitor the deformations in the pipe and the relative magnitudes of the loads applied by the two jacks. A precalibrated clip gage was used to measure the crack mouth opening displacement. The outputs of gage 1 and the clip gage were connected to an x-y recorder for continuous recording of the transverse load P vs. the crack opening displacement COD. An eight channel oscilloscope was used as a back-up to the x-y recorder and to store the information on a disk. A digital data acquisition system was used to record the outputs from the strain gages at certain values of the load. In order to detect the load level corresponding to the initiation of net ligament rupture, a photo cell was installed inside the pipe opposite the crack, the pipe was darkened by blocking the ends and the light was directed at the crack from outside.

Except for the initial fatigue-sharpening the cracks, the experimental procedure followed and essentially the results found in this study are quite similar to those reported in [23] by Wilkowski and Eiber. As in [23], the loading technique used in the present experiments was basically "displacement-controlled". This means that the experimental P vs. COD curves go through a maximum and then P starts decreasing as the load point displacement and COD increases. In a "load-controlled" experiment the maximum P thus attained would have been the fracture instability load.

Altogether six pipes were tested. In two of the pipes the fatigue crack was permitted to propagate through the entire pipe wall (Figure 81 a and c). In the remaining four some effort was made to have a part-through fatigue crack of various specific dimensions. The experimentally obtained P vs. COD curves are shown in Figures 83-95. Unlike some of the results given in [23] and except for pipe #2, the curves are all "smooth." That is, there were no "kinks" in the curves which would have been an indication of "fracture initiation" or "net ligament rupture." The reason for this is believed to be fatigue sharpening of the crack prior to static loading. Pipe #2 had a relatively short and shallow fatigue crack ($2a = 1.688$ in., $L_0/h = 0.545$) (Figure 81b). In this case the pipe "failed" as a consequence of structural instability (i.e., buckling) rather than fracture instability. After the test the crack region was cut out and fractured by "bending" it. The resulting fracture

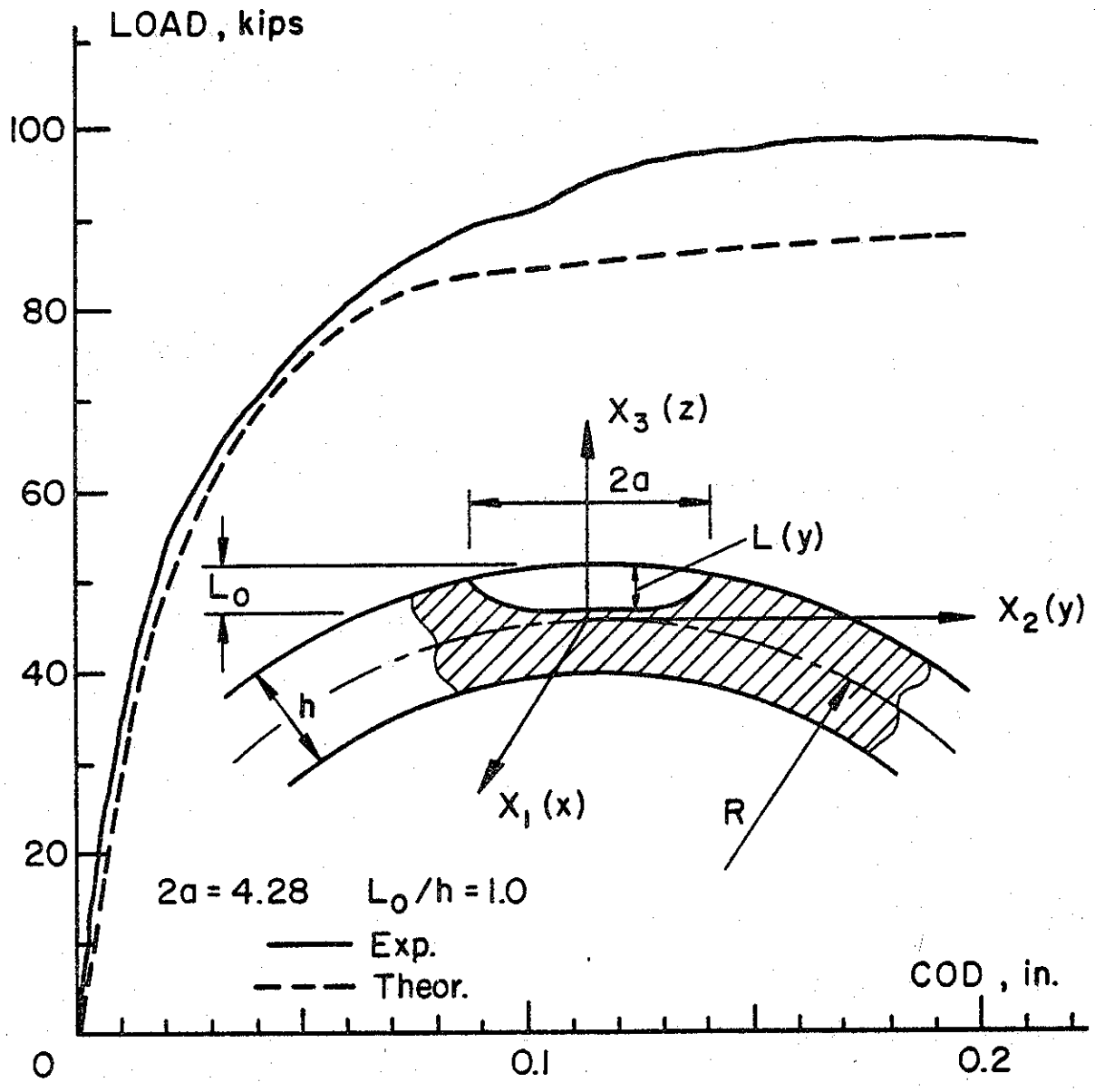


Figure 83. Transverse load P vs. COD for pipe #1.

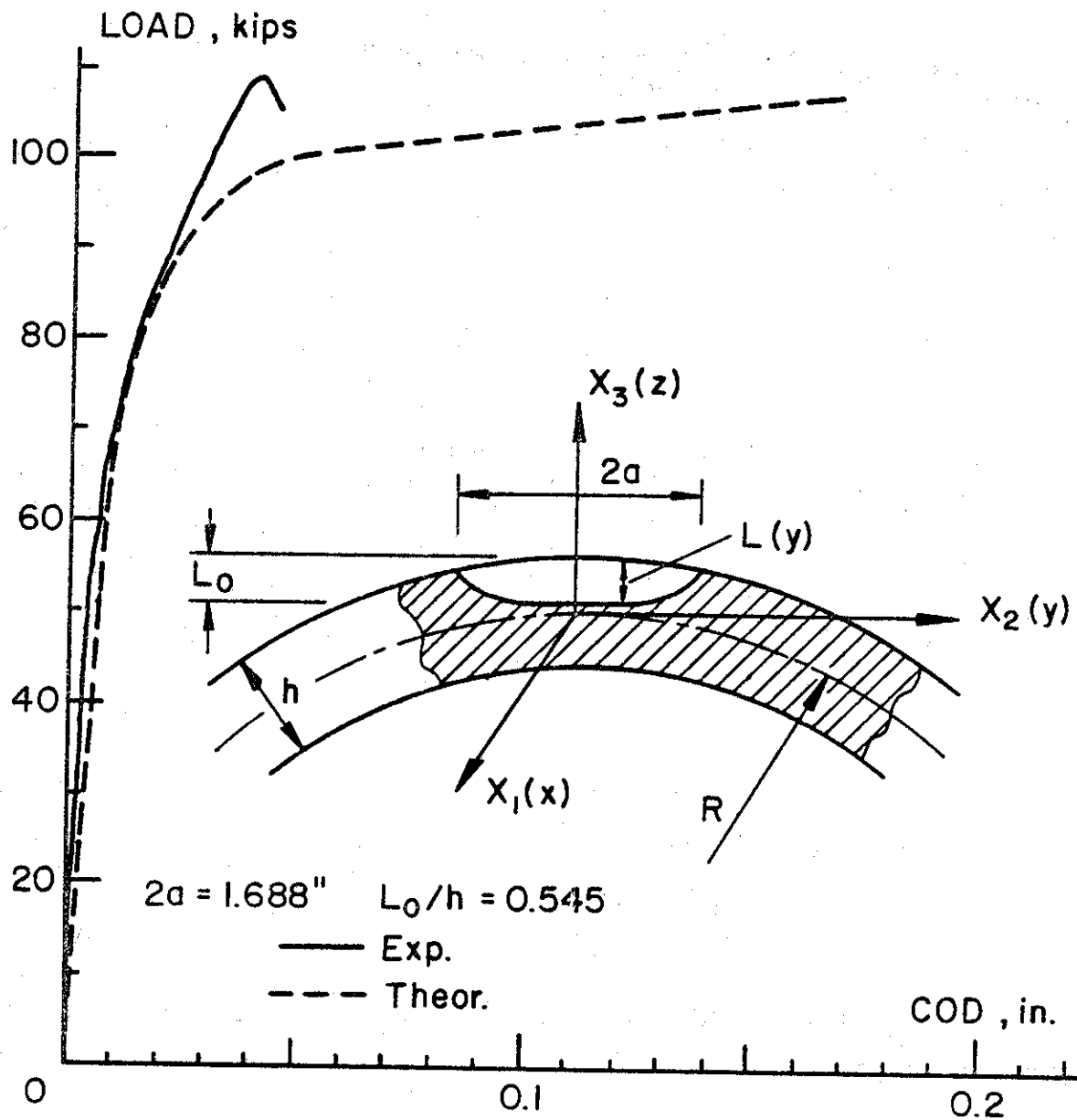


Figure 84. Transverse load P vs. COD for pipe #2

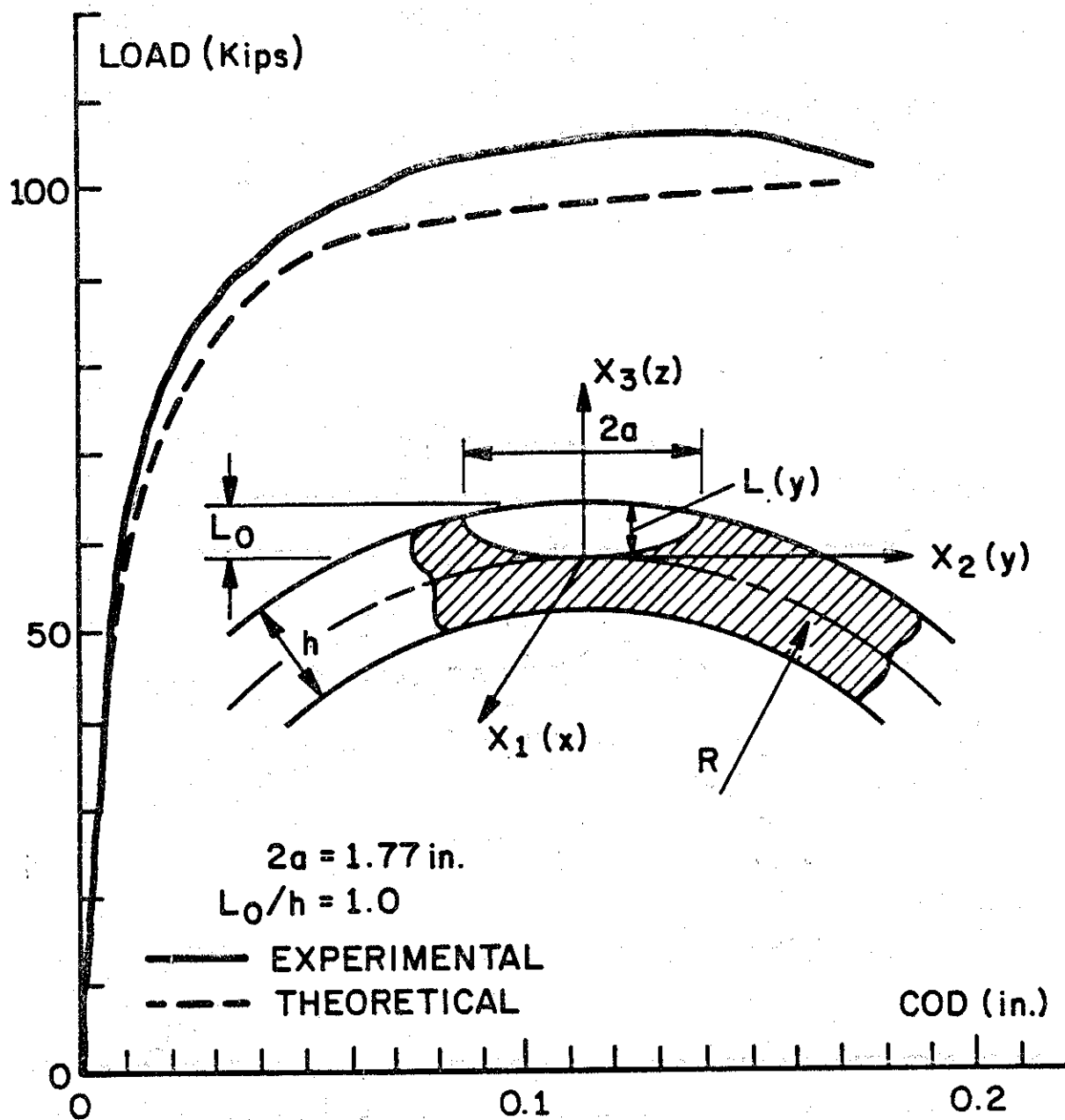


Figure 85. Transverse load P vs. COD for pipe #3

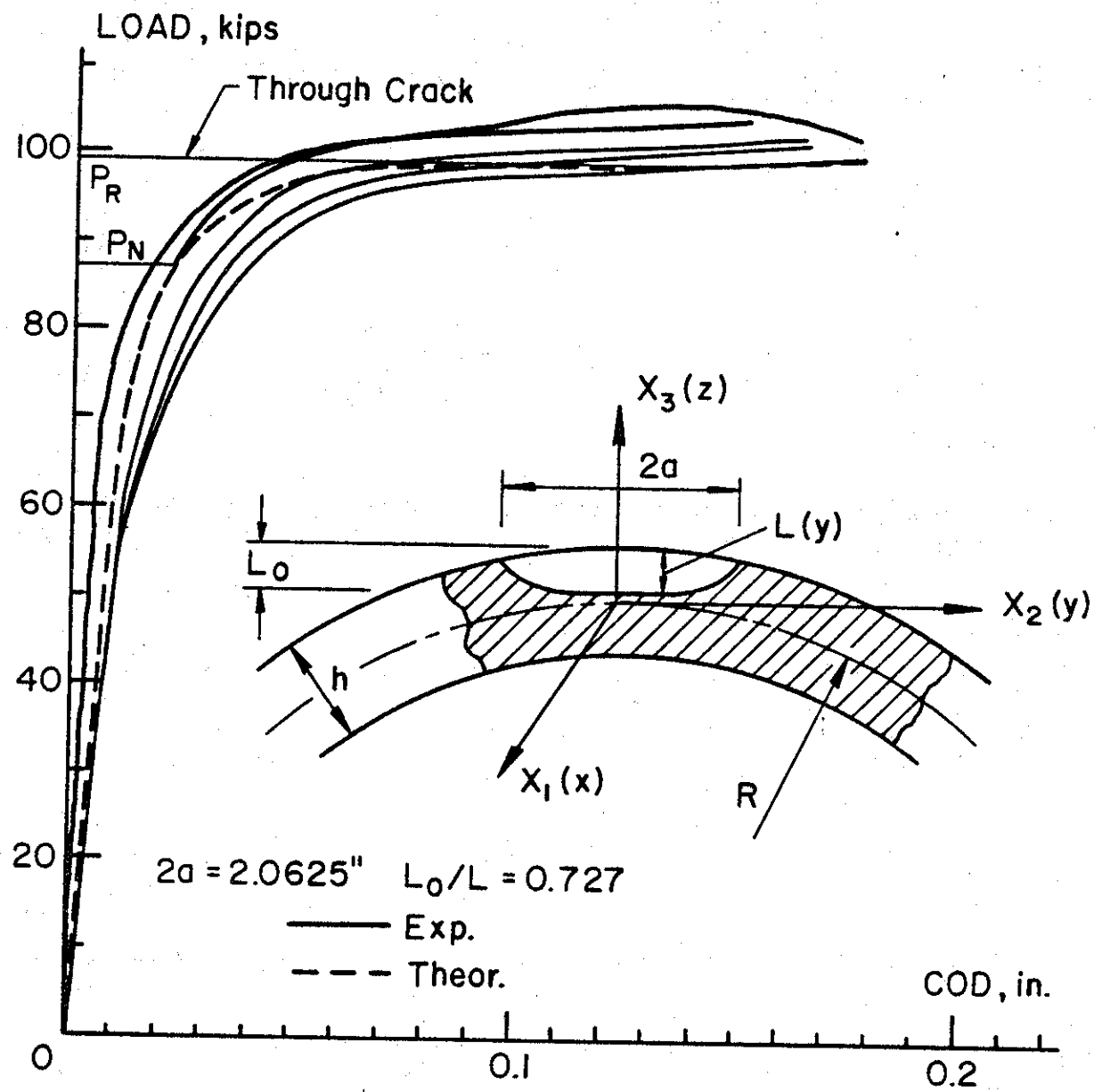


Figure 86. Transverse load P vs. COD for pipe #4

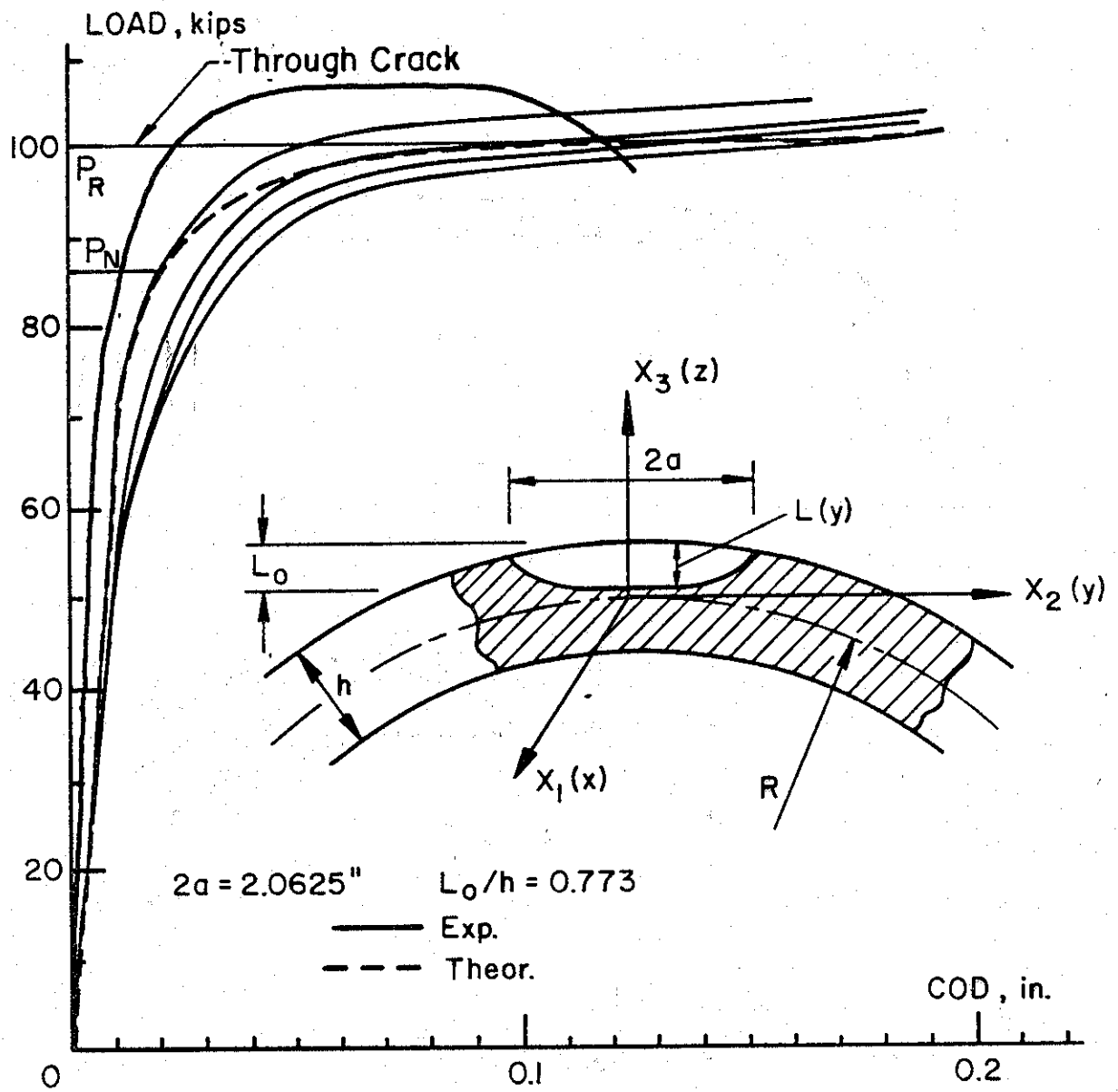


Figure 87. Transverse load P vs. COD for pipe #5

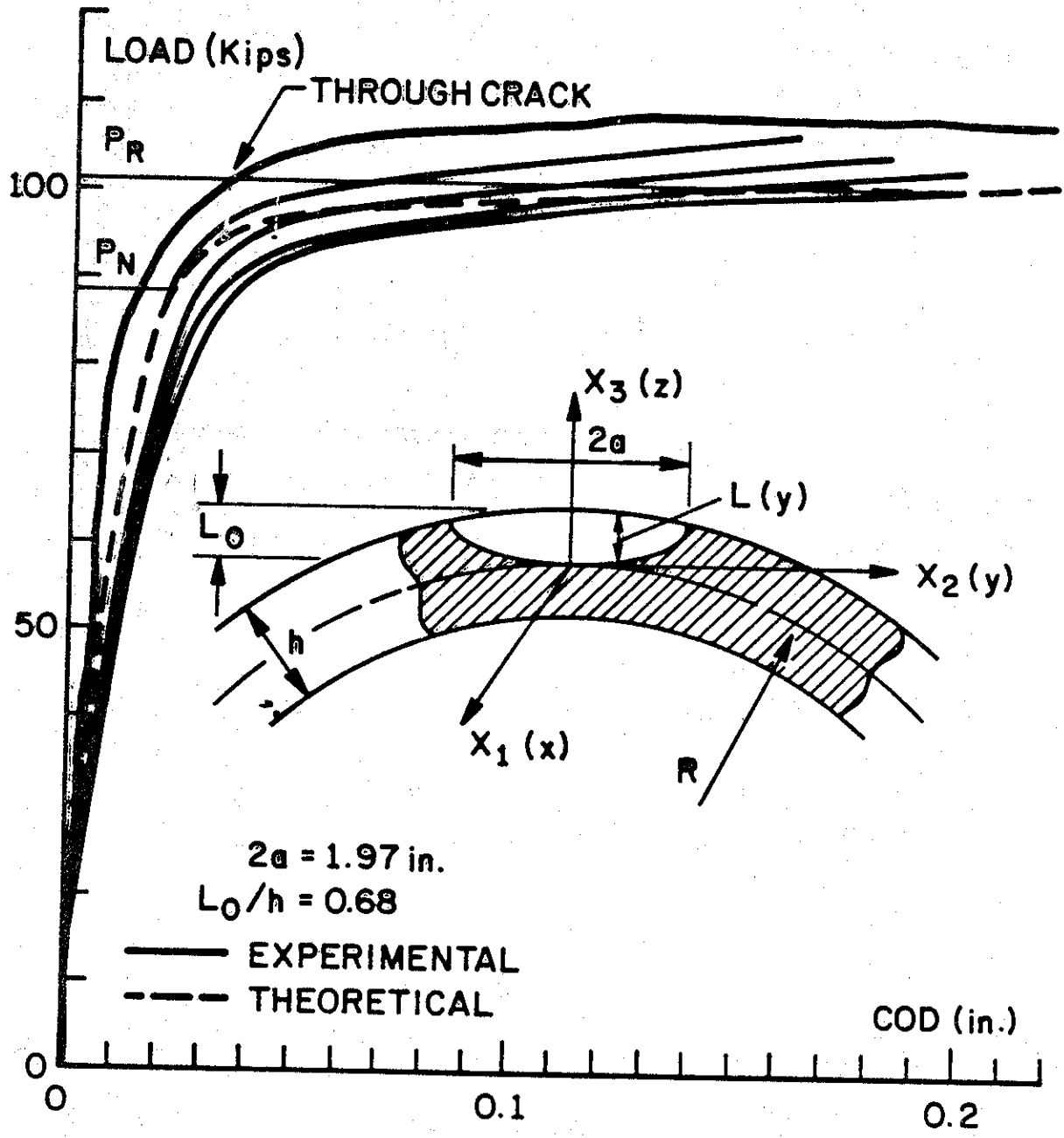


Figure 88. Transverse load P vs. COD for pipe #6

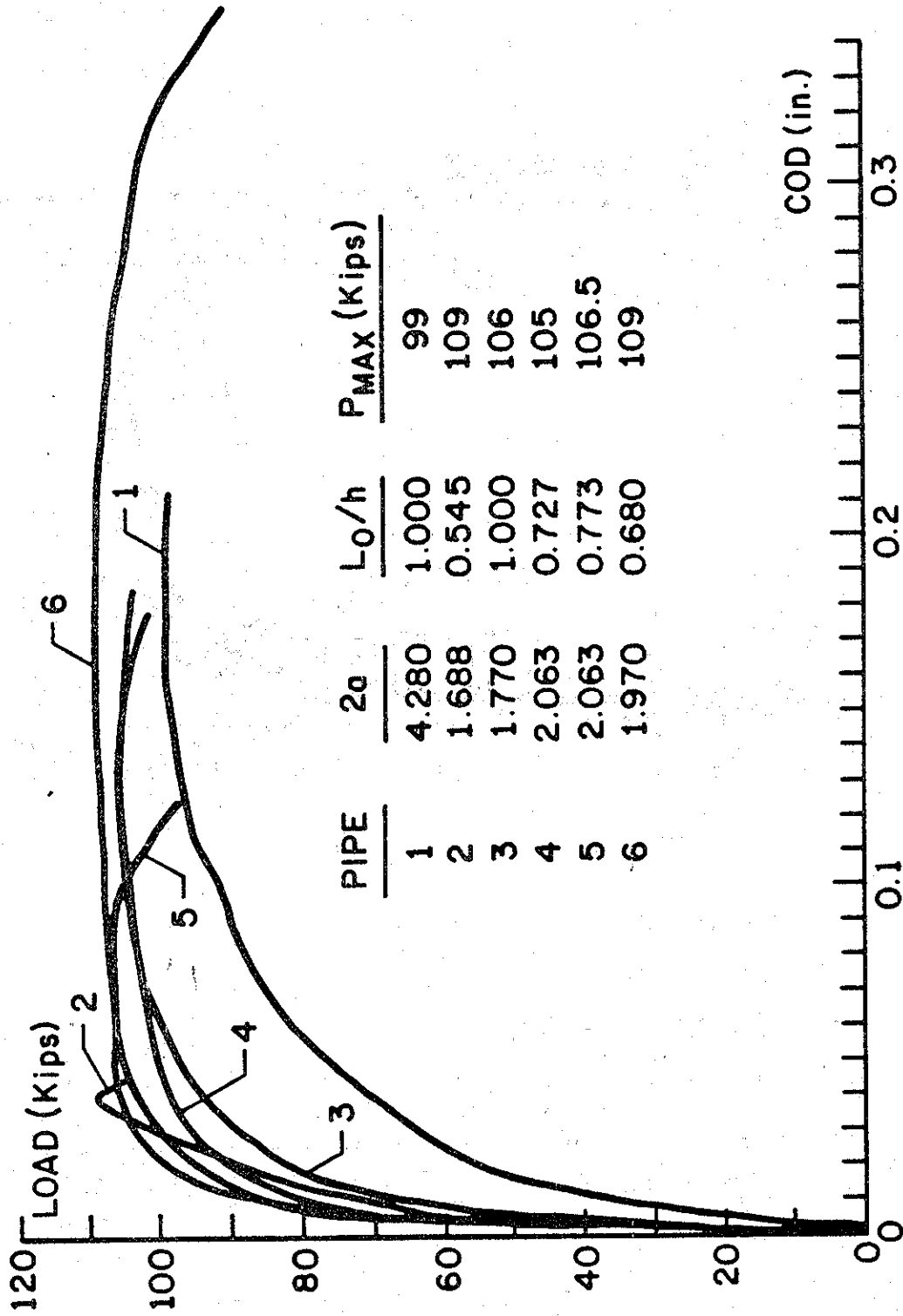


Figure 89. Transverse load P vs. COD in the pipes tested as reproduced from the x-y recorder.

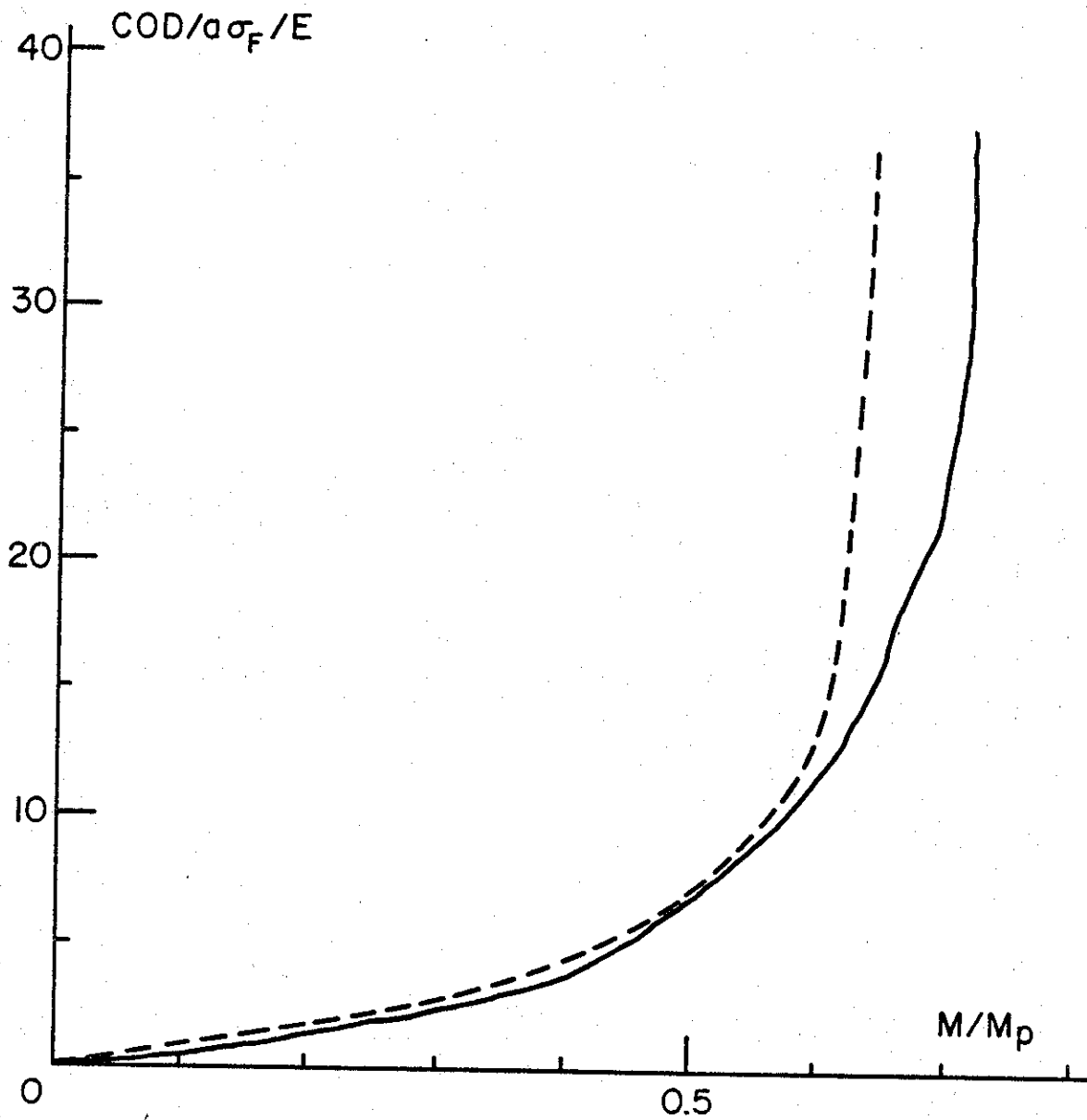


Figure 90. Normalized COD vs. moment ratio for pipe #1

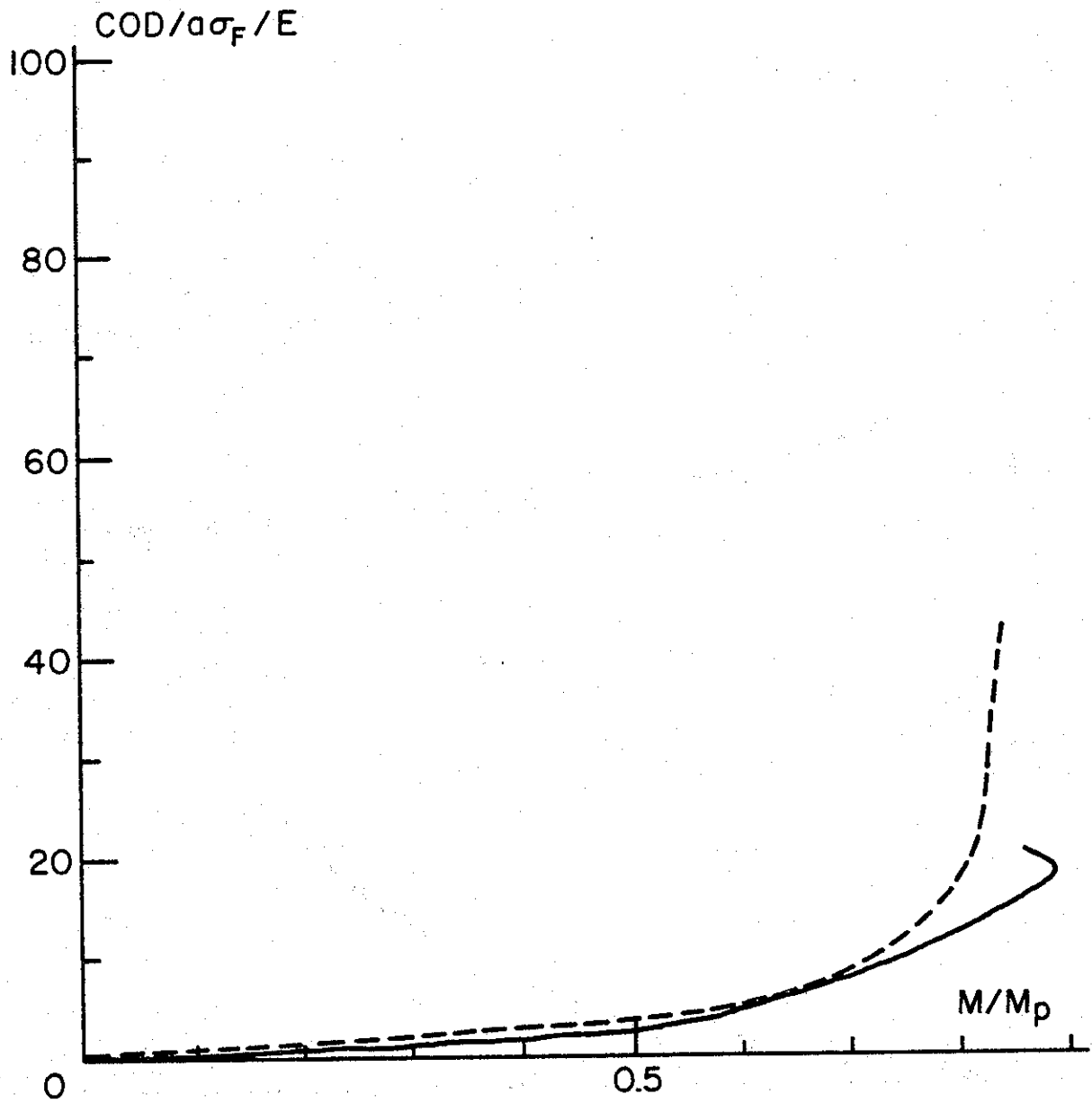


Figure 91. Normalized COD vs. moment ratio for pipe #2

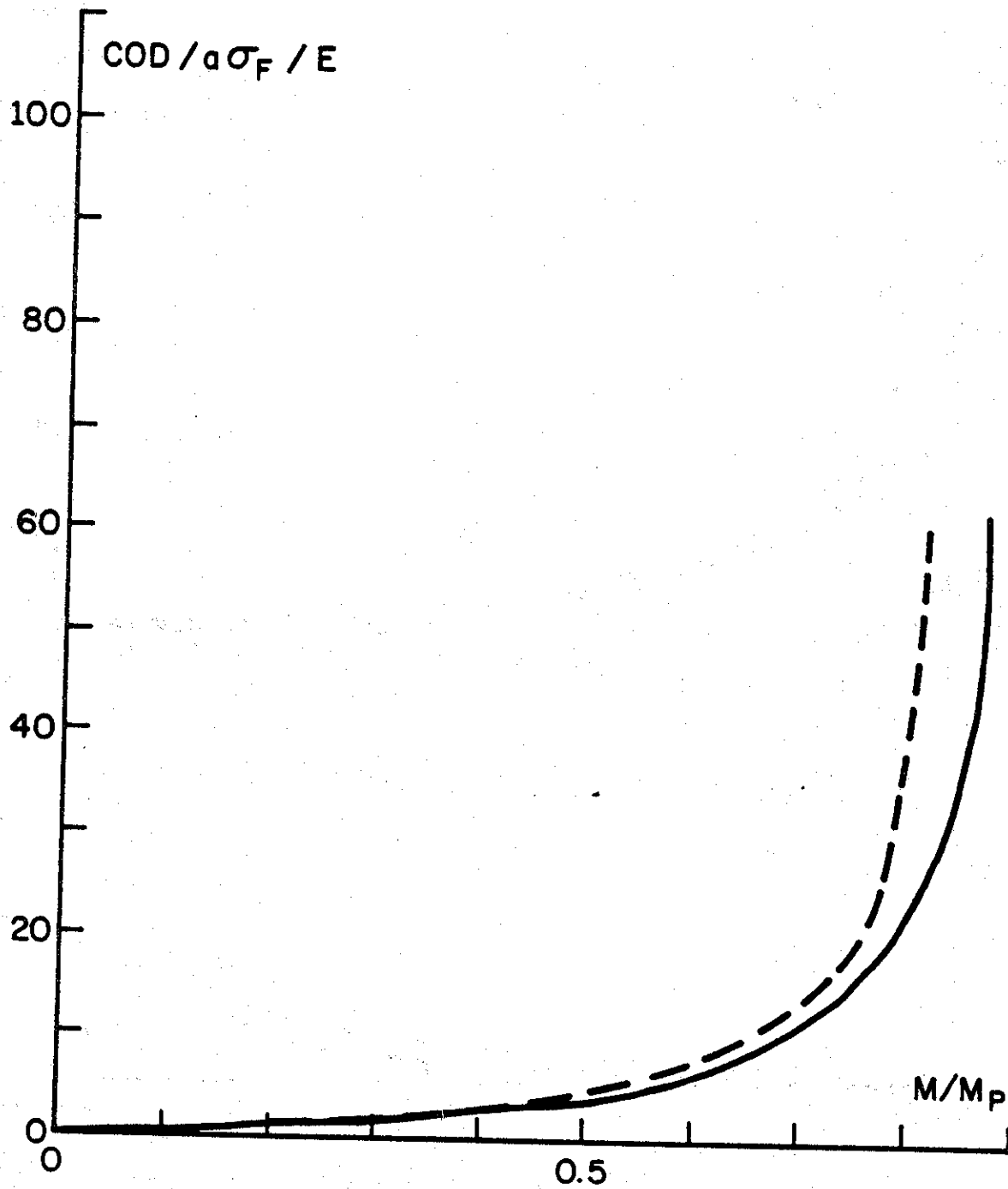


Figure 92. Normalized COD vs. moment ratio for pipe #3

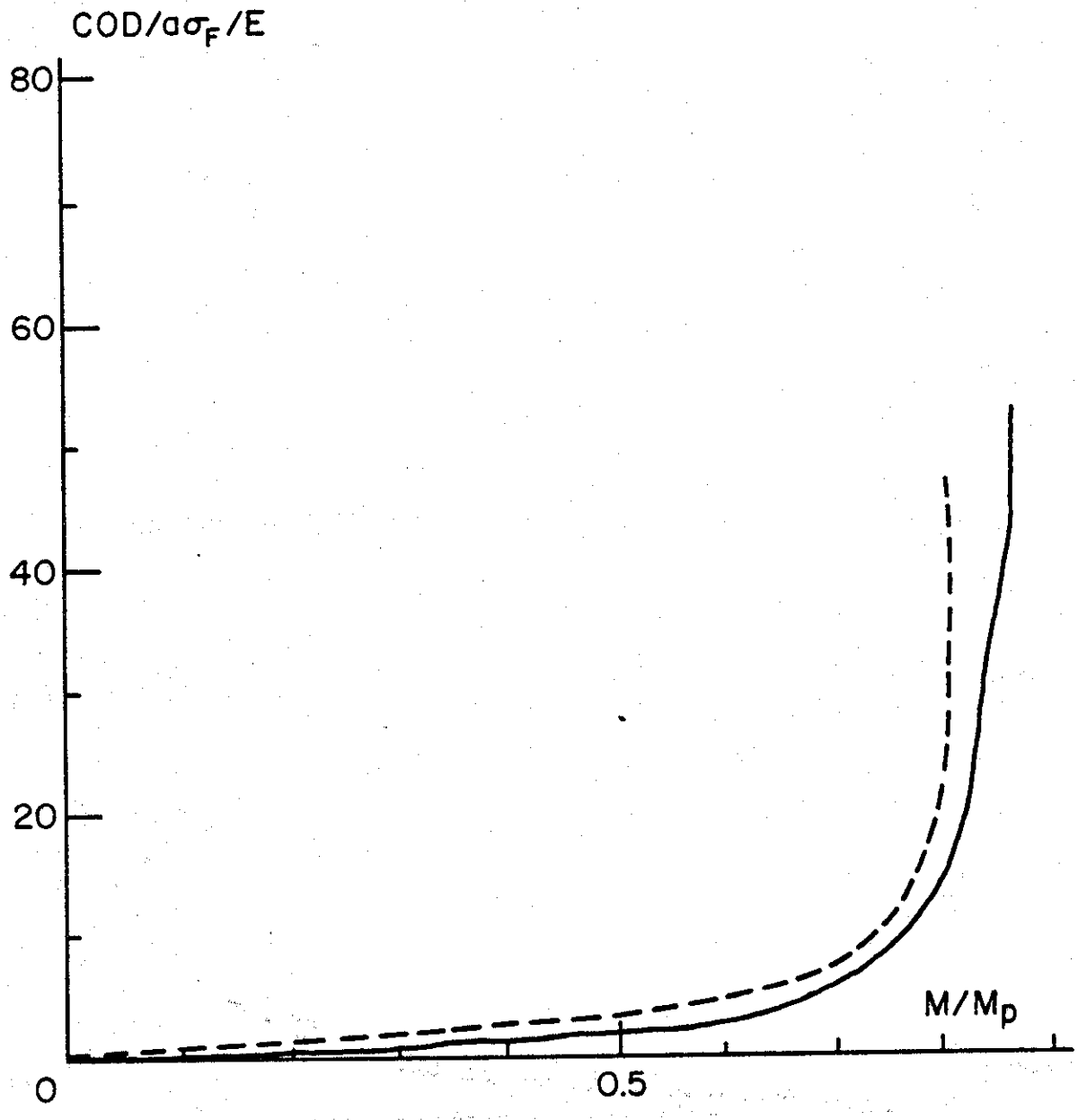


Figure 93. Normalized COD vs. moment ratio for pipe #4

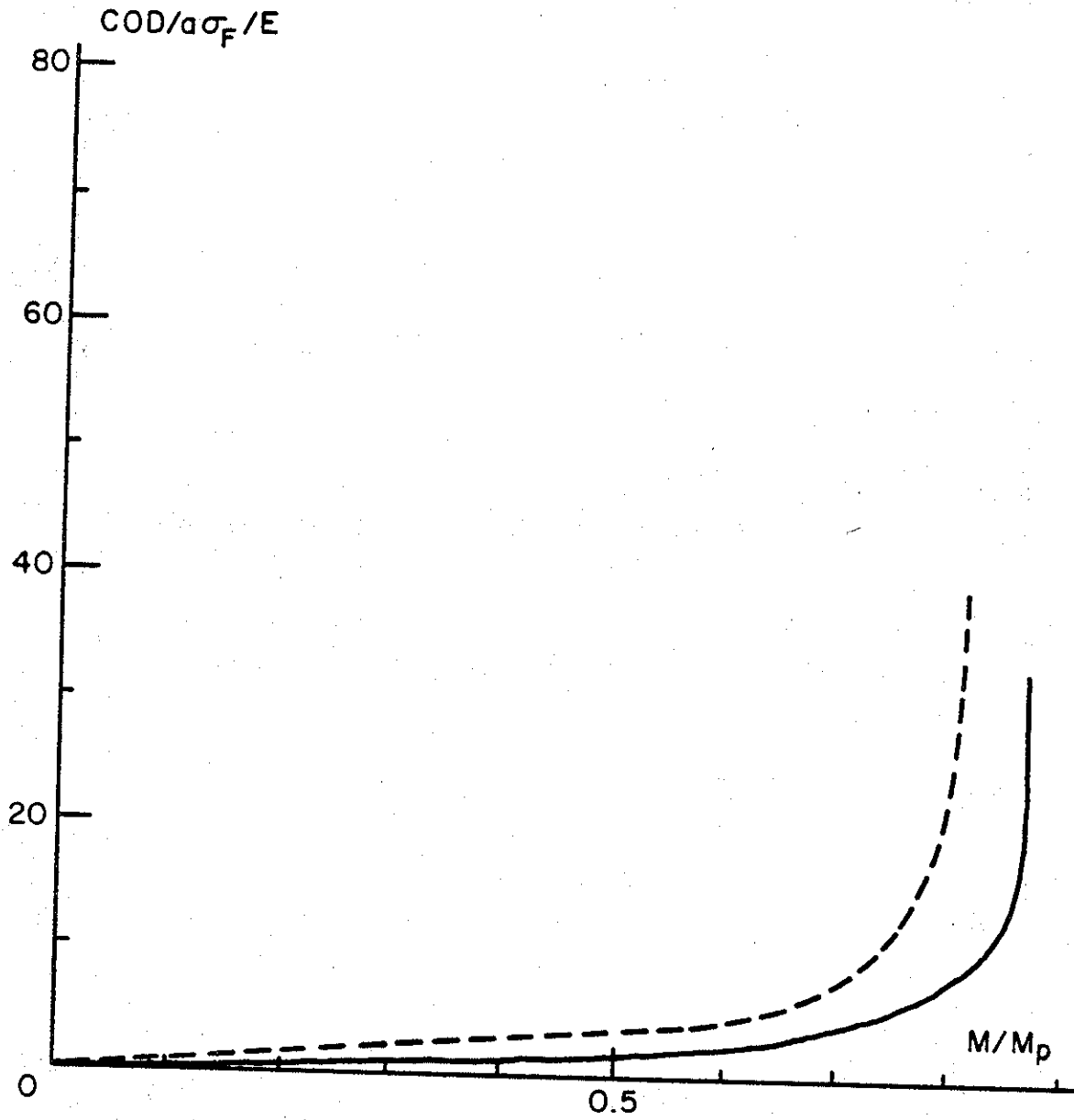


Figure 94. Normalized COD vs. moment ratio for pipe #5

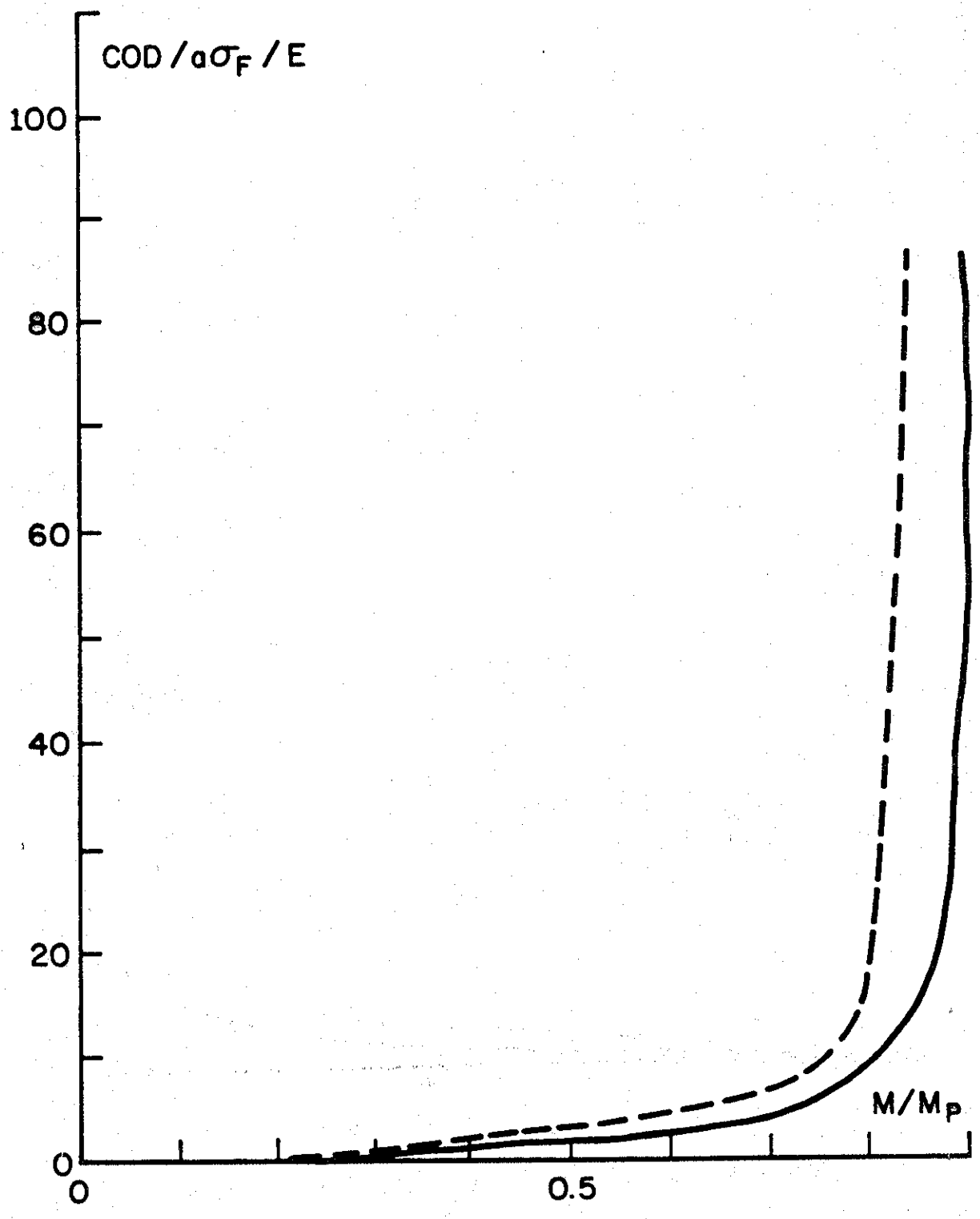


Figure 95. Normalized COD vs. moment ratio for pipe #6

surface in the net ligament is shown in Figure 81b (which, as expected, has no resemblance to that of the remaining pipes). There was no evidence of crack growth in the pipe wall during the loading process on the test bench. Severe nonlinearity observed in Figure 84 in the P vs. COD curve prior to reaching the peak load is an indication of plastic deformations in the crack region, particularly, in the net ligament. The load fell off sharply upon reaching the structural instability value (Figure 84). The actual development of the buckling of the pipe wall may be seen in Figure 96.

As pointed out earlier, the elastic instability in the pipes was not a likely mode of failure, that is, the calculated instability loads were much too high for the material strength to sustain them. However, as seen from Figure 96, the instability observed in the pipe #2 is inelastic buckling. Even though the peak load in the pipe #6 was the same as that in #2, there was no visible sign of buckling in #6. This may be due to the compliance change in the pipe #6 resulting from the propagation of the through crack on the tension side and perhaps more likely to the highly imperfection sensitivity of the buckling process. An important factor in the inelastic buckling of pipes in the present study is the nearly rigid saddles used to transmit the load from the hydraulic jacks to the specimens. There was indeed an indication of slight buckling initiation in all pipes tested. They were all on one side and very near the saddle. The local "bending" in the pipe wall near and at the leading edge of the saddle seems to be one of the main factors for the reduction in the observed instability load. The degree of buckling instability was also responsible for the difference in behavior of the measured load vs. COD curves obtained from pipes #4 and #5 which had nearly identical initial part through fatigue cracks. The buckling in the pipe #5 started at a smaller COD value than in #4 which consequently resulted in the reduction of the load at a comparatively smaller COD value (Figure 89). To give an idea about the comparative behavior of the measured P vs. COD curves obtained from various pipes they are reproduced in Figure 89 in superimposed form. Except for the pipe #1 which had a relatively long initial through crack (and to some extent #3 which had an initial through crack), the elastic behaviors (that is the initial parts of the curve) in all pipes seem to be quite similar, whereas buckling played a major role in the inelastic range. Of the six pipes tested

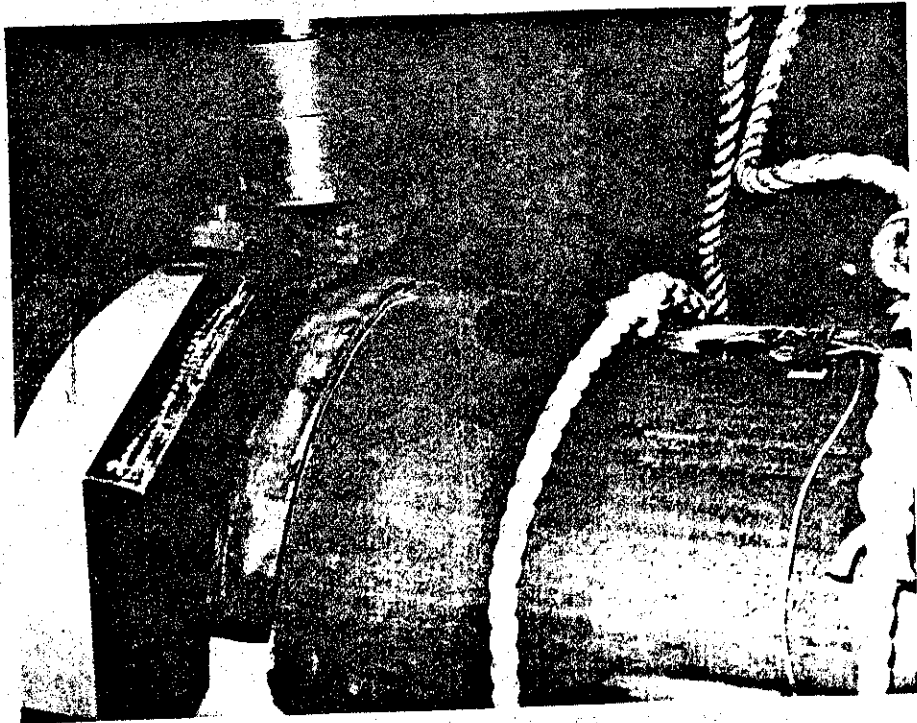


Figure 96. Buckling of the pipe #2 on the compression side.

only in one (pipe #6) there was no evidence of any structural buckling on the compression side. In this pipe after the net ligament rupture the through crack continued to grow in a slow stable fashion. At some point the clip gage ran out of space and fell and the test was terminated. When the test was stopped the crack (which had an original length of 1.97 in.) was approximately 7 in. long. In the remaining pipes there was very small stable growth of the through crack. In these tests generally the load started to fall because of structural (i.e., buckling) rather than fracture instability.

For the pipes tested, Figures 83-88 also show the load vs. COD relationship obtained from the elastic-plastic analysis described in the Section 4.3 of Part I of this report (see, also, Appendix H for other results). For part-through cracks shown in Figures 86-88 four calculated curves are given: one for the part-through crack with the profile as given by the fatigue experiment, the second for the corresponding through crack and the third and fourth for intermediate net ligament thicknesses. For a given COD the curve based on the fatigue crack has the highest and that based on the through crack the lowest values of the load P . The curves corresponding to the intermediate crack depth fall between these two limiting values. The "net ligament rupture" point (or the load corresponding to the "through crack" initiation) P_R is marked on the experimental curve (which was obtained from the photocell). Clearly, for loads greater than P_R , the crack should be treated as a through crack. The initial linear portion of the curves correspond to elastic loading. Between the load P_N corresponding to the plastic necking or tearing initiation of the net ligament and P_R corresponding to total net ligament rupture, intermediate values of net ligament thickness must be used to obtain the theoretical P vs. COD curve.

Again, it should be emphasized that the ductile fracture process involving relatively thin-walled structures and large flaws is very highly geometry-dependent and cannot be characterized by a single parameter. The empirical or semi-empirical models designed for this purpose would generally be satisfactory only for the geometry they were developed. The simple idea underlying the current study is that if one can define or designate a certain parameter which is an adequate measure of the intensity of the applied loads and of the severity of the flaw under conditions of large scale plastic deformations, and the value of which may not be highly sensitive to the details of the

elastic-plastic model assumed for the purpose of calculating it, then the asymptotic behavior of this parameter may be used to estimate a gross stability load for the flawed component. As argued in the previous section COD comes perhaps closest to fulfilling the conditions of such a parameter.

The asymptotic behaviors of the experimental and the theoretical P vs. COD curves are expected to be different. The experimental curve is obtained from a displacement controlled test and hence exhibits a maximum for the load (P_{max}). The theoretical COD curves on the other hand possess a true asymptote ($P = P_{max}$). These asymptotic values of P are the theoretical estimates of the instability load in each pipe. For the six pipes tested Table 4.1 shows the comparison of measured and estimated instability loads.

Table 4.1 Experimentally measured and theoretically estimated fracture instability values of Transverse load P in pipes.

Pipe #	$2a$	L_0/h	$(P_{max})_{exp}$ (kips)	$(P_{max})_{Theor.}$
1	4.280	1.0	99	91
(*) 2	1.688	0.545	109	112
3	1.770	1.0	106	103
4	2.063	0.727	105	102
5	2.063	0.773	106.5	102
6	1.970	0.680	109	105

(*) Inelastic buckling, no fracture.

An alternative way of presenting the results may be seen in Figures 90-95 where the normalized COD (with respect to $a\sigma_F/E$, a , σ_F and E being the half crack length, the flow stress, and the Young's modulus) is plotted against the moment ratio M/M_p . Here M is the moment applied to the pipe and M_p is the fully plastic (or hinge) value of M which is given by

$$M_p = 2\sigma_F \int_0^\pi \int_{R-h/2}^{R+h/2} r^2 \sin \theta dr d\theta = \frac{4\sigma_F}{3} \left[\left(R + \frac{h}{2}\right)^3 - \left(R - \frac{h}{2}\right)^3 \right]. \quad (24)$$

In all pipes tested for ductile fracture, at peak value of the load the region of the shell containing the crack was fully yielded, and after the tests were terminated permanent deformations in the form of gross bending could be observed in all pipe specimens. However, the elastic plastic analysis of the crack problem in the pipe was still valid. Considered as a beam, the pipe still had a very large "elastic core" after the extremities were plastically deformed. Thus, unlike the plate problem under similar situations, there was no "net section collapse". Also, in the elastic-plastic shell analysis the end points of the plastic zone in the plane of the crack extended into the elastic region in the pipe.

Originally, it was thought that the net ligament would suddenly become unstable and one may have some dynamic effects on the tearing of the resulting through crack. However, it now appears that in the type of problems under consideration the tearing or necking-tearing process in the net ligament is gradual and, for the circumferential cracks, stable. Therefore, it does not seem to be practical to talk about a "net ligament instability" load. Since the development of the through crack and its initial growth are stable, the only meaningful instability load is that of the through crack.

The main conclusion of this study is that in shell structures containing a relatively large initial crack generally the fracture instability load is highly dependent on the overall mechanics of the problem (i.e., the geometry and loading conditions) as well as on the fracture resistance characteristics of the material, and a properly selected and fairly accurately calculated parameter such as COD may be used to estimate the instability load. By examining the results given in Figures 90-95 and in Table 4.1 it may be observed that the estimate which may be obtained from the current analysis appears to be sufficiently close to the instability load and furthermore seems to be consistently conservative. One should also remark that if the tests were performed under "load-controlled" conditions, qualitatively the experimental P vs. COD curves would have been very similar in behavior to the theoretical curves, in that they would not have had a maximum and would have been asymptotic to $P = P_{\max}$ lines.

4.3 Examination of Fracture Surfaces

As in plates containing a surface crack, in fatigue-cracked pipes subjected to fracture the evidence of considerable necking was observable in the net ligament, particularly from the inside surface of the pipe opposite to the crack. The examination of the two halves of the fractured specimen indicated that after the development of the stretch zone the crack started along the front and slowly propagated in thickness direction. The stability of this phase of the crack propagation was stable was evident from the fact that prior to and during the net ligament rupture (initiation of which was detected by the photo cell) the load was still on the rise. The direction of the crack propagation was perpendicular to the pipe surface. This may easily be seen from the fact that in the net ligament region the two halves of the fractured pipe wall were perfectly symmetric with respect to the original plane of the crack. There is every indication that upon the initiation of ductile tear the crack profile near and at the leading edge maintained its (symmetric) V shape as it propagated through the net ligament.

One of the basic microscopic fracture mechanisms that almost always presents itself in cases of ductile fracture is microvoid coalescence. The stress induced fracture and, in some cases, complex dislocation interactions lead to the formation of microcracks or pores within the stressed component. As the stress level increases these voids grow larger and start coalescing to form a broad crack front. There are, roughly speaking, three main processes for void formation and coalescence which depend on the stress state existing in the component. Under simple uniaxial loading conditions, the microvoids will tend to form in association with fractured particles and/or interfaces and grow out in a plane generally normal to the direction of the applied stress. The resulting "equiaxial dimples" are believed to be related in some fashion to the fracture energy. However, when the failure is predominantly influenced by shear stresses, the voids that nucleate in the manner cited above grow and subsequently coalesce along planes of maximum shear stress. Consequently, these voids tend to be elongated and result in the formation of parabolic depressions on the fracture surface. Finally, if the state of stress is that of combined membrane and bending stresses, again the voids would be elongated, pointing back at the origin of the crack.

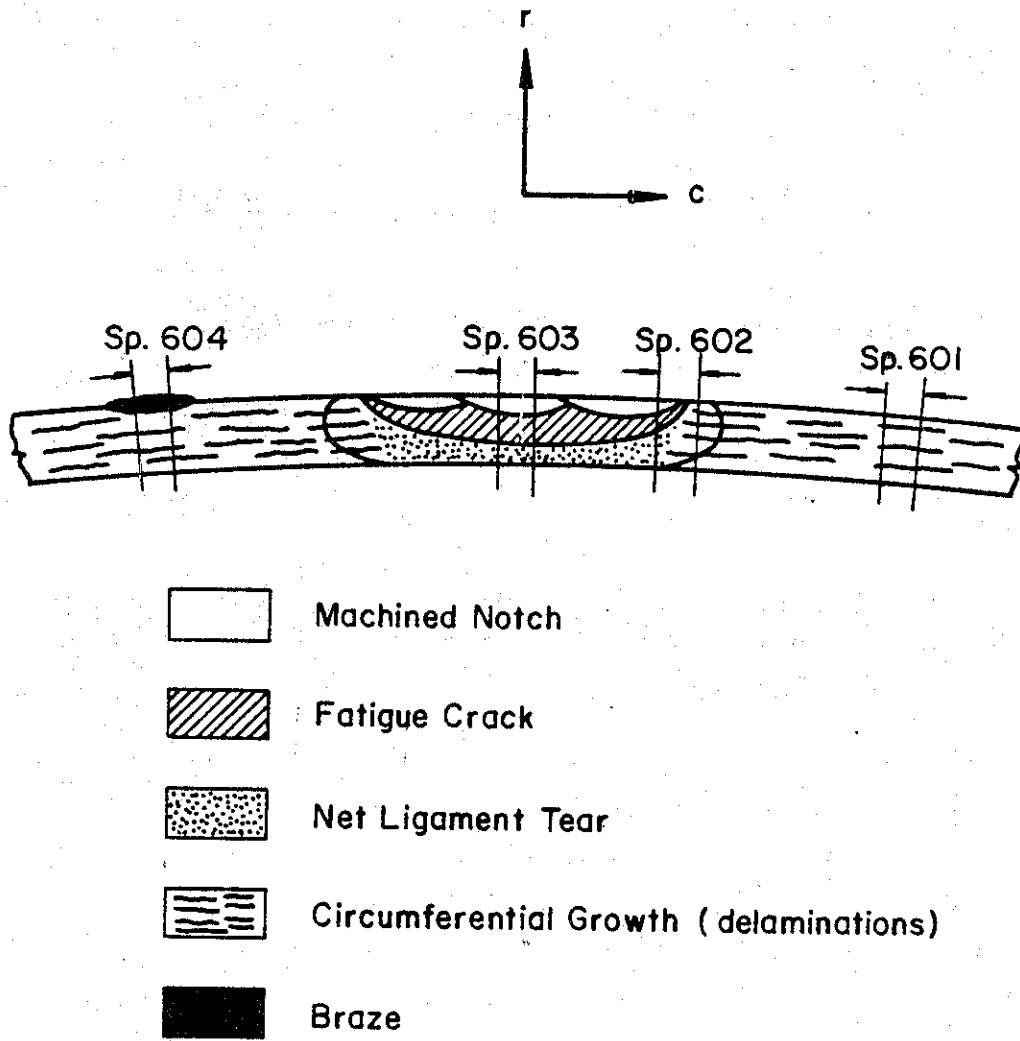


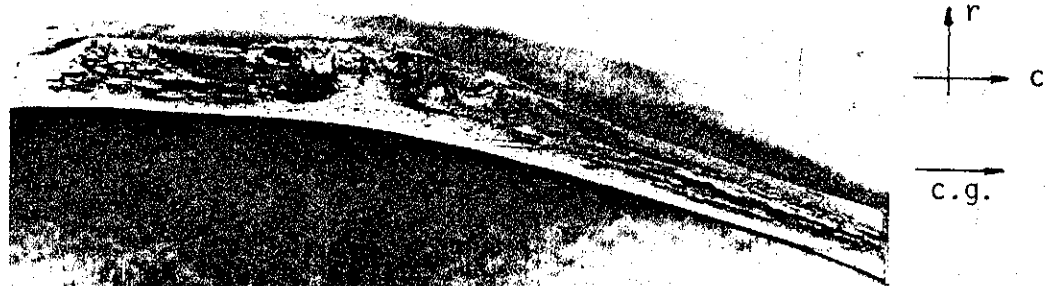
Figure 97. A sketch of the fracture surface of pipe #6 showing the locations of various specimens used in the scanning electron microscope.

From Figure 82 one may easily distinguish three different zones on the fracture surface, namely the fatigue crack, net ligament rupture, and the through-thickness shear fracture of the pipe wall. Even though both the net ligament and the pipe wall were undergone ductile fracture, their appearance were quite different. The net ligament appeared to have the structure of a fine-textured dimple fracture and had no signs of delamination. On the other hand, the through-thickness fracture beyond the crack tips had much coarser surfaces and had the appearance of shear fracture of a laminated material with clearly observable delamination cracks (Figure 82, see, also, Figure 79b).

For a closer examination of various fracture surfaces photomicrographs were taken at various locations in pipe #6 by scanning electron microscope (SEM). Figure 97 shows a sketch of the fracture surface of the pipe #6 which indicates the locations of the samples (601, 602, 603, 604) used in SEM. The symbols r, c, and c.g. shown in Figures 97-108 refer to the (outward) radial, circumferential, and macroscopic crack growth directions, respectively. The views of the fracture surface opposite to that used in SEM study are shown in Figure 98. The braze shown in Figure 97 which may also be seen in Figure 98a was part of an effort to use an acoustic emission device for detecting the crack initiation. This attempt did not prove to be very reliable and successful.

Figures 99-108 show SEM photomicrographs of the four different samples (designated by 602, 602, 603, and 604 in Figure 97) taken at various magnifications, but mostly at 1000X. The photomicrographs of the sample 601 are shown in Figures 99 and 100. Figure 99a shows the view from a "valley" between delaminations where the voids tend to be more equiaxial. As one climbs along the side of a delamination the shearing effect becomes more visible and the dimples tend to be more elongated (Figure 99b, see also Figure 100 a and b).

Figures 101-103 show various views of the sample 602. Figure 101 shows low magnification photomicrographs of the whole pipe wall and a portion of the peculiar band which was developed during the fracture process. In the section of the pipe wall shown in Figure 101a the regions of machined surface, fatigue crack, and the ductile fracture surface including the delaminations and the "band" are clearly visible. The band is also seen in Figure 101b. Figure 102a shows a photomicrograph of the fatigue surface. The stretch zone adjacent to the fatigue surface and the transition region (to ductile fracture) are shown



(a)



(b)

Figure 98. Views of the fracture surface of pipe #6 opposite to that used in the fractographic study.

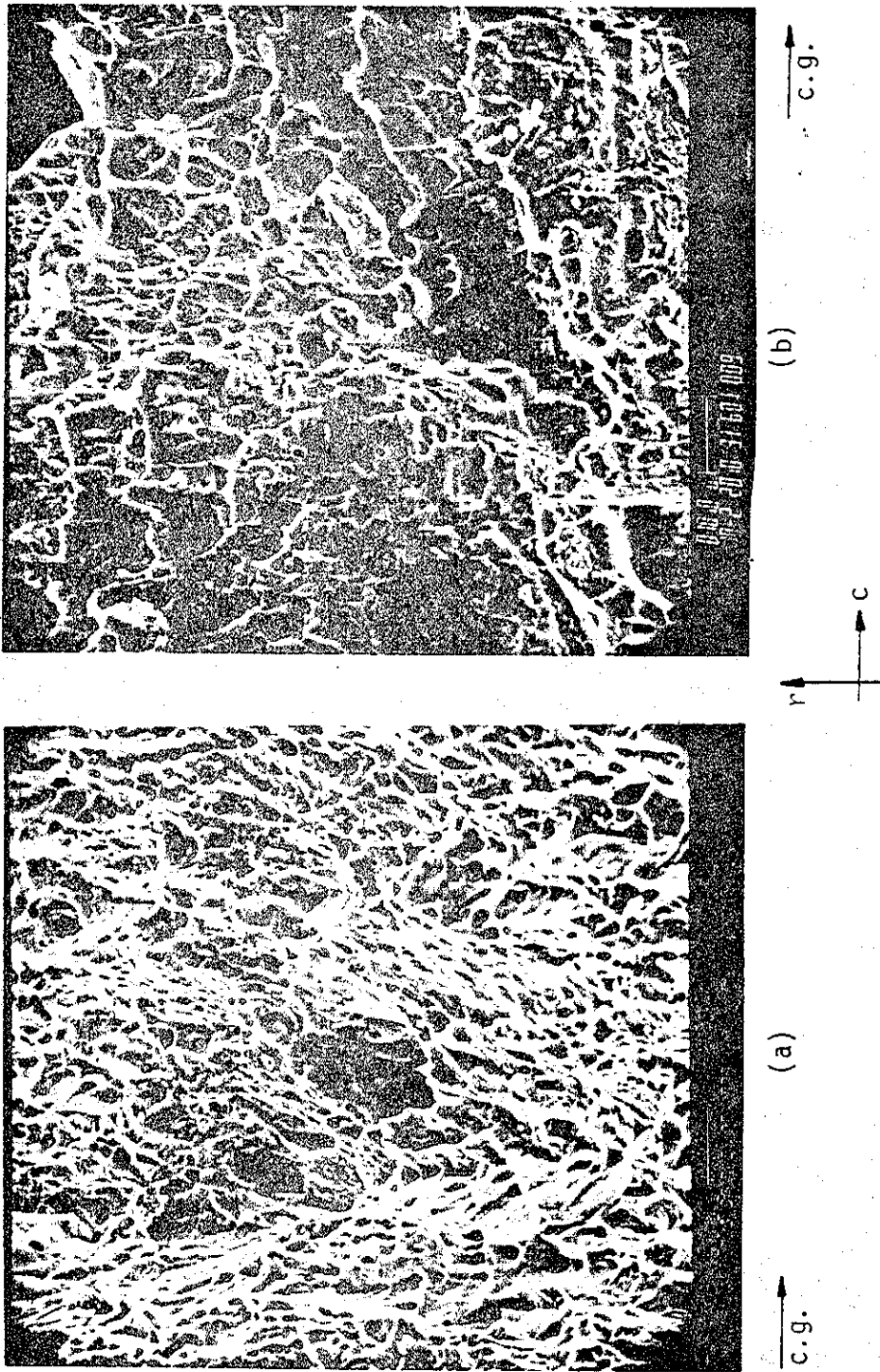


Figure 99. Scanning electron micrographs (SEM) of the fracture surface at the location 601 (See Figure 96), (a) in a valley between delaminations, (b) along the side of a delamination. (r: outward radial direction, c: circumferential direction, c.g.: crack growth direction) (1000X)

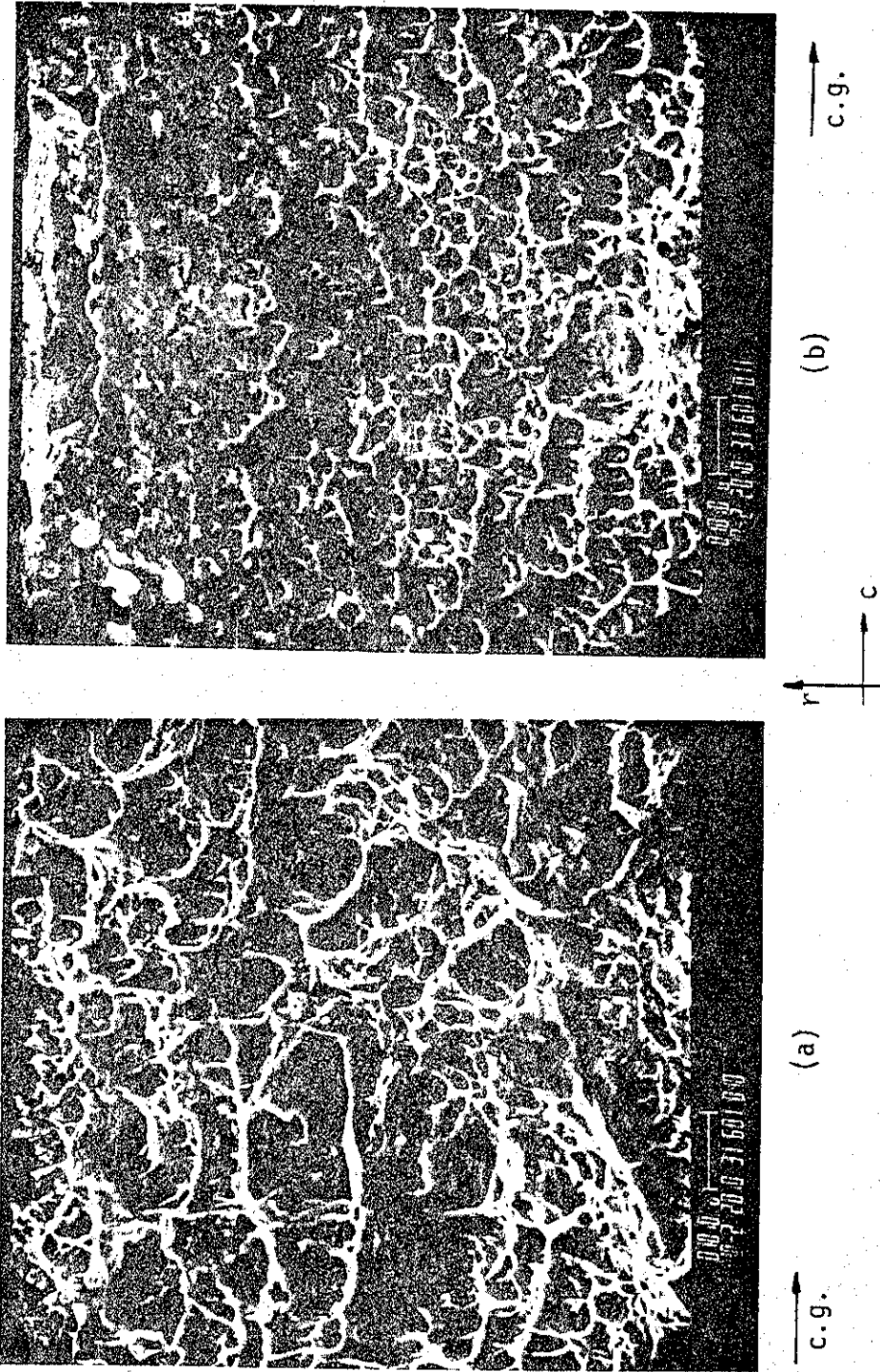


Figure 100. Scanning electron micrographs of the fracture surface at the location 60I. (a) along the side of a delamination closer to the edge, (b) near the pipe surface. (1000X)

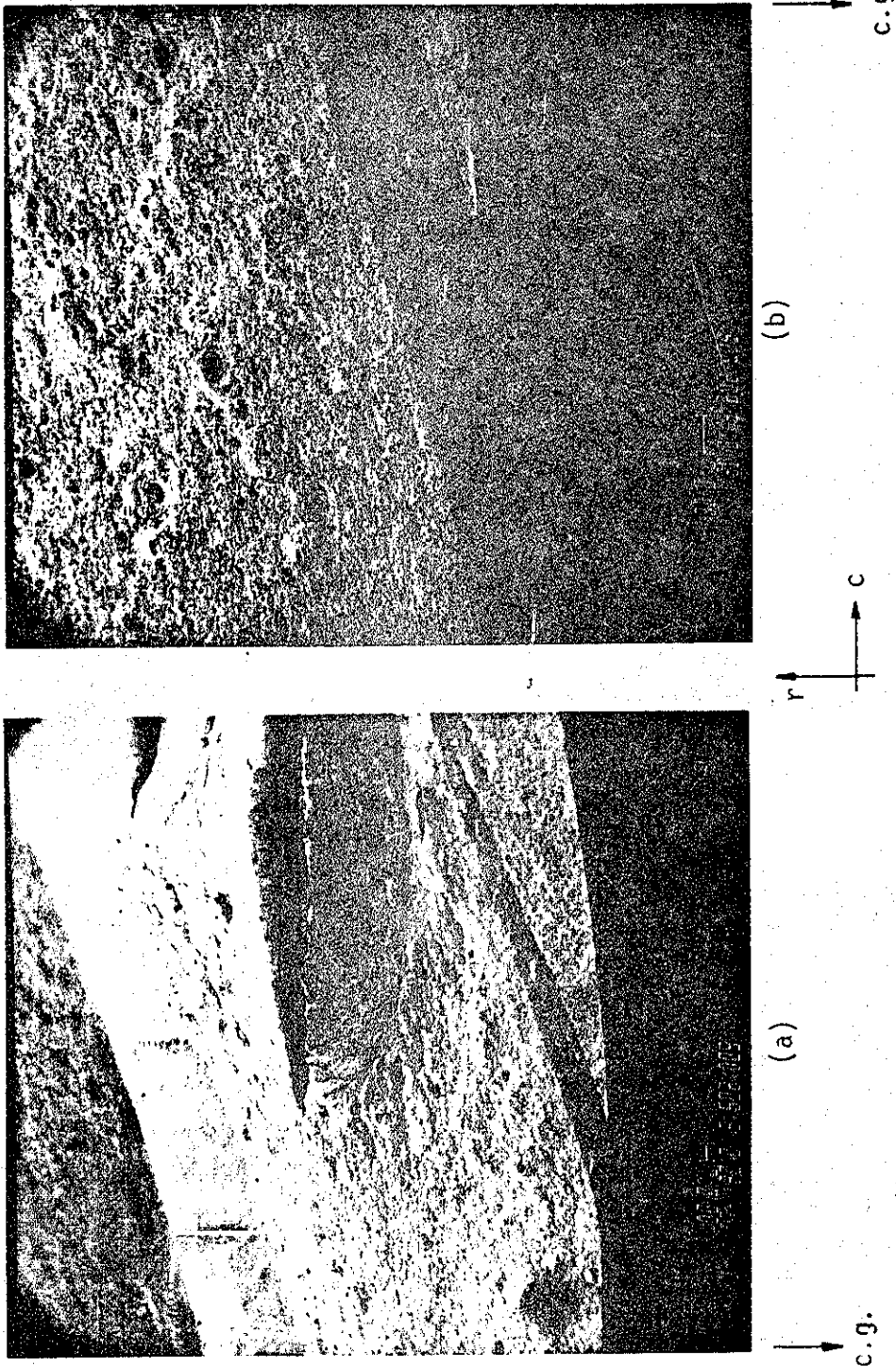


Figure 101. Low magnification SEMs of the fracture surface at the location 602. (a) 20X (from the top: machined surface, fatigue crack, tear region which includes delaminations, the "band", further tear region), (b) 50X.

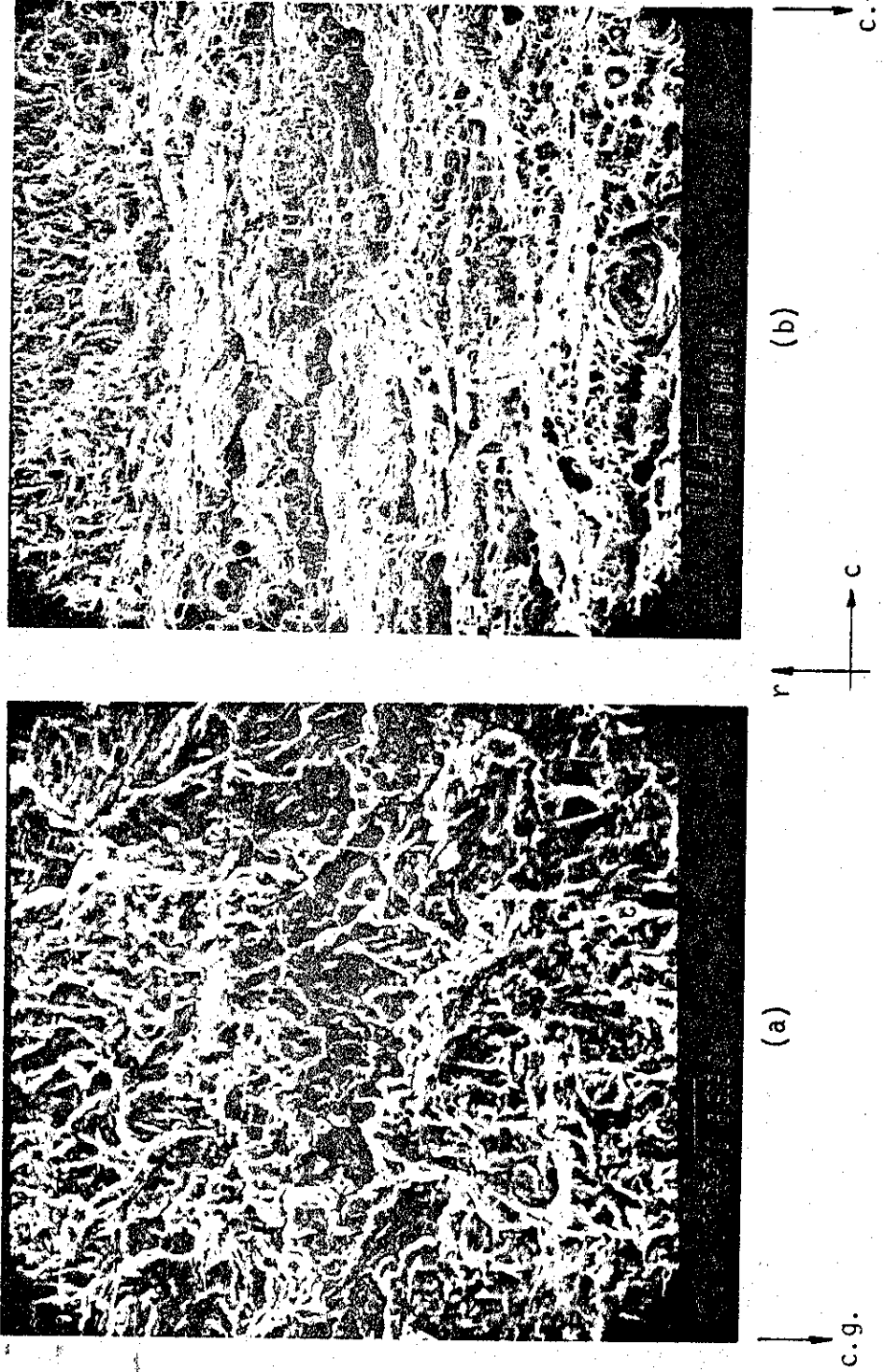


Figure 102. SEMs of the fracture surface at the location 602. (a) fatigue surface, (b) stretch or transition from fatigue to ductile fracture region. (1000X)

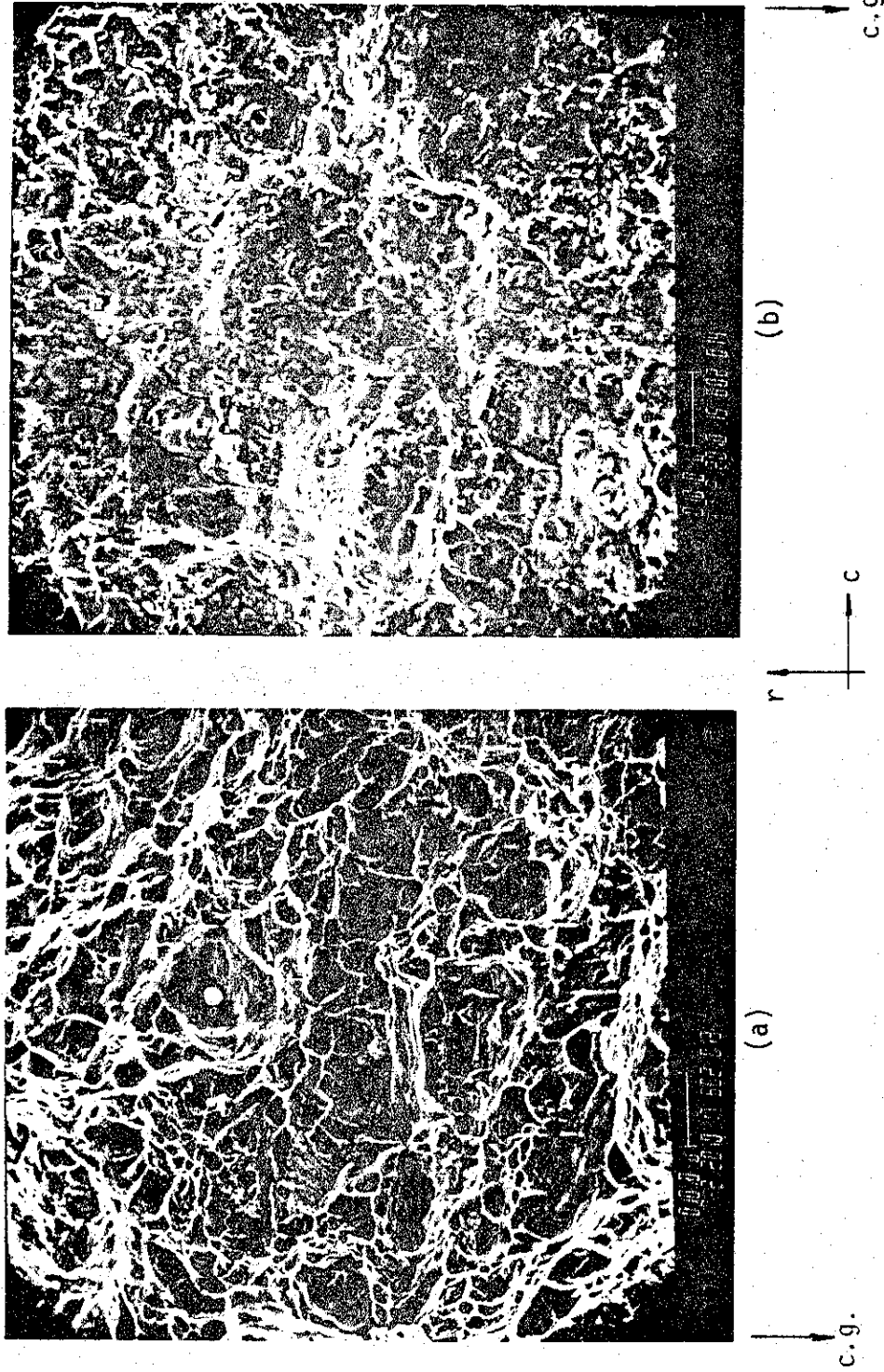


Figure 103. SEMs of the fracture surface at the location 602. (a) equiaxial dimples in the initial phase of through-thickness tear, (b) the (dark) band seen in Figure 101. (1000X)

in Figure 102b. Figure 103a shows a typical photomicrograph of equiaxial dimples corresponding to the initial phase of the through-thickness fracture. A higher magnification view of the "band" which may be observed in Figure 101 is shown in Figure 103b. Note that the same band (this time in light color) is also visible near the crack tips in Figure 82a and c. The band is believed to be due to the interruption of the test momentarily for manual readjustment of the loading jacks^(*). This may have caused a crack closure, resulting in "smearing" or "flattening" of the dimples. It is, nevertheless, clear that the bands seen in Figure 82 along the entire thickness of the pipe correspond to the crack front at a particular time during the propagation of the through thickness fracture.

The series of photomicrographs shown in Figures 104-106 are taken from the sample 603. Figure 104a shows fatigue surface and part of the stretch zone (marked by A). The stretch zone and the beginning of the tear region are shown in Figure 104b. Views further into the tear region and closer to the back surface are shown in Figures 105 and 106. The orientation of the dimples in these figures indicate that the direction of the crack propagation was radial. On the fracture surface there was no evidence of shear fracture in the net ligament propagating in circumferential direction.

Figures 107 and 108 taken from the braze area (604) at various magnifications. From the top toward the bottom of the figure the three regions seen in Figure 107b to correspond to the flat fracture in the braze material, the fatigue crack propagation in the pipe material, and the ductile fracture zone. The higher magnification photographs of the first two, namely the flat fracture surface in the braze and the fatigue surface in the steel are shown in Figures 108b and 108a, respectively. The initiation of local brittle fracture at the braze and the subsequent fatigue crack propagation in the pipe wall shown in Figure 108 indicates the importance and the possible role of, for example, are burns in initiating surface cracks in pipes and other welded structures.

(*) The drop of the load P to zero and reloading is not shown in Figure 88. Figure 88 was reproduced from the oscilloscope record in which unloading and loading was ignored. However, the corresponding trace in the x-y recorder shows that the unloading and loading were perfectly elastic, followed the same straight line (in P vs. COD plane), and there was no sign of any discontinuity or kink in P vs. COD record.

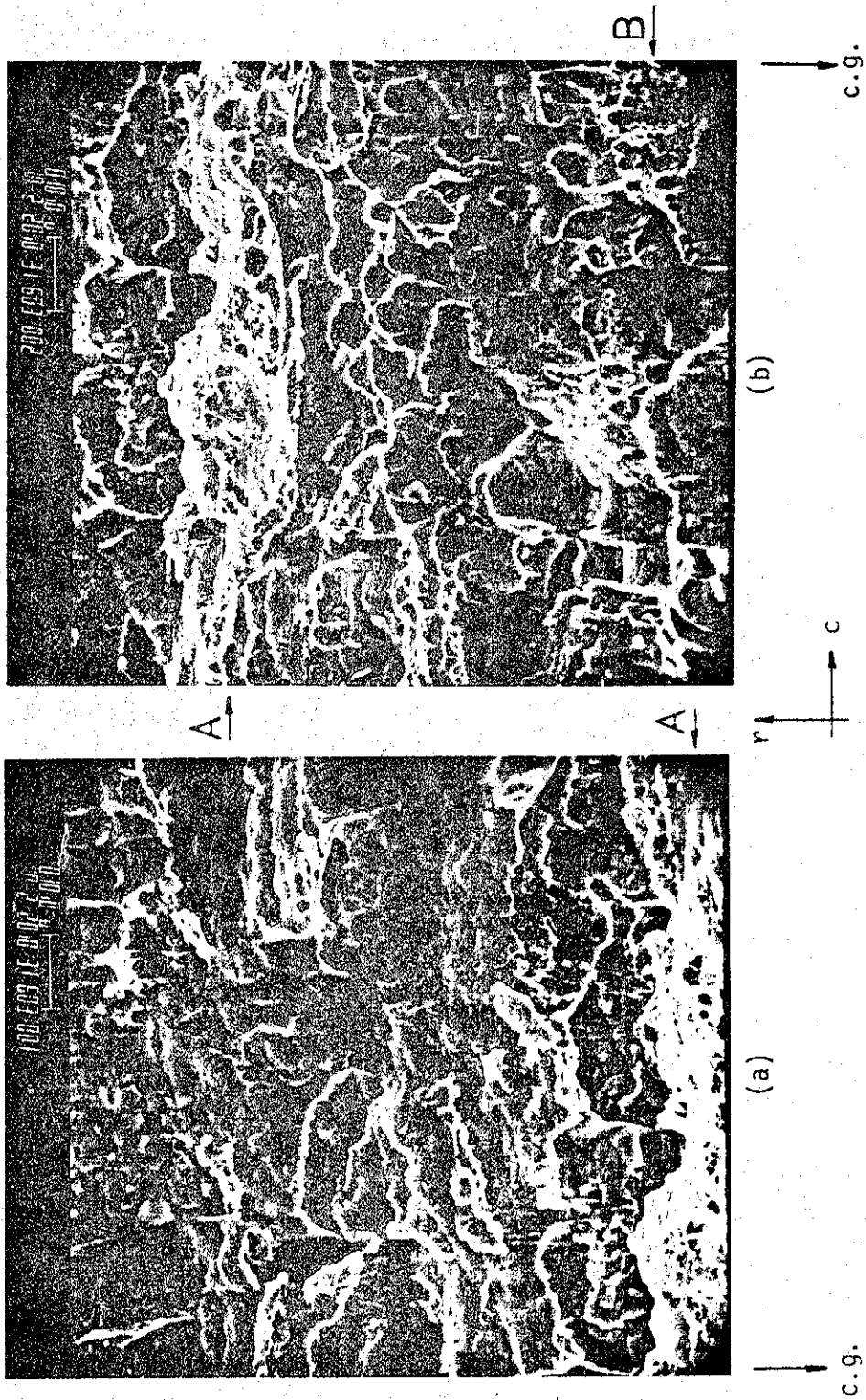


Figure 104. SEMs of the fracture surface at the location 603. (a) fatigue surface and stretch zone (A), (b) stretch zone (A) and tear region (A: line of overlap). (1000X)

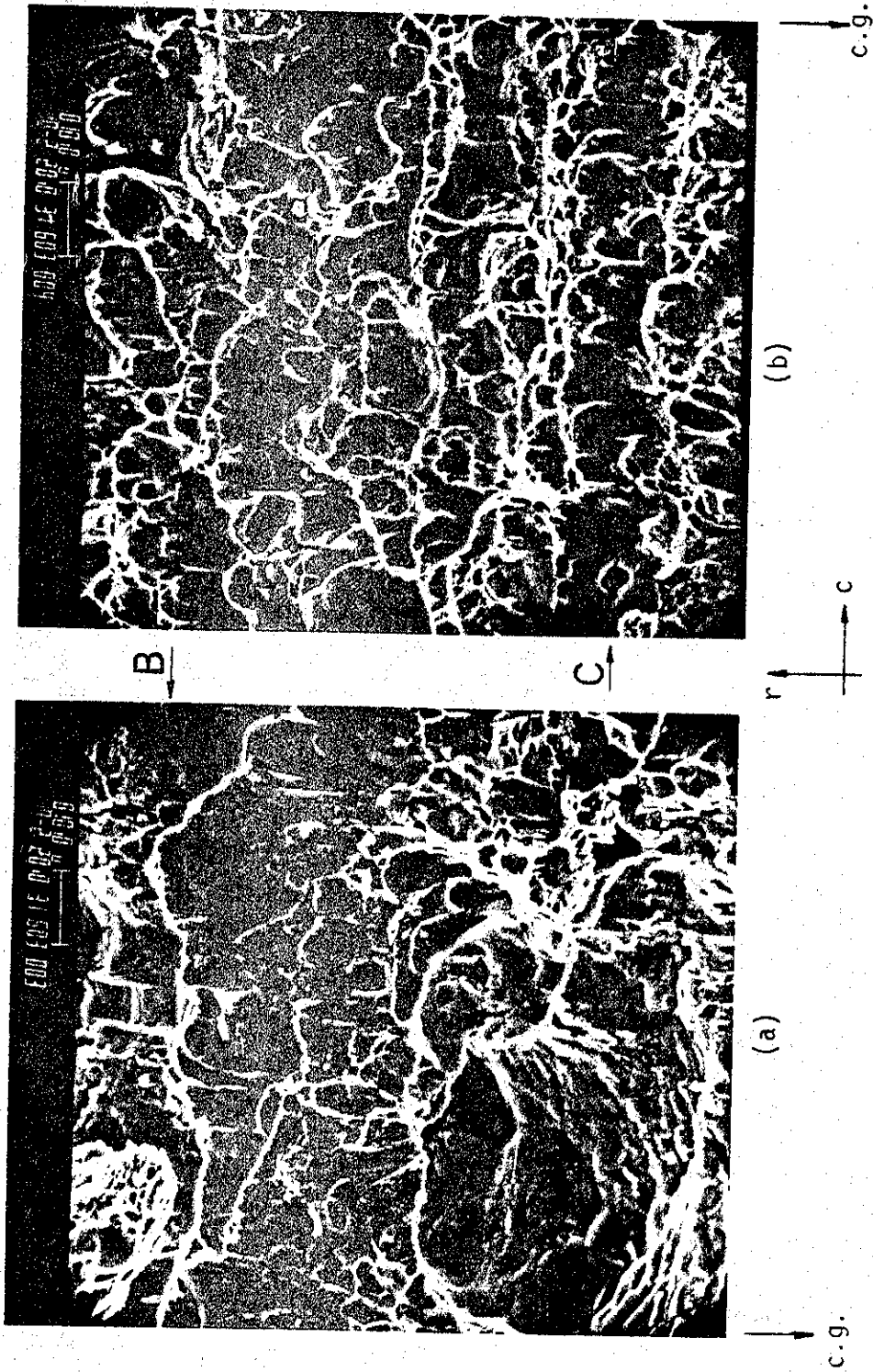


Figure 105. SEMs of the fracture surface at the location 603. (a) tear region, (b) further into the same tear region. (1000X)

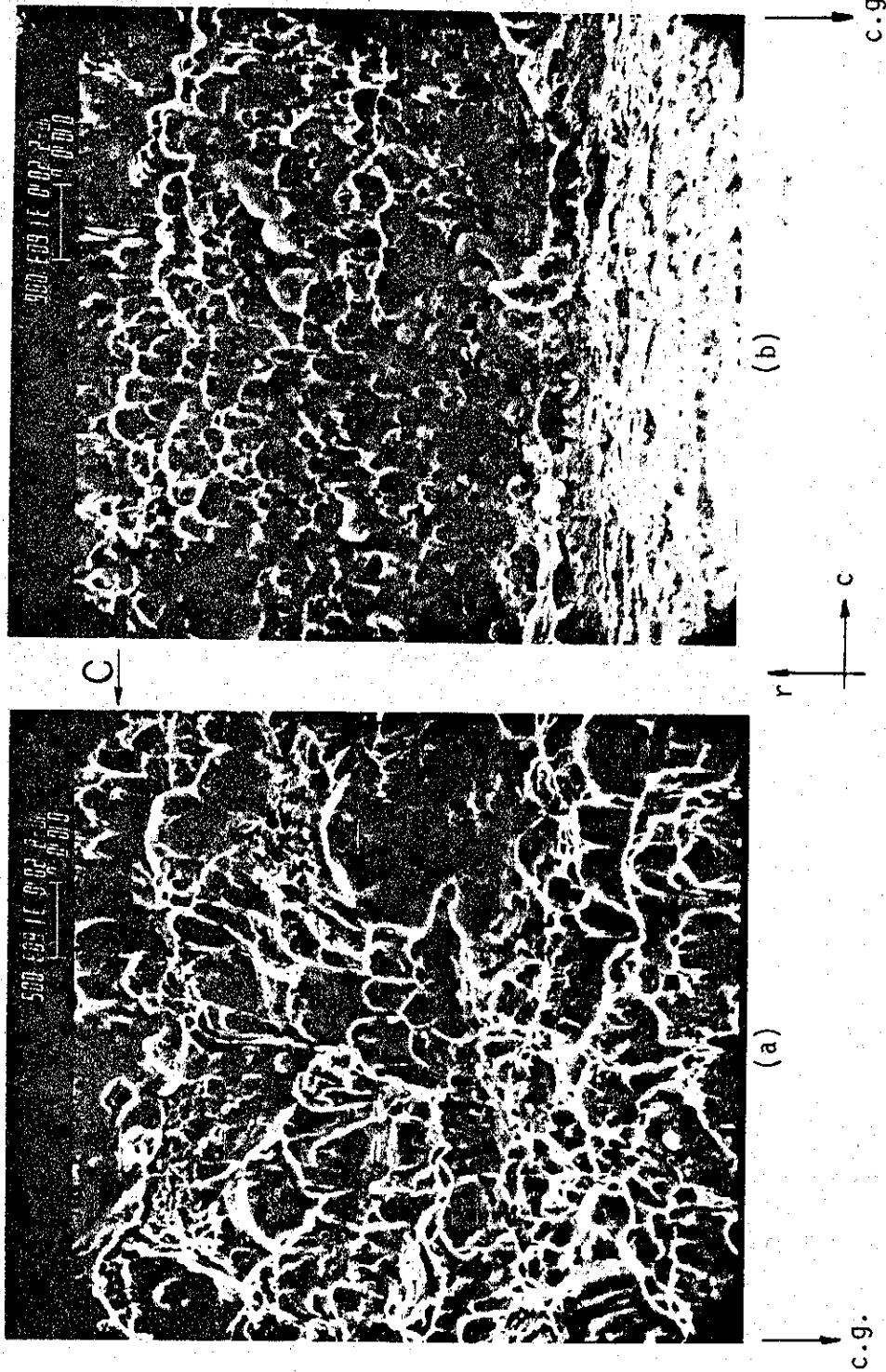


Figure 106. SEMs of the fracture surface at the location 603. (a) tear region, (b) same tear region closer to the pipe surface. (A, B and C in Figures 104-106 correspond to the lines of overlap.) (1000X)

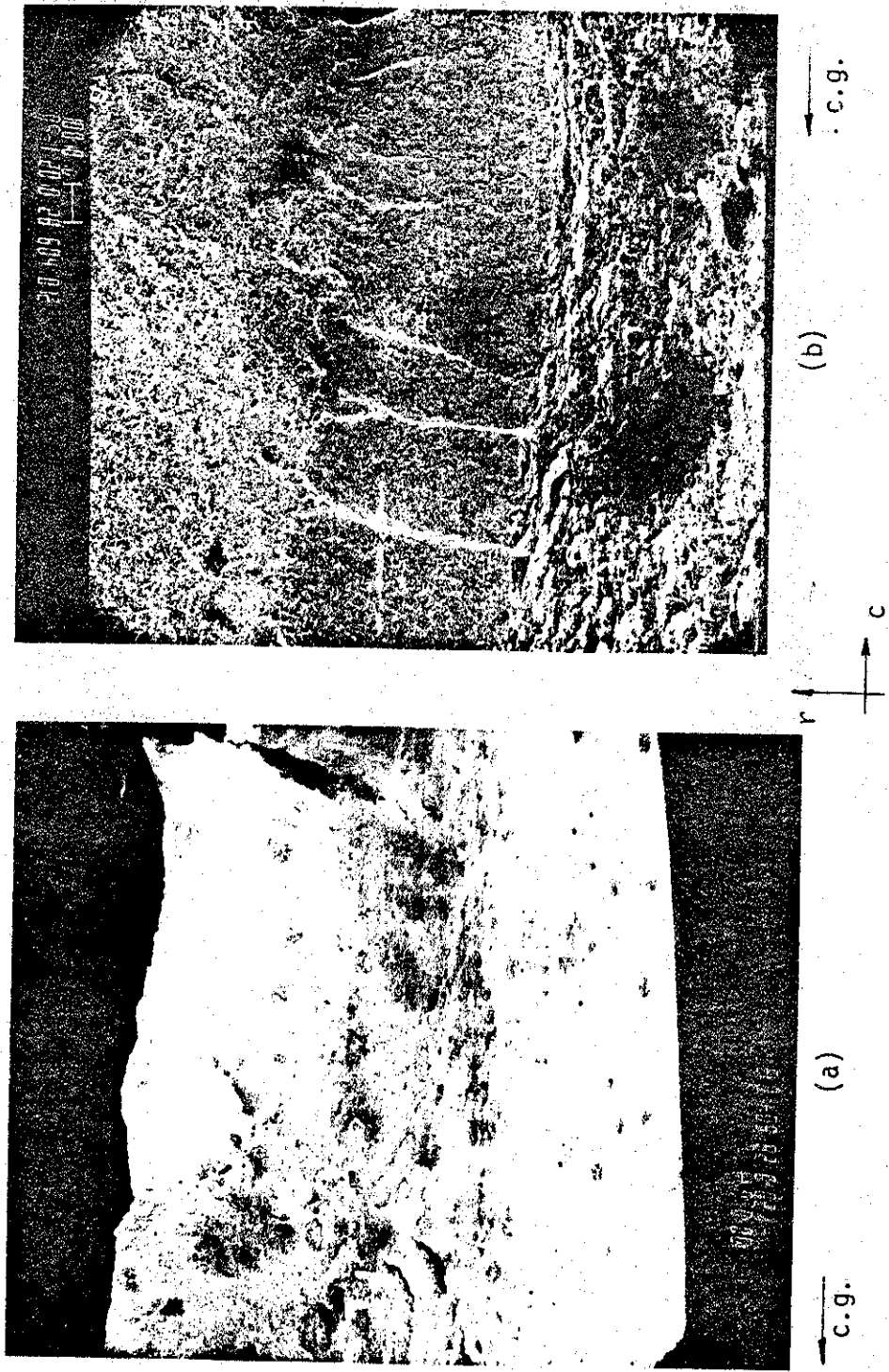


Figure 107. Low magnification SEMs of the brazed area, location 604. (a) 10X (fracture surface in braze, fatigue surface in pipe material, tear region in pipe wall), (b) 50X (braze, fatigue surface, tear region).

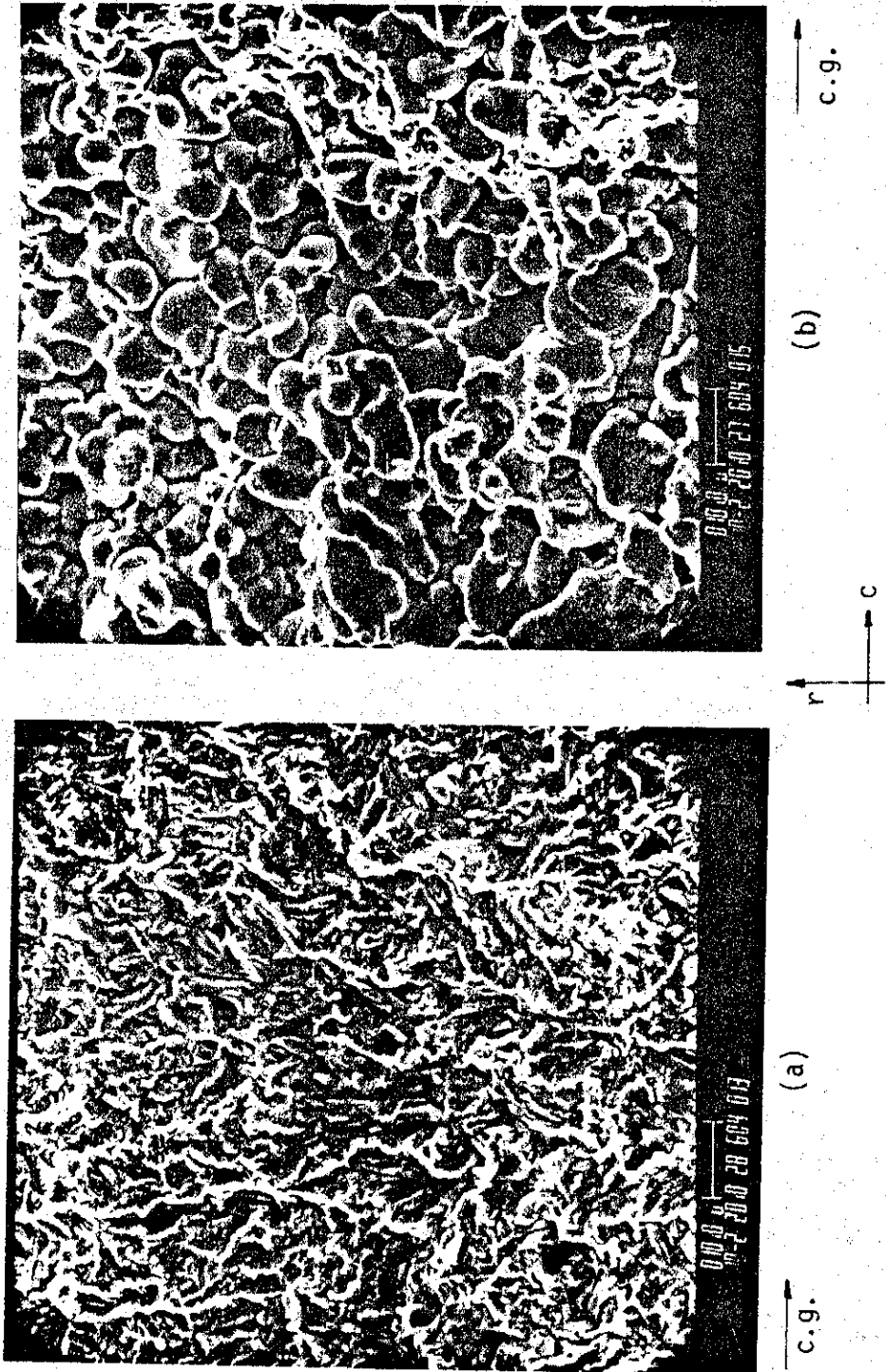


Figure 108. SEMs of the fracture surface at the location 604. (a) fatigue surface in the pipe material, (b) microstructure of the brazing material (brass). (1000X)

It may be pointed out that the difference between the through-thickness tear in the net ligament and the circumferential tear in the pipe wall is purely a matter of stress state and geometric constraints. These are very highly pronounced delaminations in the circumferential tear region initiating from the impurities in the steel, whereas the net ligament is completely free of such delaminations.

CONCLUSIONS

The primary objectives of the present research program were (a) to develop the methodology and the necessary analytical tools for application to the problems of fatigue crack propagation and ductile fracture in pipelines containing circumferential flaws, and (b) to carry out a properly conceived experimental program in order to verify the validity of the theoretical models and to establish the limitations of such models. From the outset it was useful to separate the two phases (namely, the fatigue crack growth and the ductile fracture) of the failure process. They are both equally important. To study the fatigue crack propagation phenomenon in any structural component for any crack geometry and to perform a predictive analysis the information needed is the following: the cyclic nature of the applied loads as a function of time, the baseline fatigue crack propagation data for the particular material and the environment, and an accurate knowledge of the stress intensity factors at the crack front.

In the present study a great deal of analytical effort was devoted to develop the methods for an accurate calculation of the stress intensity factors in pipes and flat plates containing a through or a part-through crack. This research was necessary for providing the tools in fatigue studies. It also formed the basis of the theoretical work for the elastic-plastic problem in pipes.

The experimental fatigue work on pipes as well as on the flat plates showed that the fatigue crack propagation rate in such structures can indeed be predicted from the baseline laboratory data obtained for simple standard specimens provided a correct estimate of the stress intensity factors is available.

In studying the ductile fracture of the three basic geometries considered, namely the single edge notched specimen, the plate with a surface crack, and the pipe with a circumferential crack, it was assumed that the part undergoes large scale plastic deformations. The crack opening and the crack tip opening displacements (COD and CTOD) were used as the correlation parameters in the analysis of the experimental results. The theoretical model developed for this purpose was based on the shell theory and elastic-plastic analysis. The model may be used in estimating the fracture instability load in pipes and flat plates. It may also be used, with the critical crack tip opening concept, to obtain a conservative estimate for the load level initiating the ductile fracture.

The particular X60 line pipes which were subjected four point bending and which contained a part-through circumferential fatigue crack on the tension side proved to be very highly resistant to ductile fracture. Even though it was possible to rupture the net ligament (i.e., the pipe wall under the crack) in all but one of the pipe specimens, the gross failure under gradually increased static bending occurred mostly as a result of inelastic buckling of the pipe wall on the compression side rather than fracture instability (i.e., unstable crack growth) on the tension side. The one pipe specimen in which the net ligament did not rupture and in which there was severe buckling on the compression side contained a relatively shallow fatigue crack. In one specimen there was no sign of buckling and the structural failure resulted from fracture instability. In all cases the theoretical model gave conservative estimates for the fracture instability load.

The report contains the analytical details of all the models developed and gives extensive calculated results for standard line pipes with a circumferential part-through crack which may be used in fatigue crack growth and ductile fracture studies. Most of the analysis and the results are given in the Appendices.

REFERENCES

1. M. Reich and E.P. Esztergar, "Compilation of References, Data Sources, and Analysis Methods for LMFBR Piping System Components," Brookhaven National Laboratory, BNL-NUREG-50650, March 1977.
2. The Surface Crack, J.L. Swedlow, ed. ASME, New York, 1972.
3. I.S. Raju and J.C. Newman, Jr., "Improved Stress Intensity Factors for Semi-Elliptic Surface Cracks in Finite Thickness Plates", NASA TMX-72825, 1977.
4. F. Erdogan, "Crack Problems in Cylindrical and Spherical Shells", in Plates and Shells with Cracks, G.C. Sih, ed., Noordhoff Int. Publ., Leyden, 1977.
5. F. Erdogan and M. Ratwani, "Plasticity and Crack Opening Displacement in Shells", Int. J. Fracture Mechanics, Vol. 8, 1972, pp. 413-426.
6. F. Erdogan and M. Ratwani, "Fracture Initiation and Propagation in a Cylindrical Shell Containing an Initial Flaw", Nuclear Engng. and Design, Vol. 27, 1974, pp. 265-286.
7. F. Erdogan, G.R. Irwin, and M. Ratwani, "Ductile Fracture of Cylindrical Vessels Containing a Large Flaw", ASTM-STP 601, 1976, pp. 191-208.
8. S.N. Atluri and K. Kathiresan, "Outer and Inner Surface Flaws in Thick-Walled Pressure Vessels", Proceed. 4th SMIRT, G5/4, San Francisco, 1977.
9. A.S. Kobayashi, N. Polvanich, A.F. Emery, and W.J. Love, "Inner and Outer Cracks in Internally Pressurized Cylinders", J. Pressure Vessel Technology, Trans. ASME, Vol. 99, 1977, pp. 83-89.
10. S.T. Rolfe and J.M. Barsom, Fracture and Fatigue Control in Structures, Prentice-Hall, 1977.
11. Review and Developments in Plane Strain Fracture Toughness Testing, ASTM-STP 463, 1970.
12. Fatigue Crack Propagation, ASTM-STP 415, 1967.
13. Progress in Flaw Growth and Fracture Toughness Testing, ASTM-STP 563, 1973.
14. Fracture Toughness Evaluation by R-Curve Methods, ASTM-STP 527, 1973.
15. J.C. Newman, Jr., "Fracture Analysis of Surface and Through-Cracked Sheets and Plates", J. Engng. Fracture Mechanics, Vol. 5, 1973, pp. 667-689.
16. J.C. Newman, Jr., "Fracture Analysis of Surface and Through Cracks in Cylindrical Vessels", NASA-TN D-8325, 1976.

17. F. Erdogan, "Ductile Fracture Theories for Pressurized Pipes and Containers", Int. J. Pressure Vessels and Piping, Vol. 4, 1976, pp. 253-283.
18. R. Roberts, J.M. Barsom, J.W. Fisher, and S.T. Rolfe, "Fracture Mechanics for Bridge Design", Final Report, Contract No. P.O. No. 5-3-0209, Prepared for DOT Federal Highway Administration, Lehigh University, July 1977.
19. "Consideration of Fracture Mechanics Analysis and Defect Dimension Measurement Assessment for the Trans-Alaska Oil Pipeline Girth Welds, "Volumes I and II, Final Report NBS IR 76-1154, Prepared for DOT Materials Transportation Bureau, October 1976.
20. J.F. Kiefner, W.A. Maxey, R.J. Eiber, and A.R. Duffy, "Failure Stress Levels of Flaws in Pressurized Cylinders", in ASTM-STP 536, 1973, pp. 461-481.
21. G.M. Wilkowski, A. Zahoor, and M.F. Kanninen, "A Plastic Fracture Mechanics Prediction of Fracture Instability in a Circumferentially Cracked Pipe in Bending-Part II: Experimental Verification on a Type 304 Stainless Steel Pipe", Journal of Pressure Vessel Technology, ASME, Dec. 1981.
22. G.M. Wilkowski and R.J. Eiber, "Review of Fracture Mechanics Approaches to Defining Critical Size Girth Weld Discontinuities", Welding Research Council Bulletin 239, July 1978.
23. G.M. Wilkowski and R.J. Eiber, "Evaluation of Tensile Failure of Girth Weld Repair Grooves in Pipe Subjected to Offshore Laying Stresses", Journal of Energy Resources Technology, Trans. ASME, Vol. 103, pp. 48-55, 1981.
24. J.D. Harrison, "The Welding Institute Studies the Significance of Alyeska Pipeline Defects", TWI Res. Bull., Vol. 18, No. 4, pp. 93-95, 1977.
25. H.I. McHenry, D.J. Read, and J.A. Begley, "Fracture Mechanics Analysis of Pipeline Girth Welds", in Elastic-Plastic Fracture, ASTM-STP-668, pp. 632-642, 1979.
26. E.L. von Rosenberg, "Alternative Girth Weld Defect Assessment Criteria for Pipelines", Proc. of Int. Conf. on Pipeline and Energy Plant Piping-Design and Technology", Calgary, Alberta, Canada, Pergamon Press, Toronto 1980.
27. R.P. Reed, H.I. McHenry, and M.B. Kasen, "A Fracture Mechanics Evaluation of Flaws in Pipeline Girth Welds", Welding Research Council Bulletin, 245, Jan. 1979.
28. G.D. Fearnehough and D.G. Jones", "An Approach to Defect Tolerance in Pipelines", Institution of Mechanical Engineers, C97/78, pp. 205-227, 1978.
29. G.D. Fearnehough and J.M. Greig, "Experience in the Gas Industry, Phil. Trans. R. Soc. Lond., Vol. A299, pp. 203-215, 1981.
30. C.I. Chang, M. Nagagaki, C.A. Griffis, and R.A. Masumura, "Piping Inelastic Fracture Mechanics Analysis", NUREG/CR 1119, NRL Memorandum Report 4259 June 1980.

31. Crack Propagation in Pipelines, Inst, Gas Eng., London, 1974.
32. C. Popelar, A.R. Rosenfield, and M.F. Kanninen, "Steady-State Crack Propagation in Pressurized Pipelines", J. Pressure Vessel Technology, Trans. ASME, Vol. 99, 1977, pp. 112-121.
33. F. Erdogan, F. Delale, and J.A. Owczarek, "Crack Propagation and Arrest in Pressurized Containers", J. Pressure Vessel Technology, Trans. ASME, Vol. 99, 1977, pp. 90-99.
34. F. Erdogan and M. Ratwani, "Fatigue and Fracture of Cylindrical Shells Containing a Circumferential Crack", Int. J. Fracture Mechanics, Vol. 6, 1970, pp. 379-387.
35. G.D. Fearnhough, et al. "Practical Application of Fracture Mechanics to Pressure Vessel Technology" Institution of Mechanical Engineering Conference, London (1971), pp. 119-127.
36. C.G. Chipperfield, J.F. Knott, and R.F. Smith, Third International Conference on Fracture, Munich (1973), Vol. 1, p. 233.
37. J.D. Landes and J.A. Begley, in Fracture Toughness, ASTM STP 514, 1972, pp. 24-39.
38. Newman, J.C. and Raju, I.S., "Stress Intensity Factors for Internal Surface Cracks in Cylindrical Pressure Vessels", NASA Technical Memorandum 80073, July 1979.
39. McGowan, J.J. and Raymund, M., "Stress Intensity Factor Solutions for Internal Longitudinal Semi-Elliptical Surface Flaws in a Cylinder under Arbitrary Loadings", Fracture Mechanics, ASTM, STP 677, 1979.
40. Heliot, J. and Labbens, R.C. and Pellisier-Tanon, A., "Semi-Elliptic Cracks in a Cylinder Subjected to Stress Gradients", Fracture Mechanics, ASTM, STP 677, pp. 341-364, 1979.
41. Raju, I.S. and Newman, J.C., Jr., "Stress-Intensity Factors for a Wide Range of Semi-Elliptical Surface Cracks in Finite-Thickness Plates", Journal of Engr. Fracture Mechanics, Vol. 11, pp. 817-829, 1979.
42. Newman, J.C., Jr., A Review and Assessment of the Stress-Intensity Factors for Surface Cracks, NASA, Technical Memorandum 78805, Nov. 1978.
43. Atluri, S.N. Kathiresan, K., Kobayashi, A.S., and Nakagaki, M., "Inner Surface Cracks in an Internally Pressurized Cylinder Analyzed by a Three-Dimensional Displacement-Hybrid Finite Element Method", Proc. of the Third Int. Conf. on Pressure Vessel Technology, Part III, pp. 526-533, ASME, New York, 1977.
44. Smith, F.W. and Sorensen, D.R., "The Semi-Elliptical Surface Crack - A Solution by the Alternating Method", Int. J. of Fracture, Vol. 12, pp. 47-57, 1976.

45. Shah, R.C. and Kobayashi, A.S., On the Surface Flaw Problem, The Surface Crack: Physical Problems and Computational Solutions, ed, J.L. Swedlow, 1972, pp. 79-124.
46. Rice, J.R. and Levy, N., "The Part-Through Surface Crack in an Elastic Plate", *Journal of Applied Mechanics*, Vo. 39, 1972, pp. 185-194.
47. Delale, F. and Erdogan, F., "Line-Spring Model for Surface Cracks in a Reissner Plate", *Int. J. Engineering Science*, Vol. 19, pp. 1331-1340, 1981.
48. S. Timoshenko, Theory of Plates and Shells, McGraw-Hill, New York, 1940.
49. F. Erdogan and M. Bakioglu, "Crack Opening Stretch in a Plate of Finite Width", *Int. J. Fracture*, Vol. 11, 1975, pp. 1031-1039.
50. R. de Wit and J.H. Smith, "Development of Analytical Fracture Mechanics Models for Pipeline Girth Welds", paper presented at the 12th National Symposium on Fracture Mechanics, May 21-23, 1979, St. Louis, Missouri.
51. J. Carlsson, "A Fracture Model for Surface Flaws and Certain Types of Weld Defects in Ductile Materials", Publication No. 176, Institutionen för hållfasthetslära, Royal Institute of Technology, Stockholm, 1972.
52. G.R. Irwin, V.G. Krishna, and B.T. Yen, "Flat-Plate Testing of Part-Through Cracks in Line-Pipe Steel Plates", Fritz Engineering Laboratory Report No. 373.1, prepared for Battelle Memorial Institute, 1972.
53. O. Vosikovsky, "Effects of Stress Ratio on Fatigue Crack Growth Rates in X70 Pipeline Steels in Air and Salt Water", *Journal of Testing and Evaluation*, Vol. 8, pp. 68-73, 1980.
54. V. Kumar, M.D. German, and C.F. Shih, "An Engineering Approach for Elastic-Plastic Fracture Analysis" (EPRI Handbook), EPRI NP-1931, Project 1237-1 Topical Report, July 1981.
55. S.P. Timoshenko and J.M. Gere, Theory of Elastic Stability, 2nd Ed., McGraw-Hill, New York, 1961.
56. J. Vinson, Structural Mechanics: Behaviour of Plates and Shells, J. Wiley, 1974.



APPENDICES



APPENDIX A
CYLINDRICAL SHELL WITH A CIRCUMFERENTIAL THROUGH CRACK

1. INTRODUCTION

The aim of this Appendix is to give complete details of the solution of a circumferentially cracked cylindrical shell problem by taking into account the effect of transverse shear deformations. A higher order shell theory compatible with the number of independent boundary conditions is used in the analysis.

2. FORMULATION OF THE PROBLEM

In this problem the general shallow shell equations developed in [1] for an isotropic medium will be used. However, as shown in [2] and [3] for the classical shell theory, in this case too it can be shown that the related differential equations of the orthotropic shells can be factorized and reduced to the equations of isotropic shells if one assumes the material to be "specially orthotropic".

Referring to Figure 12 and following [1] the equilibrium equations for a shallow shell may be expressed as

$$N_{ij,j} = 0 \quad (2.1)$$

$$V_{i,i} + (Z_{,i} N_{ij}),_j + q(X_1, X_2) = 0 \quad (2.2)$$

$$M_{ij,j} - V_i = 0 \quad , (i=1,2, j=1,2) \quad (2.3)$$

where N_{ij} , M_{ij} , and V_i , ($i, j=1,2$) are, respectively, membrane, moment and transverse shear resultants, and the indicial notation and the summation convention are used. The components of strains are given by

$$\epsilon_{ij} = \frac{1}{2}[U_{i,j} + U_{j,i} + Z_{,i} W_{,j} + Z_{,j} W_{,i}], \quad (i, j=1,2) \quad (2.4)$$

where U_1 , U_2 and W are, respectively, X_1 , X_2 , and X_3 -components of the

displacement vector, and the function $Z(X_1, X_2)$ giving the equation of the middle surface is known. Let β_1 and β_2 be the angles of rotation of the normal to the shell surface. The (transverse) shear strains may then be expressed as

$$\theta_i = W_{,i} + \beta_i, \quad i = 1, 2 \quad (2.5)$$

With the Hooke's law

$$\epsilon_{ij} = a_{ijkl} N_{kl} / h \quad (2.6)$$

and the relations giving M_{ij} and V_i in terms of β_i and θ_i , respectively, the formulation of the problem would be complete, technically the ten equations (2.1) - (2.5) accounting for the ten variables ϵ_{ij} , β_i , θ_i , U_i , and W .

First, eliminating U_1 and U_2 from (2.4) one obtains the following compatibility equation:

$$e_{ik} e_{jl} (\epsilon_{ij,kl} + Z_{,ij} W_{,kl}) = 0 \quad (2.7)$$

where e_{jk} is the permutation symbol^(*). Next, defining the stress function $F(X_1, X_2)$ by

$$N_{ij} = e_{ik} e_{jl} F_{,kl} \quad (2.8)$$

it is seen that (2.1) is satisfied and (2.2) and (2.7) reduce to

$$M_{ij,ij} + Z_{,ij} e_{ik} e_{jl} F_{,kl} + q = 0 \quad (2.9)$$

$$e_{im} e_{jn} e_{kp} e_{lq} a_{ijkl} F_{,mpq} + h Z_{,ij} e_{ik} e_{jl} W_{,kl} = 0 \quad (2.10)$$

Even for simple shell geometries for anisotropic materials the

^(*) $e_{11} = 0 = e_{22}$, $e_{12} = 1 = -e_{21}$.

differential equations are not tractable. However, as in [2] if one assumes a special orthotropy, the related differential operators in these equations can be factorized and the problem can be made analytically tractable. Let the material be orthotropic and the stress strain relations be

$$\begin{aligned} \epsilon_{11} &= \frac{1}{hE_1} (N_{11} - \nu_1 N_{22}) , & \epsilon_{12} &= \frac{N_{12}}{2hG_{12}} , \\ \epsilon_{22} &= \frac{1}{hE_2} (N_{22} - \nu_2 N_{11}) , & \frac{\nu_1}{E_1} &= \frac{\nu_2}{E_2} \end{aligned} \quad (2.11)$$

In this case too the following is the condition for the factorization of the operators:

$$2G_{12} = \frac{\sqrt{E_1 E_2}}{1 + \sqrt{\nu_1 \nu_2}} \quad (2.12)$$

The material satisfying the condition (2.12) is said to be "specially orthotropic". It has been shown that for certain orthotropic materials the value of the shear modulus calculated from (2.12) and that measured experimentally are very nearly the same and consequently with the assumption of special orthotropy, the analysis can be simplified quite considerably [3]. If we now define

$$E = \sqrt{E_1 E_2} , \quad \nu = \sqrt{\nu_1 \nu_2} , \quad c = (E_1/E_2)^{1/2} \quad (2.13)$$

the stress-strain relations (2.11) become

$$\begin{aligned} \epsilon_{11} &= \frac{1}{hE} \left(\frac{N_{11}}{c^2} - \nu N_{22} \right) , & \epsilon_{12} &= \frac{1+\nu}{hE} N_{12} , \\ \epsilon_{22} &= \frac{1}{hE} (c^2 N_{22} - \nu N_{11}) . \end{aligned} \quad (2.14)$$

From the linear thickness variation of the stress components σ_{ij} one obtains

$$\begin{aligned} M_{11} &= D(c^2 \beta_{1,1} + \nu \beta_{2,2}) , & M_{12} &= \frac{D(1-\nu)}{2} (\beta_{1,2} + \beta_{2,1}) , \\ M_{22} &= D(\nu \beta_{1,1} + \beta_{2,2}/c^2) , & D &= \frac{Eh^3}{12(1-\nu^2)} . \end{aligned} \quad (2.15)$$

Also, assuming a linear transverse shear stress-strain relationship, one finds

$$\theta_1 = \frac{1}{chB} V_1, \quad \theta_2 = \frac{c}{hB} V_2, \quad (2.16)$$

where B is the effective shear modulus. Referring to [5], it will be assumed that

$$B = \frac{5}{6} \frac{E}{2(1+\nu)} \quad (2.17)$$

Defining now the operator

$$\nabla_c^2 = c \frac{\partial^2}{\partial X_1^2} + \frac{\partial^2}{c \partial X_2^2}, \quad (2.18)$$

equations (2.9), (2.10), and (2.3) may be reduced to

$$\nabla_c^2 \nabla_c^2 F + hE \left(\frac{\partial^2 Z}{\partial X_1^2} \frac{\partial^2}{\partial X_2^2} - 2 \frac{\partial^2 Z}{\partial X_1 \partial X_2} \frac{\partial^2}{\partial X_1 \partial X_2} + \frac{\partial^2 Z}{\partial X_2^2} \frac{\partial^2}{\partial X_1^2} \right) W = 0, \quad (2.19)$$

$$\begin{aligned} D \nabla_c^2 \nabla_c^2 W - \left(1 - \frac{D}{Bh} \nabla_c^2 \right) \left(\frac{\partial^2 Z}{\partial X_1^2} \frac{\partial^2}{\partial X_2^2} - 2 \frac{\partial^2 Z}{\partial X_1 \partial X_2} \frac{\partial^2}{\partial X_1 \partial X_2} \right. \\ \left. + \frac{\partial^2 Z}{\partial X_2^2} \frac{\partial^2}{\partial X_1^2} \right) F = \left(1 - \frac{D}{Bh} \nabla_c^2 \right) q, \end{aligned} \quad (2.20)$$

$$\beta_1 + \frac{\partial W}{\partial X_1} = \frac{D}{hB} \left[\nabla_c^2 \beta_1 + \frac{1+\nu}{2c} \frac{\partial}{\partial X_2} \left(\frac{\partial \beta_2}{\partial X_1} - \frac{\partial \beta_1}{\partial X_2} \right) \right], \quad (2.21)$$

$$\beta_2 + \frac{\partial W}{\partial X_2} = \frac{D}{hB} \left[\nabla_c^2 \beta_2 + c \frac{1+\nu}{2} \frac{\partial}{\partial X_1} \left(\frac{\partial \beta_1}{\partial X_2} - \frac{\partial \beta_2}{\partial X_1} \right) \right]. \quad (2.22)$$

Equations (2.19) - (2.22) provide the formulation for an arbitrary shallow shell in terms of the unknown functions F, W, β_1 , and β_2 .

Now let us assume that in the domain of interest the curvatures of the shell are constant. Then in (2.19) and (2.20) the terms involving Z may be replaced by

$$\frac{\partial^2 Z}{\partial X_1^2} = -\frac{1}{R_1}, \quad \frac{\partial^2 Z}{\partial X_2^2} = -\frac{1}{R_2}, \quad \frac{\partial^2 Z}{\partial X_1 \partial X_2} = -\frac{1}{R_{12}}. \quad (2.23)$$

Also, following [4], if one introduces the dimensionless quantities given in Appendix A1, equations (2.19) - (2.22) may further be simplified as

$$\nabla^4 \phi - \frac{1}{\lambda^2} (\lambda_1^2 \frac{\partial^2}{\partial y^2} - 2\lambda_1^2 \frac{\partial^2}{\partial x \partial y} + \lambda_2^2 \frac{\partial^2}{\partial x^2}) w = 0 \quad (2.24)$$

$$\begin{aligned} \nabla^4 w + \lambda^2(1-\kappa\nabla^2) (\lambda_1^2 \frac{\partial^2}{\partial y^2} - 2\lambda_1^2 \frac{\partial^2}{\partial x \partial y} + \lambda_2^2 \frac{\partial^2}{\partial x^2}) \phi \\ = \lambda^4(1-\kappa\nabla^2) \frac{a}{h} q \quad , \end{aligned} \quad (2.25)$$

$$(1-\kappa\nabla^2) \beta_x + \frac{\partial w}{\partial x} = \kappa \frac{1+\nu}{2} \frac{\partial}{\partial y} \left(\frac{\partial \beta_y}{\partial x} - \frac{\partial \beta_x}{\partial y} \right) \quad , \quad (2.26)$$

$$(1-\kappa\nabla^2) \beta_y + \frac{\partial w}{\partial y} = \kappa \frac{1+\nu}{2} \frac{\partial}{\partial x} \left(\frac{\partial \beta_x}{\partial y} - \frac{\partial \beta_y}{\partial x} \right) \quad . \quad (2.27)$$

The constant a used in Appendix A1 to normalize various quantities is a characteristic length parameter in the shell. Usually in crack problems the shell is assumed to be "infinitely large" and a is taken to be the half crack length.

Defining now a new function Ω by

$$\Omega(x,y) = \frac{\partial \beta_x}{\partial y} - \frac{\partial \beta_y}{\partial x} \quad (2.28)$$

equations (2.26) and (2.27) may be expressed as

$$\left. \begin{aligned} \beta_x &= \kappa \nabla^2 \beta_x - \frac{\partial w}{\partial x} - \kappa \frac{1+\nu}{2} \frac{\partial \Omega}{\partial y} \quad , \\ \beta_y &= \kappa \nabla^2 \beta_y - \frac{\partial w}{\partial y} + \kappa \frac{1+\nu}{2} \frac{\partial \Omega}{\partial x} \quad . \end{aligned} \right\} \quad (2.29)$$

and, it may easily be shown that

$$\left. \begin{aligned} \nabla^2 \beta_x &= \frac{\partial \Omega}{\partial y} + \frac{\partial^2 \beta_x}{\partial x^2} + \frac{\partial^2 \beta_y}{\partial x \partial y} \quad , \\ \nabla^2 \beta_y &= -\frac{\partial \Omega}{\partial x} + \frac{\partial^2 \beta_x}{\partial x \partial y} + \frac{\partial^2 \beta_y}{\partial y^2} \quad . \end{aligned} \right\} \quad (2.30)$$

Also, if we define the function ψ by

$$\psi(x,y) = \kappa \left(\frac{\partial \beta_x}{\partial x} + \frac{\partial \beta_y}{\partial y} \right) - w \quad , \quad (2.31)$$

from (2.29) and (2.30) we obtain

$$\begin{aligned} \beta_x &= \frac{\partial \psi}{\partial x} + \kappa \frac{1-\nu}{2} \frac{\partial \Omega}{\partial y} \quad , \\ \beta_y &= \frac{\partial \psi}{\partial y} - \kappa \frac{1-\nu}{2} \frac{\partial \Omega}{\partial x} \quad . \end{aligned} \quad (2.32)$$

In (2.32) eliminating Ω and then using (2.31) we find

$$\kappa \nabla^2 \psi - \psi - w = 0 \quad . \quad (2.33)$$

Similarly, eliminating w , (2.29) yields

$$\kappa \frac{1-\nu}{2} \nabla^2 \Omega - \Omega = 0 \quad . \quad (2.34)$$

The solution of the shell problem must then satisfy the differential equations (2.24), (2.25), (2.33) and (2.34) and all the necessary boundary conditions.

3. CYLINDRICAL SHELL WITH A CIRCUMFERENTIAL CRACK

Consider now a cylindrical shell containing a circumferential through crack of length $2a$ shown in Figure 11. In this case $\lambda_1 = 0 = \lambda_{12}$, and if we further assume that $q = 0$, (2.24) and (2.25) become

$$\nabla^4 \phi - (\lambda_2/\lambda)^2 \frac{\partial^2 w}{\partial x^2} = 0 \quad , \quad (3.1)$$

$$\nabla^4 w + (\lambda \lambda_2)^2 (1-\kappa \nabla^2) \frac{\partial^2 \phi}{\partial x^2} = 0 \quad . \quad (3.2)$$

Eliminating ϕ , from (3.1) and (3.2) it follows that

$$\nabla^4 \nabla^4 w + \lambda_2^4 (1-\kappa \nabla^2) \frac{\partial^4 w}{\partial x^4} = 0 \quad . \quad (3.3)$$

The problem will be solved by using Fourier transforms. It will be assumed that through a proper superposition the original shell problem has been reduced to a perturbation problem in which self-equilibrating force and moment resultants acting on the crack surfaces are the only nonzero external loads (hence, the assumption $q = 0$). Thus, in some neighborhood of the crack in which the stresses are expected to be nonzero, the transform of w and its inversion may be expressed as

$$f(x, \alpha) = \int_{-\infty}^{\infty} w(x, y) e^{i\alpha y} dy \quad , \quad (3.4)$$

$$w(x, y) = \frac{1}{2\pi} \int_{-\infty}^{\infty} f(x, \alpha) e^{-i\alpha y} d\alpha \quad . \quad (3.5)$$

Substituting from (3.5) into (3.3) one obtains an 8th order ordinary linear differential equation in f . Looking for a solution in the form $f = R(\alpha) \exp(mx)$, the characteristic equation of the problem is found to be

$$m^8 - (\kappa \lambda_2^4 + 4\alpha^2)m^6 + (6\alpha^4 + \lambda_2^4 - \kappa \lambda_2^4 \alpha^2)m^4 - 4\alpha^6 m^2 + \alpha^8 = 0 \quad . \quad (3.6)$$

If we define

$$p = m^2 - \alpha^2 \quad (3.7)$$

equation (3.6) can be written in terms of p as follows:

$$p^4 - \kappa \lambda_2^4 p^3 + \lambda_2^4 (1 - 2\kappa \alpha^2) p^2 + \lambda_2^4 (2\alpha^2 - \kappa \alpha^4) p + \lambda_2^4 \alpha^4 = 0 \quad (3.8)$$

It should be emphasized that the roots of (3.8) are in general complex and, of course, are not known as a function of α in closed form. Appendix A2 describes a convenient procedure for solving (3.8). After solving (3.8) let the roots of (3.6) be ordered such that

$$\text{Re}(m_j) < 0 \quad , \quad m_{j+4} = -m_j, \quad j = 1, \dots, 4 \quad . \quad (3.9)$$

The solution $f(x, \alpha)$ of the resulting, ordinary differential equation satisfying the regularity conditions at $x = \pm\infty$ may then be expressed as

$$f(x, \alpha) = \begin{cases} \sum_{j=1}^4 R_j(\alpha) \exp(m_j x) & , \quad x > 0 \\ \sum_{j=5}^8 R_j(\alpha) \exp(m_j x) & , \quad x < 0 \end{cases} \quad (3.10)$$

If we let

$$\phi(x, y) = \frac{1}{2\pi} \int_{-\infty}^{\infty} g(x, \alpha) e^{-iy\alpha} d\alpha \quad (3.11)$$

from (3.1), (3.2) and (3.10) we find

$$g(x, \alpha) = \begin{cases} (\lambda_2/\lambda)^2 \sum_1^4 (m_j/p_j)^2 R_j(\alpha) \exp(m_j x) & , \quad x > 0 \\ (\lambda_2/\lambda)^2 \sum_5^8 (m_j/p_j)^2 R_j(\alpha) \exp(m_j x) & , \quad x < 0 \end{cases} \quad (3.12)$$

Similarly, assuming

$$\omega(x, y) = \frac{1}{2\pi} \int_{-\infty}^{\infty} h(x, \alpha) e^{-iy\alpha} d\alpha \quad (3.13)$$

from (2.34) we obtain

$$h(x, \alpha) = \begin{cases} A_1(\alpha) \exp(r_1 x) & , \quad x > 0 \\ A_2(\alpha) \exp(r_2 x) & , \quad x < 0 \end{cases} \quad (3.14)$$

where

$$r_1 = -[\alpha^2 + \frac{2}{\kappa(1-\nu)}]^{1/2} \quad , \quad r_2 = [\alpha^2 + \frac{2}{\kappa(1-\nu)}]^{1/2} \quad (3.15)$$

Also, let us assume that

$$\psi(x,y) = \frac{1}{2\pi} \int_{-\infty}^{\infty} \theta(x,\alpha) e^{-iy\alpha} d\alpha, \quad (3.16)$$

it can be shown that the remaining differential equation (2.33) is satisfied if θ is assumed to be

$$\theta(x,\alpha) = \begin{cases} \sum_{i=1}^4 \frac{R_j(\alpha)}{\kappa p_j - 1} \exp(m_j x) & , \quad x > 0 \\ \sum_{i=5}^8 \frac{R_j(\alpha)}{\kappa p_j - 1} \exp(m_j x) & , \quad x < 0 \end{cases} \quad (3.17)$$

The expressions given by (3.10), (3.12), (3.14), and (3.17) satisfy the differential equations of the problem^(*). If one now determines the arbitrary functions $R_j(\alpha)$, ($j=1, \dots, 8$) and $A_i(\alpha)$, ($i=1, 2$) in such a way that the boundary conditions of the problem are also satisfied, one then has the solution.

4. BOUNDARY CONDITIONS

As mentioned earlier, the only external loads in the problem are the self-equilibrating force and moment resultants on the crack surfaces. These forces can be decomposed in such a way that in solving the problem one needs to consider (with respect to $x=0$ plane) either symmetric or antisymmetric loading only. In these two cases the following conditions of symmetry will be satisfied:

$$\begin{aligned} N_{xx}(x,y) &= N_{xx}(-x,y) \quad , \quad N_{xy}(x,y) = -N_{xy}(-x,y) \quad , \\ M_{xx}(x,y) &= M_{xx}(-x,y) \quad , \quad M_{xy}(x,y) = -M_{xy}(-x,y) \quad , \\ V_x(x,y) &= -V_x(-x,y) \quad , \end{aligned} \quad (4.1)$$

^(*) It should perhaps be pointed out that (3.17) is a solution satisfying the differential equation (2.33), and is not the most general solution. However, with (3.17), since the solution thus found satisfies all the differential equations and, as will be shown, all the boundary conditions, it must be the solution of the physical problem.

for the symmetric problem, and

$$\begin{aligned} N_{xx}(x,y) &= -N_{xx}(-x,y) \quad , \quad N_{xy}(x,y) = N_{xy}(-x,y) \quad , \\ M_{xx}(x,y) &= -M_{xx}(-x,y) \quad , \quad M_{xy}(x,y) = M_{xy}(-x,y) \quad , \\ V_x(x,y) &= V_x(-x,y) \quad , \end{aligned} \quad (4.2)$$

for the antisymmetric problem. One may note that (4.1) and (4.2) are valid for all values of x and y , and in the odd functions the discontinuity at $x=0$ may be allowed only on the crack surface, outside the crack all these functions (indeed, all field quantities) must be continuous. It is therefore clear that in solving the problem one needs to consider only one half of the cylinder, say $x > 0$. Symmetry conditions similar to (4.1) and (4.2) are, of course valid for all the remaining field quantities. Thus, there are only five unknown functions R_1, \dots, R_4 , and A_1 which may be determined from five conditions specified at $x = +0$.

Consider now the symmetric problem for a circumferentially cracked shell. Noting that before the superposition which led to the perturbation problem the crack surfaces were free from all external loads, and since outside the crack all quantities are continuous, from (4.1) it may be concluded that

$$N_{xy}(0,y) = 0 \quad , \quad M_{xy}(0,y) = 0 \quad , \quad V_x(0,y) = 0 \quad , \quad -\infty < y < \infty \quad , \quad (4.3)$$

and $N_{xx}(+0,y)$ and $M_{xx}(+0,y)$ are known functions in $-1 < y < 1$. The problem is then a mixed boundary value problem. Using (4.3) three of the five unknowns (R_1, \dots, R_4, A_1) can be eliminated. The remaining two may be determined either from a system of dual integral equations or a system of singular integral equations arising from the mixed boundary conditions.

In terms of the normalized quantities the relevant force and moment resultants are given by

$$N_{xx} = \frac{\partial^2 \phi}{\partial y^2} \quad , \quad N_{xy} = - \frac{\partial^2 \phi}{\partial x \partial y} \quad ,$$

$$\begin{aligned}
M_{xx} &= \frac{a}{h\lambda^4} \left(\frac{\partial \beta_x}{\partial x} + \nu \frac{\partial \beta_y}{\partial y} \right) , \\
M_{xy} &= \frac{a}{h\lambda^4} \frac{1-\nu}{2} \left(\frac{\partial \beta_x}{\partial y} + \frac{\partial \beta_y}{\partial x} \right) , \\
\frac{\partial V_x}{\partial y} &= \frac{\partial^2 w}{\partial x \partial y} + \frac{\partial \beta_x}{\partial y} .
\end{aligned} \tag{4.4}$$

Using (4.4) and the results obtained in Sections 2 and 3, for $x > 0$ these quantities may be expressed in terms of R_1, \dots, R_4 and A_1 as follows:

$$N_{xx}(x, y) = -\frac{1}{2\pi} \int_{-\infty}^{\infty} \left[\left(\frac{\lambda^2}{\lambda} \right)^2 \alpha^2 \sum_1^4 \left(\frac{m_j}{p_j} \right)^2 R_j(\alpha) e^{m_j x} \right] e^{-iy\alpha} d\alpha , \tag{4.5}$$

$$N_{xy}(x, y) = \frac{i}{2\pi} \int_{-\infty}^{\infty} \left[\left(\frac{\lambda^2}{\lambda} \right)^2 \alpha \sum_1^4 \frac{m_j^3}{p_j^2} R_j(\alpha) e^{m_j x} \right] e^{-iy\alpha} d\alpha , \tag{4.6}$$

$$\begin{aligned}
M_{xx}(x, y) &= \frac{1}{2\pi} \frac{a}{h\lambda^4} \left[\int_{-\infty}^{\infty} \sum_1^4 \frac{m_j^2 - \nu \alpha^2}{\kappa p_j - 1} R_j(\alpha) e^{m_j x} e^{-iy\alpha} d\alpha \right. \\
&\quad \left. - \frac{\kappa(1-\nu)^2}{2} \int_{-\infty}^{\infty} i\alpha r_1 A_1(\alpha) e^{r_1 x} e^{-iy\alpha} d\alpha \right] ,
\end{aligned} \tag{4.7}$$

$$\begin{aligned}
M_{xy}(x, y) &= -\frac{1}{2\pi} \frac{a(1-\nu)}{h\lambda^4} \int_{-\infty}^{\infty} i\alpha \sum_1^4 \frac{m_j R_j(\alpha)}{\kappa p_j - 1} e^{m_j x} e^{-iy\alpha} d\alpha \\
&\quad - \frac{1}{2\pi} \frac{a\kappa}{h\lambda^4} \frac{(1-\nu)^2}{4} \int_{-\infty}^{\infty} (\alpha^2 + r_1^2) A_1(\alpha) e^{r_1 x} e^{-iy\alpha} d\alpha ,
\end{aligned} \tag{4.8}$$

$$\begin{aligned}
\frac{\partial}{\partial y} V_x(x, y) &= -\frac{1}{2\pi} \int_{-\infty}^{\infty} i\alpha \sum_1^4 \frac{\kappa p_j m_j}{\kappa p_j - 1} R_j(\alpha) e^{m_j x} e^{-iy\alpha} d\alpha \\
&\quad - \frac{1}{2\pi} \kappa \frac{1-\nu}{2} \int_{-\infty}^{\infty} \alpha^2 A_1(\alpha) e^{r_1 x} e^{-iy\alpha} d\alpha .
\end{aligned} \tag{4.9}$$

We will attempt to solve the problem by reducing it to a system of singular integral equations. The problem is "symmetric" and the "normal" membrane and moment resultants are specified on the crack surface. Therefore, the natural "dual" quantities which should be considered as the new unknown functions are

$$\frac{\partial}{\partial y} u(+0,y) = G_1(y) \quad , \quad \frac{\partial}{\partial y} \beta_x(+0,y) = G_2(y) \quad , \quad (4.10)$$

corresponding to the "normal" displacement and rotation on the crack surface, respectively. In (4.10) the derivatives of the dual quantities are used to make them dimensionally consistent with N_{xx} and M_{xx} and in order to insure that the resulting integral equations will have Cauchy type singularities [6]. The mixed boundary condition along $x=0$, $-\infty < y < \infty$ may now be expressed as follows:

$$\lim_{x \rightarrow +0} N_{xx}(x,y) = F_1(y) \quad , \quad -1 < y < 1 \quad , \quad (4.11)$$

$$\lim_{x \rightarrow +0} M_{xx}(x,y) = F_2(y) \quad , \quad -1 < y < 1 \quad , \quad (4.12)$$

$$u(0,y) = 0 \quad , \quad 1 < |y| < \infty \quad , \quad (4.13)$$

$$\beta_x(0,y) = 0 \quad , \quad 1 < |y| < \infty \quad . \quad (4.14)$$

Referring to the definitions (4.10) and the physical conditions (4.13) and (4.14), it is clear that the functions G_1 and G_2 must satisfy the following single-valuedness conditions:

$$\int_{-1}^1 G_1(y) dy = 0 \quad , \quad \int_{-1}^1 G_2(y) dy = 0 \quad . \quad (4.15)$$

From (2.4), (2.14), (2.8), and (2.1) it may be shown that

$$\frac{\partial^2}{\partial y^2} u(+0,y) = - \frac{\partial^3}{\partial x^3} \phi(+0,y) + (\lambda_2/\lambda)^2 \frac{\partial}{\partial x} w(+0,y) \quad . \quad (4.16)$$

Then, after some manipulations, the quantities defined by (4.10) may be obtained as follows:

$$G_1(y) = \left(\frac{\lambda_2}{\lambda}\right)^2 \frac{i}{2\pi} \int_{-\infty}^{\infty} \frac{1}{\alpha} \sum_1^4 \left(m_j - \frac{m_j^5}{p_j^2}\right) R_j(\alpha) e^{-iy\alpha} d\alpha \quad , \quad (4.17)$$

$$G_2(y) = - \frac{i}{2\pi} \int_{-\infty}^{\infty} \alpha \sum_1^4 \frac{m_j R_j(\alpha)}{\kappa p_j^{-1}} e^{-iy\alpha} d\alpha$$

$$-\frac{1}{2\pi} \kappa \frac{1-\nu}{2} \int_{-\infty}^{\infty} \alpha^2 A_1(\alpha) e^{-iy\alpha} d\alpha \quad (4.18)$$

Now, using (4.3) and inverting (4.6), (4.8), (4.9), (4.17), and (4.18), we obtain five linear algebraic equations in R_1, \dots, R_4 , and A_1 which, after some modifications and by using (4.13) and (4.14), may be expressed as

$$A_1(\alpha) = 2 \int_{-1}^1 G_2(t) e^{i\alpha t} dt \quad (4.19)$$

$$\sum_{j=1}^4 \frac{m_j^3}{p_j^2} R_j(\alpha) = 0 \quad (4.20)$$

$$\sum_{j=1}^4 \frac{m_j^5}{p_j^3} R_j(\alpha) = \frac{1-\nu}{\lambda_2^4} i\alpha \int_{-1}^1 G_2(t) e^{i\alpha t} dt \quad (4.21)$$

$$\sum_{j=1}^4 \frac{m_j^5}{p_j^4} R_j(\alpha) = i \frac{\kappa}{\lambda_2^4} \frac{1-\nu}{2\alpha} (\alpha^2 + r_1^2) \int_{-1}^1 G_2(t) e^{i\alpha t} dt \quad (4.22)$$

$$\sum_{j=1}^4 \frac{m_j}{p_j^2} R_j(\alpha) = -i(\lambda/\lambda_2)^2 \frac{1}{\alpha^3} \int_{-1}^1 G_1(t) e^{i\alpha t} dt \quad (4.23)$$

The solution of the system of equations (4.20) - (4.23) is given in Appendix A3. By substituting from (4.19), Appendix A3, (4.5) and (4.7) into (4.11) and (4.12), we obtain two integral equations to determine the unknown functions G_1 and G_2 of the following form:

$$\lim_{x \rightarrow +0} \int_{-1}^1 \sum_{j=1}^2 G_j(t) dt \int_{-\infty}^{\infty} H_{ij}(\alpha, x) e^{i(t-y)\alpha} d\alpha = F_i(y) \quad (4.24)$$

$$i = 1, 2, \quad -1 < y < 1$$

By examining the functions H_{ij} , it can be seen that they are bounded everywhere in $-\infty < \alpha < \infty$. Therefore any possible singularity of the kernels in (4.24) at $y = t$ must be due to the behavior of $H_{ij}(\alpha, x)$ as $\alpha \rightarrow \pm\infty$. Note also that H_{ij} contains exponential damping terms of the form $\exp(m_j x)$ and $\exp(r_1 x)$, where $\text{Re}(m_j) < 0$, $\text{Re}(r_1) < 0$. However, since in limit x will go to zero, for $y = t$ this damping does not insure the convergence of the inner integrals in (4.24).

The major difficulty in this problem, of course, is that the functions $m_j(\alpha)$ are not known explicitly in terms of α . For the purpose of examining the singular behavior of the kernels in (4.24) and for extracting the singular parts, all one needs, however, is the asymptotic behavior of m_j and r_1 as $|\alpha| \rightarrow \infty$. Thus, from (3.6) - (3.8) and (3.15) it can be shown that for large values of $|\alpha|$ we have

$$m_j(\alpha) = -|\alpha| \left(1 + \frac{p_j}{2\alpha^2} - \frac{p_j^2}{8\alpha^4} + \dots \right) , \quad (4.25)$$

$$r_1(\alpha) = -|\alpha| \left(1 + \frac{1}{\kappa(1-\nu)\alpha^2} - \dots \right) . \quad (4.26)$$

Using now the relations (4.25) and (4.26) and separating the asymptotic values of H_{ij} for large $|\alpha|$, the kernels in (4.24) may be expressed as

$$\begin{aligned} \int_{-\infty}^{\infty} H_{ij} e^{i(t-y)\alpha} d\alpha &= \int_{-\infty}^{\infty} H_{ij}^{\infty}(\alpha, x) e^{i(t-y)\alpha} d\alpha \\ &+ \int_{-\infty}^{\infty} [H_{ij}(\alpha, x) - H_{ij}^{\infty}(\alpha, x)] e^{i(t-y)\alpha} d\alpha . \end{aligned} \quad (4.27)$$

where H_{ij}^{∞} is the asymptotic value of H_{ij} for $|\alpha| \rightarrow \infty$. On the right hand side of (4.27) the first term gives Cauchy type kernels $1/(t-y)$ on the main diagonal terms, and the second integrals are uniformly convergent for all t and y (in which, the limit $x=0$ can therefore be put under the integral sign). After the asymptotic analysis and some lengthy but straightforward manipulations the integral equations and the kernels may then be expressed as follows:

$$\int_{-1}^1 \frac{1G_1(t)}{t-y} dt + \sum_1^2 \int_{-1}^1 k_{1j}(y, t) G_j(t) dt = 2\pi F_1(y) , \quad -1 < y < 1 , \quad (4.28)$$

$$\begin{aligned} \frac{1-\nu^2}{\lambda^4} \int_{-1}^1 \frac{G_2(t)}{t-y} dt + \sum_1^2 \int_{-1}^1 k_{2j}(y, t) G_j(t) dt \\ = 2\pi \frac{h}{a} F_2(y) , \quad -1 < y < 1 , \end{aligned} \quad (4.29)$$

$$k_{11}(y,t) = \int_0^{\infty} \left[\left(\frac{\lambda_2}{\lambda} \right)^2 \alpha^2 \sum_1^4 \frac{2m_j^2}{p_j^2} Q_j(\alpha) - 1 \right] \sin \alpha(t-y) d\alpha, \quad (4.30)$$

$$k_{12}(y,t) = 2 \left(\frac{\lambda_2}{\lambda} \right)^2 \int_0^{\infty} \alpha^2 \sum_1^4 \frac{m_j^2}{p_j^2} N_j(\alpha) \sin \alpha(t-y) d\alpha, \quad (4.31)$$

$$k_{21}(y,t) = - \frac{2\lambda_2^4}{\lambda^4} \int_0^{\infty} \sum_1^4 \frac{1}{p_j^2} (m_j^2 - v\alpha^2) m_j^4 Q_j(\alpha) \sin \alpha(t-y) d\alpha, \quad (4.32)$$

$$k_{22}(y,t) = -2 \frac{1}{\lambda} \int_0^{\infty} \left[\sum_1^4 \frac{\lambda_2^2}{p_j^2} (m_j^2 - v\alpha^2) m_j^4 N_j(\alpha) \right. \\ \left. - \kappa(1-v)^2 \alpha r_1 + \frac{1-v^2}{2} \right] \sin \alpha(t-y) d\alpha, \quad (4.33)$$

where the functions $N_j(\alpha)$ and $Q_j(\alpha)$ are given in the Appendix A3. Using the results of Appendix A3 it can be shown that $k_{12}(y,t) = k_{21}(y,t)$.

5. THE ASYMPTOTIC STRESS FIELD AROUND THE CRACK TIPS

The solutions of the singular integral equations (4.28) and (4.29) have integrable singularities at the end points $y = \pm 1$ and are of the following form:

$$G_i(y) = g_i(y)(1-y^2)^{-1/2}, \quad i=1,2, \quad (5.1)$$

where g_1 and g_2 are bounded in $-1 \leq y \leq 1$. Similar to the plane problems, it can be shown that the behavior of the stress distribution in the immediate neighborhood of the crack tips is dependent on $g_i(\pm 1)$ only. To show this, one needs to substitute (5.1) through the expressions of R_1, \dots, R_4 given in Appendix A3 and A_1 given by (4.19) into the original expressions for N_{ij} and M_{ij} , ($i, j = x, y$), such as those given by (4.5) - (4.8). Using now the relation [7]

$$\int_0^{\infty} \alpha^{\mu-1} e^{-b\alpha} \left\{ \begin{matrix} \sin \\ \cos \end{matrix} \right\} (c\alpha) d\alpha = \frac{\Gamma(\mu)}{(b^2+c^2)^{\mu/2}} \left\{ \begin{matrix} \sin \\ \cos \end{matrix} \right\} (\mu \tan^{-1} \frac{c}{b}), \quad (b>0, \mu>0), \quad (5.2)$$

and [4, 2, 3] for large values of $|\alpha|$

$$\int_{-1}^1 \frac{g(t)}{\sqrt{1-t^2}} e^{i\alpha t} dt = \left(\frac{\pi}{2|\alpha|}\right)^{1/2} \{g(1)\exp[i(\alpha - \frac{\pi}{4} \text{sign}(\alpha))] + g(-1)\exp[-i(\alpha - \frac{\pi}{4} \text{sign}(\alpha))] + 0 \left(\frac{1}{|\alpha|}\right)\} , \quad (5.3)$$

around the end point $y=1$, $x=0$ the leading terms of the asymptotic stress and moment resultants may be expressed as

$$N_{xx}(x,y) \equiv \frac{g_1(1)}{2\sqrt{2\pi}} \int_0^\infty \frac{1}{\sqrt{\alpha}} (1 + \alpha|x|) e^{-|x|\alpha} \sin[(1-y)\alpha - \frac{\pi}{4}] d\alpha , \quad (5.4)$$

$$N_{yy}(x,y) \equiv \frac{g_1(1)}{2\sqrt{2\pi}} \int_0^\infty \frac{1}{\sqrt{\alpha}} (1 - \alpha|x|) e^{-|x|\alpha} \sin[(1-y)\alpha - \frac{\pi}{4}] d\alpha , \quad (5.5)$$

$$N_{xy}(x,y) \equiv \frac{g_1(1)}{2\sqrt{2\pi}} \int_0^\infty \sqrt{\alpha} x e^{-|x|\alpha} \cos[(1-y)\alpha - \frac{\pi}{4}] d\alpha , \quad (5.6)$$

$$M_{xx}(x,y) \equiv \frac{g_2(1)}{2\sqrt{2\pi}} \frac{h}{12a} \int_0^\infty \frac{1}{\sqrt{\alpha}} (1 + \alpha|x|) e^{-|x|\alpha} \sin[(1-y)\alpha - \frac{\pi}{4}] d\alpha , \quad (5.7)$$

$$M_{yy}(x,y) \equiv \frac{g_2(1)}{2\sqrt{2\pi}} \frac{h}{12a} \int_0^\infty \frac{1}{\sqrt{\alpha}} (1 - \alpha|x|) e^{-|x|\alpha} \sin[(1-y)\alpha - \frac{\pi}{4}] d\alpha , \quad (5.8)$$

$$M_{xy}(x,y) \equiv \frac{g_2(1)}{2\sqrt{2\pi}} \frac{h}{12a} \int_0^\infty \sqrt{\alpha} x e^{-|x|\alpha} \cos[(1-y)\alpha - \frac{\pi}{4}] d\alpha , \quad (5.9)$$

From (5.4) - (5.9) it is seen that, aside from the magnitudes as represented by $g_1(1)$ and $g_2(1)$, the asymptotic behavior of the membrane and bending stress distributions around the crack tip will be identical. This is, of course, in agreement with the uncoupled in-plane and bending results for flat plates [8-10]. Defining the polar coordinates r, θ by

$$x = r \sin \theta , \quad y - 1 = r \cos \theta , \quad (5.10)$$

evaluating the integrals, and observing that in dimensionless quantities (see Appendix A1)

$$\frac{12az}{h} M_{ij} = \sigma_{ij}, \quad (i, j = x, y), \quad (5.11)$$

from (5.4) - (5.9) the asymptotic stress distribution may be obtained as

$$\sigma_{xx}(r, \theta, z) \cong - \frac{g_1(1) + zg_2(1)}{2\sqrt{2r}} \left[\frac{5}{4} \cos \frac{\theta}{2} - \frac{1}{4} \cos \frac{5\theta}{2} \right], \quad (5.12)$$

$$\sigma_{yy}(r, \theta, z) \cong - \frac{g_1(1) + zg_2(1)}{2\sqrt{2r}} \left[\frac{3}{4} \cos \frac{\theta}{2} + \frac{1}{4} \cos \frac{5\theta}{2} \right], \quad (5.13)$$

$$\sigma_{xy}(r, \theta, z) \cong - \frac{g_1(1) + zg_2(1)}{2\sqrt{2r}} \left[-\frac{1}{4} \sin \frac{\theta}{2} + \frac{1}{4} \sin \frac{5\theta}{2} \right]. \quad (5.14)$$

In this "symmetric" problem the stress intensity factor is defined by

$$k_1(x_3) = \lim_{x_2 \rightarrow a} \sqrt{2(x_2 - a)} \sigma_{11}(0, x_2, x_3), \quad (5.15)$$

which, referring to Appendix A1 and (5.12) may be obtained in terms of $g_1(1)$ and $g_2(1)$ as follows:

$$k_1(x_3) = - \frac{E\sqrt{a}}{2} [g_1(1) + \frac{z}{a} g_2(1)] \quad (5.16)$$

It should be noted that even though the analysis given in the previous sections is valid for specially orthotropic as well as isotropic shells, (a) because of the dependence of x and y on the orthotropy constant $c = (E_1/E_2)^{1/2}$, r and θ defined by (5.10) are not the physical coordinates, and consequently the angular distribution of the stress state in orthotropic shells would be different from that of isotropic shells as given by (5.12) - (5.14); and (b) since the roots m_j and r_i are very heavily dependent on c , the numerical results obtained for the isotropic shells by assuming $c = 1$ cannot be readily adopted to the orthotropic shells.

6. CRACK SURFACE DISPLACEMENTS

After obtaining the functions G_1 and G_2 upon solving the integral equations (4.28) and (4.29), through the expressions for R_1, \dots, R_4 , and

A_1 , any desired field quantity in the shell can be expressed in terms of G_1 and G_2 and be easily evaluated. One such group of quantities of some practical interest is the components of crack surface displacement vector. In the symmetric problem under consideration, referring to the definition (4.10), the in-plane component of the crack surface displacement (i.e., the crack opening displacement) may easily be obtained as

$$u(+0,y) = - \int_y^1 G_1(t) dt \quad , \quad -1 < y < 1 \quad . \quad (6.1)$$

The component of the displacement vector which is perpendicular to the shell surface, i.e., $w(x,y)$, is given by (3.5) and (3.10). Expressing again R_1, \dots, R_4 in terms of G_1 and G_2 (Appendix A3), w may be obtained as follows:

$$\begin{aligned} w(+0,y) = & - \frac{1}{\pi} \int_{-1}^1 G_1(t) dt \int_0^\infty \sum_1^4 Q_j(\alpha) \sin \alpha(t-y) d\alpha \\ & - \frac{1}{\pi} \int_{-1}^1 G_2(t) dt \int_0^\infty \sum_1^4 N_j(\alpha) \sin \alpha(t-y) d\alpha \quad , \\ & -1 < y < 1 \quad , \quad (6.2) \end{aligned}$$

where Q_j and N_j are given in Appendix A3.

7. NUMERICAL SOLUTION AND RESULTS

The singular integral equations (4.28) and (4.29) subject to single-valuedness conditions (4.15) are solved by using Gauss-Chebyshev integration formulas. Thus, equations (4.28), (4.29) and (4.15) are, respectively, replaced by

$$\begin{aligned} \sum_{j=1}^n w_j \left[\frac{g_1(t_j)}{t_j - y_i} + \sum_{m=1}^2 k_{1m}(y_i, t_j) g_m(t_j) \right] = 2\pi F_1(y_i) \quad , \\ i = 1, \dots, n-1 \quad . \quad (7.1) \end{aligned}$$

$$\sum_{j=1}^n W_j \left[\frac{1-\nu^2}{\lambda^4} \frac{g_2(t_j)}{t_j - y_i} + \sum_{m=1}^2 k_{2m}(y_i, t_j) g_m(t_j) \right] \\ = 2\pi \frac{h}{a} F_2(y_i) \quad , \quad i=1, \dots, n-1 \quad , \quad (7.2)$$

$$\sum_{j=1}^n W_j g_1(t_j) = 0 \quad , \quad \sum_{j=1}^n W_j g_2(t_j) = 0 \quad , \quad (7.3)$$

where

$$t_j = \cos\left(\frac{j-1}{n-1} \pi\right) \quad , \quad j=1, \dots, n \quad , \quad (7.4)$$

$$y_i = \cos\left(\frac{2i-1}{2n-2} \pi\right) \quad , \quad i=1, \dots, n-1 \quad , \quad (7.5)$$

$$W_1 = W_n = \frac{\pi}{2(n-1)} \quad , \quad W_j = \frac{\pi}{n-1} \quad , \quad j=2, \dots, n-1 \quad . \quad (7.6)$$

As a numerical example a cracked cylindrical shell under uniform membrane and bending loads is considered. To make the practical applications of the results more convenient, these two loads are considered separately. The calculated results for the stress intensity factors are normalized with respect to the corresponding flat plate values. For example, if the applied loads are

$$N_{11}(0, X_2) = -N_{11} = -h\sigma_m \quad , \quad M_{11}(0, X_2) = 0 \quad , \quad -a < X_2 < a \quad , \quad (7.7)$$

the input functions in the integral equations (4.28) and (4.29) become

$$F_1(y) = -N_{11}/hE \quad , \quad F_2(y) = 0 \quad , \quad (7.8)$$

and the corresponding flat plate stress intensity factor is $\sigma_m \sqrt{a}$. Then the membrane and bending stress intensity ratios k_{mm} and k_{bm} are obtained from (5.16) as follows:

$$k_{mm} = \frac{k_1(0)}{\sigma_m \sqrt{a}} = -\frac{E}{2\sigma_m} g_1(1) \quad , \quad (7.9)$$

$$k_{bm} = \frac{k_1(h/2) - k_1(0)}{\sigma_m \sqrt{a}} = -\frac{E}{2\sigma_m} \frac{h}{2a} g_2(1) \quad (7.10)$$

The "bending stress intensity factor" is thus based on the bending stresses at the outer layer of the shell, $x_3 = +h/2$.

Similarly, if the external loads are

$$N_{11}(0, x_2) = 0, \quad M_{11}(0, x_2) = -M_{11} = -\frac{h^2}{6} \sigma_b, \quad -a < x_2 < a \quad (7.11)$$

Then the input functions become

$$F_1(y) = 0, \quad F_2(y) = -\frac{M_{11}}{Eh^2}, \quad -1 < y < 1 \quad (7.12)$$

In this case too the corresponding flat plate stress intensity factor is defined by $\sigma_b \sqrt{a}$, and the stress intensity factor ratios are obtained as follows:

$$k_{mb} = \frac{k_1(0)}{\sigma_b \sqrt{a}} = -\frac{E}{2\sigma_b} g_1(1), \quad (7.13)$$

$$k_{bb} = \frac{k_1(h/2) - k_1(0)}{\sigma_b \sqrt{a}} = -\frac{E}{2\sigma_b} \frac{h}{2a} g_2(1) \quad (7.14)$$

In the numerical calculations the effective transverse shear modulus for the shell is assumed to be $B = 5G/6$, G being the shear modulus of the material. Also, the Poisson's ratio is taken as $\nu = 1/3$ in all calculations except for one set of results where the effect of ν is investigated. One may note that λ_2 is used in this analysis is the standard shell parameter λ defined in the formulation of the problem by using the classical (i.e., the 8th order) shell theory. Also note that in the present analysis there is an additional parameter a/h , which, within the confines of the shallow shell theory, gives the thickness effect.

The numerical results are shown in Tables 1-4. To help visualizing the trends some of the results are also shown in Figures 14-17. Tables 1-4 show the stress intensity factor ratios k_{mm} , k_{bm} , k_{mb} , and k_{bb} defined by

(7.9), (7.10), (7.13) and (7.14), respectively. In this table the values given for $\lambda_2 = [12(1-\nu^2)]^{\frac{1}{4}} a/\sqrt{Rh} = 0$ correspond to the flat plate. Both λ_2 and a/h have been varied from 0 to 10. For $\lambda_2 > 10$ and $a/h > 10$ the linearized shallow shell theory used in this study is probably not valid. For very thin shells (i.e., $a/h = 10$) under uniform membrane loading (Table 1a,b and Figures 14, 15) it is found that the membrane component of the stress intensity factor k_{mm} is indistinguishable from the results found by using the classical theory [11]. However, the bending stress intensity factor k_{bm} is quite different. The results given in Table 1 show that, particularly for large values of λ_2 , the thickness parameter a/h may have considerable effect on the stress intensity factors. Table 1 and Figure 16 show that when $\lambda_2 \rightarrow 0$ the results are in good agreement with the flat plate bending results given in [9] and [10] and the axially cracked shell results given in [4].

For a specific geometry $\lambda_2 = 3$ and $a/h = 5$, Table 2 shows the effect of the Poisson's ratio ν on the stress intensity factors. For the two most important components k_{mm} and k_{bb} (i.e., for the primary stress intensity factors under membrane and bending loads) the effect of ν does not seem to be significant. Hence the results given in Table 1 and calculated for $\nu = 1/3$ can be used for materials with a Poisson's ratio $0.2 < \nu < 0.4$, which may cover nearly all structural materials.

Even though the numerical results given in this report regarding the stress intensity factors are for uniform membrane loading and for pure bending, the formulation is quite general and the results may easily be obtained for any symmetric loading condition. For example, Table 3 gives the stress intensity factors for two simple loading conditions which may have some practical applications, namely a concentrated wedge force and a concentrated bending moment acting at the center section of the crack.

In pipelines and tank cars an important loading condition which gives axial stresses in the cylinder is gross bending. Referring to Figure 13, let the cylinder be subjected to a bending moment M_0 acting in X_1X_3 plane and having a neutral plane going through the cylinder axis parallel to the X_1X_2 plane. Let the crack be located on the tensile

side. Thus, the stress in the cylinder wall (which must be used with the opposite sign as the crack surface traction in solving the crack problem) is given by

$$\sigma_{11} = \frac{M_0 z_0}{I}, \quad I = Rh(4R^2 + h^2), \quad (7.15)$$

where I is the area moment of inertia of the cylinder cross-section and z_0 is the distance from the neutral plane. From the shell geometry z_0 may be expressed as

$$z_0 = (R + X_3)\cos\theta, \quad 0 \leq \theta \leq \pi, \quad |X_3| \leq h/2 \quad (7.16)$$

where R is the mean radius, X_3 is the thickness coordinate measured from the midsurface of the cylinder, h is the thickness and the circumferential angle θ is measured from the location of the maximum tensile stress (i.e., from $X_2=0$ plane). For relatively small values of θ we have

$$\cos\theta \cong 1 - \frac{\theta^2}{2} \cong 1 - \frac{X_2^2}{2R^2} \quad (7.17)$$

From (7.15)-(7.17) it follows that

$$\sigma_{11} = \frac{M_0 R}{I} \left(1 - \frac{X_2^2}{2R^2}\right) + \frac{M_0 X_3}{I} \left(1 - \frac{X_2^2}{2R^2}\right) \quad (7.18)$$

In (7.18) the first term is a membrane stress σ_{11}^m and the second term is a (local) bending stress σ_{11}^b . From (7.18) these stresses may be expressed as

$$\sigma_{11}^m = \frac{M_0 R}{I} \left(1 - \frac{a^2}{2R^2}\right) + \frac{M_0 R}{I} \frac{a^2}{2R^2} (1 - y^2), \quad (7.19)$$

$$\sigma_{11}^b = \frac{M_0 X_3}{I} \left(1 - \frac{a^2}{2R^2}\right) + \frac{M_0 X_3}{I} \frac{a^2}{2R^2} (1 - y^2), \quad y = \frac{X_2}{a} \quad (7.20)$$

Thus, it is seen that to obtain the gross bending results the integral equations must be solved by using y -independent crack surface loads as shown by the first terms in (7.19) and (7.20) and parabolic load distributions given by the second terms in (7.19) and (7.20). The results for the uniform membrane and bending loads are given in Table 1. Table 4 shows the stress intensity factor ratios for (see Eqs. (7.7)-(7.14))

$$N_{11}(0, X_2) = -h \sigma_m (1-y^2), \quad M_{11}(0, X_2) = 0, \quad y = \frac{X_2}{a} \quad (7.21)$$

and

$$N_{11}(0, X_2) = 0, \quad M_{11}(0, X_2) = -\frac{h^2}{6} \sigma_b (1-y^2), \quad y = \frac{X_2}{a}, \quad (7.22)$$

where

$$\sigma_m = \frac{M_o R}{I} \frac{a^2}{2R^2}, \quad \sigma_b = \frac{M_o h}{2I} \frac{a^2}{2R^2} \quad (7.23)$$

The final stress intensity factor may be obtained by a proper superposition of the results given in Tables 1 and 4.

REFERENCES

1. P. M. Naghdi, "Note on the Equations of Shallow Elastic Shells", Quart. Appl. Math., Vol. 14, p. 331 (1956).
2. U. Yuceoglu and F. Erdogan, "A Cylindrical Shell with an Axial Crack under Skew-Symmetric Loading", Int. J. Solids Structures, Vol. 9, p. 347 (1973).
3. F. Erdogan, "Crack Problems in Cylindrical and Spherical Shells", in Plates and Shells with Cracks, G. C. Sih, ed., Noordhoff International Publishing, Leyden, pp. 161-199 (1977).
4. S. Krenk, "Influence of Transverse Shear on an Axial Crack in a Cylindrical Shell", Int. Journal of Fracture, Vol. 14, pp. 123-143 (1978).
5. E. Reissner, "On Bending of Elastic Plates", Quart. Appl. Math., Vol. 5, p. 55 (1947).
6. F. Erdogan, "Complex Function Technique", in Continuum Physics, Vol. II, A. C. Eringen, ed., Academic Press, pp. 523-603 (1975).
7. I. S. Gradshteyn and I. M. Ryzhik, Table of Integrals, Series and Products, Academic Press (1965).
8. J. K. Knowles and N. M. Wang, "On the Bending of an Elastic Plate Containing a Crack", J. of Mathematics and Physics, Vol. 39, p. 223 (1960).
9. N. M. Wang, "Effects of Plate Thickness on the Bending of an Elastic Plate Containing a Crack", J. of Mathematics and Physics, Vol. 47, p. 371 (1968).
10. R. J. Hartranft and G. C. Sih, "Effect of Plate Thickness on the Bending Stress Distribution Around Through Cracks", J. of Mathematics and Physics, Vol. 47, p. 276 (1968).
11. F. Erdogan and M. Ratwani, "Fatigue and Fracture of Cylindrical Shells Containing a Circumferential Crack", Int. J. Fracture Mechanics, Vol. 6, pp. 379-392 (1970).

APPENDIX A1. The Dimensionless Quantities

$$x = \frac{1}{\sqrt{c}} \frac{X_1}{a}, \quad y = \sqrt{c} \frac{X_2}{a}, \quad z = \frac{X_3}{a}, \quad (\text{A.1})$$

$$\left. \begin{aligned} u &= \sqrt{c} \frac{U_1}{a}, \quad v = \frac{1}{\sqrt{c}} \frac{U_2}{a}, \quad w = \frac{W}{a}, \end{aligned} \right\} (\text{A.2})$$

$$\left. \begin{aligned} \beta_x &= \sqrt{c} \beta_1, \quad \beta_y = \frac{1}{\sqrt{c}} \beta_2, \quad \phi = \frac{F}{a^2 h E} \end{aligned} \right\}$$

$$\sigma_{xx} = \frac{\sigma_{11}}{cE}, \quad \sigma_{yy} = \frac{c\sigma_{22}}{E}, \quad \sigma_{xy} = \frac{\sigma_{12}}{E} \quad (\text{A.3})$$

$$N_{xx} = \frac{N_{11}}{chE}, \quad N_{yy} = \frac{cN_{22}}{hE}, \quad N_{xy} = \frac{N_{12}}{hE} \quad (\text{A.4})$$

$$M_{xx} = \frac{M_{11}}{ch^2E}, \quad M_{yy} = \frac{cM_{22}}{h^2E}, \quad M_{xy} = \frac{M_{12}}{h^2E} \quad (\text{A.5})$$

$$V_x = \frac{V_1}{\sqrt{c} hB}, \quad V_y = \frac{\sqrt{c} V_2}{hB}, \quad (\text{A.6})$$

$$\lambda_1^4 = 12(1-\nu^2) \frac{c^2 a^4}{h^2 R_1^2}, \quad \lambda_2^4 = 12(1-\nu^2) \frac{a^4}{c^2 h^2 R_2^2},$$

$$\lambda_{12}^4 = 12(1-\nu^2) \frac{a^4}{h^2 R_{12}^2}, \quad \lambda^4 = 12(1-\nu^2) \frac{a^2}{h^2}, \quad \kappa = \frac{E}{B\lambda^4} \quad (\text{A.7})$$

APPENDIX A2. Procedure for Solving a Quartic Equation

Consider the following quartic equation:

$$p^4 + a_3p^3 + a_2p^2 + a_1p + a_0 = 0 \quad (\text{B.1})$$

Although in the shell problem the coefficients a_0, \dots, a_3 are real, for the sake of generality, here it will be assumed that they are complex. Therefore the roots of (B.1) are in general complex. Assume that (B.1) can be written as the difference of two squares:

$$(p^2 + Ap + B)^2 - (Cp + D)^2 = 0 \quad , \quad (\text{B.2})$$

Then, from (B.2) it follows that

$$p^2 + (A + C)p + (B + D) = 0 \quad , \quad (\text{B.3})$$

$$p^2 + (A - C)p + (B - D) = 0 \quad . \quad (\text{B.4})$$

If the constants A, B, C, D can be determined in terms of a_3, a_2, a_1, a_0 , then the four roots can be found in a straight-forward manner by solving equations (B.3) and (B.4).

Comparing (B.1) and (B.2), one can write:

$$2A = a_3 \quad , \quad (\text{B.5})$$

$$2B + A^2 - C^2 = a_2 \quad , \quad (\text{B.6})$$

$$2AB - 2CD = a_1 \quad , \quad (\text{B.7})$$

$$B^2 - D^2 = a_0 \quad . \quad (\text{B.8})$$

Eliminating C and D in (B.6) - (B.8) and defining $2B = u$, one finds:

$$u^3 + b_2 u^2 + b_1 u + b_0 = 0 \quad (\text{B.9})$$

where

$$b_2 = -a_2, \quad b_1 = a_1 a_3 - 4a_0, \quad b_0 = 4a_0 a_2 - a_1^2 - a_0 a_3^2. \quad (\text{B.10})$$

Let u_1 be a root of the cubic equation (B.9), (see, for example [15] for determining the roots of a cubic). Then

$$B = \frac{u_1}{2} \quad (\text{B.11})$$

and from (B.5)

$$A = \frac{a_3}{2}. \quad (\text{B.12})$$

Once A and B are known, one can determine C and D from (B.6) and (B.8) as follows:

$$C^2 = u_1 + \frac{a_3^2}{4} - a_2 \quad (\text{B.13})$$

$$D^2 = \frac{u_1^2}{4} - a_0 \quad (\text{B.14})$$

It is seen that C and D are multiple-valued functions and one should choose the correct branch in order to obtain the correct solution.

C^2 and D^2 can be written in the complex form as follows:

$$C^2 = \rho_1 e^{i\theta_1}, \quad D^2 = \rho_2 e^{i\theta_2} \quad (\text{B.15})$$

where ρ_1 , ρ_2 , θ_1 and θ_2 can be determined by using (B.13) and (B.14). Thus

$$C_1 = \sqrt{\rho_1} e^{i\theta_1/2}, \quad C_2 = \sqrt{\rho_1} e^{i(\theta_1/2 + \pi)}$$

$$D_1 = \sqrt{\rho_2} e^{i\theta_2/2}, \quad D_2 = \sqrt{\rho_2} e^{i(\theta_2/2 + \pi)} \quad (\text{B.16})$$

All pairs of (C,D) satisfy equations (B.6) and (B.8) but not (B.7). Therefore C and D must be selected such that equation (B.7) is satisfied, i.e.,

$$2CD = \frac{u_1 a_3}{2} - a_1 \quad (B.17)$$

APPENDIX A3. Expressions for $R_j(\alpha)$, $j = 1, \dots, 4$

$$R_j(\alpha) = i[Q_j(\alpha) \int_{-1}^1 G_1(t) e^{i\alpha t} dt + N_j(\alpha) \int_{-1}^1 G_2(t) e^{i\alpha t} dt] \quad (C.1)$$

$$\begin{aligned} N_1(\alpha) = & \frac{1}{D(\alpha)} \frac{m_2 m_3 m_4}{(p_2 p_3 p_4)^2} \left\{ -\alpha \frac{1-\nu}{\lambda_2^4} \left[m_2^2 \left(\frac{m_3^4}{p_3^2} - \frac{m_4^4}{p_4^2} \right) \right. \right. \\ & - m_3^2 \left(\frac{m_2^4}{p_2^2} - \frac{m_4^4}{p_4^2} \right) + m_4^2 \left(\frac{m_2^4}{p_2^2} - \frac{m_3^4}{p_3^2} \right) \\ & + \frac{\kappa}{\lambda_2^4} \frac{1-\nu}{2\alpha} (\alpha^2 + r_1^2) \left[m_2^2 \left(\frac{m_3^4}{p_3} - \frac{m_4^4}{p_4} \right) \right. \\ & \left. \left. - m_3^2 \left(\frac{m_2^4}{p_2} - \frac{m_4^4}{p_4} \right) + m_4^2 \left(\frac{m_2^4}{p_2} - \frac{m_3^4}{p_3} \right) \right] \right\} \quad (C.2) \end{aligned}$$

$$\begin{aligned} Q_1(\alpha) = & \frac{1}{D(\alpha)} \left(\frac{\lambda}{\lambda_2} \right)^2 \frac{1}{\alpha^3} \frac{(m_2 m_3 m_4)^3}{(p_2 p_3 p_4)} \left[\left(\frac{m_3^2}{p_3} \frac{m_4^2}{p_4} - \frac{m_4^2}{p_4} \frac{m_3^2}{p_3} \right) \right. \\ & \left. - \left(\frac{m_2^2}{p_2} \frac{m_4^2}{p_4} - \frac{m_4^2}{p_4} \frac{m_2^2}{p_2} \right) + \left(\frac{m_2^2}{p_2} \frac{m_3^2}{p_3} - \frac{m_3^2}{p_3} \frac{m_2^2}{p_2} \right) \right] \quad (C.3) \end{aligned}$$

$$\begin{aligned} D(\alpha) = & \frac{m_1 m_2 m_3 m_4}{(p_1 p_2 p_3 p_4)^2} \left\{ (m_1^2 - m_2^2)(m_3^2 - m_4^2) \left(\frac{m_1^4 m_2^4}{(p_1 p_2)^2} + \frac{m_3^4 m_4^4}{(p_3 p_4)^2} \right) \right. \\ & + (m_1^2 - m_3^2)(m_4^2 - m_2^2) \left(\frac{m_1^4 m_3^4}{(p_1 p_3)^2} + \frac{m_2^4 m_4^4}{(p_2 p_4)^2} \right) \\ & \left. + (m_1^2 - m_4^2)(m_2^2 - m_3^2) \left(\frac{m_1^4 m_4^4}{(p_1 p_4)^2} + \frac{m_2^4 m_3^4}{(p_2 p_3)^2} \right) \right\} \quad (C.4) \end{aligned}$$

The expressions of N_2 and Q_2 are obtained from (C.2) and (C.3) by replacing the indices in m_j and p_j sequentially from 2, 3, 4 to 3, 4, 1. Similarly for N_3 and Q_3 the indices are replaced by 4, 1, 2, and for N_4 and Q_4 by 1, 2, 3.

Table A-1. Stress intensity factor ratios in a cylindrical shell containing a circumferential through crack ($\nu = 1/3$)

	λ_2	a/h=0.5	a/h=1	a/h=2	a/h=5	a/h=10
k_{mm}	0.0	1.000	1.000	1.000	1.000	1.000
	0.5	1.015	1.013	1.012	1.012	1.012
	1.0		1.055	1.050	1.048	1.048
	1.5			1.108	1.103	1.102
	2.0			1.179	1.169	1.168
	3.0				1.317	1.314
	4.0				1.467	1.462
	5.0				1.610	1.604
	6.0					1.735
	8.0					1.970
	10.0					2.181
k_{bm}	0.0	0.000	0.000	0.000	0.000	0.000
	0.5	0.048	0.044	0.043	0.041	0.041
	1.0		0.093	0.092	0.092	0.092
	1.5			0.114	0.119	0.123
	2.0			0.107	0.119	0.125
	3.0				0.057	0.071
	4.0				-0.042	-0.024
	5.0				-0.143	-0.126
	6.0					-0.220
	8.0					-0.374
	10.0					-0.493
k_{bb}	0.0	0.822	0.752	0.704	0.667	0.652
	0.5	0.782	0.718	0.676	0.644	0.631
	1.0		0.646	0.613	0.590	0.581
	1.5			0.542	0.526	0.520
	2.0			0.481	0.466	0.463
	3.0				0.376	0.373
	4.0				0.322	0.317
	5.0				0.288	0.281
	6.0					0.256
	8.0					0.225
	10.0					0.204
k_{mb}	0.0	0.000	0.000	0.000	0.000	0.000
	0.5	0.016	0.014	0.012	0.010	0.010
	1.0		0.030	0.027	0.024	0.022
	1.5			0.037	0.034	0.032
	2.0			0.042	0.039	0.037
	3.0				0.041	0.040
	4.0				0.039	0.037
	5.0				0.035	0.034
	6.0					0.031
	8.0					0.027
	10.0					0.025

Table A2. The effect of Poisson's ratio on the stress intensity factors, $a/h = 5$, $\lambda_2 = 3$.

ν	k_{mm}	k_{bm}	k_{bb}	k_{mb}
0.0	1.301	0.058	0.395	0.029
0.1	1.305	0.061	0.395	0.033
0.2	1.310	0.061	0.390	0.036
0.3	1.315	0.058	0.381	0.040
1/3	1.317	0.057	0.376	0.041
0.4	1.321	0.051	0.366	0.043
0.5	1.329	0.037	0.346	0.046

Table A3. Stress intensity factors for concentrated membrane and moment resultants on the crack surface, $a/h=5$, $\lambda_2=3$, $\nu=1/3$.

	$N_{11} = -\delta(X_2)$ $M_{11} = 0$	$N_{11} = 0$ $M_{11} = -\frac{1}{6} \delta(X_2)$
k_{mm}	0.536	
k_{bm}	0.007	
k_{bb}		0.018
k_{mb}		0.025

Table A-4. Stress intensity factor ratios in a cylindrical shell with a circumferential through crack under parabolic membrane stresses ($\nu=1/3$)

λ_2	a/h=1	a/h=2	a/h=5	a/h=10
k_{mm}				
0.5	0.510	0.510	0.509	0.509
1	0.541	0.538	0.536	0.536
1.5		0.582	0.578	0.577
2		0.635	0.628	0.627
3			0.741	0.738
4			0.855	0.852
6				1.057
8				1.229
k_{bm}				
0.5	0.034	0.032	0.031	0.031
1	0.069	0.068	0.068	0.069
1.5		0.083	0.088	0.090
2		0.075	0.085	0.091
3			0.031	0.043
4			-0.053	-0.038
6				-0.203
8				-0.327
k_{bb}				
0.5	0.301	0.287	0.288	0.292
1	0.248	0.240	0.248	0.255
1.5		0.189	0.200	0.210
2		0.143	0.156	0.167
3			0.091	0.102
4			0.052	0.061
6				0.024
8				0.012
k_{mb}				
0.5	0.010	0.009	0.007	0.007
1	0.022	0.020	0.017	0.016
1.5		0.027	0.025	0.023
2		0.031	0.028	0.027
3			0.029	0.028
4			0.026	0.026
6				0.019
8				0.014

1. The first part of the document discusses the importance of maintaining accurate records of all transactions and activities. It emphasizes that this is crucial for ensuring transparency and accountability in the organization's operations.

2. The second part of the document outlines the various methods and tools used to collect and analyze data. It highlights the need for consistent and reliable data collection processes to support informed decision-making.

3. The third part of the document focuses on the role of technology in data management and analysis. It discusses how modern software solutions can streamline data collection, storage, and reporting, thereby improving efficiency and accuracy.

4. The fourth part of the document addresses the challenges associated with data management, such as data quality, security, and privacy. It provides strategies to mitigate these risks and ensure that data is used responsibly and ethically.

5. The fifth part of the document concludes by summarizing the key findings and recommendations. It stresses the importance of ongoing monitoring and evaluation to ensure that data management practices remain effective and aligned with the organization's goals.

6. The sixth part of the document provides a detailed overview of the data collection process, including the identification of data sources, the design of data collection instruments, and the implementation of data collection procedures.

7. The seventh part of the document discusses the importance of data validation and quality control. It outlines the steps involved in checking the accuracy and reliability of the collected data to ensure that the analysis is based on high-quality information.

8. The eighth part of the document explores the various methods used for data analysis, including descriptive statistics, inferential statistics, and qualitative analysis. It provides a brief overview of each method and its application in different contexts.

9. The ninth part of the document discusses the importance of data visualization in presenting the results of data analysis. It highlights the use of various charts, graphs, and tables to make the data more accessible and understandable to stakeholders.

10. The tenth part of the document concludes by emphasizing the need for continuous improvement in data management practices. It encourages organizations to regularly review and update their data management processes to stay current with best practices and technological advancements.

APPENDIX B

THE PART-THROUGH CRACK PROBLEM IN PIPES

1. Introduction

In recent years there has been some renewed interest in the line spring model which was developed in [1] for obtaining an approximate solution of a plate containing a part-through surface crack. There are a number of reasons for this. First, the accuracy of the results obtained from the model turned out to be better than that shown by the early comparisons with the solutions found from the finite element and the alternating methods [2-6] (see, for example, [7]). Secondly, the technique appears to have the potential for important applications to a great variety of shell structures of rather complex geometries with a relatively small computational effort. Finally, it can be quite useful to study certain aspects of the part-through crack problem in the presence of large scale plastic deformations (see, for example, the interesting recent work by Parks [7,9], and [8] and [10]).

In this Appendix the elastic problem for a relatively thin-walled cylinder containing a semi-elliptic part-through crack is considered. It is assumed that the crack lies in a plane perpendicular to or containing the axis of the cylinder and may be an external or an internal surface crack. In formulating the problem, the cylinder is approximated by a shallow shell and the effect of transverse shear deformations are taken into account [11,12]. The edge-cracked strip results used in the line-spring model are obtained from an integral equation solution given in [13].

The stress intensity factor for a part-through axial crack located inside the cylinder is given in [14-16] where in [14] and [15] the finite element and in [16] the boundary integral equation method is used to solve the problem. The results found in this paper are compared with those given in [14] as well as the related plane strain and axisymmetric elasticity solutions.

2. General Formulation

The part-through crack geometry for the cylindrical shell under consideration is shown in Figure 1. It is assumed that the external loads are symmetric with respect to the plane of the crack. Thus, the only nonzero net ligament stress and moment resultants which have a constraining effect on the crack surface displacements would be the membrane resultant N_{11} and the moment resultant M_{11} . The basic idea underlying the line-spring model consists of (a) representing the net ligament stresses by a membrane load N and a bending moment M , and the crack surface displacements by a crack opening δ and a relative rotation θ , all referred to the midplane of the shell and continuously distributed along the length of the crack, (b) approximating the relationship between (N, M) and (δ, θ) by the corresponding plane strain results obtained from the solution of an edge-cracked strip or a ring, and (c) reducing the problem to a pair of integral equations for the unknown functions N and M or δ and θ by using the boundary and the continuity conditions for the shell in the plane of the crack.

In the formulation of the crack problem for the shell, the derivatives of the crack surface displacement and rotation are used as the unknown functions which are defined by

$$\frac{\partial}{\partial y} u(+0, y) = G_1(y), \quad \frac{\partial}{\partial y} \beta_x(+0, y) = G_2(y) \quad (1a, b)$$

The notation and the dimensionless quantities used in the formulation are given in Figure 1 and in Appendix A. It is shown in [17] that the general problem for a symmetrically loaded shell containing a through crack may be reduced to the following system of integral equations:

$$\int_{-1}^1 \frac{G_1(t)}{t-y} dt + \int_{-1}^1 \sum_1^2 k_{1j}(y, t) G_j(t) dt = 2\pi F_1(y), \quad -1 < y < 1, \quad (2a)$$

$$\frac{1-\nu^2}{\lambda^4} \int_{-1}^1 \frac{G_2(t)}{t-y} dt + \int_{-1}^1 \sum_1^2 k_{2j}(y, t) G_j(t) dt = 2\pi \frac{h}{a} F_2(y), \quad -1 < y < 1, \quad (2b)$$

$$k_{11}(y,t) = \int_0^{\infty} [2 \sum_1^4 \alpha^2 Q_j(\alpha) - 1] \sin \alpha(t-y) d\alpha ,$$

$$k_{12}(y,t) = \int_0^{\infty} 2\alpha^2 \sum_1^4 N_j(\alpha) \sin \alpha(t-y) d\alpha ,$$

$$k_{21}(y,t) = - \frac{2}{\lambda^2} \int_0^{\infty} \sum_1^4 \frac{p_j^2(m_j^2 - v\alpha^2) Q_j(\alpha)}{(\kappa p_j - 1)(\lambda_2^2 m_j^2 - \lambda_1^2 \alpha^2)} \sin \alpha(t-y) d\alpha ,$$

$$k_{22}(y,t) = - \frac{2}{\lambda^4} \int_0^{\infty} [\lambda^2 \sum_1^4 \frac{p_j^2(m_j^2 - v\alpha^2) N_j(\alpha)}{(\kappa p_j - 1)(\lambda_2^2 m_j^2 - \lambda_1^2 \alpha^2)} - \kappa(1-v)^2 \alpha r_1 + (1-v^2)/2] \sin \alpha(t-y) d\alpha \quad (3a-d)$$

subject to

$$\int_{-1}^1 G_1(y) dy = 0 , \quad \int_{-1}^1 G_2(y) dy = 0 . \quad (4a,b)$$

The problem is formulated as a stress disturbance problem in which a homogeneous stress solution for the uncracked shell is separated through a superposition and it is assumed that the stress and moment resultants applied to the crack surfaces are the only external loads. Thus, F_1 and F_2 appearing in (2) are

$$F_1(y) = N_{xx}(+0,y) , \quad F_2(y) = M_{xx}(+0,y) , \quad -1 < y < 1 . \quad (5a,b)$$

The parameters r_j , m_j , and p_j , ($j=1, \dots, 4$) are functions of the transform variable α and are given by

$$r_1 = - \left[\alpha^2 + \frac{2}{\kappa(1-v)} \right]^{1/2} , \quad (6)$$

$$m_j^2 = p_j + \alpha^2 , \quad \text{Re}(m_j) < 0 , \quad (j=1, \dots, 4) . \quad (7)$$

and p_1, \dots, p_4 are the roots of

$$p^4 - \kappa \lambda_2^4 p^3 + (2\kappa \lambda_1^2 \lambda_2^2 \alpha^2 - 2\kappa \lambda_2^4 \alpha^2 + \lambda_2^4) p^2 + (2\kappa \lambda_1^2 \lambda_2^2 \alpha^2 - \kappa \lambda_2^4 \alpha^2 - \kappa \lambda_1^4 \alpha^2 + 2\lambda_2^4 - 2\lambda_1^2 \lambda_2^2) \alpha^2 p + (\lambda_2^2 - \lambda_1^2)^2 \alpha^4 = 0 \quad (8)$$

From (6-8) it may be shown that for large values of $|\alpha|$ we have

$$r_1(\alpha) = -|\alpha| \left[1 + \frac{1}{\kappa(1-\nu)\alpha^2} + O\left(\frac{1}{\alpha^4}\right) \right], \quad (9)$$

$$m_j(\alpha) = -|\alpha| \left[1 + \frac{p_j}{2\alpha^2} - \frac{p_j^2}{8\alpha^4} + O\left(\frac{1}{\alpha^6}\right) \right], \quad (10)$$

where the roots p_j of the characteristic equation (8) are bounded for all values of α .

The functions Q_j and N_j , ($j=1, \dots, 4$) which appear in the kernels (3) are found from

$$R_j(\alpha) = i[Q_j(\alpha)f_1(\alpha) + N_j(\alpha)f_2(\alpha)], \quad (j = 1, \dots, 4), \quad (11)$$

where

$$f_k(\alpha) = \int_{-1}^1 G_k(t) e^{i\alpha t} dt, \quad (k=1,2) \quad (12)$$

and R_1, \dots, R_4 are obtained from

$$\sum_1^4 m_j R_j(\alpha) = 0,$$

$$\sum_1^4 \frac{R_j(\alpha) (\lambda_2^2 p_j^2 m_j - \lambda_2^2 m_j^5 + \lambda_1^2 \alpha^2 m_j^3)}{\lambda_2^2 m_j^2 - \lambda_1^2 \alpha^2} = -i\alpha f_1(\alpha),$$

$$\sum_1^4 \frac{R_j(\alpha) p_j^2 m_j}{(\kappa p_j - 1) (\lambda_2^2 m_j^2 - \lambda_1^2 \alpha^2)} = \frac{i(1-\nu)\kappa}{2\alpha\lambda^2} (r_1^2 + \alpha^2) f_2(\alpha),$$

$$\sum_1^4 \frac{R_j(\alpha) p_j^3 m_j}{(\kappa p_j - 1) (\lambda_2^2 m_j^2 - \lambda_1^2 \alpha^2)} = \frac{i(1-\nu)}{\lambda^2} \alpha f_2(\alpha), \quad (13a-d)$$

The formulation given above refer to a shallow shell containing a crack along the principal plane of curvature coinciding with X_2X_3 plane (Figure 1). The principal radii of curvature R_1 and R_2 are defined by

$$\frac{1}{R_1} = -\frac{\partial^2 Z}{\partial X_1^2}, \quad \frac{1}{R_2} = -\frac{\partial^2 Z}{\partial X_2^2}, \quad (14a,b)$$

where $Z(X_1, X_2)$ is the distance of the point on the middle surface to the tangent plane X_1X_2 . Thus, for the circumferential crack shown in Figure 1a, $R_2=R$ and $R_1=\infty$ (giving $\lambda_1=0$), and for the axial crack shown in Figure 1b $R_1=R$ and $R_2=\infty$ (giving $\lambda_2=0$).

Let now

$$N_{11} = N_\infty, \quad M_{11} = M_\infty \quad (15a,b)$$

be the uniform membrane load and the bending moment applied to the shell away from the crack region and $N(X_2)$ and $M(X_2)$ the stress and moment resultants which are equivalent to the net ligament stresses in $-a < X_2 < a$ or $-1 < y < 1$. The "input" functions which appear in the integral equations (2) may then be expressed as

$$F_1(y) = \frac{1}{E} (-\sigma_\infty + \sigma), \quad F_2(y) = \frac{1}{6E} (-m_\infty + m), \quad (16a,b)$$

for the crack located on the outside and

$$F_1(y) = \frac{1}{E} (-\sigma_\infty + \sigma), \quad F_2(y) = \frac{1}{6E} (m_\infty - m), \quad (17a,b)$$

for the crack located inside the cylinder^(*) where

$$\sigma_\infty = \frac{N_\infty}{h}, \quad m_\infty = \frac{6M_\infty}{h^2}, \quad (18a,b)$$

(*) In both cases the applied moment M is such that the crack tends to open under bending of the shell, and the net ligament moment is assumed to constrain the crack surface rotation, hence the change in sign of F_2 in (16) and (17).

and

$$\sigma(y) = \frac{N(X_2)}{h} = \frac{N(ay)}{h}, \quad m(y) = \frac{6M(X_2)}{h^2} = \frac{6M(ay)}{h^2}. \quad (19a,b)$$

The stresses σ and m are linearly related to the crack surface displacement $u(+0,y) = \delta/2$ and rotation $\beta_x(+0,y) = \theta/2$. This relationship may be obtained from the related plane strain problem by expressing the rate of change of the potential energy in terms of the crack closure energy and the change in gross compliance as follows:

$$\frac{1-\nu^2}{E} K^2 = \frac{1}{2} \left[\sigma h \frac{\partial \delta}{\partial L} + \frac{mh^2}{6} \frac{\partial \theta}{\partial L} \right] \quad (20)$$

where K is the total mode I stress intensity factor at the crack tip and L is the length of the edge crack. If we now let

$$K = \sqrt{h} (\sigma g_t + m g_b), \quad (21)$$

from (20) we obtain

$$\sigma(y) = E[\gamma_{tt}(y)u(+0,y) \pm \gamma_{tb}(y)\beta_x(+0,y)],$$

$$m(y) = 6E[\gamma_{bt}(y)u(+0,y) \pm \gamma_{bb}(y)\beta_x(+0,y)], \quad (22a,b)$$

where + and - signs are to be used for the outer and the inner cracks, respectively and

$$\gamma_{tt} = \frac{a}{h(1-\nu^2)} \frac{\alpha_{bb}}{\Delta}, \quad \gamma_{bb} = \frac{1}{36(1-\nu^2)} \frac{\alpha_{tt}}{\Delta},$$

$$\gamma_{tb} = -\frac{1}{6(1-\nu^2)} \frac{\alpha_{tb}}{\Delta}, \quad \gamma_{bt} = -\frac{a}{6h(1-\nu^2)} \frac{\alpha_{bt}}{\Delta},$$

$$\Delta = \alpha_{tt} \alpha_{bb} - \alpha_{tb}^2, \quad (23a-e)$$

$$\alpha_{ij} = \frac{1}{h} \int_0^L g_i g_j dL, \quad (i,j = t,b). \quad (24)$$

The crack depth L is assumed to be a known function of y (Figure 1).

Referring to the definitions (1), u and β_x may be expressed as

$$u(+0,y) = \int_{-1}^y G_1(t) dt, \quad \beta_x(+0,y) = \int_{-1}^y G_2(t) dt. \quad (25a,b)$$

Substituting from (25) and (22) into (2) the final form of the integral equations is found to be

$$\begin{aligned} & -\gamma_{tt}(y) \int_{-1}^y G_1(t) dt \mp \gamma_{tb}(y) \int_{-1}^y G_2(t) dt + \frac{1}{2\pi} \int_{-1}^1 \frac{G_1(t)}{t-y} dt \\ & + \frac{1}{2\pi} \int_{-1}^1 [k_{11}(y,t)G_1(t) + k_{12}(y,t)G_2(t)] dt = -\frac{\sigma_\infty}{E}, \quad -1 < y < 1, \\ & \mp \gamma_{bt}(y) \int_{-1}^y G_1(t) dt - \gamma_{bb}(y) \int_{-1}^y G_2(t) dt + \frac{a(1-\nu^2)}{2\pi h \lambda^4} \int_{-1}^1 \frac{G_2(t)}{t-y} dt \\ & + \frac{a}{2\pi h} \int_{-1}^1 [k_{21}(y,t)G_1(t) + k_{22}(y,t)G_2(t)] dt = \mp \frac{m_\infty}{6E}, \quad -1 < y < 1 \end{aligned} \quad (26a,b)$$

where the upper (i.e., -) and the lower (i.e., +) signs are to be used for the outer and the inner crack, respectively.

3. Compliance Coefficients

The functions g_t and g_b which appear in (21) and which give the membrane and bending components of the stress intensity factor are obtained from the corresponding plane strain crack geometry.

For the circumferential crack, the appropriate geometry is that of an infinite strip with an edge crack. On the other hand, for the axial crack the proper plane strain problem would be that of a ring having a radial edge crack. In a recent study the ring problem was formulated in terms of a singular integral equation [18]. The results

given in [18] show that for cylinders with values of h/R which may be considered a "shallow shell", the ring results are reasonably close to the strip results. Also for small values of h/R the convergence of the numerical solution of the ring problem is not very good. Hence, the complete parametrization of the problem for the purpose of obtaining g_t and g_b (which would be functions of h/R as well as L/h) becomes rather complicated. In this paper, therefore, the edge-cracked strip results will be used for both the axial and the circumferential crack problem.

For the strip the functions g_t and g_b are obtained from the results given in [13] which are valid for $0 < L/h < 0.8$ and may be expressed as

$$\begin{aligned}
 g_t(\xi) &= \sqrt{\pi\xi} (1.1216 + 6.5200\xi^2 - 12.3877\xi^4 + 89.0554\xi^6 \\
 &\quad - 188.6080\xi^8 + 207.3870\xi^{10} - 32.0524\xi^{12}) , \\
 g_b(\xi) &= \sqrt{\pi\xi} (1.1202 - 1.8872\xi + 18.0143\xi^2 - 87.3851\xi^3 \\
 &\quad + 241.9124\xi^4 - 319.9402\xi^5 + 168.0105\xi^6) \quad (27a,b)
 \end{aligned}$$

where $\xi = L(X_2)/h = L(ay)/h$. From (27) and (24) the functions α_{ij} , ($i,j=t,b$) may be determined as follows:

$$\begin{aligned}
 \alpha_{tt} &= \xi^2 \sum_{n=0}^{12} C_{tt}^{(n)} \xi^{2n} , \quad \alpha_{bb} = \xi^2 \sum_{n=0}^{12} C_{bb}^{(n)} \xi^n , \\
 \alpha_{tb} &= \alpha_{bt} = \xi^2 \sum_{n=0}^{18} C_{tb}^{(n)} \xi^n . \quad (28a-c)
 \end{aligned}$$

The coefficients $C_{ij}^{(n)}$ are given in Table 1.

4. Solution for the Cylindrical Shell

The solution of the problem is obtained for a uniform membrane loading N_∞ and for a bending moment M_∞ applied to the shell away from the crack region and for the Poisson's ratio $\nu = 0.3$. Even though $L(X_2) = L(ay)$ describing the crack shape can be any single-valued function, the problem is solved only for a semi-elliptic surface crack given by

$$L = L_0 \sqrt{1 - (X_2/a)^2} = L_0 \sqrt{1 - y^2} \quad (29)$$

The solution of the integral equations (26) is of the form

$$G_i(t) = \frac{\phi_i(t)}{(1-t^2)^{\frac{1}{2}}}, \quad (i=1,2) \quad (-1 < t < 1) \quad (30)$$

where ϕ_1 and ϕ_2 are bounded functions. The functions ϕ_i may be determined from (26) to any desired degree of accuracy by using the Gauss-Chebyshev integration procedure [19]. After obtaining ϕ_1 and ϕ_2 the unknowns σ and m representing the net ligament stresses may be determined from (22) by using (23-25), (27) and (28). The stress intensity factor $K(y)$ may then be obtained from (21) and (27). For a Poisson's ratio $\nu = 0.3$ and for various crack geometries and loading conditions the calculated results are shown in Figures 2-7 and Tables 2-11. Tables 2-9 give the normalized stress intensity factor at the deepest penetration point $y=0$, $L=L_0$ of a semi-elliptic surface crack in a cylindrical shell under uniform membrane loading or bending. The normalizing stress intensity factor k_0 is the corresponding value for the plane strain problem under tension or bending and is given by

$$k_0 = \frac{K_0}{\sqrt{\pi}} = \frac{N_\infty}{\sqrt{\pi} h} \sqrt{h} g_t(\xi_0), \quad \xi_0 = \frac{L_0}{h}, \quad (31)$$

for membrane loading, and

$$k_0 = \frac{K_0}{\sqrt{\pi}} = \frac{6M_\infty}{h^2\sqrt{\pi}} \sqrt{h} g_b(\epsilon_0), \quad \epsilon_0 = \frac{L_0}{h} \quad (32)$$

for bending.

Figures 2 and 3 show the comparison of the shell results with the stress intensity factors obtained from the corresponding axisymmetric and plane strain problems. As $(R_i/R_0) \rightarrow 1$ the shell results approach the flat plate solution k_p [21] having a part-through semi-elliptic crack of the same geometry and relative dimensions. It may be noted that, as expected, the shell stress intensity factors are generally smaller than the corresponding two-dimensional values. Even though the shell results are given for $0.74 < (R_i/R_0) < 1$, because of the nature of the theory used in the shell analysis, namely the shallow shell theory, for $(R_i/R_0) < 0.9$ the results may not be very accurate. From Figure 3 one may also observe that the difference between shell and the plane strain results decrease with decreasing crack depth $(L_0/h)^*$.

Some sample results for the distribution of the stress intensity factor along the crack front are given in Tables 10 and 11 and in Figures 4-6. The normalization factors k_0 used in these tables and figures are also those given by (31) and (32). The variable ϕ used in the presentation of these results is the usual parametric angle of the ellipse shown in the insert of Figure 4. For small values of ϕ the stress intensity factors given by the line-spring model are neither reliable nor meaningful and therefore are not presented.

The only shell results which exist in literature and which are obtained by using a method other than that of the line-spring are the stress intensity factors in a pressurized cylinder containing an internal semi-elliptic axial crack [14-16]. Figure 7 shows the comparison of the stress intensity factors obtained from the line-spring model and those given in [14] which are found by using the finite element method. The parameter ϕ is again defined by the insert in

(*) The plane strain cylinder results given in Figure 3 are obtained from [18] and the axisymmetric crack results shown in Figure 2 are from [20].

Figure 4. The stress intensity factor ratio F shown in Figure 7 is defined by

$$F = \frac{K}{\frac{pR_i}{h} \sqrt{\pi L_0/Q}}, \quad (33)$$

where $K = k\sqrt{\pi}$ is the stress intensity factor along the crack front, p is the internal pressure and $Q = [E(k)]^2$, E being the complete elliptic integral of the second kind. The results given in Figure 7 include the effect of the pressure p acting on the crack surface. Considering the gross approximations involved in the formulation of the problem by using the line-spring model, and the fact that the finite element results themselves may contain a few percent error, the agreement between the two results seems to be quite good. The plane strain results given in Figure 3 suggest that the accuracy of the results given by the line-spring model could perhaps be improved further if the ring rather than the flat plate solution is used to derive the functions g_t and g_b to express the stress intensity factor (see equations (21) and (27)).

REFERENCES

1. Rice, J.R. and Levy, N., "The Part-Through Surface Crack in an Elastic Plate," *Journal of Applied Mechanics*, V. 39, 1972, pp. 185-194.
2. Raju, I.S. and Newman, J.C., Jr., "Stress-Intensity Factors for a Wide Range of Semi-Elliptical Surface Cracks in Finite-Thickness Plates", *Journal of Engr. Fracture Mechanics*, Vol. 11, pp. 817-829, 1979.
3. Newman, J.C., Jr., A Review and Assessment of the Stress-Intensity Factors for Surface Cracks, NASA, Technical Memorandum 78805, Nov. 1978.
4. Atluri, S.N., Kathiresan, K., Kobayashi, A.S., and Nakagaki, M., "Inner Surface Cracks in an Internally Pressurized Cylinder Analyzed by a Three-Dimensional Displacement-Hybrid Finite Element Method", *Proc. of the Third Int. Conf. on Pressure Vessel Technology, Part III*, pp. 527-533, ASME, New York, 1977.
5. Smith, F.W. and Sorensen, D.R., "The Semi-Elliptical Surface Crack - A Solution by the Alternating Method", *Int. J. of Fracture*, Vol. 12, pp. 47-57, 1976.
6. Shah, R.C. and Kobayashi, A.S., On the Surface Flaw Problem, The Surface Crack: Physical Problems and Computational Solutions, ed. J.L. Swedlow, 1972, pp. 79-124.
7. Parks, D.M., "The Inelastic Line-Spring: Estimates of Elastic-Plastic Fracture Mechanics Parameters for Surface-Cracked Plates and Shells", Paper 80-C2/PVP-109, ASME, 1980.
8. Rice, J.R., "The Line-Spring Model for Surface Flaws", The Surface Crack: Physical Problems and Computational Solutions, ed. J.L. Swedlow, pp. 171-185, ASME, New York, 1972.
9. Parks, D.M., "Inelastic Analysis of Surface Flaws Using the Line-Spring Model", *Proceedings of the 5th International Conference on Fracture*, Cannes, France, 1981.
10. Erdogan, F. and Ratwani, M., "Plasticity and Crack Opening Displacement in Shells", *Int. J. of Fracture Mechanics*, Vol. 8, pp. 413-426, 1972.
11. Reissner, E. and Wan, F.Y.M., "On the Equations of Linear Shallow Shell Theory", Studies in Applied Mathematics, Vol. 48, pp. 132-145, 1969.

12. Naghdi, P.M., "Note on the Equations of Elastic Shallow Shells", *Quart. Appl. Math.*, Vol. 14, pp. 331-333 (1956).
13. Kaya, A.C. and Erdogan, F., "Stress Intensity Factors and COD in an Orthotropic Strip", *Int. J. Fracture*, Vol. 16, pp. 171-190, 1980.
14. Newman, J.C. and Raju, I.S., "Stress Intensity Factors for Internal Surface Cracks in Cylindrical Pressure Vessels", NASA Technical Memorandum 80073, July 1979.
15. McGowan, J.J. and Raymund, M., "Stress Intensity Factor Solutions for Internal Longitudinal Semi-Elliptical Surface Flaws in a Cylinder under Arbitrary Loadings", Fracture Mechanics, ASTM, STP 677, 1979.
16. Heliot, J. and Labbens, R.C. and Pellisier-Tanon, A., "Semi-Elliptic Cracks in a Cylinder Subjected to Stress Gradients", Fracture Mechanics, ASTM, STP 677, pp. 341-364, 1979.
17. Delale, F. and Erdogan, F., "Effect of Transverse Shear and Material Orthotropy in a Cracked Spherical Cap", *Int. J. Solids Structures*, Vol. 15, pp. 907-926, 1979.
18. Delale, F. and Erdogan, F., "Stress Intensity Factors in a Hollow Cylinder Containing a Radial Crack", NASA Project Report, NGR 39-007-011, November 1980.
19. Erdogan, F., "Mixed Boundary-Value Problems in Mechanics", Mechanics Today, Nemat-Nasser, S., ed., Vol. 4, Pergamon Press, Oxford, pp. 1-86, 1978.
20. Nied, H.F., "A Hollow Cylinder with an Axisymmetric Internal or Surface Crack under Nonaxisymmetric Arbitrary Loading", Ph.D. Dissertation, Lehigh University, June 1981.
21. Delale, F. and Erdogan, F., "Line-Spring Model for Surface Cracks in a Reissner Plate", NASA, Technical Report, Lehigh University, November 1980.

APPENDIX A

The notation and dimensionless quantities (Fig. 1)

$$x = \frac{X_1}{a}, \quad y = \frac{X_2}{a}, \quad z = \frac{X_3}{a}, \quad (\text{A.1})$$

$$u = \frac{U_1}{a}, \quad v = \frac{U_2}{a}, \quad w = \frac{W}{a}, \quad (\text{A.2})$$

$$\beta_x = \beta_1, \quad \beta_y = \beta_2, \quad (\text{A.3})$$

$$N_{xx} = \frac{N_{11}}{hE}, \quad N_{yy} = \frac{N_{22}}{hE}, \quad N_{xy} = \frac{N_{12}}{hE} \quad (\text{A.4})$$

$$M_{xx} = \frac{M_{11}}{h^2E}, \quad M_{yy} = \frac{M_{22}}{h^2E}, \quad M_{xy} = \frac{M_{12}}{h^2E} \quad (\text{A.5})$$

$$V_x = \frac{V_1}{hB}, \quad V_y = \frac{V_2}{hB}, \quad (\text{A.6})$$

$$\lambda_1^4 = 12(1-\nu^2) \frac{a^4}{h^2 R_1^2}, \quad \lambda_2^4 = 12(1-\nu^2) \frac{a^4}{h^2 R_2^2},$$

$$B = \frac{5}{6} \frac{E}{2(1+\nu)}, \quad \lambda^4 = 12(1-\nu^2) \frac{a^2}{h^2}, \quad \kappa = \frac{E}{B\lambda^4} \quad (\text{A.7})$$

U_1, U_2, W : components of the displacement vector,

β_1, β_2 : rotations of the normal,

$N_{ij}, (i,j=1,2)$: Membrane stress resultants

$M_{ij}, (i,j=1,2)$: Moment resultants

$V_i, (i=1,2)$: Transverse shear resultants

R_1, R_2 : Principal radii of curvature

Table B-1. Coefficients $C_{ij}^{(n)}$ which appear in eqs. (28)

n	$C_{tt}^{(n)}$	$C_{tb}^{(n)}$	$C_{bb}^{(n)}$
0	1.9761	1.9735	1.9710
1	11.4870	-2.2166	-4.4277
2	7.7086	21.6051	34.4952
3	15.0143	-69.3133	-165.7321
4	280.1207	196.3000	626.3926
5	-1099.7200	-406.2608	-2144.4651
6	3418.9795	644.9350	7043.4169
7	-7686.9237	-408.9569	-19003.2199
8	12794.1279	-159.6927	37853.3028
9	-13185.0403	-988.9879	-52595.4681
10	7868.2682	4266.5487	48079.2948
11	-1740.2463	-2997.1408	-25980.1559
12	124.1360	-6050.7849	6334.2425
13		8855.3615	
14		3515.4345	
15		-11744.1116	
16		4727.9784	
17		1695.6087	
18		-845.8958	

Table B-2. Normalized stress intensity factor k/k_0 at the deepest penetration point $L=L_0$, $y=0$ of an outer semielliptic circumferential crack in a cylinder under uniform membrane loading N_∞ ; $\lambda_2 = [12(1-\nu^2)]^{1/4} a/\sqrt{Rh}$, $\nu=0.3$.

λ_2	$L_0 = 0.2h$				$L_0 = 0.4h$			
	$a=h$	$a=2h$	$a=4h$	$a=8h$	$a=h$	$a=2h$	$a=4h$	$a=8h$
0	0.817	0.883	0.930	0.961	0.507	0.627	0.741	0.837
0.5	0.817	0.883	0.930	0.961	0.509	0.628	0.742	0.837
0.75	0.816	0.882	0.930	0.961	0.509	0.628	0.742	0.837
1.0		0.880	0.929	0.960		0.626	0.741	0.836
1.5		0.876	0.926	0.959		0.620	0.736	0.833
2.0			0.922	0.956			0.727	0.827
4.0			0.893	0.939			0.670	0.784
6.0				0.916				0.728
8.0				0.893				0.676
	$L_0 = 0.6h$				$L_0 = 0.8h$			
0	0.245	0.336	0.451	0.582	0.073	0.104	0.149	0.216
0.5	0.248	0.339	0.454	0.583	0.074	0.106	0.151	0.219
0.75	0.250	0.341	0.455	0.585	0.076	0.107	0.152	0.220
1.0		0.341	0.455	0.585		0.109	0.154	0.221
1.5		0.341	0.453	0.583		0.112	0.157	0.223
2.0			0.448	0.577			0.158	0.224
4.0			0.408	0.532			0.158	0.214
6.0				0.476				0.197
8.0				0.428				0.182

Table B-3. Normalized stress intensity factor k/k_0 at the deepest penetration point $L=L_0$, $y=0$ of an outer semi-elliptic circumferential crack in a cylindrical shell under uniform bending moment M_∞ .

λ_2	$L_0 = 0.2h$				$L_0 = 0.4h$				
	$a=h$	$a=2h$	$a=4h$	$a=8h$	$a=h$	$a=2h$	$a=4h$	$a=8h$	
0	0.804	0.875	0.926	0.959	0.441	0.579	0.710	0.819	
0.5	0.804	0.875	0.926	0.959	0.443	0.581	0.712	0.819	
0.75	0.803	0.874	0.925	0.958	0.443	0.580	0.711	0.819	
1.0		0.872	0.924	0.958		0.578	0.709	0.818	
1.5		0.867	0.921	0.956		0.570	0.703	0.814	
2.0			0.916	0.953			0.692	0.806	
4.0			0.884	0.934			0.621	0.753	
6.0				0.909				0.686	
8.0				0.883				0.624	
		$L_0 = 0.6h$				$L_0 = 0.8h$			
0	0.132	0.238	0.373	0.526	-0.012	0.017	0.065	0.140	
0.5	0.135	0.241	0.376	0.529	-0.010	0.019	0.068	0.143	
0.75	0.137	0.243	0.377	0.529	-0.008	0.021	0.069	0.145	
1.0		0.243	0.377	0.529		0.023	0.071	0.146	
1.5		0.242	0.374	0.526		0.027	0.074	0.148	
2.0			0.367	0.519			0.075	0.148	
4.0			0.313	0.459			0.072	0.132	
6.0				0.386				0.108	
8.0				0.326				0.088	

TableB-4. Normalized stress intensity factor k/k_0 at the deepest penetration point $y=0$, $L=L_0$ of an inner semi-elliptic circumferential surface crack in a cylindrical shell under uniform membrane loading N_∞ .

λ_2	$L_0 = 0.2h$				$L_0 = 0.4h$			
	$a=h$	$a=2h$	$a=4h$	$a=8h$	$a=h$	$a=2h$	$a=4h$	$a=8h$
0	0.817	0.883	0.930	0.961	0.507	0.627	0.741	0.837
0.5	0.810	0.879	0.928	0.960	0.497	0.618	0.735	0.833
0.75	0.804	0.875	0.926	0.959	0.487	0.610	0.729	0.829
1.0		0.870	0.923	0.957		0.600	0.722	0.824
1.5		0.858	0.916	0.953		0.579	0.704	0.812
2.0			0.907	0.948			0.685	0.798
4.0			0.870	0.926			0.613	0.739
6.0				0.902				0.687
8.0				0.881				0.646
	$L_0 = 0.6h$				$L_0 = 0.8h$			
0	0.245	0.336	0.451	0.582	0.073	0.104	0.149	0.216
0.5	0.240	0.330	0.444	0.576	0.073	0.103	0.147	0.213
0.75	0.236	0.324	0.438	0.570	0.073	0.102	0.145	0.210
1.0		0.318	0.431	0.563		0.101	0.143	0.207
1.5		0.305	0.414	0.546		0.101	0.140	0.200
2.0			0.398	0.529			0.137	0.194
4.0			0.350	0.467			0.133	0.177
6.0				0.422				0.168
8.0				0.392				0.163

Table B-5. Normalized stress intensity factor k/k_0 at the deepest penetration point $y=0$, $L=L_0$ of an inner semi-elliptic circumferential surface crack in a cylindrical shell under uniform bending moment M_0 .

λ_2	$L_0 = 0.2h$				$L_0 = 0.4h$				
	$a=h$	$a=2h$	$a=4h$	$a=8h$	$a=h$	$a=2h$	$a=4h$	$a=8h$	
0	0.804	0.875	0.926	0.959	0.441	0.579	0.710	0.819	
0.5	0.797	0.870	0.923	0.957	0.429	0.569	0.703	0.814	
0.75	0.789	0.866	0.921	0.956	0.418	0.559	0.696	0.809	
1.0		0.860	0.917	0.954		0.547	0.687	0.803	
1.5		0.847	0.909	0.950		0.522	0.666	0.789	
2.0			0.900	0.945			0.643	0.772	
4.0			0.859	0.920			0.557	0.702	
6.0				0.894				0.640	
8.0				0.871				0.592	
		$L_0 = 0.6h$				$L_0 = 0.8h$			
0	0.132	0.238	0.373	0.526	-0.012	0.017	0.065	0.140	
0.5	0.125	0.230	0.364	0.518	-0.013	0.015	0.062	0.136	
0.75	0.119	0.222	0.356	0.511	-0.013	0.014	0.060	0.133	
1.0		0.214	0.347	0.502		0.013	0.057	0.129	
1.5		0.197	0.326	0.481		0.012	0.053	0.120	
2.0			0.306	0.460			0.049	0.112	
4.0			0.244	0.382			0.042	0.089	
6.0				0.327				0.078	
8.0				0.289				0.070	

Table B-6. Normalized stress intensity factor k/k_0 at the deepest penetration point $y=0$, $L=L_0$ of an outer semi-elliptic axial surface crack in a cylindrical shell under uniform membrane loading N_∞

λ_1	$L_0 = 0.2h$				$L_0 = 0.4h$			
	$a=h$	$a=2h$	$a=4h$	$a=8h$	$a=h$	$a=2h$	$a=4h$	$a=8h$
0	0.817	0.883	0.930	0.961	0.507	0.627	0.741	0.837
0.5	0.822	0.886	0.932	0.962	0.518	0.635	0.748	0.841
0.75	0.826	0.888	0.933	0.963	0.527	0.642	0.752	0.844
1.0		0.890	0.934	0.963		0.649	0.757	0.847
1.5		0.894	0.936	0.964		0.663	0.766	0.853
2.0			0.938	0.965			0.773	0.857
4.0			0.935	0.964			0.775	0.860
6.0				0.959				0.848
8.0				0.954				0.834
	$L_0 = 0.6h$				$L_0 = 0.8h$			
0	0.245	0.336	0.451	0.582	0.073	0.104	0.149	0.216
0.5	0.255	0.346	0.461	0.590	0.076	0.108	0.154	0.223
0.75	0.264	0.355	0.468	0.597	0.080	0.112	0.159	0.229
1.0		0.364	0.477	0.604		0.118	0.165	0.235
1.5		0.384	0.494	0.619		0.130	0.178	0.250
2.0			0.509	0.631			0.192	0.264
4.0			0.532	0.651			0.225	0.299
6.0				0.641				0.303
8.0				0.622				0.294

Table B-7. Normalized stress intensity factor k/k_0 at the deepest penetration point $y=0$, $L=L_0$ of an outer semi-elliptic axial surface crack in a cylindrical shell under uniform bending moment M_0 .

λ_1	$L_0 = 0.2h$				$L_0 = 0.4h$			
	$a=h$	$a=2h$	$a=4h$	$a=8h$	$a=h$	$a=2h$	$a=4h$	$a=8h$
0	0.804	0.875	0.926	0.959	0.441	0.579	0.710	0.819
0.5	0.810	0.878	0.927	0.960	0.445	0.590	0.718	0.823
0.75	0.814	0.880	0.929	0.960	0.465	0.598	0.723	0.827
1.0		0.883	0.930	0.961		0.606	0.729	0.831
1.5		0.887	0.932	0.962		0.621	0.740	0.837
2.0			0.934	0.963			0.747	0.842
4.0			0.930	0.961			0.747	0.843
6.0				0.956				0.828
8.0				0.951				0.812
	$L_0 = 0.6h$				$L_0 = 0.8h$			
0	0.132	0.238	0.373	0.526	-0.012	0.017	0.065	0.140
0.5	0.143	0.250	0.385	0.536	-0.008	0.022	0.072	0.148
0.75	0.154	0.260	0.394	0.544	-0.003	0.027	0.078	0.155
1.0		0.272	0.405	0.553		0.034	0.085	0.163
1.5		0.295	0.425	0.570		0.047	0.100	0.180
2.0			0.442	0.585			0.115	0.197
4.0			0.464	0.605			0.148	0.232
6.0				0.588				0.231
8.0				0.563				0.217

Table B-8. Normalized stress intensity factor k/k_0 at the deepest penetration point $L=L_0$, $y=0$ of an inner semi-elliptic axial surface crack in a cylindrical shell under uniform membrane loading N_∞ .

λ_1	$L_0 = 0.2h$				$L_0 = 0.4h$			
	$a=h$	$a=2h$	$a=4h$	$a=8h$	$a=h$	$a=2h$	$a=4h$	$a=8h$
0	0.817	0.883	0.930	0.961	0.507	0.627	0.741	0.837
0.5	0.813	0.880	0.929	0.960	0.501	0.621	0.737	0.834
0.75	0.810	0.878	0.927	0.960	0.498	0.618	0.734	0.832
1.0		0.876	0.926	0.959		0.615	0.732	0.830
1.5		0.873	0.924	0.958		0.611	0.728	0.827
2.0			0.922	0.957			0.725	0.825
4.0			0.916	0.953			0.718	0.819
6.0				0.950				0.811
8.0				0.946				0.802
	$L_0 = 0.6h$				$L_0 = 0.8h$			
0	0.245	0.336	0.451	0.582	0.073	0.104	0.149	0.216
0.5	0.243	0.333	0.447	0.578	0.074	0.104	0.148	0.215
0.75	0.243	0.331	0.445	0.576	0.075	0.105	0.149	0.215
1.0		0.331	0.443	0.574		0.107	0.150	0.215
1.5		0.333	0.444	0.572		0.112	0.153	0.217
2.0			0.444	0.571			0.158	0.221
4.0			0.451	0.570			0.177	0.237
6.0				0.569				0.242
8.0				0.561				0.241

Table B-9. Normalized stress intensity factor k/k_0 at the deepest penetration point $L = L_0$, $y = 0$ of an inner semi-elliptic axial surface crack in a cylindrical shell under uniform bending moment M_0 .

λ_1	$L_0 = 0.2h$				$L_0 = 0.4h$			
	$a=h$	$a=2h$	$a=4h$	$a=8h$	$a=h$	$a=2h$	$a=4h$	$a=8h$
0	0.804	0.875	0.926	0.959	0.441	0.579	0.710	0.819
0.5	0.799	0.872	0.924	0.958	0.434	0.573	0.706	0.815
0.75	0.796	0.869	0.923	0.957	0.430	0.568	0.702	0.813
1.0		0.867	0.921	0.956		0.565	0.699	0.811
1.5		0.864	0.919	0.955		0.560	0.694	0.807
2.0			0.917	0.954			0.691	0.805
4.0			0.911	0.950			0.682	0.797
6.0				0.946				0.788
8.0				0.942				0.777
		$L_0 = 0.6h$			$L_0 = 0.8h$			
0	0.132	0.238	0.373	0.526	-0.012	0.017	0.065	0.140
0.5	0.128	0.233	0.368	0.521	-0.012	0.017	0.064	0.139
0.75	0.128	0.231	0.365	0.518	-0.010	0.018	0.064	0.138
1.0		0.230	0.363	0.516		0.019	0.065	0.138
1.5		0.233	0.363	0.513		0.024	0.069	0.141
2.0			0.363	0.513			0.074	0.145
4.0			0.369	0.515			0.091	0.161
6.0				0.507				0.164
8.0				0.495				0.161

Table B-10. Distribution of the normalized stress intensity factor k/k_0 along the crack front in a cylindrical shell containing an inner or outer semi-elliptic circumferential surface crack (see insert in Fig. 4), $\lambda_2 = 2$, $a=4h$, $L_0=0.4h$, $\nu=0.3$.

$\frac{2\phi}{\pi}$	Outer Crack		Inner Crack	
	Membrane Loading	Bending	Membrane Loading	Bending
1.0	0.727	0.692	0.685	0.643
0.894	0.719	0.689	0.678	0.641
0.789	0.694	0.680	0.658	0.637
0.684	0.655	0.665	0.625	0.628
0.578	0.604	0.643	0.580	0.615
0.473	0.544	0.618	0.527	0.597
0.367	0.477	0.583	0.465	0.569
0.263	0.406	0.538	0.399	0.529

Table 11. Distribution of the normalized stress intensity factor k/k_0 along the crack front in a cylindrical shell containing an inner or outer axial semi-elliptic surface crack (see insert in Fig. 4), $\nu=0.3$.

$\frac{2\phi}{\pi}$	Inner Crack $a=h, R_i=10h, L_0=0.2h$		Inner Crack $a=4h, R_i=10h, L_0=0.8h$		Outer Crack $a=4h, L_0=0.4h, \lambda_1=2$	
	Tension	Bending	Tension	Bending	Tension	Bending
1.0	0.812	0.799	0.161	0.078	0.773	0.747
0.894	0.807	0.797	0.160	0.082	0.764	0.743
0.789	0.792	0.792	0.157	0.094	0.736	0.731
0.684	0.766	0.782	0.153	0.109	0.693	0.710
0.578	0.730	0.765	0.147	0.124	0.637	0.683
0.473	0.685	0.739	0.138	0.139	0.572	0.652
0.367	0.628	0.700	0.126	0.149	0.500	0.612
0.263	0.559	0.642	0.114	0.154	0.426	0.562

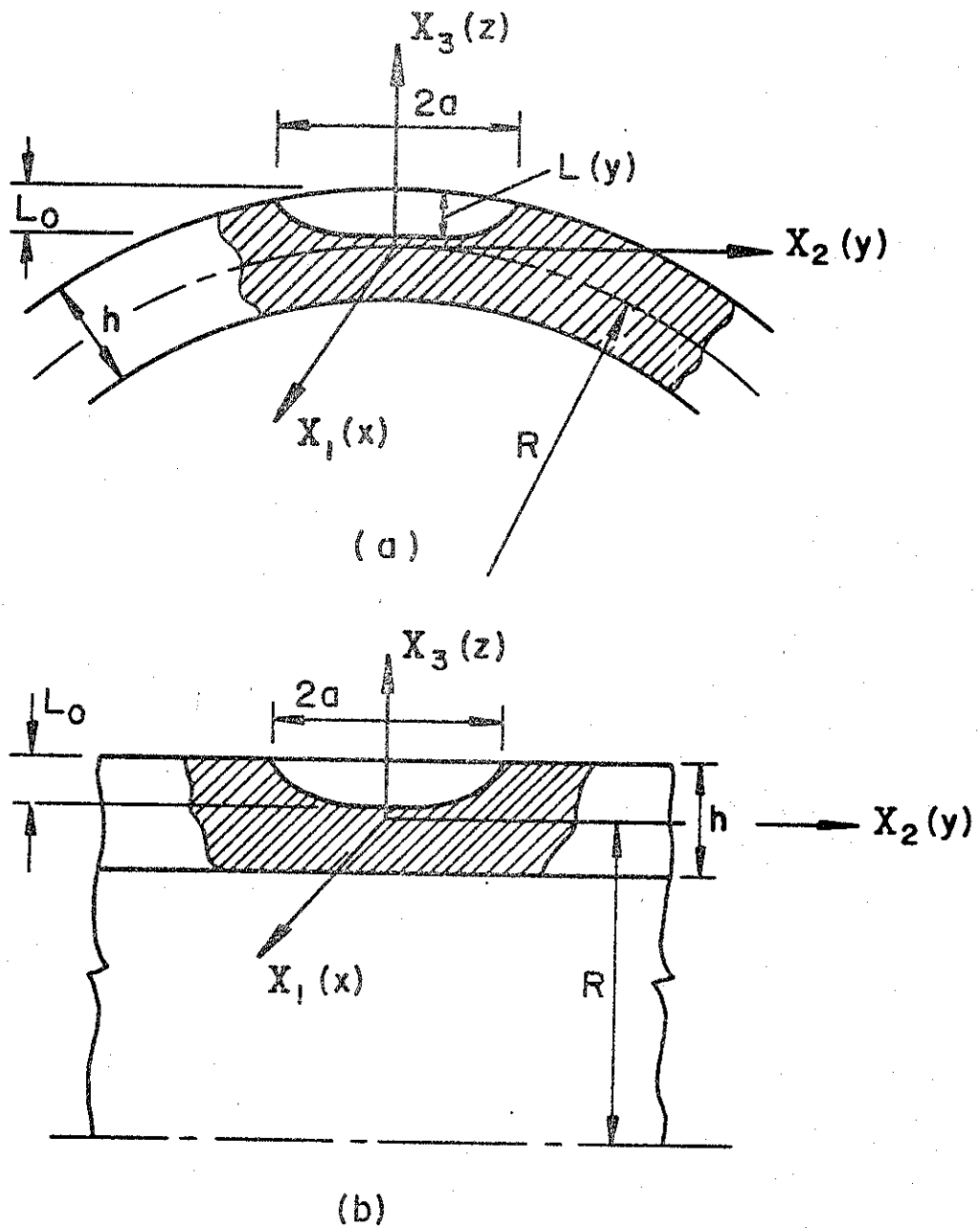


Figure B1. The geometry of a circumferential or an axial part-through surface crack in a cylindrical shell.

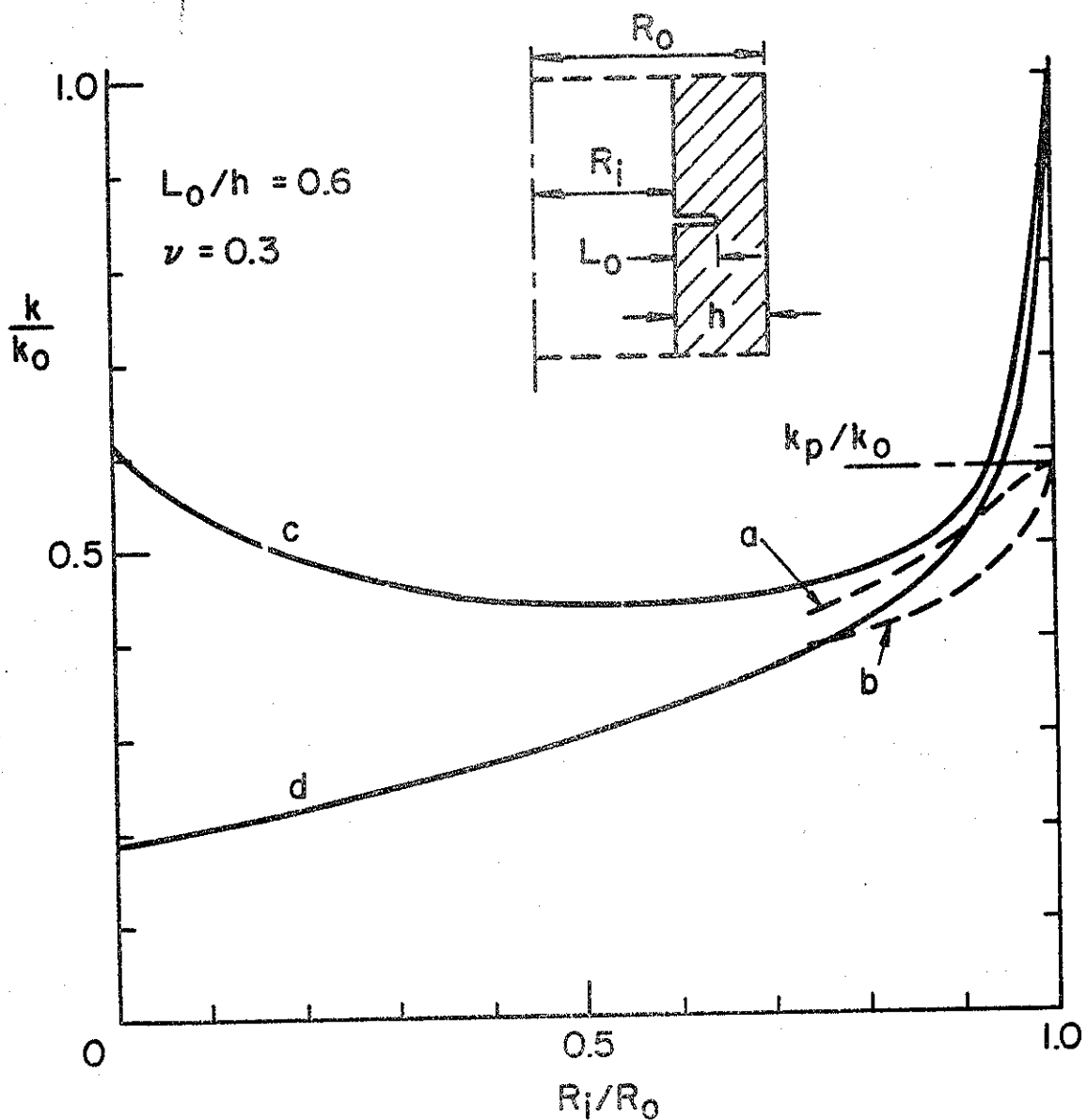


Figure B2. Comparison of the stress intensity factors obtained from the line-spring shell model and the axisymmetric elasticity solution [20]. (a) Stress intensity factor at the deepest penetration point of an external semi-elliptic circumferential crack in the shell, (b) same as (a) for an internal surface crack, (c) elasticity solution for the external axisymmetric crack, (d) the internal axisymmetric crack. (For $L_0=0.6h$, $k_0=4.035 \sigma_0 \sqrt{L_0}$, $k_p=0.582 k_0$, σ_0 : uniform axial stress, $a=8h$)

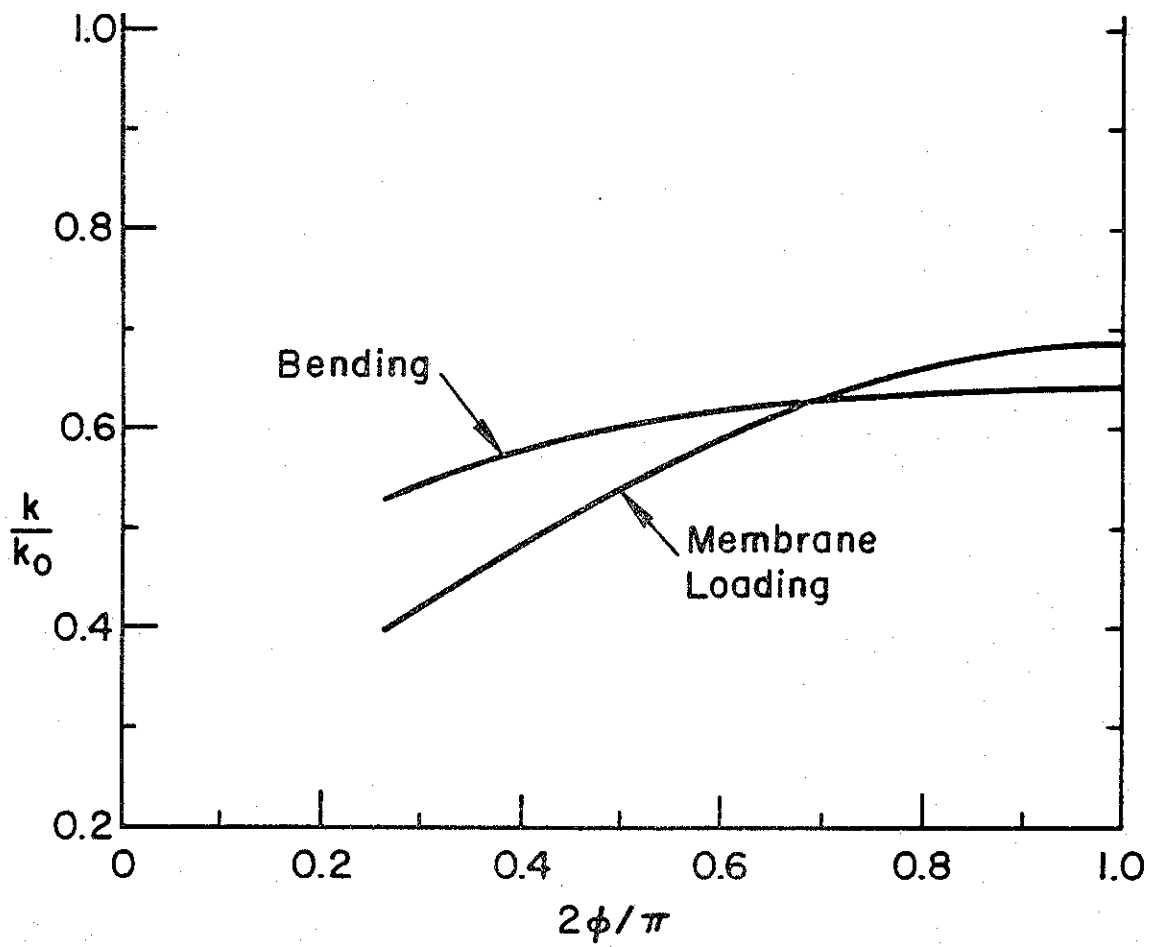


Figure B5. Same as Figure 4, for internal surface crack ($\lambda_2=2$, $a=4h$, $L_0=0.4h$).

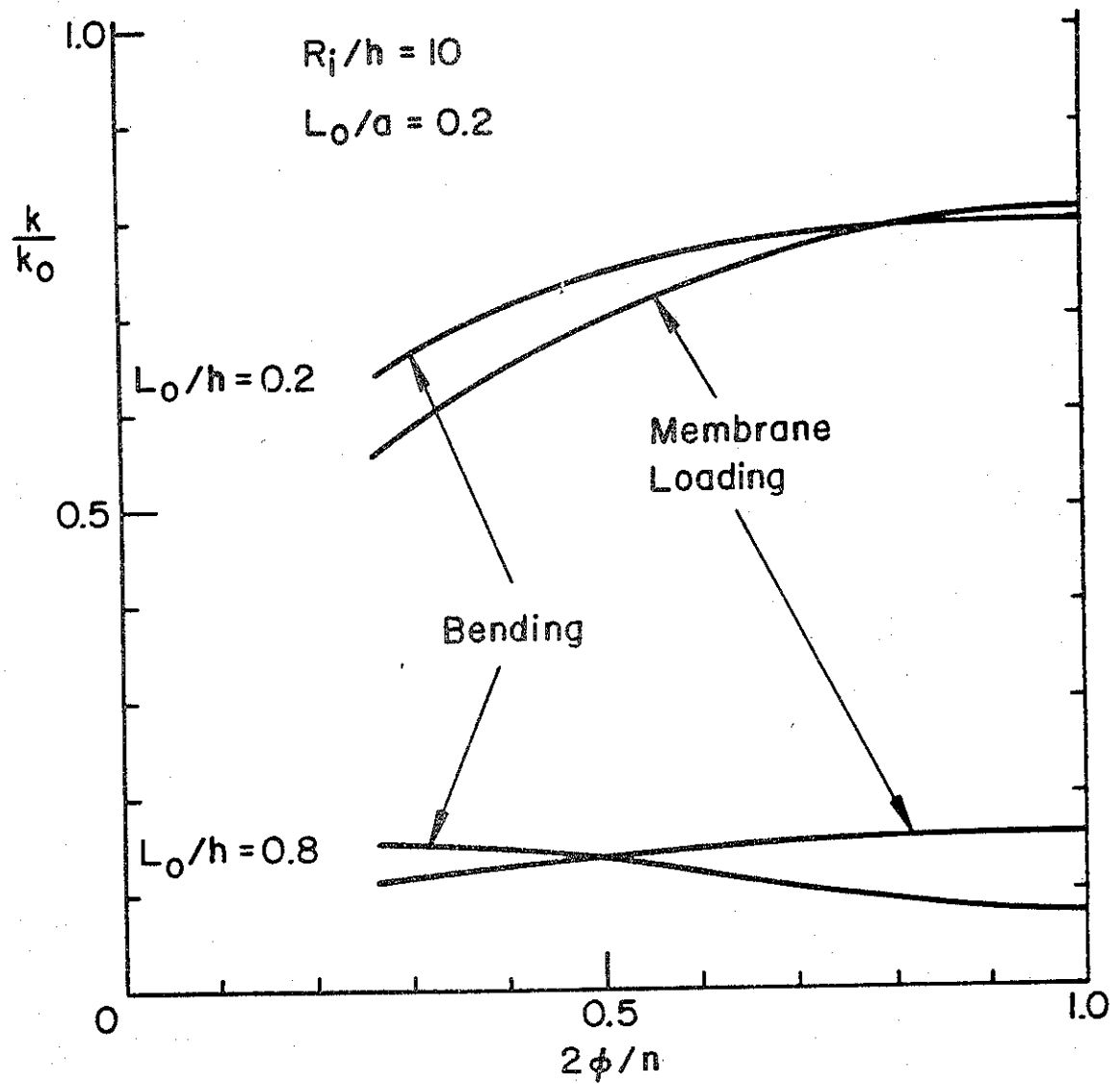


Figure B6. Variation of the stress intensity factor for a semi-elliptic internal axial surface crack in a cylindrical shell.

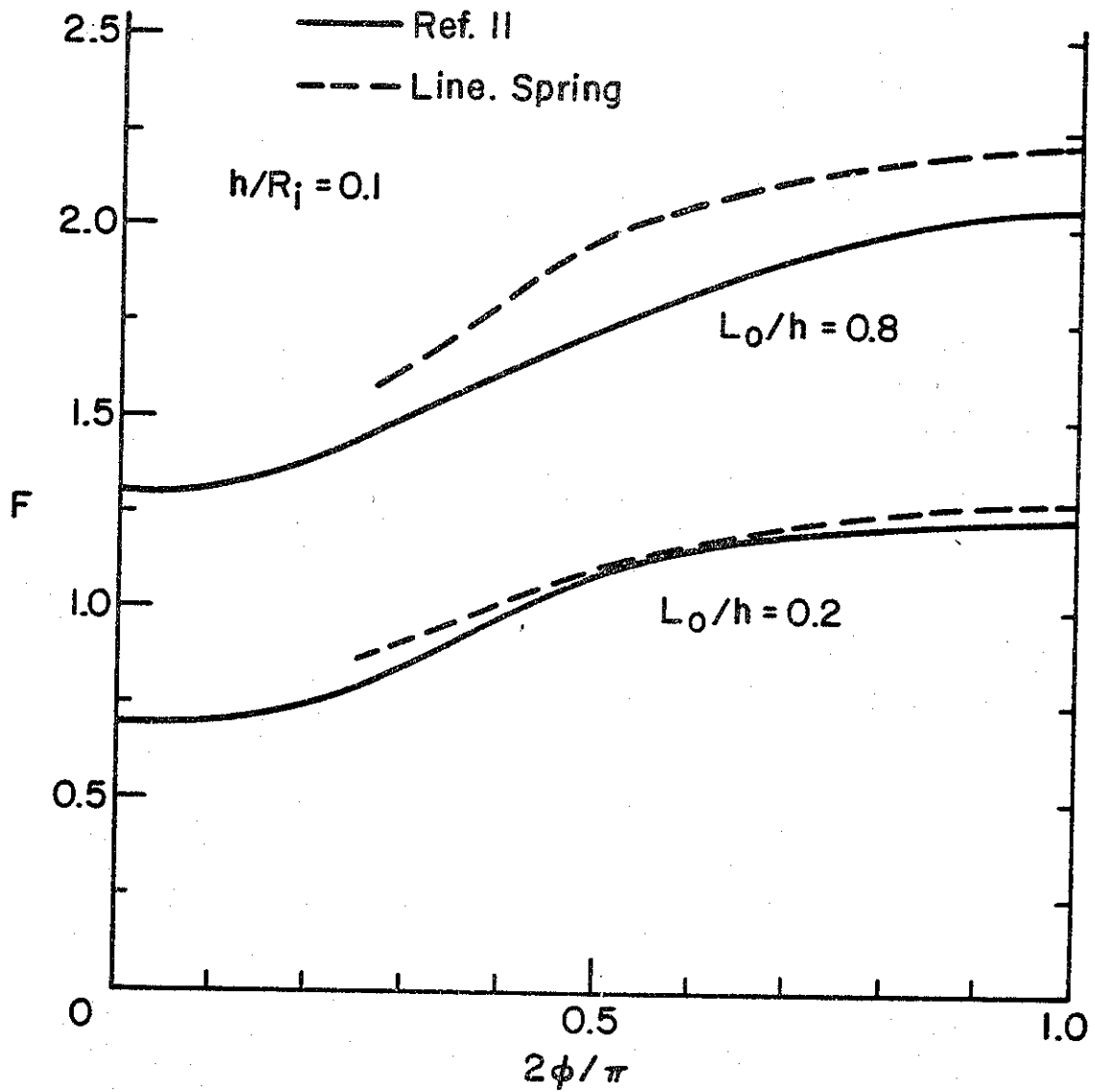


Figure B7. Comparison of the line spring shell results (dashed lines) with the finite element solution (full lines) [14] for a pressurized cylinder containing a semi-elliptic internal axial surface crack.

APPENDIX C

STRESS INTENSITY FACTORS FOR STANDARD LINE PIPES CONTAINING A PART-THROUGH SURFACE CRACK

The solution and some general results for a cylinder containing an inner or an outer surface crack are given in Appendix B. In this appendix we tabulate the stress intensity factors for standard line pipes containing an axial or a circumferential inner or outer crack. Referring to Fig. 1 of Appendix B for notation, let R , h , L_0 , and $2a$ be the mean radius, the thickness, the crack depth (at the deepest penetration point) and the crack length in the pipe. Also, let X_1 , X_2 , X_3 be the local coordinates, and $N_{11}(X_2)$ and $M_{11}(X_2)$ be the local membrane and bending resultants acting on the pipe along $X_1 = 0$, $|X_2| < a$ in the absence of the crack, where X_2 is taken along the crack in the tangent plane.

In most cases the stress state in the neighborhood of the part-through crack is approximately uniform and one may solve the problem by assuming that

$$N_{11}(X_2) = N_\infty = \text{constant}, M_{11}(X_2) = 0, \quad \text{or} \quad (1)$$

$$M_{11}(X_2) = M_\infty = \text{constant}, N_{11}(X_2) = 0. \quad (2)$$

For loading conditions (1) and (2) the Mode I stress intensity factors calculated at the deepest penetration point of a semi-elliptic surface crack in standard steel pipes (i.e., for the Poisson's ratio of 0.3) are given in Tables 1-16. The normalizing stress intensity factors K_0 in this analysis is the corresponding plane strain value for an edge cracked plate of thickness h and crack depth L_0 , and are given by

$$K_0 = K_{0t} = \frac{N_\infty}{h} \sqrt{h} g_t(\xi), \quad \xi = L_0/h, \quad (3)$$

for membrane loading, and

$$K_0 = K_{0b} = \frac{6M_\infty}{h^2} \sqrt{h} g_b(\xi), \quad \xi = L_0/h, \quad (4)$$

for (local) bending. The functions $g_t(\xi)$ and $g_b(\xi)$ are obtained from the plane strain solution and are given in Appendix B.

In addition to the uniform axial loading for which $N_{\infty} = \text{constant}$ and $M_{\infty} = 0$, in pipes the loading which is of considerable practical interest is the gross bending with bending moment M_0 . In this case, ignoring the crack, the axial stress in the pipe is given by

$$\sigma_{11} = \frac{M_0 z_0}{I}, \quad I = Rh(4R^2 + h^2), \quad (5)$$

where I is the area moment of inertia and z_0 is the distance from the neutral plane and is given by

$$z_0 = (R + X_3)\cos\theta, \quad 0 \leq \theta \leq \pi, \quad |X_3| \leq h/2, \quad (6)$$

X_3 being the local thickness coordinate. The circumferential angle θ is measured from the location of maximum tensile stress. For relatively small values of θ we observe that

$$\cos\theta \cong 1 - \frac{\theta^2}{2} = 1 - \frac{X_2^2}{2R^2}. \quad (7)$$

Combining (5), (6) and (7) we find

$$\sigma_{11} = \frac{M_0 R}{I} \left(1 - \frac{X_2^2}{2R^2}\right) + \frac{M_0 X_3}{I} \left(1 - \frac{X_2^2}{2R^2}\right). \quad (8)$$

The first term in (8) is independent of the thickness coordinate X_3 and hence represents a membrane loading whereas the second term is linear in X_3 and represents a local bending. By observing that the local membrane and bending stresses are related to the stress and moment resultants by

$$\sigma_{11}^m = \frac{N_{11}}{h}, \quad \sigma_{11}^b = \frac{12M_{11}X_3}{h^3}, \quad (9)$$

and by letting $\sigma_{11} = \sigma_{11}^m + \sigma_{11}^b$, from (8) and (9) we obtain

$$N_{11}(X_2) = \frac{M_0 Rh}{I} \left(1 - \frac{X_2^2}{2R^2}\right) = N_{\infty} \left(1 - \frac{X_2^2}{2R^2}\right), \quad (10)$$

$$M_{11}(X_2) = \frac{M_0 h^3}{12I} \left(1 - \frac{X_2^2}{2R^2}\right) = M_{\infty} \left(1 - \frac{X_2^2}{2R^2}\right). \quad (11)$$

From (10) and (11) it is seen that the stress intensity factor may be found by adding the results obtained from the following four loading conditions:

$$\begin{aligned} & \text{(a) } N_{11} = N_{\infty}, M_{11} = 0, \quad \text{(b) } N_{11} = 0, M_{11} = M_{\infty}, \\ & \text{(c) } N_{11} = -N_{\infty} X_2^2 / 2R^2, M_{11} = 0, \quad \text{(d) } N_{11} = 0, M_{11} = -M_{\infty} X_2^2 / 2R^2. \end{aligned} \quad (12)$$

The stress intensity factors due to the uniform loads (12) (a) and (b)

$$N_{\infty} = M_0 Rh / I, \quad M_{\infty} = M_0 h^3 / 12I \quad (13)$$

are given in Tables 1-16. Since $|X_2| < a$, the contribution of the nonuniform terms would be of the order a^2/R^2 or less compared to the results given by the corresponding uniform loads. Particularly, at the deepest penetration point of the crack since $X_2 = 0$, this contribution is expected to be much smaller than the order a^2/R^2 . To give some idea about such curvature effects on the stress intensity factors Table 17 shows the calculated results for a 20 in. diameter pipe. In this table, too, the respective normalizing stress intensity factors are given by (3) and (4). Note that the results are three to four orders of magnitude smaller than the corresponding stress intensity factors under uniform loading conditions and may, therefore, be neglected.

The tables give the stress intensity factor at the deepest penetration point of a part-through semi-elliptic surface crack. Since the fatigue crack propagation is generally self-similar, correlating the results at one point on the crack front is usually sufficient. However, if necessary the stress intensity factor at other locations on the crack front in a cylindrical shell under membrane loading may be obtained from the following approximate formula:

$$K(\phi) = K\left(\frac{\pi}{2}\right) [1 - (1 + \cos 2\phi)(0.2323 - 0.0615 \frac{L_0}{h})], \quad (14)$$

where the angle ϕ which determines the points along the semi-elliptic crack front is defined in Figure 4 of Appendix B, h is the wall thickness and L_0 is the maximum crack depth.

Table 1. K/K_0 in a line pipe with OD = 48 in., $h = 0.625$ in.

L/h	0.1	0.2	0.3	0.4	0.5	0.6	0.7	0.8	0.9
Outer circumferential crack, $N_\infty \neq 0, M_\infty = 0$									
1.0	0.945	0.817	0.664	0.508	0.366	0.247	0.147	0.074	0.033
2.0	0.967	0.882	0.766	0.628	0.481	0.340	0.209	0.106	0.048
3.0	0.976	0.911	0.817	0.695	0.554	0.405	0.257	0.132	0.060
4.0	0.980	0.928	0.848	0.739	0.605	0.455	0.296	0.155	0.070
5.0	0.983	0.939	0.868	0.770	0.643	0.494	0.329	0.175	0.079
6.0	0.985	0.946	0.882	0.792	0.672	0.525	0.357	0.193	0.088
7.0	0.987	0.951	0.893	0.809	0.694	0.551	0.381	0.209	0.096
8.0	0.988	0.954	0.900	0.821	0.712	0.572	0.401	0.223	0.104
Outer circumferential crack, $N_\infty = 0, M_\infty \neq 0$									
1.0	0.944	0.805	0.627	0.443	0.273	0.133	0.040	-0.011	-0.034
2.0	0.966	0.874	0.741	0.581	0.407	0.242	0.109	0.020	-0.028
3.0	0.975	0.906	0.798	0.658	0.492	0.318	0.163	0.047	-0.021
4.0	0.980	0.923	0.832	0.708	0.551	0.377	0.209	0.072	-0.017
5.0	0.983	0.934	0.855	0.742	0.595	0.422	0.246	0.094	-0.004
6.0	0.985	0.942	0.870	0.767	0.628	0.485	0.278	0.114	0.004
7.0	0.986	0.947	0.882	0.785	0.653	0.488	0.304	0.131	0.012
8.0	0.987	0.951	0.890	0.800	0.673	0.511	0.327	0.147	0.020
Inner circumferential crack, $N_\infty \neq 0, M_\infty = 0$									
1.0	0.944	0.814	0.660	0.503	0.361	0.243	0.145	0.073	0.033
2.0	0.965	0.877	0.757	0.616	0.468	0.328	0.202	0.102	0.048
3.0	0.974	0.905	0.804	0.677	0.532	0.384	0.242	0.124	0.058
4.0	0.978	0.920	0.832	0.716	0.575	0.425	0.273	0.142	0.066
5.0	0.981	0.930	0.850	0.742	0.607	0.456	0.297	0.156	0.073
6.0	0.983	0.937	0.864	0.762	0.631	0.480	0.318	0.169	0.080
7.0	0.984	0.941	0.873	0.776	0.650	0.500	0.335	0.180	0.086
8.0	0.985	0.945	0.880	0.787	0.664	0.517	0.350	0.190	0.091
Inner circumferential crack, $N_\infty = 0, M_\infty \neq 0$									
1.0	0.943	0.801	0.621	0.436	0.267	0.129	0.037	-0.012	-0.034
2.0	0.964	0.869	0.730	0.566	0.391	0.227	0.099	0.015	-0.030
3.0	0.973	0.898	0.783	0.635	0.465	0.292	0.144	0.037	-0.024
4.0	0.978	0.915	0.814	0.679	0.516	0.339	0.179	0.056	-0.018
5.0	0.981	0.925	0.835	0.709	0.552	0.375	0.207	0.071	-0.013
6.0	0.982	0.932	0.849	0.731	0.579	0.403	0.230	0.085	-0.007
7.0	0.984	0.937	0.859	0.747	0.600	0.426	0.249	0.096	-0.002
8.0	0.985	0.941	0.867	0.759	0.616	0.444	0.265	0.107	0.003

Table 2. K/K_0 in a line pipe with OD = 48 in., $h = 0.625$ in.

L_0/h	0.1	0.2	0.3	0.4	0.5	0.6	0.7	0.8	0.9
Outer axial crack, $N_{\infty} \neq 0, M_{\infty} = 0$									
a/h									
1.0	0.946	0.820	0.667	0.512	0.369	0.249	0.148	0.074	0.033
2.0	0.968	0.886	0.773	0.628	0.491	0.349	0.216	0.109	0.049
3.0	0.977	0.917	0.828	0.711	0.572	0.423	0.272	0.141	0.063
4.0	0.982	0.935	0.862	0.761	0.632	0.483	0.321	0.170	0.076
5.0	0.986	0.947	0.885	0.796	0.678	0.533	0.365	0.198	0.089
6.0	0.988	0.955	0.902	0.823	0.714	0.574	0.404	0.225	0.102
7.0	0.989	0.961	0.914	0.844	0.743	0.609	0.438	0.250	0.115
8.0	0.991	0.965	0.924	0.860	0.766	0.638	0.469	0.274	0.128
Outer axial crack, $N_{\infty} = 0, M_{\infty} \neq 0$									
1.0	0.944	0.807	0.631	0.447	0.277	0.137	0.042	-0.011	-0.034
2.0	0.967	0.879	0.750	0.592	0.420	0.253	0.117	0.024	-0.027
3.0	0.977	0.912	0.811	0.677	0.515	0.341	0.182	0.057	-0.017
4.0	0.982	0.931	0.849	0.733	0.584	0.412	0.239	0.090	-0.0058
5.0	0.985	0.944	0.874	0.774	0.637	0.470	0.289	0.122	+0.007
6.0	0.988	0.952	0.893	0.804	0.679	0.519	0.335	0.152	0.0203
7.0	0.989	0.958	0.906	0.827	0.712	0.559	0.374	0.180	0.034
8.0	0.991	0.963	0.917	0.845	0.739	0.593	0.410	0.207	0.048
Inner axial crack, $N_{\infty} \neq 0, M_{\infty} = 0$									
1.0	0.945	0.815	0.660	0.504	0.352	0.244	0.145	0.073	0.034
2.0	0.966	0.879	0.760	0.620	0.472	0.332	0.205	0.104	0.049
3.0	0.975	0.908	0.811	0.686	0.542	0.394	0.250	0.129	0.060
4.0	0.980	0.925	0.842	0.730	0.593	0.443	0.287	0.151	0.0703
5.0	0.983	0.937	0.864	0.762	0.633	0.483	0.321	0.171	0.080
6.0	0.985	0.945	0.880	0.787	0.664	0.517	0.350	0.190	0.089
7.0	0.987	0.951	0.893	0.807	0.691	0.546	0.377	0.208	0.098
8.0	0.988	0.956	0.903	0.824	0.713	0.572	0.401	0.225	0.107
Inner axial crack, $N_{\infty} = 0, M_{\infty} \neq 0$									
1.0	0.943	0.802	0.622	0.438	0.268	0.130	0.038	-0.012	-0.034
2.0	0.965	0.871	0.734	0.571	0.397	0.232	0.103	0.017	-0.029
3.0	0.974	0.902	0.791	0.646	0.478	0.305	0.154	-0.43	-0.022
4.0	0.979	0.920	0.826	0.697	0.538	0.362	0.197	0.066	-0.014
5.0	0.983	0.933	0.850	0.734	0.583	0.409	0.236	0.089	-0.006
6.0	0.985	0.941	0.868	0.762	0.620	0.449	0.270	0.109	-0.003
7.0	0.987	0.948	0.882	0.785	0.651	0.483	0.301	0.130	0.012
8.0	0.988	0.953	0.893	0.803	0.676	0.513	0.329	0.149	0.021

Table 3. K/K_0 in a line pipe with OD = 48 in., $h = 0.75$ in.

L_0/h	0.1	0.2	0.3	0.4	0.5	0.6	0.7	0.8	0.9
a/h									
Outer circumferential crack, $N_{\infty} \neq 0, M_{\infty} = 0$									
1.0	0.945	0.817	0.664	0.508	0.366	0.247	0.147	0.074	0.033
2.0	0.967	0.882	0.766	0.628	0.481	0.340	0.210	0.106	0.048
3.0	0.976	0.911	0.816	0.695	0.553	0.405	0.258	0.133	0.060
4.0	0.980	0.927	0.847	0.738	0.604	0.454	0.297	0.156	0.070
5.0	0.983	0.938	0.867	0.768	0.641	0.493	0.329	0.176	0.080
6.0	0.985	0.944	0.881	0.790	0.669	0.523	0.356	0.193	0.089
7.0	0.986	0.949	0.890	0.805	0.690	0.548	0.379	0.209	0.097
8.0	0.987	0.952	0.897	0.817	0.707	0.567	0.398	0.222	0.105
Outer circumferential crack, $N_{\infty} = 0, M_{\infty} \neq 0$									
1.0	0.944	0.805	0.627	0.443	0.273	0.133	0.040	-0.011	-0.034
2.0	0.966	0.874	0.741	0.580	0.407	0.242	0.110	0.020	-0.028
3.0	0.975	0.905	0.797	0.657	0.492	0.318	0.164	0.048	-0.020
4.0	0.980	0.922	0.831	0.706	0.550	0.376	0.209	0.073	-0.012
5.0	0.983	0.933	0.853	0.740	0.593	0.421	0.246	0.095	-0.003
6.0	0.985	0.941	0.868	0.764	0.624	0.456	0.276	0.114	0.006
7.0	0.986	0.946	0.879	0.781	0.648	0.483	0.302	0.131	0.014
8.0	0.987	0.949	0.886	0.794	0.666	0.505	0.323	0.146	0.021
Inner circumferential crack, $N_{\infty} \neq 0, M_{\infty} = 0$									
1.0	0.944	0.814	0.659	0.502	0.361	0.243	0.145	0.073	0.033
2.0	0.965	0.876	0.755	0.614	0.466	0.327	0.201	0.102	0.048
3.0	0.973	0.903	0.802	0.674	0.529	0.382	0.240	0.124	0.058
4.0	0.978	0.919	0.829	0.712	0.571	0.421	0.270	0.141	0.066
5.0	0.981	0.928	0.847	0.737	0.602	0.451	0.294	0.155	0.074
6.0	0.982	0.934	0.860	0.756	0.625	0.475	0.314	0.168	0.080
7.0	0.984	0.939	0.869	0.770	0.642	0.493	0.330	0.178	0.086
8.0	0.985	0.942	0.875	0.781	0.656	0.509	0.344	0.187	0.091
Inner circumferential crack, $N_{\infty} = 0, M_{\infty} \neq 0$									
1.0	0.943	0.801	0.621	0.436	0.266	0.128	0.037	-0.013	-0.034
2.0	0.964	0.868	0.729	0.563	0.389	0.225	0.098	0.015	-0.030
3.0	0.973	0.897	0.780	0.632	0.461	0.289	0.142	0.036	-0.024
4.0	0.977	0.913	0.811	0.675	0.510	0.335	0.176	0.054	-0.018
5.0	0.980	0.923	0.831	0.704	0.545	0.369	0.203	0.070	-0.012
6.0	0.982	0.930	0.844	0.724	0.571	0.396	0.224	0.082	-0.007
7.0	0.983	0.934	0.854	0.740	0.591	0.417	0.243	0.094	-0.002
8.0	0.984	0.938	0.861	0.751	0.606	0.434	0.258	0.104	0.003

Table 4. K/K_0 in a line pipe with OD = 48 in., h = 0.75 in.

$L_0/\eta \rightarrow$	0.1	0.2	0.3	0.4	0.5	0.6	0.7	0.8	0.9	
Outer axial crack, $N_{\infty} \neq 0, M_{\infty} = 0$										
a/h+	1.0	0.946	0.820	0.668	0.513	0.370	0.250	0.149	0.074	0.034
	2.0	0.968	0.887	0.774	0.639	0.493	0.351	0.218	0.111	0.050
	3.0	0.977	0.918	0.829	0.713	0.575	0.427	0.275	0.142	0.064
	4.0	0.983	0.936	0.863	0.763	0.635	0.487	0.325	0.173	0.077
	5.0	0.985	0.947	0.886	0.798	0.681	0.537	0.370	0.202	0.091
	6.0	0.988	0.955	0.902	0.825	0.717	0.579	0.409	0.230	0.105
	7.0	0.990	0.961	0.915	0.845	0.745	0.613	0.444	0.255	0.119
	8.0	0.991	0.965	0.924	0.861	0.768	0.642	0.474	0.279	0.132
Outer axial crack, $N_{\infty} = 0, M_{\infty} \neq 0$										
	1.0	0.945	0.807	0.631	0.448	0.278	0.137	0.423	-0.010	-0.034
	2.0	0.967	0.879	0.751	0.594	0.423	0.256	0.119	0.025	-0.027
	3.0	0.977	0.912	0.812	0.679	0.518	0.345	0.185	0.060	-0.016
	4.0	0.982	0.932	0.850	0.736	0.588	0.417	0.243	0.094	-0.004
	5.0	0.985	0.944	0.875	0.776	0.641	0.476	0.295	0.126	0.010
	6.0	0.988	0.952	0.893	0.805	0.682	0.524	0.341	0.157	0.024
	7.0	0.989	0.959	0.907	0.828	0.715	0.564	0.380	0.186	0.038
	8.0	0.990	0.963	0.917	0.846	0.741	0.597	0.415	0.212	0.052
Inner axial crack, $N_{\infty} \neq 0, M_{\infty} = 0$										
	1.0	0.944	0.815	0.660	0.503	0.362	0.244	0.145	0.0731	0.034
	2.0	0.966	0.879	0.759	0.619	0.472	0.332	0.205	0.104	0.049
	3.0	0.975	0.908	0.810	0.685	0.541	0.394	0.250	0.129	0.061
	4.0	0.980	0.925	0.841	0.729	0.592	0.443	0.288	0.152	0.071
	5.0	0.983	0.936	0.863	0.762	0.632	0.483	0.321	0.172	0.081
	6.0	0.985	0.944	0.880	0.787	0.664	0.517	0.351	0.192	0.091
	7.0	0.987	0.951	0.892	0.807	0.690	0.547	0.378	0.210	0.100
	8.0	0.988	0.956	0.902	0.823	0.713	0.572	0.403	0.227	0.109
Inner axial crack, $N_{\infty} = 0, M_{\infty} \neq 0$										
	1.0	0.943	0.802	0.622	0.437	0.268	0.129	0.038	-0.012	-0.034
	2.0	0.965	0.870	0.733	0.570	0.396	0.232	0.103	0.017	-0.029
	3.0	0.974	0.901	0.790	0.645	0.477	0.305	0.154	0.043	-0.021
	4.0	0.979	0.920	0.825	0.696	0.537	0.362	0.198	0.067	-0.013
	5.0	0.982	0.932	0.849	0.733	0.583	0.409	0.236	0.090	-0.004
	6.0	0.985	0.941	0.867	0.761	0.619	0.449	0.271	0.111	0.005
	7.0	0.987	0.947	0.881	0.784	0.650	0.484	0.302	0.132	0.014
	8.0	0.988	0.953	0.892	0.802	0.676	0.514	0.330	0.151	0.023

Table 5. K/K_0 in a line pipe with OD = 36 in., h = 0.5 in.

L_0/h	0.1	0.2	0.3	0.4	0.5	0.6	0.7	0.8	0.9
Outer circumferential crack, $N_\infty \neq 0, M_\infty = 0$									
a/h									
1.0	0.945	0.817	0.664	0.508	0.366	0.247	0.147	0.073	0.033
2.0	0.967	0.882	0.766	0.628	0.481	0.340	0.210	0.106	0.048
3.0	0.976	0.911	0.817	0.695	0.554	0.405	0.257	0.132	0.060
4.0	0.980	0.928	0.848	0.739	0.605	0.455	0.297	0.155	0.070
5.0	0.983	0.938	0.868	0.769	0.642	0.494	0.330	0.175	0.079
6.0	0.985	0.945	0.882	0.791	0.671	0.525	0.357	0.193	0.088
7.0	0.987	0.950	0.892	0.808	0.693	0.550	0.380	0.209	0.096
8.0	0.988	0.954	0.900	0.820	0.710	0.570	0.400	0.223	0.104
Outer circumferential crack, $N_\infty = 0, M_\infty \neq 0$									
1.0	0.944	0.805	0.627	0.443	0.273	0.133	0.040	-0.011	-0.034
2.0	0.966	0.874	0.741	0.581	0.407	0.242	0.109	0.020	-0.028
3.0	0.975	0.905	0.798	0.657	0.492	0.318	0.164	0.048	-0.021
4.0	0.980	0.923	0.832	0.707	0.551	0.376	0.209	0.072	-0.012
5.0	0.983	0.934	0.854	0.741	0.594	0.422	0.246	0.094	-0.004
6.0	0.985	0.941	0.870	0.766	0.627	0.458	0.277	0.114	0.005
7.0	0.986	0.947	0.881	0.784	0.652	0.486	0.304	0.131	0.013
8.0	0.987	0.950	0.889	0.798	0.671	0.509	0.326	0.146	0.020
Inner circumferential crack, $N_\infty \neq 0, M_\infty = 0$									
1.0	0.944	0.814	0.659	0.503	0.361	0.243	0.145	0.073	0.033
2.0	0.965	0.877	0.756	0.615	0.467	0.328	0.201	0.102	0.048
3.0	0.974	0.904	0.803	0.676	0.531	0.383	0.241	0.124	0.058
4.0	0.978	0.920	0.831	0.714	0.574	0.424	0.272	0.142	0.066
5.0	0.981	0.929	0.850	0.741	0.605	0.454	0.296	0.156	0.074
6.0	0.983	0.936	0.862	0.760	0.629	0.478	0.316	0.169	0.080
7.0	0.984	0.940	0.872	0.774	0.647	0.498	0.333	0.179	0.086
8.0	0.985	0.944	0.879	0.785	0.662	0.514	0.348	0.189	0.091
Inner circumferential crack, $N_\infty = 0, M_\infty \neq 0$									
1.0	0.943	0.801	0.621	0.436	0.267	0.129	0.037	-0.012	-0.034
2.0	0.964	0.868	0.730	0.565	0.390	0.226	0.099	0.015	-0.030
3.0	0.973	0.898	0.782	0.634	0.464	0.291	0.143	0.037	-0.024
4.0	0.978	0.914	0.813	0.678	0.514	0.338	0.178	0.055	-0.018
5.0	0.980	0.924	0.833	0.707	0.549	0.373	0.205	0.071	-0.013
6.0	0.982	0.931	0.847	0.729	0.576	0.401	0.228	0.084	-0.007
7.0	0.984	0.936	0.857	0.745	0.597	0.423	0.247	0.095	-0.002
8.0	0.985	0.940	0.865	0.757	0.613	0.441	0.262	0.106	0.003

Table 6. K/K_0 in a line pipe with OD = 36 in., $h = 0.5$ in.

$L_0/h \rightarrow$	0.1	0.2	0.3	0.4	0.5	0.6	0.7	0.8	0.9
a/h \downarrow									
Outer axial crack, $N_{\infty} \neq 0, M_{\infty} = 0$									
1.0	0.946	0.820	0.668	0.512	0.370	0.250	0.149	0.074	0.033
2.0	0.968	0.887	0.774	0.638	0.492	0.350	0.217	0.110	0.050
3.0	0.977	0.917	0.828	0.712	0.573	0.425	0.273	0.141	0.063
4.0	0.983	0.935	0.862	0.761	0.633	0.485	0.322	0.171	0.076
5.0	0.986	0.947	0.885	0.797	0.679	0.534	0.366	0.199	0.090
6.0	0.988	0.955	0.902	0.824	0.715	0.576	0.405	0.226	0.103
7.0	0.990	0.961	0.914	0.844	0.744	0.610	0.440	0.252	0.116
8.0	0.991	0.965	0.924	0.860	0.767	0.640	0.471	0.276	0.129
Outer axial crack, $N_{\infty} = 0, M_{\infty} \neq 0$									
1.0	0.944	0.807	0.631	0.448	0.277	0.137	0.042	-0.010	-0.034
2.0	0.967	0.879	0.750	0.593	0.421	0.254	0.118	0.024	-0.027
3.0	0.977	0.912	0.811	0.677	0.516	0.343	0.183	0.058	-0.017
4.0	0.982	0.931	0.849	0.734	0.586	0.414	0.240	0.091	-0.005
5.0	0.985	0.944	0.875	0.774	0.639	0.472	0.291	0.123	0.008
6.0	0.988	0.952	0.893	0.804	0.680	0.520	0.337	0.154	0.022
7.0	0.989	0.959	0.906	0.827	0.713	0.561	0.377	0.182	0.035
8.0	0.991	0.963	0.917	0.845	0.739	0.594	0.412	0.209	0.049
Inner axial crack, $N_{\infty} \neq 0, M_{\infty} = 0$									
1.0	0.945	0.815	0.660	0.504	0.362	0.244	0.145	0.073	0.034
2.0	0.966	0.879	0.760	0.620	0.472	0.332	0.205	0.104	0.049
3.0	0.975	0.908	0.810	0.685	0.542	0.394	0.250	0.129	0.060
4.0	0.980	0.925	0.842	0.730	0.593	0.443	0.288	0.151	0.071
5.0	0.983	0.937	0.864	0.762	0.632	0.483	0.321	0.171	0.080
6.0	0.985	0.945	0.880	0.787	0.664	0.517	0.351	0.190	0.090
7.0	0.987	0.951	0.893	0.807	0.691	0.546	0.377	0.208	0.099
8.0	0.988	0.956	0.903	0.823	0.713	0.572	0.402	0.225	0.108
Inner axial crack, $N_{\infty} = 0, M_{\infty} \neq 0$									
1.0	0.943	0.802	0.622	0.437	0.268	0.129	0.038	-0.012	-0.034
2.0	0.965	0.871	0.734	0.571	0.396	0.232	0.103	0.017	-0.030
3.0	0.974	0.902	0.790	0.646	0.478	0.305	0.154	0.043	-0.022
4.0	0.980	0.920	0.826	0.697	0.537	0.362	0.197	0.067	-0.014
5.0	0.983	0.932	0.850	0.734	0.583	0.409	0.236	0.089	-0.005
6.0	0.985	0.941	0.868	0.762	0.620	0.449	0.270	0.110	0.004
7.0	0.987	0.948	0.882	0.784	0.650	0.483	0.301	0.130	0.013
8.0	0.988	0.953	0.893	0.803	0.676	0.514	0.329	0.149	0.022

Table 7. K/K_0 in a line pipe with OD = 36 in., $h = 0.625$ in.

L_0/h	0.1	0.2	0.3	0.4	0.5	0.6	0.7	0.8	0.9
$a/h \downarrow$	Outer circumferential crack, $N_{\infty} \neq 0, M_{\infty} = 0$								
1.0	0.945	0.817	0.664	0.508	0.366	0.247	0.147	0.074	0.033
2.0	0.967	0.882	0.766	0.628	0.481	0.340	0.210	0.107	0.049
3.0	0.975	0.911	0.816	0.695	0.553	0.405	0.258	0.133	0.060
4.0	0.980	0.927	0.846	0.737	0.603	0.454	0.297	0.156	0.071
5.0	0.983	0.987	0.866	0.767	0.640	0.492	0.329	0.176	0.081
6.0	0.985	0.944	0.879	0.788	0.667	0.522	0.356	0.193	0.090
7.0	0.986	0.948	0.889	0.803	0.688	0.545	0.378	0.209	0.098
8.0	0.987	0.951	0.895	0.814	0.704	0.564	0.396	0.222	0.105
	Outer circumferential crack, $N_{\infty} = 0, M_{\infty} \neq 0$								
1.0	0.944	0.805	0.627	0.443	0.273	0.134	0.040	-0.011	-0.034
2.0	0.966	0.874	0.741	0.580	0.407	0.242	0.110	0.021	-0.028
3.0	0.975	0.905	0.797	0.656	0.491	0.318	0.164	0.048	-0.020
4.0	0.980	0.922	0.830	0.705	0.549	0.375	0.209	0.073	-0.011
5.0	0.982	0.933	0.852	0.738	0.591	0.419	0.245	0.095	-0.002
6.0	0.984	0.940	0.866	0.761	0.622	0.453	0.275	0.114	0.006
7.0	0.986	0.944	0.877	0.778	0.645	0.480	0.300	0.130	0.014
8.0	0.986	0.948	0.884	0.790	0.662	0.401	0.320	0.145	0.022
	Inner circumferential crack, $N_{\infty} \neq 0, M_{\infty} = 0$								
1.0	0.944	0.814	0.658	0.502	0.360	0.243	0.145	0.073	0.033
2.0	0.965	0.876	0.754	0.613	0.465	0.326	0.200	0.102	0.048
3.0	0.973	0.903	0.800	0.672	0.527	0.380	0.239	0.123	0.058
4.0	0.978	0.918	0.827	0.709	0.568	0.419	0.269	0.140	0.067
5.0	0.980	0.927	0.845	0.734	0.598	0.448	0.292	0.155	0.074
6.0	0.982	0.933	0.857	0.752	0.620	0.471	0.311	0.167	0.081
7.0	0.983	0.937	0.866	0.766	0.638	0.489	0.327	0.177	0.086
8.0	0.984	0.941	0.872	0.760	0.651	0.504	0.341	0.186	0.092
	Inner circumferential crack, $N_{\infty} = 0, M_{\infty} \neq 0$								
1.0	0.942	0.801	0.620	0.435	0.266	0.128	0.037	-0.013	-0.034
2.0	0.964	0.867	0.727	0.562	0.387	0.224	0.097	0.015	-0.030
3.0	0.972	0.896	0.777	0.629	0.459	0.287	0.141	0.036	-0.024
4.0	0.977	0.912	0.809	0.671	0.507	0.332	0.174	0.054	-0.018
5.0	0.980	0.922	0.828	0.700	0.541	0.365	0.200	0.069	-0.012
6.0	0.981	0.928	0.841	0.720	0.566	0.391	0.221	0.081	-0.007
7.0	0.983	0.933	0.851	0.735	0.585	0.412	0.239	0.092	-0.001
8.0	0.984	0.936	0.858	0.746	0.600	0.429	0.254	0.102	0.004

Table 8. K/K_0 in a line pipe with OD = 36 in., h = 0.625 in.

$L_0/h \rightarrow$	1.0	2.0	3.0	4.0	5.0	6.0	7.0	8.0	9.0
a/h \downarrow									
Outer axial crack, $N_{\infty} \neq 0, M_{\infty} = 0$									
1.0	0.946	0.820	0.668	0.513	0.371	0.250	0.149	0.075	0.034
2.0	0.968	0.887	0.775	0.640	0.495	0.352	0.219	0.111	0.050
3.0	0.978	0.918	0.830	0.714	0.577	0.429	0.277	0.144	0.064
4.0	0.983	0.936	0.864	0.764	0.637	0.490	0.328	0.175	0.079
5.0	0.986	0.947	0.887	0.799	0.683	0.540	0.373	0.204	0.093
6.0	0.988	0.955	0.903	0.826	0.718	0.581	0.412	0.232	0.107
7.0	0.990	0.961	0.915	0.846	0.747	0.616	0.447	0.258	0.121
8.0	0.991	0.965	0.924	0.861	0.769	0.644	0.477	0.282	0.134
Outer axial crack, $N_{\infty} = 0, M_{\infty} \neq 0$									
1.0	0.945	0.808	0.632	0.449	0.279	0.138	0.043	-0.010	-0.034
2.0	0.967	0.880	0.752	0.595	0.424	0.257	0.121	0.026	-0.026
3.0	0.977	0.913	0.813	0.680	0.520	0.348	0.187	0.061	-0.015
4.0	0.982	0.932	0.851	0.737	0.590	0.420	0.246	0.096	-0.002
5.0	0.986	0.944	0.876	0.777	0.643	0.479	0.299	0.129	0.012
6.0	0.988	0.953	0.894	0.807	0.684	0.527	0.344	0.160	0.026
7.0	0.989	0.959	0.907	0.829	0.716	0.566	0.384	0.189	0.041
8.0	0.990	0.963	0.917	0.846	0.742	0.599	0.418	0.216	0.055
Inner axial crack, $N_{\infty} \neq 0, M_{\infty} = 0$									
1.0	0.944	0.815	0.660	0.503	0.361	0.244	0.145	0.073	0.034
2.0	0.966	0.878	0.759	0.619	0.471	0.332	0.205	0.105	0.049
3.0	0.975	0.907	0.809	0.684	0.541	0.394	0.250	0.130	0.061
4.0	0.980	0.925	0.841	0.729	0.592	0.443	0.288	0.152	0.072
5.0	0.983	0.936	0.863	0.761	0.632	0.483	0.322	0.173	0.082
6.0	0.985	0.944	0.879	0.786	0.664	0.517	0.352	0.193	0.092
7.0	0.987	0.950	0.892	0.806	0.690	0.547	0.379	0.211	0.102
8.0	0.988	0.955	0.902	0.822	0.712	0.573	0.404	0.228	0.111
Inner axial crack, $N_{\infty} = 0, M_{\infty} \neq 0$									
1.0	0.943	0.801	0.621	0.437	0.267	0.129	0.037	-0.012	-0.034
2.0	0.965	0.870	0.733	0.569	0.395	0.232	0.103	0.017	-0.029
3.0	0.974	0.901	0.789	0.645	0.477	0.304	0.154	0.043	-0.021
4.0	0.979	0.919	0.824	0.695	0.536	0.362	0.198	0.068	-0.012
5.0	0.982	0.932	0.849	0.732	0.582	0.409	0.237	0.090	-0.003
6.0	0.985	0.941	0.867	0.761	0.619	0.449	0.272	0.112	0.006
7.0	0.986	0.947	0.881	0.783	0.650	0.484	0.303	0.133	0.016
8.0	0.988	0.952	0.892	0.802	0.675	0.514	0.331	0.152	0.025

Table 9. K/K_0 in a line pipe with OD = 30 in., $h = 0.375$ in.

L_0/h	0.1	0.2	0.3	0.4	0.5	0.6	0.7	0.8	0.9	
Outer circumferential crack, $N_{\infty} \neq 0, M_{\infty} = 0$										
a/h	1.0	0.945	0.817	0.664	0.508	0.366	0.247	0.147	0.073	0.033
	2.0	0.967	0.883	0.766	0.628	0.481	0.340	0.209	0.106	0.048
	3.0	0.976	0.912	0.817	0.696	0.554	0.405	0.257	0.132	0.060
	4.0	0.981	0.928	0.848	0.740	0.605	0.455	0.296	0.158	0.070
	5.0	0.983	0.939	0.869	0.770	0.643	0.494	0.329	0.175	0.078
	6.0	0.985	0.946	0.883	0.793	0.672	0.526	0.357	0.193	0.088
	7.0	0.987	0.951	0.893	0.810	0.695	0.552	0.381	0.209	0.096
	8.0	0.988	0.954	0.901	0.822	0.713	0.573	0.401	0.223	0.103
Outer circumferential crack, $N_{\infty} = 0, M_{\infty} \neq 0$										
	1.0	0.944	0.805	0.627	0.447	0.273	0.133	0.040	-0.011	-0.034
	2.0	0.966	0.874	0.741	0.581	0.407	0.242	0.109	0.020	-0.099
	3.0	0.975	0.906	0.798	0.658	0.492	0.318	0.163	0.047	-0.021
	4.0	0.980	0.923	0.833	0.708	0.552	0.377	0.209	0.072	-0.013
	5.0	0.983	0.935	0.855	0.743	0.595	0.423	0.246	0.094	-0.004
	6.0	0.985	0.942	0.871	0.768	0.629	0.459	0.278	0.114	0.004
	7.0	0.986	0.947	0.882	0.786	0.654	0.488	0.305	0.132	0.012
	8.0	0.987	0.951	0.891	0.800	0.674	0.512	0.328	0.147	0.019
Inner circumferential crack, $N_{\infty} \neq 0, M_{\infty} = 0$										
	1.0	0.944	0.815	0.660	0.503	0.361	0.243	0.145	0.073	0.033
	2.0	0.965	0.878	0.757	0.616	0.468	0.328	0.202	0.103	0.048
	3.0	0.974	0.905	0.805	0.677	0.532	0.385	0.242	0.124	0.058
	4.0	0.978	0.921	0.833	0.716	0.576	0.426	0.273	0.142	0.066
	5.0	0.981	0.930	0.852	0.743	0.608	0.457	0.298	0.157	0.073
	6.0	0.983	0.937	0.865	0.763	0.632	0.482	0.319	0.169	0.080
	7.0	0.984	0.942	0.874	0.778	0.651	0.502	0.336	0.181	0.086
	8.0	0.985	0.945	0.881	0.789	0.666	0.518	0.351	0.190	0.091
Inner circumferential crack, $N_{\infty} = 0, M_{\infty} \neq 0$										
	1.0	0.943	0.802	0.622	0.437	0.267	0.129	0.037	-0.012	-0.034
	2.0	0.964	0.869	0.731	0.566	0.391	0.227	0.099	0.015	-0.030
	3.0	0.973	0.898	0.784	0.636	0.466	0.293	0.144	0.037	-0.024
	4.0	0.978	0.921	0.833	0.716	0.576	0.340	0.180	0.056	-0.018
	5.0	0.981	0.925	0.836	0.712	0.553	0.377	0.208	0.072	-0.013
	6.0	0.983	0.933	0.850	0.733	0.581	0.405	0.231	0.085	-0.007
	7.0	0.984	0.938	0.860	0.749	0.602	0.428	0.250	0.097	-0.002
	8.0	0.985	0.941	0.868	0.761	0.618	0.446	0.266	0.107	0.003

Table 10. K/K_0 in a line pipe with OD = 30 in., $h = 0.375$ in.

L_0/h	0.1	0.2	0.3	0.4	0.5	0.6	0.7	0.8	0.9
a/h									
Outer axial crack, $N_{\infty} \neq 0, M_{\infty} = 0$									
1.0	0.946	0.820	0.667	0.512	0.369	0.249	0.148	0.074	0.033
2.0	0.968	0.886	0.773	0.637	0.491	0.349	0.216	0.109	0.050
3.0	0.977	0.917	0.828	0.711	0.572	0.423	0.271	0.140	0.063
4.0	0.982	0.935	0.862	0.760	0.631	0.482	0.320	0.169	0.075
5.0	0.986	0.947	0.885	0.796	0.677	0.532	0.364	0.197	0.088
6.0	0.988	0.955	0.902	0.823	0.713	0.573	0.402	0.224	0.101
7.0	0.990	0.961	0.914	0.843	0.742	0.608	0.437	0.249	0.114
8.0	0.991	0.965	0.923	0.859	0.766	0.637	0.468	0.273	0.127
Outer axial crack, $N_{\infty} = 0, M_{\infty} \neq 0$									
1.0	0.944	0.807	0.630	0.447	0.277	0.136	0.042	-0.010	-0.034
2.0	0.967	0.879	0.749	0.592	0.420	0.253	0.117	0.024	-0.027
3.0	0.977	0.912	0.810	0.676	0.514	0.341	0.181	0.057	-0.018
4.0	0.982	0.931	0.848	0.733	0.584	0.411	0.238	0.089	-0.006
5.0	0.985	0.943	0.874	0.773	0.637	0.469	0.288	0.121	0.006
6.0	0.988	0.952	0.892	0.803	0.678	0.517	0.333	0.151	0.020
7.0	0.989	0.958	0.906	0.826	0.711	0.558	0.373	0.179	0.033
8.0	0.991	0.963	0.916	0.844	0.738	0.592	0.408	0.205	0.046
Inner axial crack, $N_{\infty} \neq 0, M_{\infty} = 0$									
1.0	0.945	0.815	0.660	0.504	0.362	0.244	0.145	0.073	0.033
2.0	0.966	0.879	0.760	0.620	0.472	0.332	0.205	0.104	0.048
3.0	0.975	0.908	0.811	0.686	0.542	0.394	0.250	0.129	0.060
4.0	0.980	0.925	0.842	0.730	0.593	0.443	0.287	0.151	0.070
5.0	0.983	0.937	0.864	0.763	0.633	0.483	0.320	0.171	0.080
6.0	0.985	0.945	0.880	0.788	0.665	0.517	0.350	0.190	0.089
7.0	0.987	0.951	0.893	0.807	0.691	0.546	0.377	0.207	0.098
8.0	0.988	0.956	0.903	0.824	0.713	0.572	0.401	0.224	0.106
Inner axial crack, $N_{\infty} = 0, M_{\infty} \neq 0$									
1.0	0.943	0.802	0.622	0.438	0.268	0.130	0.038	-0.012	-0.034
2.0	0.965	0.871	0.734	0.571	0.397	0.232	0.103	0.017	-0.030
3.0	0.974	0.902	0.791	0.647	0.479	0.305	0.154	0.043	-0.022
4.0	0.979	0.921	0.826	0.697	0.538	0.362	0.197	0.066	-0.014
5.0	0.983	0.933	0.850	0.734	0.584	0.409	0.235	0.088	-0.006
6.0	0.985	0.941	0.868	0.762	0.620	0.449	0.270	0.109	0.003
7.0	0.987	0.948	0.882	0.785	0.651	0.483	0.300	0.129	0.012
8.0	0.988	0.953	0.893	0.803	0.676	0.513	0.328	0.148	0.020

Table 11. K/K_0 in a line pipe with OD = 30 in., $h = 0.5$ in.

L_0/h	0.1	0.2	0.3	0.4	0.5	0.6	0.7	0.8	0.9
Outer circumferential crack, $N_\infty \neq 0, M_\infty = 0$									
1.0	0.945	0.817	0.664	0.508	0.366	0.247	0.147	0.074	0.033
2.0	0.967	0.882	0.766	0.628	0.481	0.340	0.210	0.107	0.049
3.0	0.975	0.911	0.816	0.695	0.553	0.405	0.258	0.133	0.060
4.0	0.980	0.927	0.847	0.738	0.604	0.454	0.297	0.156	0.071
5.0	0.983	0.937	0.866	0.767	0.640	0.492	0.329	0.176	0.080
6.0	0.985	0.944	0.880	0.788	0.668	0.522	0.356	0.193	0.089
7.0	0.986	0.949	0.890	0.804	0.689	0.546	0.378	0.209	0.098
8.0	0.987	0.952	0.896	0.815	0.705	0.565	0.397	0.222	0.105
Outer circumferential crack, $N_\infty = 0, M_\infty \neq 0$									
1.0	0.944	0.805	0.627	0.443	0.273	0.134	0.040	-0.011	-0.034
2.0	0.966	0.874	0.741	0.580	0.407	0.242	0.110	0.020	-0.028
3.0	0.975	0.905	0.797	0.657	0.491	0.318	0.164	0.048	-0.020
4.0	0.980	0.922	0.831	0.706	0.549	0.376	0.209	0.073	-0.011
5.0	0.983	0.933	0.852	0.739	0.592	0.420	0.245	0.095	-0.002
6.0	0.984	0.940	0.867	0.762	0.623	0.454	0.276	0.114	0.006
7.0	0.986	0.945	0.877	0.779	0.646	0.481	0.301	0.131	0.014
8.0	0.987	0.948	0.885	0.792	0.664	0.503	0.321	0.145	0.022
Inner circumferential crack, $N_\infty \neq 0, M_\infty = 0$									
1.0	0.944	0.814	0.659	0.502	0.360	0.243	0.145	0.073	0.033
2.0	0.965	0.876	0.755	0.613	0.465	0.326	0.201	0.102	0.048
3.0	0.973	0.903	0.801	0.673	0.527	0.381	0.240	0.124	0.058
4.0	0.978	0.918	0.828	0.710	0.569	0.420	0.269	0.141	0.067
5.0	0.980	0.927	0.846	0.736	0.600	0.450	0.293	0.155	0.074
6.0	0.982	0.934	0.858	0.754	0.622	0.472	0.312	0.167	0.080
7.0	0.983	0.938	0.867	0.767	0.639	0.491	0.328	0.177	0.086
8.0	0.984	0.941	0.874	0.778	0.653	0.506	0.342	0.187	0.092
Inner circumferential crack, $N_\infty = 0, M_\infty \neq 0$									
1.0	0.942	0.801	0.620	0.435	0.266	0.128	0.037	-0.013	-0.034
2.0	0.964	0.867	0.728	0.562	0.388	0.225	0.098	0.015	-0.030
3.0	0.972	0.896	0.779	0.630	0.460	0.288	0.141	0.036	-0.024
4.0	0.977	0.912	0.809	0.673	0.508	0.333	0.175	0.054	-0.018
5.0	0.980	0.922	0.829	0.701	0.542	0.367	0.201	0.069	-0.012
6.0	0.982	0.929	0.842	0.722	0.568	0.393	0.223	0.082	-0.007
7.0	0.983	0.933	0.852	0.737	0.587	0.414	0.240	0.093	-0.001
8.0	0.984	0.937	0.859	0.748	0.602	0.431	0.255	0.102	0.004

Table 12. K/K_0 in a line pipe with OD = 30 in., $h = 0.5$ in.

L_0/h	0.1	0.2	0.3	0.4	0.5	0.6	0.7	0.8	0.9
Outer axial crack, $N_{\infty} \neq 0, M_{\infty} = 0$									
1.0	0.946	0.820	0.668	0.513	0.370	0.250	0.149	0.744	0.034
2.0	0.968	0.887	0.775	0.640	0.494	0.352	0.218	0.111	0.050
3.0	0.978	0.918	0.830	0.714	0.576	0.428	0.276	0.143	0.064
4.0	0.983	0.936	0.864	0.764	0.636	0.489	0.327	0.174	0.078
5.0	0.986	0.947	0.886	0.799	0.682	0.539	0.371	0.204	0.092
6.0	0.988	0.955	0.903	0.825	0.718	0.580	0.411	0.231	0.106
7.0	0.990	0.961	0.915	0.845	0.746	0.615	0.446	0.257	0.120
8.0	0.991	0.965	0.924	0.861	0.769	0.643	0.476	0.281	0.133
Outer axial crack, $N_{\infty} = 0, M_{\infty} \neq 0$									
1.0	0.945	0.808	0.632	0.449	0.278	0.138	0.043	-0.010	-0.034
2.0	0.967	0.880	0.751	0.595	0.423	0.257	0.120	0.026	-0.026
3.0	0.977	0.913	0.812	0.680	0.519	0.347	0.186	0.061	-0.016
4.0	0.982	0.932	0.850	0.737	0.590	0.419	0.245	0.095	-0.003
5.0	0.985	0.944	0.876	0.777	0.642	0.477	0.297	0.128	0.011
6.0	0.988	0.925	0.894	0.807	0.683	0.526	0.343	0.159	0.026
7.0	0.989	0.959	0.907	0.829	0.816	0.565	0.383	0.188	0.040
8.0	0.990	0.963	0.917	0.846	0.741	0.598	0.417	0.214	0.054
Inner axial crack, $N_{\infty} \neq 0, M_{\infty} = 0$									
1.0	0.944	0.815	0.660	0.503	0.362	0.244	0.145	0.073	0.034
2.0	0.966	0.879	0.759	0.619	0.471	0.332	0.205	0.105	0.049
3.0	0.975	0.908	0.809	0.685	0.541	0.394	0.250	0.130	0.061
4.0	0.980	0.925	0.841	0.729	0.592	0.443	0.288	0.152	0.072
5.0	0.983	0.936	0.863	0.761	0.632	0.483	0.322	0.173	0.082
6.0	0.985	0.944	0.879	0.786	0.664	0.517	0.352	0.192	0.092
7.0	0.987	0.951	0.892	0.806	0.690	0.547	0.379	0.210	0.101
8.0	0.988	0.955	0.902	0.823	0.712	0.572	0.403	0.228	0.110
Inner axial crack, $N_{\infty} = 0, M_{\infty} \neq 0$									
1.0	0.943	0.802	0.622	0.437	0.267	0.129	0.038	-0.012	-0.034
2.0	0.965	0.870	0.733	0.570	0.395	0.232	0.103	0.017	-0.029
3.0	0.974	0.901	0.789	0.645	0.477	0.304	0.154	0.042	-0.021
4.0	0.979	0.920	0.825	0.696	0.536	0.362	0.198	0.067	-0.013
5.0	0.982	0.932	0.849	0.732	0.582	0.409	0.237	0.090	-0.004
6.0	0.985	0.941	0.867	0.761	0.619	0.449	0.271	0.112	0.006
7.0	0.987	0.947	0.881	0.784	0.650	0.484	0.303	0.132	0.015
8.0	0.988	0.952	0.892	0.802	0.675	0.514	0.331	0.151	0.024

Table 13. K/K_0 in a line pipe with OD = 24 in., $h = 0.344$ in.

L_0/h	0.1	0.2	0.3	0.4	0.5	0.6	0.7	0.8	0.9
Outer circumferential crack, $N_\infty \neq 0, M_\infty = 0$									
1.0	0.945	0.817	0.664	0.508	0.366	0.247	0.147	0.073	0.033
2.0	0.967	0.882	0.766	0.628	0.481	0.340	0.210	0.106	0.048
3.0	0.976	0.911	0.817	0.695	0.553	0.405	0.257	0.132	0.060
4.0	0.980	0.928	0.847	0.739	0.604	0.455	0.297	0.155	0.070
5.0	0.983	0.938	0.868	0.769	0.642	0.493	0.329	0.175	0.080
6.0	0.985	0.945	0.882	0.791	0.670	0.524	0.357	0.193	0.088
7.0	0.987	0.950	0.892	0.807	0.692	0.549	0.380	0.209	0.097
8.0	0.987	0.953	0.899	0.819	0.709	0.570	0.400	0.223	0.104
Outer circumferential crack, $N_\infty = 0, M_\infty \neq 0$									
1.0	0.944	0.805	0.627	0.443	0.273	0.133	0.040	-0.011	-0.034
2.0	0.966	0.874	0.741	0.581	0.407	0.242	0.109	0.020	-0.028
3.0	0.975	0.905	0.798	0.657	0.492	0.318	0.164	0.048	-0.021
4.0	0.980	0.923	0.832	0.707	0.551	0.376	0.209	0.072	-0.012
5.0	0.983	0.934	0.854	0.741	0.594	0.421	0.246	0.094	-0.004
6.0	0.985	0.941	0.869	0.765	0.626	0.457	0.277	0.114	0.005
7.0	0.986	0.946	0.880	0.783	0.651	0.485	0.303	0.131	0.013
8.0	0.987	0.950	0.888	0.797	0.670	0.508	0.325	0.146	0.020
Inner circumferential crack, $N_\infty \neq 0, M_\infty = 0$									
1.0	0.944	0.814	0.659	0.503	0.361	0.243	0.145	0.073	0.033
2.0	0.965	0.877	0.756	0.615	0.467	0.327	0.201	0.102	0.048
3.0	0.974	0.904	0.803	0.675	0.530	0.383	0.241	0.124	0.058
4.0	0.978	0.919	0.831	0.714	0.573	0.423	0.271	0.141	0.066
5.0	0.981	0.929	0.849	0.740	0.604	0.453	0.296	0.156	0.074
6.0	0.983	0.935	0.862	0.759	0.628	0.477	0.316	0.168	0.080
7.0	0.984	0.940	0.871	0.773	0.646	0.497	0.332	0.179	0.086
8.0	0.985	0.943	0.878	0.784	0.660	0.513	0.347	0.189	0.091
Inner circumferential crack, $N_\infty = 0, M_\infty \neq 0$									
1.0	0.943	0.801	0.621	0.436	0.267	0.129	0.037	-0.012	-0.034
2.0	0.964	0.868	0.729	0.565	0.390	0.226	0.099	0.015	-0.030
3.0	0.973	0.897	0.782	0.634	0.463	0.291	0.143	0.037	-0.024
4.0	0.977	0.914	0.813	0.677	0.513	0.337	0.177	0.055	-0.018
5.0	0.980	0.924	0.833	0.706	0.548	0.372	0.204	0.070	-0.012
6.0	0.982	0.931	0.846	0.728	0.575	0.399	0.227	0.084	-0.007
7.0	0.983	0.936	0.856	0.743	0.595	0.421	0.246	0.095	-0.002
8.0	0.984	0.939	0.864	0.755	0.611	0.439	0.261	0.105	0.003

Table 16. K/K_0 in a line pipe with OD = 20 in., $h = 0.344$ in.

$L_0/h \rightarrow$	0.1	0.2	0.3	0.4	0.5	0.6	0.7	0.8	0.9
Outer axial crack, $N_{\infty} \neq 0, M_{\infty} = 0$									
a/h \downarrow									
1.0	0.946	0.820	0.668	0.513	0.371	0.250	0.149	0.074	0.034
2.0	0.968	0.887	0.775	0.640	0.494	0.352	0.219	0.111	0.050
3.0	0.978	0.918	0.830	0.714	0.577	0.428	0.276	0.144	0.064
4.0	0.983	0.936	0.864	0.764	0.637	0.490	0.327	0.175	0.079
5.0	0.986	0.947	0.887	0.799	0.683	0.540	0.372	0.204	0.093
6.0	0.988	0.955	0.903	0.826	0.718	0.581	0.412	0.232	0.107
7.0	0.990	0.961	0.915	0.845	0.747	0.615	0.446	0.258	0.121
8.0	0.991	0.965	0.924	0.861	0.769	0.644	0.477	0.282	0.134
Outer axial crack, $N_{\infty} = 0, M_{\infty} \neq 0$									
1.0	0.944	0.808	0.632	0.448	0.279	0.138	0.043	-0.010	-0.034
2.0	0.967	0.880	0.752	0.595	0.424	0.257	0.120	0.026	-0.026
3.0	0.977	0.913	0.813	0.680	0.520	0.347	0.187	0.061	-0.015
4.0	0.982	0.932	0.851	0.737	0.590	0.420	0.246	0.095	-0.002
5.0	0.985	0.944	0.876	0.777	0.643	0.478	0.298	0.129	0.012
6.0	0.988	0.955	0.894	0.807	0.684	0.526	0.344	0.160	0.026
7.0	0.989	0.959	0.907	0.829	0.716	0.566	0.383	0.189	0.041
8.0	0.990	0.963	0.917	0.846	0.742	0.599	0.418	0.215	0.055
Inner axial crack, $N_{\infty} \neq 0, M_{\infty} = 0$									
1.0	0.944	0.815	0.660	0.503	0.361	0.244	0.145	0.073	0.034
2.0	0.966	0.879	0.759	0.619	0.471	0.332	0.205	0.105	0.049
3.0	0.975	0.907	0.809	0.684	0.541	0.394	0.250	0.130	0.061
4.0	0.980	0.925	0.841	0.729	0.592	0.443	0.288	0.152	0.072
5.0	0.983	0.936	0.863	0.761	0.632	0.483	0.322	0.173	0.082
6.0	0.985	0.944	0.879	0.786	0.664	0.517	0.352	0.192	0.092
7.0	0.987	0.950	0.892	0.806	0.690	0.547	0.379	0.211	0.101
8.0	0.988	0.955	0.902	0.822	0.712	0.573	0.403	0.228	0.111
Inner axial crack, $N_{\infty} = 0, M_{\infty} \neq 0$									
1.0	0.943	0.801	0.622	0.437	0.267	0.129	0.038	-0.012	-0.034
2.0	0.965	0.870	0.733	0.569	0.395	0.232	0.103	0.017	-0.029
3.0	0.974	0.901	0.789	0.645	0.477	0.304	0.154	0.043	-0.021
4.0	0.979	0.920	0.824	0.695	0.536	0.362	0.198	0.068	-0.013
5.0	0.982	0.932	0.849	0.732	0.582	0.409	0.237	0.091	-0.003
6.0	0.985	0.941	0.867	0.761	0.619	0.449	0.272	0.112	0.006
7.0	0.986	0.947	0.881	0.783	0.650	0.484	0.303	0.133	0.015
8.0	0.988	0.952	0.892	0.802	0.675	0.514	0.331	0.152	0.025

Table 17. The stress intensity factor ratio $10^4(K/K_0)$ at the deepest penetration point of a semi-elliptic outer circumferential crack in a pipe subjected to parabolic loadings. OD = 20 in., $h = 0.344$ in., $\nu = 0.3$.

$$N_{11} = N_{\infty} X_2^2 / 2R^2, M_{11} = 0$$

$a/h \backslash L_0/h$	0.1	0.2	0.3	0.4	0.5	0.6	0.7	0.8	0.9
1.0	0.024	0.062	0.080	0.078	0.063	0.043	0.026	.012	0.004
1.5	0.032	0.089	0.129	0.138	0.121	0.089	0.055	0.026	0.010
2.0	0.083	0.247	0.379	0.432	0.400	0.311	0.200	0.096	0.035
2.5	0.175	0.538	0.863	1.032	1.003	0.813	0.542	0.271	0.097
3.0	0.320	1.006	0.673	2.077	2.098	1.764	1.217	0.625	0.227
3.5	0.529	1.699	2.896	3.711	3.875	3.366	2.396	1.263	0.467
4.0	0.810	2.645	4.616	6.076	6.530	5.843	4.277	2.312	0.875
4.5	1.169	3.882	6.904	9.302	10.261	9.429	7.088	3.928	1.526
5.0	1.618	5.429	9.822	13.514	15.254	14.366	11.064	6.281	2.512

$$N_{11} = 0, M_{11} = M_{\infty} X_2^2 / 2R^2$$

$a/h \backslash L_0/h$	0.1	0.2	0.3	0.4	0.5	0.6	0.7	0.8	0.9
1.0	0.025	0.069	0.097	0.098	0.082	0.057	0.032	0.013	.002
1.5	0.033	0.100	0.154	0.173	0.157	0.119	0.072	0.311	0.066
2.0	0.127	0.402	0.659	0.786	0.756	0.604	0.385	0.175	0.043
2.5	0.184	0.602	1.032	1.290	1.300	1.082	0.723	0.344	0.093
3.0	0.336	1.129	1.997	2.591	2.715	2.358	1.628	0.805	0.236
3.5	0.555	1.899	3.453	4.620	5.003	4.491	3.207	1.641	0.518
4.0	0.850	2.956	5.495	7.547	8.410	7.780	5.724	3.026	1.015
4.5	1.229	4.333	8.205	11.531	13.182	12.521	9.468	5.154	1.828
5.0	1.698	6.053	11.653	16.709	19.540	19.020	14.751	8.251	3.077

APPENDIX D

CIRCUMFERENTIALLY CRACKED CYLINDERS UNDER EXTENSION OR BENDING

I. Introduction

The solution for cylinders containing a part-through surface crack given in Appendices B and C of this report is based on a shell theory. Even though no solution has appeared yet, the problem can also be solved numerically by using the finite element method. Since the analytical solution of the surface crack problem itself is intractable, the next best thing would be to obtain an exact upper bound to its results analytically. Such a bound can be obtained by assuming that the part-through crack goes along the entire circumference of the cylinder, that is, the geometry of the problem is axisymmetric. The general problem considered in this Appendix is three-dimensional in the sense that the external loads are assumed to be nonaxisymmetric. Thus the results are given for a cylinder under bending as well as under axial tension.

Elasticity solutions for penny-shaped and ring-shaped cracks in an infinite medium or in long cylinders with uniform symmetric tractions acting on the crack surface abound in the literature [1]-[4]. The circumferentially cracked thick-walled cylinder subjected to symmetric loading has recently been solved by R. Erdol and F. Erdogan [5] using integral transform techniques in a very straightforward manner. Their numerical solutions coincide with the first term of the general solution presented in this study.

The problem of a penny-shaped crack in an infinite medium opened by the application of a nonsymmetrical pressure has been solved by using a variety of techniques starting with the method used by Kobayashi in 1931 [6]. The nonaxisymmetrically loaded penny-shaped crack is also formulated in [7] and [8] by expanding the load in terms of a Fourier series and using integral transform techniques. More recently, M.K. Kassir and M. Singh have solved the problem of a solid cylinder with a penny-shaped crack subjected to bending [9] by expanding the load in a Fourier cosine series. The numerical results presented by Kassir and Singh represent the limiting values of stress intensity factors for small inner radius, hollow, thick-walled cylinders with internal edge cracks in bending. The numerical results presented here for this special case are in excellent agreement with Kassir and Singh.

The formulation presented in the following investigation represents a general technique for the solution of a three-dimensional elasticity problem in cylindrical coordinates with mixed boundary conditions imposed along a plane perpendicular to the z axis. Mathematically, direct reduction of the problem to a singular integral equation is accomplished in a straightforward manner after the boundary conditions have been applied and the dominant singular behavior extracted. The resulting

integral equation of the Fredholm type is solved numerically for a variety of problems by reducing the problem to a system of simultaneous linear algebraic equations. Consideration of edge cracks in the cylinder present no theoretical difficulties and are also handled in a direct manner without the introduction of any additional conditions or constraints.

The numerical results presented are of useful engineering significance. Stress intensity factors obtained for axial loading and pure bending are of direct interest to the design engineer and are useful in the correlation and development of various numerical and analytical models used in the determination of structural failure.

The effect of transient thermal stress fields on a cracked hollow cylinder is pertinent in the design of nuclear reactor coolant systems and components. The numerical results presented for this transient form of loading are for the particularly critical situation when the coolant is suddenly introduced into a pipe with a circumferential crack on the inner surface. In this situation, which is usually difficult to inspect visually, high tensile stresses develop in a thin layer on the inner radius and may cause significant crack growth radially outwards.

Another interesting example of nonuniform loading presented in this study, is the effect residual stresses in the cylinder

wall have on varying crack lengths. These residual stresses usually develop after sudden cooling of the cylinder during manufacture or welding. A circumferential flaw in the cylinder wall under such residual loading, is extremely difficult to detect due to the closure of the crack in the compressive stress field near the cylinder surface. In some cases residual stresses may be the only stress state in the body. For example, in considering the problem of subcritical crack growth due to static fatigue in glass pipes and other ceramics which do not normally carry any external loads, the crack driving force is mainly provided by the residual stresses.

II. Formulation

The problem which is to be formulated mathematically is that of a long thick-walled cylinder which contains a concentric ring-shaped crack in the $z=0$ plane, z being the axis of the cylinder (see figure 1). The cylinder is subjected to external loads which may be mechanical, thermal or residual and are independent of z .

Since the applied loading $p(r,\theta)$ is in general nonsymmetric the problem must be formulated as a three-dimensional elasticity problem. The usual superposition technique, which results in a traction free crack surface, is employed to express the problem in terms of an infinite region with a crack plus a hollow cylinder without a crack. The crack surface tractions in the infinite media are equal in magnitude and opposite in sign to the stresses on the $z=0$ plane in the uncracked hollow cylinder.

Two shear stress symmetry conditions,

$$\tau_{zr}(r,\theta,0) = \tau_{z\theta}(r,\theta,0) = 0, \quad a \leq r \leq b, \quad 0 \leq \theta \leq 2\pi, \quad (1)$$

six stress boundary conditions,

$$\tau_{rz}(a,\theta,z) = \tau_{rz}(b,\theta,z) = 0, \quad (2)$$

$$\tau_{r\theta}(a,\theta,z) = \tau_{r\theta}(b,\theta,z) = 0, \quad (3)$$

$$\sigma_{rr}(a,\theta,z) = \sigma_{rr}(b,\theta,z) = 0, \quad 0 \leq \theta \leq 2\pi, \quad 0 \leq z < \infty, \quad (4)$$

and the mixed boundary conditions,

$$u_z(r,\theta,0) = 0, \quad a \leq r \leq c, \quad d \leq r \leq b, \quad 0 \leq \theta \leq 2\pi, \quad (5)$$

$$\sigma_{zz}(r,\theta,0) = -p(r,\theta), \quad c \leq r \leq d, \quad 0 \leq \theta \leq 2\pi, \quad (6)$$

where u_z is the displacement in the z direction, must be satisfied for the complete solution of the perturbation or crack problem in the infinite region. This is accomplished by expanding the applied load $p(r,\theta)$ on the $z=0$ plane in terms of a cosine Fourier series. Of course, the loading could have been expanded in a general Fourier series, but since the problems of primary interest in this investigation are axial extension and pure bending, assuming loading to be even in θ is not a serious restriction and simplifies the analysis.

The applied load is represented in series form as

$$-p(r,\theta) = -\sum_{n=0}^{\infty} P_n(r)\cos(n\theta), \quad (7)$$

with

$$P_0(r) = \frac{1}{\pi} \int_0^{\pi} p(r,\theta) d\theta \quad (8)$$

$$P_n(r) = \frac{2}{\pi} \int_0^{\pi} p(r,\theta)\cos(n\theta) d\theta. \quad (9)$$

The solutions of most three-dimensional elasticity problems are obtained in terms of displacement potentials. It can be shown, Green and Zerna [10] or Sih [11], that the solution for an infinite medium with a crack may be obtained in terms of one potential function only. The displacements and stresses in terms of a single potential function ϕ may be expressed as [10]-[11];

$$2\mu u_r = (1-2\nu) \frac{\partial \phi}{\partial r} + z \frac{\partial^2 \phi}{\partial r \partial z} , \quad (10)$$

$$2\mu u_\theta = (1-2\nu) \frac{1}{r} \frac{\partial \phi}{\partial \theta} + \frac{z}{r} \frac{\partial^2 \phi}{\partial \theta \partial z} , \quad (11)$$

$$2\mu u_z = -2(1-\nu) \frac{\partial \phi}{\partial z} + z \frac{\partial^2 \phi}{\partial z^2} , \quad (12)$$

$$\sigma_{rr} = z \frac{\partial^3 \phi}{\partial r^2 \partial z} + \frac{\partial^2 \phi}{\partial r^2} - 2\nu \left(\frac{\partial^2 \phi}{\partial r^2} + \frac{\partial^2 \phi}{\partial z^2} \right) , \quad (13)$$

$$\sigma_{\theta\theta} = -(1-2\nu) \frac{\partial^2 \phi}{\partial r^2} + \frac{z}{r^2} \frac{\partial^3 \phi}{\partial \theta^2 \partial z} + \frac{z}{r} \frac{\partial^2 \phi}{\partial r \partial z} - \frac{\partial^2 \phi}{\partial z^2} , \quad (14)$$

$$\sigma_{zz} = z \frac{\partial^3 \phi}{\partial z^3} - \frac{\partial^2 \phi}{\partial z^2} , \quad (15)$$

$$\tau_{zr} = z \frac{\partial^3 \phi}{\partial r \partial z^2} , \quad (16)$$

$$\tau_{z\theta} = \frac{z}{r} \frac{\partial^3 \phi}{\partial \theta \partial z^2} \quad (17)$$

$$\tau_{r\theta} = (1-2\nu) \left(\frac{1}{r} \frac{\partial^2 \phi}{\partial r \partial \theta} - \frac{1}{r^2} \frac{\partial \phi}{\partial \theta} \right) - \frac{z}{r^2} \frac{\partial^2 \phi}{\partial \theta \partial z} + \frac{z}{r} \frac{\partial^3 \phi}{\partial r \partial \theta \partial z} , \quad (18)$$

where μ is the shear modulus, ν the Poisson's ratio and ϕ satisfies Laplace's equation in cylindrical coordinates

$$\frac{\partial^2 \phi}{\partial r^2} + \frac{1}{r} \frac{\partial \phi}{\partial r} + \frac{1}{r^2} \frac{\partial^2 \phi}{\partial \theta^2} + \frac{\partial^2 \phi}{\partial z^2} = 0 \quad (19)$$

If it is assumed that the displacement potential is of the form

$$\phi(r, \theta, z) = \sum_{n=0}^{\infty} \phi_n(r, z) \cos(n\theta), \quad (20)$$

then the application of Hankel integral transforms to (19) would show that the harmonic function $\phi(r, \theta, z)$ may be expressed as

$$\phi(r, \theta, z) = \sum_{n=0}^{\infty} \cos(n\theta) \int_0^{\infty} A_n(\alpha) J_n(\alpha r) \alpha e^{-\alpha z} d\alpha. \quad (21)$$

If body forces are neglected, Lure [12], Green and Zerna [10] and Kassir [9], demonstrate that the general problem of a cylinder without a crack can be expressed in terms of four harmonic functions. The displacement vector expressed in terms of these Papkovitch-Neuber displacement potentials is given by [12] as

$$\vec{u} = 4(1-\nu)\vec{B} - \text{grad}(\vec{R} \cdot \vec{B} + B_0), \quad (22)$$

where

$$\vec{R} = r \vec{i}_r + z \vec{i}_z \quad (23)$$

and

$$\vec{B} = B_r \vec{i}_r + B_\theta \vec{i}_\theta + B_z \vec{i}_z \quad (24)$$

Since B_r and B_θ are not necessarily harmonic [12], the example of [9], [10] and [12] is followed and the form of the four potential functions is chosen in such a manner as to ensure that the functions are harmonic in cylindrical coordinates. The displacements and stresses expressed in terms of these four new functions are ([9]-[10]):

$$2\mu u_r = (3-4\nu)[B_1 \cos\theta + B_2 \sin\theta] - r \left[\frac{\partial B_1}{\partial r} \cos\theta + \frac{\partial B_2}{\partial r} \sin\theta \right] - \frac{\partial B_0}{\partial r} + \frac{2}{r} \frac{\partial \psi}{\partial \theta} \quad (25)$$

$$2\mu u_\theta = (3-4\nu)[B_2 \cos\theta - B_1 \sin\theta] - \left[\frac{\partial B_1}{\partial \theta} \cos\theta + \frac{\partial B_2}{\partial \theta} \sin\theta \right] - \frac{1}{r} \frac{\partial B_0}{\partial \theta} - 2 \frac{\partial \psi}{\partial r} \quad (26)$$

$$2\mu u_z = -r \frac{\partial B_1}{\partial z} \cos\theta - r \frac{\partial B_2}{\partial z} \sin\theta - \frac{\partial B_0}{\partial z} \quad (27)$$

$$\frac{\sigma_{rr}}{2\mu} = \frac{\nu \Delta}{1-2\nu} + \frac{\partial u_r}{\partial r} \quad (28)$$

$$\frac{\sigma_{\theta\theta}}{2\mu} = \frac{\nu \Delta}{1-2\nu} + \frac{1}{r} \left(\frac{\partial u_\theta}{\partial \theta} + u_r \right) \quad (29)$$

$$\frac{\sigma_{zz}}{2\mu} = \frac{\nu \Delta}{1-2\nu} + \frac{\partial u_z}{\partial z} \quad (30)$$

$$\frac{\tau_{\theta z}}{\mu} = \frac{1}{r} \frac{\partial u_z}{\partial \theta} + \frac{\partial u_\theta}{\partial z} \quad (31)$$

$$\frac{\tau_{rz}}{\mu} = \frac{\partial u_r}{\partial z} + \frac{\partial u_z}{\partial r} \quad (32)$$

$$\frac{\tau_{r\theta}}{\mu} = \frac{1}{r} \frac{\partial u_r}{\partial \theta} + \frac{\partial u_\theta}{\partial r} - \frac{u_\theta}{r} \quad (33)$$

where

$$\begin{aligned} \Delta &= \frac{\partial u_r}{\partial r} + \frac{u_r}{r} + \frac{1}{r} \frac{\partial u_\theta}{\partial \theta} + \frac{\partial u_z}{\partial z} \\ &= \frac{1-2\nu}{\mu} \left[\left(\frac{\partial B_1}{\partial r} + \frac{1}{r} \frac{\partial B_2}{\partial \theta} \right) \cos \theta + \left(\frac{\partial B_2}{\partial r} - \frac{1}{r} \frac{\partial B_1}{\partial \theta} \right) \sin \theta \right]. \end{aligned} \quad (34)$$

Since σ_{zz} is assumed to be even in θ , B_1 and B_0 must be even in θ ; and B_2 and ψ must be odd in θ . Thus the functions may be expressed in the following form ([9] & [12]),

$$\begin{bmatrix} B_1 \\ B_2 \end{bmatrix} = \sum_{n=0}^{\infty} \begin{Bmatrix} \cos(n\theta) \\ \sin(n\theta) \end{Bmatrix} G_1(r, z), \quad (35)$$

$$B_0 = \sum_{n=0}^{\infty} \cos(n\theta) G_2(r, z), \quad (36)$$

$$\psi = \sum_{n=0}^{\infty} \sin(n\theta) G_3(r, z). \quad (37)$$

From (19) and (35)-(37) the final form of the displacement potentials are determined. As an example, for u_z to be an odd

function in z and B_1 , an even function in z a cosine transform solution in the z -direction is assumed. This yields,

$$B_1 = \sum_{n=0}^{\infty} \cos[(n+1)\theta] \frac{2}{\pi} \int_0^{\infty} [C_{1n}(s)I_{n+1}(sr) + C_{2n}(s)K_{n+1}(sr)] \cos(sz) ds, \quad (38)$$

where $I_n(sr)$ and $K_n(sr)$ are modified Bessel functions of the first and the second kind. In the same manner B_2 , B_0 and ψ are determined.

$$B_2 = \sum_{n=0}^{\infty} \sin[(n+1)\theta] \frac{2}{\pi} \int_0^{\infty} [C_{1n}(s)I_{n+1}(sr) + C_{2n}(s)K_{n+1}(sr)] \cos(sz) ds \quad (39)$$

$$B_0 = \sum_{n=0}^{\infty} \cos(n\theta) \frac{2}{\pi} \int_0^{\infty} [C_{3n}(s)I_n(sr) + C_{4n}(s)K_n(sr)] \cos(sz) ds, \quad (40)$$

$$\psi = \sum_{n=0}^{\infty} \sin(n\theta) \frac{2}{\pi} \int_0^{\infty} [C_{5n}(s)I_n(sr) + C_{6n}(s)K_n(sr)] \cos(sz) ds \quad (41)$$

The displacement relations (10)-(12) and (25)-(27) when added together represent the displacement field for the superimposed problem. Thus, with the introduction of the displacement potential functions defined by (21) and (38)-(41), the displacements for the cracked cylinder may be expressed by:

$$\begin{aligned}
2\mu u_z &= \sum_{n=0}^{\infty} \cos(n\theta) \left\{ \int_0^{\infty} (2-2\nu+\alpha z) A_n(\alpha) \alpha^2 J_n(\alpha r) e^{-\alpha z} d\alpha \right. \\
&+ \frac{2}{\pi} \int_0^{\infty} [C_{1n}(s) r I_{n+1}(sr) + C_{2n}(s) K_{n+1}(sr) + C_{3n}(s) I_n(sr) \\
&+ C_{4n}(s) K_n(sr)] s \sin(sz) ds \left. \right\} \quad (42)
\end{aligned}$$

$$\begin{aligned}
2\mu u_r &= \sum_{n=0}^{\infty} \cos(n\theta) \left\{ \int_0^{\infty} (1-2\nu-\alpha z) A_n(\alpha) J_n'(\alpha r) \alpha e^{-\alpha z} d\alpha \right. \\
&+ \frac{2}{\pi} \int_0^{\infty} [C_{1n}(s) [(3-4\nu) I_{n+1}(sr) - r I_{n+1}'(sr)] + C_{2n}(s) [\\
&(3-4\nu) K_{n+1}(sr) - r K_{n+1}'(sr)] - C_{3n}(s) I_n'(sr) - C_{4n}(s) K_n'(sr) \\
&+ C_{5n}(s) \frac{2n}{r} I_n(sr) + C_{6n}(s) \frac{2n}{r} K_n(sr)] \cos(sz) ds \left. \right\} \quad (43)
\end{aligned}$$

$$\begin{aligned}
2\mu u_{\theta} &= \sum_{n=0}^{\infty} \sin(n\theta) \left\{ \int_0^{\infty} \frac{n}{r} (\alpha z + 2\nu - 1) A_n(\alpha) J_n(\alpha r) \alpha e^{-\alpha z} d\alpha \right. \\
&+ \frac{2}{\pi} \int_0^{\infty} [(4-4\nu+n) [C_{1n}(s) I_{n+1}(sr) + C_{2n}(s) K_{n+1}(sr)] \\
&+ \frac{n}{r} C_{3n}(s) I_n(rs) + \frac{n}{r} C_{4n}(s) K_n(rs) - 2C_{5n}(s) I_n'(sr) \\
&- 2C_{6n}(s) K_n'(sr)] \cos(sz) ds \left. \right\} \quad (44)
\end{aligned}$$

where $J_n(\alpha r)$ is the Bessel function of the first kind and the primes represent differentiation with respect to r .

The stresses are expressed in a similar manner by combining the stress relations (13)-(18) and (28)-(33). The stress field is described by:

$$\begin{aligned} \sigma_{zz} = & \sum_{n=0}^{\infty} \cos(n\theta) \left\{ \int_0^{\infty} -(1+\alpha z) A_n(\alpha) J_n(\alpha r) \alpha^3 e^{-\alpha z} d\alpha \right. \\ & + \frac{2}{\pi} \int_0^{\infty} \{ C_{1n}(s) [2\nu I_n(sr) + rs I_{n+1}(sr)] + C_{2n}(s) [-2\nu K_n(sr) \\ & + rs K_{n+1}(sr)] + s C_{3n}(s) I_n(sr) + s C_{4n}(s) K_n(sr) \} s \cos(sz) ds \} \end{aligned} \quad (45)$$

$$\begin{aligned} \sigma_{rr} = & \sum_{n=0}^{\infty} \cos(n\theta) \left\{ \int_0^{\infty} \left[[(1-2\nu-\alpha z) \left(\frac{n(n-1)}{r^2} - \alpha^2 \right) - 2\nu\alpha^2] J_n(\alpha r) \right. \right. \\ & + \frac{\alpha}{r} (1-2\nu-\alpha z) J_{n+1}(\alpha r) \} A_n(\alpha) \alpha e^{-\alpha z} d\alpha + \frac{2}{\pi} \int_0^{\infty} \{ C_{1n}(s) * \\ & * \{ (3-2\nu)s I_n(sr) - \left[\frac{(n+1)}{r} (4-4\nu+n) + rs^2 \right] I_{n+1}(sr) \} - C_{2n}(s) * \\ & * \{ (3-2\nu)s K_n(sr) + \left[\frac{(n+1)}{r} (4-4\nu+n) + rs^2 \right] K_{n+1}(sr) \} - C_{3n}(s) * \\ & * \left\{ \left[\frac{n(n-1)}{r^2} + s^2 \right] I_n(sr) - \frac{s}{r} I_{n+1}(sr) \right\} - C_{4n}(s) \left\{ \left[\frac{n(n-1)}{r^2} + s^2 \right] * \right. \\ & * K_n(sr) + \frac{s}{r} K_{n+1}(sr) \} + C_{5n}(s) \frac{2n}{r} \left[\frac{(n-1)}{r} I_n(sr) + s I_{n+1}(sr) \right] \\ & \left. + C_{6n}(s) \frac{2n}{r} \left[\frac{(n-1)}{r} K_n(sr) - s K_{n+1}(sr) \right] \right\} \cos(sz) ds \} \end{aligned} \quad (46)$$

$$\begin{aligned}
\tau_{rz} &= \sum_{n=0}^{\infty} \cos(n\theta) \left\{ \int_0^{\infty} A_n(\alpha) \left[\frac{n}{r} J_n(\alpha r) - \alpha J_{n+1}(\alpha r) \right] z \alpha^3 e^{-\alpha z} d\alpha \right. \\
&+ \frac{2}{\pi} \int_0^{\infty} \{ C_{1n}(s) [rs I_n(sr) - (2-2\nu+n) I_{n+1}(sr)] - C_{2n}(s) [rs K_n(sr) \\
&+ (2-2\nu+n) K_{n+1}(sr)] + C_{3n}(s) [s I_{n+1}(sr) + \frac{n}{r} I_n(sr)] \\
&+ C_{4n}(s) \left[\frac{n}{r} K_n(sr) - s K_{n+1}(sr) \right] - C_{5n}(s) \frac{n}{r} I_n(sr) \\
&\left. - C_{6n}(s) \frac{n}{r} K_n(sr) \} s \sin(sz) ds \right\} \quad (47)
\end{aligned}$$

$$\begin{aligned}
\tau_{\theta z} &= \sum_{n=0}^{\infty} \sin(n\theta) \left\{ \int_0^{\infty} -\frac{n}{r} A_n(\alpha) z \alpha^3 e^{-\alpha z} J_n(\alpha r) d\alpha \right. \\
&+ \frac{2}{\pi} \int_0^{\infty} \{ (2\nu-2-n) [C_{1n}(s) I_{n+1}(rs) + C_{2n}(s) K_{n+1}(rs)] - C_{3n}(s) \frac{n}{r} I_n(rs) \\
&- C_{4n}(s) \frac{n}{r} K_n(sr) + C_{5n}(s) [s I_{n+1}(rs) + \frac{n}{r} I_n(sr)] \\
&\left. + C_{6n}(s) \left[\frac{n}{r} K_n(sr) - s K_{n+1}(sr) \right] \} s \sin(sz) ds \right\} \quad (48)
\end{aligned}$$

$$\begin{aligned}
\tau_{r\theta} &= \sum_{n=0}^{\infty} \sin(n\theta) \left\{ \int_0^{\infty} \frac{n}{r} (\alpha z + 2\nu - 1) \left(\frac{n-1}{r} J_n(\alpha r) - \alpha J_{n+1}(\alpha r) \right) * \right. \\
&\left. * A_n(\alpha) \alpha e^{-\alpha z} d\alpha + \frac{2}{\pi} \int_0^{\infty} \{ C_{1n}(s) \left[-\frac{(n+1)}{r} (4-4\nu+n) I_{n+1}(sr) \right. \right. \right.
\end{aligned}$$

$$\begin{aligned}
& + (2-2\nu+n)s I_n(sr)] + C_{2n}(s)\left[-\frac{(n+1)}{r} (4-4\nu+n)K_{n+1}(sr)\right. \\
& - (2-2\nu+n)s K_n(sr)] + C_{3n}(s)\left[\frac{sn}{r} I_{n+1}(sr) + \frac{n}{r^2} (n-1)I_n(sr)\right] \\
& + C_{4n}(s)\left[-\frac{ns}{r} K_{n+1}(sr) + \frac{n}{r^2} (n-1)K_n(sr)\right] + C_{5n}(s)\left[-\frac{2n}{r^2} (n-1)\right. \\
& + s^2)I_n(sr) + \frac{2s}{r} I_{n+1}(sr)] + C_{6n}(s)\left[-\frac{2n}{r^2} (n-1)+s^2)K_n(sr)\right. \\
& \left. - \frac{2s}{r} K_{n+1}(sr)\right]\} \cos(sz) ds \quad . \quad (49)
\end{aligned}$$

From the above expressions it can readily be seen that the symmetry condition $\tau_{zr}(r, \theta, 0) = \tau_{z\theta}(r, \theta, 0) = 0$ is identically satisfied.

The unknown coefficients $A_n(\alpha)$ and $C_{in}(s)$ ($i=1,6$) are determined from the boundary conditions (2)-(6) for each value of n ($n=0,1,2,\dots$). Direct application of the mixed boundary conditions (5) and (6) may be implemented by introducing a new unknown function $\phi_n(r)$. Thus, the displacement $u_z(r, \theta, 0)$ is given by,

$$u_z(r, \theta, 0) = \sum_{n=0}^{\infty} \phi_n(r) \cos(n\theta), \quad c < r < d, \quad 0 \leq \theta \leq 2\pi, \quad (50)$$

$$u_z(r, \theta, 0) = 0, \quad a \leq r \leq c, \quad d \leq r \leq b, \quad 0 \leq \theta \leq 2\pi. \quad (51)$$

Application of the displacement boundary condition gives the unknown coefficient $A_n(\alpha)$ in terms of ϕ_n . Equation (42) in conjunction with (50)-(51) and the Hankel inversion yield

$$A_n(\alpha) = \frac{\mu}{1-\nu} \left[\frac{1}{\alpha} \int_c^d t \phi_n(t) J_n(\alpha t) dt \right] \quad (52)$$

The six unknown coefficients $C_{in}(s)$ ($i=1,6$), which occur in the stress and displacement equations (42)-(49) for each value of n , are obtained by application of the six boundary conditions (2)-(4) to the three stress equations (46), (47) and (49). For each equation the inverse Fourier transform is taken and the resulting six equations are solved for the six unknown coefficients. Obviously, due to the complexity of the matrix which must be inverted for the solution of the coefficients $C_{in}(s)$, this inversion is not attempted algebraically. The general expression which describes the coefficients $C_{in}(s)$ is given by,

$$C_{in}(s) = - \frac{\mu}{1-\nu} m_{ij}(s,a,b) \int_c^d t \phi_n(t) G_j(s,t) dt, \quad \begin{matrix} i=1,6 \\ j=1,6 \end{matrix}, \quad (53)$$

where the matrix $m_{ij}(s,a,b)$ is defined as $m_{ij}(s,a,b) = f_{ij}^{-1}(s,a,b)$ and the coefficient matrix $f_{ij}(s,a,b)$ is obtained from the stress equations (46), (47) and (49) and is given in appendix A. The terms $G_j(s,t)$ are obtained by integrating in

α the Bessel integrals which result from the substitution of (52) into the stress equations (46), (47) and (49). These definite Bessel integrals are evaluated in closed form by differentiating a related integral given by Erdélyi [13] and the resulting expressions for $G_j(s,t)$ are listed in appendix A.

Application of the last mixed boundary condition (6) yields the following integral equation,

$$\sum_{n=0}^{\infty} \left\{ \lim_{z \rightarrow 0} \int_0^{\infty} -(1+\alpha z) A_n(\alpha) J_n(\alpha r) \alpha^3 e^{-\alpha z} d\alpha \right. \\ \left. + \frac{2}{\pi} \int_0^{\infty} \left(\sum_{i=1}^4 C_{in}(s) N_i(s,r) \right) s ds \right\} = - \sum_{n=0}^{\infty} P_n(r) \quad (54)$$

where the terms $N_i(s,r)$ are given by

$$N_1(s,r) = 2\nu I_n(sr) + rs I_{n+1}(sr) \quad (55)$$

$$N_2(s,r) = -2\nu K_n(sr) + rs K_{n+1}(sr) \quad (56)$$

$$N_3(s,r) = s I_n(sr) \quad (57)$$

$$N_4(s,r) = s K_n(sr) \quad (58)$$

The asymptotic behavior of the first integral in (54) is extracted after the substitution of (52). This behavior is added and subtracted and the added portion of the asymptotic

integral is evaluated in closed form. Taking the $\lim_{z \rightarrow 0}$, a strong singular form for the first integral term is obtained. This is expressed as,

$$\frac{\mu}{1-\nu} \int_c^d \phi_n(t) \left[\frac{1}{\pi} \left(\frac{t}{r}\right)^{\frac{1}{2}} \frac{1}{(t-r)^2} - L_0(t,r) \right] dt \quad (59)$$

where $L_0(t,r)$ is given by,

$$L_0(t,r) = \int_0^\infty \alpha^2 \{ t J_n(\alpha t) J_n(\alpha r) - \frac{1}{\pi \alpha} \left(\frac{t}{r}\right)^{\frac{1}{2}} (\cos[\alpha(t-r)] + (-1)^n \sin[\alpha(t+r)]) \} d\alpha \quad (60)$$

The singular behavior in (59) is stronger than the Cauchy type singularity and is in general nonintegrable. This does not present a difficulty though, since integration by parts weakens the order of the singularity and enables one to express (59) in terms of the derivative of the unknown function, $\phi_n'(t)$. After integration by parts (59) becomes

$$\begin{aligned} & \frac{\mu}{1-\nu} \phi_n(t) \left\{ \frac{-\sqrt{t}}{t-r} + \frac{1}{2\sqrt{r}} \log \left[\frac{(t^{\frac{1}{2}} - r^{\frac{1}{2}})^2}{|t-r|} \right] \right\} \Big|_c^d \\ & + \frac{\mu}{1-\nu} \int_c^d \left[\frac{1}{\pi} \left(\frac{t}{r}\right)^{\frac{1}{2}} \frac{1}{t-r} + L_1(t,r) \right] \phi_n'(t) dt, \end{aligned} \quad (61)$$

with $L_1(t,r)$ given by,

$$\begin{aligned}
L_1(t,r) = & -\frac{1}{\pi} \frac{1}{2r} \log \left[\frac{(t^{\frac{1}{2}} - r^{\frac{1}{2}})^2}{|t-r|} \right] + \int_0^\infty \{ \alpha t [n J_n(\alpha t) S_{0,n-1}(\alpha t) \\
& - J_{n-1}(\alpha t) S_{1,n}(\alpha t)] J_n(\alpha r) - \frac{1}{\pi} \frac{\sqrt{t}}{r} [\sin \alpha(t-r) - (-1)^n \cos \alpha(t+r)] \\
& - \frac{1}{\sqrt{2\pi r \alpha}} [C(\sqrt{\alpha t})(\sin(\alpha r) + (-1)^n \cos(\alpha r)) - S(\sqrt{\alpha t})(\cos(\alpha r) \\
& + (-1)^n \sin(\alpha r))] \} d\alpha, \tag{62}
\end{aligned}$$

In the preceding equation $S_{\mu,\nu}(z)$ is the standard notation for Lommel's function. The introduction of this function results from the evaluation of indefinite integrals which contain Bessel functions [14], [15]. Appendix C contains a brief summary of the properties of these functions and convenient methods for calculating their values numerically. The functions $C(x)$ and $S(x)$ are forms of the Fresnel integrals given by [16] and are expressed as;

$$C(x) = \frac{1}{\sqrt{2\pi}} \int_0^{x^2} \frac{\cos t}{\sqrt{t}} dt \tag{63}$$

$$S(x) = \frac{1}{\sqrt{2\pi}} \int_0^{x^2} \frac{\sin t}{\sqrt{t}} dt. \tag{63}$$

Careful examination of equation (61) indicates that the first, or constant term is zero if the crack is embedded in the

cylinder wall since the displacement at the crack tips is zero and from (50), (51) $\phi_n(c) = \phi_n(d) = 0$. If the crack is a penny shaped crack the constant term is also zero since the terms in brackets are zero at $t=0$. The only situation in which the constant terms, which result from the integration by parts, are nonzero is when the problem of an edge crack is considered. In this particular case $\phi(c)$ and $\phi(d)$ may be expressed as;

for an inner edge crack:

$$\phi(d) = 0 \quad , \quad \phi(c) = - \int_c^d \phi'(t) dt \quad (65)$$

and for an outer edge crack:

$$\phi(c) = 0 \quad , \quad \phi(d) = \int_c^d \phi'(t) dt \quad (66)$$

The problem of edge cracks is considered separately and for the sake of simplicity the final form of the integral equation is derived assuming the constant term in (61) equals zero.

Integration by parts of the second term in (54) is now performed and combining this result with the expression given in (61) the singular integral equation becomes:

$$\begin{aligned} \sum_{n=0}^{\infty} \frac{1}{\pi} \int_c^d \left(\frac{t}{r}\right)^{\frac{1}{2}} \frac{\phi_n'(t)}{t-r} dt + \int_c^d [L_1(t,r) + L_2(t,r)] \phi_n'(t) dt \\ = - \frac{1-\nu}{\mu} \sum_{n=0}^{\infty} P_n(r) \quad , \quad c < r < d. \end{aligned} \quad (67)$$

The Fredholm Kernel $L_2(t,r)$ is the term which modifies the infinite space crack solution and is the resulting effect of finite cylinder boundaries. $L_2(t,r)$ is given by,

$$L_2(t,r) = \frac{2}{\pi} \int_0^{\infty} \sum_{i=1}^4 \sum_{j=1}^6 m_{ij}(s,a,b) v_j(s,t) N_i(s,r) s \, ds, \quad (68)$$

where $N_i(s,r)$ has been previously defined (55)-(58) and the matrix m_{ij} is given by the inverse of f_{ij} which is expressed in appendix A. The terms $v_j(s,t)$ are expressed in terms of modified Bessel functions and Lommel's function of imaginary argument and are recorded in appendix B.

The formulation of the singular integral equation of the first kind (67), has been quite general. No restrictions have been placed on the crack location and the dimensions of the inner and outer radii. Thus, for instance, with the omission of the Fredholm kernel $L_2(t,r)$, (67) becomes the singular integral equation for a concentric ring-shaped crack in an infinite medium subjected to general loading. If $c=0$ this is the equation for a penny-shaped crack. Inclusion of kernel $L_2(t,r)$ yields the equation for cylinder problems, hollow or solid.

III. Numerical Solution

The singular integral equation (67) with a Cauchy-type singularity is a standard form which can be solved in a direct manner numerically [17]. When normalized with respect to the crack length, (67) may be expressed as

$$\sum_{n=0}^{\infty} \frac{1}{\pi} \int_{-1}^{+1} \left[\frac{\frac{d-c}{2} \tau + \frac{d+c}{2}}{\frac{d-c}{2} \rho + \frac{d+c}{2}} \right]^{\frac{1}{2}} \frac{F_n(\tau)}{\tau - \rho} d\tau$$

$$+ \frac{d-c}{2} \int_{-1}^{+1} [L_1(t, r) + L_2(t, r)] F_n(\tau) d\tau = - \frac{1-\nu}{\mu} \sum_{n=0}^{\infty} P_n(r),$$

$$-1 < \tau, \rho < 1, \quad c < t, r < d, \quad (69)$$

where the unknown function

$$F_n(\tau) = \phi_n'(t), \quad (70)$$

and

$$t = \frac{d-c}{2} \tau + \frac{d+c}{2}, \quad (71)$$

$$r = \frac{d-c}{2} \rho + \frac{d+c}{2}. \quad (72)$$

For situations where internal cracks are considered an additional single-valuedness condition is given by

$$\int_c^d \phi_n'(t) dt = 0, \quad n = 0, 1, 2, \dots, \quad (73)$$

which, in normalized form, becomes

$$\int_{-1}^{+1} F_n(\tau) d\tau = 0, \quad n = 0, 1, 2, \dots, \quad (74)$$

The integral equations in this normalized form are readily solved using the methods detailed in [18].

Internal Crack

Examination of kernels $L_1(t, r)$ and $L_2(t, r)$ defined by (62) and (68) indicates that $L_1(t, r)$ has a logarithmic singularity, whereas $L_2(t, r)$ is bounded in the closed interval $c \leq (r, t) \leq d$ provided $a < c < d < b$, that is if the crack is a fully embedded internal crack. If this is the case, the Cauchy kernel $1/(\tau - \rho)$ is the dominant kernel. The index of the integral equation is +1 and the solution of the integral equation (69) has integrable singularities at the end points. Thus the solution is of the form [5],

$$\phi_n'(r) = \phi_n'(r) [(r-c)(d-r)]^{-\frac{1}{2}}. \quad (75)$$

Following the standard procedure for an integral equation of index +1 [17], [18], the solution of (69) and (74) reduces to

solving the following system of linear algebraic equations,

$$\sum_{k=1}^m W_k f_n(\tau_k) \left\{ \left[\frac{\frac{d-c}{2} \tau_k + \frac{d+c}{2}}{\frac{d-c}{2} \rho_i + \frac{d+c}{2}} \right]^{\frac{1}{2}} \frac{1}{\tau_k^{-\rho_i}} + K(\tau_k, \rho_i) \right\} = -p_n(\rho_i), \quad i = 1, \dots, m-1 \quad (76)$$

$$\sum_{k=1}^m W_k f_n(\tau_k) = 0, \quad \text{for } n = 0, 1, 2, \dots, \quad (77)$$

where

$$\frac{f_n(\tau)}{\sqrt{1-\tau^2}} = \frac{1}{\sigma_n(b)} \frac{\mu}{1-\nu} F_n(\tau), \quad (78)$$

$$K(\tau, \rho) = \frac{d-c}{2} \pi(L_2(t, r) + L_3(t, r)), \quad (79)$$

$$p_n(\rho) = P_n(r)/\sigma_n(b), \quad n = 0, 1, 2, \dots \quad (80)$$

The weights and abscissas for (76) and (77) are given by [18] as,

$$W_1 = W_m = \frac{1}{2(m-1)}, \quad W_k = \frac{1}{m-1}, \quad k = 2, \dots, m-1 \quad (81)$$

$$\tau_k = \cos\left(\pi \frac{k-1}{m-1}\right), \quad k = 1, \dots, m \quad (82)$$

$$\rho_i = \cos\left(\pi \frac{2i-1}{2m-2}\right), \quad i = 1, \dots, m-1 \quad (83)$$

Once the integral equation has been solved the quantities of particular interest are the stress intensity factors, which are defined by ,

$$k_n(c) = \lim_{r \rightarrow c} \sqrt{2(c-r)} \sigma_{zz_n}(r, \theta, 0) , \quad (84)$$

$$k_n(d) = \lim_{r \rightarrow d} \sqrt{2(r-d)} \sigma_{zz_n}(r, \theta, 0) , \quad n=0,1,2,\dots, \quad (85)$$

which may also be expressed as

$$k_n(c) = \lim_{r \rightarrow c} \sqrt{2(r-c)} \frac{\mu}{1-\nu} \frac{\partial u_z(r)}{\partial r} \cos n\theta \quad (86)$$

or

$$k_n(c) = \lim_{r \rightarrow c} \sqrt{2(r-c)} f_n(\rho) (1-\rho^2)^{-\frac{1}{2}} \cos n\theta \sigma_n(b) . \quad (87)$$

Thus the final form for the stress intensity factor becomes

$$k_n(c) = \sqrt{\frac{d-c}{2}} f_n(-1) \cos n\theta \sigma_n(b) \quad (88)$$

$$k_n(d) = - \sqrt{\frac{d-c}{2}} f_n(1) \cos n\theta \sigma_n(b) , \quad n = 0,1,2,\dots \quad (89)$$

where $f(1)$ and $f(-1)$ are obtained from the solution of (76)

and (77) and $\sigma_n(b)$ is defined for $n=0$ and $n=1$ as

$$\sigma_0(b) = \frac{P_\infty}{\pi(b^2-a^2)} \quad (90)$$

$$\sigma_1(b) = \frac{4Mb}{\pi(b^4 - a^4)} \quad , \quad (91)$$

with P_∞ the applied axial load at infinity and M the applied bending moment.

Edge Cracks

When the crack is an edge crack, the constant terms which are obtained from integration by parts are no longer zero (61). Using the expressions given in (65) and (66) the integral equation (67) for an edge crack becomes,

$$\begin{aligned} & \sum_{n=0}^{\infty} \left\{ \frac{1}{\pi} \int_c^d \left(\frac{t}{r}\right)^{\frac{1}{2}} \frac{\phi_n'(t)}{t-r} dt + \int_c^d \left[\frac{-1}{\pi} \left(\frac{\epsilon}{r}\right)^{\frac{1}{2}} \frac{1}{\epsilon-r} \right. \right. \\ & \quad \left. \left. + L_1(t,r) - L_1(\epsilon,r) + L_2(t,r) - L_2(\epsilon,r) \right] \phi_n'(t) dt \right\} \\ & = - \frac{1-\nu}{\mu} \sum_{n=0}^{\infty} P_n(r) \quad , \quad c < r < d \quad . \quad (92) \end{aligned}$$

An inner edge crack in the hollow cylinder opens on the inner radius and $\epsilon=c$. For outer edge cracks, $\epsilon=d$.

Casting the integral equation in this form clearly demonstrates that all coefficients of the unknown values $\phi'(c)$ or $\phi'(d)$ are equal to zero for the inner edge crack and the outer edge crack respectively. This is an important result since it

demonstrates that for edge cracks there is one less unknown. It is only natural that this is the case, since the auxiliary equation associated with the internal crack problem is no longer applicable. Thus, the solution of an edge crack problem will involve the simultaneous solution of $m-1$ linear algebraic equations as opposed to m equations for an internal crack. This means such statements or additional equations as $\phi'(c) < \infty$ or $\phi'(d) < \infty$, which have been previously employed in the solution of edge crack problems, are redundant and unnecessary.

When the case of edge cracks is being considered the Fredholm kernel $L_2(t,r)$ becomes very difficult to evaluate numerically since when both t and r simultaneously go to an endpoint the kernel becomes unbounded. To obtain any reasonable degree of accuracy in the numerical solution of the edge crack problem the generalized Cauchy kernel must be extracted. This is virtually impossible analytically since L_2 is not known in closed form, but instead calculated numerically. In this investigation the asymptotic behavior of the integrand in (68) was obtained by modifying the closed form asymptotic expression for symmetric loading given in [5]. This was done in such a manner as to ensure that the numerical values calculated for the integrand in (68) for large values of s and the asymptotic expression were identical.

Numerically, excellent agreement was obtained for large values of the integrand of L_2 in comparison with the modified closed form asymptotic behavior from [5]. Numerical values for the infinite integral in $L_2(t,r)$ were obtained by integrating numerically from 0 to A, where A is a finite number, and then adding the asymptotic "tail" which was determined by integrating in closed form the asymptotic behavior. Symbolically this process is described by,

$$L_2(t,r) = \frac{2}{\pi} \int_0^A \sum_{i=1}^4 \sum_{j=1}^6 m_{ij} v_j N_i s ds + k_s(t,r), \quad (93)$$

where

$$k_s(t,r) = k_{sa}(t,r) + k_{sb}(t,r), \quad (94)$$

with

$$k_{sa}(t,r) = \sqrt{\frac{t}{r}} \left\{ \frac{4(r-a)(t-a)}{(r+t-2a)^3} + \frac{4A(r-a)(t-a)-3(t-a)-(r-a)}{(r+t-2a)^2} \right. \\ \left. + \frac{2A^2(r-a)(t-a)-[3(t-a)+(r-a)]A+2}{(r+t-2a)} \right\} \frac{e^{-A(r+t-2a)}}{2} \quad (95)$$

$$k_{sb}(t,r) = - \sqrt{\frac{t}{r}} \left\{ \frac{4(b-r)(b-t)}{(2b-r-t)^3} + \frac{4A(b-r)(b-t)-3(b-t)-(b-r)}{(2b-r-t)^2} \right. \\ \left. + \frac{2A^2(b-r)(b-t)-[3(b-t)+(b-r)]A+2}{(2b-r-t)} \right\} \frac{e^{-A(2b-r-t)}}{2}. \quad (96)$$

Besides the stress intensity factor, another quantity of particular interest is the crack opening displacement or COD at the mouth of the crack. This displacement for an inner edge crack is defined by

$$\delta(c) = u_z(c, \theta, +0) - u_z(c, \theta, -0), \quad (97)$$

where $u_z(r, \theta, 0)$ is given by (50). Using expressions (65), (70) and (78), the crack opening displacement at the crack mouth c , $\delta(c)$, is written in terms of the following normalized expression.

$$\frac{\mu}{1-\nu} \frac{\delta(c)}{h\sigma_n(b)} = -\cos(n\theta) \frac{d-c}{h} \int_{-1}^1 \frac{f_n(\tau)}{\sqrt{1-\tau^2}} d\tau, \quad (98)$$

$$n = 0, 1, 2, \dots$$

In a similar manner the crack opening displacement for an outer edge crack is written as

$$\frac{\mu}{1-\nu} \frac{\delta(d)}{h\sigma_n(b)} = \cos(n\theta) \frac{d-c}{h} \int_{-1}^1 \frac{f_n(\tau)}{\sqrt{1-\tau^2}} d\tau, \quad (99)$$

$$n = 0, 1, 2, \dots,$$

where $h = b-a$.

When edge cracks are considered, very accurate numerical results are obtained for stress intensity factors and crack opening displacements. Equation (92) is solved in the same

manner as (67), by making use of the same numerical scheme summarized in equations (76)-(83).

Numerical Techniques

Numerical evaluation of the integral equations (67) and (92) present certain difficulties which will be explained in greater detail. First, numerical evaluation of the Fredholm kernel $L_1(t,r)$ involves the computation of Lommel's function for both small and large values of the product αt . The methods used to accomplish this are outlined in appendix C.

Another difficulty in the evaluation of kernel $L_1(t,r)$ is that the infinite integral in this expression converges very slowly for virtually all values of t and r . The reason for this can be easily seen by examining the first grouping of Bessel functions in expression (62). Since the Bessel function decays asymptotically as $\sim \frac{1}{\sqrt{\alpha}}$ and the product of Bessel functions in (62) is multiplied by α , no decay in amplitude occurs in this integrand. Convergence in this infinite integral occurs for very large α when the asymptotic oscillatory behavior of the Bessel terms is identical but opposite in sign to the trigonometric terms given in (62). This suggests that direct numerical integration of the integral in (62) would be unwise, since either very large upper limits must be set for a finite Gauss-Legendre quadrature or a great number

of quadrature points must be used for the Gauss-Laguerre quadrature technique usually employed when evaluating well behaved infinite integrals. In this investigation the infinite integral in (62) was evaluated by determining an analytic expression for the asymptotic behavior of the integrand which included higher order terms. This expression was integrated in closed form from A to ∞ and added to the original integral evaluated numerically between the finite limits 0 and A. The resulting form of $L_1(t,r)$ to be calculated numerically is then given by

$$\begin{aligned}
 L_1(t,r) = & \frac{-1}{\pi} \frac{1}{2r} \log \left[\frac{(t^{\frac{1}{2}} - r^{\frac{1}{2}})^2}{|t-r|} \right] - \frac{1}{\pi} \left[\frac{1}{t-r} \right. \\
 & \left. - \frac{\cos A(t-r)}{t-r} - (-1)^n \frac{\sin A(t+r)}{t+r} \right] + \int_0^A \{ \alpha t [n J_n(\alpha t) S_{0,n-1}(\alpha t) \\
 & - J_{n-1}(\alpha t) S_{1,n}(\alpha t)] J_n(\alpha r) - \frac{1}{\sqrt{2\pi r \alpha}} [C(\sqrt{\alpha t}) (\sin(\alpha r) + (-1)^n \cos(\alpha r)) \\
 & - S(\sqrt{\alpha t}) (\cos(\alpha r) + (-1)^n \sin(\alpha r))] \} d\alpha + [A_1 + A_2 + A_3], \\
 & n = 0, 1, 2, \dots, \quad (100)
 \end{aligned}$$

where the terms A_1 , A_2 and A_3 are given in appendix D. The finite integral expressed in (100) was evaluated numerically using Gauss-Legendre quadrature with the upper limit A usually set at 200.

Fredholm kernel $L_2(t,r)$, (68) or (93), is evaluated numerically without difficulty for internal and edge cracks. When edge cracks are investigated the asymptotic analysis given by (93)-(96) greatly improves the rate of convergence. Gauss-Legendre quadrature was used with the upper limit in (93) set at 150 and the 6x6 matrix m_{ij} determined by numerical inversion of f_{ij} .

IV. Results

Extensive numerical results are given in tables 1 through 33. Most of these results were obtained by solving the set of simultaneous linear algebraic equations designated by (76) and (77). In most cases it was found that 20 Chebyshev abscissa points ($m=20$) were sufficient for 3 significant figure accuracy. Unless otherwise noted, all values were calculated for Poisson's ratio equal to 0.3.

Stress intensity factors for ring shaped concentric cracks in an infinite medium subjected to axial tension ($n=0$) and pure bending ($n=1$) are determined by omitting the Fredholm Kernel $L_2(t,r)$ in (67). Numerical and graphical results for this problem are given in table 1 and in figure 2. For inner crack radius $c=0$ the problem becomes that of a penny-shaped crack in an infinite medium. The numerical results obtained for this special geometry are identical to values obtained from exact closed form solutions. As clearly indicated in figure 2, in axial extension the normalized stress intensity factor at the inner crack tip is always greater than at the outer crack tip. It is also observed that in pure bending this situation is reversed, with the outer crack tip having the greater normalized stress intensity factor.

Tables 2, 3 and 4 give stress intensity factors for concentric cracks fully embedded in the cylinder wall, where the crack

is symmetrically located between unbroken ligaments of equal radial thickness. Results for this geometry are given for axial loading and pure bending, where the ratio of crack length to wall thickness $(d-c)/(b-a)$ is 0.1 and 0.5. For $(d-c)/(b-a) = 0.9$, results are presented for axial loading only. When the loading is uniform axial tension $\sigma_0 = P_\infty / \pi(b^2 - a^2)$, where P_∞ is the load at infinity acting in the z direction and for pure bending, $\sigma_1 = 4Mb / \pi(b^4 - a^4)$, with M equal to the applied bending moment. The stress intensity factors for $(d-c)/(b-a) = 0.5$ are displayed graphically for axial tension in figure 3. It can clearly be seen from tables 2, 3, 4, and figure 3 that the stress intensity factor at the inner crack tip is always greater than at the outer crack tip for equal net ligament thickness when the loading is axial tension. Also, it can be seen in figure 3 that as the a/b ratio approaches 1.0 the stress intensity factor approaches the value given for a flat strip with a centrally located embedded crack. It thus becomes apparent that this plane strain solution is not a bad approximation for small crack lengths and a/b ratios which are not excessively small.

The bulk of the numerical results were obtained for cylinders with edge cracks (internal and external) in axial extension and pure bending and are presented in tables 5 through 16. The stress intensity factors and crack opening displacements at the crack mouth (COD) presented in the tables were calculated for

a/b ratios from 0 to 1.0. The values tabulated are for internal and external edge cracks with the crack length ℓ to wall thickness h ratios from $\ell/h=0.1$ to $\ell/h=0.6$.

When $a/b = 0$ these tabulated crack solutions correspond to solid cylinders with either internal penny-shaped cracks or external circumferential cracks. In pure bending the results for a penny-shaped crack in a solid cylinder are identical to the results given by the investigators in [9].

As in the embedded crack problem, in the limit as the a/b ratio goes to 1.0, the edge crack stress intensity factor is identical to stress intensity factors for the cracked strip solution. Figure 4 clearly indicates that for small edge crack length to wall thickness ratios (specifically $\ell/h=0.01$), under axial loading, the plain strain cracked strip solution is a very good approximation for a broad range of a/b .

Figures 5, 6, 7, and 8 are plots of the values of stress intensity factors vs. a/b for ℓ/h ratios equal to 0.1 and 0.5 where the loading is uniform axial tension or pure bending. It can be seen that for longer crack lengths the strip solution is no longer valid over a large range of a/b and is only a good approximation when the ratio a/b is very close to 1.0.

Comparison of figures 5, 6, 7, 8, 9, and 10 also demonstrates that while the curves for stress intensity factors of internal edge cracks are fairly similar for various crack lengths, this

is not the case for the external edge crack. The variation is particularly noticeable in bending. Also, in pure bending for ℓ/h ratios equal to or greater than 0.5 the solid cylinder with an external edge crack has a maximum normalized stress intensity factor which is greater than the plane strain crack solution in a strip. This is not the case in axial tension, where the plane strain solution is the maximum value of the stress intensity factor for all ℓ/h ratios greater than 0.01.

Figure 9 also indicates that for certain a/b ratios the quantity $k(d)/\sigma_0\sqrt{\ell}$, which is the stress intensity factor for an internal edge crack, may decrease with increasing crack length ℓ/h before increasing. It is also clear that this behavior only occurs for very thick-walled cylinders where $a/b < 0.6$. Figure 10 indicates that a similar type of variation does not occur for the internal edge crack in pure bending and that for any value of a/b the quantity $k(d)/\sigma_1\sqrt{\ell} \cos\theta$ increases with increasing ℓ/h ratios.

Tables 17 through 26 contain numerical results for temperature fields and stresses generated for the transient thermal stress problem described in appendix E. These numerical results are given for 5 different a/b ratios and are tabulated with respect to the nondimensional Fourier number $Fo=Dt/b^2$, where D is the thermal diffusivity, t is the time and b is the outer radius of the hollow cylinder.

When a fluid or vapor suddenly cools the inner surface of a heated cylinder, the results given represent the most severe thermal transient conditions and thus an upper bound on the actual elastic thermal stresses.

Figures 11, 13, 15, and 17 are plots of nondimensional temperature vs. $(r-a)/h$ for a/b ratios of 0.3, 0.5, 0.7, and 0.9 respectively. Figures 12, 14, 16, and 18 graphically display nondimensional thermal stress vs. $(r-a)/h$ for the same a/b ratios. It can be seen in all plots, but especially in the very thick walled cylinders, that for very small Fo the thermal stresses are represented by a sharp tensile spike of magnitude $E\alpha\theta_{\infty}/(1-\nu)$ restricted to a material layer very close to the inner radius. The coefficient of expansion is given by α and θ_{∞} is the initial temperature difference at the inner radius. For small Fo the stresses are compressive in most of the cylinder wall. As Fo increases, the tensile stressed region moves deeper into the wall thickness but decreases in magnitude while the compressive stress increases in magnitude. As can be clearly seen in figures 16 and 18, when Fo begins to approach steady state conditions the magnitude of the tensile and compressive stresses decrease as expected.

From these thermal stress curves it can be seen that from the point of view of fracture very small internal edge cracks are the most severely loaded due to the thermal transience.

examined in this example. This rather obvious observation is born out by the numerical results presented in tables 27-31. In these tables stress intensity factors $k_T(d)$ are determined for various a/b and λ/h ratios using the transient thermal stress loading determined in appendix E and recorded with respect to F_0 . These results show that for a fixed crack length the stress intensity factor generally increases for increasing F_0 , reaches a maximum and then decreases. It is also interesting to note that for fixed λ/h the stress intensity factors reach a maximum "sooner" for a/b ratios which are close to 1.0 (i.e. thin-walled cylinders).

Figure 19 depicts the crack geometry in a hollow cylinder with residual stresses. These residual stresses usually develop after sudden cooling of the cylinder during manufacture or welding and are highly compressive at the free surface. Approximating the residual stresses with a parabolic distribution which satisfies the self-equilibrium condition

$$\int_a^b \sigma_z(r) r dr = 0 \quad , \quad (101)$$

yields an internal stress distribution of the form

$$\sigma_z(r) = \sigma_s \left[1 - \frac{6(r-a)(b-r)}{(b-a)^2} \right] \quad , \quad (102)$$

where σ_s is the stress at the surface. It is obvious that for circumferential edge cracks under such residual loading, crack closure and contact will occur in the compressive stress field near the cylinder surface. The edge crack under this type of loading will be cusped shaped and equivalent to an eccentric embedded crack (figure 1) with the condition that

$$k(c) = 0 \quad (103)$$

Thus, the residual stress problem is solved by determining the stress intensity factor for an eccentric embedded crack from equation (67) and (73) with the loading determined by equation (102). The location of the crack tip furthest from the surface is fixed and by iteration the location of the crack tip closest to the surface is determined when condition (103) is satisfied.

The resulting stress intensity factors at the fixed crack tip are presented in normalized form in figure 20. In this graph the quantity $k/\sqrt{\ell}|\sigma_s|$ is plotted for internal and external edge cracks for cylinders with a/b ratios equal to 0.7 and 0.9. It can be seen that differences in the normalized stress intensity factor are not great for the two different a/b ratios. Also, external edge cracks have a slightly higher maximum stress intensity factor than internal edge cracks, when subjected

to the same assumed residual stress distribution. Both crack geometries have a maximum k value when the crack depth is about $0.63(b-a)$.

Figure 21 is a plot of the crack contact length ϵ in the compressive zone, which is equivalent to $(c-a)$ for the internal crack model and $(b-d)$ for the external crack model. The figure is for $a/b=0.9$ and demonstrates that for crack lengths between $0.21(b-a)$ and $0.7(b-a)$ the contact length decreases in a linear manner.

Unlike the situation in plane stress or plane strain where the stresses are usually independent of Poisson's ratio, the stress field in three-dimensional problems depends on the value chosen for Poisson's ratio. Tables 32 and 33 show the effect Poisson's ratio has on the stress intensity factor and COD in both axial tension and pure bending. In the example chosen $a/b = 0.5$ and $\lambda/h = 0.3$. It can be seen that Poisson's ratio has a very slight effect on the stress intensity factor. When $\nu=0$ the stress intensity factor is a minimum and for $\nu=0.5$ the stress intensity factor reaches a maximum. Small changes in ν at large values of Poisson's ratio apparently have a greater effect on the stress intensity factor than changes in ν for small Poisson's ratio. Also it is noticed that varying Poisson's ratio has a slightly greater effect on COD than on stress intensity factor.

It should be emphasized that the solution in this investigation was obtained in terms of a sum of Fourier terms. Thus, strictly speaking, the bending results should not be considered independently from the values given for axial tension. Referring to tables 5 - 16 it is obvious that for $\pi/2 < \theta < 3\pi/2$ the stress intensity factors resulting from the bending terms are negative. For these quantities to have a physical significance the axial load must be of sufficient magnitude to cause a positive stress intensity factor around the entire crack periphery when the axial problem is superposed on the bending problem.

Since this investigation does not admit the solution of crack problems where the crack surfaces are in nonaxisymmetric contact, it is important that the axial loading is of sufficient magnitude to prevent crack surface contact when superposed with the bending component. The stress intensity factor is a quantity at the crack tip which is determined by the local stress field. Thus, requiring the stress intensity factor to be positive does not alone ensure that crack surface contact will not take place.

It is also necessary to monitor the crack displacement along the entire length of the crack using expressions similar to (98) and (99) to ensure that no crack surfaces are in contact when the axial problem is superposed with the bending problem. For external edge cracks the maximum displacements are at the

mouth of the crack and thus the COD's given in the tables are useful in checking to see that this condition is satisfied.

In any case, the above conditions do not appear to be a severe restriction on the usefulness of the results since in many problems of interest the loading is dominated by axial loading which, for instance, may be the result of internal pressurization.

V. Conclusion

In conclusion, it can be stated that the mathematical methods in this investigation are quite general and the techniques employed may be used in the solution of many other three-dimensional elasticity problems, especially problems of the so-called "mixed" type. Reduction to a singular integral equation of the first kind is straightforward and the numerical analysis yields very accurate results.

The results presented in this investigation are of great practical interest. These results may be incorporated directly in any calculations which are being used to predict fracture in cylindrical pressure vessels and piping with circumferential flaws. Also, the numerical trends and actual values should be of use to programmers and users of the finite element method who wish to check special cases and verify accuracy in their three-dimensional code.

As noted in the introduction, the results presented in this study for cylinders with axisymmetric edge cracks can be considered a reasonable upper bound on solutions for cylinders with circumferential part-through surface flaws of finite arc length. Recent results by Delale and Erdogan [20] using the line-spring model confirm this for part-through elliptic surface cracks in thin-walled cylinders.

This investigation has shown, for small crack lengths and sufficiently large radius to thickness ratios, the plane strain cracked strip solution is of adequate accuracy when considering circumferential cracks and it is often unnecessary to make use of the general three-dimensional calculations.

Future areas of investigation in the circumferential cracking of hollow cylinders should examine the coupling effect between nonaxisymmetric crack surface contact and the stress intensity factor and crack opening displacement.

Other areas of interest, which would probably be most easily investigated using finite element techniques, would be the important problems where the crack is not axisymmetric and situations where plastic phenomena are included.

Table D1. Stress intensity factors for concentric ring shaped cracks in an infinite medium subjected to axial tension ($n=0$) and pure bending ($n=1$). The inner crack tip is located at c and the outer crack tip at d (see figure 2). σ_0 is the uniform applied stress in axial tension and σ_m is the maximum linear bending stress at point d .

c/d	n=0	n=1	n=0	n=1
	$\frac{k(c)}{\sigma_0 \sqrt{\frac{d-c}{2}}}$	$\frac{k(c)}{\sigma_m \sqrt{\frac{d-c}{2}} \cos \theta}$	$\frac{k(d)}{\sigma_0 \sqrt{\frac{d-c}{2}}}$	$\frac{k(d)}{\sigma_m \sqrt{\frac{d-c}{2}} \cos \theta}$
0	$\rightarrow \infty$	$\rightarrow 0$	0.900	0.600
0.01	5.922	0.070	0.900	0.604
0.1	1.972	0.250	0.909	0.633
0.2	1.502	0.370	0.918	0.669
0.3	1.310	0.470	0.927	0.708
0.4	1.204	0.560	0.936	0.749
0.5	1.137	0.643	0.946	0.792
0.6	1.089	0.721	0.957	0.835
0.7	1.057	0.796	0.967	0.878
0.8	1.032	0.867	0.978	0.920
0.9	1.014	0.935	0.988	0.961
0.99	1.001	0.994	0.999	0.996
$\rightarrow 1.0$	$\rightarrow 1.0$	$\rightarrow 1.0$	$\rightarrow 1.0$	$\rightarrow 1.0$

Table D2. Stress intensity factors for a symmetric embedded crack in a thick-walled cylinder subjected to axial tension and pure bending. $((d-c)/(b-a)=0.1, \sigma_0 = P_\infty/[\pi(b^2-a^2)], \sigma_1=4Mb/[\pi(b^4-a^4)])$.

$\frac{a}{b}$	$\frac{d-c}{b}$	$\frac{c}{b}$	$\frac{k(c)}{\sigma_0 \sqrt{\frac{d-c}{2}}}$	$\frac{k(d)}{\sigma_0 \sqrt{\frac{d-c}{2}}}$	$\frac{k(c)}{\sigma_1 \sqrt{\frac{d-c}{2}} \cos \theta}$	$\frac{k(d)}{\sigma_1 \sqrt{\frac{d-c}{2}} \cos \theta}$
0.1	0.09	0.505	1.028	0.989	0.538	0.562
0.2	0.08	0.56	1.024	0.991	0.590	0.612
0.3	0.07	0.515	1.020	0.994	0.643	0.662
0.4	0.06	0.67	1.017	0.996	0.695	0.711
0.5	0.05	0.725	1.014	0.998	0.747	0.761
0.6	0.04	0.78	1.012	1.000	0.799	0.810
0.7	0.03	0.835	1.010	1.002	0.851	0.859
0.8	0.02	0.89	1.009	1.003	0.903	0.908
0.9	0.01	0.945	1.007	1.005	0.954	0.957
→1.0	→0	→1	→1.006	→1.006	→1.006	→1.006

Table D3. Stress intensity factors for a symmetric embedded crack in a thick-walled cylinder subjected to axial tension and pure bending. $((d-c)/(b-a)=0.5, \sigma_0 = P_\infty/[\pi(b^2-a^2)], \sigma_1=4Mb/[\pi(b^4-a^4)])$.

$\frac{a}{b}$	$\frac{d-c}{b}$	$\frac{c}{b}$	$\frac{k(c)}{\sigma_0 \sqrt{\frac{d-c}{2}}}$	$\frac{k(d)}{\sigma_0 \sqrt{\frac{d-c}{2}}}$	$\frac{k(c)}{\sigma_1 \sqrt{\frac{d-c}{2}} \cos \theta}$	$\frac{k(d)}{\sigma_1 \sqrt{\frac{d-c}{2}} \cos \theta}$
0.1	0.45	0.325	1.383	1.117	0.506	0.671
0.2	0.40	0.40	1.330	1.124	0.593	0.733
0.3	0.35	0.475	1.294	1.131	0.677	0.795
0.4	0.30	0.55	1.268	1.139	0.758	0.856
0.5	0.25	0.625	1.247	1.147	0.836	0.914
0.6	0.20	0.70	1.231	1.155	0.911	0.971
0.7	0.15	0.775	1.217	1.162	0.984	1.026
0.8	0.10	0.85	1.206	1.170	1.054	1.080
0.9	0.05	0.925	1.196	1.178	1.121	1.133
→1.0	→0	→1	→1.187	→1.187	→1.187	→1.187

Table D4. Stress intensity factors for a symmetric embedded crack in a thick-walled cylinder subjected to axial tension. $((d-c)/(b-a)=0.9, \sigma_0 = P_\infty / [\pi(b^4 - a^4)])$.

$\frac{a}{b}$	$\frac{d-c}{b}$	$\frac{c}{b}$	$\frac{k(c)}{\sigma_0 \frac{d-c}{2}}$	$\frac{k(d)}{\sigma_0 \frac{d-c}{2}}$
0.1	0.81	0.145	3.740	2.412
0.2	0.72	0.24	3.300	2.404
0.3	0.63	0.335	3.081	2.410
0.4	0.54	0.43	2.945	2.422
0.5	0.45	0.525	2.850	2.437
0.6	0.36	0.62	2.778	2.456
0.7	0.27	0.715	2.720	2.479
0.8	0.18	0.81	2.671	2.506
0.9	0.09	0.905	2.627	2.536
$\rightarrow 1.0$	$\rightarrow 0$	$\rightarrow 1$	$\rightarrow 2.585$	$\rightarrow 2.585$

Table D5. Stress intensity factors and crack opening displacements for an internal edge crack in a thick-walled cylinder subjected to axial tension and pure bending. $(\ell/h=0.1, h=b-a, \sigma_0 = P_\infty / [\pi(b^2 - a^2)], \sigma_1 = 4Mb / [\pi(b^4 - a^4)])$.

$\frac{a}{b}$	$\frac{k(d)}{\sigma_0 \sqrt{\ell}}$	$\frac{k(d)}{\sigma_1 \sqrt{\ell} \cos \theta}$	$\frac{\mu}{1-\nu} \frac{\delta(c)}{h \sigma_0}$	$\frac{\mu}{1-\nu} \frac{\delta(c)}{h \sigma_1 \cos \theta}$
0	0.637	0.042	0.128	0
0.1	0.842	0.123	0.212	0.021
0.2	0.940	0.225	0.244	0.050
0.3	1.000	0.334	0.261	0.080
0.4	1.042	0.447	0.272	0.111
0.5	1.073	0.563	0.281	0.142
0.6	1.097	0.680	0.287	0.174
0.7	1.119	0.800	0.292	0.206
0.8	1.138	0.922	0.297	0.239
0.9	1.158	1.048	0.302	0.273
$\rightarrow 1.0$	$\rightarrow 1.189$	$\rightarrow 1.189$	$\rightarrow 0.310$	$\rightarrow 0.310$

Table D6. Stress intensity factors and crack opening displacements for an external edge crack in a thick-walled cylinder subjected to axial tension and pure bending. ($\ell/h=0.1$, $h=b-a$, $\sigma_0=P_\infty/[\pi(b^2-a^2)]$, $\sigma_1=4Mb/[\pi(b^4-a^4)]$).

$\frac{a}{b}$	$\frac{k(c)}{\sigma_0\sqrt{\ell}}$	$\frac{k(c)}{\sigma_1\sqrt{\ell} \cos\theta}$	$\frac{\mu}{1-\nu} \frac{\delta(d)}{h \sigma_c}$	$\frac{\mu}{1-\nu} \frac{\delta(d)}{h \sigma_1 \cos\theta}$
0	1.181	1.166	0.302	0.308
0.1	1.176	1.159	0.302	0.306
0.2	1.172	1.153	0.302	0.304
0.3	1.170	1.149	0.302	0.303
0.4	1.168	1.147	0.302	0.302
0.5	1.167	1.147	0.302	0.301
0.6	1.167	1.149	0.303	0.301
0.7	1.168	1.152	0.303	0.302
0.8	1.169	1.158	0.304	0.303
0.9	1.173	1.166	0.306	0.305
→1.0	→1.189	→1.189	→0.310	→0.310

Table D7. Stress intensity factors and crack opening displacements for an internal edge crack in a thick-walled cylinder subjected to axial tension and pure bending. ($\ell/h=0.2$, $h=b-a$, $\sigma_0=P_\infty/[\pi(b^2-a^2)]$, $\sigma_1=4Mb/[\pi(b^4-a^4)]$).

$\frac{a}{b}$	$\frac{k(d)}{\sigma_0\sqrt{\ell}}$	$\frac{k(d)}{\sigma_1\sqrt{\ell} \cos\theta}$	$\frac{\mu}{1-\nu} \frac{\delta(c)}{h \sigma_0}$	$\frac{\mu}{1-\nu} \frac{\delta(c)}{h \sigma_1 \cos\theta}$
0	0.644	0.085	0.258	0
0.1	0.775	0.153	0.373	0.036
0.2	0.869	0.241	0.441	0.089
0.3	0.942	0.342	0.488	0.148
0.4	1.003	0.452	0.524	0.212
0.5	1.055	0.571	0.555	0.280
0.6	1.104	0.699	0.582	0.353
0.7	1.150	0.833	0.608	0.429
0.8	1.198	0.978	0.635	0.511
0.9	1.253	1.139	0.666	0.602
→1.0	→1.367	→1.367	→0.732	→0.732

Table D8. Stress intensity factors and crack opening displacements for an external edge crack in a thick-walled cylinder subjected to axial tension and pure bending. ($l/h=0.2$, $h=b-a$, $\sigma_0=P_\infty/[\pi(b^2-a^2)]$, $\sigma_1=4Mb/[\pi(b^4-a^4)]$).

$\frac{a}{b}$	$\frac{k(c)}{\sigma_0\sqrt{l}}$	$\frac{k(c)}{\sigma_1\sqrt{l} \cos\theta}$	$\frac{\mu}{1-\nu} \frac{\delta(d)}{h \sigma_0}$	$\frac{\mu}{1-\nu} \frac{\delta(d)}{h \sigma_1 \cos\theta}$
0	1.260	1.314	0.625	0.705
0.1	1.244	1.279	0.622	0.685
0.2	1.235	1.253	0.623	0.669
0.3	1.231	1.234	0.626	0.658
0.4	1.230	1.222	0.630	0.651
0.5	1.232	1.217	0.635	0.647
0.6	1.238	1.218	0.643	0.648
0.7	1.247	1.226	0.652	0.652
0.8	1.261	1.243	0.663	0.661
0.9	1.285	1.274	0.680	0.677
→1.0	→1.367	→1.367	→0.732	→0.732

Table D9. Stress intensity factors and crack opening displacements for an internal edge crack in a thick-walled cylinder subjected to axial tension and pure bending. ($l/h=0.3$, $h=b-a$, $\sigma_0=P_\infty/[\pi(b^2-a^2)]$, $\sigma_1=4Mb/[\pi(b^4-a^4)]$).

$\frac{a}{b}$	$\frac{k(d)}{\sigma_0\sqrt{l}}$	$\frac{k(d)}{\sigma_1\sqrt{l} \cos\theta}$	$\frac{\mu}{1-\nu} \frac{\delta(c)}{h \sigma_0}$	$\frac{\mu}{1-\nu} \frac{\delta(c)}{h \sigma_1 \cos\theta}$
0	0.651	0.127	0.390	0
0.1	0.753	0.188	0.526	0.050
0.2	0.840	0.266	0.626	0.123
0.3	0.918	0.359	0.707	0.210
0.4	0.991	0.466	0.776	0.308
0.5	1.060	0.587	0.841	0.419
0.6	1.130	0.724	0.906	0.543
0.7	1.203	0.876	0.973	0.681
0.8	1.286	1.053	1.050	0.841
0.9	1.392	1.267	1.150	1.038
→1.0	→1.660	→1.660	→1.410	→1.410

Table D10. Stress intensity factors and crack opening displacements for an external edge crack in a thick-walled cylinder subjected to axial tension and pure bending. ($l/h=0.3$, $h=b-a$, $\sigma_0=P_\infty/[\pi(b^2-a^2)]$, $\sigma_1=4Mb/[\pi(b^4-a^4)]$).

$\frac{a}{b}$	$\frac{k(c)}{\sigma_0\sqrt{l}}$	$\frac{k(c)}{\sigma_1\sqrt{l}\cos\theta}$	$\frac{\mu}{1-\nu} \frac{\delta(d)}{h\sigma_0}$	$\frac{\mu}{1-\nu} \frac{\delta(d)}{h\sigma_1\cos\theta}$
0	1.388	1.592	0.987	1.307
0.1	1.350	1.450	0.976	1.225
0.2	1.328	1.431	0.975	1.165
0.3	1.316	1.381	0.983	1.122
0.4	1.313	1.347	0.996	1.093
0.5	1.317	1.327	1.015	1.078
0.6	1.329	1.323	1.040	1.077
0.7	1.350	1.334	1.073	1.089
0.8	1.384	1.365	1.117	1.120
0.9	1.442	1.428	1.185	1.181
→1.0	→1.660	→1.660	→1.410	→1.410

Table D11. Stress intensity factors and crack opening displacements for an internal edge crack in a thick-walled cylinder subjected to axial tension and pure bending. ($l/h=0.4$, $h=b-a$, $\sigma_0=P_\infty/[\pi(b^2-a^2)]$, $\sigma_1=4Mb/[\pi(b^4-a^4)]$).

$\frac{a}{b}$	$\frac{k(d)}{\sigma_0\sqrt{l}}$	$\frac{k(d)}{\sigma_1\sqrt{l}\cos\theta}$	$\frac{\mu}{1-\nu} \frac{\delta(c)}{h\sigma_0}$	$\frac{\mu}{1-\nu} \frac{\delta(c)}{h\sigma_1\cos\theta}$
0	0.665	0.171	0.531	0
0.1	0.754	0.226	0.686	0.062
0.2	0.838	0.296	0.817	0.155
0.3	0.920	0.383	0.935	0.269
0.4	1.001	0.487	1.046	0.404
0.5	1.085	0.611	1.158	0.563
0.6	1.174	0.757	1.277	0.752
0.7	1.275	0.928	1.412	0.973
0.8	1.397	1.141	1.580	1.254
0.9	1.568	1.426	1.821	1.638
→1.0	→2.112	→2.112	→2.614	→2.614

Table D12. Stress intensity factors and crack opening displacements for an external edge crack in a thick-walled cylinder subjected to axial tension and pure bending. ($\ell/h=0.4$, $h=b-a$, $\sigma_0=P_\infty/[\pi(b^2-a^2)]$, $\sigma_1=4Mb/[\pi(b^4-a^4)]$).

$\frac{a}{b}$	$\frac{k(c)}{\sigma_0\sqrt{\ell}}$	$\frac{k(c)}{\sigma_1\sqrt{\ell} \cos\theta}$	$\frac{\mu}{1-\nu} \frac{\delta(d)}{h \sigma_0}$	$\frac{\mu}{1-\nu} \frac{\delta(d)}{h \sigma_1 \cos\theta}$
0	1.593	2.077	1.422	2.337
0.1	1.513	1.865	1.388	2.078
0.2	1.465	1.715	1.381	1.899
0.3	1.437	1.606	1.392	1.774
0.4	1.425	1.531	1.419	1.692
0.5	1.427	1.486	1.459	1.646
0.6	1.443	1.467	1.516	1.633
0.7	1.475	1.476	1.594	1.658
0.8	1.533	1.520	1.706	1.730
0.9	1.641	1.626	1.891	1.890
→1.0	→2.112	→2.112	→2.614	→2.614

Table D13. Stress intensity factors and crack opening displacements for an internal edge crack in a thick-walled cylinder subjected to axial tension and pure bending. ($\ell/h=0.5$, $h=b-a$, $\sigma_0=P_\infty/[\pi(b^2-a^2)]$, $\sigma_1=4Mb/[\pi(b^4-a^4)]$).

$\frac{a}{b}$	$\frac{k(d)}{\sigma_0\sqrt{\ell}}$	$\frac{k(d)}{\sigma_1\sqrt{\ell} \cos\theta}$	$\frac{\mu}{1-\nu} \frac{\delta(c)}{h \sigma_0}$	$\frac{\mu}{1-\nu} \frac{\delta(c)}{h \sigma_1 \cos\theta}$
0	0.691	0.217	0.689	0
0.1	0.775	0.267	0.864	0.074
0.2	0.859	0.333	1.029	0.187
0.3	0.945	0.415	1.189	0.329
0.4	1.035	0.517	1.351	0.503
0.5	1.131	0.643	1.523	0.718
0.6	1.239	0.799	1.718	0.985
0.7	1.366	0.989	1.954	1.318
0.8	1.529	1.243	2.267	1.775
0.9	1.779	1.612	2.765	2.472
→1.0	→2.826	→2.826	→4.950	→4.950

Table D14. Stress intensity factors and crack opening displacements for an external edge crack in a thick-walled cylinder subjected to axial tension and pure bending. ($\ell/h=0.5$, $h=b-a$, $\sigma_0=P_\infty/[\pi(b^2-a^2)]$, $\sigma_1=4Mb/[\pi(b^4-a^4)]$).

$\frac{a}{b}$	$\frac{k(c)}{\sigma_0\sqrt{\ell}}$	$\frac{k(c)}{\sigma_1\sqrt{\ell} \cos\theta}$	$\frac{\mu}{1-\nu} \frac{\delta(d)}{h \sigma_0}$	$\frac{\mu}{1-\nu} \frac{\delta(d)}{h \sigma_1 \cos\theta}$
0	1.922	2.929	1.989	4.291
0.1	1.762	2.468	1.901	3.548
0.2	1.667	2.163	1.873	3.076
0.3	1.610	1.946	1.884	2.753
0.4	1.580	1.780	1.924	2.546
0.5	1.572	1.707	1.994	2.426
0.6	1.586	1.660	2.097	2.382
0.7	1.627	1.658	2.248	2.417
0.8	1.709	1.712	2.478	2.558
0.9	1.878	1.867	2.888	2.904
→1.0	→2.826	→2.826	→4.950	→4.950

Table D15. Stress intensity factors and crack opening displacements for an internal edge crack in a thick-walled cylinder subjected to axial tension and pure bending. ($\ell/h=0.6$, $h=b-a$, $\sigma_0=P_\infty/[\pi(b^2-a^2)]$, $\sigma_1=4Mb/[\pi(b^4-a^4)]$).

$\frac{a}{b}$	$\frac{k(d)}{\sigma_0\sqrt{\ell}}$	$\frac{k(d)}{\sigma_1\sqrt{\ell} \cos\theta}$	$\frac{\mu}{1-\nu} \frac{\delta(c)}{h \sigma_0}$	$\frac{\mu}{1-\nu} \frac{\delta(c)}{h \sigma_1 \cos\theta}$
0	0.736	0.265	0.877	0
0.1	0.820	0.314	1.077	0.087
0.2	0.908	0.378	1.283	0.222
0.3	1.000	0.459	1.493	0.393
0.4	1.099	0.561	1.716	0.611
0.5	1.208	0.691	1.966	0.890
0.6	1.333	0.856	2.261	1.253
0.7	1.484	1.066	2.636	1.729
0.8	1.688	1.359	3.166	2.431
0.9	2.025	1.824	4.091	3.623
→1.0	→4.035	→4.035	→9.965	→9.965

Table D16. Stress intensity factors and crack opening displacements for an external edge crack in a thick-walled cylinder subjected to axial tension and pure bending. ($l/h=0.6$, $h=b-a$, $\sigma_0=P_\infty/[\pi(b^2-a^2)]$, $\sigma_1=4Mb/[\pi(b^4-a^4)]$).

$\frac{a}{b}$	$\frac{k(c)}{\sigma_0\sqrt{l}}$	$\frac{k(c)}{\sigma_1\sqrt{l} \cos\theta}$	$\frac{\mu}{1-\nu} \frac{\delta(d)}{h \sigma_0}$	$\frac{\mu}{1-\nu} \frac{\delta(d)}{h \sigma_1 \cos\theta}$
0	2.478	4.579	2.798	8.542
0.1	2.159	3.527	2.589	6.365
0.2	1.977	2.880	2.510	5.095
0.3	1.866	2.460	2.506	4.307
0.4	1.802	2.194	2.557	3.833
0.5	1.773	2.021	2.661	3.550
0.6	1.776	1.923	2.826	3.424
0.7	1.818	1.895	3.080	3.455
0.8	1.918	1.949	3.491	3.692
0.9	2.153	2.155	4.289	4.354
→1.0	→4.035	→4.035	→9.965	→9.965

Table D17. Transient temperature distribution θ/θ_∞ in a hollow cylinder due to a sudden temperature change on the inner radius. ($a/b=0.1$, $Fo=Dt/b^2$, $\theta/\theta_\infty=(T(r,t)-T_0)/(T_\infty-T_0)$).

$\frac{r-a}{h}$	$Fo=.0001$ θ/θ_∞	$Fo=.0005$ θ/θ_∞	$Fo=.001$ θ/θ_∞	$Fo=.005$ θ/θ_∞	$Fo=.01$ θ/θ_∞
0	1.000	0.999	0.997	0.987	0.974
0.05	0.001	0.129	0.263	0.545	0.618
0.10	0	0.003	0.032	0.271	0.383
0.15	0	0	0.002	0.118	0.225
0.20	0	0	0	0.044	0.124
0.25	0	0	0	0.138	0.063
0.30	0	0	0	0.004	0.030
0.35	0	0	0	0.001	0.131
0.40	0	0	0	0	0.005
0.45	0	0	0	0	0.002
0.50	0	0	0	0	0.001
0.55	0	0	0	0	0
0.60	0	0	0	0	0
0.65	0	0	0	0	0
0.70	0	0	0	0	0
0.75	0	0	0	0	0
0.80	0	0	0	0	0
0.85	0	0	0	0	0
0.90	0	0	0	0	0
0.95	0	0	0	0	0
1.00	0	0	0	0	0

Table D18. Stress distribution σ^* in a hollow cylinder due to a sudden temperature change on the inner radius. ($a/b=0.1$, $Fo=Dt/b^2$, $\sigma^*=(1-\nu/E\alpha)\sigma_{zz}/\theta_\infty$, $\theta_\infty=T_\infty-T_0$).

$\frac{r-a}{h}$	$Fo=.0001$ σ^*	$Fo=.0005$ σ^*	$Fo=.001$ σ^*	$Fo=.005$ σ^*	$Fo=.01$ σ^*
0	-.997	-.993	-.989	-.966	-.943
0.05	.001	-.123	-.254	-.524	-.587
0.10	.002	.002	-.024	-.250	-.353
0.15	.002	.006	.006	-.097	-.195
0.20	.002	.006	.008	-.023	-.093
0.25	.002	.006	.008	.007	-.033
0.30	.002	.006	.008	.017	.001
0.35	.002	.006	.008	.020	.018
0.40	.002	.006	.008	.020	.026
0.45	.002	.006	.008	.020	.029
0.50	.002	.006	.008	.020	.030
0.55	.002	.006	.008	.020	.031
0.60	.002	.006	.008	.020	.031
0.65	.002	.006	.008	.020	.031
0.70	.002	.006	.008	.020	.031
0.75	.002	.006	.008	.020	.031
0.80	.002	.006	.008	.020	.031
0.85	.002	.006	.008	.020	.031
0.90	.002	.006	.008	.020	.031
0.95	.002	.006	.008	.020	.031
1.00	.002	.006	.008	.020	.031

Table D19. Transient temperature distribution θ/θ_∞ in a hollow cylinder due to a sudden temperature change on the inner radius. ($a/b=0.3$, $Fo=Dt/b^2$, $\theta/\theta_\infty = (T(r,t)-T_0)/(T_\infty-T_0)$).

$\frac{r-a}{h}$	$Fo=.0001$	$Fo=.0005$	$Fo=.001$	$Fo=.005$	$Fo=.01$	$Fo=.05$
	θ/θ_∞	θ/θ_∞	θ/θ_∞	θ/θ_∞	θ/θ_∞	θ/θ_∞
0	1.000	1.000	0.999	0.997	0.994	0.969
0.05	0.013	0.254	0.411	0.687	0.760	0.842
0.10	0	0.024	0.106	0.437	0.559	0.729
0.15	0	0.001	0.016	0.254	0.395	0.629
0.20	0	0	0.001	0.134	0.267	0.539
0.25	0	0	0	0.064	0.173	0.459
0.30	0	0	0	0.027	0.106	0.389
0.35	0	0	0	0.011	0.062	0.327
0.40	0	0	0	0.004	0.035	0.272
0.45	0	0	0	0.001	0.018	0.225
0.50	0	0	0	0	0.009	0.185
0.55	0	0	0	0	0.004	0.151
0.60	0	0	0	0	0.002	0.122
0.65	0	0	0	0	0.001	0.098
0.70	0	0	0	0	0	0.079
0.75	0	0	0	0	0	0.063
0.80	0	0	0	0	0	0.051
0.85	0	0	0	0	0	0.042
0.90	0	0	0	0	0	0.036
0.95	0	0	0	0	0	0.033
1.00	0	0	0	0	0	0.032

Table D20. Stress distribution σ^* in a hollow cylinder due to a sudden temperature change on the inner radius. ($a/b=0.3$, $Fo=Dt/b^2$, $\sigma^*=(1-\nu/E\alpha)\sigma_{zz}/\theta_\infty$, $\theta_\infty=T_\infty-T_0$).

$\frac{r-a}{h}$	$Fo=.0001$	$Fo=.0005$	$Fo=.001$	$Fo=.005$	$Fo=.01$	$Fo=.05$
	σ^*	σ^*	σ^*	σ^*	σ^*	σ^*
0	-.992	-.982	-.975	-.939	-.909	-.758
0.05	-.005	-.237	-.386	-.630	-.675	-.631
0.10	.007	-.007	-.081	-.379	-.475	-.518
0.15	.007	.016	.008	-.196	-.311	-.418
0.20	.007	.017	.023	-.076	-.183	-.328
0.25	.007	.017	.024	-.006	-.088	-.249
0.30	.007	.017	.025	.030	-.022	-.178
0.35	.007	.017	.025	.047	.022	-.116
0.40	.007	.017	.025	.054	.050	-.061
0.45	.007	.017	.025	.057	.066	-.014
0.50	.007	.017	.025	.057	.075	.026
0.55	.007	.017	.025	.058	.080	.060
0.60	.007	.017	.025	.058	.082	.089
0.65	.007	.017	.025	.058	.084	.113
0.70	.007	.017	.025	.058	.084	.132
0.75	.007	.017	.025	.058	.084	.148
0.80	.007	.017	.025	.058	.084	.160
0.85	.007	.017	.025	.058	.084	.168
0.90	.007	.017	.025	.058	.084	.175
0.95	.007	.017	.025	.058	.084	.178
1.00	.007	.017	.025	.058	.084	.179

Table D21. Transient temperature distribution θ/θ_∞ in a hollow cylinder due to a sudden temperature change on the inner radius. ($a/b=0.5$, $F_0=Dt/b^2$, $\theta/\theta_\infty=(T(r,t)-T_0)/(T_\infty-T_0)$)

$\frac{r-a}{h}$	$F_0=.0001$	$F_0=.0005$	$F_0=.001$	$F_0=.005$	$F_0=.01$	$F_0=.05$
	θ/θ_∞	θ/θ_∞	θ/θ_∞	θ/θ_∞	θ/θ_∞	θ/θ_∞
0	1.000	1.000	1.000	0.998	0.996	0.980
0.05	0.075	0.419	0.562	0.783	0.837	0.900
0.10	0	0.109	0.251	0.588	0.689	0.824
0.15	0	0.016	0.087	0.423	0.556	0.752
0.20	0	0.001	0.023	0.290	0.438	0.684
0.25	0	0	0.005	0.189	0.337	0.620
0.30	0	0	0.001	0.117	0.254	0.561
0.35	0	0	0	0.069	0.186	0.506
0.40	0	0	0	0.038	0.133	0.455
0.45	0	0	0	0.020	0.093	0.409
0.50	0	0	0	0.010	0.063	0.367
0.55	0	0	0	0.005	0.042	0.329
0.60	0	0	0	0.002	0.027	0.296
0.65	0	0	0	0.001	0.017	0.266
0.70	0	0	0	0	0.010	0.241
0.75	0	0	0	0	0.006	0.220
0.80	0	0	0	0	0.003	0.203
0.85	0	0	0	0	0.002	0.190
0.90	0	0	0	0	0.001	0.181
0.95	0	0	0	0	0.001	0.176
1.0	0	0	0	0	0.001	0.174

Table D22. Stress distribution σ^* in a hollow cylinder due to a sudden temperature change on the inner radius. ($a/b=0.5$, $Fo=Dt/b^2$, $\sigma^*=(1-\nu/E\alpha)\sigma_{zz}/\theta_\infty$, $\theta_\infty=T_\infty-T_0$)

$\frac{r-a}{h}$	$Fo=.0001$	$Fo=.0005$	$Fo=.001$	$Fo=.005$	$Fo=.01$	$Fo=.05$
	σ^*	σ^*	σ^*	σ^*	σ^*	σ^*
0	-.985	-.965	-.951	-.885	-.833	-.587
0.05	-.060	-.385	-.513	-.670	-.674	-.507
0.10	.015	-.074	-.202	-.476	-.526	-.431
0.15	.015	.018	-.038	-.310	-.393	-.359
0.20	.015	.033	.026	-.177	-.275	-.291
0.25	.015	.034	.044	-.076	-.175	-.227
0.30	.015	.034	.048	-.005	-.091	-.168
0.35	.015	.034	.049	.044	-.023	-.113
0.40	.015	.034	.049	.074	.030	-.062
0.45	.015	.034	.049	.092	.070	-.016
0.50	.015	.034	.049	.103	.100	.026
0.55	.015	.034	.049	.108	.121	.064
0.60	.015	.034	.049	.111	.136	.097
0.65	.015	.034	.049	.112	.146	.127
0.70	.015	.034	.049	.112	.153	.152
0.75	.015	.034	.049	.113	.157	.173
0.80	.015	.034	.049	.113	.159	.190
0.85	.015	.034	.049	.113	.161	.203
0.90	.015	.034	.049	.113	.162	.212
0.95	.015	.034	.049	.113	.162	.217
1.00	.015	.034	.049	.113	.162	.219

Table D23. Transient temperature distribution θ/θ_∞ in a hollow cylinder due to a sudden temperature change on the inner radius. ($a/b=0.7$, $Fo=Dt/b^2$, $\theta/\theta_\infty=(T(r,t)-T_0)/(T_\infty-T_0)$)

$\frac{r-a}{h}$	$Fo=.0001$	$Fo=.0005$	$Fo=.001$	$Fo=.005$	$Fo=.01$	$Fo=.05$
	θ/θ_∞	θ/θ_∞	θ/θ_∞	θ/θ_∞	θ/θ_∞	θ/θ_∞
0	1.000	1.000	1.000	0.998	0.997	0.985
0.05	0.286	0.628	0.729	0.870	0.904	0.953
0.10	0.033	0.336	0.492	0.748	0.813	0.922
0.15	0.001	0.150	0.305	0.632	0.726	0.892
0.20	0	0.055	0.172	0.526	0.644	0.863
0.25	0	0.017	0.089	0.431	0.566	0.835
0.30	0	0.004	0.042	0.347	0.494	0.808
0.35	0	0.001	0.018	0.274	0.427	0.783
0.40	0	0	0.007	0.213	0.367	0.759
0.45	0	0	0.002	0.162	0.312	0.737
0.50	0	0	0.001	0.121	0.264	0.717
0.55	0	0	0	0.089	0.221	0.698
0.60	0	0	0	0.064	0.184	0.681
0.65	0	0	0	0.045	0.153	0.666
0.70	0	0	0	0.031	0.126	0.653
0.75	0	0	0	0.021	0.104	0.642
0.80	0	0	0	0.014	0.087	0.633
0.85	0	0	0	0.010	0.074	0.626
0.90	0	0	0	0.007	0.065	0.621
0.95	0	0	0	0.005	0.060	0.618
1.00	0	0	0	0.005	0.058	0.617

Table D24. Stress distribution σ^* in a hollow cylinder due to a sudden temperature change on the inner radius. ($a/b=0.7$, $Fo=Dt/b^2$, $\sigma^*=(1-\nu/E\alpha)\sigma_{zz}/\theta_\infty$, $\theta_\infty=T_\infty-T_0$)

$\frac{r-a}{h}$	$Fo=.0001$	$Fo=.0005$	$Fo=.001$	$Fo=.005$	$Fo=.01$	$Fo=.05$
	σ^*	σ^*	σ^*	σ^*	σ^*	σ^*
0	-.969	-.930	-.900	-.770	-.669	-.250
0.05	-.225	-.558	-.630	-.642	-.575	-.219
0.10	-.002	-.265	-.392	-.519	-.485	-.188
0.15	.030	-.080	-.205	-.404	-.398	-.157
0.20	.031	.015	-.073	-.298	-.316	-.128
0.25	.031	.053	.011	-.202	-.238	-.100
0.30	.031	.066	.058	-.118	-.166	-.074
0.35	.031	.069	.082	-.046	-.099	-.049
0.40	.031	.070	.093	.016	-.039	-.025
0.45	.031	.070	.097	.066	.016	-.003
0.50	.031	.070	.099	.107	.064	.018
0.55	.031	.070	.100	.139	.107	.036
0.60	.031	.070	.100	.164	.144	.053
0.65	.031	.070	.100	.183	.176	.068
0.70	.031	.070	.100	.197	.202	.081
0.75	.031	.070	.100	.207	.224	.092
0.80	.031	.070	.100	.214	.241	.101
0.85	.031	.070	.100	.219	.254	.108
0.90	.031	.070	.100	.222	.263	.113
0.95	.031	.070	.100	.223	.268	.116
1.00	.031	.070	.100	.224	.270	.117

Table D25. Transient temperature distribution θ/θ_∞ in a hollow cylinder due to a sudden temperature change on the inner radius. ($a/b=0.9$, $Fo=Dt/b^2$, $\theta/\theta_\infty=(T(r,t)-T_0)/(T_\infty-T_0)$)

$\frac{r-a}{h}$	$Fo=.0001$ θ/θ_∞	$Fo=.0005$ θ/θ_∞	$Fo=.001$ θ/θ_∞	$Fo=.005$ θ/θ_∞
0	1.000	1.000	1.000	0.999
0.05	0.723	0.872	0.908	0.967
0.10	0.477	0.748	0.818	0.937
0.15	0.286	0.630	0.731	0.906
0.20	0.156	0.521	0.648	0.877
0.25	0.076	0.423	0.568	0.848
0.30	0.033	0.337	0.494	0.820
0.35	0.013	0.263	0.426	0.794
0.40	0.005	0.201	0.363	0.769
0.45	0.001	0.151	0.307	0.745
0.50	0	0.111	0.257	0.723
0.55	0	0.080	0.213	0.703
0.60	0	0.056	0.176	0.685
0.65	0	0.038	0.144	0.668
0.70	0	0.026	0.117	0.654
0.75	0	0.017	0.095	0.641
0.80	0	0.011	0.078	0.631
0.85	0	0.007	0.065	0.623
0.90	0	0.005	0.056	0.617
0.95	0	0.003	0.050	0.614
1.00	0	0.003	0.048	0.613

Table D26. Stress distribution σ^* in a hollow cylinder due to a sudden temperature change on the inner radius. ($a/b=0.9$, $F_0=Dt/b^2$, $\sigma^*=(1-\nu/E\alpha)\sigma_{zz}/\theta_\infty$, $\theta_\infty=T_\infty-T_0$)

$\frac{r-a}{h}$	$F_0=.0001$ σ^*	$F_0=.0005$ σ^*	$F_0=.001$ σ^*	$F_0=.005$ σ^*
0	-.892	-.758	-.656	-.251
0.05	-.614	-.630	-.565	-.220
0.10	-.369	-.506	-.475	-.189
0.15	-.179	-.388	-.388	-.159
0.20	-.048	-.280	-.304	-.129
0.25	.031	-.182	-.225	-.100
0.30	.074	-.096	-.151	-.073
0.35	.094	-.022	-.083	-.046
0.40	.103	.040	-.020	-.021
0.45	.106	.091	.036	.002
0.50	.107	.131	.086	.025
0.55	.107	.162	.130	.045
0.60	.107	.186	.167	.063
0.65	.107	.203	.200	.080
0.70	.107	.216	.226	.094
0.75	.107	.224	.248	.106
0.80	.107	.230	.265	.117
0.85	.107	.234	.279	.125
0.90	.107	.237	.288	.130
0.95	.107	.238	.293	.134
1.00	.107	.239	.295	.135

Table D27. Stress intensity factors for internal edge cracks subjected to transient thermal stresses ($k_T(d) = -\frac{k(d)}{\sqrt{d}} \frac{1-\nu}{E\alpha\theta_\infty}$, $\frac{a}{b} = 0.1$, $Fo = \frac{Dt}{b^2}$, $h=b-a$, $\theta_\infty = T_\infty - T_0$)

$\frac{d}{h}$	$Fo = .0001$	$Fo = .0005$	$Fo = .001$	$Fo = .005$	$Fo = .01$	$Fo = .05$
	$\frac{k_T(d)}{\sqrt{d}}$	$\frac{k_T(d)}{\sqrt{d}}$	$\frac{k_T(d)}{\sqrt{d}}$	$\frac{k_T(d)}{\sqrt{d}}$	$\frac{k_T(d)}{\sqrt{d}}$	$\frac{k_T(d)}{\sqrt{d}}$
0.01	0.721	0.885	0.923	0.957	0.945	0.789
0.1	0.045	0.110	0.169	0.364	0.427	0.414
0.2	0.014	0.032	0.048	0.135	0.198	0.261
0.3	0.006	0.015	0.022	0.059	0.095	0.173
0.4	0.004	0.008	0.012	0.031	0.050	0.114
0.5	0.002	0.005	0.007	0.018	0.029	0.075
0.6	0.002	0.003	0.005	0.012	0.018	0.049

Table D28. Stress intensity factors for internal edge cracks subjected to transient thermal stresses. ($k_T(d) = -\frac{k(d)}{\sqrt{d}} \frac{1-\nu}{E\alpha\theta_\infty}$, $\frac{a}{b} = 0.3$, $Fo = \frac{Dt}{b^2}$, $h=b-a$, $\theta_\infty = T_\infty - T_0$)

$\frac{d}{h}$	$Fo = .0001$	$Fo = .0005$	$Fo = .001$	$Fo = .005$	$Fo = .01$	$Fo = .05$
	$\frac{k_T(d)}{\sqrt{d}}$	$\frac{k_T(d)}{\sqrt{d}}$	$\frac{k_T(d)}{\sqrt{d}}$	$\frac{k_T(d)}{\sqrt{d}}$	$\frac{k_T(d)}{\sqrt{d}}$	$\frac{k_T(d)}{\sqrt{d}}$
0.01	0.832	0.961	0.987	0.994	0.972	0.820
0.1	0.094	0.235	0.329	0.566	0.624	0.601
0.2	0.035	0.080	0.117	0.288	0.373	0.437
0.3	0.018	0.041	0.059	0.150	0.220	0.318
0.4	0.011	0.025	0.035	0.086	0.131	0.231
0.5	0.007	0.016	0.023	0.054	0.082	0.165
0.6	0.005	0.012	0.016	0.037	0.054	0.117

Table D29. Stress intensity factors for internal edge cracks subjected to transient thermal stresses. $(k_T(d) = \frac{k(d)}{\sqrt{\lambda}} \frac{1-\nu}{E\alpha\theta_\infty}, \frac{a}{b} = 0.5, Fo = \frac{Dt}{b^2}, h=b-a, \theta_\infty=T_\infty-T_0)$

$\frac{\lambda}{h}$	Fo=.0001	Fo=.0005	Fo=.001	Fo=.005	Fo=.01	Fo=.05
	$k_T(d)$	$k_T(d)$	$k_T(d)$	$k_T(d)$	$k_T(d)$	$k_T(d)$
0.01	0.906	0.988	0.997	0.957	0.907	0.644
0.1	0.154	0.364	0.485	0.671	0.686	0.525
0.2	0.064	0.146	0.214	0.435	0.495	0.420
0.3	0.037	0.082	0.117	0.277	0.351	0.334
0.4	0.024	0.054	0.076	0.179	0.246	0.262
0.5	0.018	0.038	0.053	0.121	0.173	0.203
0.6	0.013	0.029	0.040	0.087	0.123	0.154

Table D30. Stress intensity factors for internal edge cracks subjected to transient thermal stresses. $(k_T(d) = \frac{k(d)}{\sqrt{\lambda}} \frac{1-\nu}{E\alpha\theta_\infty}, \frac{a}{b} = 0.7, Fo = \frac{Dt}{b^2}, h=b-a, \theta_\infty=T_\infty-T_0)$

$\frac{\lambda}{h}$	Fo=.0001	Fo=.0005	Fo=.001	Fo=.005	Fo=.01	Fo=.05
	$k_T(d)$	$k_T(d)$	$k_T(d)$	$k_T(d)$	$k_T(d)$	$k_T(d)$
0.01	0.968	0.988	0.969	0.844	0.736	0.276
0.1	0.285	0.562	0.650	0.689	0.622	0.237
0.2	0.125	0.292	0.399	0.548	0.519	0.202
0.3	0.079	0.176	0.253	0.432	0.431	0.171
0.4	0.057	0.124	0.175	0.337	0.354	0.144
0.5	0.045	0.095	0.131	0.263	0.288	0.119
0.6	0.036	0.076	0.104	0.205	0.230	0.097

Table D31. Stress intensity factors for internal edge cracks subjected to transient thermal stresses. $(k_T(d) = \frac{k(d)}{\sqrt{\ell}} \frac{1-\nu}{E\alpha\theta_\infty}, \frac{a}{b} = 0.9, Fo = \frac{Dt}{b^2}, h=b-a, \theta_\infty=T_\infty-T_0)$

$\frac{\ell}{h}$	Fo=.0001 $\frac{k_T(d)}{k_T(d)}$	Fo=.0005 $\frac{k_T(d)}{k_T(d)}$	Fo=.001 $\frac{k_T(d)}{k_T(d)}$	Fo=.005 $\frac{k_T(d)}{k_T(d)}$
0.01	0.962	0.833	0.724	0.277
0.1	0.657	0.701	0.633	0.247
0.2	0.426	0.589	0.560	0.224
0.3	0.300	0.501	0.502	0.206
0.4	0.238	0.432	0.453	0.190
0.5	0.205	0.378	0.408	0.174
0.6	0.185	0.334	0.367	0.158

Table D32. The effect of Poisson's ratio on stress intensity factors and $\delta(c)$ when loading is uniform tension ($a/b=0.5, \ell/h=0.3, \sigma_0=P_\infty/[\pi(b^2-a^2)], h=b-a$).

	$\nu=0$	$\nu=0.1$	$\nu=0.2$	$\nu=0.3$	$\nu=0.4$	$\nu=0.5$
$\frac{k(d)}{\sigma_0\sqrt{\ell}}$	1.048	1.051	1.055	1.060	1.067	1.076
$\frac{\mu}{1-\nu} \frac{\delta(c)}{h\sigma_0}$	0.814	0.821	0.831	0.841	0.854	0.870

Table D33. The effect of Poisson's ratio on stress intensity factors and $\delta(c)$ when loading is pure bending ($a/b=0.5, \ell/h=0.3, \sigma_1=4Mb/[\pi(b^4-a^4)], h=b-a$).

	$\nu=0$	$\nu=0.1$	$\nu=0.2$	$\nu=0.3$	$\nu=0.4$	$\nu=0.5$
$\frac{k(d)}{\sigma_1\sqrt{\ell} \cos\theta}$	0.574	0.577	0.582	0.587	0.594	0.602
$\frac{\mu}{1-\nu} \frac{\delta(c)}{h\sigma_1 \cos\theta}$	0.395	0.402	0.410	0.419	0.430	0.443

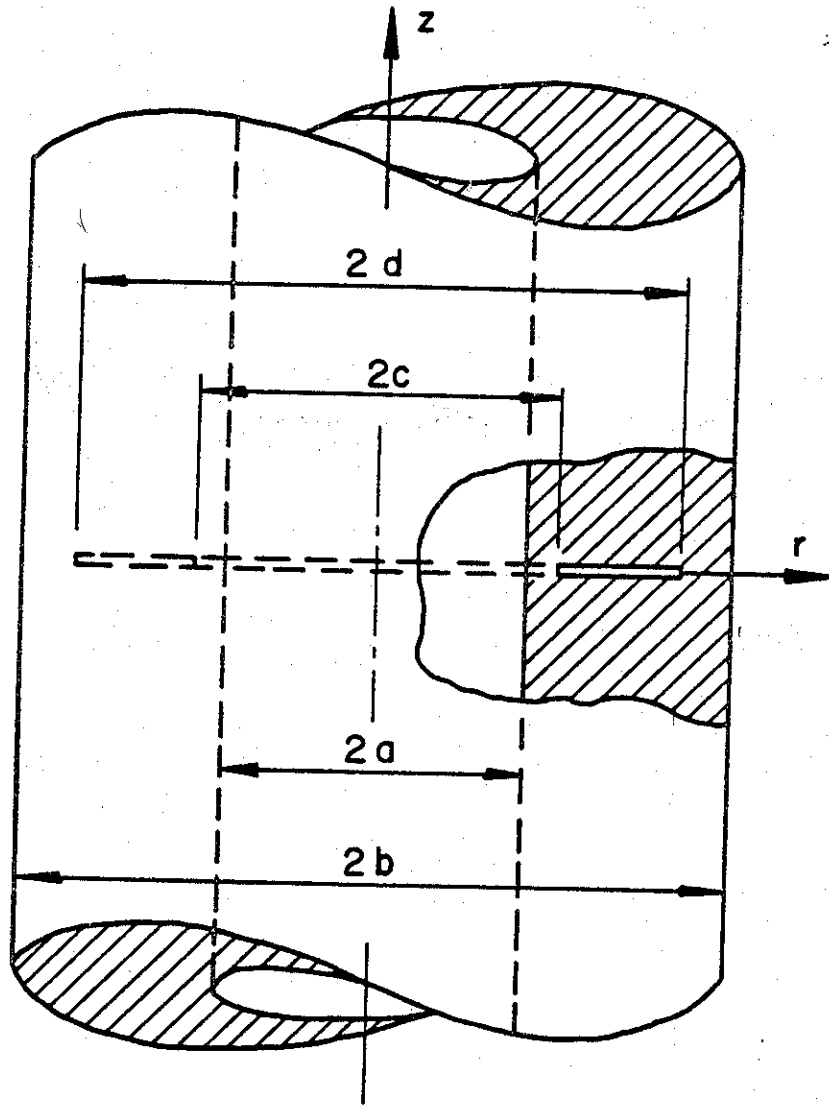


Fig.D1 Geometry of a thick-walled cylinder containing an axisymmetric circumferential crack.

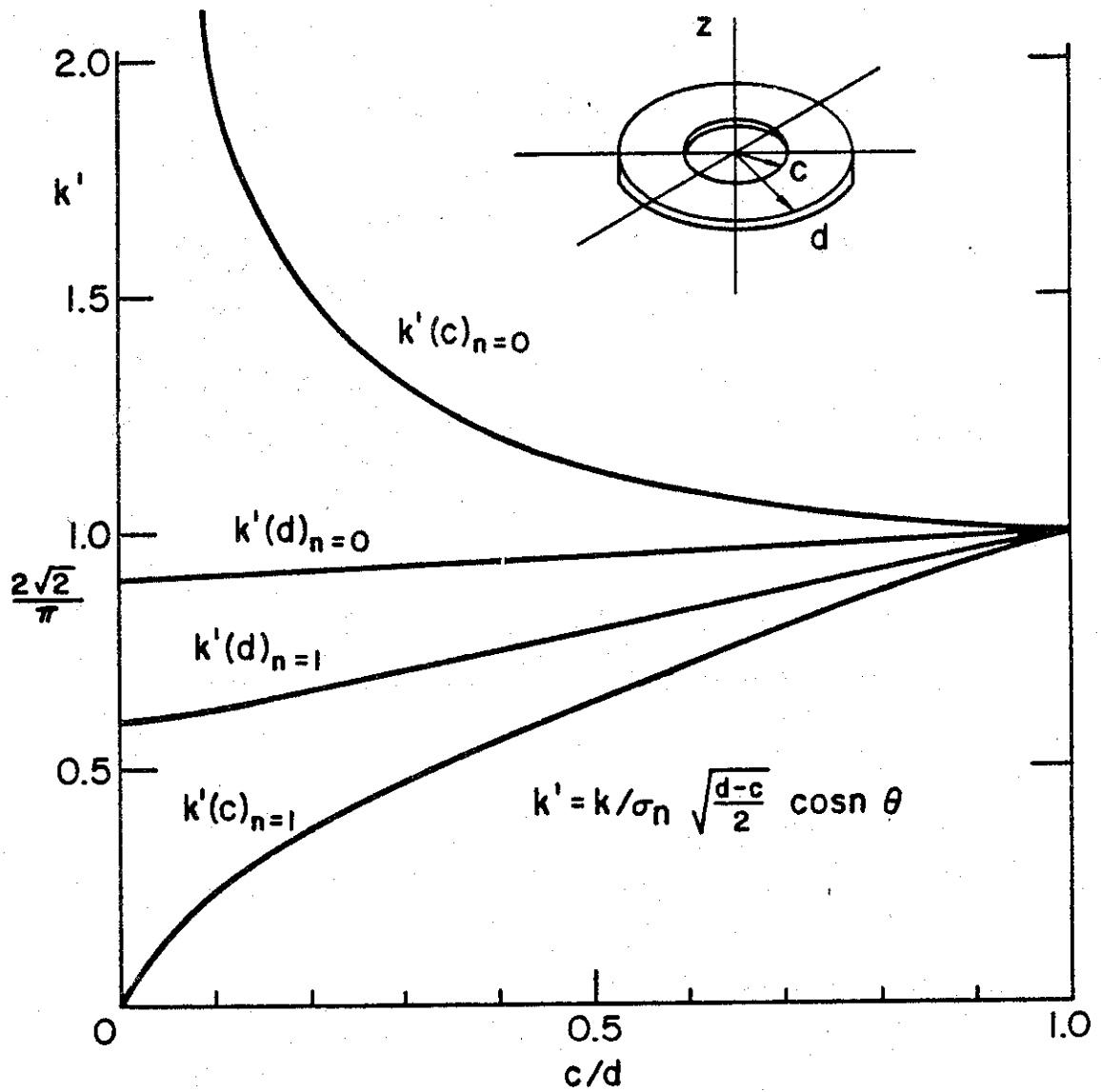


Fig.D2 Stress intensity factors for concentric ring shaped cracks in an infinite medium subjected to axial extension ($n=0$) and pure bending ($n=1$).

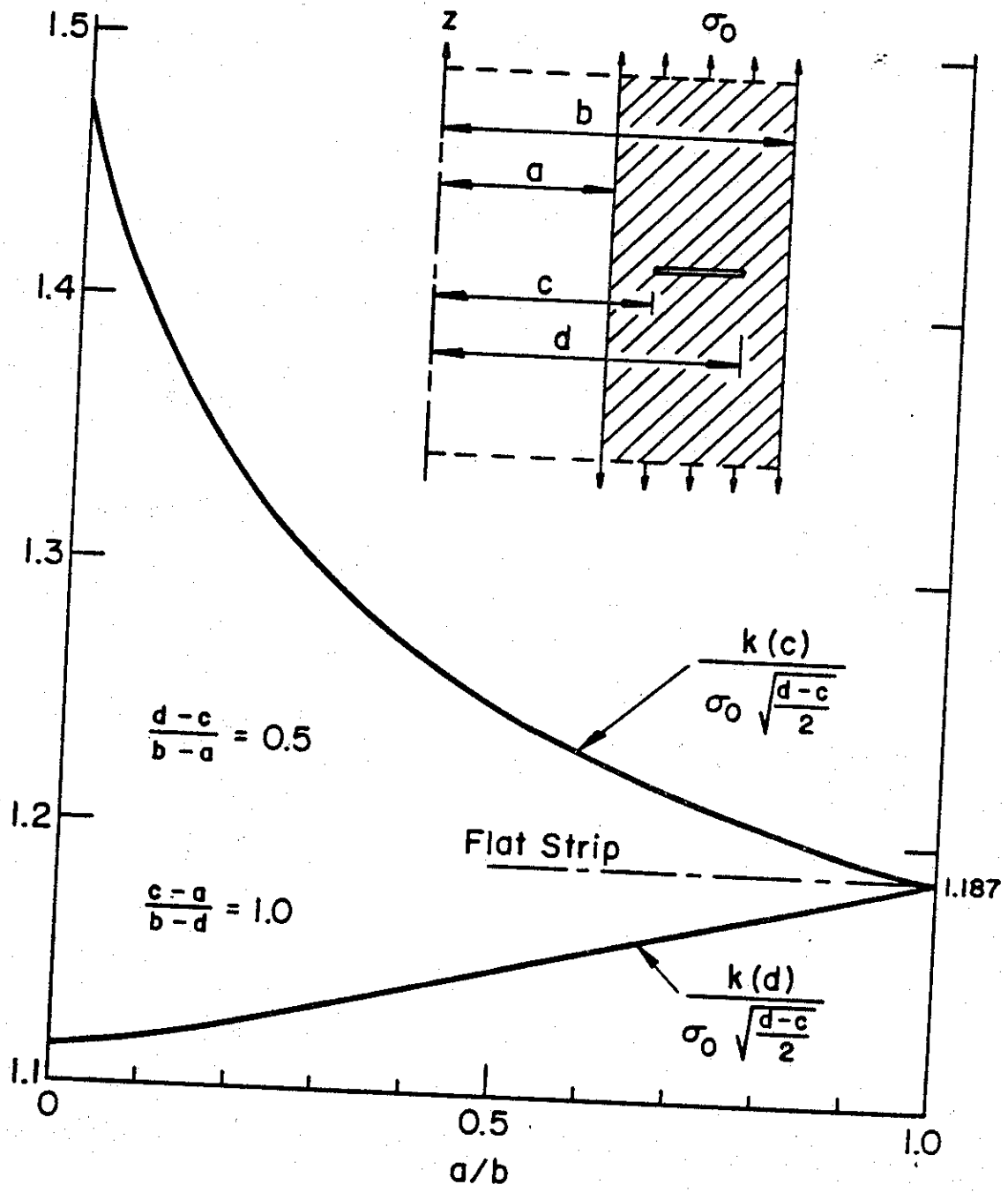


Fig.D3 Stress intensity factors for a symmetric embedded crack in a thick-walled cylinder subjected to axial tension. $(d-c)/(b-a)=0.4$.

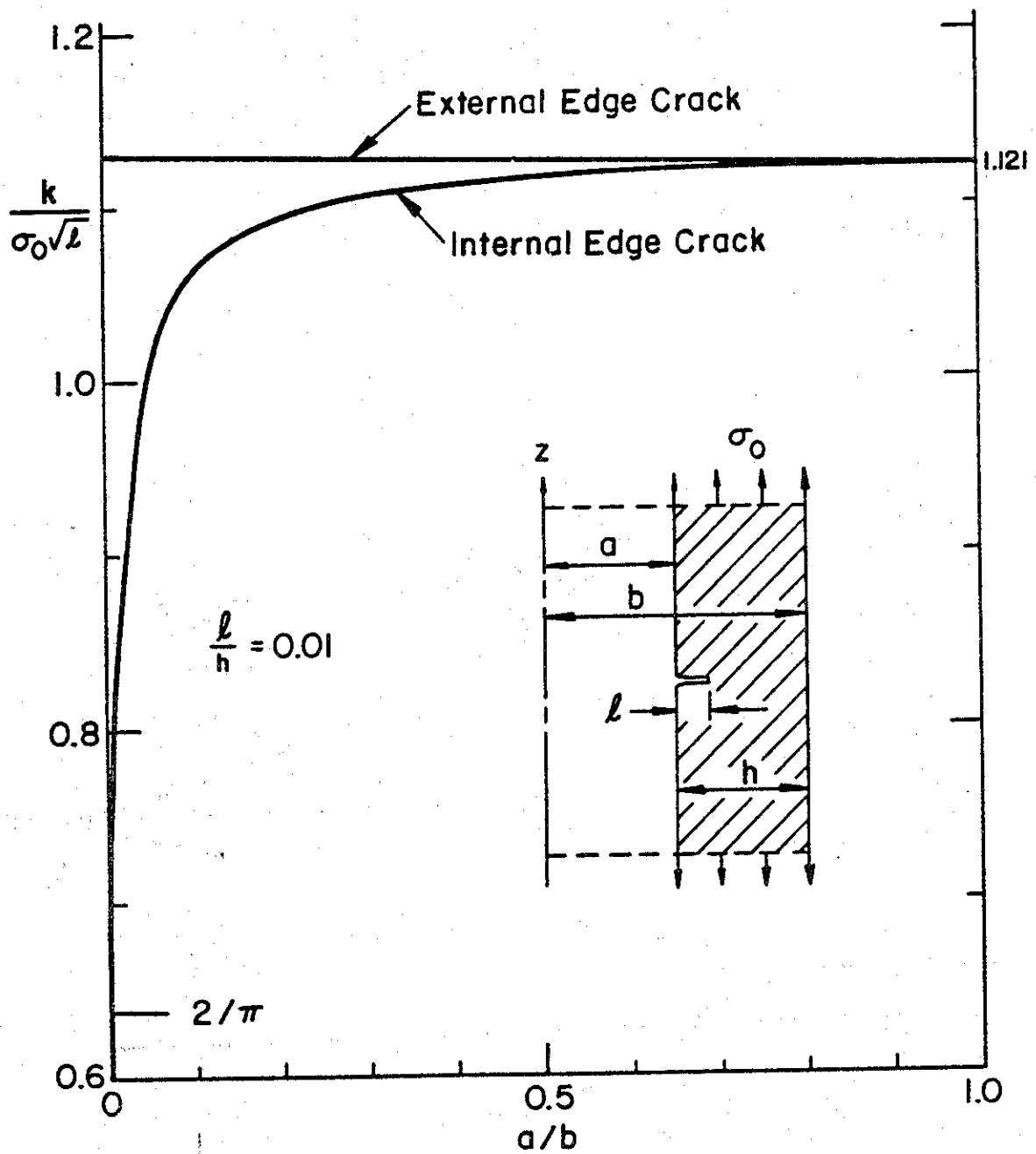


Fig.D4 Stress intensity factors for edge cracks in a thick-walled cylinder subjected to axial tension. $l/h = 0.01$.

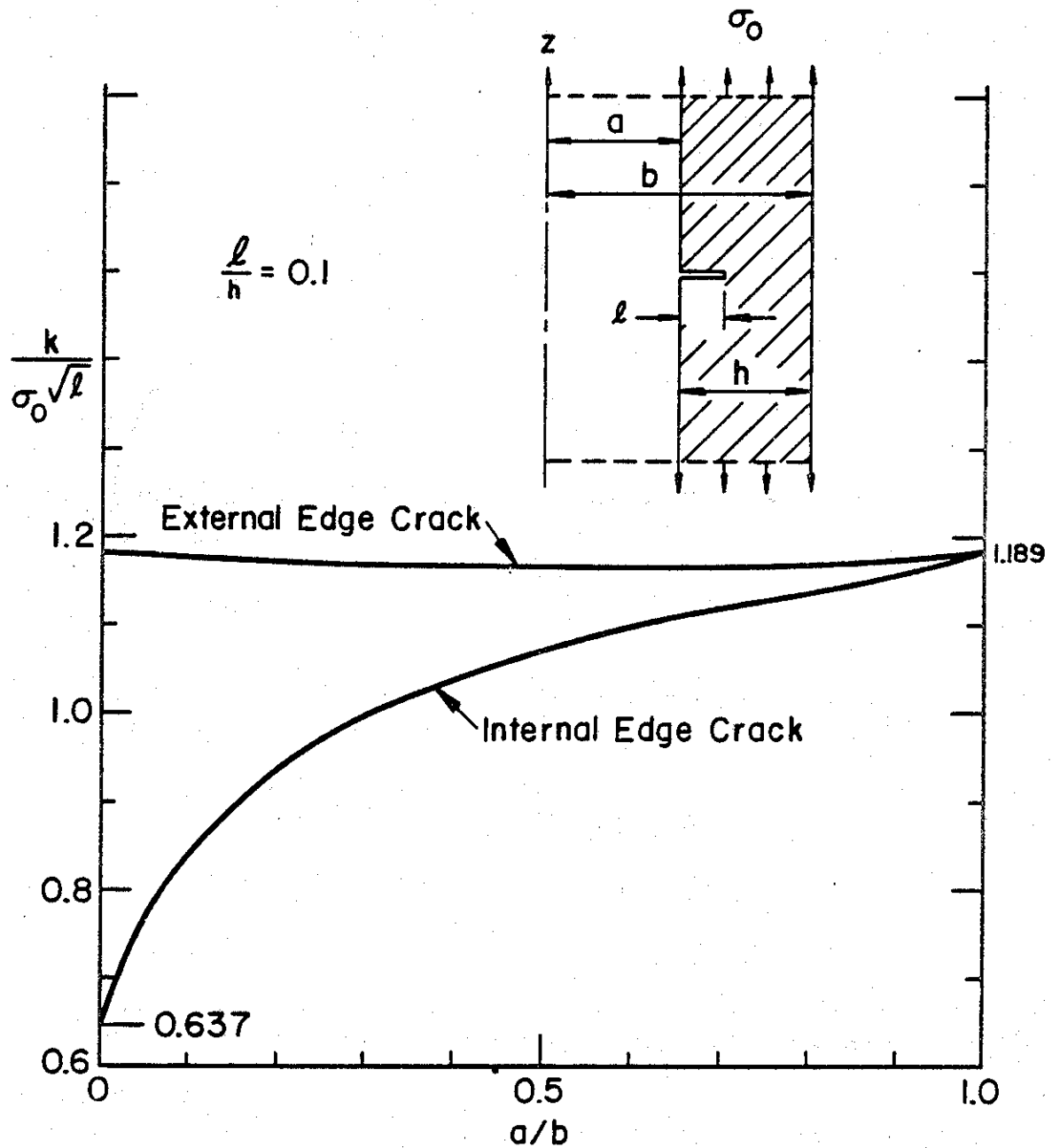


Fig.D5 Stress intensity factors for edge cracks in a thick-walled cylinder subjected to axial tension. $l/h = 0.1$.

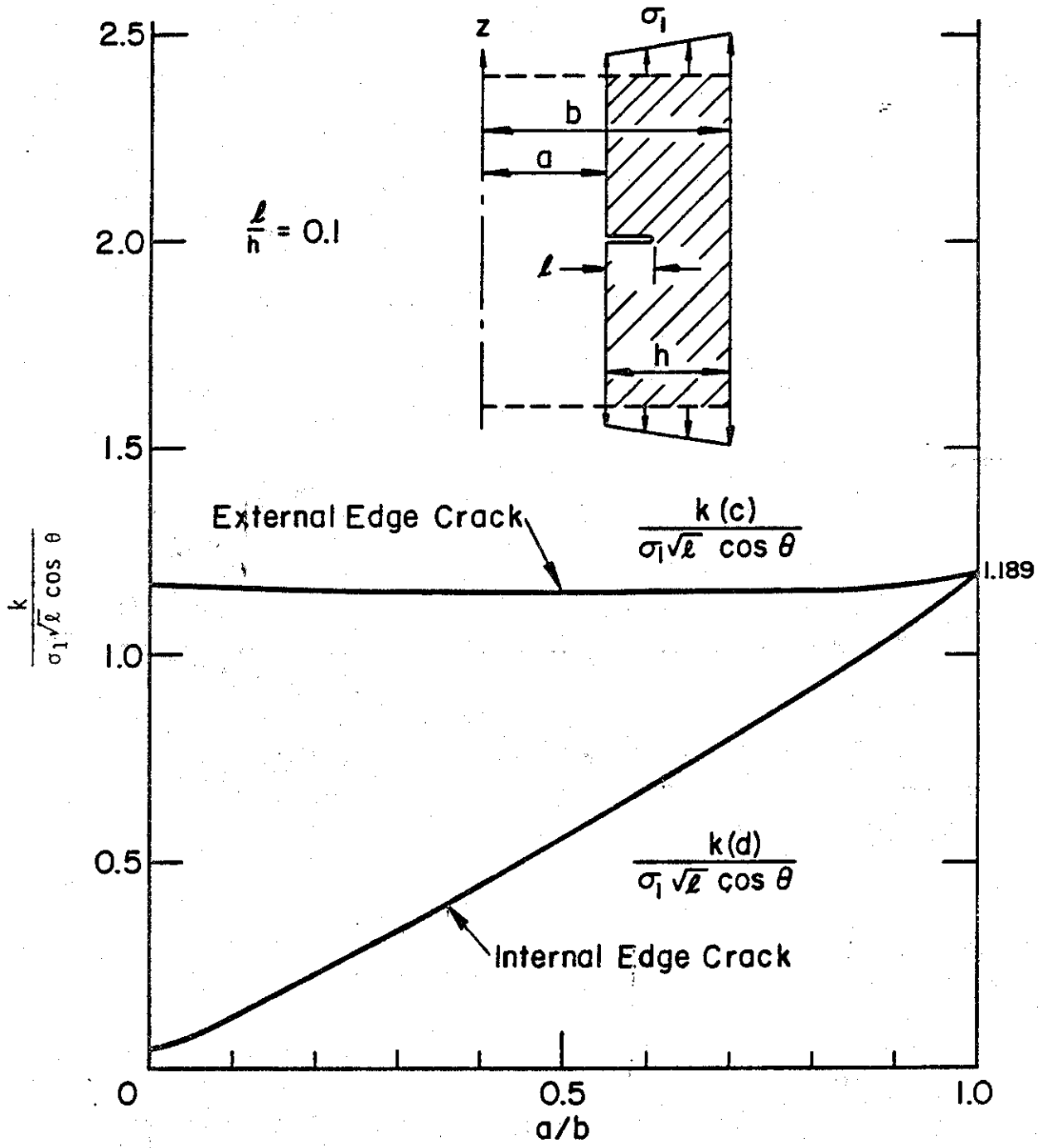


Fig.D6 Stress intensity factors for edge cracks in a thick-walled cylinder subjected to pure bending. $l/h = 0.1$.

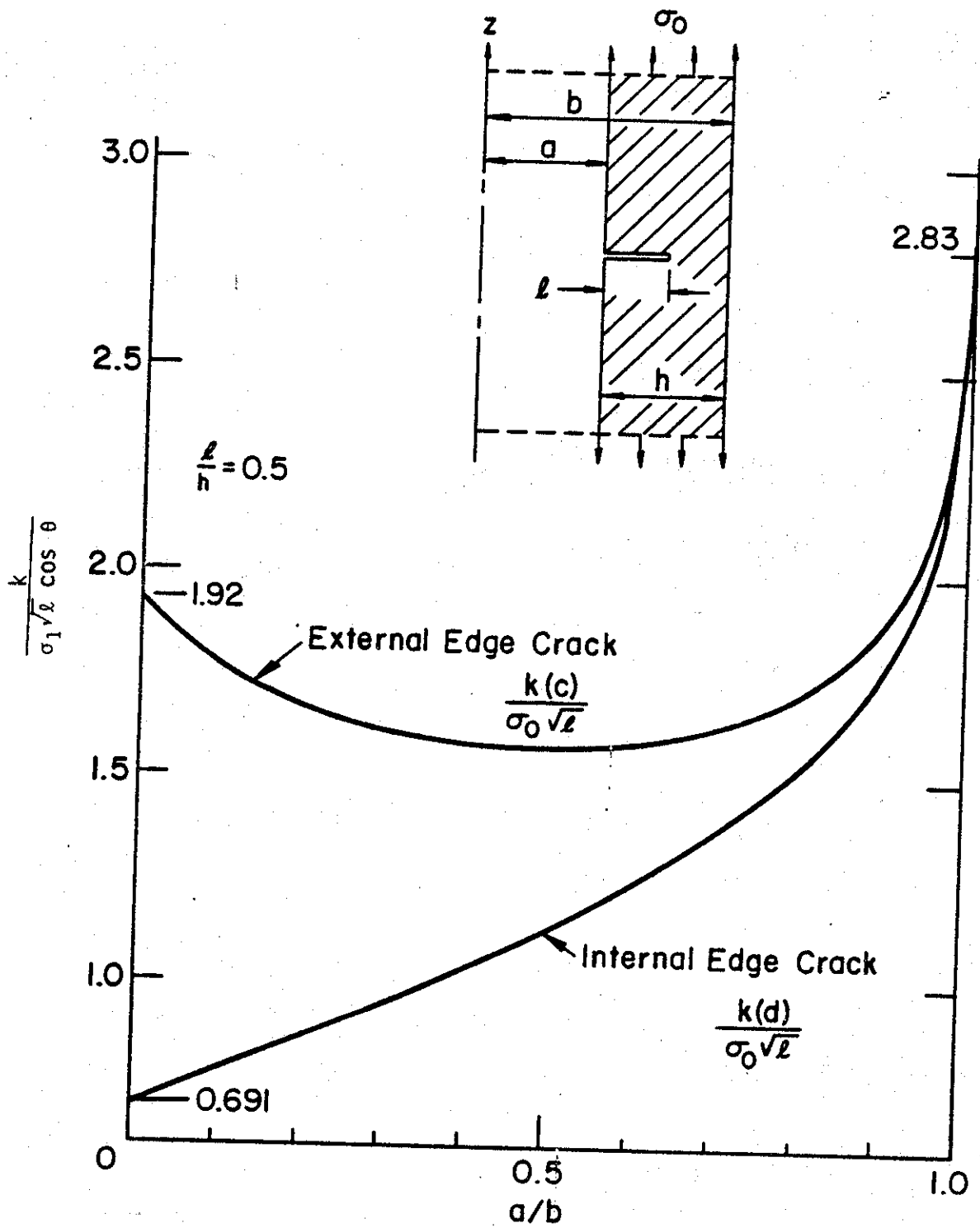


Fig.D7 Stress intensity factors for edge cracks in a thick-walled cylinder subjected to axial tension. $l/h = 0.5$.

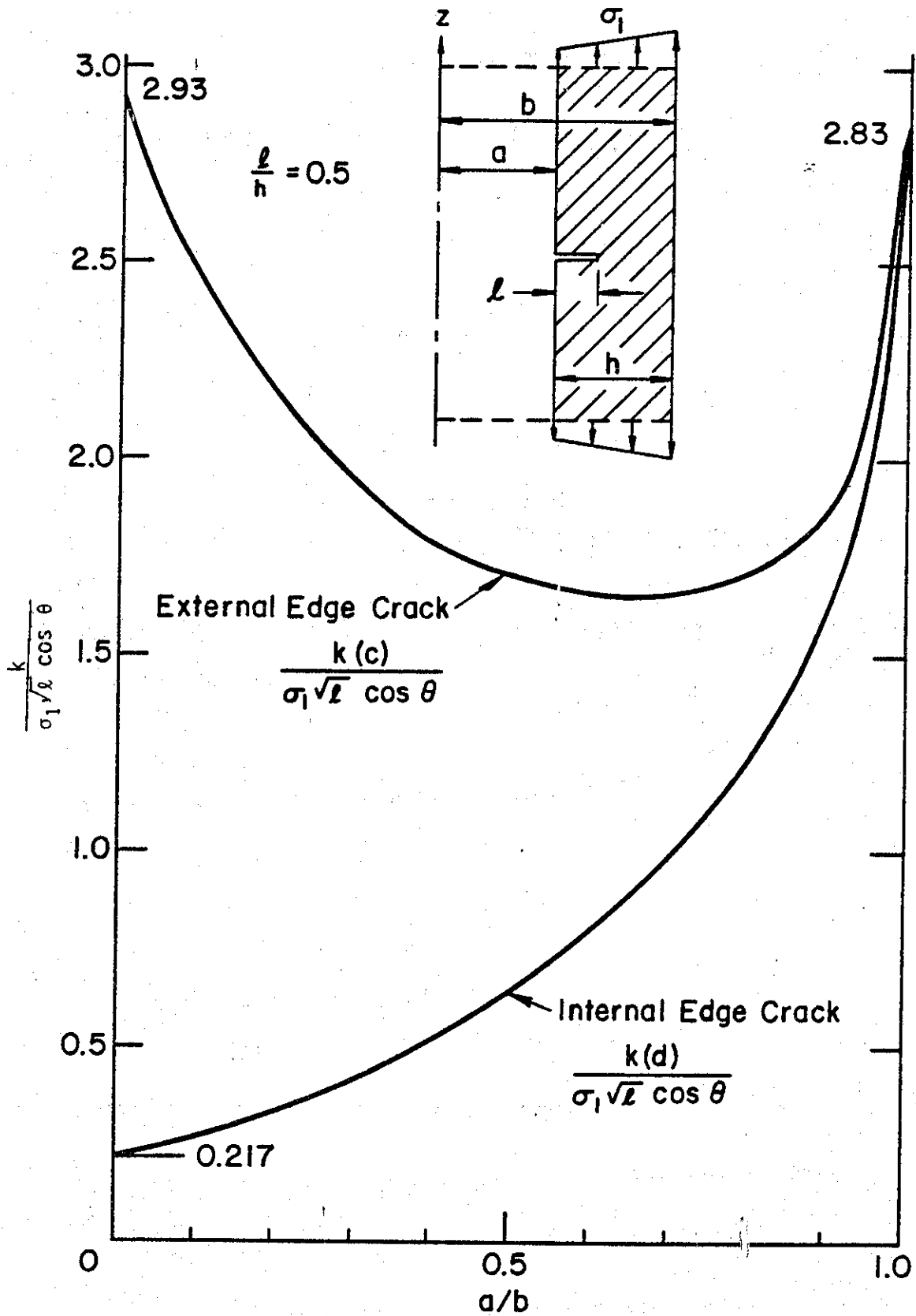


Fig.D8 Stress intensity factors for edge cracks in a thick-walled cylinder subjected to pure bending. $l/h = 0.5$.

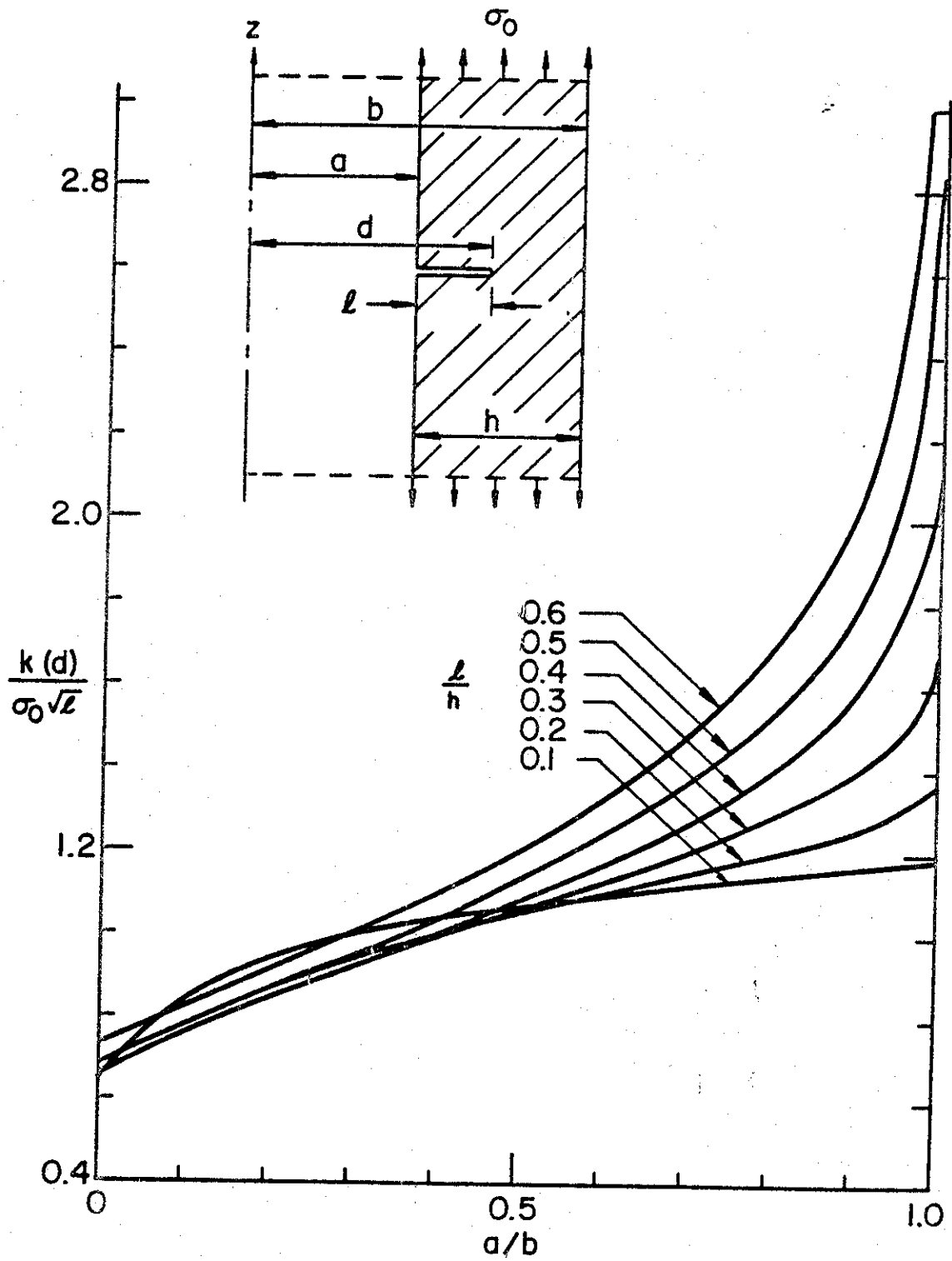


Fig.D9 Stress intensity factors for internal edge-cracks in thick-walled cylinders subjected to axial tension.

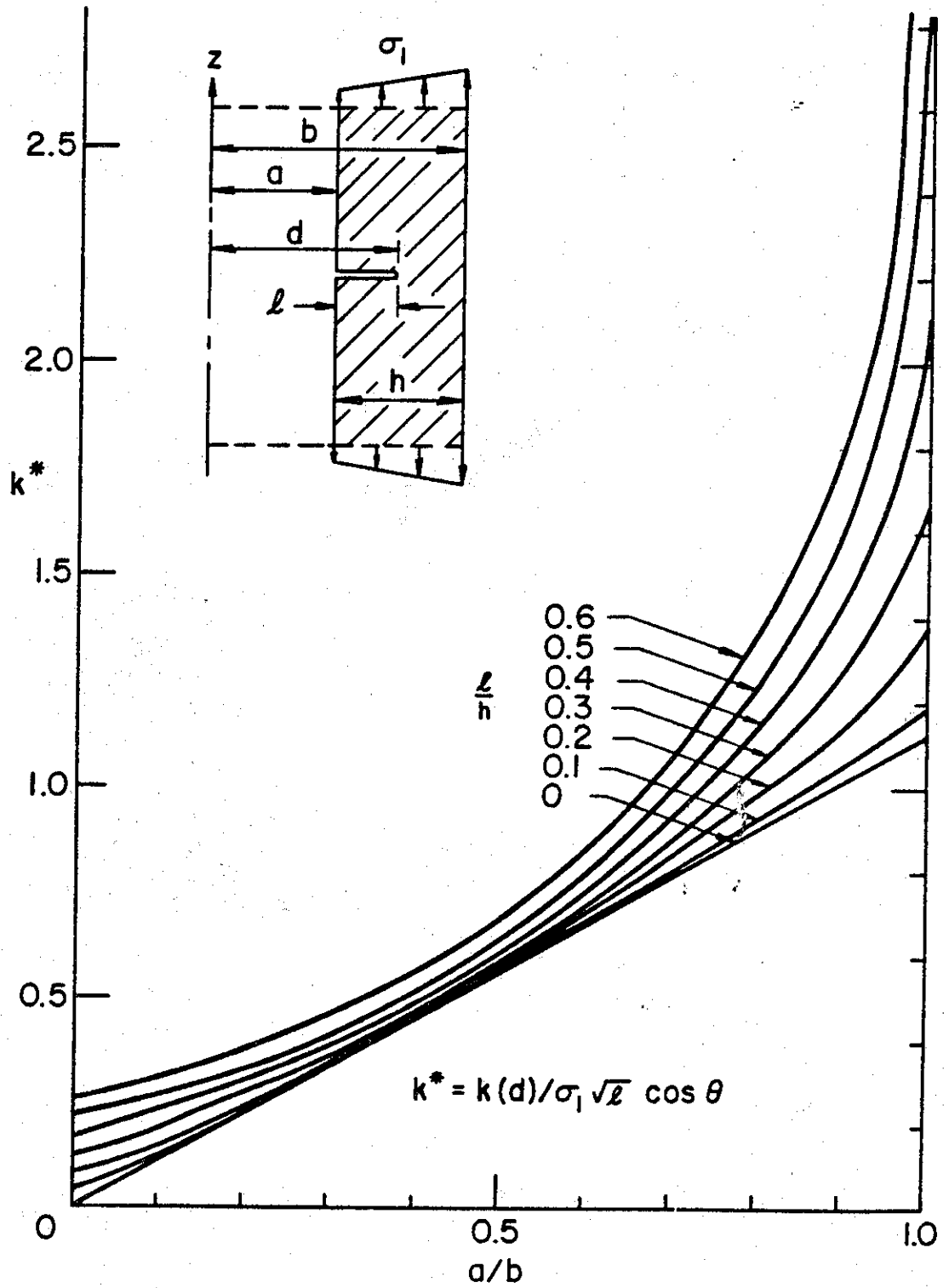


Fig.D10 Stress intensity factors for internal edge cracks in thick-walled cylinders subjected to pure bending.

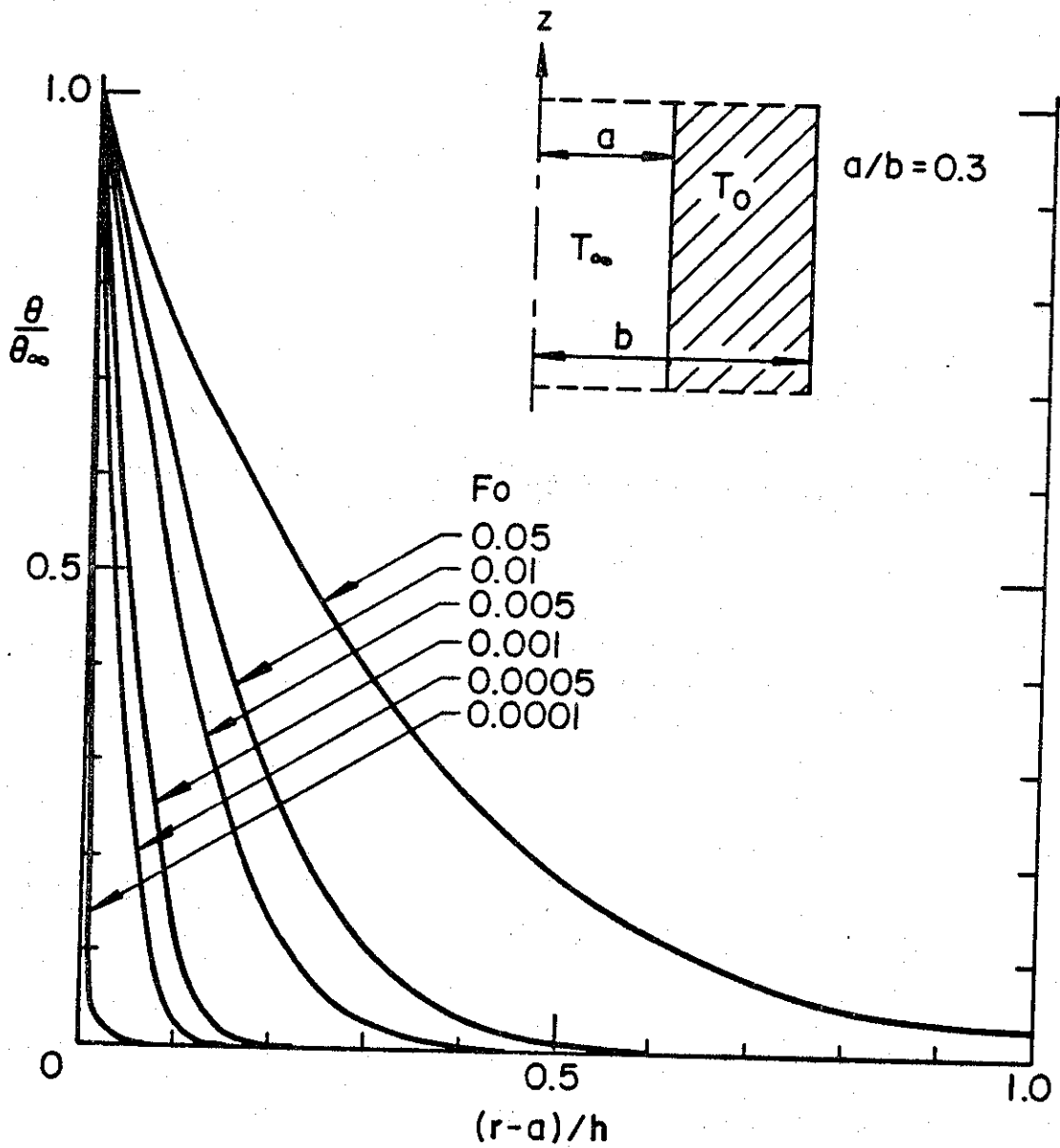


Fig.D11 Transient temperature distribution θ/θ_{∞} in a hollow cylinder due to a sudden temperature change on the inner radius. $a/b=0.3$, $h=b-a$, $Fo=Dt/b^2$, $\theta/\theta_{\infty} = (T(r,t)-T_0)/(T_{\infty}-T_0)$.

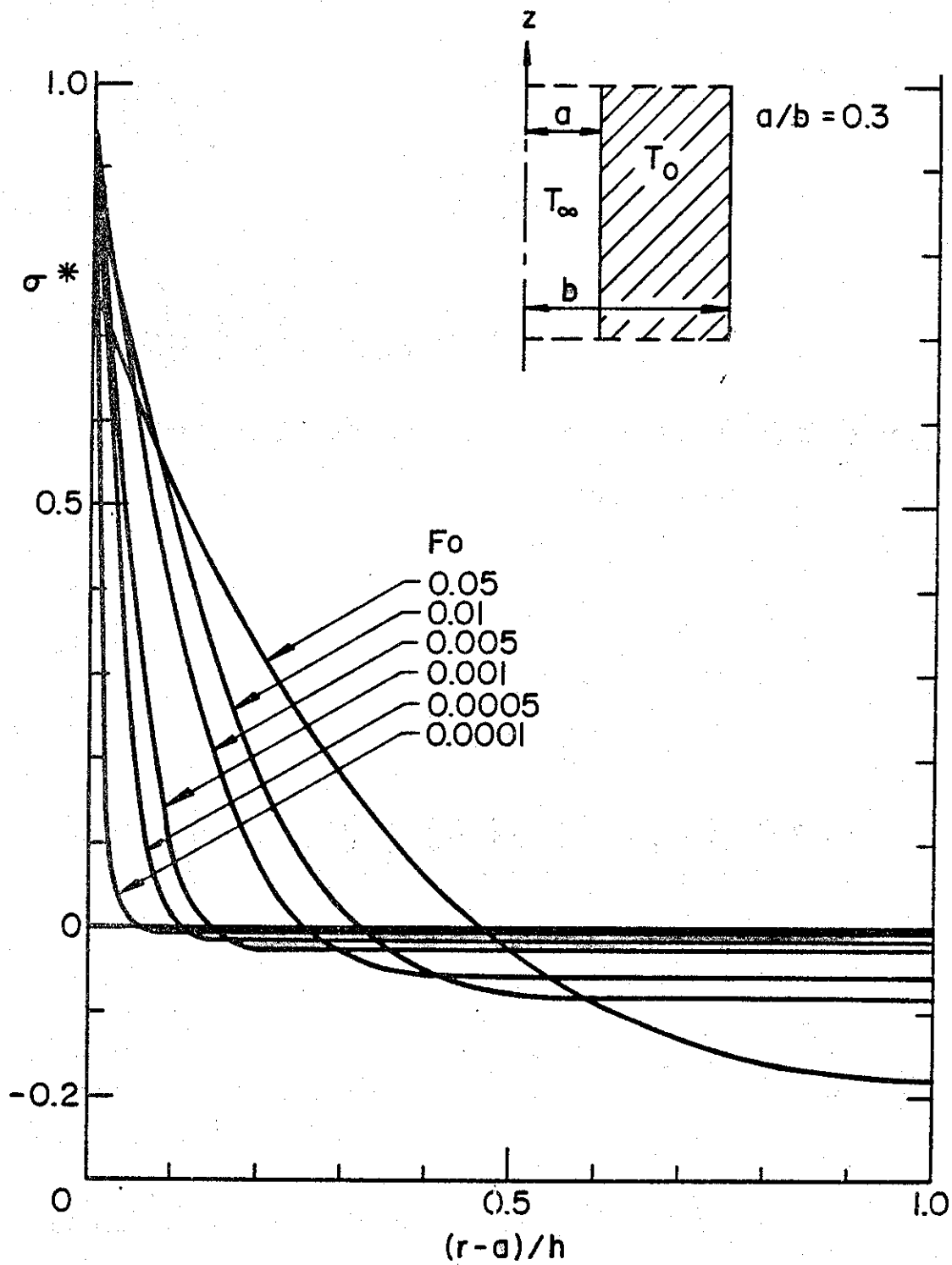


Fig.D12 Transient thermal stresses in a hollow cylinder which has been suddenly cooled by a temperature T_∞ on its inner radius. $a/b=0.3$, $h=b-a$, $Fo=Dt/b^2$, $\sigma^* = -\left(\frac{1-\nu}{E\alpha}\right) \sigma_{zz}/\theta_\infty$.

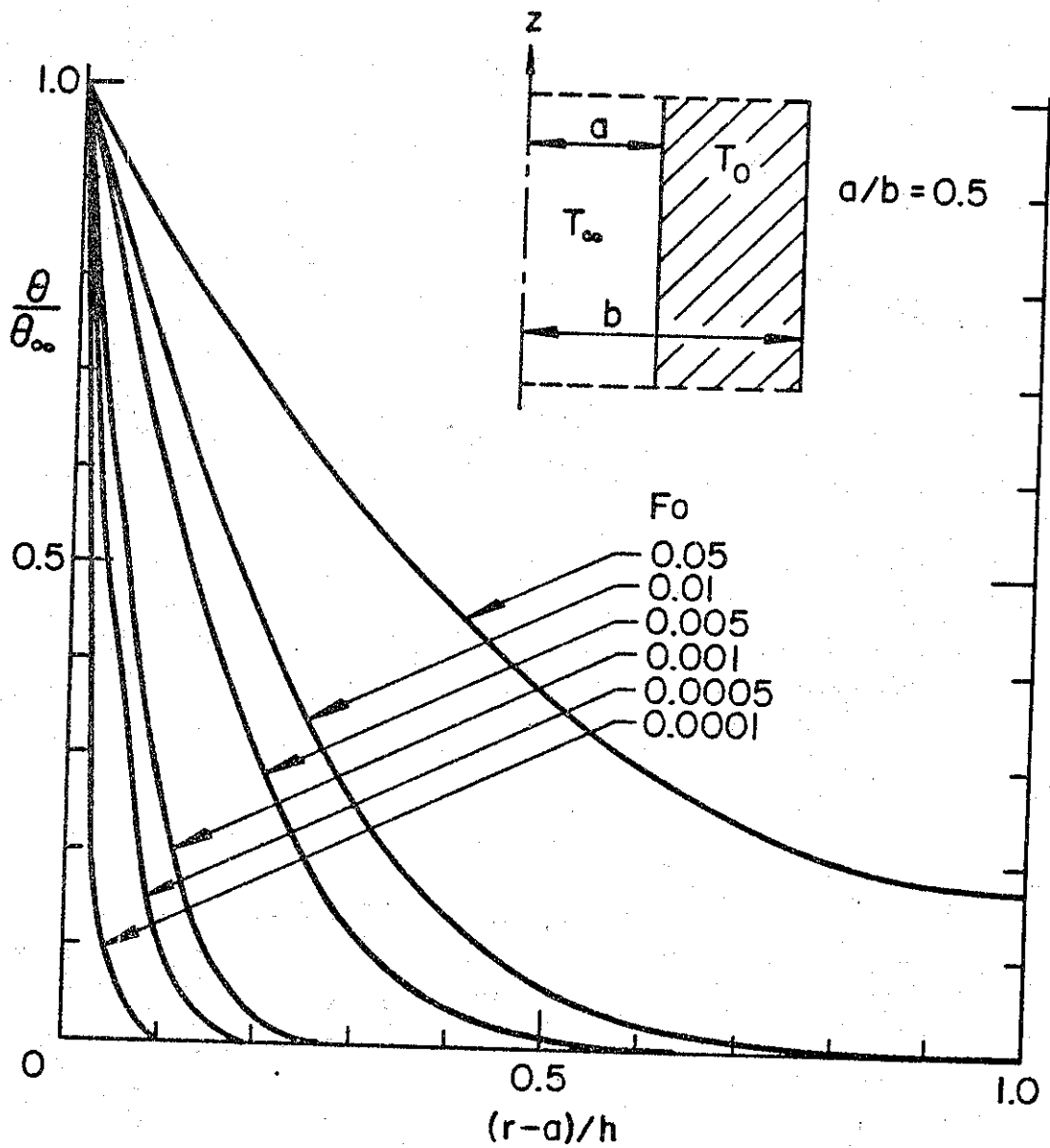


Fig.D13 Transient temperature distribution θ/θ_{∞} in a hollow cylinder due to a sudden temperature change on the inner radius. $a/b=0.5$, $h=b-a$, $Fo=Dt/b^2$, $\theta/\theta_{\infty} = (T(r,t)-T_0)/(T_{\infty}-T_0)$.

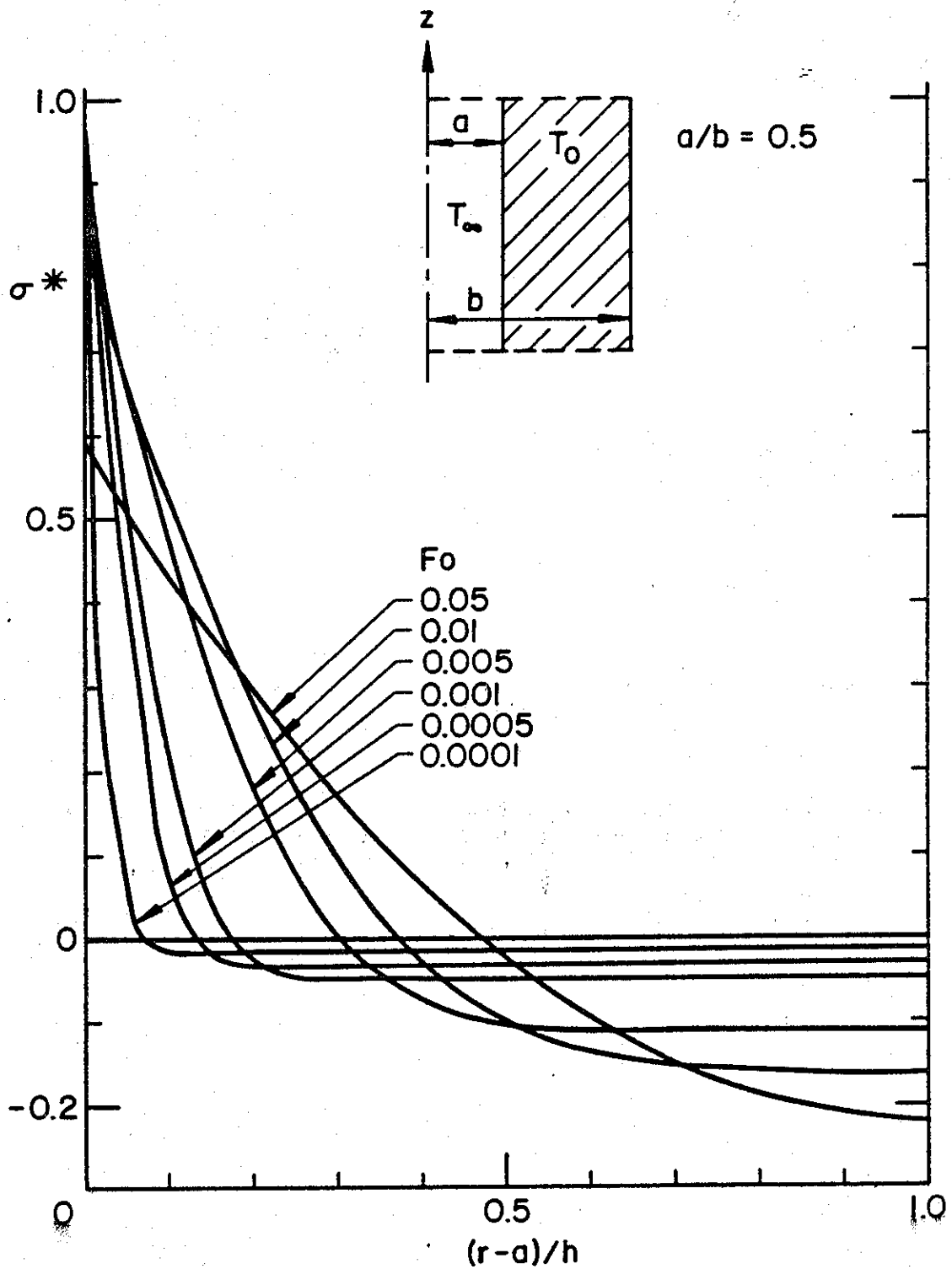


Fig.D14 Transient thermal stresses in a hollow cylinder which has been suddenly cooled by a temperature T_∞ on its inner radius. $a/b = 0.5$, $h=b-a$, $F_0=Dt/b^2$, $\sigma^* = -\left(\frac{1-\nu}{E\alpha}\right) \sigma_{zz}/\theta_\infty$.

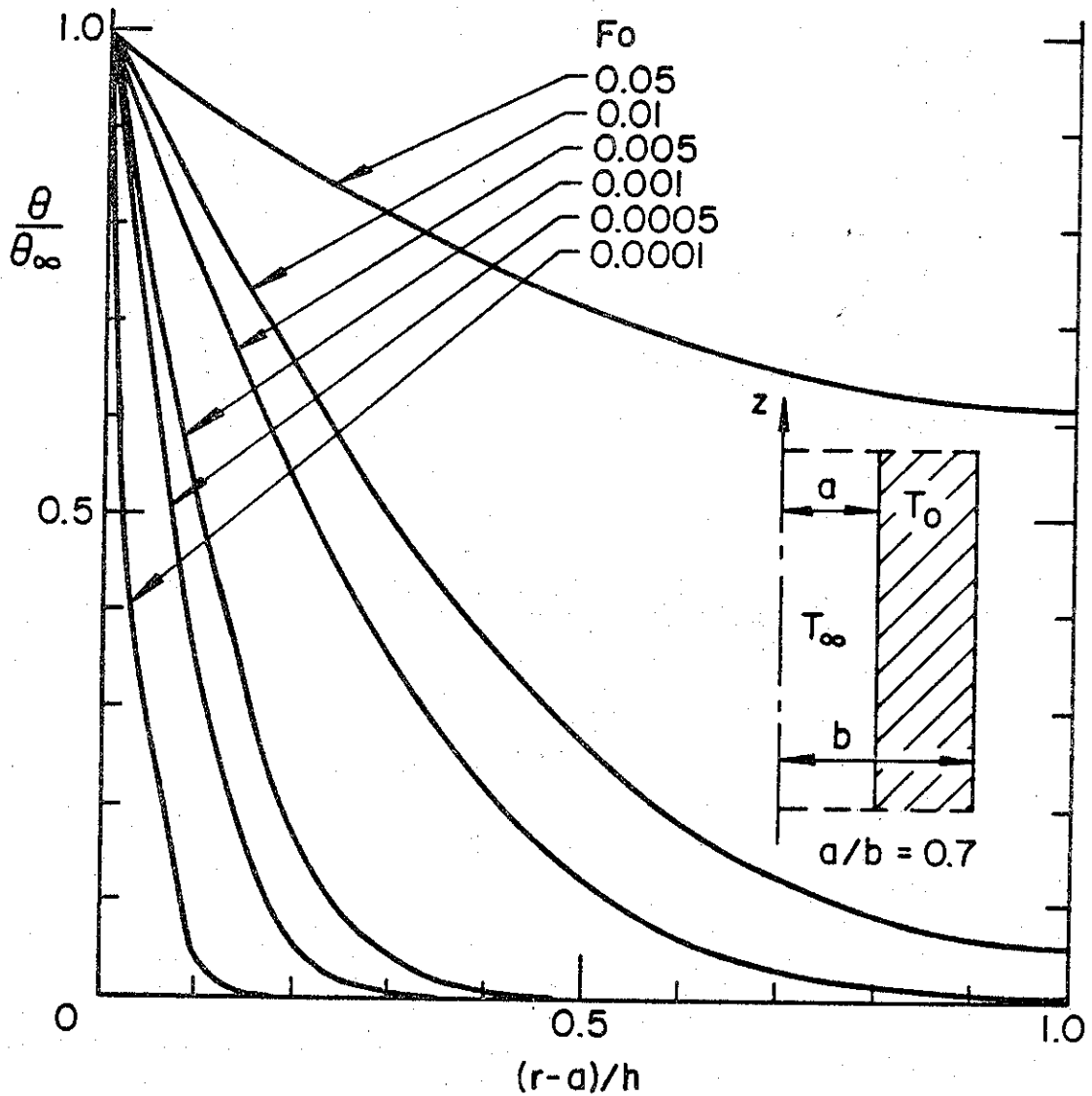


Fig.D15 Transient temperature distribution θ/θ_{∞} in a hollow cylinder due to a sudden temperature change on the inner radius. $a/b=0.7$, $h=b-a$, $Fo=Dt/b^2$, $\theta/\theta_{\infty} = (T(r,t)-T_0)/(T_{\infty}-T_0)$.

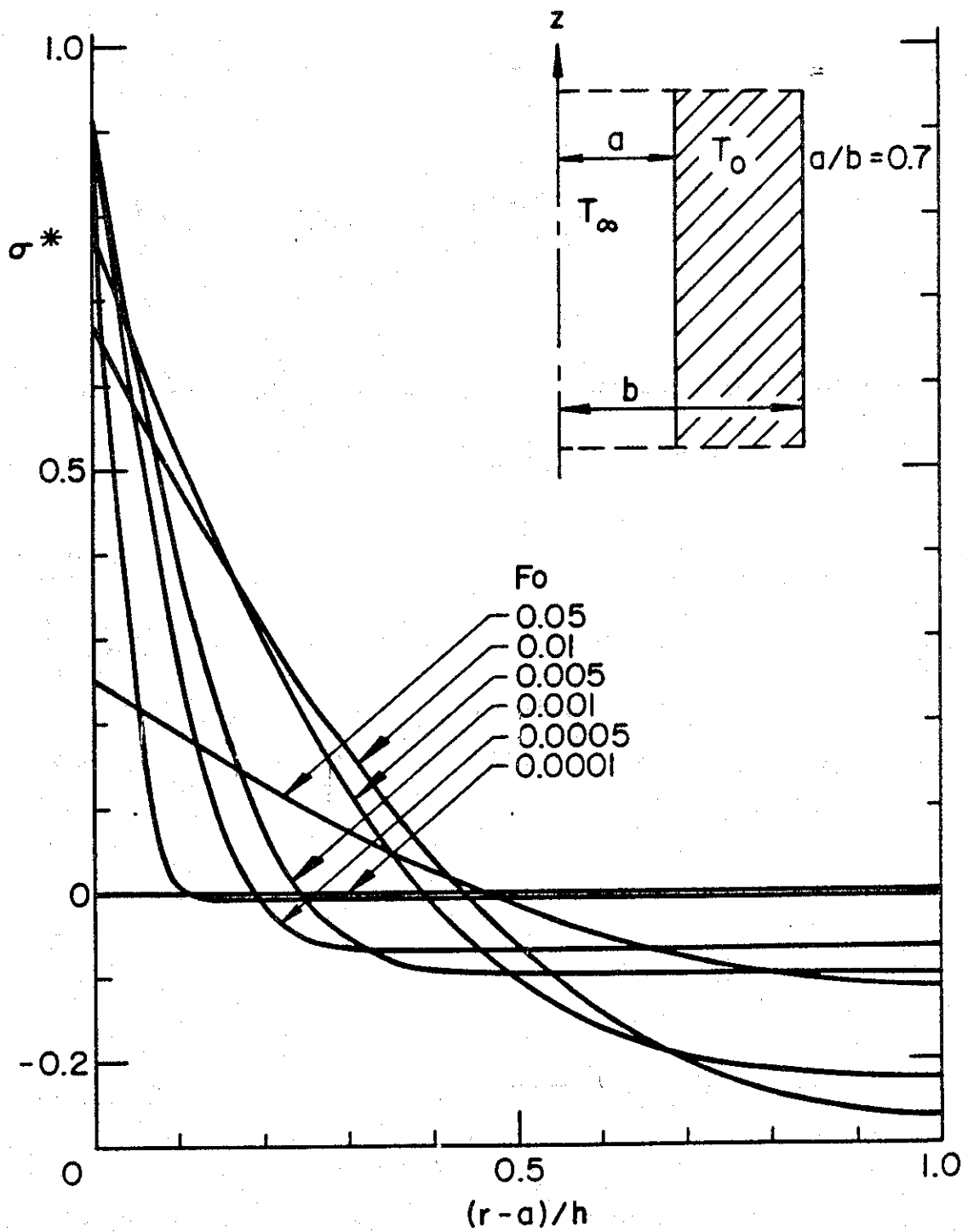


Fig.D16 Transient thermal stresses in a hollow cylinder which has been suddenly cooled by a temperature T_∞ on its inner radius. $a/b = 0.7$, $h=b-a$, $F_0=Dt/b^2$, $\sigma^* = -\left(\frac{1-\nu}{E\alpha}\right) \sigma_{zz}/\theta_\infty$.

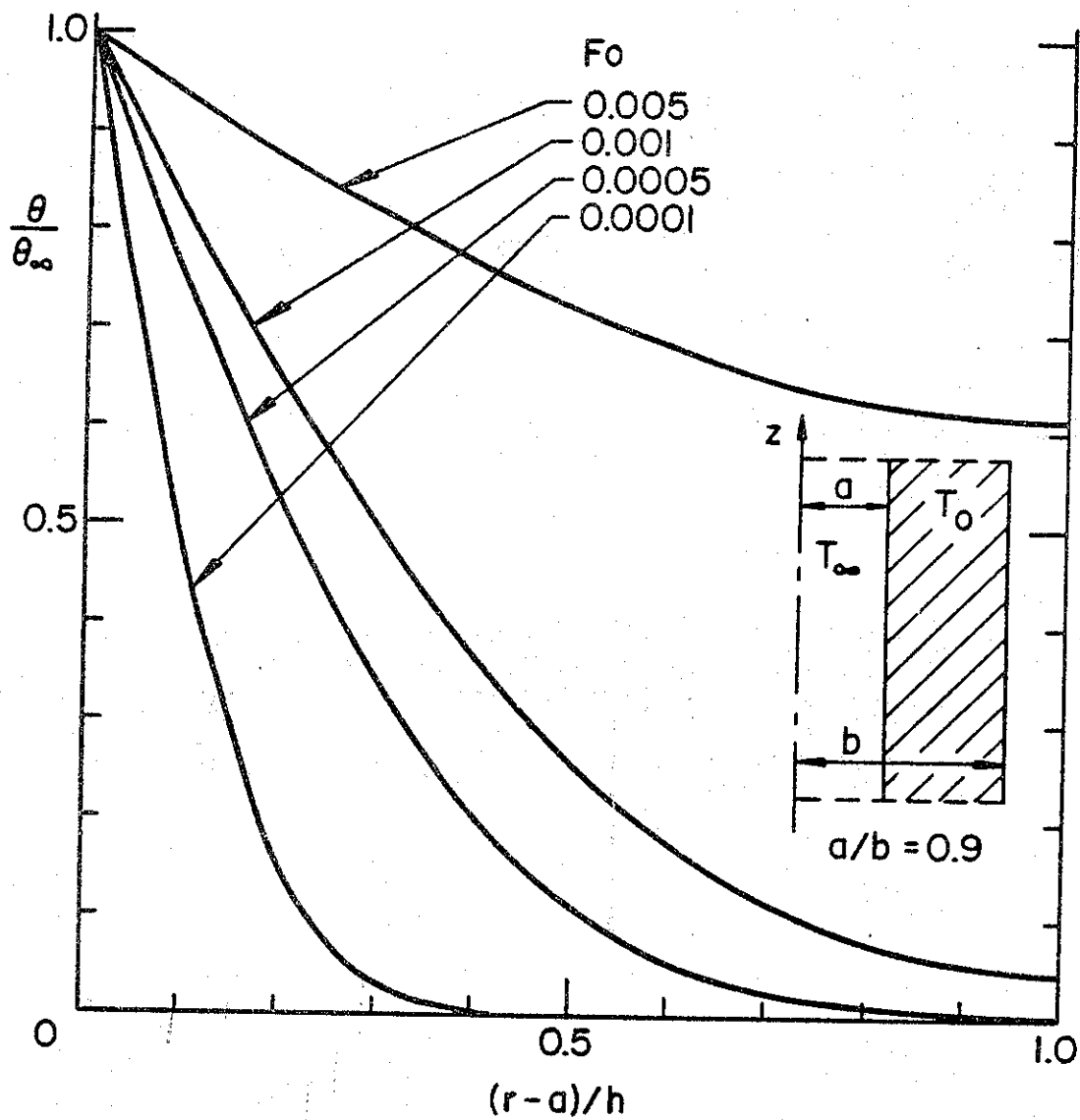


Fig.D17 Transient temperature distribution θ/θ_{∞} in a hollow cylinder due to a sudden temperature change on the inner radius. $a/b=0.9$, $h=b-a$, $Fo=Dt/b^2$, $\theta/\theta_{\infty} = (T(r,t)-T_0)/(T_{\infty}-T_0)$.

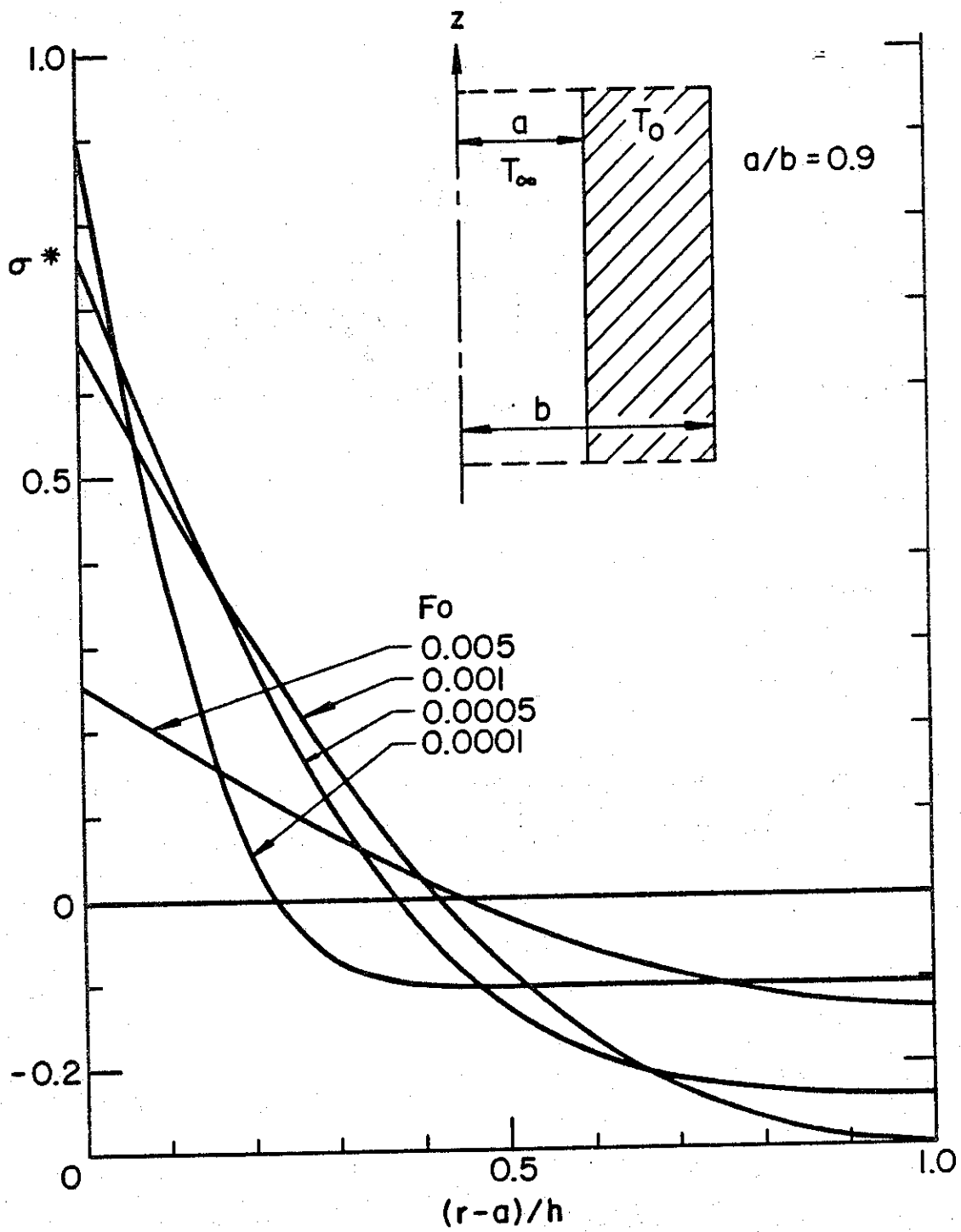


Fig. D18 Transient thermal stresses in a hollow cylinder which has been suddenly cooled by a temperature T_∞ on its inner radius. $a/b = 0.9$, $h = b - a$, $Fo = Dt / b^2$, $\sigma^* = -\left(\frac{1-\nu}{E\alpha}\right) \sigma_{zz} / \theta_\infty$.

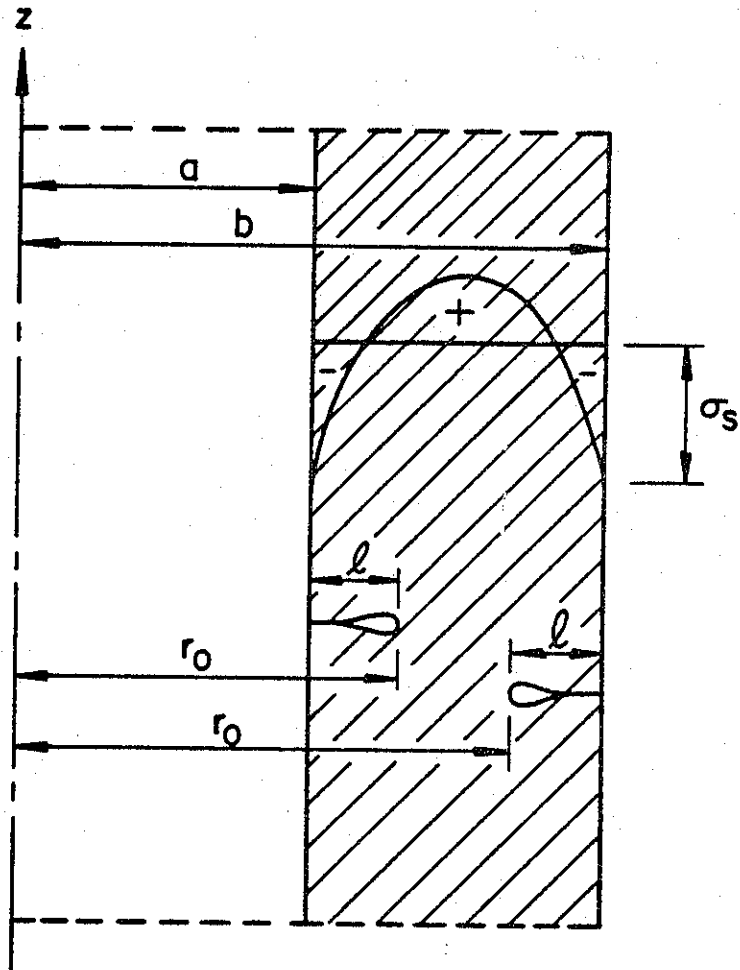


Fig.D19 Geometry of edge cracks in a cylinder wall subjected to residual stresses.

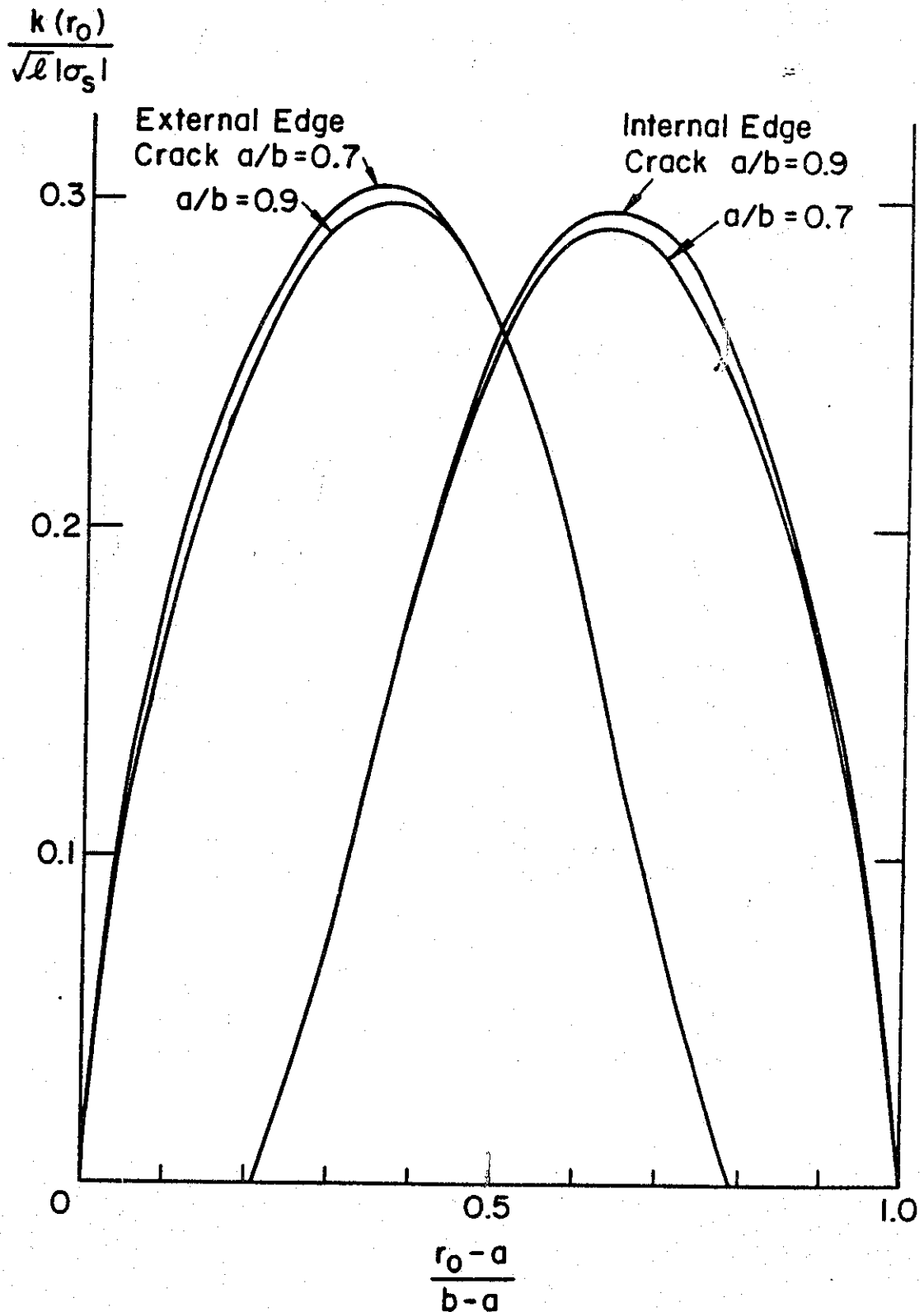


Fig.D20 Stress intensity factors for edge cracks in a hollow cylinder subjected to residual stresses. $a/b = 0.9$, $a/b = 0.7$.

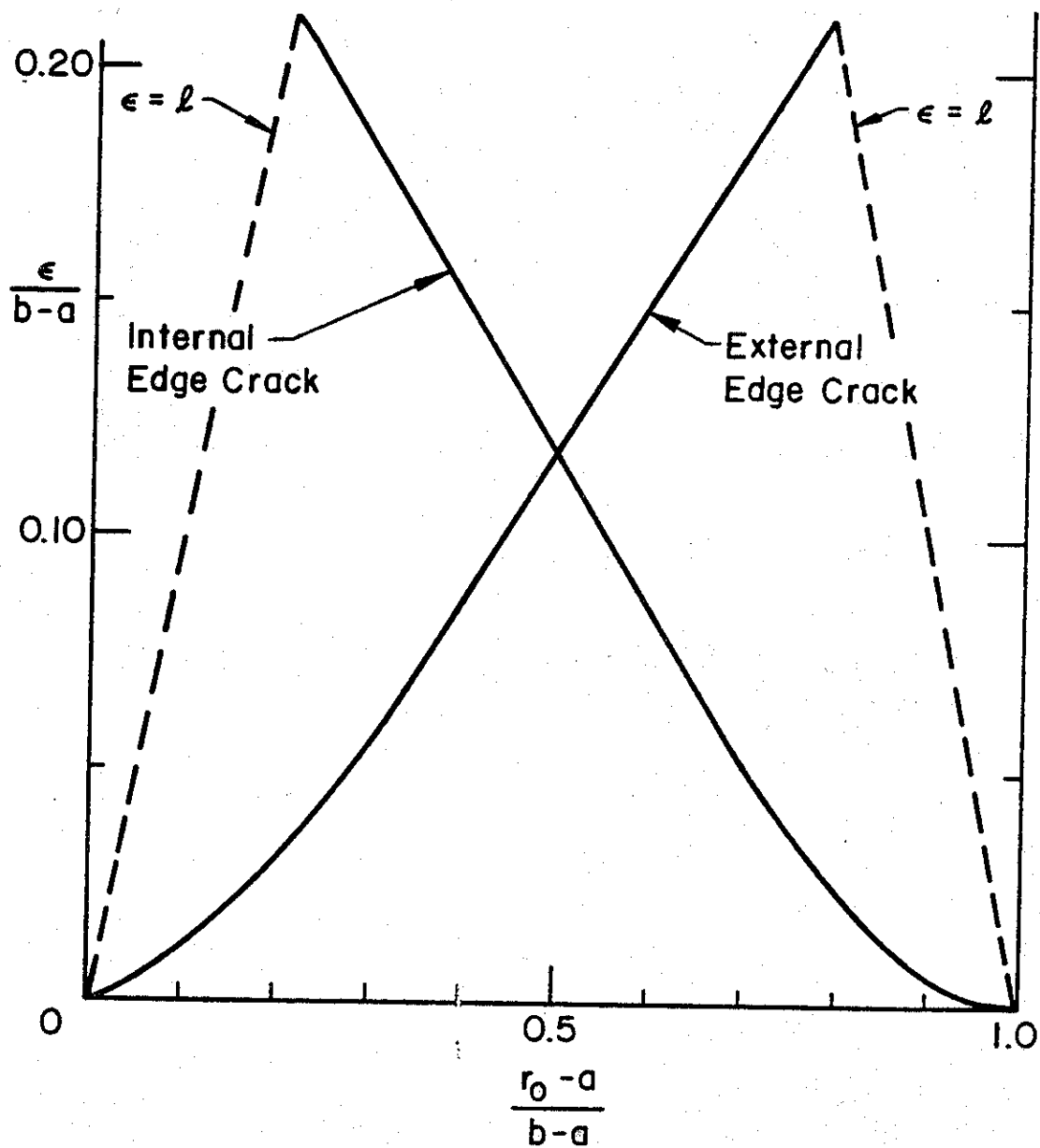


Fig.D21 Crack contact length ϵ for a hollow cylinder under residual stresses with either internal or external circumferential edge crack. $a/b = 0.9$.

Bibliography

1. Sneddon, I.N. and Lowengrub, M., Crack Problems in the Classical Theory of Elasticity, SIAM Series in Applied Mathematics, John Wiley & Sons, Inc., 1969.
2. Collins, W.D., "Some Axially Symmetric Stress Distributions in Elastic Solids Containing Penny-shaped Cracks", Proc. Edinburgh Math. Soc. (2), Vol. 13, pp. 69-78, 1962.
3. Sneddon, I.N. and Tait, J.T., "The Effect of a Penny-shaped Crack on the Distribution of Stress in a Long Circular Cylinder", Int. J. Engng. Sci., Vol. 1, pp. 391-409, 1963.
4. Sneddon, I.N. and Welch, J.T., "A Note on the Distribution of Stress in a Cylinder Containing a Penny-shaped Crack", Int. J. Engng. Sci., Vol. 1, pp. 411-419, 1963.
5. Erdol, R. and Erdogan, F., "A Thick-walled Cylinder with an Axisymmetric Internal or Edge Crack", J. Appl. Mech., Vol. 45, Trans. ASME, pp. 281-286, 1978.
6. Kobayashi, I., "Darstellung eines Potentials in Zylinderschen Koordinaten das sich aus einer Ebene innerhalb und ausserhalb einer Kreisbegrenzung verschiedenen Grenzbedingung unterwirft", Sci. Rep. Tohoku Imp. Univ. 20, 197.
7. Keer, L.M., "A Class of Nonsymmetrical Punch and Crack Problems", Quart. Journ. Mech. and Applied Math., Vol. XVII, Pt. 4, 1964.
8. Pacella, A.H. and Erdogan, F., "A Penny-shaped Crack in a Filament-Reinforced Matrix-II. The Crack Problem", Int. J. Solids Structures, Vol. 10, pp. 807-819, 1974.
9. Kassir, M.K. and Singh, M., "Non-Axisymmetric Loadings of a Crack Cylinder", Int. J. Solids Structures, Vol. 14, pp. 153-160, 1978.
10. Green, A.E. and Zerna, W., Theoretical Elasticity, Oxford University Press, London, 1968.
11. Sih, G.C., ed., Mechanics of Fracture II: Three-Dimensional Crack Problems, Noordhoff International Publishing, Leyden, Netherlands, 1975.

12. Luré, A.I., Three-Dimensional Problems of the Theory of Elasticity, Interscience Publishers, 1964.
13. Erdélyi, A., ed., Table of Integral Transforms - Bateman Manuscript Project, Vol. 2, McGraw-Hill, New York, 1954.
14. Magnus, W., Oberhettinger, F., Soni, R.P., Formulas and Theorems for the Special Functions of Mathematical Physics, Die Grundlehren der mathematischen Wissenschaften, Vol. 52, Springer-Verlag, New York, 1966.
15. Watson, G.N., A Treatise on the Theory of Bessel Functions, 2nd ed., Cambridge University Press, London, 1944.
16. Gradshteyn, I.S. and Ryzhik, I.M., Tables of Integrals, Series and Products, 4th ed., Academic Press, New York, 1966.
17. Erdogan, F., Gupta, G.D. and Cook, T.S., "Numerical Solution of Singular Integral Equations", Mechanics of Fracture I: Methods of Analysis and Solutions of Crack Problems, pp. 368-425, ed. G.C. Sih, Noordhoff International Publishing, Leyden, Netherlands, 1973.
18. Krenk, S., "On Quadrature Formulas for Singular Integral Equations of the First and Second Kind", Quart. of Applied Math., Vol. XXXIII, No. 3, Oct., 1975.
19. Abramowitz, M. and Stegun, I., Handbook of Mathematical Functions, Dover Publications, New York, 1965.
20. Delale, F. and Erdogan, F., "Application of the Line-Spring Model to a Cylindrical Shell Containing a Circumferential or Axial Part-Through Crack", U.S. Department of Transportation Technical Report, Lehigh University, DOT-RC-82007, April 1981.

Appendix A

The coefficient matrix $f_{ij}(s,a,b)$ whose inverse $m_{ij}(s,a,b)$ is used to calculate the unknown coefficients in the stress and displacement equations.

$$f_{i1} = rs I_n(sr) - (2-2\nu+n) I_{n+1}(sr) \quad (A-1)$$

$$f_{i2} = -[rs K_n(sr) + (2-2\nu+n) K_{n+1}(sr)] \quad (A-2)$$

$$f_{i3} = s I_{n+1}(sr) + \frac{n}{r} I_n(sr) \quad (A-3)$$

$$f_{i4} = \frac{n}{r} K_n(sr) - s K_{n+1}(sr) \quad (A-4)$$

$$f_{i5} = -\frac{n}{r} I_n(sr) \quad (A-5)$$

$$f_{i6} = -\frac{n}{r} K_n(sr), \quad i = 1, 2, \quad (A-6)$$

for $i = 1$, $r = a$ and for $i = 2$, $r = b$.

$$f_{i1} = -\frac{(n+1)}{r} (4-4\nu+n) I_{n+1}(sr) + (2-2\nu+n)s I_n(sr) \quad (A-7)$$

$$f_{i2} = -\frac{(n+1)}{r} (4-4\nu+n) K_{n+1}(sr) - (2-2\nu+n)s K_n(sr) \quad (A-8)$$

$$f_{i3} = \frac{sn}{r} I_{n+1}(sr) + \frac{n}{r^2} (n-1) I_n(sr) \quad (A-9)$$

$$f_{i4} = -\frac{sn}{r} K_{n+1}(sr) + \frac{n}{r^2} (n-1) K_n(sr) \quad (A-10)$$

$$f_{i5} = -\left(\frac{2n}{r^2} (n-1) + s^2\right) I_n(sr) + \frac{2s}{r} I_{n+1}(sr) \quad (A-11)$$

$$f_{i6} = -\left(\frac{2n}{r^2} (n-1) + s^2\right) K_n(sr) - \frac{2s}{r} K_{n+1}(sr) \quad (A-12)$$

for $i = 3, 4$; when $i = 3$, $r = a$ and when $i = 4$, $r = b$.

$$f_{i1} = (3-2\nu)s I_n(sr) - \left[\frac{(n+1)}{r} (4-4\nu+n) + rs^2 \right] I_{n+1}(sr) \quad (A-13)$$

$$f_{i2} = - \left\{ (3-2\nu)s K_n(sr) + \left[\frac{(n+1)}{r} (4-4\nu+n) + rs^2 \right] K_{n+1}(sr) \right\} \quad (A-14)$$

$$f_{i3} = - \left\{ \left[\frac{n(n-1)}{r^2} + s^2 \right] I_n(sr) - \frac{s}{r} I_{n+1}(sr) \right\} \quad (A-15)$$

$$f_{i4} = - \left\{ \left[\frac{n(n-1)}{r^2} + s^2 \right] K_n(sr) + \frac{s}{r} K_{n+1}(sr) \right\} \quad (A-16)$$

$$f_{i5} = \frac{2n}{r} \left[\frac{(n-1)}{r} I_n(sr) + s I_{n+1}(sr) \right] \quad (A-17)$$

$$f_{i6} = \frac{2n}{r} \left[\frac{(n-1)}{r} K_n(sr) - s K_{n+1}(sr) \right] \quad (A-18)$$

for $i = 5, 6$; when $i = 5$, $r = a$ and when $i = 6$, $r = b$.

The terms $G_j(s, t)$ in (53) are obtained by integrating the Bessel integrals which result from the substitution of (52) into the stress equations (46), (47) and (49). These definite Bessel integrals are evaluated by differentiating a related integral given by Erdélyi, v2. p. 49.

Erdélyi gives:

$$\int_0^{\infty} \alpha^{\nu-\mu+2n+1} (s^2+\alpha^2)^{-1} J_{\mu}(a\alpha) J_{\nu}(t\alpha) d\alpha = (-1)^n s^{\nu-\mu+2n} I_{\mu}(as) K_{\nu}(ts)$$

$$a > 0, \operatorname{Re} s > 0, a < t < \infty,$$

$$\operatorname{Re} \mu - 2n + 1 > \operatorname{Re} \nu > -n - 1, n = \text{integer}. \quad (A-19)$$

Taking the derivative with respect to s on both sides, the integral becomes,

$$\int_0^{\infty} \alpha^{v-\mu+2n+1} (s^2+\alpha^2)^{-2} J_{\mu}(a\alpha) J_{\nu}(t\alpha) d\alpha = \frac{(-1)^n}{-2} \{ (v-\mu+2n) * \\ * s^{v-\mu+2n-2} I_{\mu}(as) K_{\nu}(ts) + s^{v-\mu+2n-1} [a I_{\mu+1}(sa) + \frac{\mu}{s} I_{\mu}(sa)] * \\ * K_{\nu}(ts) + s^{v-\mu+2n-1} I_{\mu}(as) [\frac{v}{s} K_{\nu}(st) - t K_{\nu+1}(st)] \}$$

$$a > 0, \text{Re } s > 0, a < t < \infty, \quad (\text{A-20})$$

$$\text{Re } \mu-2n+4 > \text{Re } \nu > -n-1$$

Thus, the terms $G_j(s,t)$ ($j=1,6$) are expressed as:

$$G_1(s,t) = K_n(st) \{ \frac{2n(n+1)}{a} I_n(as) + (4+3n)s I_{n+1}(as) \\ + s^2 a I_{n+2}(as) \} - t K_{n+1}(st) \{ \frac{ns}{a} I_n(as) + s^2 I_{n+1}(as) \} \quad (\text{A-21})$$

$$G_2(s,t) = I_n(st) \{ \frac{2n(n+1)}{b} K_n(bs) - (4+3n)s K_{n+1}(bs) \\ + s^2 b K_{n+2}(bs) \} + t I_{n+1}(st) \{ \frac{ns}{b} K_n(bs) - s^2 K_{n+1}(bs) \} \quad (\text{A-22})$$

$$G_3(s,t) = \frac{n}{a} \{ K_n(st) [\frac{2(n-1)(v+n)}{a} I_n(as) + s(2v+3n+1) I_{n+1}(as) \\ + s^2 a I_{n+2}(as)] - t K_{n+1}(st) [\frac{s(n-1)}{a} I_n(as) + s^2 I_{n+1}(as)] \} \quad (\text{A-23})$$

$$\begin{aligned}
G_4(s,t) = & \frac{n}{b} \{I_n(st) \left[\frac{2(n-1)(v+n)}{b} K_n(bs) - s(2v+3n+1)K_{n+1}(bs) \right. \\
& \left. + s^2b K_{n+2}(bs) \right] + t I_{n+1}(st) \left[\frac{s(n-1)}{b} K_n(bs) - s^2K_{n+1}(bs) \right] \} \\
\end{aligned} \tag{A-24}$$

$$\begin{aligned}
G_5(s,t) = & K_n(st) \left\{ - \left[\frac{2n(n-1)(n+v)}{a^2} + 2(n+1)s^2 \right] I_n(sa) \right. \\
& \left. + \left[\frac{s}{a} (-n^2+3n+2(v+1)) - s^3a \right] I_{n+1}(sa) + s^2 I_{n+2}(sa) \right\} \\
& - t K_{n+1}(st) \left\{ - \left[\frac{n(n-1)}{a^2} + s^2 \right] s I_n(as) + \frac{s^2}{a} I_{n+1}(as) \right\} \\
\end{aligned} \tag{A-25}$$

$$\begin{aligned}
G_6(s,t) = & I_n(st) \left\{ - \left[\frac{2n(n-1)(n+v)}{b^2} + 2(n+1)s^2 \right] K_n(bs) \right. \\
& \left. + \left[\frac{s}{b} (n^2-3n-2(v+1)) + s^3b \right] K_{n+1}(bs) + s^2 K_{n+2}(bs) \right\} \\
& + t I_{n+1}(st) \left\{ - \left[\frac{n(n-1)}{b^2} + s^2 \right] s K_n(bs) - \frac{s^2}{b} K_{n+1}(bs) \right\} \\
\end{aligned} \tag{A-26}$$

Appendix B

The terms $v_j(s,t)$ in equation (68).

$$v_j = \gamma_{jK} Q_K \quad \text{for } j = 1,3,5, \quad K = 1,2 \quad (\text{B-1})$$

$$v_j = \gamma_{jK} Q_{K+2} \quad \text{for } j = 2,4,6, \quad K = 1,2 \quad (\text{B-2})$$

For example,

$$v_1 = \gamma_{11} Q_1 + \gamma_{12} Q_2$$

$$v_2 = \gamma_{21} Q_3 + \gamma_{22} Q_4$$

$$v_3 = \gamma_{31} Q_1 + \gamma_{32} Q_2, \text{ etc.}$$

$$\gamma_{11} = \frac{2n(n+1)}{a} I_n(as) + (4+3n)s I_{n+1}(as) + s^2 a I_{n+2}(as) \quad (\text{B-3})$$

$$\gamma_{12} = \frac{ns}{a} I_n(as) + s^2 I_{n+1}(as) \quad (\text{B-4})$$

$$\gamma_{21} = \frac{2n(n+1)}{b} K_n(bs) - (4+3n)s K_{n+1}(bs) + s^2 b K_{n+2}(bs) \quad (\text{B-5})$$

$$\gamma_{22} = \frac{ns}{b} K_n(bs) - s^2 K_{n+1}(bs) \quad (\text{B-6})$$

$$\gamma_{31} = \frac{n}{a} \left[\frac{2(n-1)(v+n)}{a} I_n(as) + s(2v+3n+1) I_{n+1}(as) + s^2 a I_{n+2}(as) \right]$$

(B-7)

$$\gamma_{32} = \frac{n}{a} \left[\frac{s(n-1)}{a} I_n(as) + s^2 I_{n+1}(as) \right] \quad (\text{B-8})$$

$$\gamma_{41} = \frac{n}{b} \left[\frac{2(n-1)(v+n)}{b} K_n(bs) - s(2v+3n+1) K_{n+1}(bs) + s^2 b K_{n+2}(bs) \right]$$

(B-9)

$$\gamma_{42} = \frac{n}{b} \left[\frac{s(n-1)}{b} K_n(bs) - s^2 K_{n+1}(bs) \right] \quad (B-10)$$

$$\begin{aligned} \gamma_{51} = & - \left[\frac{2n(n-1)(n+v)}{a^2} + 2(n+1)s^2 \right] I_n(sa) + \left[\frac{s}{a} (-n^2+3n+2(v+1)) \right. \\ & \left. - s^3 a \right] I_{n+1}(sa) + s^2 I_{n+2}(sa) \end{aligned} \quad (B-11)$$

$$\gamma_{52} = - \left[\frac{n(n-1)}{a^2} + s^2 \right] s I_n(as) + \frac{s^2}{a} I_{n+1}(as) \quad (B-12)$$

$$\begin{aligned} \gamma_{61} = & - \left[\frac{2n(n-1)(n+v)}{b^2} + 2(n+1)s^2 \right] K_n(bs) + \left[\frac{s}{b} (n^2-3n-2(v+1)) \right. \\ & \left. + s^3 b \right] K_{n+1}(bs) + s^2 K_{n+2}(bs) \end{aligned} \quad (B-13)$$

$$\gamma_{62} = - \left[\frac{n(n-1)}{b^2} + s^2 \right] s K_n(bs) - \frac{s^2}{b} K_{n+1}(bs) \quad (B-14)$$

The terms in (B-1) and (B-2) denoted by Q_K are defined as,

$$Q_1(s,t) = - \frac{i}{s} [nt K_n(st) S_{0,n-1}(ist) - it K_{n-1}(st) S_{1,n}(ist)] \quad (B-15)$$

$$Q_2(s,t) = \frac{1}{s^2} [(n+2)t K_{n+1}(st) S_{1,n}(ist) - it K_n(st) S_{2,n+1}(ist)] \quad (B-16)$$

$$Q_3(s,t) = - \frac{i}{s} [nt I_n(st) S_{0,n-1}(ist) + it I_{n-1}(st) S_{1,n}(ist)] \quad (B-17)$$

$$Q_4(s,t) = - \frac{1}{s^2} [(n+2)t I_{n+1}(st) S_{1,n}(ist) + it I_n(st) S_{2,n+1}(ist)]. \quad (B-18)$$

The Lommel functions of imaginary argument which are encountered in Q_K are not in a form which is convenient for numerical

computation, but with the aid of certain identities involving the Struve function (see Appendix C) Q_K may be expressed in terms of real functions with real arguments. The terms Q_K $K=1, \dots, 4$ for five harmonics $n=0, \dots, 4$ are given.

$$\begin{array}{c} \underline{n=0} \\ Q_1(s, t) = \frac{-t}{s} K_1(st) \end{array} \quad (B-19)$$

$$Q_2(s, t) = \frac{2t}{s^2} K_1(st) + \frac{t^2}{s} K_0(st) \quad (B-20)$$

$$Q_3(s, t) = \frac{t}{s} I_1(st) \quad (B-21)$$

$$Q_4(s, t) = -\frac{2t}{s^2} I_1(st) + \frac{t^2}{s} I_0(st) \quad (B-22)$$

$$\text{let: } u_0(z) = \int_0^1 e^{-zp} (1-p^2)^{-1/2} dp \quad (B-23)$$

$$u_1(z) = \int_0^1 e^{-zp} (1-p^2)^{1/2} dp \quad (B-24)$$

$$u_2(z) = z^2 \int_0^1 e^{-zp} (1-p^2)^{3/2} dp, \quad (B-25)$$

then for $\underline{n=1}$:

$$Q_1(s, t) = \frac{-t}{s} [K_1(st)u_0(st) + K_0(st)u_1(st)] \quad (B-26)$$

$$Q_2(s, t) = \frac{t}{s^2} [3K_2(st)u_1(st) + K_1(st)u_2(st)] \quad (B-27)$$

$$Q_3(s, t) = \frac{t}{s} [I_0(st)u_1(st) - I_1(st)u_0(st)] \quad (B-28)$$

$$Q_4(s, t) = \frac{-t}{s^2} [3I_2(st)u_1(st) - I_1(st)u_2(st)] \quad (B-29)$$

n=2

$$Q_1(s, t) = \frac{-2}{s^2} K_2(st) - \frac{t}{s} [1 - \frac{4}{(st)^2}] K_1(st) \quad (B-30)$$

$$Q_2(s, t) = \frac{4t}{s^2} [1 - \frac{4}{(st)^2}] K_3(st) + \frac{t}{s^2} [st - \frac{8}{st} + \frac{64}{(st)^3}] K_2(st) \quad (B-31)$$

$$Q_3(s, t) = -\frac{2}{s^2} I_2(st) + \frac{t}{s} [1 - \frac{4}{(st)^2}] I_1(st) \quad (B-32)$$

$$Q_4(s, t) = \frac{-4t}{s^2} [1 - \frac{4}{(st)^2}] I_3(st) + \frac{t}{s^2} [st - \frac{8}{st} + \frac{64}{(st)^3}] I_2(st) \quad (B-33)$$

n=3

$$Q_1(s, t) = \frac{t}{s} \{K_3(st)[3u_0(st) - \frac{6}{st} u_1(st)] + K_2(st)[3u_1(st) - \frac{4}{st} u_2(st)]\} \quad (B-34)$$

$$Q_2(s, t) = \frac{t}{s^2} \{K_4(st)[\frac{20}{st} u_2(st) - 15 u_1(st)] + K_3(st)[st - 15 u_0(st) + \frac{120}{st} u_1(st) - \frac{120}{(st)^2} u_2(st)]\} \quad (B-35)$$

$$Q_3(s, t) = \frac{t}{s} \{I_3(st)[3 u_0(st) - \frac{6}{st} u_1(st)] - I_2(st)[3u_1(st) - \frac{4}{st} u_2(st)]\} \quad (B-36)$$

$$Q_4(s, t) = \frac{-t}{s^2} \{I_4(st)[\frac{20}{st} u_2(st) - 15u_1(st)] + I_3(st)[-st + 15u_0(st) - \frac{120}{st} u_1(st) + \frac{120}{(st)^2} u_2(st)]\} \quad (B-37)$$

n=4

$$Q_1(s,t) = \frac{4t}{s} \left[-\frac{1}{st} + \frac{8}{(st)^3} \right] K_4(st) - \frac{t}{s} \left[1 - \frac{16}{(st)^2} \right] + \frac{192}{(st)^4} K_3(st) \quad (B-38)$$

$$Q_2(s,t) = \frac{6t}{s^2} \left[1 - \frac{16}{(st)^2} + \frac{192}{(st)^4} \right] K_5(st) + \frac{t}{s^2} \left[st - \frac{24}{st} \right] + \frac{576}{(st)^3} - \frac{9216}{(st)^5} K_4(st) \quad (B-39)$$

$$Q_3(s,t) = \frac{4t}{s} \left[-\frac{1}{st} + \frac{8}{(st)^3} \right] I_4(st) + \frac{t}{s} \left[1 - \frac{16}{(st)^2} \right] + \frac{192}{(st)^4} I_3(st) \quad (B-40)$$

$$Q_4(s,t) = \frac{-6t}{s^2} \left[1 - \frac{16}{(st)^2} + \frac{192}{(st)^4} \right] I_5(st) + \frac{t}{s^2} \left[st - \frac{24}{st} + \frac{576}{(st)^3} - \frac{9216}{(st)^5} \right] I_4(st) \quad (B-41)$$

Appendix C - Some Properties of Lommel Functions.

A brief summary of certain properties associated with Lommel's functions are included. These functions occur quite frequently in this investigation and are generally associated with indefinite integrals of Bessel functions. For more complete information see [14], [15] and [16].

Lommel's functions were first encountered in this investigation when it became necessary to evaluate indefinite integrals of the following type [14];

$$\int z^\mu J_\nu(z) dz = (\mu+\nu-1)z J_\nu(z) S_{\mu-1, \nu-1}(z) - z J_{\nu-1}(z) S_{\mu, \nu}(z) \quad (C-1)$$

where $S_{\mu, \nu}(z)$ is known as Lommel's function.

When either of the numbers $\mu \pm \nu$ is an odd positive integer $S_{\mu, \nu}(z)$ can be represented by the following series which terminates [15].

$$S_{\mu, \nu}(z) = z^{\mu-1} \left[1 - \frac{(\mu-1)^2 - \nu^2}{z^2} + \frac{[(\mu-1)^2 - \nu^2][(\mu-3)^2 - \nu^2]}{z^4} - \dots \right] \quad (C-2)$$

When $\mu = \nu$ Lommel's function is given by [14],

$$S_{\nu, \nu}(z) = \pi^{1/2} 2^{\nu-1} \Gamma\left(\frac{1}{2} + \nu\right) [H_\nu(z) - Y_\nu(z)], \quad (C-3)$$

where $H_\nu(z)$ is the Struve function and $Y_\nu(z)$ is the Bessel function of the second kind.

Also from [14]

$$\Gamma\left(\frac{1}{2} + \nu\right)[H_\nu(z) - Y_\nu(z)] = 2\pi^{-1/2}\left(\frac{1}{2}z\right)^\nu \int_0^\infty (1+t^2)^{\nu-1/2} e^{-zt} dt$$

Re $z > 0$. (C-4)

Thus,

$$S_{\nu,\nu}(z) = 2^\nu \left(\frac{1}{2}z\right)^\nu \int_0^\infty (1+t^2)^{\nu-1/2} e^{-zt} dt \quad \text{Re } z > 0 . \quad (C-5)$$

Two useful recursion relationships are given by

$$\left(\frac{2\nu}{z}\right)S_{\mu,\nu}(z) = (\mu+\nu-1)S_{\mu-1,\nu-1}(z) - (\mu-\nu-1)S_{\mu-1,\nu+1}(z) \quad (C-6)$$

$$S_{\mu+2,\nu}(z) = z^{\mu+1} - [(\mu+1)^2 - \nu^2]S_{\mu,\nu}(z) . \quad (C-7)$$

Using the relationships described above Lommel's functions of real argument which are encountered in $L_1(t,r)$ can be determined from the following expressions for $n=0, \dots, 5$.

$$n = 0 \quad S_{1,0}(z) = 1 \quad (C-8)$$

$$n = 1 \quad \begin{cases} S_{0,0}(z) = \int_0^\infty (1+t^2)^{-1/2} e^{-zt} dt & (C-9) \\ S_{1,1}(z) = z \int_0^\infty (1+t^2)^{1/2} e^{-zt} dt & (C-10) \end{cases}$$

$$n = 2 \quad \begin{cases} S_{0,1}(z) = z^{-1} & (C-11) \\ S_{1,2}(z) = 1 + 4z^{-2} & (C-12) \end{cases}$$

$$n=3 \quad \begin{cases} S_{0,2}(z) = 2z^{-1} S_{1,1}(z) - S_{0,0}(z) & (C-13) \\ S_{1,3}(z) = 4 + (24z^{-2}-3)S_{1,1}(z) - 12z^{-1}S_{0,0}(z) & (C-14) \end{cases}$$

$$n=4 \quad \begin{cases} S_{0,3}(z) = z^{-1} + 8z^{-3} & (C-15) \\ S_{1,4}(z) = 1 + 16z^{-2} + 192z^{-4} & (C-16) \end{cases}$$

$$n=5 \quad \begin{cases} S_{0,4}(z) = 8z^{-1} + (48z^{-3} - 8z^{-1})S_{1,1}(z) + (1 - 24z^{-2})S_{0,0}(z) & (C-17) \end{cases}$$

$$S_{1,5}(z) = -4 + 320z^{-2} + (1920z^{-4} - 360z^{-2} + 5)S_{1,1}(z) + (60z^{-1} - 960z^{-3})S_{0,0}(z) \quad (C-18)$$

Lommel's functions of imaginary argument are encountered in the Fredholm Kernel $L_2(t,r)$ through the terms $Q_k(s,t)$ (see (68) and appendix B). For n an even positive integer Q_k can be calculated in a straight forward manner since in this case the necessary Lommel's functions satisfy the property that $\mu \pm \nu$ is an odd positive integer. Thus, (C-2) may be used to determine the finite series. The resulting expressions for Q_k are always real.

For odd values of n , determination of Lommel's function for imaginary argument is facilitated by equation (C-3) in conjunction with the following expressions:

$$L_\nu(z) = -i e^{-i\pi/2 \nu} H_\nu(z e^{i\pi/2}) \quad (C-19)$$

$$\Gamma(\frac{1}{2} + \nu)[I_\nu(z) - L_\nu(z)] = 2\pi^{-1/2} (\frac{1}{2}z)^\nu \int_0^1 e^{-zt} (1-t^2)^{\nu-1/2} dt \quad (C-20)$$

$$Y_\nu(z e^{i\pi/2}) = i e^{i\pi/2} I_\nu(z) - \frac{2}{\pi} e^{-i\nu\pi/2} K_\nu(z), \quad (C-21)$$

where $L_\nu(z)$ is known as the modified Struve function.

After simple substitution $S_{\nu,\nu}(iz)$ may be expressed as

$$S_{\nu,\nu}(iz) = \pi^{1/2} 2^{\nu-1} \Gamma(\frac{1}{2} + \nu) i e^{i\pi/2 \nu} \left[-\frac{2\pi^{-1/2}}{\Gamma(1/2+\nu)} (\frac{1}{2}z)^\nu * \right. \\ \left. * \int_0^1 e^{-zt} (1-t^2)^{\nu-1/2} dt - \frac{2}{\pi} i e^{-i\pi\nu} K_\nu(z) \right], \quad (C-22)$$

which is in a form convenient for numerical computation.

Defining the following integrals

$$u_0(z) = \int_0^1 e^{-zt} (1-t^2)^{-1/2} dt \quad (C-23)$$

$$u_1(z) = z \int_0^1 e^{-zt} (1-t^2)^{1/2} dt \quad (C-24)$$

$$u_2(z) = z^2 \int_0^1 e^{-zt} (1-t^2)^{3/2} dt, \quad (C-25)$$

Lommel's functions for odd values of n with imaginary arguments can be expressed in terms of these integrals. For example,

$$S_{0,0}(iz) = -i u_0(z) + K_0(z) \quad (C-26)$$

$$S_{1,1}(iz) = u_1(z) - i K_1(z) \quad (C-27)$$

Again, as in the case of even n the resulting expressions for $Q_k(s,t)$ are real.

Numerical evaluation of the Fredholm kernel $L_1(t,r)$ involves the computation of Lommel's function for both small and large argument. When $\mu \pm \nu$ is odd, no difficulties are encountered, since Lommel's function can be expressed by the truncated series given by (C-2). It is when $\mu = \nu$ that certain difficulties arise. In this case it was found that for small values of z the representation of Lommel's function given by (C-3) was the most convenient, with the necessary Struve function for small argument given by the series [19]:

$$H_0(z) = \frac{2}{\pi} \left[z - \frac{z^3}{1^2 \cdot 3^2} + \frac{z^5}{1^2 \cdot 3^2 \cdot 5^2} - \dots \right] \quad (C-28)$$

$$H_1(z) = \frac{2}{\pi} \left[\frac{z^2}{1^2 \cdot 3} - \frac{z^4}{1^2 \cdot 3^2 \cdot 5} + \frac{z^6}{1^2 \cdot 3^2 \cdot 5^2 \cdot 7} - \dots \right] \quad (C-29)$$

When Lommel's function for intermediate and large argument is to be determined, the integral representations (C-9) and (C-10) were found to be most useful. These integrals were evaluated numerically using Gauss-Legendre quadrature.

Numerical evaluation of the Fredholm kernel $L_2(t,r)$ involves computation of Lommel's function for imaginary argument (C-26)-

(C-27). To perform the necessary calculations, the integrals (C-23)-(C-25) must be evaluated. For small values of z this can easily be accomplished by expanding the integrand in a series and the result is,

$$u_0(z) = \frac{\pi}{2} - z + \frac{\pi}{8} z^2 - \frac{z^3}{9} + \frac{\pi}{128} z^4 - \frac{z^5}{225} + \frac{\pi}{4608} z^6 \\ - \frac{z^7}{11025} + \frac{\pi}{294912} z^8 - \frac{z^9}{893025} \quad (\text{C-30})$$

$$u_1(z) = \frac{\pi}{4} z - \frac{z^2}{3} + \frac{\pi}{32} z^3 - \frac{z^4}{45} + \frac{\pi}{768} z^5 - \frac{z^6}{1575} \\ + \frac{\pi}{36864} z^7 - \frac{z^8}{99225} \quad (\text{C-31})$$

$$u_2(z) = \frac{3\pi}{16} z^2 - \frac{z^3}{5} + \frac{\pi}{64} z^4 - \frac{z^5}{105} + \frac{\pi}{2048} z^6 \\ - \frac{z^7}{4725} + \frac{\pi}{122880} z^8 - \frac{z^9}{363825} \quad (\text{C-32})$$

In actual calculations expression (C-30) was used for $z < 2$ and expressions (C-31), (C-32) were used for $z < 1$. For all other values of z , u_0 , u_1 and u_2 were calculated by numerical quadrature using the integral expressions given in (C-23)-(C-25). Thirty Gauss-Legendre quadrature points were found to give sufficient accuracy.

Appendix D

With the aid of asymptotic expressions given by Watson [15] and Magnus [14] the asymptotic behavior of the integrand in (62) can be expressed and evaluated in closed form. Important asymptotic expansions are given by:

$$J_n(z) \sim \left(\frac{1}{2} \pi z\right)^{-1/2} \left\{ \cos\left(z - \frac{n\pi}{2} - \frac{\pi}{4}\right) \left[1 - \frac{(4n^2-1)(4n^2-a)}{128} z^{-2} + \dots \right] \right. \\ \left. - \sin\left(z - \frac{n\pi}{2} - \frac{\pi}{4}\right) \left[\frac{4n^2-1}{8} z^{-1} - \frac{(4n^2-1)(4n^2-a)(4n^2-25)}{3072} z^{-3} \dots \right] \right\} \quad (D-1)$$

$$S_{0,n-1}(z) \sim z^{-1} - (-n^2+2n)z^{-3} + \dots, \quad n=0,1,2,\dots, \quad (D-2)$$

$$S_{1,n}(z) \sim 1 + \frac{n^2}{2} z^{-2} - \dots, \quad n=0,1,2,\dots, \quad (D-3)$$

$$S(x) \sim \frac{1}{2} - \frac{1}{\sqrt{2\pi}} \frac{1}{x} \cos x^2 + \frac{1}{2} \frac{1}{\sqrt{2\pi}} \frac{1}{x^3} \sin x^2 + \frac{3}{4} \frac{1}{\sqrt{2\pi}} \frac{1}{x^5} \cos x^2 \quad (D-4)$$

$$C(x) \sim \frac{1}{2} + \frac{1}{\sqrt{2\pi}} \frac{1}{x} \sin x^2 + \frac{1}{2} \frac{1}{\sqrt{2\pi}} \frac{1}{x^3} \cos x^2 - \frac{3}{4} \frac{1}{\sqrt{2\pi}} \frac{1}{x^5} \sin x^2 \quad (D-5)$$

After substitution of the above asymptotic expressions in (62) and integrating, the portion of the integral which is evaluated in closed form becomes

$$\begin{aligned}
A_1 = & \frac{n}{\pi} \left(\frac{t}{r}\right)^{\frac{1}{2}} \{-\text{Ci}(A(t-r)) + (-1)^n [\frac{\pi}{2} - \text{Si}(A(t+r))]\} \\
& + \left[\frac{4n^2-1}{8} \frac{1}{tr} - \frac{(4n^2-1)(4n^2-9)}{128} \left(\frac{1}{t^2} + \frac{1}{r^2}\right) \right] * \\
& * \left[\frac{\cos A(t-r)}{2A^2} + (-1)^n \frac{\sin A(t+r)}{2A^2} - \frac{(t-r)}{2} \frac{\sin A(t-r)}{A} \right. \\
& + (-1)^n \frac{(t+r)}{2} \frac{\cos A(t+r)}{A} + \frac{(t-r)^2}{2} \text{Ci}(A(t-r)) \\
& - (-1)^n \frac{(t+r)^2}{2} [\frac{\pi}{2} - \text{Si}(A(t+r))] \left. \right] + \frac{4n^2-1}{8} \left(\frac{1}{r} - \frac{1}{t}\right) * \\
& * \left[\frac{\sin A(t-r)}{A} + (-1)^n \frac{\cos A(t+r)}{A} - (t-r)\text{Ci}(A(t-r)) \right. \\
& \left. - (-1)^n (t+r) [\frac{\pi}{2} - \text{Si}(A(t+r))] \right] \quad (D-6)
\end{aligned}$$

$$\begin{aligned}
A_2 = & \frac{1}{\pi} \left(\frac{t}{r}\right)^{\frac{1}{2}} \left\{ \left[-\frac{(4n^2-1)(4n^2-9)}{128} r^{-2} \right. \right. \\
& - \left. \frac{(4(n-1)^2-1)(4(n-1)^2-9)-64n^2}{128} t^{-2} \right] \left[\frac{\sin A(t-r)}{A} \right. \\
& - (t-r)\text{Ci}(A(t-r)) - (-1)^n \frac{\cos A(t+r)}{A} + (-1)^n (t+r) \left(\frac{\pi}{2} \right. \\
& \left. - \text{Si}(A(t+r))) \right] + \frac{4(n-1)^2-1}{8} t^{-1} [-\text{Ci}(A(t-r)) \\
& + (-1)^n \left(\frac{\pi}{2} - \text{Si}(A(t+r))\right)] + \frac{4n^2-1}{8} r^{-1} [\text{Ci}(A(t-r)) \\
& + (-1)^n \left(\frac{\pi}{2} - \text{Si}(A(t+r))\right)] + \frac{(4n^2-1)(4(n-1)^2-1)}{64} (rt)^{-1} * \\
& * \left[\frac{\sin A(t-r)}{A} - (t-r)\text{Ci}(A(t-r)) + (-1)^n \frac{\cos A(t+r)}{A} \right. \\
& \left. - (-1)^n (t+r) \left(\frac{\pi}{2} - \text{Si}(A(t+r))\right) \right] \quad (D-7)
\end{aligned}$$

$$\begin{aligned}
A_3 = & -\frac{1-(-1)^n}{2r} [C(\sqrt{Ar}) - S(\sqrt{Ar})] - \frac{1}{2\pi} (rt)^{-\frac{1}{2}} * \\
& * [(-1)^n [\frac{\pi}{2} - Si(A(t+r))] - Ci(A(t-r))] - \frac{1}{4\pi} r^{-\frac{1}{2}} t^{-\frac{3}{2}} * \\
& * [-\frac{\sin A(t-r)}{A} + (t-r)Ci(A(t-r)) + (-1)^n \frac{\cos A(t+r)}{A} \\
& - (-1)^n (t+r)(\frac{\pi}{2} - Si(A(t+r)))] , \quad n = 0,1,2,\dots, \quad (D-8)
\end{aligned}$$

where Ci and Si are the standard notations for cosine and sine integrals defined [16]

$$Ci(x) = \int_{\infty}^x \frac{\cos v}{v} dv \quad (D-9)$$

$$Si(x) = \int_0^x \frac{\sin v}{v} dv \quad (D-10)$$

Appendix E - Transient Thermal Stress Problem

The transient thermal stress problem for a cracked hollow cylinder is an interesting example where the axial stress is nonuniform. Consider the following problem: A fluid or vapor at temperature T_∞ suddenly fills an insulated pipe of inner and outer radii a and b , respectively (see figure 1). The initial temperature of the pipe is T_0 . Find the unsteady temperature and thermal stress.

The unsteady temperature field

$$\theta(r,t) = T(r,t) - T_0 \quad (E-1)$$

in the idealized, uncoupled, linear model is determined from

$$\nabla^2 \theta(r,t) = \frac{1}{D} \frac{\partial \theta(r,t)}{\partial t} \quad , \quad (E-2)$$

where D , the thermal diffusivity, is expressed as

$$D = \frac{\kappa}{\rho c} \quad , \quad (E-3)$$

with κ = coefficient of thermal conductivity, ρ = density and c = specific heat. The initial temperature condition and idealized thermal boundary conditions may be expressed by

$$\theta(r,0) = 0 \quad (E-4)$$

$$\theta(a,t) = \theta_\infty = T_\infty - T_0 \quad (E-5)$$

$$\frac{\partial \theta(b,t)}{\partial r} = 0 \quad (E-6)$$

The thermal stresses σ_{zz} in a hollow cylinder where the ends are traction free is given by

$$\sigma_{zz}(r,t) = \left(\frac{E\alpha}{1-\nu}\right) \left[\frac{2}{b^2-a^2} \int_a^b \theta(r,t)r \, dr - \theta(r,t) \right] \quad (E-7)$$

where E = modulus of elasticity, ν = Poisson's ratio and α = coefficient of thermal expansion.

Using Laplace transforms and asymptotic expansions of the modified Bessel functions, solutions were obtained which are valid for small time. The temperature for small time is given by

$$\begin{aligned} \frac{\theta(r,t)}{\theta_\infty} = & \sum_{n=1}^4 E_n \operatorname{erfc} \left[\frac{x_n}{2(Dt)^{1/2}} \right] + F_n \left[2 \left(\frac{Dt}{\pi} \right)^{1/2} e^{-x_n^2/4Dt} \right. \\ & \left. - x_n \operatorname{erfc} \left[\frac{x_n}{2(Dt)^{1/2}} \right] \right] + G_n D \left[\left(t + \frac{x_n^2}{2D} \right) \operatorname{erfc} \left[\frac{x_n}{2(Dt)^{1/2}} \right] \right. \\ & \left. - x_n \left(\frac{t}{\pi D} \right)^{1/2} e^{-x_n^2/4Dt} \right] \quad (E-8) \end{aligned}$$

$$x_1 = r-a$$

$$x_2 = 2b-r-a$$

$$x_3 = 2b+r-3a$$

$$x_4 = 4b-r-3a$$

(E-9)-(E-12)

$$E_1 = E_2 = \frac{A_1}{B_1}$$

(E-13)-(E-16)

$$E_3 = E_4 = -\frac{A_1}{B_1}$$

$$F_1 = \frac{A_2 B_1 - A_1 B_2}{B_1^2}$$

(E-17)-(E-20)

$$F_2 = -\frac{A_1 B_2 + A_2 B_1}{B_1^2}$$

$$F_3 = \frac{3A_1 B_2 - A_2 B_1}{B_1^2}$$

$$F_4 = \frac{3A_1 B_2 + A_2 B_1}{B_1^2}$$

$$G_1 = \frac{B_1 A_3 - A_1 B_3 - A_2 B_2}{B_1^2}$$

$$G_2 = \frac{B_1 A_3 - A_1 B_3 + A_2 B_2}{B_1^2}$$

(E-21)-(E-24)

$$G_3 = \frac{-B_1 A_3 + A_1 B_3 + 3A_2 B_2}{B_1^2} - \frac{2A_1 B_2^2}{B_1^3}$$

$$G_4 = \frac{-B_1 A_3 + A_1 B_3 - 3A_2 B_2}{B_1^2} - \frac{2A_1 B_2^2}{B_1^3}$$

$$A_1 = (rb)^{-\frac{1}{2}}$$

$$A_2 = -\frac{(3r+b)}{8(br)^{\frac{3}{2}}} \quad (E-24)-(E-27)$$

$$A_3 = \frac{3(5r+3b)(b-r)}{128(br)^{\frac{5}{2}}}$$

$$B_1 = (ab)^{-\frac{1}{2}}$$

$$B_2 = -\frac{(3a+b)}{8(ab)^{\frac{3}{2}}} \quad (E-28)-(E-30)$$

$$B_3 = \frac{3(5a+3b)(b-a)}{128(ab)^{\frac{5}{2}}}$$

Using the same small time approximation to obtain the thermal stress, from (E-7) we obtain

$$\begin{aligned} \left(\frac{1-\nu}{E\alpha}\right) \frac{\sigma_{zz}(r,t)}{\theta_{\infty}} &= \frac{-2a}{b^2-a^2} \{-2\sqrt{D} \left(\frac{t}{\pi}\right)^{\frac{1}{2}} + D H_1 t \\ &+ \frac{4}{3} H_2 \frac{(Dt)^{\frac{3}{2}}}{\pi^{\frac{1}{2}}} + 2\lambda_1(x_5) + H_7\lambda_2(x_5) + \lambda_1(x_6) \\ &+ H_9\lambda_2(x_6)\} - \frac{\theta(r,t)}{\theta_{\infty}} \end{aligned} \quad (E-31)$$

where

$$x_5 = 2(b-a)$$

$$x_6 = 4(b-a)$$

(E-32)-(E-33)

$$\lambda_1(x) = 2\left(\frac{Dt}{\pi}\right)^{\frac{1}{2}} e^{-x^2/4Dt} - x \operatorname{erfc}\left[\frac{x}{2(Dt)^{\frac{1}{2}}}\right] \quad (\text{E-34})$$

$$\lambda_2(x) = D\left(t + \frac{x^2}{2D}\right) \operatorname{erfc}\left[\frac{x}{2(Dt)^{\frac{1}{2}}}\right] - Dx\left(\frac{t}{\pi D}\right)^{\frac{1}{2}} e^{-x^2/4Dt} \quad (\text{E-35})$$

From equations (E-8) and (E-31) numerical values for the temperature field and thermal stress are easily calculated. Once the thermal stress is known it may be used as an input load function in the integral equation (92). In this manner, stress intensity factors and crack opening displacements are determined at various nondimensional time intervals.

It was found that for small values of the quantity $F_0 = \frac{Dt}{b^2}$, equation (E-31) gave very accurate results. For larger values of F_0 more accurate stress results were obtained by evaluating the integral in (E-7) numerically. This integration was done using 60 Gauss-Legendre quadrature points.

APPENDIX E

STRESS INTENSITY FACTORS IN A HOLLOW CYLINDER CONTAINING A RADIAL CRACK

1. Introduction

In this paper we reconsider the plane problem of a hollow cylinder containing an arbitrarily oriented radial crack and subjected to arbitrary normal tractions on the crack surfaces. Aside from its direct applications to plane problems such as cracked rings and rotating disks, the problem has potentially important applications to pressure vessels and piping containing a relatively long part-through crack in a meridional plane. In this latter group of three dimensional problems the plane strain solution provides an upper bound for the stress intensity factor in the mid-region of the longitudinal part-through crack in the cylinder wall. Because of the importance of the crack geometry, the problem has been studied rather extensively (see, for example, [1-7]). After Bueckner's early work in which the technique of complex potentials was used [1], most of the subsequent analytical studies were based on the mapping technique originally developed by Bowie [2-4]. In [1] the problem of a rotating disk having a radial edge crack on its inner boundary is considered. The same crack geometry under uniform tensile tractions applied to the outer boundary of the ring is studied in [2]. The problem of multiple cracks located on the inner or outer boundary of the ring is considered in [3]. The problem of a curved beam or a ring segment containing a radial crack is studied in [4]. In [5] the problem of a hollow cylinder containing an external edge crack is considered for various loading conditions where a numerical technique similar to finite difference approximations is used for the solution. In [6] the ring problem with an inner edge crack is solved by using the method of weight functions. However, it may be observed that the existing solutions in one form or another are all restricted with regard to loading and/or geometry.

In the plane strain or the generalized plane stress problem considered in this Appendix it is assumed that the external loads are symmetric with respect to the plane of the crack and the basic ring problem without

the crack has been solved. Thus the main problem of interest is the Mode I crack problem in which the self-equilibrating arbitrary normal crack surface tractions are the only external loads (Figure 1a).

It should be pointed out that in the special cases of solid disk (Figure 1a, $a=0$, $b<\infty$) and the infinite plane with a circular hole ($0<a<\infty$, $b=\infty$), the problem may readily be formulated in terms of a singular integral equation by using the basic dislocation solutions given in [8] as the Green's functions.

2. Formulation of the Problem

The geometry and loading for the problem under consideration is shown in Figure 1a. In crack problems involving finite geometries, almost invariably the basic technique to formulate the problem is to express the solution as the sum of certain number of suitable solutions satisfying the differential equations of the problem in such a way that at least one of the solutions contains the main features of the general crack problem and the total solution contains sufficient number of arbitrary functions or sets of arbitrary constants to account for all boundary conditions. In this problem the solution is expressed as the sum of a crack or dislocation solution for an infinite plane and the general solution for a circular ring. In order to facilitate the application of the boundary conditions, the dislocation solution is expressed in polar rather than in rectangular coordinates. Let, then, the stress state in the cracked ring problem be of the following form:

$$\sigma_{ij}(r,\theta) = \sigma_{1ij}(r,\theta) + \sigma_{2ij}(r,\theta), \quad (i,j = r,\theta) \quad (1)$$

where σ_{1ij} and σ_{2ij} , ($i,j = r,\theta$) respectively refer to an infinite plane containing an edge dislocation or a crack along $\theta=0$ line and to a concentric circular cylinder.

a) *The infinite plane solution.*

Consider an infinite plane with an edge dislocation having a Burger's vector $b_y = -f$ located at the point $r=t$, $\theta=0$ (Figure 1b). The plane

elasticity problem may be solved by assuming that

$$\sigma_{1r\theta} = 0, \quad 0 \leq r < \infty, \quad \theta = 0, \quad \theta = \pi \quad (2)$$

$$\frac{\partial}{\partial r} [u_{1\theta}(r, +0) - u_{1\theta}(r, -0)] = f\delta(r-t), \quad 0 \leq r < \infty. \quad (3)$$

Referring to [8] the Airy stress function of the problem may be expressed as (Figure 1b)

$$\begin{aligned} \psi_1(r, \theta) &= -\frac{2\mu}{\pi(1+\kappa)} f r_1 \log r_1 \cos \theta_1 \\ &= -\frac{\mu}{\pi(1+\kappa)} f (r \cos \theta - t) \log (r^2 + t^2 - 2rt \cos \theta), \end{aligned} \quad (4)$$

where μ is the shear modulus, $\kappa=3-4\nu$ for plane strain and $\kappa=(3-\nu)/(1+\nu)$ for the generalized plane stress, ν being the Poisson's ratio. From (4) the stresses are obtained to be

$$\begin{aligned} \sigma_{1rr}(r, \theta) &= \frac{1}{r} \frac{\partial \psi_1}{\partial r} + \frac{1}{r^2} \frac{\partial^2 \psi_1}{\partial \theta^2} \\ &= -\frac{2\mu f}{\pi(\kappa+1)} \left[\frac{r \cos \theta - t - 2t \sin^2 \theta}{r^2 + t^2 - 2rt \cos \theta} \right. \\ &\quad \left. - \frac{2t^2 \sin^2 \theta (r \cos \theta - t)}{(r^2 + t^2 - 2rt \cos \theta)^2} \right], \end{aligned} \quad (5)$$

$$\begin{aligned} \sigma_{1r\theta}(r, \theta) &= -\frac{\partial}{\partial r} \left(\frac{1}{r} \frac{\partial \psi_1}{\partial \theta} \right) \\ &= \frac{2\mu f}{\pi(\kappa+1)} \left[\frac{\sin \theta (2t \cos \theta - r)}{r^2 + t^2 - 2rt \cos \theta} \right. \\ &\quad \left. - \frac{2t \sin \theta (r \cos \theta - t)(r - t \cos \theta)}{(r^2 + t^2 - 2rt \cos \theta)^2} \right], \end{aligned} \quad (6)$$

$$\begin{aligned} \sigma_{1\theta\theta}(r, \theta) &= \frac{\partial^2 \psi_1}{\partial r^2} \\ &= -\frac{2\mu f}{\pi(\kappa+1)} \left[\frac{2 \cos \theta (r - t \cos \theta) + r \cos \theta - t}{r^2 + t^2 - 2rt \cos \theta} \right. \\ &\quad \left. - \frac{2(r \cos \theta - t)(r - t \cos \theta)^2}{(r^2 + t^2 - 2rt \cos \theta)^2} \right]. \end{aligned} \quad (7)$$

With an eye on combining the infinite plane solution with the ring solution, we now express the normal and shear components of the stress state along the circles $r=a$ and $r=b$ in the plane in terms of the following Fourier series:

$$\sigma_{1r\theta}(a,\theta) = \frac{\mu f}{\pi(1+\kappa)} \sum_1^{\infty} A_n(t) \sin n\theta, \quad (8)$$

$$\sigma_{1rr}(a,\theta) = -\frac{\mu f}{\pi(1+\kappa)} \sum_0^{\infty} B_n(t) \cos n\theta, \quad (9)$$

$$\sigma_{1r\theta}(b,\theta) = \frac{\mu f}{\pi(1+\kappa)} \sum_1^{\infty} C_n(t) \sin n\theta, \quad (10)$$

$$\sigma_{1rr}(b,\theta) = -\frac{\mu f}{\pi(1+\kappa)} \sum_0^{\infty} D_n(t) \cos n\theta, \quad (11)$$

where the Fourier coefficients are given by

$$A_n(t) = \frac{2}{\pi} \int_0^{\pi} \left[\frac{2 \sin\theta(2t \cos\theta - a)}{a^2 + t^2 - 2at \cos\theta} - \frac{4t \sin\theta(a \cos\theta - t)(a - t \cos\theta)}{(a^2 + t^2 - 2at \cos\theta)^2} \right] \sin n\theta \, d\theta, \quad (12)$$

$$B_0(t) = \left(-\frac{\pi(1+\kappa)}{\mu f}\right) \frac{1}{\pi} \int_0^{\pi} \sigma_{1rr}(a,\theta) \, d\theta,$$

$$B_n(t) = \left(-\frac{\pi(1+\kappa)}{\mu f}\right) \frac{2}{\pi} \int_0^{\pi} \sigma_{1rr}(a,\theta) \cos n\theta \, d\theta; \quad (13a,b)$$

$$C_n(t) = \left(\frac{\pi(1+\kappa)}{\mu f}\right) \frac{2}{\pi} \int_0^{\pi} \sigma_{1r\theta}(b,\theta) \sin n\theta \, d\theta, \quad (14)$$

$$D_0(t) = \left(1 \frac{\pi(1+\kappa)}{\mu f}\right) \frac{1}{\pi} \int_0^{\pi} \sigma_{1rr}(b,\theta) \, d\theta,$$

$$D_n(t) = \left(-\frac{\pi(1+\kappa)}{\mu f}\right) \frac{2}{\pi} \int_0^{\pi} \sigma_{1rr}(b,\theta) \cos n\theta \, d\theta \quad (15a,b)$$

After some manipulations and combining some of the terms, the integrals which appear in (12-15) can be evaluated in closed form, giving

$$A_n(t) = \frac{1}{a} \left\{ \frac{a^2}{t^2-a^2} \left[n \left(\frac{a}{t}\right)^{n+1} - (n-4) \left(\frac{a}{t}\right)^{n-3} \right] + 2n \left(\frac{a}{t}\right)^{n+1} - \frac{2a^4}{(t^2-a^2)^2} \left[\left(\frac{a}{t}\right)^{n-5} - \left(\frac{a}{t}\right)^{n-1} \right] \right\}, n \geq 2, \quad (16)$$

$$B_0(t) = -\frac{2}{t},$$

$$B_n(t) = \frac{1}{a} \left\{ \frac{4a^4}{(t^2-a^2)^2} \left[\left(\frac{a}{t}\right)^{n-3} - \frac{1}{2} \left(\frac{a}{t}\right)^{n-1} - \frac{1}{2} \left(\frac{a}{t}\right)^{|n-2|-3} \right] + 2 \left(\frac{a}{t}\right)^{n+1} \frac{t^2+a^2}{t^2-a^2} - \frac{a^2}{t^2-a^2} \left[n \left(\frac{a}{t}\right)^{n+1} - (2n-8) \left(\frac{a}{t}\right)^{n-1} + (|n-2|-2) \left(\frac{a}{t}\right)^{|n-2|-1} \right] \right\}, n \geq 1, \quad (17a,b)$$

$$C_n(t) = \frac{1}{b} \left\{ \frac{2b^4}{(b^2-t^2)^2} \left[\left(\frac{t}{b}\right)^{n+1} - \left(\frac{t}{b}\right)^{n+5} \right] - 2n \left(\frac{t}{b}\right)^{n-1} + \frac{b^2}{b^2-t^2} \left[n \left(\frac{t}{b}\right)^{n-1} - (n+4) \left(\frac{t}{b}\right)^{n+3} \right] \right\}, n \geq 2, \quad (18)$$

$$D_0(t) = -\frac{2t}{b^2},$$

$$D_n(t) = \frac{1}{b} \left\{ -\frac{2b^2}{b^2-t^2} \left[(n+3) \left(\frac{t}{b}\right)^{n+1} - \frac{n+4}{2} \left(\frac{t}{b}\right)^{n+3} - \frac{1}{2} (|n-2|+2) \left(\frac{t}{b}\right)^{|n-2|+1} \right] + \frac{2b^2}{b^2-t^2} \left(\frac{t}{b}\right)^{n-1} - \frac{4b^4}{(b^2-t^2)^2} \left[\left(\frac{t}{b}\right)^{n+3} - \frac{1}{2} \left(\frac{t}{b}\right)^{n+5} - \frac{1}{2} \left(\frac{t}{b}\right)^{|n-2|+3} \right] \right\}, n \geq 1, \quad (19a,b)$$

b) *The ring solution.*

In this case assuming a stress function of the form

$$\psi_2(r, \theta) = F(r)e^{\beta\theta} \quad (20)$$

the general elasticity solution in polar coordinates may be obtained as [9]

$$\begin{aligned}
 \psi_2(r, \theta) = & a_0 + b_0 \log r + c_0 r^2 + d_0 r^2 \log r \\
 & + (a'_0 + b'_0 \log r + c'_0 r^2 + d'_0 r^2 \log r) \theta \\
 & + (a_1 r + b_1 r \log r + \frac{c_1}{r} + d_1 r^3) \frac{\sin \theta}{\cos \theta} \\
 & + (a'_1 r + b'_1 r \log r) \theta \frac{\sin \theta}{\cos \theta} \\
 & + \sum_{n=2}^{\infty} (a_n r^n + b_n r^{n+2} + c_n r^{-n} + d_n r^{2-n}) \frac{\sin n \theta}{\cos n \theta} . \quad (21)
 \end{aligned}$$

This is basically the solution given by Michell, except that he omitted some of the repeated roots. From (21) the stresses for an annulus are found to be

$$\begin{aligned}
 \sigma_{2rr} = & \frac{b_0}{r^2} + 2c_0 + \left(-\frac{2c_1}{r^3} + 2d_1 r\right) \frac{\sin \theta}{\cos \theta} \\
 & - \frac{3+\nu}{4\pi r} (R_y \sin \theta + R_x \cos \theta) - \sum_{n=2}^{\infty} [a_n n(n-1)r^{n-2} \\
 & + b_n(n+1)(n-2)r^n + c_n n(n+1)r^{-(n+2)} + d_n(n-1)(n+2)r^{-n}] \frac{\sin n \theta}{\cos n \theta} , \\
 \sigma_{2\theta\theta} = & -\frac{b_0}{r^2} + 2c_0 + \left(\frac{2c_1}{r^3} + 6d_1 r\right) \frac{\sin \theta}{\cos \theta} + \frac{1-\nu}{4\pi r} (R_y \sin \theta + R_x \cos \theta) \\
 & + \sum_{n=2}^{\infty} [a_n n(n-1)r^{n-2} + b_n(n+1)(n+2)r^n \\
 & + c_n n(n+1)r^{-(n+2)} + d_n(n-2)(n-1)r^{-n}] \frac{\sin n \theta}{\cos n \theta} ,
 \end{aligned}$$

$$\begin{aligned}
\sigma_{2r\theta} = & \frac{a_0'}{r^2} + \left(\frac{2c_1}{r^3} - 2d_1 r\right) \begin{matrix} \cos\theta \\ -\sin\theta \end{matrix} - \frac{1-\nu}{4\pi r} (R_y \cos\theta + R_x \sin\theta) \\
& - \sum_{n=2}^{\infty} [a_n n(n-1)r^{n-2} + b_n n(n+1)r^n - c_n n(n+1)r^{-(n+2)} \\
& - d_n n(n-1)r^{-n}] \begin{matrix} \cos n\theta \\ -\sin n\theta \end{matrix}, \tag{22a-c}
\end{aligned}$$

where R_x and R_y are the resultants of the tractions on $r=a$. In the problem under consideration $R_x=0$, $R_y=0$ and the stresses satisfy the following symmetry conditions:

$$\begin{aligned}
\sigma_{2rr}(r, \theta) &= \sigma_{2rr}(r, -\theta), \quad \sigma_{2\theta\theta}(r, \theta) = \sigma_{2\theta\theta}(r, -\theta), \\
\sigma_{2r\theta}(r, \theta) &= -\sigma_{2r\theta}(r, -\theta). \tag{23a-c}
\end{aligned}$$

Thus, from (22) and (23) it follows that

$$\begin{aligned}
\sigma_{2rr} = & \frac{b_0}{r^2} + 2c_0 + \left(-\frac{2c_1}{r^3} + 2d_1 r\right) \cos\theta - \sum_2^{\infty} [a_n n(n-1)r^{n-2} \\
& + b_n(n+1)(n-2)r^n + c_n n(n+1)r^{-n-2} + d_n(n-1)(n+2)r^{-n}] \cos n\theta, \\
\sigma_{2r\theta} = & \left(-\frac{2c_1}{r^3} + 2d_1 r\right) \sin\theta + \sum_2^{\infty} [a_n n(n-1)r^{n-2} \\
& + b_n n(n+1)r^n - c_n n(n+1)r^{-n-2} - d_n n(n-1)r^{-n}] \sin n\theta, \\
\sigma_{2\theta\theta} = & -\frac{b_0}{r^2} + 2c_0 + \left(\frac{2c_1}{r^3} + 6d_1 r\right) \cos\theta + \sum_2^{\infty} [a_n n(n-1)r^{n-2} \\
& + b_n(n+1)(n+2)r^n + c_n n(n+1)r^{-n-2} + d_n(n-2)(n-1)r^{-n}] \cos n\theta. \tag{24a-c}
\end{aligned}$$

c) *Boundary conditions.*

After determining the basic form of the solutions for the infinite plate with a dislocation and for the ring, the stresses in the ring

having a dislocation may be expressed as the sum of the two solutions (see (1), (5-7) and (24)). The combined stress state must then satisfy the following boundary conditions (Figure 1a):

$$\sigma_{1rr}(a,\theta) + \sigma_{2rr}(a,\theta) = 0, \quad 0 \leq \theta \leq \pi,$$

$$\sigma_{1r\theta}(a,\theta) + \sigma_{2r\theta}(a,\theta) = 0, \quad 0 \leq \theta \leq \pi,$$

$$\sigma_{1rr}(b,\theta) + \sigma_{2rr}(b,\theta) = 0, \quad 0 \leq \theta \leq \pi,$$

$$\sigma_{1r\theta}(b,\theta) + \sigma_{2r\theta}(b,\theta) = 0, \quad 0 \leq \theta \leq \pi \quad (25 \text{ a-d})$$

$$\sigma_{1\theta\theta}(r,0) + \sigma_{2\theta\theta}(r,0) = g(r), \quad c < r < d \quad (26)$$

where σ_{1rr} and $\sigma_{1r\theta}$ are given by (8-15) and σ_{2rr} and $\sigma_{2r\theta}$ are given by (24), and $g(r)$ is the crack surface traction. Note that each equation in (25) is a sine or cosine series in which the coefficients of $\sin n\theta$ and $\cos n\theta$, ($n=0,1,\dots$) must vanish. Thus, defining

$$a_n = -\frac{\mu f}{\pi(\kappa+1)} \alpha_n, \quad b_n = -\frac{\mu f}{\pi(\kappa+1)} \beta_n,$$

$$c_n = -\frac{\mu f}{\pi(\kappa+1)} \gamma_n, \quad d_n = -\frac{\mu f}{\pi(\kappa+1)} \delta_n, \quad (n=0,1,\dots), \quad (27 \text{ a-d})$$

we obtain

$$\frac{\beta_0}{a^2} + 2\gamma_0 = -B_0, \quad \frac{\beta_0}{b^2} + 2\gamma_0 = -D_0; \quad (28a,b)$$

$$-\frac{2\gamma_1}{a^3} + 2\delta_1 a = -B_1, \quad -\frac{2\gamma_1}{a^3} + 2\delta_1 b = -D_1; \quad (29a,b)$$

$$-\frac{2\gamma_1}{a^3} + 2\delta_1 a = A_1, \quad -\frac{2\gamma_1}{a^3} + 2\delta_1 b = C_1; \quad (30a,b)$$

$$\begin{aligned}
& \alpha_n n(n-1)a^{n-2} + \beta_n (n+1)(n-2)a^n + \gamma_n n(n+1)a^{-n-2} \\
& \quad + \delta_n (n-1)(n+2)a^{-n} = B_n, \quad (n=2,3,\dots), \\
& \alpha_n n(n-1)a^{n-2} + \beta_n n(n+1)a^n - \gamma_n n(n+1)a^{-n-2} \\
& \quad - \delta_n n(n-1)a^{-n} = A_n, \quad (n=2,3,\dots), \\
& \alpha_n n(n-1)b^{n-2} + \beta_n (n+1)(n-2)b^n + \gamma_n n(n+1)b^{-n-2} \\
& \quad + \delta_n (n-1)(n+2)b^{-n} = D_n, \quad (n=2,3,\dots), \\
& \alpha_n n(n-1)b^{n-2} + \beta_n n(n+1)b^n - \gamma_n n(n+1)b^{-n-2} \\
& \quad - \delta_n n(n-1)b^{-n} = C_n, \quad (n=2,3,\dots), \tag{31a-d}
\end{aligned}$$

where $A_n, B_n, C_n,$ and $D_n, (n=0,1,2,\dots)$ are known functions of t and are given by (16-19). Consequently, the coefficients $a_n, b_n, c_n,$ and d_n calculated from (27-31) will also be functions of t . From (24) it may be observed that the coefficients a_0, a_1, b_1 and d_0 do not appear in the expressions of σ_{2ij} . Therefore, if the series in (24) are truncated at the n th term, there would be $4n$ unknown coefficients to be determined. On the other hand, there are $4n+2$ equations in the corresponding algebraic system given by (28-31). Two of these equations must, therefore, be redundant. This is, in fact, suggested by the pairs of equations (29a, 30a) and (29b, 30b). These equations indicate that if

$$A_1 + B_1 = 0, \quad C_1 + D_1 = 0, \tag{32a,b}$$

then (29) and (30) are identical and by, for example, ignoring (30), the unknown coefficients may be determined uniquely from (28), (29), and (31). Referring to (8) and (9), it may be seen that

$$A_1 + B_1 = \frac{\pi(1+\kappa)}{\mu f} \frac{1}{\pi a} \int_0^{2\pi} [\sigma_{1r\theta}(a,\theta)\sin\theta - \sigma_{1rr}(a,\theta)\cos\theta] a d\theta. \quad (33)$$

Consider now an infinite plane containing an edge dislocation at $x=t$ (see eqs. (2,3)). If we introduce a circular hole $r=a$, $a < t$ into the plane (Fig. 1), then certain tractions σ_{1rr} and $\sigma_{1r\theta}$ must be applied along the boundary of the hole in order to maintain the equilibrium of the plane. It is clear that the integral in (33) is nothing but the x -component of the resultant of these tractions. Since the external force system due to the dislocation or the crack (which results from (2) and (3)) is self-equilibrating, this resultant must be zero, proving the validity of (32a). Equation (32b) follows from similar arguments for a disk $r \leq b$ containing a dislocation at $x=t < b$. It is because of the relations (32) that in (16-19) the expressions for A_1 and C_1 are not included.

After expressing the coefficients a_n, \dots, d_n in terms of f , the remaining boundary condition (26) may be used to determine f . If we now assume that the crack is formed by distributing the dislocations along the line $\theta=0$, $c < r < d$ with f as a function of t , $\sigma_{\theta\theta}(r,\theta)$ in the ring may be evaluated by integrating the Green's function obtained from (1), (7), (24c) and (27-32). Specifically, for $\theta=0$ from (26) we find

$$\int_c^d \frac{f(t)}{t-r} dt + \int_c^d k(r,t)f(t)dt = \frac{\pi(\kappa+1)}{2\mu} g(r), \quad c < r < d, \quad (34)$$

where

$$\begin{aligned} k(r,t) = & -\frac{1}{2} \left\{ -\frac{\beta_0}{r^2} + 2\gamma_0 + \frac{2\gamma_1}{r^3} + 6\delta_1 r + \sum_2^{\infty} [n(n-1)\alpha_n r^{n-2} \right. \\ & + (n+1)(n+2)\beta_n r^n + n(n+1)\gamma_n r^{-n-2} \\ & \left. + (n-2)(n-1)\delta_n r^{-n}] \right\}, \end{aligned} \quad (35)$$

and α_n , β_n , γ_n , and δ_n ($n=0,1,\dots$) are known functions of t which are determined from (28-32). If the crack is an embedded crack (i.e., if $a < c < d < b$) then from the definition of $f(t)$ given by (3) it follows that

$$\int_c^d f(t) dt = 0 \quad (36)$$

3. Stress Intensity Factors and Examples

If the crack is an embedded crack, the index of the integral equation (34) is +1 and the solution is of the following form

$$f(r) = \frac{F(r)}{[(r-c)(d-r)]^{\frac{1}{2}}}, \quad (c < r < d) \quad (37)$$

where $F(r)$ is a bounded function. After evaluating $F(r)$, the stress intensity factors at the crack tips $r=c$ and $r=d$ may be defined and obtained from

$$\begin{aligned} k(c) &= \lim_{r \rightarrow c} \sqrt{2(c-r)} \sigma_{\theta\theta}(r,0) \\ &= \frac{2\mu}{1+\kappa} \lim_{r \rightarrow c} \sqrt{2(r-c)} f(r) = \frac{2\mu}{1+\kappa} \frac{F(c)}{\sqrt{(d-c)/2}}, \end{aligned} \quad (38)$$

$$\begin{aligned} k(d) &= \lim_{r \rightarrow d} \sqrt{2(r-d)} \sigma_{\theta\theta}(r,0) \\ &= -\frac{2\mu}{1+\kappa} \lim_{r \rightarrow d} \sqrt{2(d-r)} f(r) = -\frac{2\mu}{1+\kappa} \frac{F(d)}{\sqrt{(d-c)/2}}. \end{aligned} \quad (39)$$

The singular integral equation (34) may be solved numerically by normalizing the interval (c,d) to $(-1,1)$ and by using the Gaussian integration formula [10]. Since the Fredholm kernel $k(r,t)$ is given in a simple form, one could obtain the results to any desired degree of accuracy with a relatively modest computational effort.

In the case of an edge crack (i.e., for $a=c < d < b$ or $a < c < d=b$) the single-valuedness condition (36) is not valid and also is not required as an additional condition for a unique solution.

For certain ring-crack geometries the convergence of the infinite series giving the Fredholm kernel (35) was rather slow. The results given in this paper were obtained by truncating the series at the N th term, solving the integral equations for $N=100, 120,$ and 140 for each ring-crack geometry and loading condition considered, calculating the stress intensity factors k as a function of N (from (38) and (39)), and by using a curve-fitting procedure of the following form

$$k(N_i) = A + \frac{B}{N_i^\alpha}, \quad (N_1 = 100, N_2 = 120, N_3 = 140). \quad (40)$$

The value of A obtained from (40) is assumed to be the calculated stress intensity factor. In the examples, for the values N_i considered, α is generally greater than unity, implying that the slope of k vs. $1/N$ curve at $(1/N) = 0$ is zero. Also, since the values $k(N_i)$ ($i=1,2,3$) differ from each other only in the third or fourth significant digits in the slowest converging cases, the extrapolated values ought to be quite reliable.

Three different loading conditions are used in the examples. Note that $g(r)$ which appear as the input function in the integral equation (34) or as the traction in the boundary condition (26) is the value of $\sigma_{\theta\theta}$ in the perturbation problem. For the loading conditions considered, $g(r)$ is given by the following expressions:

a) *Uniform crack surface pressure*

$$g(r) = -\sigma_0, \quad c < r < d. \quad (41)$$

b) *Internally pressurized cylinder*

$$g(r) = -\frac{p_0 a^2}{b^2 - a^2} \left(1 + \frac{b^2}{r^2} \right), \quad c < r < d, \quad (42)$$

where p_0 is the internal pressure (i.e., $\sigma_{rr}(a, \theta) = -p_0$). Here, it should be observed that in the case of the internal edge crack (i.e.,

for $c = a < d < b$), in addition to $g(r)$ given by (42), the crack surfaces may be subjected to uniform (fluid) pressure $g(r) = -p_0$. If that is the case, then the stress intensity factor separately obtained from $g(r) = -p_0$ should be added to that given by (42). In the examples, results due to (41) and (42) are listed separately.

c) *Rotating disk*

$$g(r) = -\frac{3+\nu}{8} \rho \omega^2 \left[a^2 + b^2 + \left(\frac{ab}{r}\right)^2 - \frac{1+3\nu}{3+\nu} r^2 \right] \quad (43)$$

where ρ is the mass density and ω is the angular velocity. The expression given in (43) is for the generalized plane stress and is valid for a rotating "disk". For a long rotating hollow cylinder, i.e., for the plane strain case, we have

$$g(r) = -\frac{1}{8} \frac{3-2\nu}{1-\nu} \rho \omega^2 \left[b^2 + a^2 + \left(\frac{ab}{r}\right)^2 - \frac{1+2\nu}{3-2\nu} r^2 \right]. \quad (44)$$

For various crack geometries the calculated stress intensity factors are shown in Tables 1-8. To give some idea about the trends, some limited results are also given in Figures 2-5. Table 1 gives the results for an embedded crack symmetrically located with respect to the boundaries of the ring or the hollow cylinder and subjected to a uniform crack surface pressure (see (41)). Here the crack length is fixed at half the wall thickness $b-a$ and the ratio of a/b is varied. The results are also displayed in Figure 2. Intuitively, it may be argued that the "constraint" at the inner crack tip $r=c$ is greater and at the outer crack tip $r=d$ is less than that of a centrally cracked infinite strip. Therefore, one may expect that $k(c)$ should be less and $k(d)$ should be greater than the corresponding stress intensity factor in the strip. This trend may also be observed in Figure 2 where the ring results seem to approach the strip value as $a \rightarrow \infty$ for constant wall thickness $b-a$.

Table 2 shows the effect of the crack length on the stress intensity factors in a ring or a hollow cylinder with a fixed radius ratio

Table E1. Stress intensity factors $k(c)$ and $k(d)$ for an embedded crack in a ring or a hollow cylinder subjected to uniform crack surface pressure $\sigma_{\theta\theta}(r,0) = -\sigma_0 \cdot \frac{d-c}{b-a} = 0.5, \frac{c-a}{b-d} = 1$ (Figure 1a)

$\frac{a}{b-a}$	$\frac{k(c)}{\sigma_0 \sqrt{(d-c)}/2}$	$\frac{k(d)}{\sigma_0 \sqrt{(d-c)}/2}$
0.05	1.1477	1.2046
0.10	1.1498	1.2030
0.25	1.1580	1.2018
0.50	1.1664	1.2007
1.0	1.1736	1.1980
2.0	1.1788	1.1943
3.0	1.1810	1.1923
4.0	1.1822	1.1911
∞	1.1867	1.1867

Table E2. Stress intensity factors $k(c)$ and $k(d)$ for an embedded crack in a ring or a hollow cylinder subjected to uniform crack surface pressure $\sigma_{\theta\theta}(r,0) = -\sigma_0$ (columns 2 and 3) or internal pressure $\sigma_{rr}(a,\theta) = -p_0$ (columns 4 and 5). $\frac{a}{b} = \frac{1}{2}, \frac{c-a}{b-d} = 1$ (Figure 1a) (The last column refers to the centrally cracked infinite strip)

$\frac{d-c}{b-a}$	$\frac{k(c)}{\sigma_0 \sqrt{(d-c)}/2}$	$\frac{k(d)}{\sigma_0 \sqrt{(d-c)}/2}$	$\frac{k(c)}{p_0 \sqrt{(d-c)}/2}$	$\frac{k(d)}{p_0 \sqrt{(d-c)}/2}$	$\frac{k}{\sigma_0 \sqrt{(d-c)}/2}$
-0.0	1.0	1.0	0.9259	0.9259	1.0
0.1	1.0060	1.0062	0.9522	0.9129	1.0060
0.2	1.0241	1.0256	0.9920	0.9139	1.0246
0.3	1.0556	1.0608	1.0468	0.9311	1.0577
0.4	1.1034	1.1158	1.1201	0.9682	1.1094
0.5	1.1736	1.1980	1.2186	1.0318	1.1867
0.6	1.2785	1.3213	1.3557	1.1341	1.3033
0.7	1.4445	1.5146	1.5606	1.3010	1.4884
0.8	1.7407	1.8536	1.9084	1.6002	1.8169
-1.0	∞	∞	∞	∞	∞

Table E3. Stress intensity factors $k(c)$ and $k(d)$ for an embedded crack in a ring or a hollow cylinder subjected to uniform crack surface pressure $\sigma_{\theta\theta}(r,0) = -\sigma_0$ (columns 2 and 3) or internal pressure $\sigma_{rr}(a,\theta) = -p_0$ (columns 4 and 5).
 $\frac{d-c}{b-a} = 0.5, \frac{a}{b} = \frac{1}{2}$ (Figure 1a)

$\frac{c-a}{b-a}$	$\frac{k(c)}{\sigma_0\sqrt{(d-c)/2}}$	$\frac{k(d)}{\sigma_0\sqrt{(d-c)/2}}$	$\frac{k(c)}{p_0\sqrt{(d-c)/2}}$	$\frac{k(d)}{p_0\sqrt{(d-c)/2}}$
0.15	1.2414	1.1755	1.4292	1.1004
0.20	1.1929	1.1777	1.3033	1.0554
0.25	1.1736	1.1980	1.2186	1.0318
0.30	1.1744	1.2391	1.1608	1.0290
0.35	1.1936	1.3118	1.1249	1.0533

$a/b = 1/2$. The crack is again symmetrically located with respect to the boundaries (i.e., $c-a = b-d$). The table shows the results for uniform crack surface pressure σ_0 (columns 2 and 3), for internal (wall) pressure p_0 (columns 4 and 5), and, for the purpose of comparison, for a centrally cracked infinite strip (column 6). Again to show the general trend of the results, the stress intensity factors for a cylinder under internal pressure p_0 are also displayed in Figure 3. In this case, as the crack length $d-c$ goes to zero, the stress intensity factors $k(c)$ and $k(d)$ approach $\sigma_{\theta\theta}(\frac{a+b}{2}, 0)\sqrt{(d-e)/2}$ which is the corresponding infinite plane result (for $a/b=1/2$, $\sigma_{\theta\theta}(\frac{a+b}{2}, 0) = (25/27) p_0 \approx 0.9259 p_0$). In this problem the initial decrease in $k(d)$ with increasing crack length is due to the decrease in $\sigma_{\theta\theta}(r,0)$ in the neighborhood of $r=d$.

The effect of the relative position of the crack in the cylinder wall is shown in Table 3. Here it is assumed that the crack length and radius ratio of the cylinder are constant ($(d-c) = (b-a)/2, a = b/2$) and the radial position of the crack $(c-a)/(b-a)$ is varied.

The results for an internal edge crack $c = a < d < b$ are given in Tables 4-6. Table 4 shows the stress intensity factor for a uniform crack surface pressure σ_0 (see (41)). The strip results given in the last column of the table are the limit of the cylinder results for

Table E4. The normalized stress intensity factor $k(d)/(\sigma_0\sqrt{d-a})$ in a hollow cylinder or a ring containing an internal edge crack ($c=a<d<b$) and subjected to uniform crack surface pressure $\sigma_{\theta\theta}(r,0) = -\sigma_0$.

$\frac{d-a}{b-a} \backslash \frac{a}{b-a}$	1/3	1/2	1	2	3	∞ (strip)
$\rightarrow 0$	1.1216	1.1216	1.1216	1.1216	1.1216	1.1216
0.1	1.153	1.155	1.157	1.159	1.167	1.1893
0.2	1.218	1.229	1.247	1.277	1.299	1.3674
0.3	1.295	1.310	1.366	1.449	1.493	1.6601
0.4	1.373	1.402	1.503	1.655	1.747	2.1119
0.5	1.465	1.508	1.658	1.901	2.066	2.8258
0.6	1.578	1.635	1.830	2.177	2.441	4.035
0.7	1.730	1.796	2.030	2.475	2.851	6.361
$\rightarrow 1.0$	∞	∞	∞	∞	∞	∞

Table E5. The normalized stress intensity factor $k(d)/[\sigma_{\theta\theta}(a,0)\sqrt{d-a}]$ for an internal edge crack ($c=a<d<b$) in a hollow cylinder under internal pressure, $\sigma_{rr}(a,\theta) = -p_0$. (The effect of pressure p on the crack surfaces is not included) $\sigma_{\theta\theta}(a,0) = p_0(b^2+a^2)/(b^2-a^2)$.

$\frac{d-a}{b-a} \backslash \frac{a}{b-a}$	1/3	1/2	1	2	3
$\rightarrow 0$	1.1216	1.1216	1.1216	1.1216	1.1216
0.1	0.878	0.957	1.058	1.113	1.137
0.2	0.756	0.878	1.057	1.189	1.239
0.3	0.685	0.834	1.089	1.305	1.397
0.4	0.643	0.813	1.138	1.461	1.613
0.5	0.620	0.808	1.199	1.635	1.883
0.6	0.611	0.816	1.273	1.834	2.189
0.7	0.626	0.841	1.359	2.046	2.527
$\rightarrow 1$	∞	∞	∞	∞	∞

Table E6. The normalized stress intensity factor $k(d)/[\sigma_{\theta\theta}(a,0)\sqrt{d-a}]$ for an internal edge crack ($c=a<d<b$) in a rotating disk ($\nu=0.3$) $\sigma_{\theta\theta}(a,0) = \frac{3+\nu}{4} \rho \omega^2 (b^2 + \frac{1-\nu}{3+\nu} a^2)$.

$\frac{d-a}{b-a} \backslash \frac{a}{b-a}$	1/3	1/2	1	2	3
→0.0	1.1216	1.1216	1.1216	1.1216	1.1216
0.1	1.008	1.040	1.089	1.120	1.139
0.2	0.962	1.018	1.114	1.202	1.240
0.3	0.944	1.018	1.168	1.324	1.401
0.4	0.943	1.032	1.235	1.477	1.617
0.5	0.956	1.058	1.315	1.664	1.879
0.6	0.981	1.096	1.405	1.867	2.196
0.7	1.025	1.153	1.508	2.082	2.526
→1.0	∞	∞	∞	∞	∞

$a \rightarrow \infty$ and for constant wall thickness $b-a$. The results of Table 4 are partly displayed in Figure 4 to show the general trend. One may again note that as $a/(b-a)$ increases, the geometric constraints decrease causing an increase in the stress intensity factors. As the crack length $d-a$ tends to zero, the stress intensity factor ratio approaches that of a half plane with an edge crack namely, 1.1216.

Table 5 and Figure 5 show the stress intensity factor $k(d)$ for a hollow cylinder with an internal edge crack and subjected to internal pressure $\sigma_{rr}(a,\theta) = -p_0$. Note that $k(d)$ is normalized with respect to the hoop stress at the inner boundary of the cylinder, $\sigma_{\theta\theta}(a,\theta) = p_0(b^2+a^2)/(b^2-a^2)$. Figure 5 also shows the variation of the hoop stress $\sigma_{\theta\theta}(r,\theta)$ through the cylinder wall, again normalized with respect to $\sigma_{\theta\theta}(a,\theta)$. Thus, the initial decrease in $k(d)$ for increasing crack length $d-a$ in cylinders having small values of $a/(b-a)$ may easily be explained by the relatively sharp decrease in $\sigma_{\theta\theta}(r,\theta)$ (which is the external load applied to the crack surface). Again, as $d-a \rightarrow 0$, the stress intensity

factor ratio tends to the half-plane value 1.1216.

The rotating disk or cylinder results are given in Table 6. Here, too, the stress intensity factor $k(d)$ is normalized with respect to the hoop stress $\sigma_{\theta\theta}$ at the inner boundary $r=a$, the expression of which is given in the table (see (43)). Note that the expressions of the hoop stress $\sigma_{\theta\theta}$ in the rotating disk and in the long hollow cylinder are different and are dependent on the Poisson's ratio ν . Therefore, the problems for the disk and the cylinder must be solved separately for a specified value of ν . The results given in Tables 6 and 8 are for the rotating disk which are obtained by using the plane stress solution with $\nu=0.3$.

The results for a hollow cylinder or a disk with an external edge crack are given in Tables 7 and 8. Table 7 shows the results for an internally pressurized hollow cylinder or disk. The stress intensity factor for a rotating disk obtained again from the plane stress solution with $\nu=0.3$ is given in Table 8.

Table E7. The normalized stress intensity factor $k(c)/[\sigma_{\theta\theta}(b,0)\sqrt{b-c}]$ for an external edge crack ($a < c < d = b$) in a hollow cylinder or a disk under internal pressure $\sigma_{rr}(a,\theta) = -p_0$; $\sigma_{\theta\theta}(b,0) = 2a^2p_0/(b^2-a^2)$.

$\frac{a}{b-a}$ \ / \ $\frac{b-c}{b-a}$	1/3	1/2	1	2	3
$\rightarrow 0$	1.1216	1.1216	1.1216	1.1216	1.1216
0.1	1.250	1.245	1.219	1.203	1.208
0.2	1.413	1.391	1.368	1.355	1.352
0.3	1.617	1.587	1.557	1.560	1.574
0.4	1.874	1.829	1.797	1.832	1.873
0.5	2.207	2.137	2.095	2.170	2.259
0.6	2.655	2.540	2.462	2.586	2.740
0.7	3.301	3.103	2.941	3.085	3.320
$\rightarrow 1.0$	$\rightarrow \infty$				

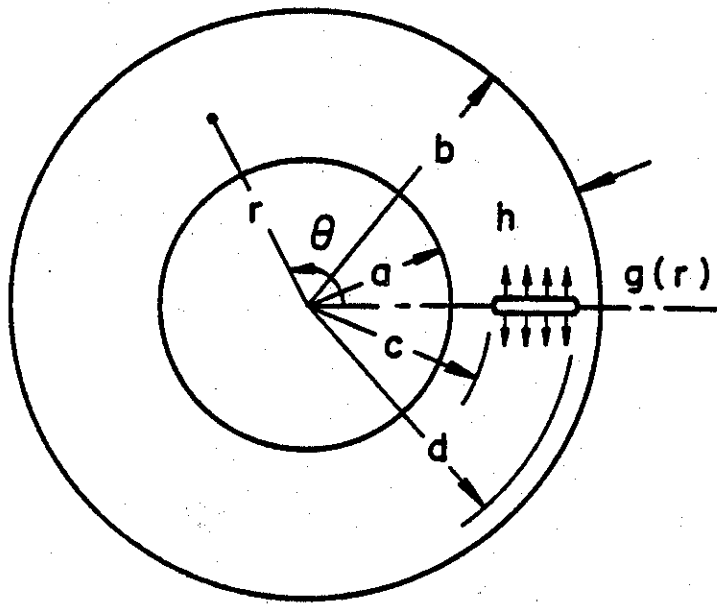
Table E8. The normalized stress intensity factor $k(c)/(\sigma_{\theta\theta}(b,0)\sqrt{b-c})$ in a rotating disk having an external edge crack ($a < c < b$).
 $\sigma_{\theta\theta}(b,0) = \frac{3+\nu}{4} \rho \omega^2 (a^2 + \frac{1-\nu}{3+\nu} b^2)$, $\nu = 0.3$.

$\frac{b-c}{b-a}$ \diagdown $\frac{a}{b-a}$	$\frac{a}{b-a}$				
	1/3	1/2	1	2	3
→0	1.1216	1.1216	1.1216	1.1216	1.1216
0.1	1.312	1.288	1.245	1.217	1.214
0.2	1.530	1.486	1.419	1.377	1.367
0.3	1.774	1.714	1.632	1.608	1.601
0.4	2.053	1.982	1.893	1.894	1.911
0.5	2.380	2.299	2.210	2.242	2.309
0.6	2.777	2.691	2.601	2.682	2.811
0.7	3.301	3.210	3.093	3.199	3.406
→1.0	→∞	→∞	→∞	→∞	→∞

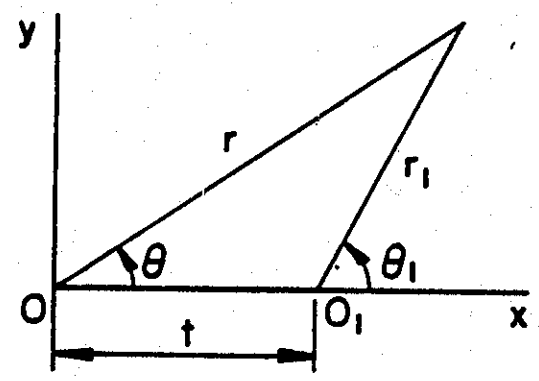
References

1. H.F. Bueckner and I. Giaever, "The stress concentration of a notched rotor subjected to centrifugal forces", ZAMM, Vol. 46, pp. 265-273, 1966.
2. O.L. Bowie and C.E. Freese, "Elastic analysis for a radial crack in a circular ring", U.S. AMMRC monograph MS-70-3, Watertown, MA., 1970.
3. P.G. Tracy, "Elastic analysis of radial cracks emanating from the outer and inner surfaces of a circular ring", J. Engng. Fracture Mechanics, Vol. 11, pp. 291-300, 1979.
4. P.G. Tracy, "Analysis of a radial crack in a circular ring segment", J. Engineering Fracture Mechanics, Vol. 7, pp. 253-260, 1975.
5. A.F. Emery and C.M. Segedin, "The evaluation of stress intensity factors for cracks subjected to tension, torsion, and flexure by an efficient numerical technique", J. Basic Engng. Trans. ASME, Vol. 94, pp. 387-393, 1972.
6. R. Labbens, A. Pellissier-Tanon, and J. Heliot, "Practical method for calculating stress intensity factors through weight functions" in Mechanics of Crack Growth, ASTM, STP 590, pp. 368-384, 1976.

7. C.B. Buchalet and W.H. Bamford, "Stress intensity factor solutions for continuous surface flaws in reactor pressure vessels", in Mechanics of Crack Growth, ASTM, STP 590, pp. 385-402, 1976.
8. J. Dundurs, "Elastic interaction of dislocations with inhomogeneities", in Mathematical Theory of Dislocations, ed. T. Mura, pp. 70-115, 1969.
9. R.W. Little, Elasticity, Prentice Hall, 1973.
10. F. Erdogan, "Mixed boundary value problems in mechanics", Mechanics Today, S. Nemat-Nasser, ed., Vol. 4, pp. 1-86, Pergammon Press, 1978.



(a)



(b)

Figure E-1. The geometry of the problem.

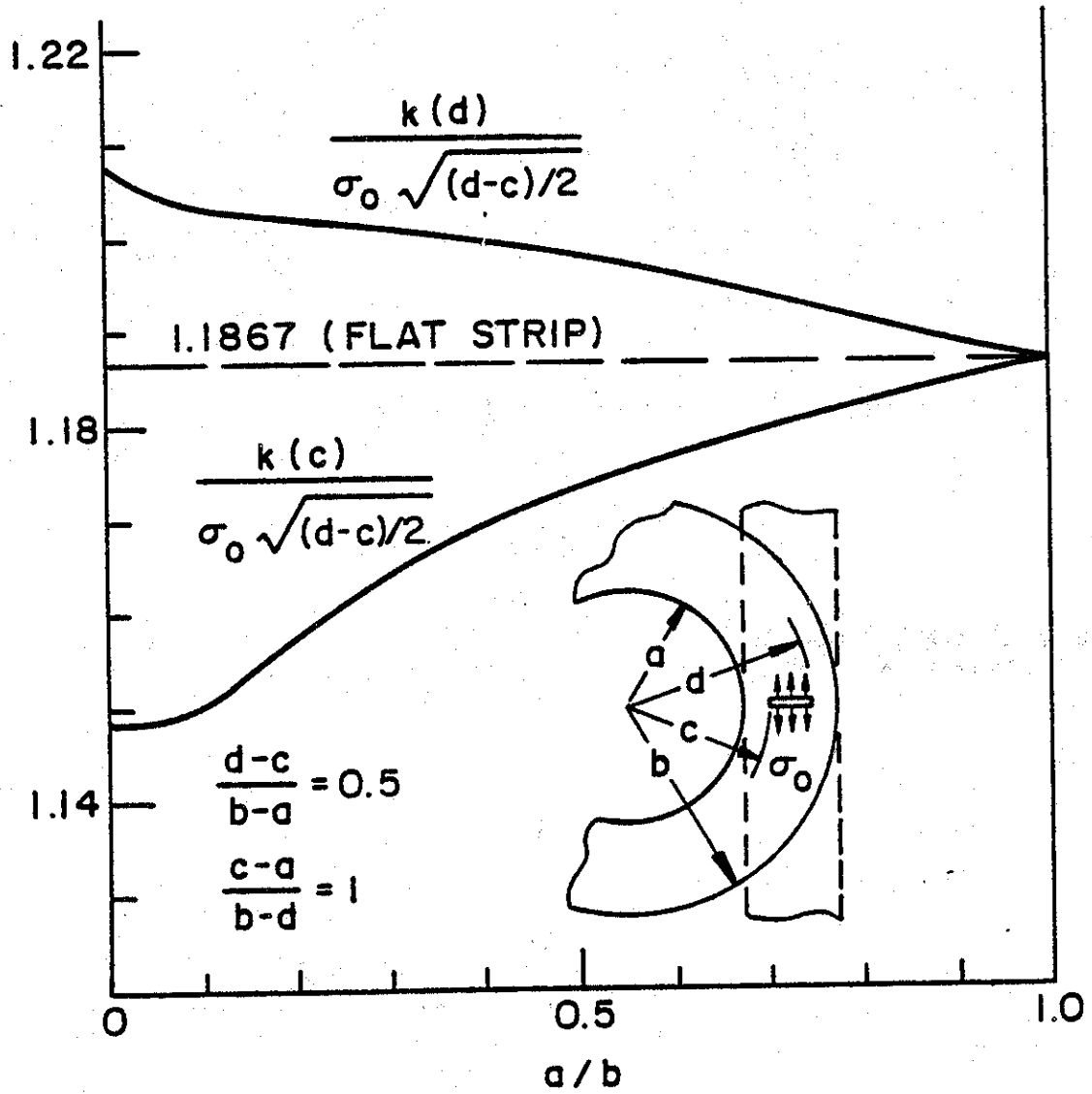


Figure E-2. Stress intensity factors for an embedded crack in a hollow cylinder or a disk loaded by a uniform crack surface pressure $\sigma_{\theta\theta}(r,0) = -\sigma_0$, $c < r < d$.

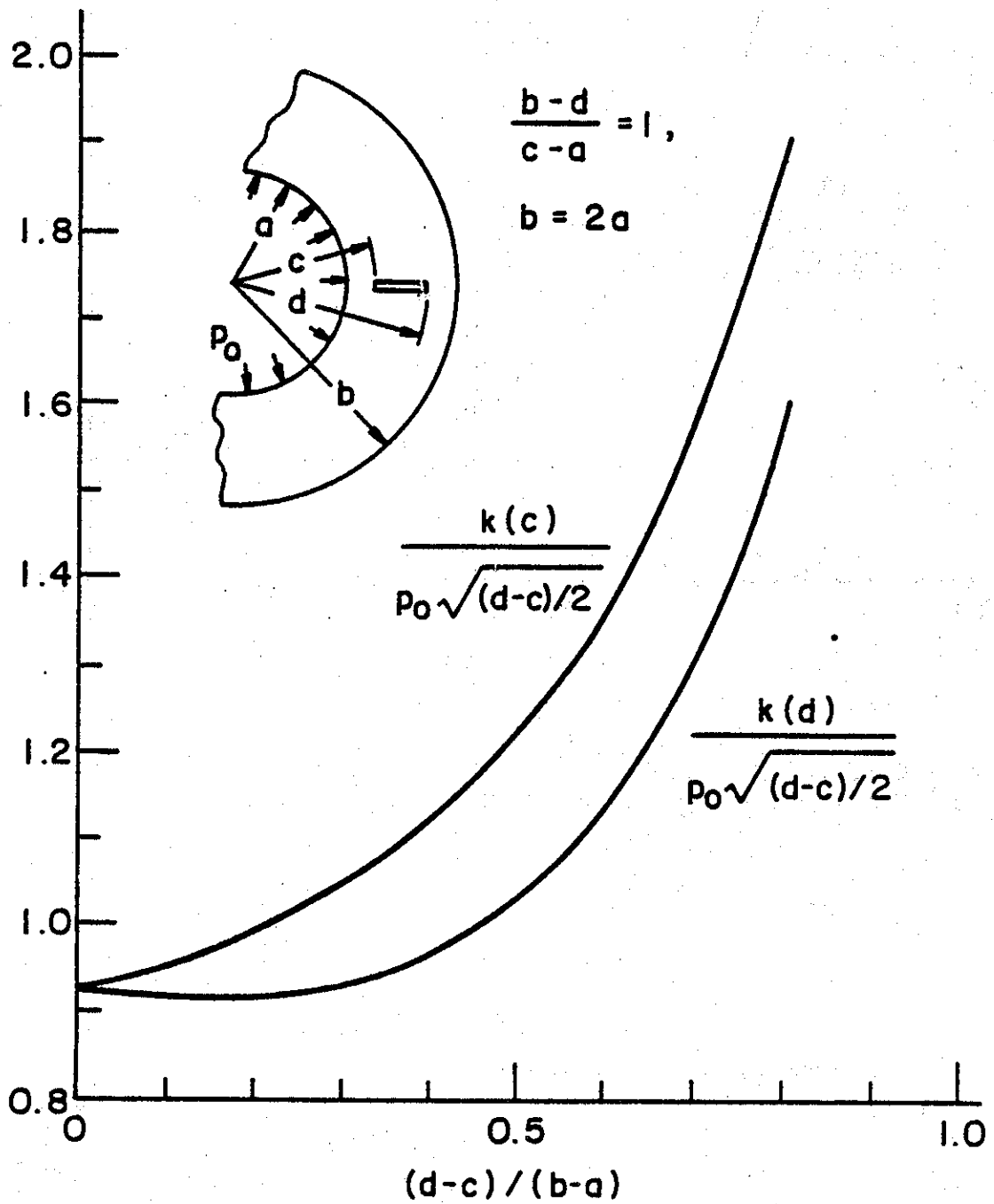


Figure E-3. Stress intensity factors for an embedded crack in a hollow cylinder or a disk under internal pressure $\sigma_{rr}(a, \theta) = -p_0$.

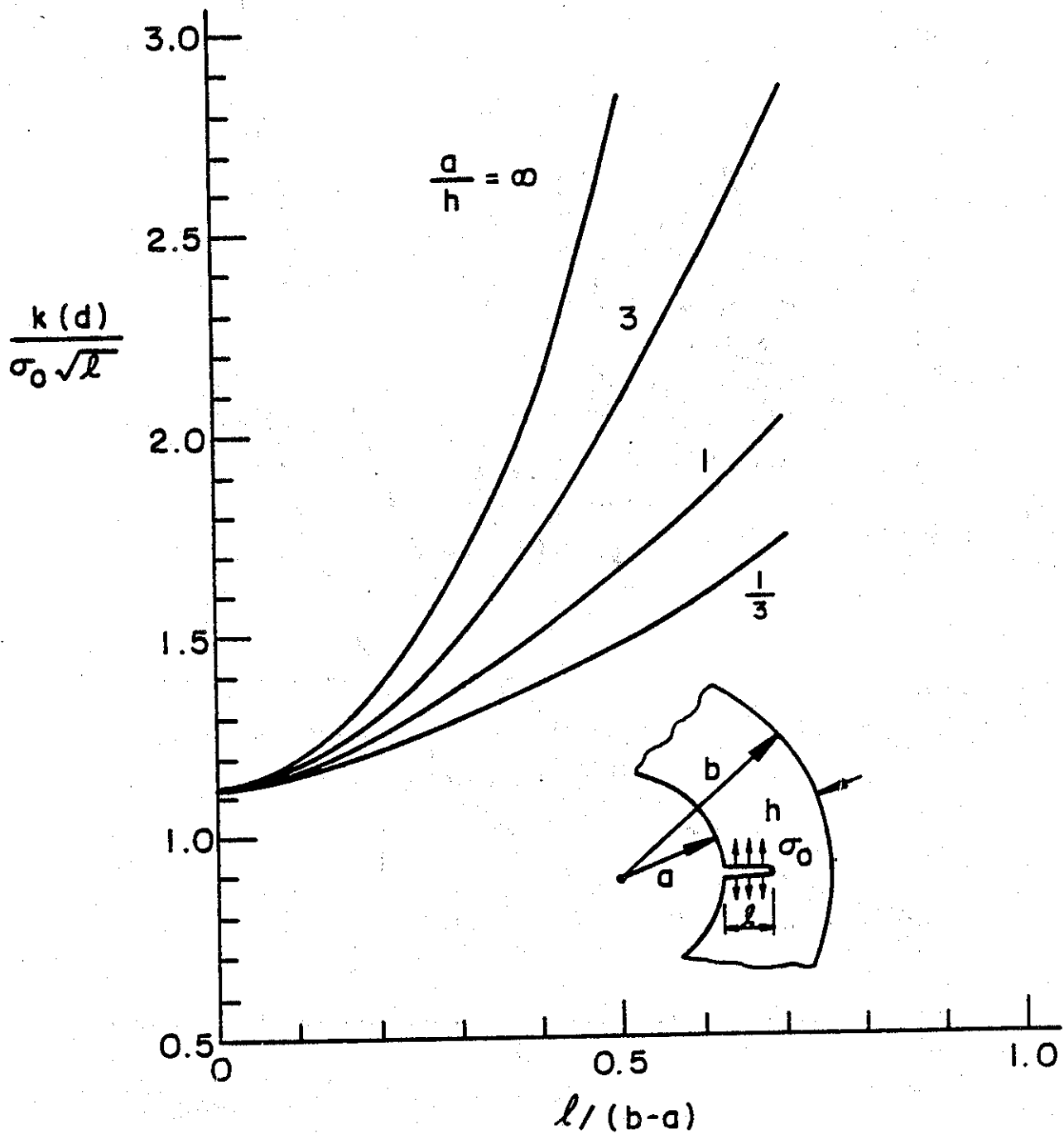


Figure E-4. The stress intensity factor for an internal edge crack in a hollow cylinder or a disk loaded by uniform crack surface pressure $\sigma_{\theta\theta}(r,0) = -\sigma_0$, $l=d-a$.

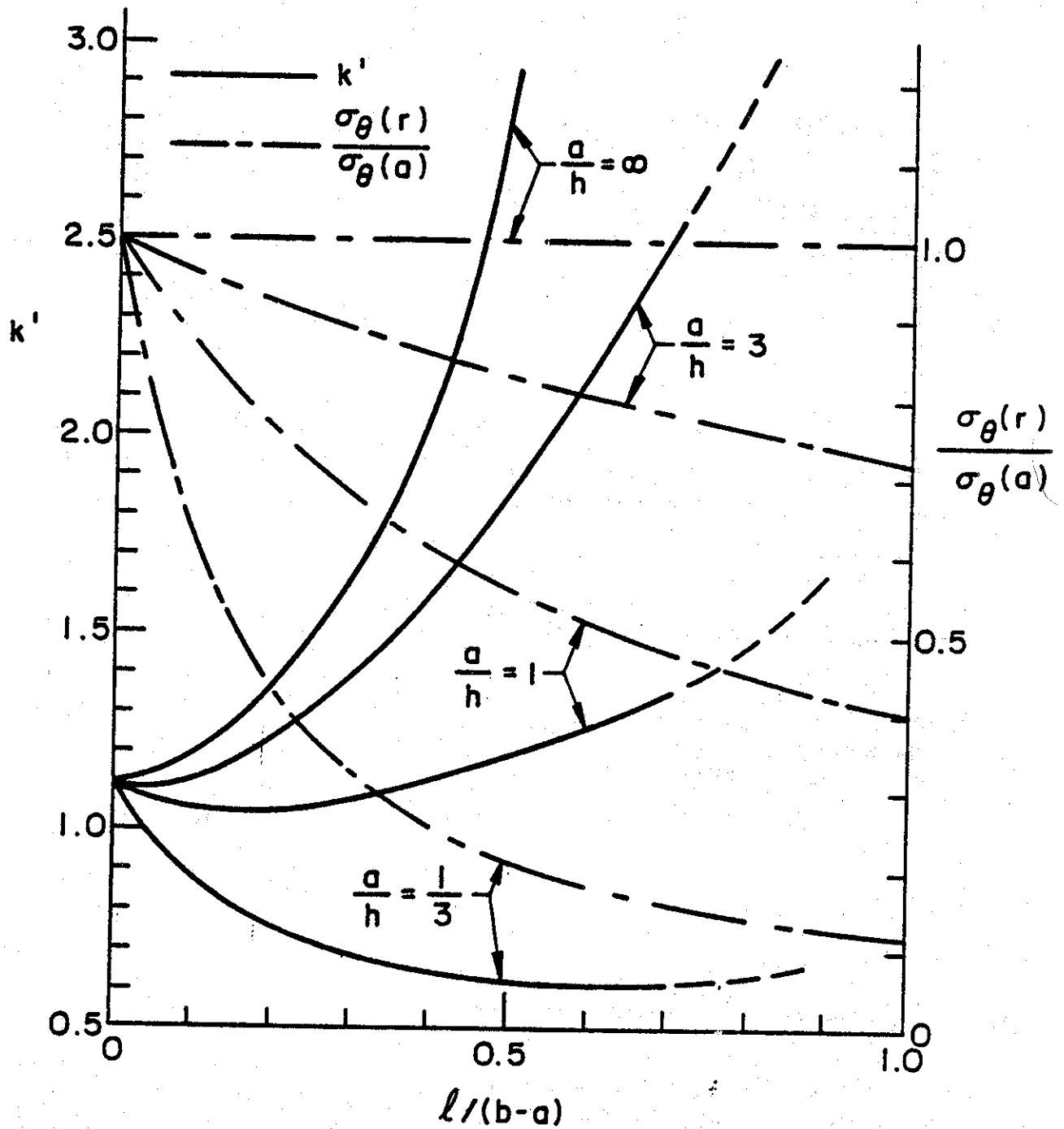


Figure E-5. The stress intensity factor ratio $k' = k(d)/[\sigma_{\theta\theta}(a,0)\sqrt{d-a}]$ and the normalized hoop stress $\sigma_{\theta\theta}(r)/\sigma_{\theta\theta}(a,0)$ in a hollow cylinder or a disk containing an internal edge crack and subjected to the internal pressure $\sigma_{rr}(a,\theta) = -p_0$; $\sigma_{\theta\theta}(a,0) = p_0(b^2+a^2)/(b^2-a^2)$ (The effect of the pressure p_0 on the crack surfaces is not included). ($l=d-a$)

Handwritten text, likely bleed-through from the reverse side of the page. The text is extremely faint and illegible due to the quality of the scan. It appears to be several lines of a letter or document, possibly containing names and dates, but the characters are too light to transcribe accurately.

APPENDIX F

AN EDGE-CRACKED PLATE OR BEAM WITH TENSILE AND COMPRESSIVE YIELD ZONES

1. Introduction

In a beam with an edge crack or in a plate containing a relatively long and deep surface crack it is known that under uniform tension and particularly under bending relatively large compressive stresses may develop in the region opposite to the crack near and at the surface. The problem is described in Figure 37. The beam problem can be approximated by the plane stress problem for an edge-cracked infinite strip. Similarly, the geometry shown in Figure 37a under plane strain conditions may represent the stress and deformation state around the midsection of the plate shown in Figure 37b. In applying the crack initiation or crack instability criteria described in Sections 3 and 4 of this report one needs a fairly accurate evaluation of the crack opening stretch at the leading edge of the crack. Previous studies of this problem have been either purely elastic calculating the crack opening displacement on the surface for use in compliance calibration analysis or have taken into consideration only the tensile yielding around the crack tip. In this study a plastic strip model has been used to take into account the plastic deformations in compressive as well as in tensile zones. The model used does not allow the consideration of strain hardening. This is usually taken care of by using a flow stress in place of the yield strength of the material. The flow stresses in tension and compression are generally different and, depending on the strain hardening behavior, are somewhat higher than the yield strength.

2. Formulation of the Problem

The basic formulation of the related elasticity problem for nonsymmetric cracks and arbitrary loading conditions is given in Reference [1]^(*). For the

(*) H.F. Nied and F. Erdogan, "A cracked beam or plate transversely loaded by a stamp", Int. J. of Solids and Structures, Vol. 15, pp. 951-965, 1979.

convenience of applications the plasticity effects have been considered for two different problems. In Problem 1 it is assumed that the magnitude of the compressive stresses is not sufficiently high to warrant the introduction of a separate compressive yield zone. This is the case in most plate or beam structures under membrane loading only. In Problem 2 yielding is considered both in tension and compression.

Problem 1

The plane elasticity problem of an infinite strip $0 < y < h$, $-\infty < x < \infty$, containing a nonsymmetric edge crack along $0 < y < c$, $x=0$ (Figure 37a) may be formulated in terms of a singular integral equation of the following form [1]

$$\int_0^c \left[\frac{1}{t-y} + k(y,t) \right] F(t) dt = \frac{\kappa+1}{4G} \sigma_{xx}(0,y) \quad (1)$$

$$F(y) = \frac{\partial u}{\partial y}(+0,y), \quad (0 < y < c) \quad (2)$$

where $\sigma_{xx}(0,y)$ is the crack surface traction and the Fredholm kernel $k(y,t)$ is given in [1]. The material constants are given by the shear modulus G and κ ($\kappa=3-4\nu$ for plane strain, $\kappa=(3-\nu)/(1+\nu)$ for plane stress, ν being Poisson's ratio). The complete statement of the elastic problem, when the crack is given as an edge crack must also include the additional condition:

$$F(0) < \infty \quad (3)$$

Implementation of the plastic strip model for Problem 1 requires the superposition of the following two loading conditions for the right side of (1).

$$\sigma_{xx}(0,y) = -\sigma_0 \quad 0 < y < c, \quad (4)$$

$$\sigma_{xx}(0,y) = \sigma_Y \quad a < y < c. \quad (5)$$

Here the applied load σ_0 and the yield strength σ_Y are known. The plastic zone size $\alpha=c-a$ is unknown and is determined by the condition that at the

fictitious crack tip c the stress must be finite. This condition may be expressed in terms of the stress intensity factors such that:

$$k_1 + k_2 = 0 \quad (6)$$

where k_1 and k_2 are the stress intensity factors resulting from loading conditions (4) and (5) respectively. The stress intensity factors themselves are expressed in terms of the density functions F_1 and F_2 which are obtained from the solution of (1). The stress intensity factors are defined by

$$k_i(c) = -\lim_{y \rightarrow c} [2(y-c)]^{\frac{1}{2}} \frac{4G}{1+\kappa} F_i(y), \quad i=1,2. \quad (7)$$

Normalizing crack lengths with respect to the thickness h , (6) becomes:

$$\sigma_0 f_1\left(\frac{c}{h}\right) + \sigma_Y f_2\left(\frac{c}{h}\right) = 0, \quad f_i(y) = F_i(y) \frac{2}{c} \sqrt{y(c-y)}. \quad (8)$$

f_1 and f_2 are determined (for unit loads) from (1) and the corresponding $\frac{\sigma_0}{\sigma_Y}$ is obtained from (8) by holding the actual crack length $\frac{a}{h}$ constant and varying the fictitious crack length $\frac{c}{h}$. Various values of $\frac{\sigma_0}{\sigma_Y}$ are obtained for various plastic zone sizes $\frac{\alpha}{h}$ at constant crack lengths $\frac{a}{h}$. This is done in a straight-forward manner by noting that the Chebyshev quadrature technique used to solve (1) locates the points at which loads are applied through the equation [1]

$$s_m = \cos\left(\frac{2m-1}{2n-2} \pi\right), \quad m=1, \dots, n-1 \quad (9)$$

where n is the total number of quadrature points and the integral in (1) is normalized from -1 to $+1$ by

$$y = \frac{c}{2}(s+1). \quad (10)$$

The values for $\frac{c}{h}$ are then determined from

$$\frac{c}{h} = \frac{2\left(\frac{a}{h}\right)}{\left[\cos\left(\pi \frac{2m-1}{2n-2}\right) + 1\right]}, \quad m=1, \dots, n-1 \quad (11)$$

where for a constant a/h the appropriate n may be chosen to give various $\frac{\alpha}{h}$ ($\frac{\alpha}{h} = \frac{c-a}{h}$) values.

Normalization and integration of the density functions F_i from -1 to $+1$ gives the crack surface displacement ($\delta(0) = u(+0,0) - u(-0,0)$), as

$$\frac{4G}{\kappa+1} \frac{1}{\sigma_Y} \frac{\delta(0)}{h} = \frac{\sigma_0}{\sigma_Y} \text{COD}_1 + \text{COD}_2 \quad (12)$$

where

$$\text{COD}_i = \frac{-c}{h} \int_{-1}^1 \phi_i(s) ds, \quad \phi_i(s) = F_i(y), \quad i = 1, 2. \quad (13)$$

It was found convenient to obtain results for the crack opening displacements δ other than the COD by using the polynomial interpolation method as follows:

$$\frac{4G}{1+\kappa} \frac{1}{\sigma_Y} \frac{\delta(0,y)}{h} = \frac{\sigma_0}{\sigma_Y} \text{CTOD}_1 + \text{CTOD}_2 \quad (14)$$

and

$$\text{CTOD}_i = \frac{-c}{h} \int_r^1 \phi_i(s) ds \quad (15)$$

with r the normalized location of the crack tip as determined from (10). In a straight-forward manner from the properties of U_j , the Chebyshev polynomial of the second kind, $\phi_i(s)$ is rewritten as

$$\phi_i(s) = (1-s^2)^{\frac{1}{2}} \sum_0^{n-3} b_j U_j(s) \quad (16)$$

with

$$b_j = \frac{2}{r-1} \sum_{k=2}^{n-1} v_i(s_k) U_j(s_k), \quad s_i = \cos\left(\frac{k-1}{n-1} \pi\right) \quad (17)$$

$$v_i(s) = \phi_i(s) (1-s^2)^{\frac{1}{2}}, \quad -1 < s < 1, \quad (18)$$

where n is the total number of quadrature points.

Observing that

$$U_j(\cos\theta) = \frac{\sin[(j+1)\theta]}{\sin\theta} \quad (19)$$

and defining $r = \cos\beta$, (15) may be rewritten as

$$CTOD_i = \frac{c}{h} \sum_{j=0}^{n-3} b_j H_j(\beta), \quad r = \cos\beta \quad (20)$$

where

$$H_j(\beta) = \begin{cases} \beta - \frac{1}{2} \sin 2\beta & j=0 \\ \frac{\sin j\beta}{j} - \frac{\sin(j+2)\beta}{j+2} & j=1, \dots, n-3. \end{cases} \quad (21)$$

From (14) and (20) it is possible to directly determine the crack opening stretch $\delta(a)$ at the crack tip ($\delta(a) = u(+0, a) - u(-0, a)$).

Another quantity of interest is the stress $\sigma_{xx}(0, y)$ ahead of the crack tip plastic zone $\frac{\alpha}{h}$. The ratio of $\sigma_{xx}(0, h)/\sigma_Y$ is especially important for when this quantity is greater than one, yielding will have occurred on the compressive side of the strip. Thus, in numerical calculations this ratio is monitored to assure that the formulation of Problem 1 is physically valid.

Once the density function $F(t)$, where

$$F(t) = \frac{\sigma_0}{\sigma_Y} F_1(t) + F_2(t), \quad (22)$$

is determined, the stress $\sigma_{xx}(0, y)/\sigma_Y$ for any value of $y > c$ may be calculated by direct integration of (1). This stress solution to the perturbation problem must be superimposed with the stress field due to the applied external loads $\sigma_0(0, y)/\sigma_Y$ to give the total stress ahead of the plastic zone $\frac{\alpha}{h}$.

Problem 2.

In both uniform tension and pure bending, for specific $\frac{a}{h}$ and $\frac{\alpha}{h}$ values, $\sigma_{xx}(0, h)/\sigma_Y$ becomes greater than one. The yielding which occurs due to the magnitude of the compressive stress must now be taken into account in the

formulation. This may be done by introducing a second plastic strip along another fictitious crack $x=0$, $b < y < h$ (Figure 37a). Similar to the plastic strip in the tensile zone $a < y < c$, this strip is also assumed to carry a constant stress in x -direction. However in this case the stress is compressive and represents the yield behavior of the material in compression. The results obtained from the solution of Problem 1 indicated that for the case of uniform tension only for very large relative crack lengths a/h and plastic zone sizes α/h (i.e., for high load ratios σ_0/σ_Y) did the medium yield on the compressive side. Thus the more interesting problem occurs in pure bending when this yield zone may develop more readily.

The formulation of Problem 2 proceeds in an identical manner as Problem 1 where now the elastic problem contains two edge cracks. The integral equation (1) is recast as a set of two coupled singular integral equations as follows:

$$\int_0^c k_{11}(y,t)F(t)dt + \int_b^h k_{12}(y,t)G(t)dt = \frac{\kappa+1}{4G} \sigma_{xx}(0,y) \quad 0 < y < c, \quad (23)$$

$$\int_0^c k_{21}(y,t)F(t)dt + \int_b^h k_{22}(y,t)G(t)dt = \frac{\kappa+1}{4G} \sigma_{xx}(0,y) \quad b < y < h, \quad (24)$$

where $k_{ij}(y,t)$, $(i,j=1,2)$ are the same expression as in (1) $(\frac{1}{t-y} + k(y,t))$. Thus, k_{11} and k_{22} have a Cauchy type singularity

$$k_{11}(y,t) \sim \frac{1}{t-y}, \quad \text{for } 0 < y < c$$

$$k_{22}(y,t) \sim \frac{1}{t-y}, \quad \text{for } b < y < h$$

and k_{12} and k_{21} are bounded in their respective domains of definition. The additional edge crack conditions are given by:

$$F(0) < \infty, \quad (25)$$

$$G(h) < \infty \quad (26)$$

It should be noted that the formulation for elastic problems with any number of cracks is thus straight-forward and involves only the introduction of a new unknown density function for each additional crack.

For pure bending the loading conditions for the right side of (23) and (24) involve the superposition of a linear traction and an opposite uniform loading equal in magnitude to either σ_Y on the tension strip $a < y < c$ or the compressive flow stress $(\sigma_Y)_c$ on the compression strip $b < y < h$ (Figure 37). These loading conditions may be expressed as:

$$\sigma_{xx}(0,y) = -\sigma_0(y) = \frac{M}{I} (y-h/2), \quad 0 < y < a \quad (27)$$

$$\sigma_{xx}(0,y) = \frac{M}{I} (y-\frac{h}{2}) + \sigma_Y \quad a < y < c, \quad (28)$$

$$\sigma_{xx}(0,y) = \frac{M}{I} (y - \frac{h}{2}) - (\sigma_Y)_c, \quad b < y < h, \quad (29)$$

where M is the applied external bending moment and I is the moment of inertia for the strip cross section. The introduction of the plastic strips, whether they are tensile or compressive, forces the condition that at both c and b the stresses must be finite in magnitude. Similar to condition (8) in Problem 1, this statement may now be expressed as

$$k(c) = \sigma_Y f_1(c/h) + (\sigma_Y)_c f_2(c/h) + \frac{hM}{2I} [f_3(c/h) + f_4(c/h)] = 0 \quad (30)$$

$$k(b) = \sigma_Y g_1(b/h) + (\sigma_Y)_c g_2(b/h) + \frac{hM}{2I} [g_3(b/h) + g_4(b/h)] = 0 \quad (31)$$

where it is assumed a and c are known (i.e. α is known) and both b and M are unknown. The functions f_i and g_i ($i=1,2,3,4$) are known from the solution of the normalized form of (23) and (24), and σ_Y , $(\sigma_Y)_c$ are given. Combining (30) and (31) the expression

$$\frac{f_1(c/h) + \tau f_2(c/h)}{f_3(c/h) + f_4(c/h)} - \frac{g_1(b/h) + \tau g_2(b/h)}{g_3(b/h) + g_4(b/h)} = 0 \quad (32)$$

is obtained where,

$$\tau = \frac{(\sigma_Y)_c}{\sigma_Y} \quad (33)$$

and M is determined from

$$m = \frac{hM}{2I} = - \frac{f_1(c/h) + \tau f_2(c/h)}{f_3(c/h) + f_4(c/h)} \quad (34)$$

By fixing a , c and τ the unknown compressive zone size $h-b$ and m may be obtained by iteration from (32) and varying these parameters in the simultaneous solution of (23) and (24).

Once the compressive plastic zone size and m have been determined all quantities calculated in Problem 1 may now be determined in a similar manner. The crack opening displacement $\delta(0)$ is given as:

$$\frac{4G}{1+\kappa} \frac{1}{\sigma_Y} \frac{\delta(0)}{h} = \text{COD}_1 + \tau \text{COD}_2 + m[\text{COD}_3 + \text{COD}_4], \quad (35)$$

where

$$\text{COD}_i = \frac{-c}{h} \int_{-1}^1 \phi_i(s) ds + \frac{(b-h)}{h} \int_{-1}^1 \psi_i(s) ds \quad (36)$$

$$-1 < s < 1, \quad i=1, \dots, 4,$$

ϕ_i and ψ_i having been determined from the solution of (23), (24).

Crack opening stretch $\delta(a)$ at the crack tip is determined as in Problem 1 using a polynomial expression. Also the stress distribution between the tensile plastic zone and the compressive plastic zone is calculated by direct integration of the normalized form of (23). Again the solution to the perturbation problem for the stress must be superimposed on the stress obtained from the externally applied moment in order to calculate the total stress.

Problem 3: The Effect of Strain Hardening

In the problems 1 and 2 described in this Appendix it is assumed that the stress in the plastic strip zone is constant. The crack problem can also be solved for a material which has linear strain hardening. For example, consider the single edge notched strip under uniform tension discussed in Problem 1. In this case, the integral equation (1) and the first loading (4) are still valid. However, the second loading condition (5) corresponding to the crack surface tractions which simulate the plastic strip must now be

replaced by

$$\sigma_{xx}(0,y) = \sigma_Y + E_p u(0,y) \quad . \quad a < y < c \quad . \quad (37)$$

The plastic ligament stress expressed by (37) assumes that at the fictitious crack tip where the crack surface displacement u is zero the stress is equal to the yield strength σ_Y and elsewhere in the yield zone the stress is linearly dependent on the stretch in the strip or on the crack opening displacement u . Again the plastic zone size $c-a$ is determined from (6) where the input function (37) rather than (5) is used to determine k_2 .

Referring to (2), the crack surface displacement may be expressed as

$$u(+0,y) = \int_y^c F(t) dt \quad . \quad (38)$$

Substituting now from (37) and (38) into (1), for the second loading condition, we obtain

$$\int_0^c \left[\frac{1}{t-y} + k(y,t) \right] F(t) dt + \frac{\kappa+1}{4G} E_p \int_y^c F(t) dt = \begin{cases} 0, & (0 < y < a) \\ \frac{\kappa+1}{4G} \sigma_Y, & (a < y < c) \end{cases} \quad , \quad 0 < y < c \quad . \quad (39)$$

The integral equation (39) may again be solved in a straightforward manner.

The results of Problem 1, i.e., for a plate under uniform tension in which plastic deformations develop only in a tensile zone are given in Table 1. For various values of the relative crack depth a/h and the stress ratio σ_0/σ_Y , the table shows the relative size of the plastic zone α/h , the crack opening stretch $\delta(a)$ at the leading edge of the crack, the crack opening displacement (COD) $\delta(0)$ on the surface of the plate, and the relative magnitude of the net ligament stress $\sigma_{xx}(0,h)/\sigma_Y$ on the surface opposite to the crack, where σ_Y is the flow stress in tension. $\sigma_{xx}(0,h)$ is listed to monitor the possibility of compressive yielding. It may indeed be seen that for greater values of a/h and σ_0/σ_Y , the magnitude of the compressive stress may exceed the flow stress in compression $(\sigma_Y)_c$. It is seen that when the external load reaches a certain value, any small increase in the load may cause a relatively large increase in the crack opening stretch $\delta(a)$ which may indicate the triggering of a crack instability or plastic collapse process in the plate.

Table 2 gives the results for the edge crack problem in a plate under pure bending. The bending stress shown in the table is defined by $\sigma_B = 6M/h^2$. In addition to the quantities listed in Table 1, Table 2 gives the size of the compressive plastic zone $(h-b)/h$ whenever relevant. To calculate the results given by Table 2 the flow stresses in tension σ_Y , and in compression $(\sigma_Y)_C$ are assumed to be equal. The effect of the flow stress ratio $\tau = \sigma_Y/(\sigma_Y)_C$ is separately studied for a specific crack depth $a/h = 0.5$ and the results are shown in Table 3. From Table 3 it may be observed that even though the compressive plastic zone size $h-b$ is rather heavily dependent on the flow stress ratio τ , the change in $\delta(0)$ and $\delta(a)$ is not very significant. One should add that for numerical convenience in the calculations as τ is varied the tensile plastic zone size α rather than the applied load σ_B was kept constant. If σ_B were to be constant the change in $\delta(0)$ and $\delta(a)$ would have been somewhat higher than the change shown in the table, but it would still not have been very significant.

Some sample results showing the effect of the strain hardening are given in Tables 4-6. For higher E_p/E values the same plastic zone size α/h seems to require higher values of the external load σ_0 . The effect of the strain hardening on the crack opening stretch $\delta(a)$ seems to be negligible. However, the crack opening displacement $\delta(0)$ and the backside stress $\sigma_{xx}(0,h)$ seem to increase slightly with the increasing E_p/E ratio. It is also interesting to note that to create the same plastic zone size α one needs to apply a smaller external load σ_0 in the plane strain than in the plane stress case.

It should be noted that in the integral equation (1) the Fredholm kernel is independent of the elastic constants. Therefore, Problems 1 and 2 and Tables 1-3 are valid for both plane stress and plane strain cases. The two cases are distinguished by properly identifying the constant κ in the tables ($\kappa=(3-\nu)/(1+\nu)$ for plane stress, $\kappa=3-4\nu$ for plane strain). However, in the case of strain hardening materials, as seen from (39), the Fredholm kernel is dependent on the Poisson's ratio and $(1+\kappa)$ does not appear as simply a multiplying factor on the right hand side. Consequently, in this case the calculations for plane stress and plane strain conditions have to be carried out separately.

TABLE F1
RESULTS FOR UNIFORM TENSION

a/h	α/h	σ_0/σ_Y	$\sigma_{xx}(0,h)/\sigma_Y$	$\frac{4G}{1+\kappa} \frac{1}{\sigma_Y} \frac{\delta(0)}{h}$	$\frac{4G}{1+\kappa} \frac{1}{\sigma_Y} \frac{\delta(a)}{h}$
.01	.0002	.109	.109	3.18×10^{-3}	2.24×10^{-4}
.01	.0018	.327	.326	1.01×10^{-2}	2.22×10^{-3}
.01	.01	.628	.627	2.33×10^{-2}	1.00×10^{-2}
.01	.0313	.820	.817	3.91×10^{-2}	2.28×10^{-2}
.01	.0540	.882	.878	4.86×10^{-2}	3.13×10^{-2}
.01	.1617	.950	.939	7.07×10^{-2}	5.21×10^{-2}
.01	.2716	.964	.947	8.34×10^{-2}	6.45×10^{-2}
.01	.3808	.970	.946	9.30×10^{-2}	7.40×10^{-2}
.01	.4739	.973	.943	1.02×10^{-1}	8.30×10^{-2}
.01	.5988	.976	.933	1.19×10^{-1}	9.92×10^{-2}
.1	.0007	.061	.056	1.91×10^{-2}	7.48×10^{-4}
.1	.0320	.387	.345	1.34×10^{-1}	3.74×10^{-2}
.1	.0516	.466	.410	1.70×10^{-1}	5.79×10^{-2}
.1	.1	.578	.492	2.38×10^{-1}	1.03×10^{-1}
.1	.1548	.646	.528	2.97×10^{-1}	1.47×10^{-1}
.1	.1938	.677	.536	3.34×10^{-1}	1.76×10^{-1}
.1	.2448	.705	.536	3.80×10^{-1}	2.13×10^{-1}
.1	.3296	.737	.515	4.54×10^{-1}	2.75×10^{-1}
.1	.4054	.755	.480	5.27×10^{-1}	3.38×10^{-1}
.1	.5272	.794	.443	6.28×10^{-1}	4.41×10^{-1}
.2	.0013	.053	.034	3.92×10^{-2}	1.50×10^{-3}
.2	.0124	.160	.100	1.20×10^{-1}	1.53×10^{-2}
.2	.0639	.333	.185	2.80×10^{-1}	7.67×10^{-2}
.2	.1032	.398	.200	3.98×10^{-1}	1.21×10^{-1}
.2	.2	.489	.175	5.35×10^{-1}	2.30×10^{-1}
.2	.3050	.541	.090	7.23×10^{-1}	3.62×10^{-1}
.2	.4025	.572	-.044	9.44×10^{-1}	5.24×10^{-1}
.2	.5	.581	-.309	1.309	8.16×10^{-1}
.2	.6	.612	-.749	1.966	1.30
.3	.0020	.044	.005	6.23×10^{-2}	2.25×10^{-3}
.3	.0283	.160	.008	2.39×10^{-1}	3.55×10^{-2}
.3	.1096	.286	-.046	5.03×10^{-1}	1.40×10^{-1}
.3	.2095	.359	-.172	7.75×10^{-1}	2.84×10^{-1}
.3	.3	.399	-.347	1.06	4.54×10^{-1}
.3	.4	.437	-.648	1.52	7.28×10^{-1}
.3	.5	.459	-1.28	2.42	1.32
.4	.1	.198	-.257	6.32×10^{-1}	1.30×10^{-1}
.4	.2	.263	-.499	1.04	2.96×10^{-1}
.4	.3	.285	-.890	1.59	6.03×10^{-1}
.4	.4	.318	-1.62	2.65	1.15

Table F1 (cont.)

a/h	α/h	σ_o/σ_Y	$\sigma_{xx}(0,h)/\sigma_Y$	$\frac{4G}{1+\kappa} \frac{1}{\sigma_Y} \frac{\delta(0)}{h}$	$\frac{4G}{1+\kappa} \frac{1}{\sigma_Y} \frac{\delta(a)}{h}$
.5	.0014	.017	-.046	8.46×10^{-2}	1.63×10^{-3}
.5	.0131	.051	-.142	2.50×10^{-1}	1.67×10^{-2}
.5	.0402	.088	-.266	4.74×10^{-1}	5.37×10^{-2}
.5	.0826	.122	-.423	7.30×10^{-1}	1.18×10^{-1}
.5	.1	.132	-.487	8.28×10^{-1}	1.50×10^{-1}
.5	.1104	.138	-.527	8.89×10^{-1}	1.67×10^{-1}
.5	.1403	.153	-.645	1.07	2.26×10^{-1}
.5	.1853	.171	-.850	1.37	3.34×10^{-1}
.5	.2617	.196	-1.34	2.07	6.14×10^{-1}
.5	.3	.203	-1.72	2.61	8.5×10^{-1}

TABLE F2- RESULTS FOR PURE BENDING

a/h	α/h	σ_B/σ_Y	$\sigma_{xx}(0,h)/\sigma_Y$	$\frac{4G}{1+\kappa} \frac{1}{\sigma_Y} \frac{\delta(0)}{h}$	$\frac{4G}{1+\kappa} \frac{1}{\sigma_Y} \frac{\delta(a)}{h}$	(h-b)/h
.01	.0002	.110	-.110	3.20×10^{-3}	2.24×10^{-4}	
.01	.0018	.331	-.332	1.02×10^{-2}	2.23×10^{-3}	
.01	.01	.644	-.645	2.37×10^{-2}	1.02×10^{-2}	
.01	.0313	.863	-.866	4.17×10^{-2}	2.47×10^{-2}	
.01	.0540	.956	-.961	5.56×10^{-2}	3.70×10^{-2}	
.01	.1617	1.18	-1	1.34×10^{-1}	1.11×10^{-1}	.142
.01	.2716	1.33	-1	2.99×10^{-1}	2.72×10^{-1}	.266
.1	.0007	.070	-.076	2.04×10^{-2}	7.49×10^{-4}	
.1	.0320	.459	-.505	1.48×10^{-1}	3.97×10^{-2}	
.1	.0516	.567	-.630	1.94×10^{-1}	6.39×10^{-2}	
.1	.1	.749	-.855	2.92×10^{-1}	1.26×10^{-1}	
.1	.1548	.899	-1	4.05×10^{-1}	2.07×10^{-1}	.043
.1	.1938	.985	-1	4.97×10^{-1}	2.76×10^{-1}	.122
.1	.3401	1.18	-1	1.07	7.31×10^{-1}	.331
.2	.0013	.069	-.091	4.43×10^{-2}	1.50×10^{-3}	
.2	.0124	.211	-.277	1.38×10^{-1}	1.56×10^{-2}	
.2	.0639	.469	-.643	3.41×10^{-1}	8.64×10^{-2}	
.2	.1032	.590	-.837	4.65×10^{-1}	1.48×10^{-1}	
.2	.2	.808	-1	8.03×10^{-1}	3.46×10^{-1}	.135

TABLE F2 (cont.)

a/h	α/h	σ_B/σ_Y	$\sigma_{xx}(0,h)/\sigma_Y$	$\frac{4G}{1+\kappa} \frac{1}{\sigma_Y} \frac{\delta(0)}{h}$	$\frac{4G}{1+\kappa} \frac{1}{\sigma_Y} \frac{\delta(a)}{h}$	(h-b)/h
.3	.0020	.065	-.110	7.35×10^{-2}	2.26×10^{-3}	
.3	.0283	.245	-.423	2.90×10^{-1}	3.73×10^{-2}	
.3	.1096	.485	-.914	6.70×10^{-1}	1.71×10^{-1}	
.3	.2098	.661	-1	1.19	4.24×10^{-1}	.172
.3	.3	.726	-1	2.10	9.03×10^{-1}	.297
.5	.0014	.032	-.107	1.03×10^{-1}	1.63×10^{-3}	
.5	.0131	.098	-.330	3.20×10^{-1}	1.70×10^{-2}	
.5	.0402	.172	-.606	5.95×10^{-1}	5.72×10^{-2}	
.5	.0826	.252	-.946	9.50×10^{-1}	1.34×10^{-1}	
.5	.1104	.294	-1	1.19	1.98×10^{-1}	.047
.5	.1403	.328	-1	1.47	2.82×10^{-1}	.106
.5	.1853	.360	-1	2.04	4.62×10^{-1}	.175
.5	.2024	.367	-1	2.36	5.65×10^{-1}	.194
.5	.2617	.376	-1	7.26	2.24	.226

TABLE F3- THE EFFECT OF THE FLOW STRESS RATIO $\tau = (\sigma_Y)_c/\sigma_Y$

a/h	α/h	τ	σ_B/σ_Y	$\frac{4G}{1+\kappa} \frac{1}{\sigma_Y} \frac{\delta(0)}{h}$	$\frac{4G}{1+\kappa} \frac{1}{\sigma_Y} \frac{\delta(a)}{h}$	(h-b)/h
.5	.1853	1.0	.360	2.04	4.62×10^{-1}	.175
.5	.1853	1.2	.379	1.98	4.50×10^{-1}	.123
.5	.1853	1.4	.389	1.97	4.46×10^{-1}	.078
.5	.1853	1.6	.393	1.96	4.45×10^{-1}	.038

TABLE F4 - THE EFFECT OF STRAIN HARDENING FOR THE EDGE NOTCHED BAR
SUBJECTED TO UNIFORM TENSION UNDER PLANE STRESS CONDITIONS

a/h	α/h	E_p/E	σ_o/σ_Y	$\sigma_{xx}(0,h)/\sigma_Y$	$\frac{E\delta(0)}{2\sigma_Y h}$	$\frac{E\delta(a)}{2\sigma_Y h}$
0.2	0.0639	0	0.333	0.185	2.80×10^{-1}	7.67×10^{-2}
0.2	0.0639	0.3	0.335	0.187	2.82×10^{-1}	7.69×10^{-2}
0.2	0.0639	0.6	0.338	0.189	2.84×10^{-1}	7.71×10^{-2}
0.2	0.2	0	0.489	0.175	5.35×10^{-1}	2.30×10^{-1}
0.2	0.2	0.3	0.511	0.191	5.50×10^{-1}	2.31×10^{-1}
0.2	0.2	0.6	0.568	0.209	5.68×10^{-1}	2.33×10^{-1}
0.2	0.3050	0	0.541	0.090	7.23×10^{-1}	3.62×10^{-1}
0.2	0.3050	0.3	0.609	0.142	7.63×10^{-1}	3.62×10^{-1}
0.2	0.3050	0.6	0.815	0.213	8.15×10^{-1}	3.62×10^{-1}

TABLE F5 - SAME AS TABLE 4, THE PLANE STRAIN CASE ($\nu = 0.3$)

a/h	α/h	E_p/E	σ_o/σ_Y	$\sigma_{xx}(0,h)/\sigma_Y$	$\frac{E\delta(0)}{2(1-\nu^2)\sigma_Y h}$	$\frac{E\delta(a)}{2(1-\nu^2)\sigma_Y h}$
0.2	0.0639	0.3	0.335	0.186	2.81×10^{-1}	7.69×10^{-2}
0.2	0.2	0.3	0.504	0.186	5.45×10^{-1}	2.31×10^{-1}
0.2	0.3050	0.3	0.587	0.125	7.50×10^{-1}	3.62×10^{-1}

TABLE F6 - THE EFFECT OF STRAIN HARDENING FOR THE EDGE-NOTCHED BAR UNDER
BENDING, PLANE STRESS CASE,

a/h	α/h	E_p/E	σ_B/σ_Y	$\sigma_{xx}(0,h)/\sigma_Y$	$\frac{E\delta(0)}{2\sigma_Y h}$	$\frac{E\delta(a)}{2\sigma_Y h}$
0.2	0.0639	0	0.469	- .643	3.41×10^{-1}	8.64×10^{-2}
0.2	0.0639	0.3	0.473	- .648	3.43×10^{-1}	8.67×10^{-2}
0.2	0.0639	0.6	0.477	- .653	3.46×10^{-1}	8.70×10^{-2}
*0.2	0.2	0	0.808	-1	8.03×10^{-1}	3.46×10^{-1}
0.2	0.2	0.3	0.856	-1.336	8.29×10^{-1}	3.52×10^{-1}
0.2	0.2	0.6	0.899	-1.395	8.60×10^{-1}	3.60×10^{-1}

*Results obtained from double plastic zone model.

APPENDIX G

ELASTIC-PLASTIC PROBLEM FOR A PLATE WITH A PART-THROUGH CRACK UNDER EXTENSION AND BENDING

1. Introduction

In plate and shell structures such as, for example, pipelines, tank cars, pressurized containers, ship hulls and a variety of bridge components a possible fracture failure may generally initiate from internal or surface defects which may have been introduced during manufacturing, installation, or service. If the applied load has a fluctuating component, the initial flaw may propagate subcritically. In most cases the subcritically growing crack may not penetrate through the wall during the entire service life of the structural component. However, in some cases it may be possible for a part-through crack to become critical under a peak load and the wall of the structure may locally rupture. The stability of the ensuing through crack would then depend on the nature of loading, geometry, and the existing constraints. Since the proper design procedure requires the operation of the component above the transition temperature, around a relatively deep and long part-through crack, the type of plate and shell structures under consideration would invariably contain large scale plastic deformations. Referring to Figure 1a and 1b, if the component wall is largely elastic and if the plastic deformations are confined to a small region along the crack front, then the problems of fatigue crack propagation and fracture are said to be K-controlled and an elastic solution is generally sufficient to study the problem. However, if the plastic zone spreads through the entire wall thickness around the crack as shown in Figure 1c, then the problem is highly three-dimensional and the crack may propagate and may lead to wall rupture as a consequence of either progressive growth and plastic strain instability (Figure 1d), or net ligament plastic necking instability (Figure 1e). In either case to study the problem one needs a relatively simple correlation parameter or load factor which is a realistic measure of the intensity of actual strains around the crack front and at the same time lends itself to a reasonably accurate analytical treatment. The crack opening displacement (COD) (or the crack opening stretch (COS)) is such a quantity which is one of the standardized parameters in fracture mechanics [1].

In this study the plate with a part-through crack shown in Figure 1e under membrane and bending loads is considered. The corresponding problem for a cylindrical shell with a circumferential or an axial part-through crack was considered in [2-4]. As in the shell problem the plastic deformations in the plate will be taken into account by introducing a plastic layer (of unknown size) in the plane of the crack. Reissner's Theory of plates will be used to treat the bending effects arising from the nonsymmetric orientation of the surface crack.

2. Plate Bending Problem.

Even though linearized membrane and bending formulations of the elastic plate are uncoupled, in this problem because of the existence of a plastic zone of unknown size, the problem is coupled. However, due to the particular nature of the strip model which is assumed to represent the plastic deformations, the coupling is through the boundary conditions only and, unlike the shell problem, the differential equations remain uncoupled. In this section a brief outline of the bending formulation of the cracked plate problem is given.

Using the Reissner's transverse shear theory, the bending of elastic plates may be formulated as follows (see, for example [5] and [6] for the general case):

$$\nabla^4 w = 0, \quad (1)$$

$$\frac{1-\nu}{2} \kappa \nabla^2 \Omega - \Omega = 0, \quad (2)$$

$$\kappa \nabla^2 \psi - \psi - w = 0, \quad (3)$$

$$\beta_x = \frac{\partial \psi}{\partial x} + \frac{1-\nu}{2} \kappa \frac{\partial \Omega}{\partial y}, \quad (4)$$

$$\beta_y = \frac{\partial \psi}{\partial y} - \frac{1-\nu}{2} \kappa \frac{\partial \Omega}{\partial x}, \quad (5)$$

$$M_{xx} = \frac{a^*}{h\lambda^4} \left[\frac{\partial^2 \psi}{\partial x^2} + \nu \frac{\partial^2 \psi}{\partial y^2} + \frac{\kappa}{2} (1-\nu)^2 \frac{\partial^2 \Omega}{\partial x \partial y} \right], \quad (6)$$

$$M_{yy} = \frac{a^*}{h\lambda^4} \left[\frac{\partial^2 \psi}{\partial y^2} + \nu \frac{\partial^2 \psi}{\partial x^2} - \frac{\kappa}{2} (1-\nu)^2 \frac{\partial^2 \Omega}{\partial x \partial y} \right], \quad (7)$$

$$M_{xy} = \frac{a^*(1-\nu)}{2h\lambda^4} \left[2 \frac{\partial^2 \psi}{\partial x \partial y} + \frac{\kappa}{2} (1-\nu) \left(\frac{\partial^2 \Omega}{\partial y^2} - \frac{\partial^2 \Omega}{\partial x^2} \right) \right], \quad (8)$$

$$V_x = \frac{\partial W}{\partial x} + \frac{\kappa}{2} (1-\nu) \frac{\partial \Omega}{\partial y} + \frac{\partial \psi}{\partial x}, \quad (9)$$

$$V_y = \frac{\partial W}{\partial y} - \frac{\kappa}{2} (1-\nu) \frac{\partial \Omega}{\partial x} + \frac{\partial \psi}{\partial y}. \quad (10)$$

The dimensionless quantities which appear in (1-10) are given in the Appendix and refer to the plate geometry shown in Figure 2. In the usual notation N_{ij} , M_{ij} , and V_i , ($i, j=1, 2$) are respectively the membrane, bending, and the transverse shear resultants, β_1 and β_2 are the components of the rotation vector, u_1 , u_2 , u_3 are the components of the displacement vector, and a^* is a length parameter representing the crack size.

Assuming that the problem has been reduced to one of perturbation and the external loads are local and self-equilibrating, using standard Fourier transforms the solution of the differential equations (1-3) may be expressed as follows:

$$w(x, y) = \frac{2}{\pi} \int_0^{\infty} (A_1 + yA_2) e^{-\alpha y} \cos \alpha x \, d\alpha, \quad (11)$$

$$\Omega(x, y) = \frac{2}{\pi} \int_0^{\infty} A_3 e^{-ry} \sin \alpha x \, d\alpha, \quad (12)$$

$$\psi(x, y) = \frac{2}{\pi} \int_0^{\infty} [-A_1 + (2\kappa\alpha - y)A_2] e^{-\alpha y} \cos \alpha x \, d\alpha, \quad (13)$$

where

$$r = \left[\alpha^2 + \frac{2}{\kappa(1-\nu)} \right]^{\frac{1}{2}} \quad (14)$$

and A_1 , A_2 and A_3 are (unknown) functions of α . In deriving (11-13) it is assumed that $x=0$ and $y=0$ are planes of symmetry with respect to loading and crack geometry. The symmetric bending problem is subject to the following boundary conditions:

$$M_{xy}(x,0) = 0, V_y(x,0) = 0, 0 \leq x < \infty, \quad (15a,b)$$

$$\left. \begin{aligned} M_{yy}(x,+0) &= g(x), x \in L, \\ \beta_y(x,0) &= 0, x \in L', \end{aligned} \right\} \quad (16)$$

where $(L+L') = (0,\infty)$, L refers to a system of collinear cracks and is finite. Two of the three unknown functions A_i may be eliminated by using the homogeneous conditions (15). The third one is then obtained from the mixed boundary conditions (16). The problem may be reduced to an integral equation for the unknown function defined by

$$\frac{\partial}{\partial x} \beta_y(x,0) = f(x), 0 \leq x < \infty. \quad (17)$$

Noting that $f(x) = 0$, for $x \in L'$, after rather straightforward manipulations (16) may be expressed as follows:

$$\begin{aligned} & \frac{a^*(1-\nu^2)}{2\pi h \lambda^4} \int_L \left\{ \frac{3+\nu}{1+\nu} \left(\frac{1}{t-x} + \frac{1}{t+x} \right) - \frac{4\kappa(1-\nu)}{1+\nu} \left[\frac{1}{(t-x)^3} + \frac{1}{(t+x)^3} \right] \right. \\ & \quad \left. + \frac{4}{1+\nu} \left[\frac{1}{t-x} K_2(\gamma|t-x|) + \frac{1}{t+x} K_2(\gamma|t+x|) \right] \right\} f(t) dt \\ & = g(x), \gamma = \frac{2}{\kappa(1-\nu)}, x \in L, \end{aligned} \quad (18)$$

where $K_2(z)$ is the modified Bessel function of the second kind. In the neighborhood of $z = 0$ observing that

$$K_2(z) = \frac{2}{z^2} - \frac{1}{2} + O(z^2 \log z), \quad (19)$$

equation (18) may be shown to be a singular integral equation with a

simple Cauchy-type singularity of the following form:

$$\frac{a^*(1-\nu^2)}{2\pi h\lambda^4} \int_L \left[\frac{1}{t-x} + \frac{1}{t+x} + k(t,x) + k(t,-x) \right] f(t) dt = g(x), \quad x \in L. \quad (20)$$

If $b_i < x_1 < c_i$, ($i=1, \dots, n$) defines the cracks along the x_1 axis, from (16) and (17) it follows that (18) must be solved under the following single-valuedness conditions:

$$\int_{b_i^1}^{c_i^1} f(x) dx = 0, \quad i = 1, \dots, n. \quad (21)$$

where $b_i^1 = b_i/a^*$, $c_i^1 = c_i/a^*$.

For example if the plate contains a single crack along $(-a, a)$ subjected to uniform bending moment $M_{22} = M_0$, selecting $a^* = a$ it is seen that $L = (0, 1)$ and the solution of the integral equation is of the following form:

$$f(t) = \frac{F_1(t)}{(1-t^2)^{1/2}}. \quad (22)$$

Defining now

$$\frac{hE}{4a\sigma_b} F_1(t) = F(t), \quad \sigma_b = \frac{6M_0}{h^2}. \quad (23)$$

equation (18) may be expressed as

$$\frac{1}{\pi} \int_{-1}^1 \frac{F(t)}{(1-t^2)^{1/2}} \left[\frac{3+\nu}{1+\nu} \frac{1}{t-x} - \frac{4\kappa(1-\nu)}{1+\nu} \frac{1}{(t-x)^3} + \frac{4}{1+\nu} \frac{1}{t-x} K_2(\gamma|t-x|) \right] dt = -1, \quad -1 < x < 1, \quad (24)$$

subject to

$$\int_{-1}^1 \frac{F(t)}{(1-t^2)^{1/2}} dt = 0 . \quad (25)$$

In the symmetric bending problem under consideration the stress intensity factor at a typical crack tip $x_1 = c_1$ is defined as follows:

$$k_1(x_3) = \lim_{x_1 \rightarrow c_1} [2(x_1 - c_1)]^{1/2} \sigma_{22}(x_1, 0, x_3) . \quad (26)$$

Referring to the definitions in the Appendix and, for example, to [6] for the procedure, in the single crack case the stress intensity factor ratio defined by

$$k_{bb} = k_1(h/2)/\sigma_b \sqrt{a} , \quad k_1(x_3) = \frac{x_3}{h/2} k_{bb} \sigma_b \sqrt{a} , \quad (27)$$

is found to be

$$k_{bb} = -F(1) . \quad (28)$$

Similarly, if the plate under uniform bending contains two identical cracks along $x_2 = 0$, $b < |x_1| < c$, and if we let $b' = b/a$, $c' = c/a$, and $a = (c-b)/2 = a^*$, it is seen that $L = (b', c')$ and, after normalizing the interval, the integral equation may be solved in a straightforward manner. Thus, letting

$$t = \frac{c'-b'}{2} s + \frac{c'+b'}{2} , \quad f(t) = \frac{4a\sigma_b}{hE} \frac{F(s)}{(1-s^2)^{1/2}} \quad (29)$$

the stress intensity factors at the crack tips b and c may be obtained as

$$k_{1b}(x_3) = \frac{x_3}{h/2} \sigma_b \sqrt{a} k_{bb}(b) , \quad k_{1c}(x_3) = \frac{x_3}{h/2} \sigma_b \sqrt{a} k_{bb}(c) ,$$

$$k_{bb}(b) = F(-1) , \quad k_{bb}(c) = -F(1) . \quad (30)$$

3. The Plasticity and COD

Consider now the plate with a part-through inner or surface crack subjected to uniform membrane loading. Figure 2 shows the surface crack case. Because of the nonsymmetric orientation of the crack in the thickness direction, the plate will be under bending as well as membrane loading and some local bulging will take place. It will be assumed that the material behavior, the load level, and the crack dimensions are such that the yielding spreads through the entire plate wall in some neighborhood of the crack. Let $2a$ and d be the dimensions of an inner planar crack, c be the distance from the centerline of the crack to the surface ($c=d/2$ for a surface crack, $c=h/2$ for a symmetrically located crack), and p be the plastic zone size. Using a plastic strip model to account for yielding effects, it will be assumed that in the net ligament $|x_1| < a$ the membrane stress σ_{22} is constant and is equal to the flow stress σ_F of the material, and in the yield zones $a < |x_1| < a + p$ the membrane and bending resultants are N and M , respectively. p , N , and M are unknown. The flow stress σ_F represents the yield behavior of the material and is generally selected between yield and ultimate strengths.

Under the stated assumptions, referring to Figure 2 the membrane problem has the following boundary conditions:

$$\sigma_{22}(x_1, +0) = \begin{cases} -\sigma_0 + \sigma_F(h-d)/h, & |x_1| < a, \\ -\sigma_0 + N/h, & a < |x_1| < a_p, \end{cases} \quad (31)$$

$$u_2(x_1, 0) = 0, \quad |x_1| > a_p, \quad a_p = a + p \quad (32)$$

$$\sigma_{12}(x_1, 0) = 0, \quad -\infty < x_1 < \infty. \quad (33)$$

Defining

$$\frac{\partial}{\partial x_1} u_2(x_1, 0) = \phi(x_1), \quad (34)$$

the membrane problem may be formulated as

$$\frac{E}{2\pi} \int_{-a_p}^{a_p} \frac{\phi(t)}{t-x_1} dt = \begin{cases} -\sigma_0 + \sigma_F(h-d)/h, & |x_1| < a, \\ -\sigma_0 + \sigma, & a < |x_1| < a_p, \sigma = \frac{N}{h}, \end{cases} \quad (35)$$

subject to

$$\int_{-a_p}^{a_p} \phi(t) dt = 0. \quad (36)$$

The general formulation of the bending problem is given by (18) and (21). Again, referring to the assumptions stated above regarding the crack geometry and the plastic strip model, these equations must be solved under

$$a^* = a_p = a+p, L = (0,1), x = x_1/a_p, g(x) = M_{22}(x_1, +0),$$

$$M_{22}(x_1, +0) = \begin{cases} -\frac{\sigma_F}{2} [(c+\frac{d}{2})(h-c-\frac{d}{2}) - (h-c+\frac{d}{2})(c-\frac{d}{2})], & |x_1| < a, \\ M, & a < |x_1| < a_p. \end{cases} \quad (37)$$

The three additional unknown constants p , N (or $\sigma = N/h$), and M which appear in the formulation of the problem are obtained from the conditions of finiteness of stresses at $x_1 = \pm a_p$ and the yield condition in $a < |x_1| < a_p$, which may be expressed as

$$k_{1m} = 0, \quad (38)$$

$$k_{1b} = 0, \quad (39)$$

$$\left(\frac{\sigma}{\sigma_F}\right)^2 + \frac{4|M|}{\sigma_F h^2} = 1 \quad (40)$$

where subscripts m and b refer to the membrane and bending components of the mode I stress intensity factor at $x_1 = a_p$.

Following, for example, [7] the solution of the membrane problem satisfying (38) may be obtained as

$$\phi(x_1) = \frac{2}{\pi E} \left(\frac{h-d}{h} \sigma_F - \sigma \right) \left(\cosh^{-1} \left| \frac{m}{a-x_1} + n \right| - \cosh^{-1} \left| \frac{m}{a+x_1} + n \right| \right), \quad (41)$$

$$u_2(x_1, 0) = \frac{2}{\pi E} \left(\frac{h-d}{h} \sigma_F - \sigma \right) \left[(x_1 - a) \cosh^{-1} \left| \frac{m}{a-x_1} + n \right| - (x_1 + a) \cosh^{-1} \left| \frac{m}{a+x_1} + n \right| \right], \quad (42)$$

$$\frac{a}{a+p} = \cos \frac{\pi[(h-d)\sigma_F - h\sigma_0]}{2[(h-d)\sigma_F - h\sigma]} = \cos \theta \quad (43)$$

where

$$m = (a_p^2 - a^2)/a_p, \quad n = a/a_p, \quad a_p = a + p. \quad (44)$$

Equation (42) corresponds to one half of the crack opening displacement contributed by the membrane loading. For example, at $x=0$ and $x=a$ we have

$$\delta_m(0) = 2 u_2(0, 0) = \frac{8}{\pi} \frac{a\sigma_F}{E} \left(\frac{\sigma}{\sigma_F} - 1 + \frac{d}{h} \right) \log \left(\frac{1+\sin\theta}{\cos\theta} \right), \quad (45)$$

$$\delta_m(a) = 2 u_2(a, 0) = - \frac{8}{\pi} \frac{a\sigma_F}{E} \left(\frac{\sigma}{\sigma_F} - 1 + \frac{d}{h} \right) \log (\cos\theta). \quad (46)$$

After solving the integral equation for bending which is given by (18) under the conditions (37), the crack opening displacement due to bending may be obtained as

$$\delta_b(x_1, x_3) = x_3 \beta_2(x_1, 0) = x_3 \int_{-1}^{x_1/a_p} f(x) dx, \quad (47)$$

where $\beta_2(x_1, 0) = \beta_y(x, 0)$ is the crack surface rotation. The total crack opening displacement at any point on the crack surface is then given by

$$\delta(x_1, x_3) = \delta_m(x_1) + \delta_b(x_1, x_3) = 2 u_2(x_1, 0) + x_3 \int_{-1}^{x_1/a_p} f(x) dx. \quad (48)$$

Assuming again that the solution of the bending problem is given as in (22), the three unknown constants of the problem, p , σ , and M are determined from (40), (43) and

$$F_1(1) = 0 \quad (49)$$

4. Results and Discussion

The elastic problem for the symmetric bending of a cracked plate has been considered before in [8-10]. In this paper some additional results are given. As in the previous studies, it is assumed that the plate is under membrane as well as bending loads so that there is no interference of the crack surfaces on the compressive side of the plate. Because of the nature of the plate theory used in the analysis the stress intensity factors are linear functions of the thickness coordinate x_3 (see (27) and (30)). Table 1 and Figure 3 show the effect of the thickness ratio a/h and Poisson's ratio ν on the stress intensity factor. The figure also shows $(1+\nu)/(3+\nu)$ which is stated to be the asymptotic value of the stress intensity factor for "thin" plates [8,10]. The results calculated up to $a/h = 100$ are accurate. Since the bending theory of plates breaks down for $h \rightarrow 0$, as may be observed from Figure 3, the "thin plate asymptotic" does not seem to have any validity.

Table 2 and Figure 4 show some results obtained for two collinear cracks in a plate under bending. Aside from the expected results

Table 1. The effect of the Poisson's ratio ν and the thickness ratio a/h on the stress intensity factors in a cracked plate under uniform bending. $\sigma_b = 6M_0/h^2$.

a/h	$k_1(h/2)/\sigma_b\sqrt{a}$			
	$\nu=0$	$\nu=0.25$	$\nu=0.3$	$\nu=0.5$
0.5	0.7804	0.8138	0.8193	0.8383
1	0.7020	0.7409	0.7475	0.7707
2	0.6518	0.6927	0.6997	0.7247
5	0.6140	0.6560	0.6633	0.6894
10	0.5984	0.6407	0.6481	0.6746
100	0.5803	0.6231	0.6305	0.6575

to the effect that for $a \rightarrow 0$ single crack results are recovered, for $b \rightarrow 0$ the stress intensity factor at the inner tip $k_{bb}(b)$ becomes unbounded, and $k_{bb}(b)$ is always greater than $k_{bb}(c)$, it may be observed that for $b \rightarrow 0$ (or for $2a \rightarrow (b+c)$) the slope of $k_{bb}(c)$ becomes quite steep. As in all limiting cases of collinear crack problems, the smooth extrapolation of the results would correspond to the stress intensity factor in a plate containing a crack of length $2c$ "pinched" in the middle where the displacement u_2 is forced to vanish. Because of the abrupt change in the crack geometry, thus, going from two cracks ($b > 0$) to a single crack ($b = 0$), steep changes in stress intensity factors at the crack tips $\mp c$ should not be unexpected. Some sample results giving the crack opening displacement at various locations in a plate containing a part-through crack and subjected to uniform tension away from the crack region are shown in Figures 5-8. The figures clearly show

Table 2. Stress intensity factors in a plate containing two identical collinear cracks along $x_2=0$, $b < |x_1| < c$ and subjected to uniform bending moment $M_{22}=M_0$.
 $a=(c-b)/2$, $\sigma_b=6M_0/h^2$, $k_{bb}(b)=k_{1b}(h/2)/\sigma_b\sqrt{a}$,
 $k_{bb}(c)=k_{1c}(h/2)/\sigma_b\sqrt{a}$, $\nu=0.3$.

$\frac{2a}{b+c}$	$(a/h)=1$		$(a/h)=2$	
	$k_{bb}(b)$	$k_{bb}(c)$	$k_{bb}(b)$	$k_{bb}(c)$
0.1	0.7491	0.7489	0.7009	0.7008
0.2	0.7544	0.7530	0.7052	0.7041
0.3	0.7644	0.7595	0.7133	0.7094
0.4	0.7805	0.7683	0.7267	0.7167
0.5	0.8046	0.7795	0.7477	0.7262
0.6	0.8390	0.7933	0.7805	0.7385
0.7	0.8874	0.8102	0.8328	0.7545
0.8	0.9594	0.8309	0.9199	0.7760
0.9	1.0981	0.8583	1.0867	0.8076
0.95	1.2785	0.8783	1.2758	0.8316
0.96	1.3495	0.8836	1.3452	0.8379
0.97	1.4520	0.8898	1.4433	0.8451
0.98	1.6208	0.8975	1.6020	0.8541
0.99	1.9879	0.9085	1.9439	0.8664
1.0	$\rightarrow \infty$	0.9895	$\rightarrow \infty$	0.9457

the effect of the bending due to the nonsymmetric orientation of the crack in thickness direction. The crack opening displacement $\delta(x_1, x_3)$ is calculated from (48) and (49). The values given in the figures and in Table 3 are normalized with respect to $4h\sigma_F/E$. Also note that δ becomes unbounded at all locations for $\sigma_0 \rightarrow \sigma_F$.

Extensive calculated results for a part-through surface crack of depth d and length $2a$ are given in Table 3. The table shows the crack opening displacements calculated at various locations for fixed values of a_p/h ($a_p = a+p$) and d/h . The notation used in the table is (see also Figure 5)

$$\begin{aligned} AP/H &= a_p/h, \quad D/H = d/h, \quad A/H = a/h, \quad S_0/S_Y = \sigma_0/\sigma_F, \\ 2 \text{ BETA} &= 2\beta_2(0)/(4\sigma_F/E), \quad \text{COD}_0 = \delta(0,0)/(4h\sigma_F/E), \\ \text{COD}_1 &= \delta(0, h/2)/(4h\sigma_F/E), \quad \text{COD}_2 = \delta(0, \frac{h}{2}-d)/(4h\sigma_F/E), \\ \text{COD}_3 &= \delta(0, -\frac{h}{2})/(4h\sigma_F/E), \quad \text{COD}_A = \delta(a, 0)/(4h\sigma_F/E), \\ \text{COD}_4 &= \delta(a, h/2)/(4h\sigma_F/E), \quad \text{COD}_5 = \delta(a, \frac{h}{2}-d)/(4h\sigma_F/E), \\ \text{COD}_6 &= \delta(a, -h/2)/(4h\sigma_F/E). \end{aligned}$$

For $d/h = 0.7, 0.8, 0.9$ the calculations have been carried out for $a_p/h = 1, 2, 3, 4, 6, 8, 10, 12, 14, 16$, for $d/h = 0.6$, $a_p/h = 2, 3, 4, 6, \dots, 16$, and for $d/h = 0.5$, $a_p/h = 4, 6, \dots, 16$. Table 3 shows some sample results only. It may be noted that for certain crack dimensions and generally for low stress ratios σ_0/σ_F the crack opening displacement at some locations is negative. For such cases the procedure outlined in this paper is not valid.

References

1. Methods for Crack Opening Displacement Testing, British Standards Institution, DD19, 1972.
2. F. Erdogan and F. Delale, "Ductile Fracture of Pipes and Cylindrical Containers with a Circumferential Flaw", ASME paper 80-C2/PVP-68, 1980.
3. F. Erdogan, G.R. Irwin, and M. Ratwani, "Ductile Fracture of Cylindrical Vessels Containing a Large Flaw", ASTM-STP 601, pp. 191-208, 1976.

4. S. Krenk, "Influence of Transverse Shear on Plasticity around an Axial Crack in a Cylindrical Shell", Trans. of the 4th Int. Conf. on SMIRT, Vol. G5-3, 1977.
5. S. Krenk, "Influence of Transverse Shear on an Axial Crack in a Cylindrical Shell", Int. J. of Fracture, Vol. 14, p. 123, 1978.
6. F. Delale and F. Erdogan, "Transverse Shear Effect in a Circumferentially Cracked Cylindrical Shell", Quart. Appl. Math., Vol. 37, p. 239, 1979.
7. N.I. Muskhelishvili, "Singular Integral Equations", Noordhoff, Groningen, The Netherlands, 1953.
8. J.K. Knowles and N.M. Wang, "On the Bending of an Elastic Plate Containing a Crack", J. of Math. and Phys., Vol. 39, p. 223, 1960.
9. N.M. Wang, "Effects of Plate Thickness on the Bending of an Elastic Plate Containing a Crack", J. of Math. and Phys., Vol. 47, p. 371, 1968.
10. R.J. Hartranft and G.C. Sih, "Effect of Plate Thickness on the Bending Stress Distribution around Through Cracks", J. of Math. and Phys., Vol. 47, p. 276, 1968.

APPENDIX G-1

The normalized quantities:

$$x = x_1/a^*, y = x_2/a^*, z = x_3/a^*,$$

$$u = u_1/a^*, v = u_2/a^*, w = u_3/a^*,$$

$$\beta_x = \beta_1, \beta_y = \beta_2,$$

$$\sigma_{xx} = \sigma_{11}/E, \sigma_{yy} = \sigma_{22}/E, \sigma_{xy} = \sigma_{12}/E,$$

$$N_{xx} = N_{11}/hE, N_{yy} = N_{22}/hE, N_{xy} = N_{12}/hE,$$

$$M_{xx} = M_{11}/h^2E, M_{yy} = M_{22}/h^2E, M_{xy} = M_{12}/h^2E,$$

$$V_x = V_1/hB, V_y = V_2/hB,$$

$$\lambda^4 = 12(1-\nu^2)a^{*2}/h^2, \kappa = E/B\lambda^4, B = 5E/12(1+\nu).$$

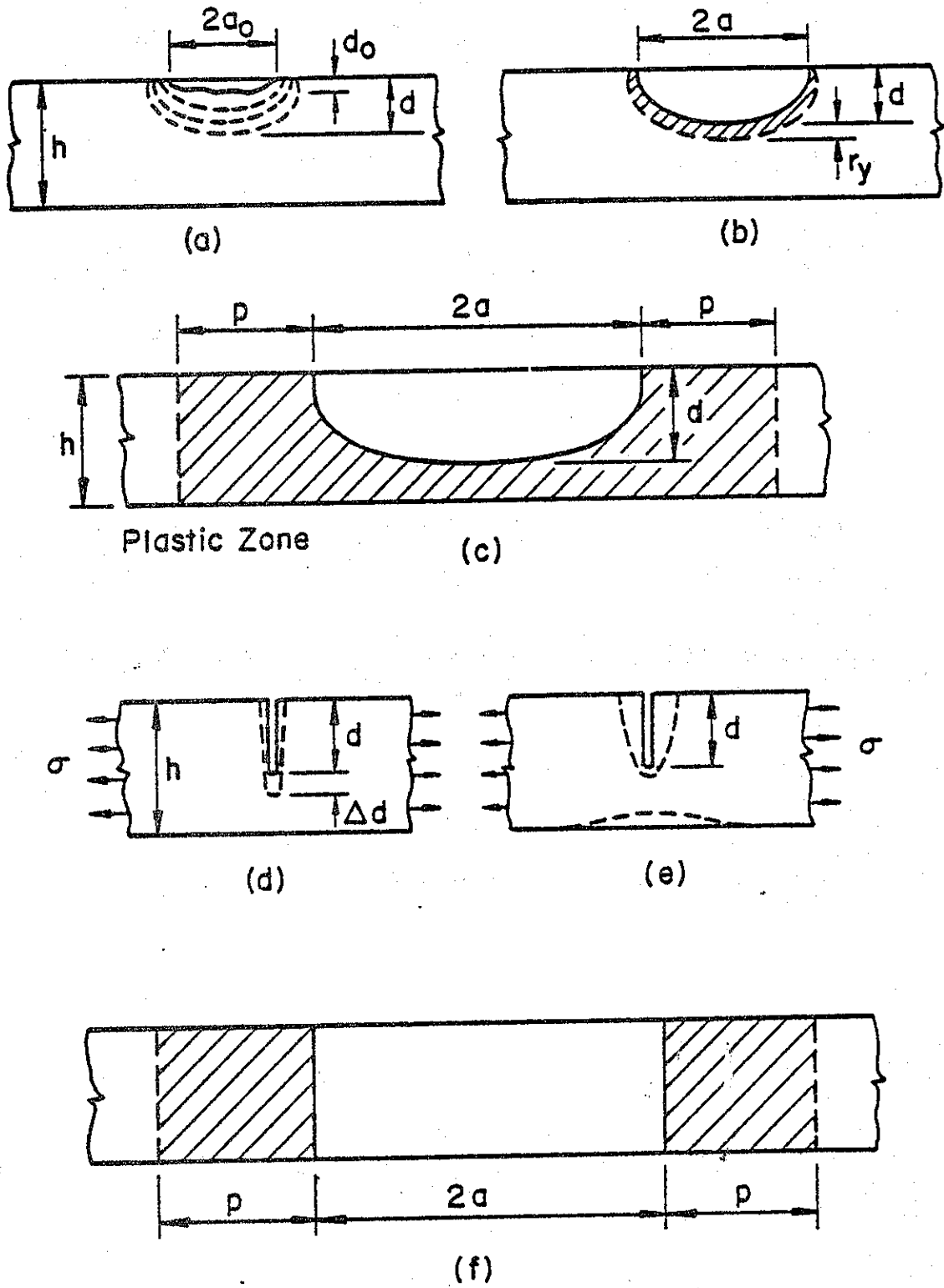


Figure G1. Formation of a through crack in plates.

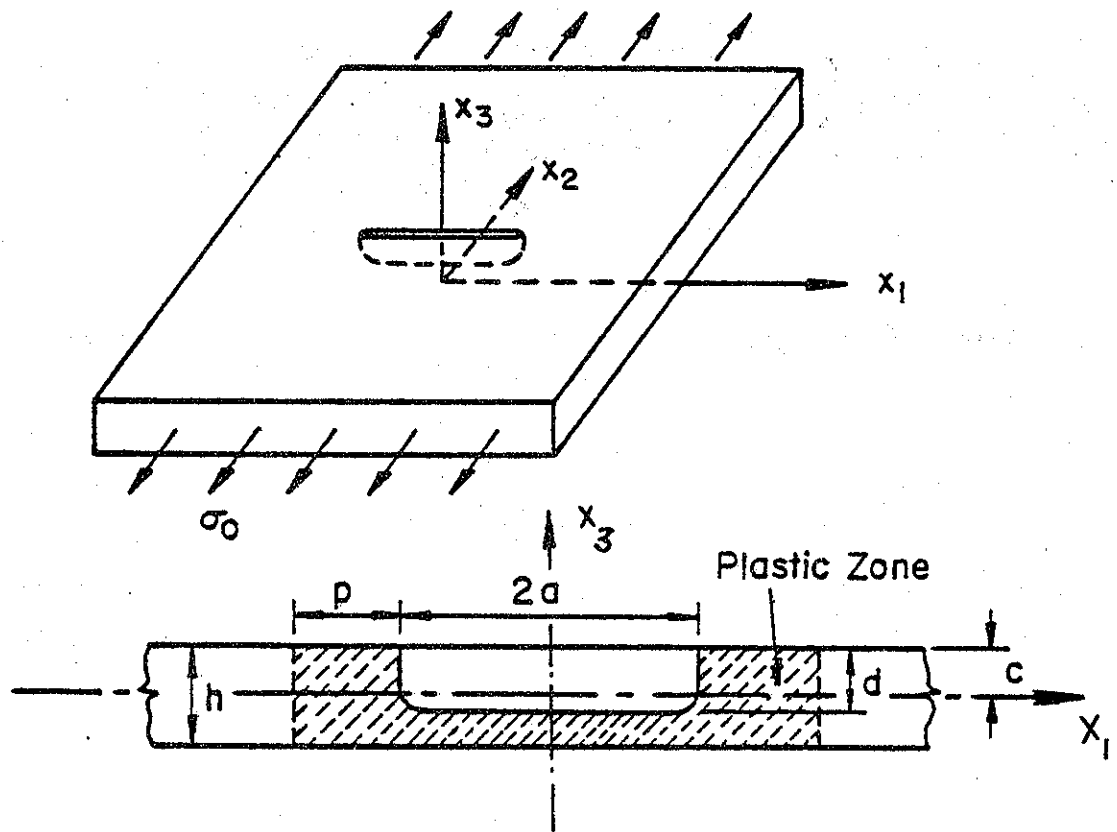


Figure G2. The plate containing a part-through crack with fully yielded net ligament.

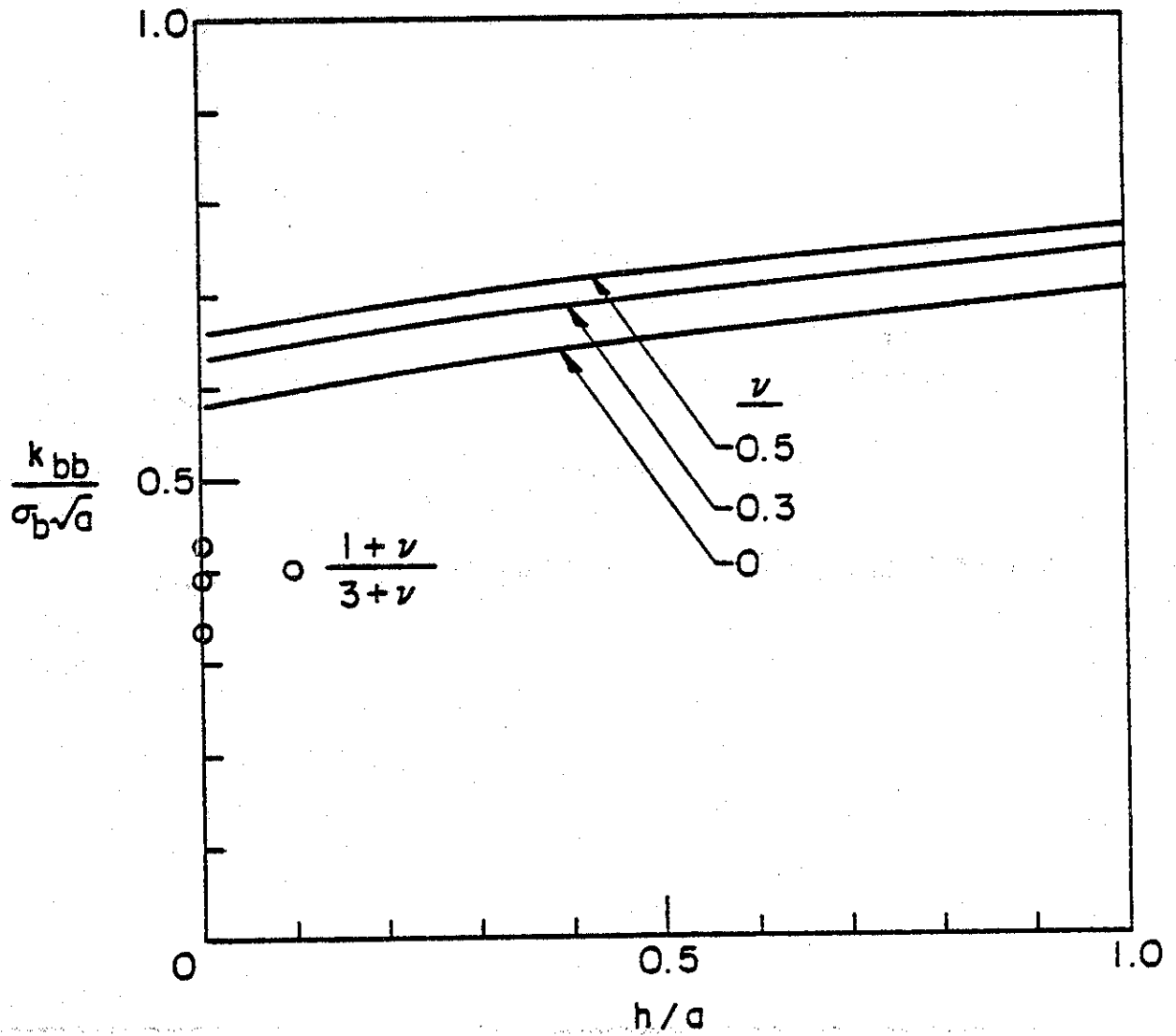


Figure G3. Stress intensity factor in a cracked plate under bending.

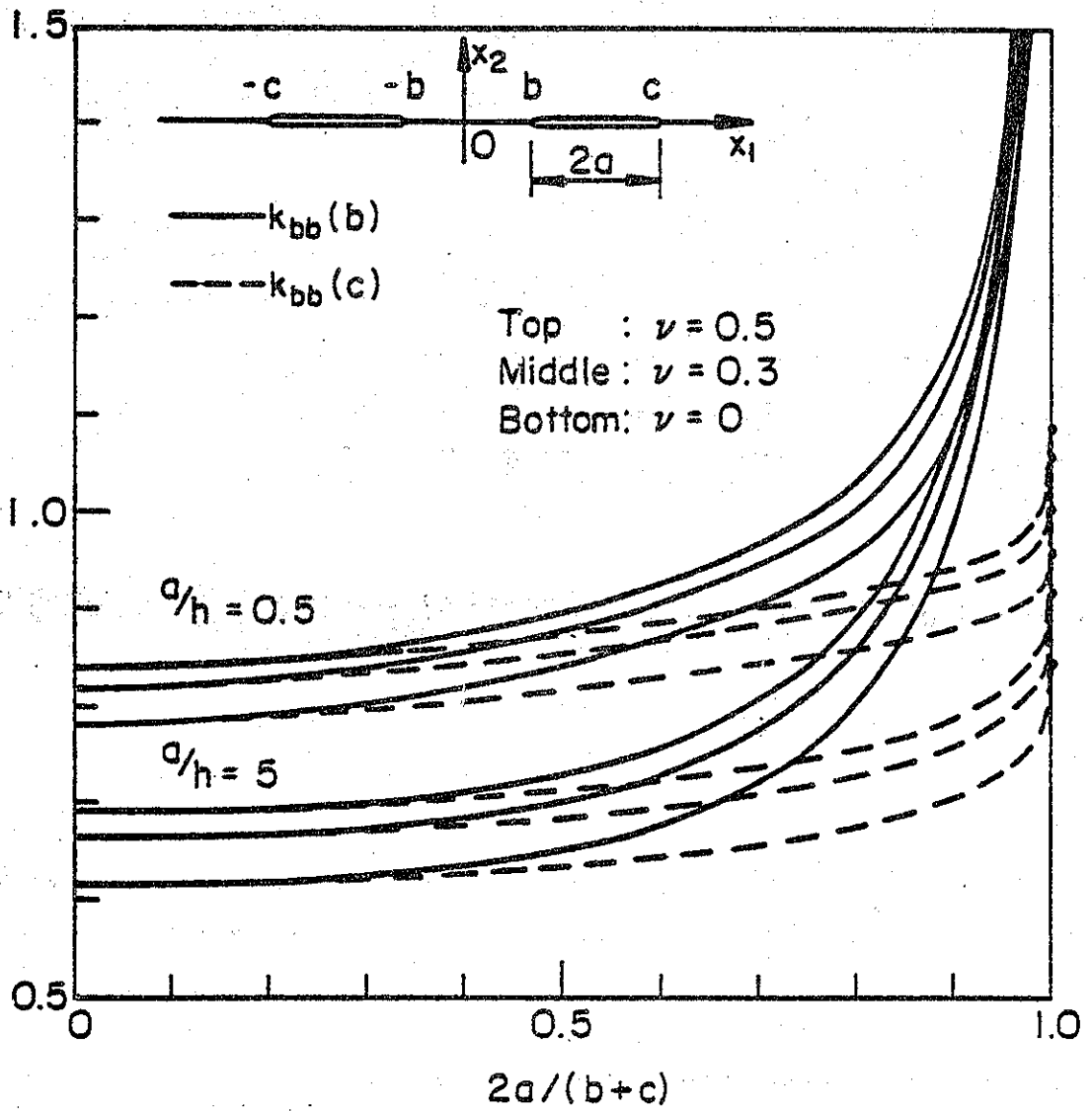


Figure G4. Stress intensity factors in a plate containing two identical collinear cracks.

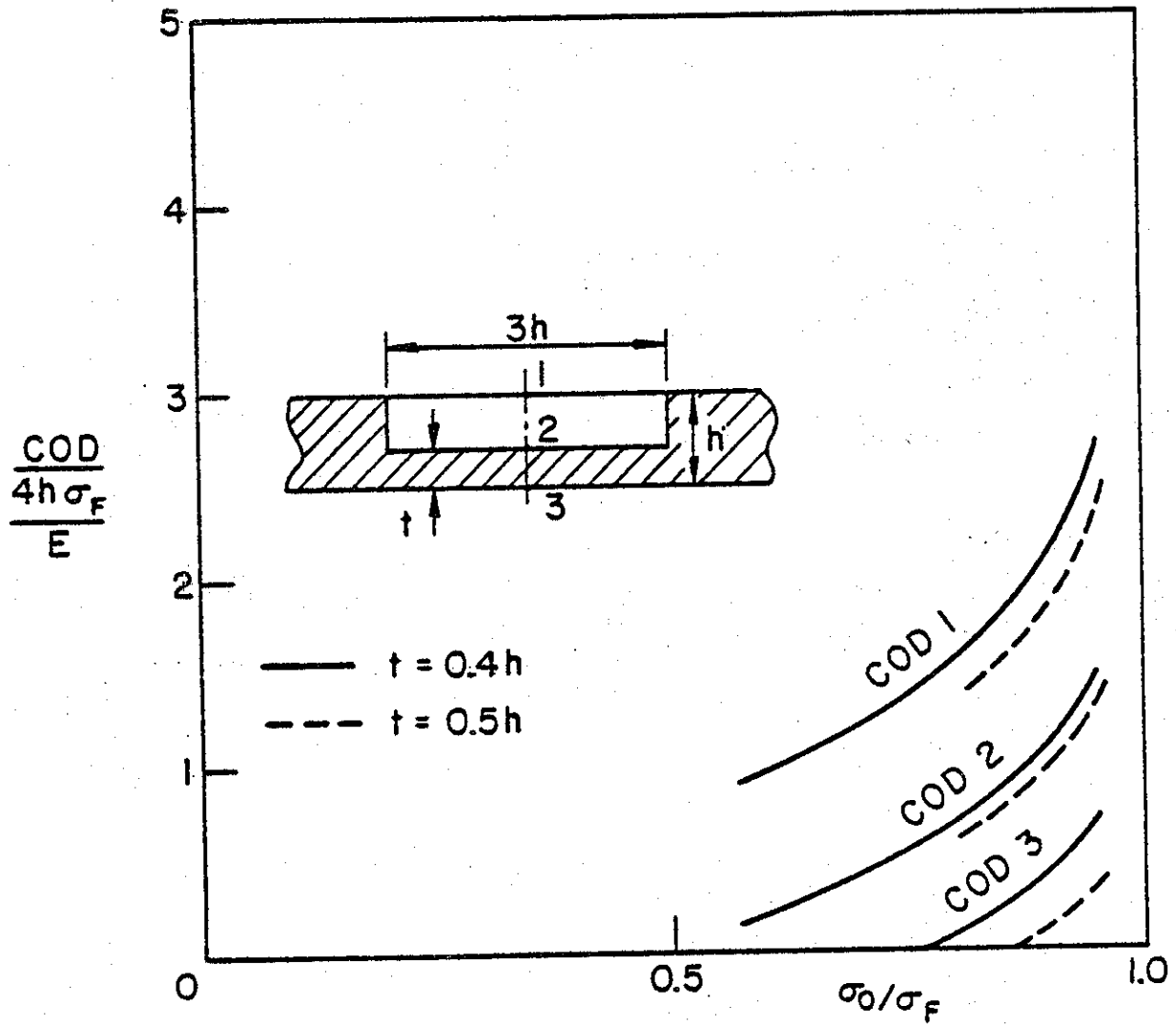


Figure G5. Crack opening displacements at locations 1, 2, and 3 in a plate under membrane stress σ_0 , $d = 0.6h$, $d = 0.5h$.

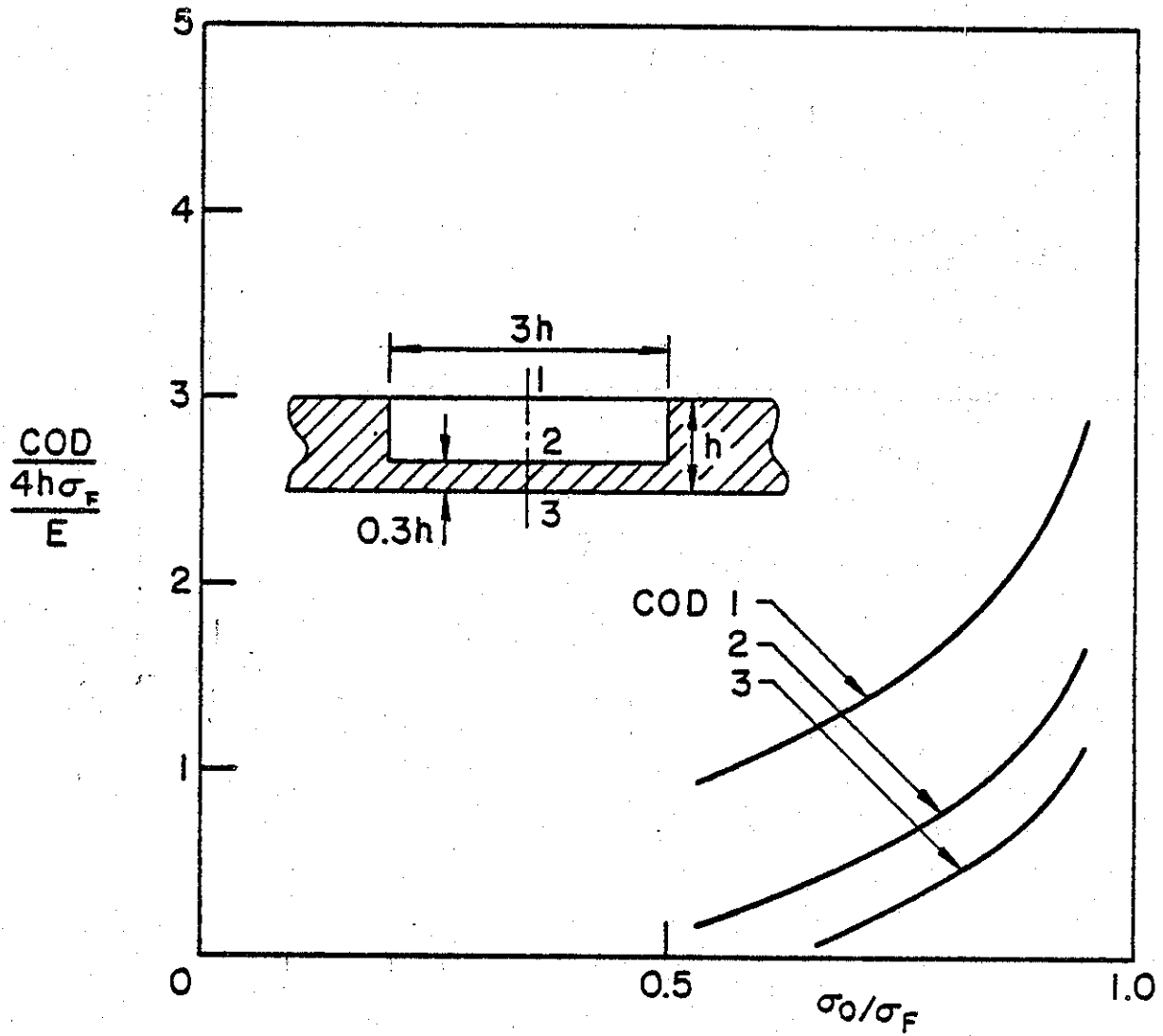


Figure G6. Same as Figure 5, $d = 0.7h$.

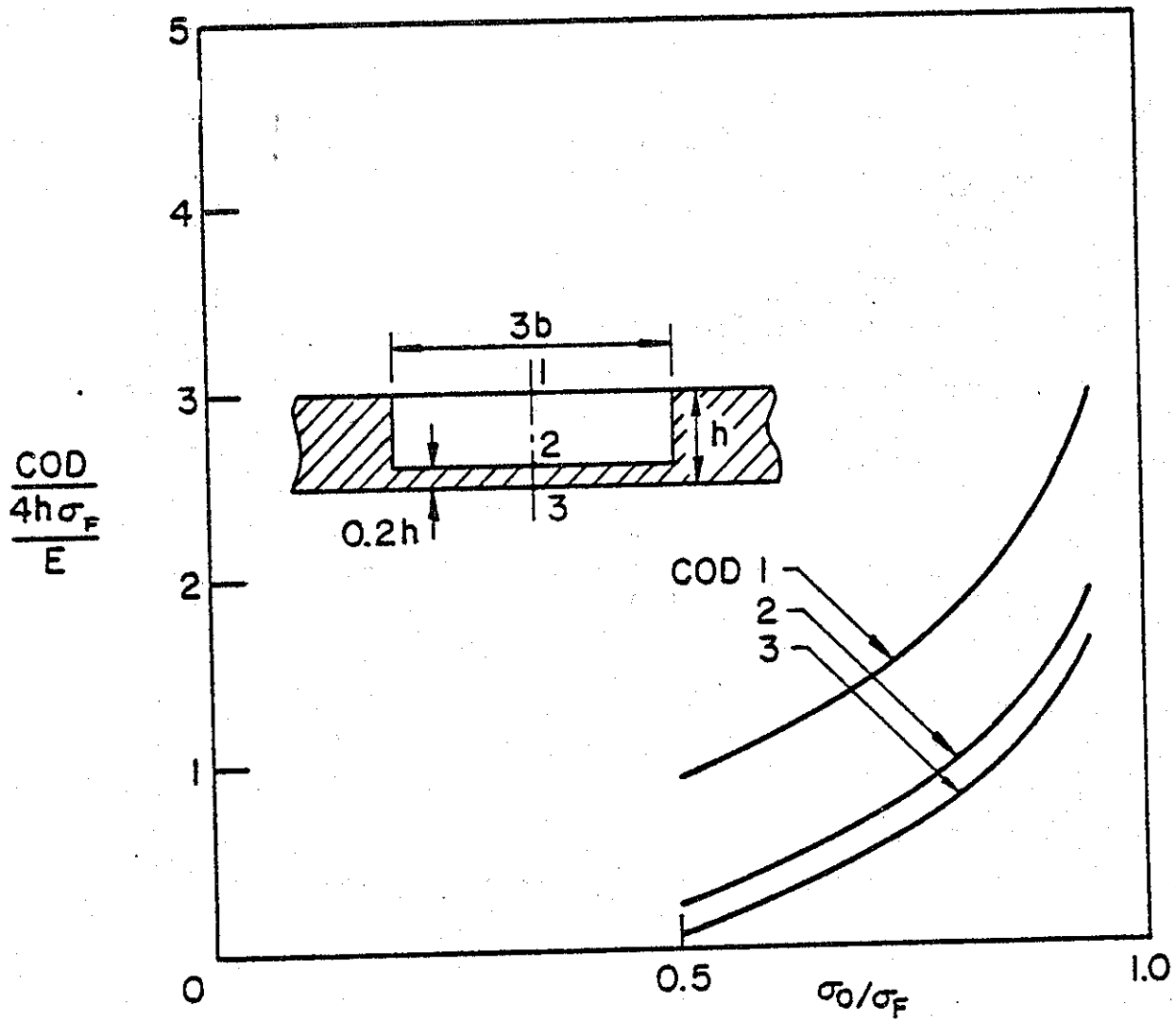


Figure G7. Same as Figure 5, $d = 0.8h$.

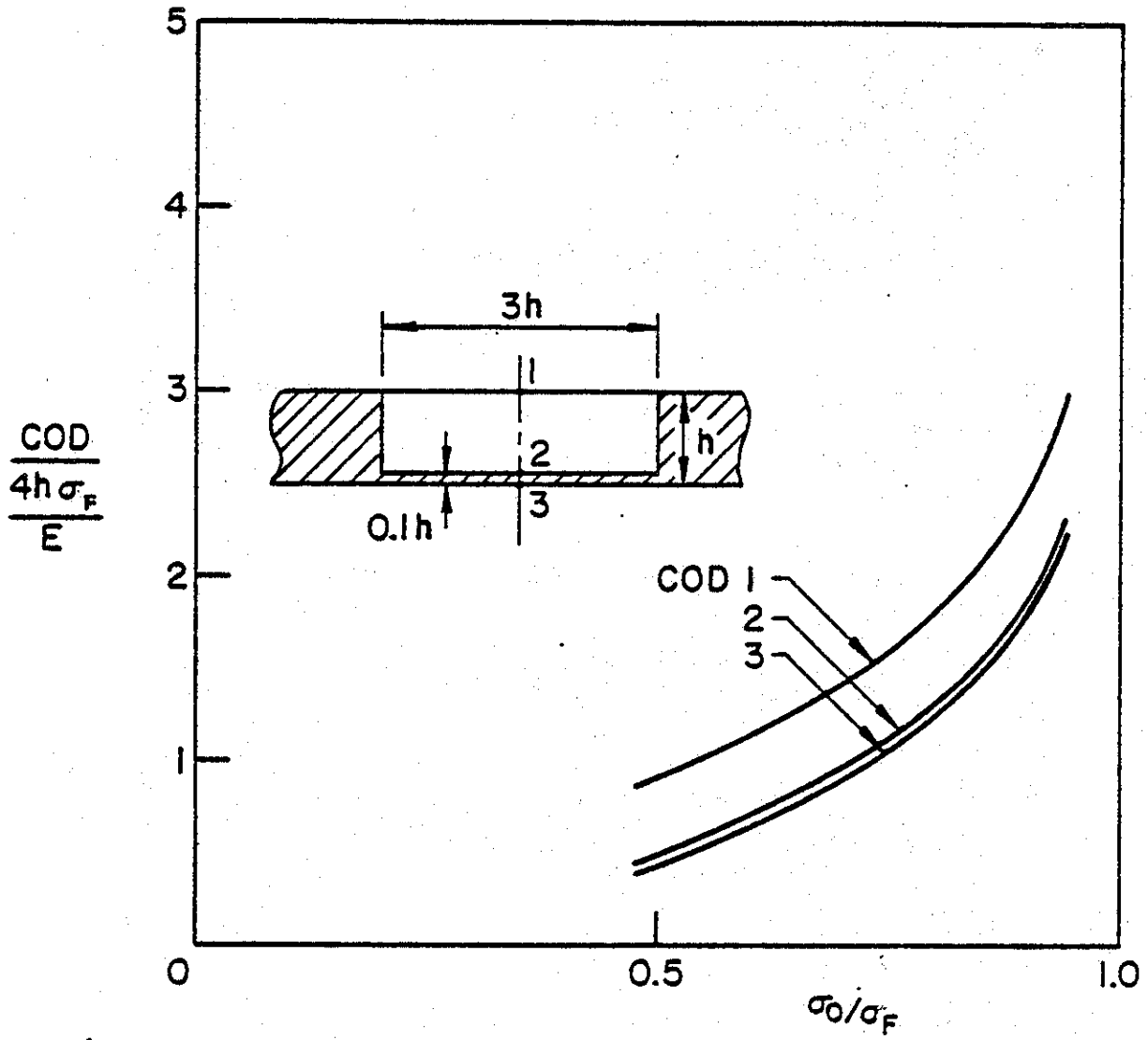


Figure G8. Same as Figure 5, $d = 0.9h$.

Table G3. CRACK SURFACE ROTATION AND CRACK OPENING DISPLACEMENTS FOR AP/H= 6.0 AND D/H= .5

A/H	S0/SY	2 BETA	G000	G001	G002	G003	G004	G005	G006
5.4578	.4076	3.7400	-.5204	1.3496	-.5204	-2.3904	-.1115	.2050	-.4287
5.3760	.4476	3.7026	-.2922	1.5592	-.2922	-2.1435	-.0672	.2785	-.4049
5.2887	.4730	3.6526	-.1487	1.6827	-.1487	-1.9808	-.0366	.3205	-.3936
5.1982	.4940	3.6200	-.0326	1.7774	-.0326	-1.8426	-.0085	.3669	-.3839
5.0984	.5120	3.5748	.0690	1.8564	.0690	-1.7184	.0192	.4120	-.3736
4.9954	.5384	3.5271	.1614	1.9249	.1614	-1.6021	.0474	.4567	-.3619
4.8875	.5472	3.4769	.2470	1.9854	.2470	-1.4914	.0765	.5014	-.3484
4.7746	.5635	3.4242	.3272	2.0393	.3272	-1.3849	.1065	.5461	-.3331
4.6569	.5795	3.3690	.4027	2.0872	.4027	-1.2818	.1375	.5909	-.3159
4.5345	.5952	3.3113	.4739	2.1296	.4739	-1.1817	.1693	.6359	-.2960
4.4076	.6108	3.2512	.5410	2.1667	.5410	-1.0846	.2019	.6799	-.2760
4.2762	.6262	3.1886	.6041	2.1984	.6041	-.9902	.2351	.7237	-.2535
4.1405	.6415	3.1235	.6630	2.2248	.6630	-.8987	.2687	.7668	-.2295
4.0006	.6568	3.0558	.7178	2.2457	.7178	-.8101	.3024	.8087	-.2040
3.8567	.6720	2.9856	.7683	2.2611	.7683	-.7245	.3359	.8493	-.1774
3.7090	.6871	2.9127	.8143	2.2706	.8143	-.6420	.3692	.8888	-.1497
3.5574	.7022	2.8370	.8557	2.2743	.8557	-.5628	.4017	.9247	-.1212
3.4024	.7173	2.7586	.8924	2.2717	.8924	-.4870	.4334	.9588	-.0921
3.2438	.7323	2.6774	.9240	2.2627	.9240	-.4147	.4637	.9900	-.0626
3.0821	.7473	2.5931	.9503	2.2469	.9503	-.3462	.4924	1.0178	-.0329
2.9172	.7623	2.5058	.9712	2.2241	.9712	-.2817	.5191	1.0417	-.0034
2.7494	.7773	2.4153	.9863	2.1939	.9863	-.2214	.5434	1.0612	.0256
2.5788	.7922	2.3214	.9953	2.1560	.9953	-.1654	.5649	1.0758	.0539
2.4056	.8072	2.2239	.9979	2.1098	.9979	-.1141	.5830	1.0849	.0812
2.2300	.8221	2.1227	.9937	2.0558	.9937	-.0677	.5973	1.0878	.1069
2.0521	.8369	2.0174	.9822	1.9909	.9822	-.0265	.6072	1.0837	.1308
1.8722	.8519	1.9076	.9630	1.9168	.9630	.0092	.6120	1.0718	.1523
1.6904	.8667	1.7930	.9354	1.8319	.9354	.0389	.6110	1.0510	.1709
1.5069	.8815	1.6729	.8988	1.7352	.8988	.0623	.6032	1.0283	.1861
1.3219	.8964	1.5465	.8522	1.6254	.8522	.0789	.5877	.9783	.1971
1.1355	.9112	1.4127	.7945	1.5000	.7945	.0882	.5631	.9231	.2031
.9480	.9260	1.2695	.7242	1.3589	.7242	.0894	.5277	.8525	.2030
.7556	.9408	1.1140	.6391	1.1961	.6391	.0821	.4793	.7634	.1952
.5703	.9556	.9404	.5361	1.0063	.5361	.0659	.4144	.6510	.1778

CRACK SURFACE ROTATION AND CRACK OPENING DISPLACEMENTS FOR AP/H= 10.0 AND D/H= .5

A/H	Sθ/SY	2 BETA	COD0	COD1	COD2	COD3	COD4	COD5	COD6
0.9599	.4083	5.9164	-.0526	2.1056	-.0526	-3.0100	-.1962	-.1962	-.7070
0.8145	.4466	5.0510	-.4911	2.4344	-.4911	-3.8166	-.4223	-.1208	-.6639
0.6603	.4720	5.7016	-.2460	2.6440	-.2460	-3.1376	.5090	-.0646	-.6303
0.4973	.4949	5.7082	-.0455	2.8006	-.0455	-2.0996	.5905	-.0126	-.6150
0.3257	.5149	5.6309	.1319	2.9474	.1319	-2.6036	.6704	.0307	-.5929
0.1458	.5336	5.5497	.2932	3.0680	.2932	-2.8016	.7496	.0900	-.5681
7.9576	.5515	5.4644	.4422	3.1744	.4422	-2.2900	.0287	.1439	-.5409
7.7615	.5684	5.3752	.5810	3.2606	.5810	-2.1066	.9076	.1983	-.5109
7.5575	.5057	5.2019	.7107	3.3517	.7107	-1.9302	.9061	.2540	-.4702
7.3459	.6022	5.1046	.8321	3.4244	.8321	-1.7602	1.0630	.3106	-.4426
7.1269	.6105	5.0030	.9455	3.4070	.9455	-1.5961	1.1404	.3600	-.4044
6.9008	.6346	4.9773	1.0510	3.5396	1.0510	-1.4377	1.2155	.4259	-.3638
6.6677	.6506	4.0674	1.1406	3.5023	1.1406	-1.2051	1.2086	.4030	-.3209
6.4279	.6664	4.7530	1.2304	3.6149	1.2304	-1.1381	1.3591	.5415	-.2761
6.1816	.6020	4.6343	1.3201	3.6373	1.3201	-.9970	1.4265	.5905	-.2295
5.9291	.6976	4.5110	1.3936	3.6491	1.3936	-.8619	1.4902	.6543	-.1816
5.6706	.7131	4.3030	1.4506	3.6502	1.4506	-.7329	1.5495	.7004	-.1320
5.4064	.7286	4.2503	1.5149	3.6400	1.5149	-.6103	1.6038	.7603	-.0833
5.1368	.7439	4.1126	1.5620	3.6103	1.5620	-.4943	1.6523	.8093	-.0336
4.8620	.7592	3.9697	1.5996	3.5845	1.5996	-.3852	1.6942	.8550	.0159
4.5823	.7745	3.0215	1.6273	3.5301	1.6273	-.2834	1.7200	.8966	.0645
4.2979	.7897	3.6676	1.6447	3.4704	1.6447	-.1891	1.7558	.9334	.1119
4.0093	.8049	3.5077	1.6510	3.4049	1.6510	-.1020	1.7719	.9647	.1574
3.7166	.8201	3.3415	1.6459	3.3166	1.6459	-.0249	1.7704	.9894	.2005
3.4202	.8352	3.1605	1.6204	3.2126	1.6204	.0442	1.7731	1.0067	.2403
3.1203	.8503	2.9800	1.5979	3.0919	1.5979	.0309	1.7540	1.0155	.2763
2.8173	.8653	2.7994	1.5533	2.9530	1.5533	.0166	1.7217	1.0145	.3074
2.5115	.8804	2.6017	1.4934	2.7942	1.4934	.0025	1.6719	1.0023	.3327
2.2031	.8954	2.3930	1.4168	2.6136	1.4168	.0199	1.6030	.9770	.3511
1.8925	.9104	2.1739	1.3215	2.4004	1.3215	.0345	1.5122	.9366	.3610
1.5800	.9254	1.9399	1.2051	2.1750	1.2051	.0491	1.3956	.8782	.3607
1.2659	.9403	1.6801	1.0639	1.9000	1.0639	.0639	1.2400	.7979	.3470
.9506	.9553	1.4122	.0920	1.5909	.0920	.0787	1.0617	.6902	.3107
.6342	.9702	1.0984	.6826	1.2310	.6826	.1334	.8239	.5456	.2674

CRACK SURFACE ROTATION AND CRACK OPENING DISPLACEMENTS FOR AP/H= 14.0 AND D/H= .5

A/H	S0/SY	Z BETA	COD0	CO01	CO02	CO03	CO04	CO05	CO06
12.3403	.4261	8.0319	-.9509	3.0658	-.9509	-4.9668	.4947	-.2339	-.9625
12.1244	.4586	7.9366	-.5267	3.4416	-.5267	-4.9950	.6348	-.1379	-.9106
11.8962	.4838	7.8358	-.2038	3.7441	-.2038	-4.1217	.7589	-.0566	-.8721
11.6560	.5057	7.7295	.0710	3.9357	.0710	-3.7938	.8776	.0208	-.8359
11.4041	.5259	7.6178	.3157	4.1246	.3157	-3.4932	.9940	.0977	-.7986
11.1407	.5448	7.5004	.5387	4.2889	.5387	-3.2415	1.1092	.1753	-.7505
10.8661	.5630	7.3774	.7445	4.4332	.7445	-2.9442	1.2234	.2542	-.7151
10.5805	.5805	7.2487	.9355	4.5539	.9355	-2.6089	1.3366	.3343	-.6661
10.2843	.5977	7.1143	1.1132	4.6704	1.1132	-2.4440	1.4484	.4155	-.6174
9.9777	.6145	6.9741	1.2785	4.7659	1.2785	-2.2806	1.5583	.4976	-.5631
9.6611	.6310	6.8279	1.4316	4.8458	1.4316	-1.9822	1.6659	.5802	-.5055
9.3348	.6473	6.6758	1.5734	4.9113	1.5734	-1.7645	1.7704	.6628	-.4449
8.9990	.6634	6.5175	1.7033	4.9621	1.7033	-1.5554	1.8711	.7448	-.3815
8.6542	.6794	6.3531	1.8215	4.9980	1.8215	-1.3558	1.9674	.8258	-.3158
8.3007	.6953	6.1822	1.9277	5.0188	1.9277	-1.1634	2.0583	.9050	-.2483
7.9388	.7110	6.0049	2.0216	5.0248	2.0216	-.9808	2.1429	.9818	-.1794
7.5690	.7266	5.8208	2.1029	5.0133	2.1029	-.8075	2.2205	1.0554	-.1097
7.1915	.7422	5.6298	2.1712	4.9861	2.1712	-.6437	2.2898	1.1250	-.0390
6.8068	.7577	5.4315	2.2268	4.9417	2.2268	-.4898	2.3499	1.1898	.0281
6.4152	.7731	5.2257	2.2666	4.8795	2.2666	-.3463	2.3996	1.2489	.0981
6.0171	.7885	5.0121	2.2925	4.7955	2.2925	-.2135	2.4376	1.3012	.1640
5.6130	.8038	4.7900	2.3029	4.6979	2.3029	-.0921	2.4624	1.3456	.2287
5.2033	.8191	4.5591	2.2970	4.5765	2.2970	.0175	2.4725	1.3809	.2892
4.7883	.8343	4.3186	2.2738	4.4331	2.2738	.1145	2.4663	1.4057	.3452
4.3625	.8495	4.0676	2.2321	4.2859	2.2321	.1983	2.4416	1.4186	.3956
3.9443	.8647	3.8053	2.1706	4.0732	2.1706	.2679	2.3962	1.4177	.4393
3.5161	.8798	3.5302	2.0875	3.8226	2.0875	.3225	2.3273	1.4011	.4748
3.0843	.8949	3.2406	1.9810	3.6013	1.9810	.3607	2.2318	1.4011	.5005
2.6495	.9100	2.9344	1.8482	3.3154	1.8482	.3818	2.1054	1.3899	.5144
2.2120	.9250	2.6082	1.6858	2.9899	1.6858	.3816	1.9429	1.2285	.5140
1.7723	.9401	2.2576	1.4886	2.6174	1.4886	.3598	1.7369	1.1164	.4959
1.3308	.9551	1.8749	1.2494	2.1868	1.2494	.3119	1.4766	.9650	.4551
.8879	.9701	1.4450	.9553	1.6778	.9553	.2320	1.1441	.7637	.3832

CRACK SURFACE ROTATION AND CRACK OPENING DISPLACEMENTS FOR AP/H= 6.0 AND O/H= .6

A/H	S0/SY	2 BETA	C000	C001	C002	C003	C004	C005	C006
5.4578	.3604	3.5904	-.2230	1.5722	-.5920	-2.0181	-.6478	.2568	-.3523
5.3760	.3920	3.5545	.0444	1.7329	-.3998	-1.6216	-.0102	.3140	-.3344
5.2807	.4163	3.5161	.0902	1.8482	-.2615	-1.6679	.0222	.3649	-.3206
5.1962	.4376	3.4752	.2052	1.9426	-.1423	-1.5324	.0537	.4141	-.3066
5.0924	.4574	3.4318	.3087	2.0246	-.0345	-1.4072	.0857	.4628	-.2913
4.9954	.4761	3.3860	.4042	2.0972	.0656	-1.2868	.1187	.5116	-.2742
4.8875	.4943	3.3378	.4935	2.1624	.1597	-1.1794	.1528	.5607	-.2551
4.7746	.5121	3.2872	.5775	2.2211	.2488	-1.0661	.1880	.6108	-.2341
4.6569	.5296	3.2342	.6568	2.2739	.3334	-.9583	.2242	.6595	-.2110
4.5345	.5470	3.1789	.7316	2.3218	.4137	-.8579	.2614	.7089	-.1861
4.4076	.5642	3.1212	.8019	2.3625	.4824	-.7587	.2993	.7581	-.1595
4.2762	.5813	3.0611	.8677	2.3983	.5616	-.6628	.3377	.8068	-.1313
4.1405	.5983	2.9986	.9291	2.4283	.6292	-.5702	.3765	.8547	-.1017
4.0006	.6153	2.9336	.9857	2.4525	.6923	-.4811	.4152	.9013	-.0709
3.8567	.6323	2.8662	1.0374	2.4705	.7508	-.3957	.4536	.9464	-.0392
3.7090	.6492	2.7962	1.0841	2.4822	.8045	-.3139	.4915	.9896	-.0066
3.5574	.6660	2.7236	1.1256	2.4874	.8532	-.2362	.5284	1.0305	-.0264
3.4024	.6829	2.6483	1.1615	2.4857	.8957	-.1626	.5641	1.0685	.0597
3.2438	.6997	2.5703	1.1917	2.4768	.9347	-.0934	.5981	1.1033	.0929
3.0821	.7165	2.4894	1.2159	2.4606	.9669	-.0288	.6300	1.1343	.1257
2.9172	.7332	2.4056	1.2337	2.4365	.9931	.0309	.6594	1.1611	.1578
2.7494	.7500	2.3187	1.2449	2.4042	1.0130	.0855	.6859	1.1830	.1880
2.5788	.7667	2.2285	1.2490	2.3633	1.0262	.1348	.7089	1.1994	.2184
2.4056	.7835	2.1350	1.2458	2.3133	1.0323	.1783	.7279	1.2097	.2461
2.2300	.8002	2.0378	1.2347	2.2536	1.0309	.2158	.7422	1.2138	.2714
2.0521	.8169	1.9367	1.2152	2.1835	1.0215	.2468	.7513	1.2087	.2939
1.8722	.8336	1.8313	1.1867	2.1024	1.0036	.2710	.7542	1.1956	.3128
1.6904	.8502	1.7213	1.1486	2.0092	.9764	.2874	.7502	1.1727	.3277
1.5069	.8669	1.6068	1.0999	1.9029	.9393	.2969	.7382	1.1386	.3378
1.3219	.8836	1.4846	1.0397	1.7820	.8912	.2973	.7170	1.0920	.3420
1.1355	.9002	1.3561	.9665	1.6446	.8309	.2884	.6850	1.0306	.3394
.9480	.9169	1.2187	.8786	1.4880	.7567	.2692	.6403	.9521	.3285
.7596	.9335	1.0695	.7735	1.3082	.6665	.2387	.5801	.8528	.3074
.5703	.9502	.9028	.6473	1.0987	.5570	.1959	.5004	.7275	.2733

CRACK SURFACE ROTATION AND CRACK OPENING DISPLACEMENTS FOR AP/H= 10.0 AND D/H= .6

A/H	S0/SY	2 BETA	CO00	CO01	CO02	CC03	CO04	CO05	CO06
0.9599	.3622	5.6797	-.3509	2.4090	-.9168	-2.1907	-.0407	-.1798	-.5719
0.8145	.3936	5.6169	-.8585	2.7500	-.6202	-2.8669	-.0144	-.1107	-.5150
0.6603	.4187	5.5503	.1782	2.9684	-.3848	-2.6049	.0446	-.0656	-.5061
0.4973	.4411	5.4873	.3684	3.1084	-.1796	-2.3715	.1023	-.0135	-.4767
0.3257	.4619	5.4057	.5755	3.2503	.0069	-2.1554	.1608	-.0395	-.4456
0.1458	.4817	5.3277	.7125	3.3764	.1798	-1.9513	.2286	.0941	-.4120
7.9576	.5009	5.2459	.8663	3.4892	.3417	-1.7567	.2819	.1584	-.3755
7.7615	.5196	5.1602	1.0191	3.5902	.4941	-1.5700	.3448	.2085	-.3361
7.5575	.5380	5.0706	1.1448	3.6801	.6377	-1.3905	.4091	.2685	-.2938
7.3459	.5561	4.9772	1.2708	3.7594	.7731	-1.2178	.4743	.3297	-.2487
7.1269	.5740	4.8797	1.3883	3.8281	.9003	-1.0516	.5404	.3920	-.2012
6.9008	.5918	4.7782	1.4972	3.8863	1.0194	-.8919	.6067	.4551	-.1514
6.6677	.6094	4.6727	1.5976	3.9339	1.1393	-.7388	.6729	.5184	-.0996
6.4279	.6269	4.5629	1.6891	3.9786	1.2628	-.5923	.7386	.5816	-.0463
6.1816	.6443	4.4489	1.7717	3.9961	1.3268	-.4528	.8032	.6442	.0003
5.9291	.6616	4.3305	1.8449	4.0102	1.4189	-.3293	.8661	.7056	.0637
5.6706	.6785	4.2077	1.9086	4.0124	1.5478	-.1953	.9269	.7654	.1194
5.4064	.6961	4.0803	1.9623	4.0024	1.6542	-.0779	.9848	.8228	.1750
5.1368	.7132	3.9481	2.0056	3.9796	1.7187	.0315	1.0392	.8773	.2300
4.8620	.7303	3.8109	2.0380	3.9434	1.8269	.1325	1.0893	.9282	.2837
4.5823	.7473	3.6686	2.0590	3.8933	1.9222	.2247	1.1345	.9747	.3357
4.2979	.7643	3.5209	2.0682	3.8286	2.0161	.3077	1.1758	1.0161	.3851
4.0093	.7813	3.3674	2.0647	3.7484	2.1280	.3810	1.2064	1.0514	.4314
3.7166	.7983	3.2078	2.0488	3.6519	2.2272	.4441	1.2312	1.0797	.4738
3.4202	.8152	3.0417	2.0171	3.5379	2.3129	.4962	1.2470	1.0999	.5113
3.1203	.8321	2.8685	1.9711	3.4053	2.3882	.5368	1.2527	1.1168	.5430
2.8173	.8490	2.6874	1.9088	3.2525	2.4400	.5651	1.2467	1.1110	.5679
2.5115	.8658	2.4976	1.8288	3.0776	2.4790	.5808	1.2274	1.0988	.5846
2.2031	.8826	2.2980	1.7294	2.8784	2.4936	.5808	1.1926	1.0724	.5917
1.8925	.8994	2.0869	1.6083	2.6527	2.4866	.5648	1.1399	1.0293	.5873
1.5800	.9162	1.8623	1.4625	2.3936	2.4583	.5314	1.0658	.9664	.5690
1.2659	.9330	1.6205	1.2879	2.0982	2.4029	.4776	.9659	.8795	.5338
.9506	.9498	1.3557	1.0781	1.7560	.9426	.4003	.8335	.7621	.4760
.6342	.9665	1.0544	.8224	1.3496	.7170	.2952	.6574	.6048	.3903

CRACK SURFACE ROTATION AND CRACK OPENING DISPLACEMENTS FOR AP/H= 14.0 AND D/H= .6

A/H	Sθ/SY	2 BETA	CO06	CO01	CO02	CO03	CO04	CO05	CO06
12.5439	.3345	7.7960	-.8522	3.8462	-1.6319	-4.7507	-.1961	-.3273	-.6521
12.3483	.3771	7.7106	-.2942	3.9631	-1.8652	-4.1494	-.0724	-.2122	-.7718
12.1244	.4063	7.6191	.0805	3.8981	-.6814	-3.7298	.0211	-.1273	-.7207
11.8962	.4310	7.5224	.3899	4.1511	-.3623	-3.3713	.1083	-.0483	-.6746
11.6560	.4535	7.4204	.6625	4.3727	-.8795	-3.0476	.1945	.0300	-.6280
11.4041	.4745	7.3131	.9100	4.5665	.1787	-2.7465	.2617	.1096	-.5788
11.1407	.4947	7.2004	1.1380	4.7382	.4180	-2.4622	.3704	.1911	-.5261
10.8661	.5142	7.0823	1.3497	4.8989	.6415	-2.1914	.4688	.2747	-.4697
10.5805	.5332	6.9588	1.5468	5.0263	.8510	-1.9325	.5527	.3683	-.4095
10.2843	.5518	6.8297	1.7304	5.1453	1.0474	-1.6845	.6459	.4476	-.3457
9.9777	.5702	6.6951	1.9009	5.2485	1.2314	-1.4466	.7399	.5362	-.2784
9.6611	.5884	6.5548	2.0587	5.3361	1.4032	-1.2187	.8342	.6258	-.2881
9.3348	.6063	6.4087	2.2037	5.4081	1.5628	-1.0007	.9283	.7156	-.1350
8.9990	.6241	6.2568	2.3359	5.4643	1.7102	-.7925	1.0214	.8052	-.0598
8.6542	.6418	6.0989	2.4550	5.5044	1.8451	-.5945	1.1138	.8938	.0170
8.3007	.6594	5.9349	2.5606	5.5281	1.9671	-.4068	1.2021	.9807	.0950
7.9388	.6768	5.7647	2.6525	5.5349	2.0781	-.2298	1.2882	1.0652	.1734
7.5690	.6942	5.5880	2.7301	5.5241	2.1713	-.0639	1.3701	1.1464	.2516
7.1915	.7115	5.4046	2.7929	5.4952	2.2525	.0906	1.4471	1.2235	.3289
6.8068	.7288	5.2143	2.8483	5.4474	2.3189	.2331	1.5182	1.2954	.4045
6.4152	.7460	5.0167	2.8715	5.3799	2.3699	.3632	1.5822	1.3612	.4775
6.0130	.7631	4.8116	2.8859	5.2917	2.4047	.4801	1.6379	1.4197	.5470
5.6130	.7802	4.5984	2.8825	5.1817	2.4226	.5833	1.6842	1.4697	.6120
5.2033	.7973	4.3767	2.8603	5.0406	2.4226	.6719	1.7195	1.5099	.6715
4.7883	.8143	4.1458	2.8182	4.8911	2.4036	.7453	1.7423	1.5387	.7242
4.3685	.8313	3.9049	2.7540	4.7072	2.3633	.8023	1.7508	1.5544	.7687
3.9443	.8483	3.6531	2.6684	4.4958	2.3031	.8419	1.7429	1.5551	.8036
3.5161	.8652	3.3690	2.5572	4.2517	2.2183	.8627	1.7163	1.5385	.8271
3.0843	.8822	3.1110	2.4187	3.9742	2.1876	.8632	1.6688	1.5018	.8370
2.6495	.8991	2.8470	2.2490	3.6583	1.9681	.8413	1.5946	1.4418	.8309
2.2120	.9159	2.5839	2.0463	3.2982	1.7359	.7943	1.4912	1.3540	.8053
1.7723	.9328	2.1673	1.8022	2.8859	1.5855	.7186	1.3516	1.2325	.7559
1.3308	.9496	1.7999	1.5089	2.4089	1.3289	.6089	1.1664	1.0684	.6761
.8879	.9664	1.3872	1.1512	1.8448	1.0124	.4576	.9202	.8472	.5550

CRACK SURFACE ROTATION AND CRACK OPENING DISPLACEMENTS FOR AP/H= 4.0 AND D/H= .7

A/H	S0/SY	2 BETA	COD0	COD1	COD2	COD3	COD4	COD5	COD6
3.7366	.2250	2.2312	-.0573	1.0583	-.5036	-1.1738	-.0305	.1544	-.1753
3.6894	.3200	2.2132	.0760	1.1027	-.3667	-1.0300	.0151	.1945	-.1644
3.6345	.3458	2.1942	.1721	1.2692	-.2667	-.9258	.0369	-.0404	-.1562
3.5840	.3682	2.1733	.2535	1.3401	-.1012	-.8332	.0563	.2642	-.1476
3.5250	.3888	2.1509	.3284	1.4018	-.1038	-.7491	.0803	.2981	-.1376
3.4641	.4083	2.1268	.3935	1.4559	-.0319	-.6639	.1030	.3320	-.1260
3.3903	.4271	2.1012	.4562	1.5069	.0360	-.5784	.1267	.3661	-.1127
3.3303	.4456	2.0741	.5153	1.5524	.1005	-.5217	.1513	.4004	-.0977
3.2583	.4637	2.0455	.5712	1.5940	.1621	-.4515	.1768	.4340	-.0812
3.1830	.4817	2.0154	.6242	1.6319	.2211	-.3835	.2031	.4695	-.0632
3.1046	.4996	1.9838	.6742	1.6661	.2774	-.3177	.2302	.5041	-.0438
3.0230	.5174	1.9508	.7214	1.6968	.3312	-.2548	.2570	.5387	-.0232
2.9384	.5352	1.9163	.7657	1.7238	.3824	-.1925	.2850	.5731	-.0015
2.8508	.5529	1.8804	.8069	1.7471	.4309	-.1332	.3141	.6070	.0211
2.7603	.5706	1.8430	.8451	1.7665	.4765	-.0764	.3425	.6404	.0446
2.6671	.5884	1.8042	.8801	1.7822	.5193	-.0228	.3707	.6729	.0666
2.5712	.6062	1.7638	.9117	1.7936	.5589	.0298	.3987	.7043	.0930
2.4725	.6239	1.7220	.9397	1.8007	.5953	.0787	.4260	.7343	.1177
2.3716	.6417	1.6787	.9640	1.8033	.6282	.1246	.4526	.7627	.1424
2.2682	.6596	1.6338	.9843	1.8012	.6576	.1674	.4780	.7892	.1668
2.1626	.6774	1.5873	1.0005	1.7942	.6831	.2069	.5021	.8136	.1909
2.0547	.6952	1.5391	1.0123	1.7819	.7045	.2428	.5245	.8349	.2142
1.9448	.7131	1.4893	1.0196	1.7642	.7217	.2749	.5450	.8534	.2365
1.8329	.7310	1.4376	1.0219	1.7407	.7344	.3031	.5631	.8695	.2576
1.7192	.7489	1.3840	1.0192	1.7112	.7424	.3271	.5784	.8837	.2772
1.6037	.7668	1.3285	1.0109	1.6752	.7452	.3467	.5907	.8965	.2948
1.4866	.7847	1.2708	.9969	1.6323	.7427	.3615	.5993	.9084	.3101
1.3681	.8026	1.2108	.9767	1.5820	.7345	.3713	.6030	.9144	.3220
1.2481	.8205	1.1482	.9498	1.5239	.7202	.3757	.6036	.9151	.3322
1.1269	.8384	1.0827	.9157	1.4570	.6992	.3744	.5981	.9141	.3360
1.0046	.8564	1.0138	.8738	1.3807	.6710	.3668	.5864	.9076	.3358
.8812	.8743	.9410	.8232	1.2937	.6350	.3526	.5677	.8966	.3350
.7570	.8923	.8633	.7629	1.1945	.5902	.3312	.5407	.8849	.3261
.6320	.9102	.7792	.6915	1.0811	.5357	.3019	.5039	.8685	.3093
.5064	.9282	.6864	.6071	.9503	.4699	.2640	.4553	.8268	.2838

CRACK SURFACE ROTATION AND CRACK OPENING DISPLACEMENTS FOR AP/H= 6.0 AND D/H= .7

A/H	S0/SY	2 .BETA	COO0	COO1	COO2	COO3	COO4	COO5	COO6
5.6049	.2638	3.1974	-.2075	1.3912	-.8470	-1.0062	-.0379	.1911	-.2668
5.5341	.3070	3.1706	.0400	1.6253	-.5941	-1.5453	.0079	.2562	-.0914
5.4578	.3345	3.1416	.1942	1.7650	-.4341	-1.3756	.0416	.3881	-.2249
5.3760	.3576	3.1102	.3212	1.8763	-.3009	-1.2339	.0739	.3576	-.2898
5.2887	.3787	3.0766	.4340	1.9723	-.1813	-1.1093	.1068	.4067	-.1932
5.1982	.3987	3.0408	.5370	2.0582	-.0703	-.9826	.1408	.4562	-.0147
5.0984	.4180	3.0028	.6350	2.1364	.0344	-.8664	.1764	.0444	-.1536
4.9954	.4369	2.9624	.7268	2.2082	.1342	-.7516	.2134	.0759	-.1304
4.8875	.4555	2.9206	.8138	2.2741	.2297	-.6405	.2519	.1091	-.1050
4.7716	.4740	2.8763	.8964	2.3345	.3211	-.5417	.2917	.1440	-.0775
4.6569	.4924	2.8299	.9746	2.3896	.4087	-.4403	.3327	.1804	-.0481
4.5345	.5106	2.7815	1.0485	2.4393	.4922	-.3423	.3746	.2160	-.0169
4.4076	.5289	2.7310	1.1179	2.4834	.5717	-.2473	.4173	.2567	.0158
4.2762	.5471	2.6785	1.1827	2.5219	.6470	-.1565	.4603	.2962	.0499
4.1405	.5653	2.6238	1.2427	2.5546	.7179	-.0692	.5036	.3362	.0851
4.0006	.5835	2.5669	1.2977	2.5811	.7843	.0142	.5466	.3765	.1212
3.8567	.6016	2.5079	1.3473	2.6013	.8458	.0934	.5892	.4167	.1580
3.7090	.6198	2.4466	1.3915	2.6148	.9022	.1682	.6304	.4565	.1950
3.5574	.6379	2.3831	1.4299	2.6215	.9533	.2384	.6713	.4956	.2320
3.4024	.6561	2.3173	1.4623	2.6289	.9980	.3037	.7101	.5336	.2680
3.2438	.6742	2.2490	1.4882	2.6127	1.0384	.3637	.7469	.5700	.3048
3.0821	.6924	2.1782	1.5075	2.5966	1.0718	.4164	.7814	.6046	.3396
2.9172	.7105	2.1049	1.5197	2.5721	1.0987	.4673	.8123	.6367	.3734
2.7494	.7286	2.0289	1.5245	2.5389	1.1187	.5101	.8400	.6660	.4050
2.5786	.7467	1.9500	1.5215	2.4965	1.1315	.5465	.8635	.6919	.4344
2.4056	.7649	1.8681	1.5102	2.4442	1.1366	.5761	.8824	.7137	.4608
2.2300	.7830	1.7831	1.4901	2.3816	1.1335	.5985	.8950	.7310	.4838
2.0521	.8011	1.6946	1.4606	2.3079	1.1216	.6133	.9030	.7429	.5027
1.8722	.8192	1.6024	1.4210	2.2222	1.1095	.6190	.9031	.7486	.5169
1.6904	.8373	1.5061	1.3785	2.1236	1.0893	.6175	.8952	.7473	.5255
1.5069	.8554	1.4052	1.3082	2.0108	1.0627	.6056	.8780	.7379	.5276
1.3219	.8735	1.2991	1.2329	1.8824	.9731	.5833	.8502	.7190	.5221
1.1355	.8915	1.1866	1.1429	1.7362	.9056	.5496	.8100	.6891	.5076
.9480	.9096	1.0664	1.0362	1.5694	.8256	.5030	.7551	.6460	.4823
.7596	.9277	.9358	.9100	1.3779	.7229	.4421	.6825	.5870	.4439
.5703	.9458	.7899	.7594	1.1548	.6019	.3649	.5074	.5079	.3886

CRACK SURFACE ROTATION AND CRACK OPENING DISPLACEMENTS FOR AF/H= 0.0 AND D/H= .7

A/H	S0/SY	2 BETA	COD0	COD1	COD2	COD3	COD4	COD5	COD6
7.378A	.2924	4.1216	-.0576	2.0032	-.8619	-2.1184	-.0114	.3811	-.3239
7.2771	.3232	4.0830	.1745	2.2160	-.6421	-1.0670	.0374	.3720	-.2981
7.1680	.3479	4.0414	.3563	2.3770	-.4520	-1.6645	.0620	.4394	-.2755
7.0516	.3701	3.9970	.5152	2.5137	-.2882	-1.4033	.1267	.5053	-.2518
6.9282	.3909	3.9498	.6604	2.6353	-.1296	-1.3145	.1729	.5718	-.2259
6.7978	.4109	3.8999	.7959	2.7458	.0159	-1.1541	.2210	.6394	-.1973
6.6606	.4304	3.8473	.9235	2.8471	.1540	-1.0802	.2712	.7082	-.1659
6.5166	.4497	3.7919	1.0443	2.9402	.2859	-.8217	.3232	.7782	-.1317
6.3661	.4687	3.7339	1.1587	3.0256	.4119	-.7083	.3771	.8490	-.0948
6.2092	.4875	3.6732	1.2669	3.1035	.5323	-.5697	.4325	.9203	-.0553
6.0460	.5063	3.6097	1.3609	3.1738	.6470	-.4359	.4891	.9919	-.0136
5.8767	.5249	3.5436	1.4646	3.2364	.7559	-.3071	.5467	1.0632	.0302
5.7816	.5435	3.4746	1.5539	3.2912	.8590	-.1834	.6048	1.1339	.0758
5.5206	.5620	3.4028	1.6364	3.3378	.9558	-.0658	.6631	1.2034	.1220
5.3342	.5805	3.3282	1.7120	3.3760	1.0463	.0479	.7211	1.2712	.1711
5.1423	.5989	3.2506	1.7803	3.4056	1.1301	.1258	.7785	1.3368	.2201
4.9453	.6172	3.1701	1.8410	3.4261	1.2070	.2050	.8346	1.3997	.2695
4.7433	.6357	3.0865	1.8939	3.4371	1.2766	.2806	.8891	1.4592	.3190
4.5365	.6540	2.9980	1.9385	3.4384	1.3385	.3586	.9414	1.5147	.3681
4.3251	.6724	2.9099	1.9744	3.4294	1.3925	.4386	.9909	1.5656	.4162
4.1894	.6907	2.8167	2.0014	3.4097	1.4300	.5195	1.0370	1.6110	.4630
3.8896	.7090	2.7200	2.0188	3.3787	1.4748	.6008	1.0791	1.6584	.5070
3.6558	.7272	2.6197	2.0262	3.3360	1.5022	.7163	1.1164	1.6827	.5500
3.4384	.7455	2.5156	2.0000	3.2808	1.5199	.7653	1.1482	1.7072	.5692
3.2874	.7637	2.4075	2.0000	3.2125	1.5273	.8351	1.1737	1.7229	.6245
2.9733	.7820	2.2951	1.9827	3.1302	1.5237	.8891	1.1919	1.7286	.6552
2.7362	.8002	2.1781	1.9440	3.0331	1.5084	.9549	1.2018	1.7232	.6805
2.4963	.8184	2.0562	1.8918	2.9199	1.4806	.9637	1.2023	1.7053	.6994
2.2539	.8366	1.9288	1.8251	2.7895	1.4393	.8607	1.1921	1.6733	.7109
2.0892	.8548	1.7954	1.7425	2.6482	1.3834	.8448	1.1695	1.6253	.7137
1.7625	.8730	1.6550	1.6424	2.4699	1.3114	.7695	1.1327	1.5590	.7063
1.5140	.8911	1.5066	1.5228	2.2761	1.2215	.6149	1.0793	1.4716	.6870
1.2648	.9093	1.3485	1.3609	2.0552	1.1112	.4707	1.0063	1.3594	.6532
1.0127	.9274	1.1780	1.2129	1.8019	.9773	.3239	.9096	1.2173	.6019
.7604	.9456	.9900	1.0128	1.5078	.8140	.1780	.7830	1.0377	.5282
.5074	.9637	.7733	.7708	1.1575	.6162	.3842	.6162	.8082	.4242

CRACK SURFACE ROTATION AND CRACK OPENING DISPLACEMENTS FOR AF/H= 10.0 AND D/H= .7

A/H	S0/SY	2 BEYA	COD0	COD1	COD2	COD3	COD4	COD5	COD6
9.2235	.2765	5.0693	-.2229	2.3110	-1.2367	-2.7575	-.8542	.3302	-.4186
9.0983	.3128	5.0213	.1204	2.6310	-.8038	-2.3902	.8298	.4283	-.3767
8.9599	.3396	4.9698	.3678	2.8527	-.6261	-2.1171	.8846	.5144	-.3451
8.8145	.3630	4.9148	.5790	3.0364	-.4039	-1.8784	.1424	.5986	-.3130
8.6603	.3847	4.8565	.7698	3.1980	-.2815	-1.6558	.2016	.6834	-.2803
8.4973	.4055	4.7949	.9465	3.3440	-.0125	-1.4518	.2629	.7696	-.2430
8.3257	.4257	4.7300	1.1122	3.4772	.1662	-1.2528	.3266	.8572	-.2040
8.1458	.4454	4.6617	1.2684	3.5993	.3361	-1.0624	.3926	.9461	-.1608
7.9576	.4649	4.5901	1.4159	3.7110	.4979	-.8791	.4608	1.0361	-.1144
7.7615	.4841	4.5152	1.5551	3.8012	.6521	-.7025	.5309	1.1266	-.0649
7.5575	.5032	4.4368	1.6860	3.9044	.7986	-.5324	.6024	1.2174	.3564
7.3459	.5222	4.3550	1.8085	3.9861	.9375	-.3690	.6751	1.3077	.6424
7.1269	.5410	4.2698	1.9227	4.0575	1.0687	-.2122	.7483	1.3972	.4889
6.9008	.5598	4.1810	2.0281	4.1186	1.1919	-.0524	.8218	1.4851	.0995
6.6677	.5785	4.0886	2.1245	4.1688	1.3068	.0802	.8949	1.5709	.2189
6.4279	.5971	3.9926	2.2117	4.2086	1.4132	.2154	.9671	1.6539	.6924
6.1816	.6157	3.8928	2.2892	4.2358	1.5187	.3628	1.0378	1.7334	.2003
5.9291	.6342	3.7892	2.3567	4.2513	1.5989	.4621	1.1064	1.8086	.3423
5.6786	.6527	3.6817	2.4137	4.2546	1.6774	.5729	1.1722	1.8787	.4042
5.4064	.6711	3.5702	2.4590	4.2450	1.7458	.6747	1.2345	1.9438	.4657
5.1368	.6896	3.4546	2.4945	4.2218	1.8036	.7672	1.2929	2.0006	.5259
4.8620	.7079	3.3345	2.5172	4.1845	1.8503	.8499	1.3455	2.0504	.5845
4.5823	.7263	3.2100	2.5273	4.1323	1.8853	.9223	1.3925	2.0919	.6406
4.2979	.7447	3.0808	2.5241	4.0645	1.9080	.9837	1.4326	2.1227	.6935
4.0093	.7630	2.9465	2.5070	3.9802	1.9177	1.0337	1.4648	2.1420	.7425
3.7166	.7813	2.8069	2.4750	3.8784	1.9177	1.0715	1.4878	2.1506	.7867
3.4202	.7996	2.6615	2.4411	3.7579	1.8949	1.0964	1.5006	2.1443	.8251
3.1283	.8179	2.5099	2.3624	3.6174	1.8665	1.1075	1.5014	2.1224	.8561
2.8173	.8361	2.3515	2.2795	3.4552	1.8092	1.1037	1.4889	2.0829	.8805
2.5115	.8544	2.1854	2.1766	3.2693	1.7395	1.0839	1.4608	2.0233	.8984
2.2031	.8726	2.0188	2.0518	3.0572	1.6497	1.0465	1.4158	1.9408	.8092
1.8925	.8909	1.8261	1.9026	2.8156	1.5374	.9996	1.3485	1.8320	.6650
1.5800	.9091	1.6295	1.7255	2.5406	1.3996	.9108	1.2574	1.6921	.4828
1.2659	.9273	1.4180	1.5151	2.2246	1.2321	.8067	1.1367	1.5147	.2586
.9506	.9455	1.1863	1.2658	1.8589	1.0285	.6726	.9785	1.2906	.0054
.6342	.9637	.9226	.9634	1.4247	.7789	.5021	.7701	1.0039	.5364

CRACK SURFACE ROTATION AND CRACK OPENING DISPLACEMENTS FOR AF/H= 12.0 AND D/H= .7

A/H	SO/SY	2 BEYA	COD0	COD1	COD2	COD3	COD4	COD5	COD6
11.0603	.2575	6.0150	-.4834	2.5241	-1.6864	-3.4909	.8959	.3393	-.5311
10.9156	.3033	5.9570	.0373	3.0162	-1.1542	-2.9415	.0080	.4769	-.4609
10.7519	.3325	5.8965	.3622	3.3105	-.8171	-2.5860	.0833	.5851	-.4184
10.5774	.3572	5.8312	.6312	3.5468	-.5351	-2.2844	.1553	.6092	-.3787
10.3923	.3799	5.7620	.8708	3.7518	-.2816	-2.0102	.2208	.7932	-.3372
10.1967	.4013	5.6888	1.0909	3.9353	-.0469	-1.7535	.3030	.8985	-.2926
9.9900	.4220	5.6117	1.2961	4.1028	.1738	-1.5097	.3806	1.0854	-.2462
9.7749	.4423	5.5306	1.4880	4.2541	.3827	-1.2765	.4688	1.1137	-.1920
9.5491	.4621	5.4455	1.6701	4.3929	.5810	-1.0526	.5436	1.2230	-.1359
9.3138	.4816	5.3564	1.8400	4.5189	.7695	-.8374	.6284	1.3330	-.0762
9.0690	.5010	5.2632	2.0089	4.6325	.9483	-.6307	.7149	1.4430	-.0132
8.8151	.5202	5.1658	2.1507	4.7336	1.1175	-.4322	.8028	1.5526	.5028
8.5523	.5392	5.0642	2.2899	4.8220	1.2771	-.2222	.8913	1.6609	.5835
8.2809	.5582	4.9585	2.4185	4.8977	1.4260	-.0508	.9808	1.7673	.6651
8.0012	.5770	4.8484	2.5360	4.9601	1.5663	.1118	1.0682	1.8711	.7471
7.7135	.5958	4.7339	2.6422	5.0091	1.6954	.2752	1.1553	1.9714	.8209
7.4179	.6145	4.6149	2.7366	5.0441	1.8136	.4291	1.2406	2.0675	.9099
7.1149	.6331	4.4914	2.8188	5.0645	1.9206	.5731	1.3233	2.1585	.9893
6.8047	.6517	4.3631	2.8884	5.0699	2.0158	.7068	1.4027	2.2433	1.0664
6.4877	.6702	4.2300	2.9447	5.0597	2.0987	.8297	1.4778	2.3211	1.1405
6.1601	.6887	4.0920	2.9872	5.0332	2.1688	.9412	1.5478	2.3907	1.2106
5.8344	.7072	3.9487	3.0152	4.9986	2.2255	1.0409	1.6117	2.4511	1.2759
5.4987	.7257	3.8000	3.0281	4.9281	2.2681	1.1281	1.6684	2.5009	1.3354
5.1575	.7441	3.6456	3.0249	4.8477	2.2958	1.2021	1.7168	2.5389	1.3880
4.8112	.7625	3.4852	3.0049	4.7475	2.3079	1.2623	1.7567	2.5635	1.4326
4.4599	.7808	3.3184	2.9671	4.6262	2.3034	1.3079	1.7837	2.5732	1.4678
4.1042	.7992	2.1447	2.9102	4.4825	2.2812	1.3378	1.7992	2.5662	1.4924
3.7444	.8175	2.9635	2.8329	4.3147	2.2402	1.3512	1.8005	2.5483	1.5045
3.3800	.8358	2.7740	2.7337	4.1207	2.1789	1.3467	1.7856	2.4932	1.5025
3.0138	.8541	2.5755	2.6106	3.8983	2.0955	1.3229	1.7521	2.4221	1.4841
2.6437	.8724	2.3665	2.4612	3.6444	1.9879	1.2779	1.6973	2.3235	1.4468
2.2710	.8907	2.1455	2.2824	3.3551	1.8533	1.2096	1.6176	2.1932	1.3874
1.8960	.9089	1.9102	2.0701	3.0252	1.6890	1.1149	1.5085	2.0256	1.3017
1.5191	.9271	1.6573	1.8184	2.6471	1.4870	.9898	1.3637	1.8151	.9144
1.1407	.9454	1.3809	1.5187	2.2092	1.2425	.8282	1.1740	1.6259	.8038
.7611	.9636	1.0690	1.1560	1.6905	.9422	.6215	.9241	1.2004	.6177

CRACK SURFACE ROTATION AND CRACK OPENING DISPLACEMENTS FOR AF/W= 14.0 AND D/W= .7

A/H	S0/SY	2 BETA	CO00	CO01	CO02	CO03	CO04	CO04	CO05	CO06
12.7340	.2946	6.0931	-.0711	3.3754	-1.4490	-3.5177	-.0152	.5199	-.2293	-.5504
12.5439	.3264	6.0222	.3437	3.7548	-1.8208	-3.0675	.0791	.6531	-.1505	-.4949
12.3403	.3525	6.7468	.6751	4.0485	-.6743	-2.6903	.1661	.7781	-.0707	-.4460
12.1244	.3759	6.6667	.9660	4.2994	-.3673	-2.3674	.2530	.9020	-.0867	-.3961
11.8922	.3980	6.5821	1.2310	4.5221	-.0854	-2.0600	.3419	1.0270	-.0679	-.3431
11.6568	.4192	6.4920	1.4768	4.7232	-.1782	-1.7696	.4336	1.1533	.1458	-.2861
11.4041	.4398	6.3989	1.7066	4.9068	-.4268	-1.4929	.5283	1.2812	-.2271	-.2246
11.1407	.4599	6.3003	1.9222	5.0724	.6622	-1.2279	.6256	1.4108	.3118	-.1588
10.8661	.4797	6.1970	2.1247	5.2232	.8853	-.9730	.7253	1.5395	.3996	-.0889
10.5805	.4993	6.0889	2.3144	5.3589	1.0966	-.7301	.8270	1.6689	.4802	-.0150
10.2843	.5186	5.9760	2.4915	5.4796	1.2963	-.4965	.9300	1.7976	.5829	.0524
9.9777	.5378	5.8582	2.6561	5.5852	1.4845	-.2730	1.0338	1.9248	.6774	.1820
9.6611	.5569	5.7355	2.8079	5.6756	1.6608	-.0590	1.1370	2.0498	.7730	.2258
9.3348	.5759	5.6077	2.9466	5.7505	1.8251	.1428	1.2412	2.1716	.8690	.3188
8.9990	.5947	5.4787	3.0719	5.8093	1.9770	.3346	1.3433	2.2894	.9648	.3972
8.6542	.6135	5.3366	3.1834	5.8517	2.1160	.5151	1.4432	2.4021	1.0596	.4842
8.3007	.6323	5.1931	3.2804	5.8770	2.2418	.6039	1.5400	2.5088	1.1525	.5713
7.9388	.6509	5.0441	3.3626	5.8946	2.3537	.8405	1.6330	2.6084	1.2428	.6576
7.5690	.6696	4.8895	3.4292	5.8739	2.4513	.9844	1.7210	2.6996	1.3295	.7423
7.1915	.6881	4.7298	3.4795	5.8448	2.5337	1.1158	1.8029	2.7814	1.4115	.8245
6.8060	.7067	4.5625	3.5130	5.7942	2.6005	1.2317	1.8770	2.8522	1.4880	.9033
6.4152	.7252	4.3896	3.5286	5.7234	2.6587	1.3338	1.9442	2.9188	1.5576	.9776
6.0171	.7436	4.2101	3.5255	5.6306	2.6835	1.4204	2.0010	2.9555	1.6191	1.0464
5.6130	.7621	4.0236	3.5027	5.5145	2.6980	1.4909	2.0466	2.9847	1.6713	1.1084
5.2033	.7805	3.8296	3.4590	5.3738	2.6931	1.5442	2.0794	2.9964	1.7126	1.1624
4.7883	.7989	3.6276	3.3931	5.2068	2.6675	1.5793	2.0977	2.9885	1.7413	1.2068
4.3685	.8172	3.4168	3.3033	5.0117	2.6199	1.5949	2.0994	2.9587	1.7557	1.2481
3.9443	.8356	3.1964	3.1879	4.7861	2.5486	1.5897	2.0822	2.9841	1.7535	1.2883
3.5161	.8539	2.9654	3.0446	4.5272	2.4515	1.5619	2.0434	2.8214	1.7321	1.2653
3.0843	.8722	2.7221	2.8705	4.2316	2.3261	1.5094	1.9796	2.7067	1.6887	1.2525
2.6495	.8905	2.4649	2.6621	3.9346	2.1691	1.4297	1.8868	2.5550	1.6195	1.2185
2.2120	.9088	2.1909	2.4166	3.5181	1.9764	1.3191	1.7596	2.3597	1.5195	1.1595
1.7723	.9271	1.8964	2.1212	3.0694	1.7419	1.1730	1.5908	2.1120	1.3823	1.0696
1.3308	.9453	1.5750	1.7716	2.5591	1.4567	.9842	1.3696	1.7986	1.1980	.9485
.8879	.9635	1.2138	1.3446	1.9555	1.1058	.7417	1.0740	1.3976	.9502	.7584

CRACK SURFACE ROTATION AND CRACK OPENING DISPLACEMENTS FOR AP/H= 16.0 AND D/H= .7

A/H	S0/SY	2 BETA	G000	G001	G002	G003	G004	G005	G006
14.5541	.2865	7.0277	- .2030	3.7108	-1.7686	-4.1169	-.0435	.5582	-.6452
14.3359	.3212	7.7473	.3150	4.1086	-1.2345	-3.5587	.0725	.7191	-.5741
14.1833	.3485	7.6617	.7129	4.5438	-.8194	-3.1179	.1754	.8660	-.5152
13.8564	.3727	7.5709	1.0571	4.0425	-.4571	-2.7284	.2768	1.0103	-.4567
13.5956	.3953	7.4748	1.3681	5.1055	-.1268	-2.3693	.3800	1.1551	-.3951
13.3211	.4169	7.3734	1.6551	5.3418	.1804	-2.0316	.4860	1.3012	-.3292
13.0332	.4378	7.2667	1.9225	5.5550	.4691	-1.7109	.5951	1.4486	-.2585
12.7322	.4581	7.1547	2.1727	5.7501	.7418	-1.4046	.7071	1.5971	-.1829
12.4183	.4782	7.0372	2.4073	5.9259	.9990	-1.1113	.8218	1.7461	-.1025
12.0920	.4979	6.9143	2.6268	6.0839	1.2439	-.8304	.9386	1.8950	-.0178
11.7535	.5174	6.7858	2.8315	6.2244	1.4743	-.5614	1.0569	2.0429	.0709
11.4031	.5367	6.6518	3.0215	6.3474	1.6912	-.3044	1.1768	2.1890	.1631
11.0413	.5559	6.5120	3.1967	6.4527	1.8943	-.0593	1.2953	2.3325	.2501
10.6683	.5750	6.3665	3.3567	6.5408	2.0834	.1734	1.4139	2.4724	.3355
10.2846	.5939	6.2152	3.5812	6.6088	2.2582	.3916	1.5310	2.6076	.4544
9.8905	.6128	6.0579	3.8297	6.6586	2.4181	.6000	1.6455	2.7378	.5540
9.4865	.6316	5.8944	3.7416	6.6889	2.5628	.7944	1.7566	2.8595	.6537
9.0730	.6503	5.7247	3.8364	6.6988	2.6915	.9741	1.8631	2.9737	.7525
8.6503	.6690	5.5485	3.9134	6.6876	2.8036	1.1391	1.9619	3.0785	.8494
8.2188	.6876	5.3657	3.9717	6.6545	2.8985	1.2888	2.0579	3.1723	.9435
7.7791	.7062	5.1760	4.0105	6.5985	2.9753	1.4225	2.1437	3.2538	1.0336
7.3316	.7248	4.9790	4.0289	6.5184	3.0332	1.5395	2.2199	3.3211	1.1187
6.8767	.7433	4.7744	4.0260	6.4132	3.0711	1.6388	2.2850	3.3726	1.1974
6.4149	.7618	4.5618	4.0004	6.2813	3.0880	1.7195	2.3373	3.4063	1.2684
5.9466	.7802	4.3406	3.9508	6.1212	3.0827	1.7805	2.3751	3.4208	1.3302
5.4723	.7986	4.1103	3.8758	5.9318	3.0538	1.8207	2.3962	3.4113	1.3818
4.9925	.8170	3.8700	3.7736	5.7086	2.9996	1.8386	2.3983	3.3775	1.4191
4.5077	.8354	3.6187	3.6528	5.4513	2.9183	1.8327	2.3788	3.3154	1.4423
4.0184	.8537	3.3551	3.4785	5.1568	2.8074	1.8009	2.3346	3.2212	1.4480
3.5250	.8721	3.0777	3.2798	4.8186	2.6642	1.7409	2.2618	3.0904	1.4333
3.0280	.8904	2.7842	3.0418	4.4339	2.4850	1.6497	2.1559	2.9172	1.3946
2.5280	.9087	2.4716	2.7591	3.9949	2.2648	1.5233	2.0107	2.6943	1.3271
2.0255	.9270	2.1354	2.4239	3.4916	1.9968	1.3562	1.8178	2.4113	1.2243
1.5209	.9453	1.7687	2.0246	2.9089	1.6708	1.1402	1.5651	2.0533	1.0768
1.0148	.9635	1.3576	1.5411	2.2199	1.2696	.8623	1.2320	1.5952	.8687
.5076	.9818	.8622	.9318	1.3628	.7593	.5007	.7759	.9857	.5662

CRACK SURFACE ROTATION AND CRACK OPENING DISPLACEMENTS FOR AP/H= 4.0 AND D/H= .8

A/H	S0/SV	2 BETA	C0D0	C0D1	C0D2	C0D3	C0D4	C0D5	C0D6
3.0196	.2226	1.7234	.0478	.9495	-.4292	-.7739	.0132	.1145	-.0475
3.7800	.2523	1.7123	.2016	1.0578	-.3121	-.6545	.0336	.1474	-.0347
3.7366	.2765	1.7000	.2926	1.1426	-.2174	-.5574	.0534	.1790	-.0220
3.6894	.2984	1.6865	.3730	1.2162	-.1330	-.4703	.0748	.2107	-.0627
3.6385	.3190	1.6718	.4469	1.2828	-.0546	-.3898	.0957	.2429	-.0075
3.5840	.3389	1.6559	.5162	1.3442	.0195	-.3117	.1100	.2757	-.0301
3.5250	.3582	1.6367	.5818	1.4012	.0902	-.2375	.1431	.3091	-.0229
3.4641	.3773	1.6204	.6442	1.4545	.1581	-.1668	.1607	.3432	-.0850
3.3989	.3961	1.6009	.7037	1.5042	.2235	-.0967	.1955	.3779	.0131
3.3303	.4148	1.5803	.7605	1.5506	.2864	-.0297	.2233	.4131	.0336
3.2583	.4335	1.5585	.8145	1.5937	.3470	.0353	.2521	.4487	.0555
3.1830	.4521	1.5356	.8658	1.6336	.4051	.0900	.2818	.4847	.0789
3.1040	.4707	1.5115	.9143	1.6701	.4609	.1586	.3121	.5209	.1034
3.0230	.4893	1.4863	.9599	1.7031	.5140	.2168	.3430	.5570	.1289
2.9384	.5079	1.4601	1.0025	1.7325	.5645	.2725	.3742	.5931	.1553
2.8508	.5265	1.4327	1.0419	1.7583	.6121	.3256	.4055	.6287	.1824
2.7603	.5452	1.4042	1.0780	1.7803	.6560	.3759	.4368	.6638	.2099
2.6671	.5639	1.3746	1.1106	1.7979	.6982	.4233	.4678	.6980	.2376
2.5712	.5827	1.3439	1.1395	1.8115	.7364	.4676	.4983	.7311	.2654
2.4726	.6014	1.3120	1.1645	1.8205	.7709	.5085	.5279	.7628	.2930
2.3716	.6203	1.2790	1.1854	1.8249	.8017	.5459	.5565	.7929	.3202
2.2682	.6391	1.2448	1.2020	1.8244	.8286	.5797	.5838	.8209	.3467
2.1626	.6579	1.2094	1.2141	1.8188	.8513	.6094	.6093	.8465	.3721
2.0547	.6768	1.1727	1.2214	1.8077	.8696	.6350	.6328	.8693	.3954
1.9448	.6957	1.1347	1.2236	1.7909	.8831	.6562	.6540	.8890	.4190
1.8329	.7147	1.0953	1.2204	1.7681	.8918	.6728	.6724	.9051	.4397
1.7152	.7336	1.0545	1.2116	1.7389	.8953	.6843	.6877	.9172	.4581
1.6037	.7526	1.0122	1.1968	1.7029	.8931	.6907	.6993	.9247	.4738
1.4866	.7716	.9682	1.1756	1.6597	.8851	.6915	.7067	.9270	.4864
1.3681	.7905	.9225	1.1476	1.6088	.8709	.6864	.7095	.9236	.4954
1.2481	.8095	.8748	1.1122	1.5496	.8498	.6749	.7069	.9137	.5001
1.1249	.8286	.8249	1.0689	1.4814	.8215	.6565	.6982	.8964	.5008
1.0046	.8476	.7724	1.0170	1.4032	.7933	.6308	.6826	.8707	.4944
.8812	.8666	.7170	.9554	1.3139	.7403	.5959	.6589	.8356	.4822
.7570	.8856	.6578	.8831	1.2120	.6850	.5543	.6259	.7894	.4625
.6320	.9047	.5937	.7986	1.0954	.6205	.5017	.5819	.7302	.4337
.5064	.9237	.5229	.6995	.9610	.5426	.4380	.5246	.6552	.3939

CRACK SURFACE ROTATION AND CRACK OPENING DISPLACEMENTS FOR AP/H= 0.0 AND D/H= .6

A/H	S0/SY	2 BETA	COD0	COD1	COD2	COD3	COD4	COD5	COD6
7.6392	.2066	3.2148	.0512	1.6586	-.9133	-1.5563	.0077	.1877	-.1723
7.5600	.2395	3.1923	.3041	1.9002	-.6536	-1.2921	.0507	.2511	-.1490
7.4732	.2643	3.1675	.6914	2.0751	-.4589	-1.0324	.6897	.3094	-.1301
7.3788	.2863	3.1403	.6544	2.2245	-.2877	-.9158	.1298	.3679	-.1003
7.2771	.3071	3.1108	.8041	2.3595	-.1291	-.7513	.1723	.4278	-.0833
7.1680	.3271	3.0792	.9450	2.4846	.0213	-.5946	.2174	.4898	-.0549
7.0516	.3467	3.0453	1.0792	2.6019	.1656	-.4435	.2655	.5539	-.0229
6.9282	.3662	3.0094	1.2077	2.7124	.3049	-.2970	.3163	.6201	.0124
6.7978	.3855	2.9714	1.3310	2.8167	.4396	-.1547	.3697	.6804	.0509
6.6606	.4047	2.9313	1.4492	2.9146	.5698	-.0165	.4255	.7585	.0925
6.5166	.4239	2.8891	1.5621	3.0067	.6954	.1176	.4835	.8301	.1370
6.3661	.4431	2.8449	1.6697	3.0922	.8163	.2873	.5434	.9029	.1839
6.2052	.4622	2.7986	1.7717	3.1710	.9321	.4926	.6048	.9765	.2331
6.0460	.4814	2.7503	1.8678	3.2429	1.0427	.6777	.6674	1.0504	.2843
5.8767	.5006	2.6999	1.9576	3.3075	1.1477	.8209	.7307	1.1242	.3372
5.7016	.5198	2.6473	2.0409	3.3645	1.2467	.9184	.7944	1.1975	.3913
5.5206	.5390	2.5926	2.1172	3.4135	1.3394	1.0093	.8579	1.2696	.4463
5.3342	.5582	2.5358	2.1863	3.4542	1.4255	1.0934	.9209	1.3400	.5018
5.1423	.5774	2.4767	2.2477	3.4860	1.5047	1.1781	.9828	1.4083	.5574
4.9453	.5966	2.4153	2.3010	3.5087	1.5764	1.2591	1.0432	1.4737	.6126
4.7433	.6158	2.3516	2.3459	3.5217	1.6404	1.3400	1.1013	1.5357	.6670
4.5365	.6350	2.2856	2.3819	3.5247	1.6962	1.4184	1.1567	1.5935	.7199
4.3251	.6542	2.2171	2.4086	3.5171	1.7434	1.4984	1.2088	1.6466	.7709
4.1094	.6735	2.1460	2.4254	3.4984	1.7816	1.5784	1.2567	1.6941	.8194
3.8896	.6927	2.0724	2.4319	3.4681	1.8102	1.6558	1.2999	1.7352	.8646
3.6658	.7119	1.9959	2.4276	3.4256	1.8288	1.7296	1.3376	1.7691	.9061
3.4384	.7311	1.9166	2.4118	3.3701	1.8368	1.8035	1.3768	1.7948	.9429
3.2074	.7503	1.8343	2.3838	3.3009	1.8335	1.8667	1.4122	1.8112	.9744
2.9733	.7695	1.7486	2.3429	3.2172	1.8183	1.9286	1.4484	1.8174	.9995
2.7362	.7887	1.6595	2.2882	3.1179	1.7903	1.9884	1.4846	1.8119	1.0174
2.4963	.8079	1.5666	2.2187	3.0020	1.7487	2.0454	1.5181	1.7933	1.0269
2.2533	.8272	1.4696	2.1331	2.8679	1.6923	2.0984	1.5526	1.7599	1.0267
2.0092	.8464	1.3679	2.0302	2.7141	1.6196	2.1462	1.5866	1.7096	1.0153
1.7625	.8656	1.2610	1.9079	2.5384	1.5296	2.1774	1.6158	1.6406	.9909
1.5140	.8848	1.1479	1.7641	2.3380	1.4197	2.1901	1.5492	1.5492	.9514
1.2640	.9040	1.0274	1.5955	2.1093	1.2873	2.1818	1.4317	1.4317	.8937
1.0127	.9232	.9075	1.3979	1.8467	1.1287	2.1484	1.2820	1.2820	.8140
.7604	.9424	.7543	1.1647	1.5418	.9384	2.0875	.9004	1.0945	.7062
.5074	.9616	.5892	.8845	1.1791	.7077	.5699	.7070	.8533	.5608

CRACK SURFACE ROTATION AND CRACK OPENING DISPLACEMENTS FOR AP/H= 12.8 AND D/H= .8

A/H	2S0/SY	2 BETA	C000	C001	C002	C003	C004	C005	C006
11.4588	1772	4.6943	2.2647	2.0824	-1.6730	-2.6119	.2102	-.1900	-.2980
11.3400	2252	4.6604	.2912	2.6214	-1.1070	-2.6391	.3267	-.1104	-.2297
11.2098	2526	4.6233	.6034	2.9151	-.7836	-1.7002	.4154	-.0731	-.1952
11.0683	2761	4.5820	.8651	3.1565	-.5097	-1.4263	.5032	-.0274	-.1600
10.9156	2979	4.5392	1.1026	3.3722	-.2592	-1.1678	.5934	.0219	-.1210
10.7519	3168	4.4926	1.3250	3.5713	-.0228	-.9213	.6872	.0755	-.0774
10.5774	3392	4.4428	1.5361	3.7576	.2033	-.6853	.7846	.1330	-.0209
10.3923	3594	4.3901	1.7370	3.9329	.4208	-.4572	.8857	.1967	.0244
10.1967	3794	4.3344	1.9308	4.0980	.6305	-.2364	.9900	.2640	.0825
9.9908	3992	4.2756	2.1152	4.2530	.8326	-.0226	1.0972	.3355	.1451
9.7749	4189	4.2138	2.2911	4.3981	1.0270	.1842	1.2066	.4108	.2118
9.5491	4366	4.1490	2.4583	4.5320	1.2136	.3030	1.3170	.4894	.2824
9.3138	4582	4.0811	2.6164	4.6569	1.3928	.5758	1.4300	.5718	.3563
9.0690	4777	4.0100	2.7650	4.7700	1.5620	.7600	1.5427	.6551	.4332
8.8151	4973	3.9358	2.9038	4.8717	1.7230	.9350	1.6551	.7411	.5126
8.5523	5168	3.8585	3.0322	4.9615	1.8747	1.1030	1.7666	.8204	.5939
8.2809	5362	3.7779	3.1499	5.0389	2.0166	1.2618	1.8762	.9165	.6765
8.0012	5557	3.6940	3.2564	5.1034	2.1482	1.4094	1.9834	1.0046	.7600
7.7135	5751	3.6068	3.3510	5.1544	2.2690	1.5476	2.0871	1.0922	.8435
7.4179	5945	3.5161	3.4333	5.1914	2.3785	1.6753	2.1865	1.1705	.9265
7.1149	6139	3.4220	3.5027	5.2137	2.4761	1.7917	2.2807	1.2626	1.0081
6.8047	6333	3.3243	3.5586	5.2208	2.5613	1.8965	2.3687	1.3439	1.0877
6.4877	6527	3.2229	3.6003	5.2118	2.6334	1.9889	2.4494	1.4213	1.1643
6.1641	6720	3.1177	3.6271	5.1860	2.6916	2.0683	2.5216	1.4941	1.2372
5.8344	6914	3.0085	3.6383	5.1426	2.7358	2.1341	2.5843	1.5610	1.3052
5.4987	7107	2.8952	3.6331	5.0807	2.7645	2.1855	2.6361	1.6212	1.3675
5.1575	7300	2.7776	3.6105	4.9993	2.7772	2.2217	2.6755	1.6734	1.4229
4.8112	7494	2.6554	3.5695	4.8972	2.7729	2.2419	2.7011	1.7163	1.4701
4.4599	7687	2.5283	3.5091	4.7733	2.7506	2.2050	2.7111	1.7486	1.5080
4.1042	7880	2.3959	3.4279	4.6253	2.7091	2.2259	2.7036	1.7686	1.5340
3.7444	8073	2.2579	3.3244	4.4533	2.6470	2.1954	2.6765	1.7746	1.5491
3.3808	8266	2.1136	3.1968	4.2535	2.5627	2.1400	2.6272	1.7645	1.5489
3.0138	8459	1.9622	3.0429	4.0240	2.4542	2.0618	2.5527	1.7360	1.5318
2.6437	8652	1.8030	2.8600	3.7616	2.3191	1.9585	2.4495	1.6061	1.4953
2.2710	8844	1.6347	2.6447	3.4621	2.1543	1.8274	2.3130	1.6113	1.4359
1.8960	9037	1.4554	2.3923	3.1200	1.9557	1.6646	2.1373	1.5070	1.3494
1.5191	9230	1.2627	2.0963	2.7276	1.7175	1.4649	1.9145	1.3667	1.2297
1.1407	9422	1.0522	1.7466	2.2727	1.4310	1.2206	1.6323	1.1610	1.0602
.7611	9615	.8145	1.3265	1.7338	1.0822	.9193	1.2718	.9341	.8498

CRACK SURFACE ROTATION AND CRACK OPENING DISPLACEMENTS FOR AP/H= 16.0 AND D/H= .8

A/H	S0/SY	2 BETA	COD0	COD1	COD2	COD3	COD4	COD5	COD6
15.1200	.2112	6.1236	.1725	3.2343	-1.6646	-2.0893	.0287	.3815	-.1829
14.9464	.2429	6.0745	.6554	3.6927	-1.1669	-2.3018	.1196	.5881	-.1135
14.7577	.2682	6.0212	1.0345	4.0451	-.7719	-1.9761	.2952	.6289	-.6289
14.5541	.2913	5.9640	1.3710	4.3530	-.4181	-1.6109	.2937	.7521	-.1547
14.3159	.3131	5.9027	1.6825	4.6339	-.0083	-1.2688	.3671	.8798	-.1055
14.1033	.3343	5.8375	1.9760	4.8948	.2248	-.9427	.4861	1.0122	-.8401
13.8564	.3551	5.7683	2.2547	5.1389	.5243	-.6294	.5904	1.1493	.0316
13.5956	.3756	5.6951	2.5202	5.3677	.8116	-.3274	.7000	1.2905	.1894
13.3211	.3958	5.6178	2.7729	5.5819	1.0876	-.0368	.8143	1.4354	.1931
13.0332	.4159	5.5366	3.0133	5.7816	1.3523	.2450	.9327	.4416	.4944
12.7322	.4359	5.4512	3.2411	5.9667	1.6057	.5155	1.0548	.5425	.2824
12.4183	.4550	5.3617	3.4561	6.1370	1.8476	.7753	1.1798	.6488	.3767
12.0920	.4756	5.2680	3.6580	6.2928	2.0776	1.0240	1.3070	.7573	.4756
11.7535	.4963	5.1702	3.8463	6.4314	2.2952	1.2612	1.4357	.8698	.5784
11.4031	.5150	5.0680	4.0205	6.5545	2.5081	1.4862	1.5649	.9849	.6844
11.0413	.5346	4.9615	4.1799	6.6607	2.6915	1.6992	1.6938	1.1010	.7931
10.6683	.5542	4.8507	4.3241	6.7495	2.8689	1.8988	1.8214	1.2196	.9035
10.2846	.5738	4.7354	4.4523	6.8200	3.0317	2.0846	1.9469	1.3376	1.0150
9.8905	.5933	4.6155	4.5639	6.8716	3.1792	2.2561	2.0690	1.4547	1.1266
9.4865	.6128	4.4910	4.6580	6.9035	3.3107	2.4125	2.1868	1.5781	1.2374
9.0730	.6323	4.3617	4.7340	6.9148	3.4255	2.5531	2.2998	1.6826	1.3465
8.6503	.6512	4.2275	4.7909	6.9046	3.5227	2.6772	2.4043	1.7913	1.4528
8.2188	.6712	4.0882	4.8278	6.8719	3.6014	2.7838	2.5015	1.8948	1.5552
7.7791	.6906	3.9436	4.8439	6.8156	3.6608	2.8721	2.5891	1.9921	1.6525
7.3316	.7100	3.7935	4.8378	6.7346	3.6998	2.9411	2.6656	2.0817	1.7434
6.8767	.7294	3.6376	4.8086	6.6274	3.7173	2.9898	2.7292	2.1622	1.8266
6.4149	.7488	3.4756	4.7548	6.4926	3.7121	3.0169	2.7781	2.2328	1.9086
5.9466	.7682	3.3072	4.6749	6.3285	3.6827	3.0213	2.8103	2.2895	1.9837
5.4723	.7876	3.1317	4.5672	6.1331	3.6277	3.0816	2.8236	2.3327	2.0142
4.9925	.8069	2.9485	4.4298	5.9041	3.5452	2.9555	2.8153	2.3595	2.0502
4.5077	.8263	2.7571	4.2601	5.6387	3.4330	2.8016	2.7826	2.3677	2.0693
4.0184	.8456	2.5563	4.0554	5.3336	3.2685	2.7773	2.7218	2.3544	2.0690
3.5250	.8649	2.3449	3.8120	4.9845	3.1085	2.7396	2.6289	2.3185	2.0463
3.0280	.8842	2.1213	3.5253	4.5859	2.8889	2.6446	2.4986	2.2582	1.9185
2.5280	.9035	1.8831	3.1890	4.1306	2.6241	2.4775	2.3240	2.1585	1.8031
2.0255	.9228	1.6270	2.7945	3.6080	2.3064	1.9810	2.0950	2.0448	1.6436
1.5209	.9421	1.3475	2.3286	3.0023	1.9243	1.6548	1.8081	1.8244	1.4281
1.0148	.9614	1.0344	1.7686	2.2858	1.4583	1.2514	1.4138	1.5769	1.1370
.5076	.9807	.6569	1.0670	1.3954	.8699	.7386	.8886	1.6905	.7288

APPENDIX H
THE CALCULATED COD vs. σ_0/σ_F FOR
SOME STANDARD PIPES

The general problem of calculating the crack opening displacement in a pipe containing a circumferential part-through crack is discussed in Section 6.3 of this report. In this Appendix the results are presented for certain standard pipe dimensions and for various crack sizes. In Figures H-1 to H-16, OD is the outer pipe diameter, h is the pipe wall thickness, 2a is the crack length (on the pipe surface), and L_0 is the depth of the crack at its maximum penetration point (or at its mid-section). Also σ_F is the flow stress, E is the Young's modulus, and the COD is the crack mouth opening displacement calculated on the surface of the pipe and at the mid-section of the crack. It is assumed that in the crack region the pipe is under uniform axial tensile stress σ_0 and the crack is on the outer surface.

Figures H-1 to H-4 show the results for a 24 in., H-5 to H-8 for a 30 in., H-9 to H-12 for a 36 in., and H-13 to H-16 for a 48 in. diameter pipe.

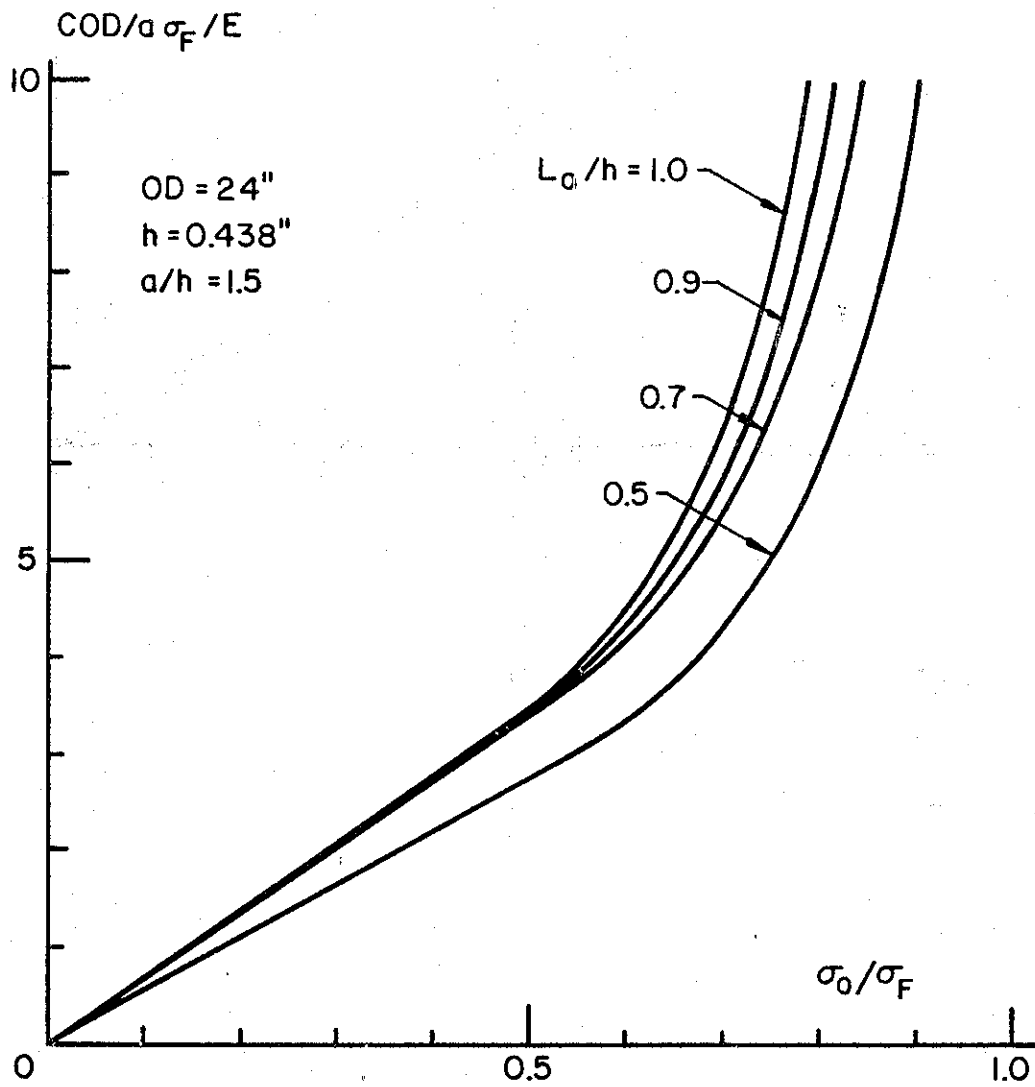


Figure H-1 COD vs. σ_0/σ_F for a 24 in. diameter pipe.

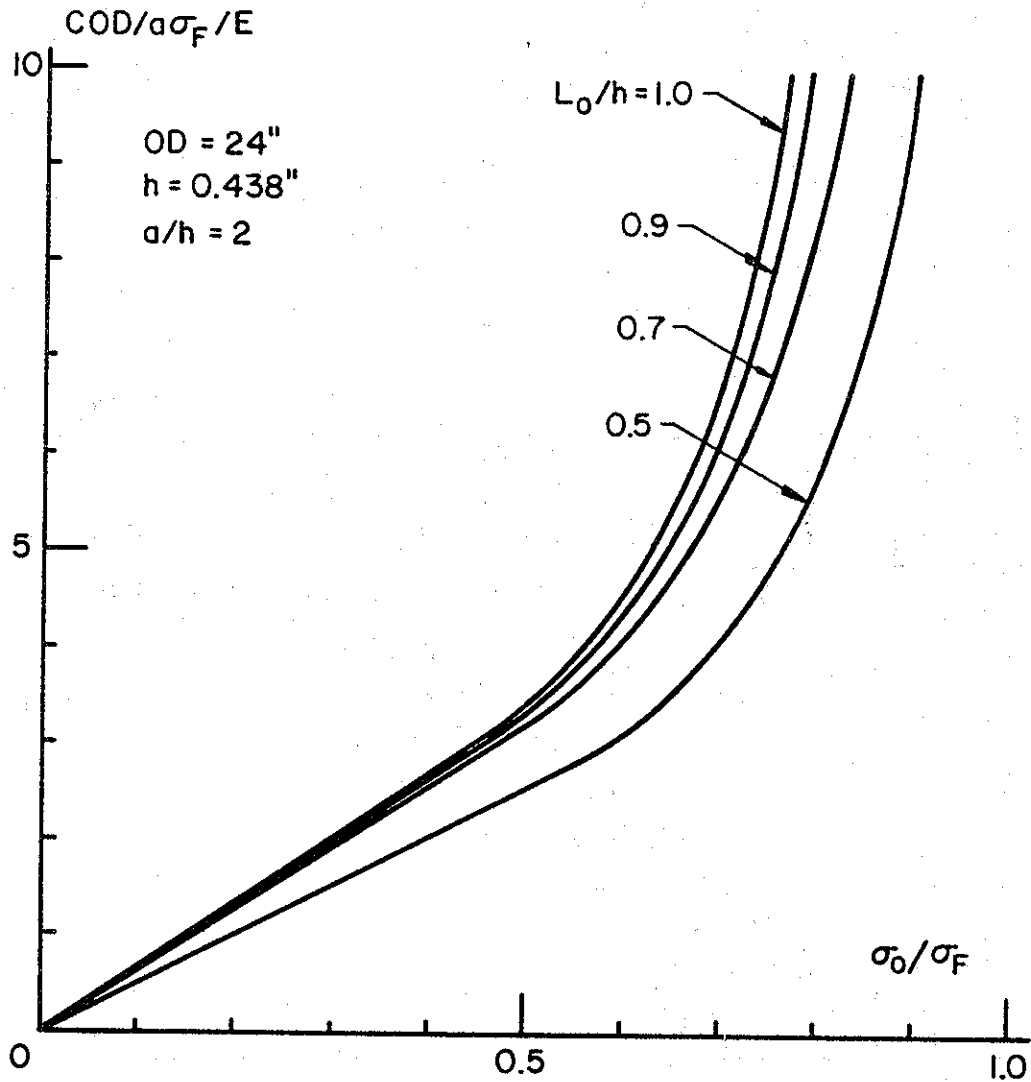


Figure H-2 COD vs. σ_0/σ_F for a 24 in. diameter pipe.

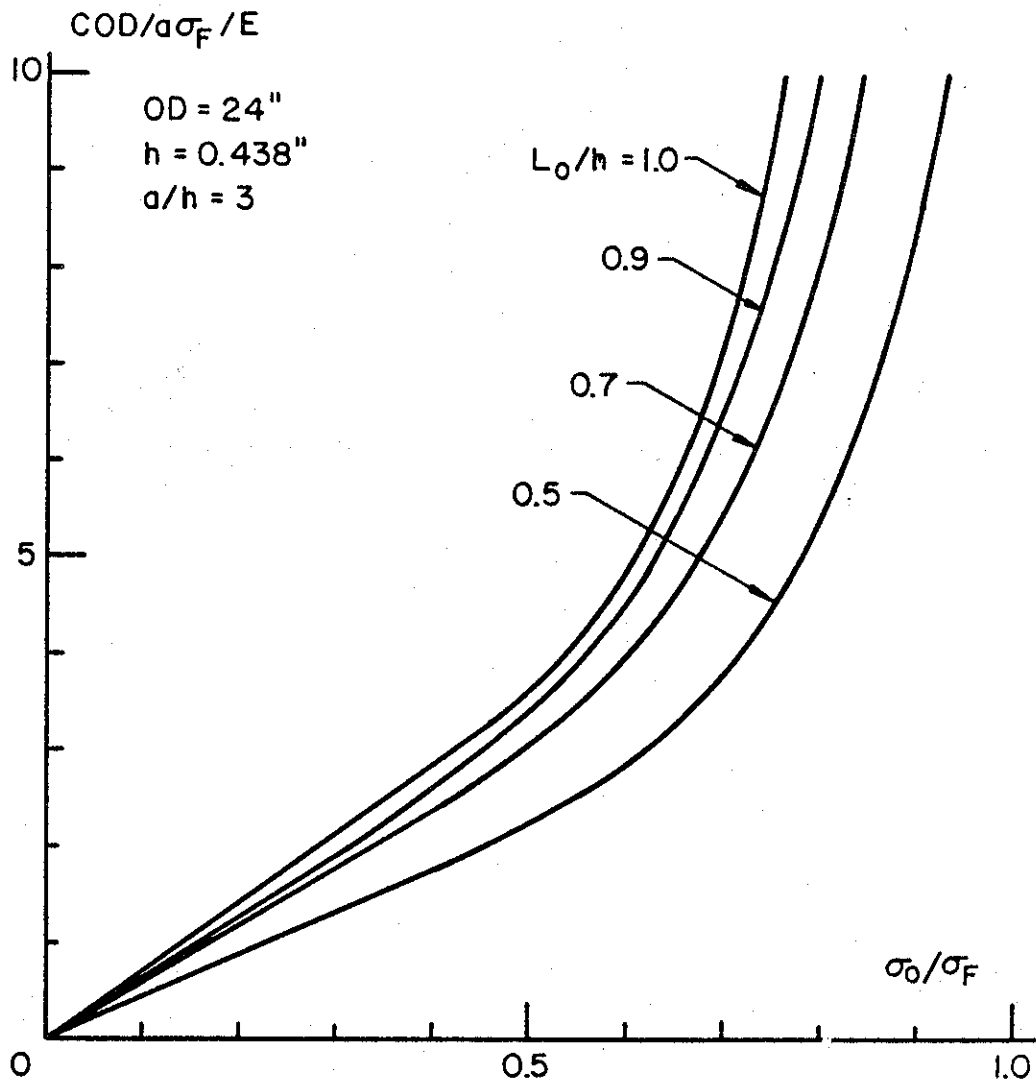


Figure H-3 COD vs. σ_0/σ_F for a 24 in. diameter pipe.

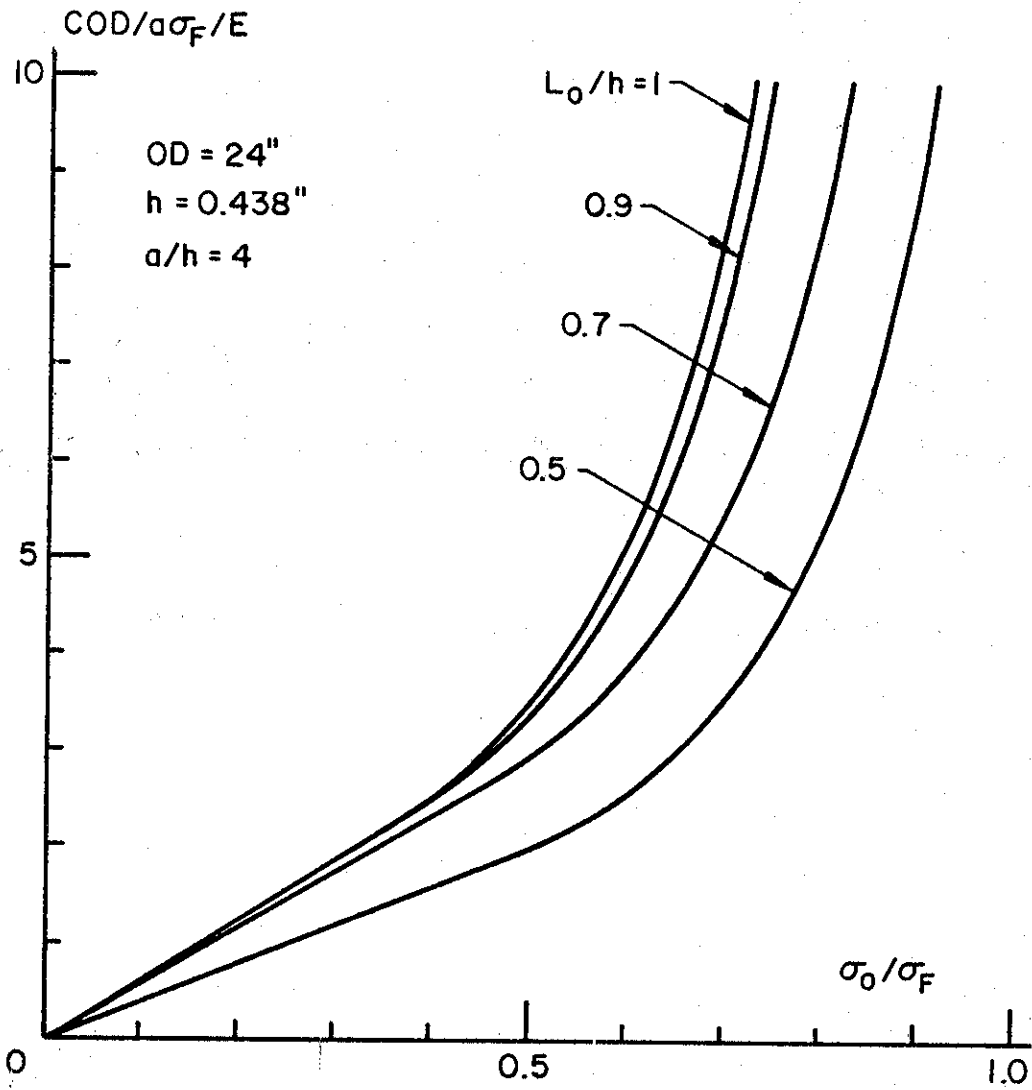


Figure H-4 COD vs. σ_0/σ_F for a 24 in. diameter pipe.

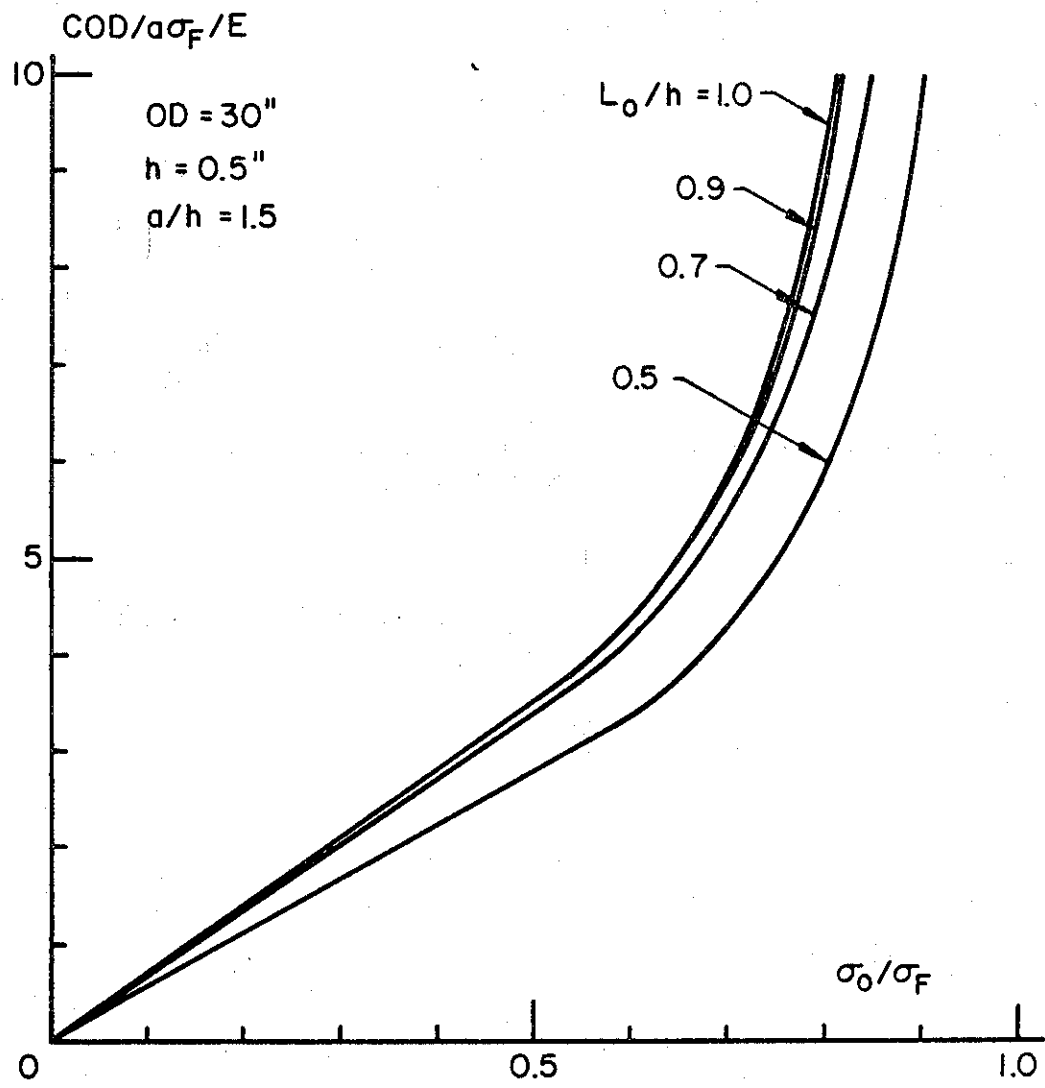


Figure H-5 COD vs. σ_0/σ_F for a 30 in. diameter pipe.

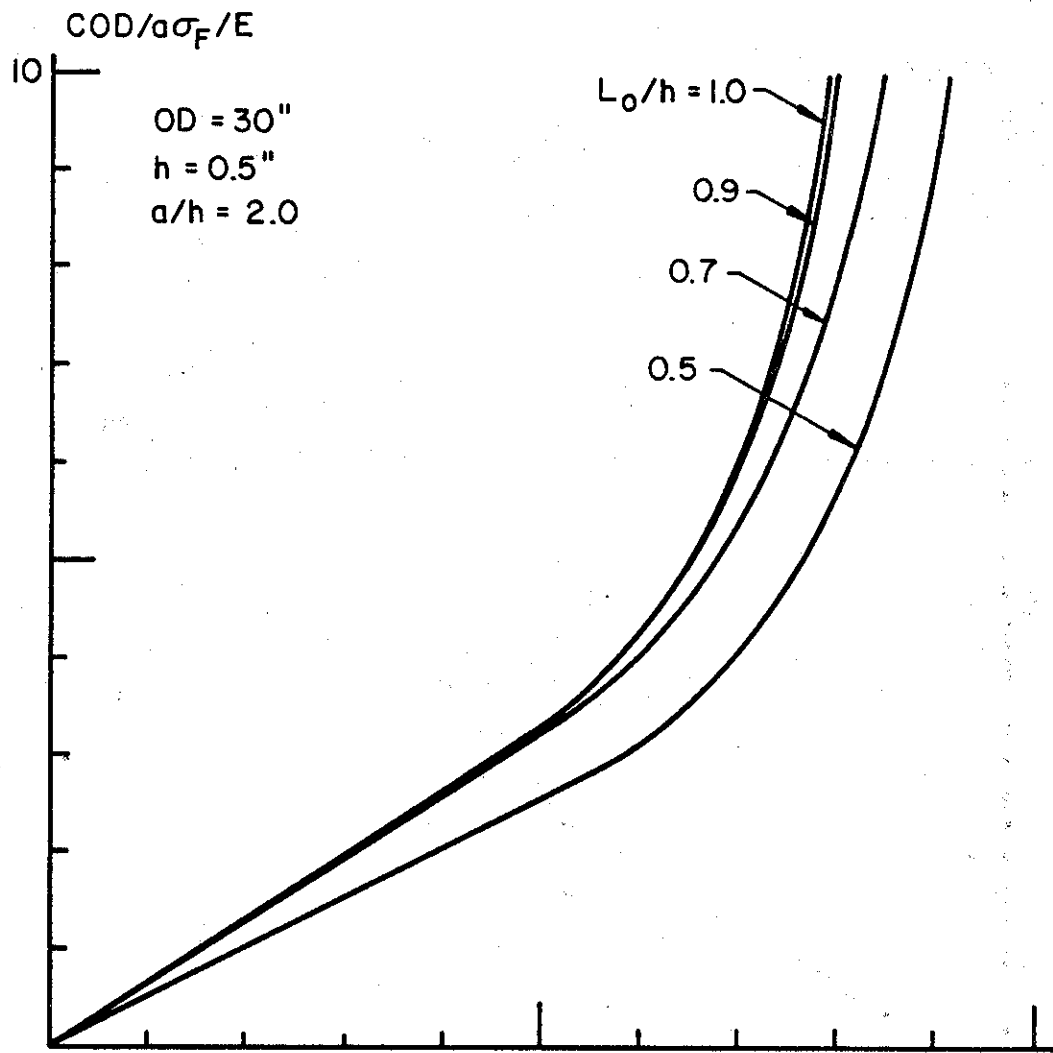


Figure H-6 COD vs. σ_0/σ_F for a 30 in. diameter pipe.

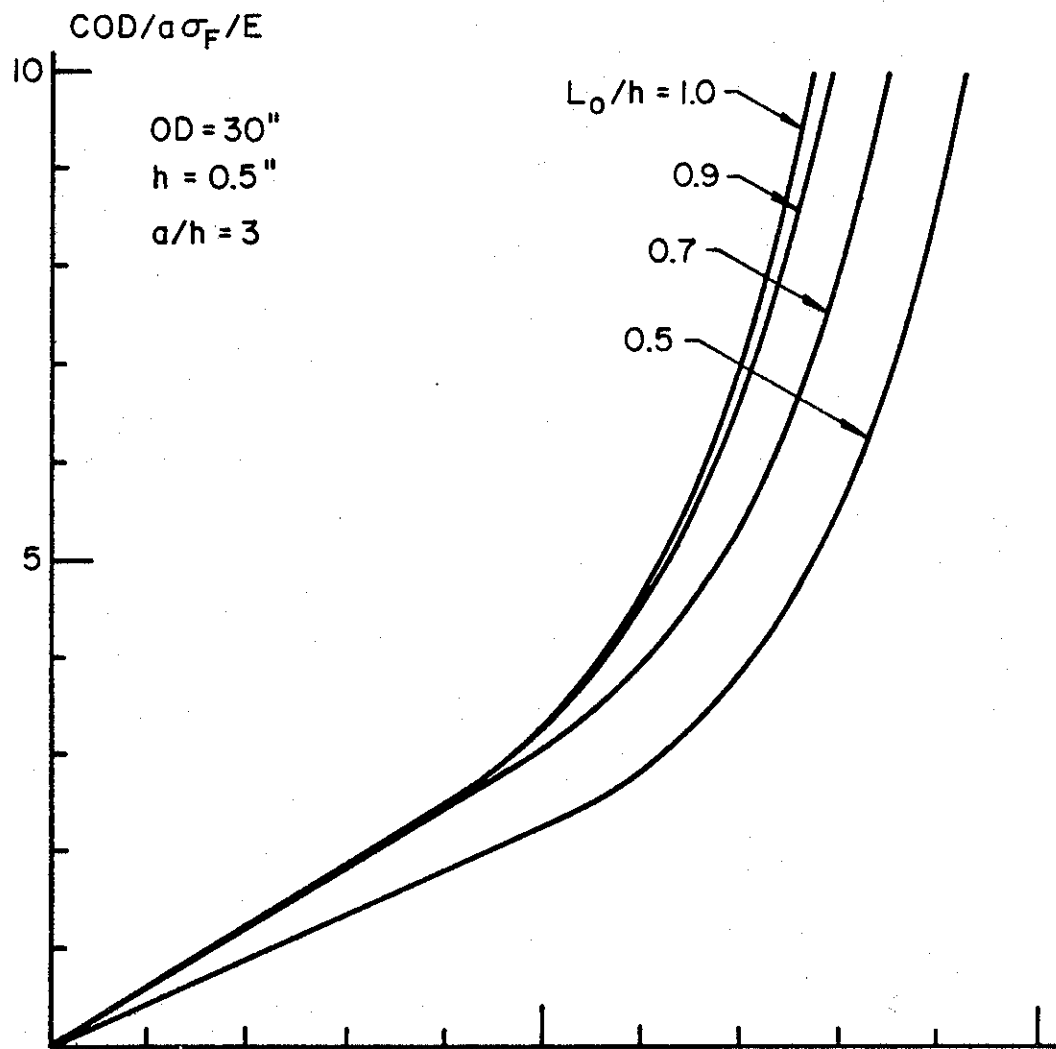


Figure H-7 COD vs. σ_0/σ_F for a 30 in. diameter pipe.

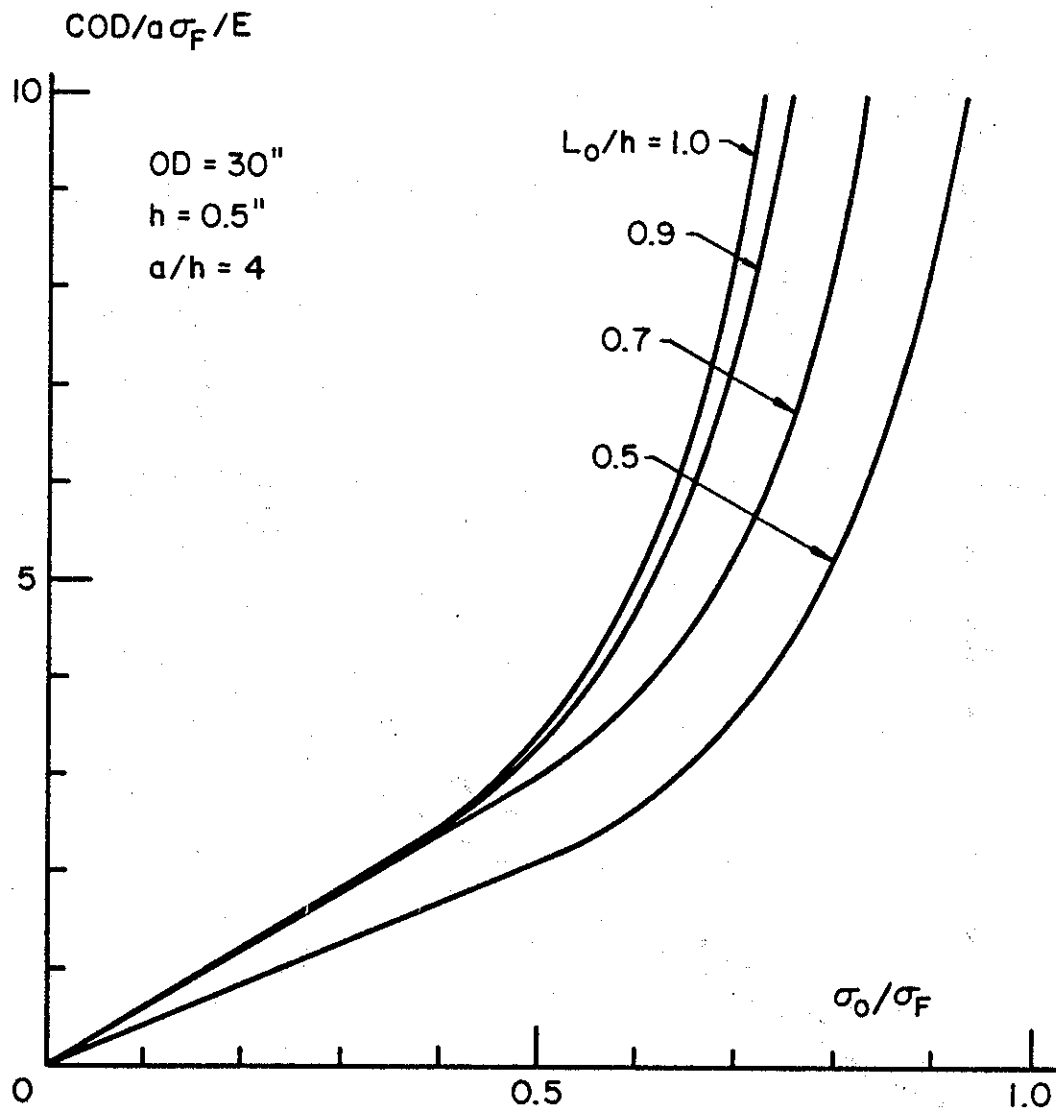


Figure H-8 COD vs. σ_0/σ_F for a 30 in. diameter pipe.

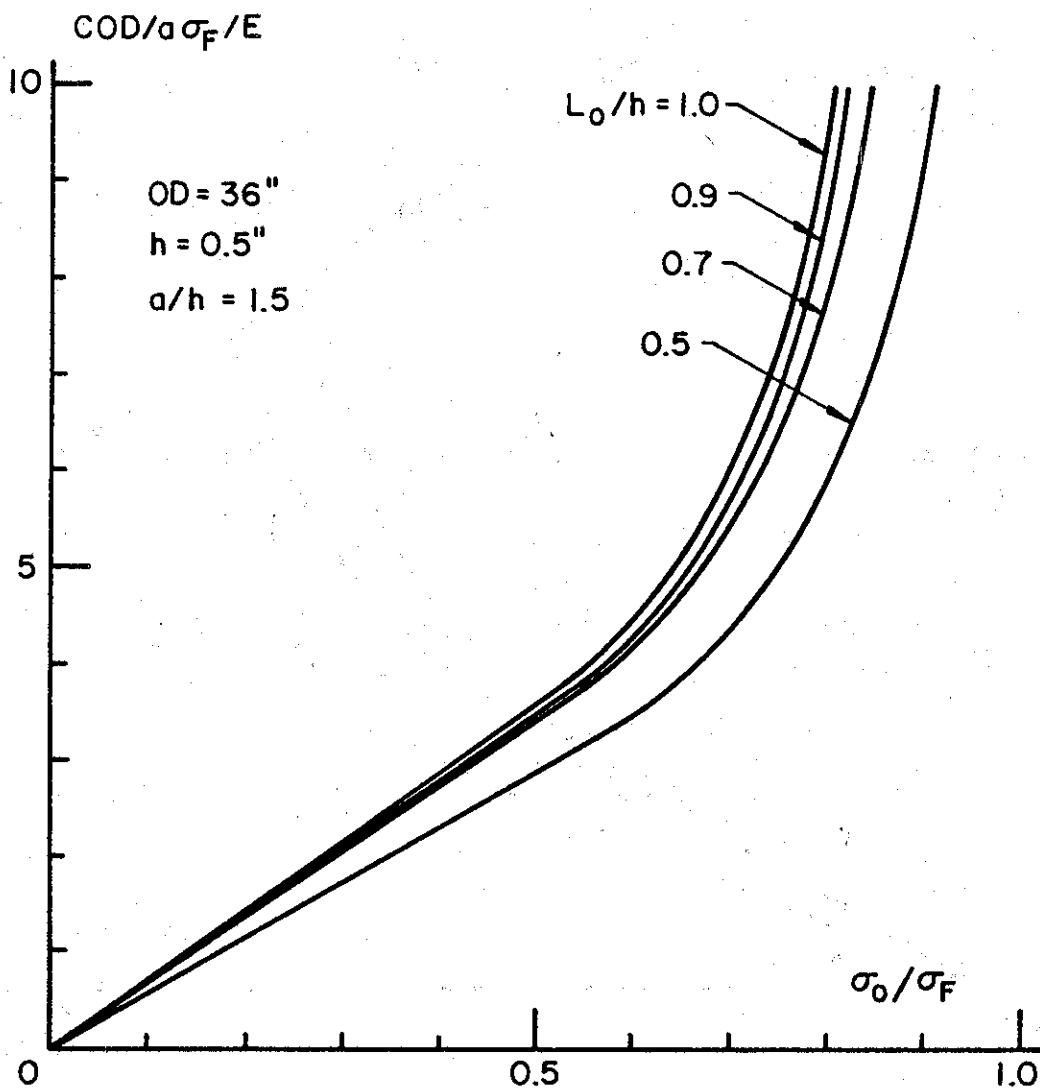


Figure H-9 COD vs. σ_0/σ_F for a 36 in. diameter pipe.

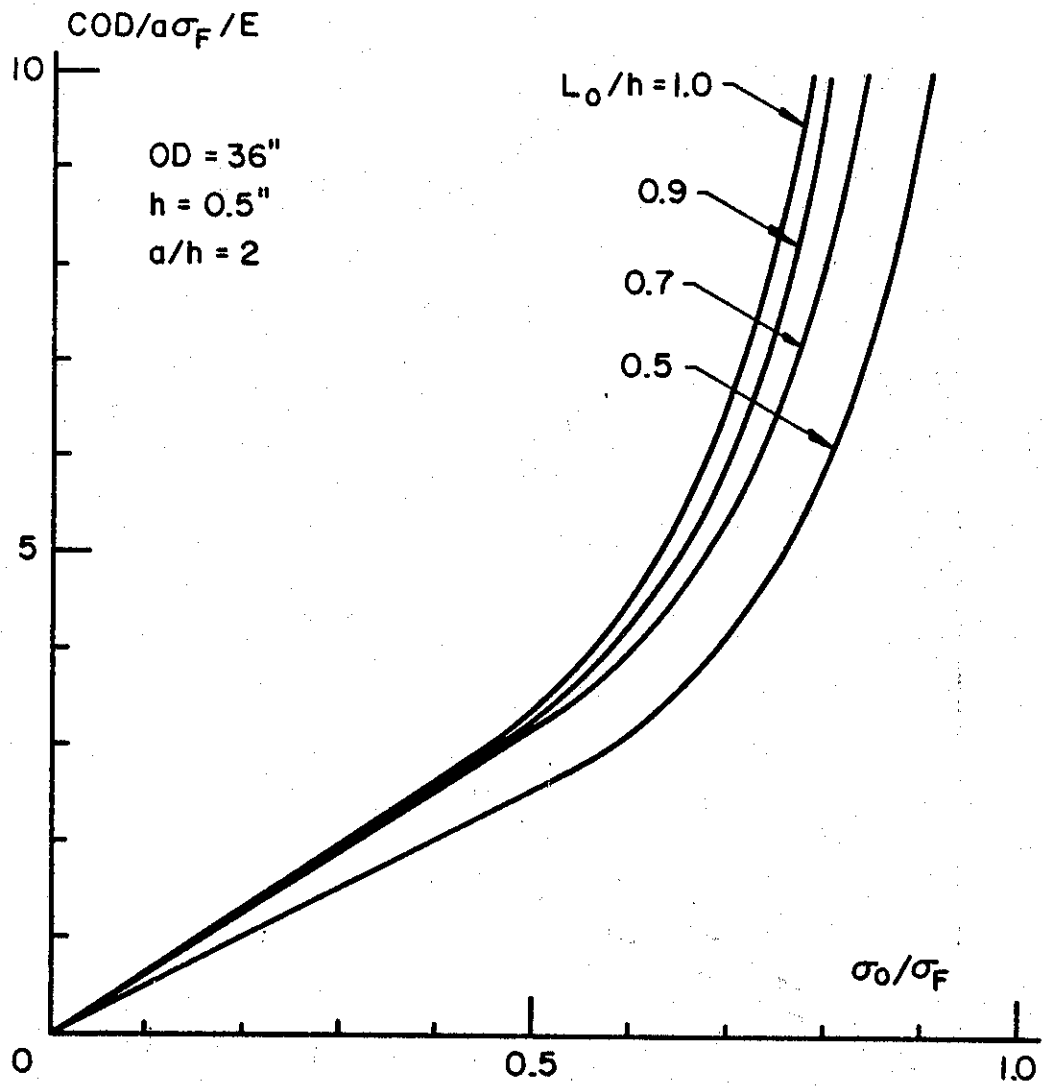


Figure H-10 COD vs. σ_0/σ_F for a 36 in. diameter pipe.

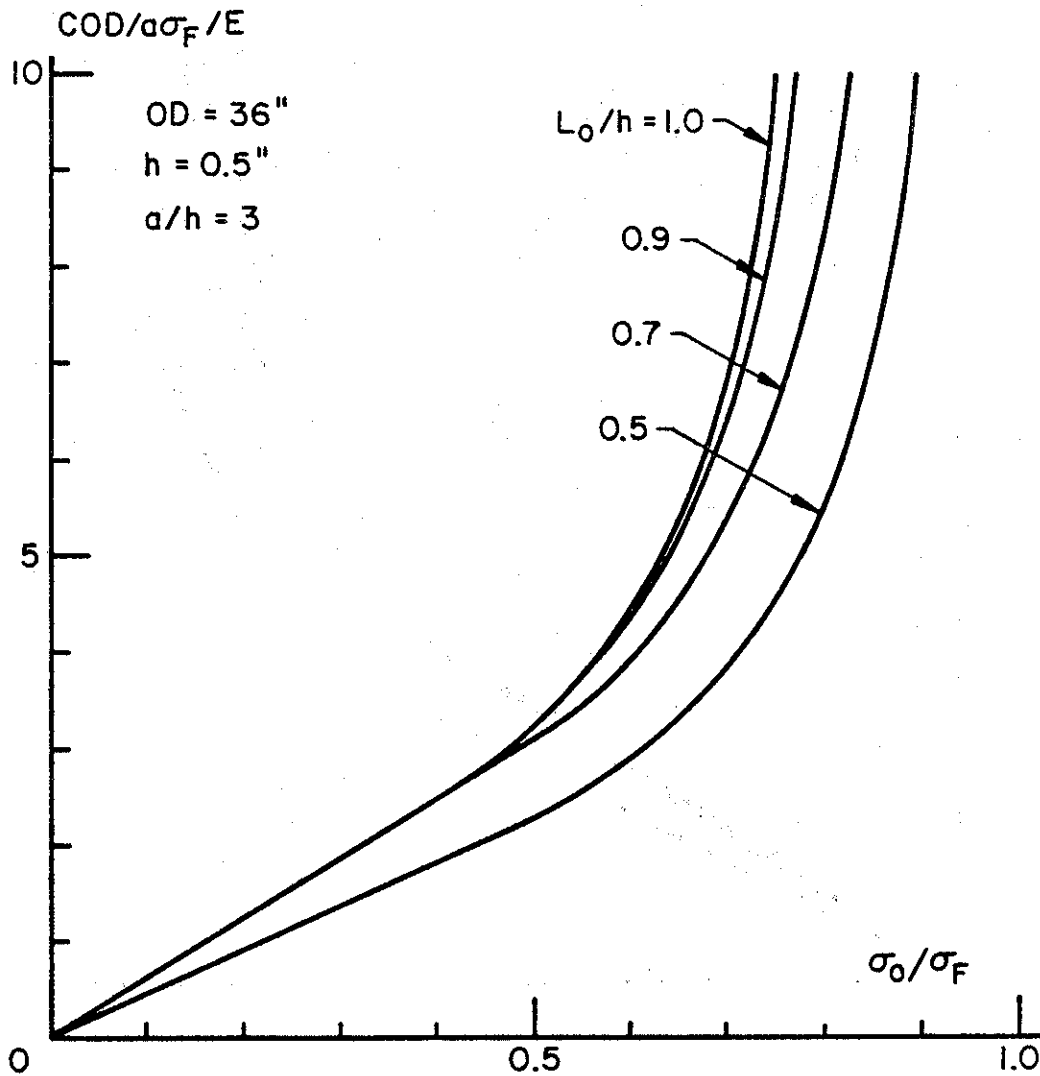


Figure H-11 COD vs. σ_0/σ_F for a 36 in. diameter pipe.

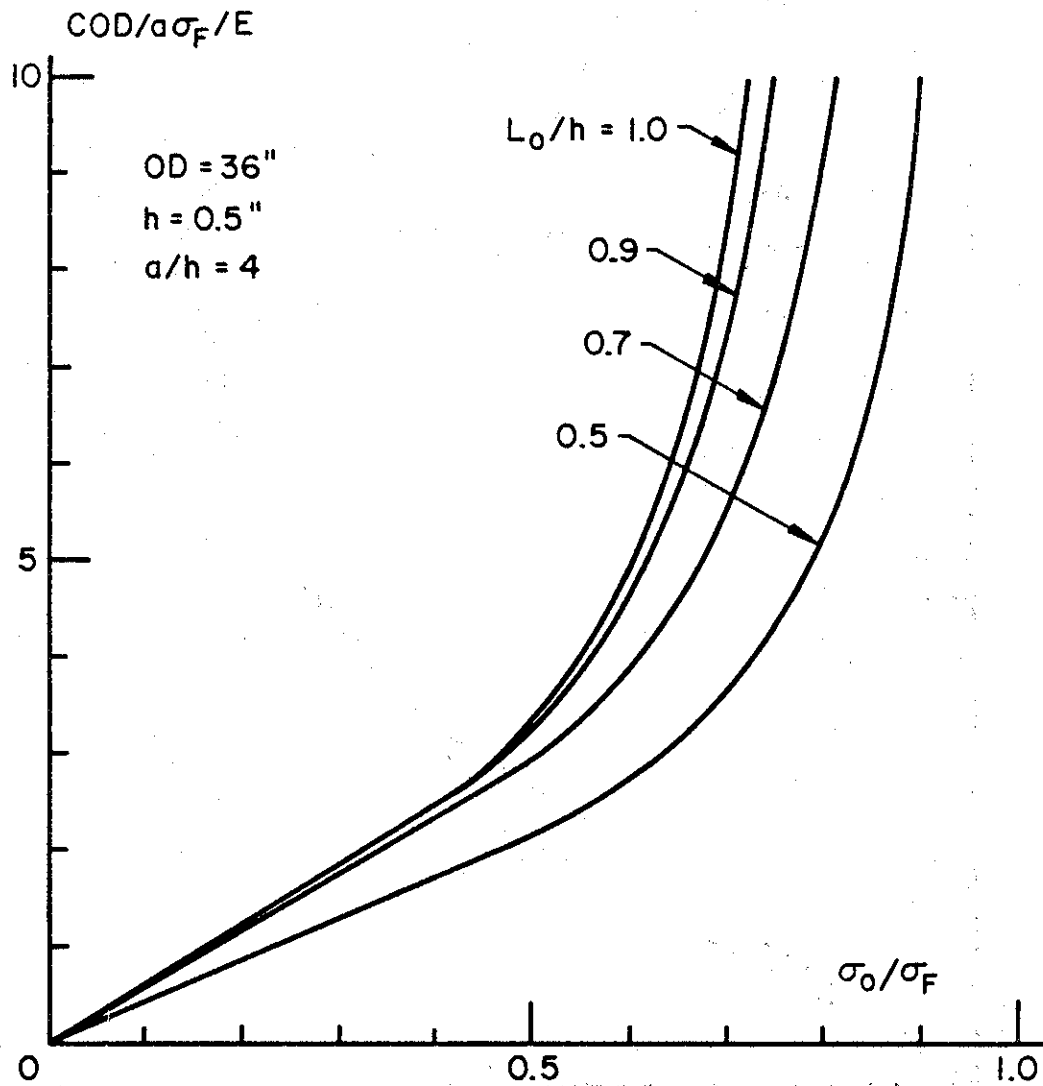


Figure H-12 COD vs. σ_0/σ_F for a 36 in. diameter pipe.

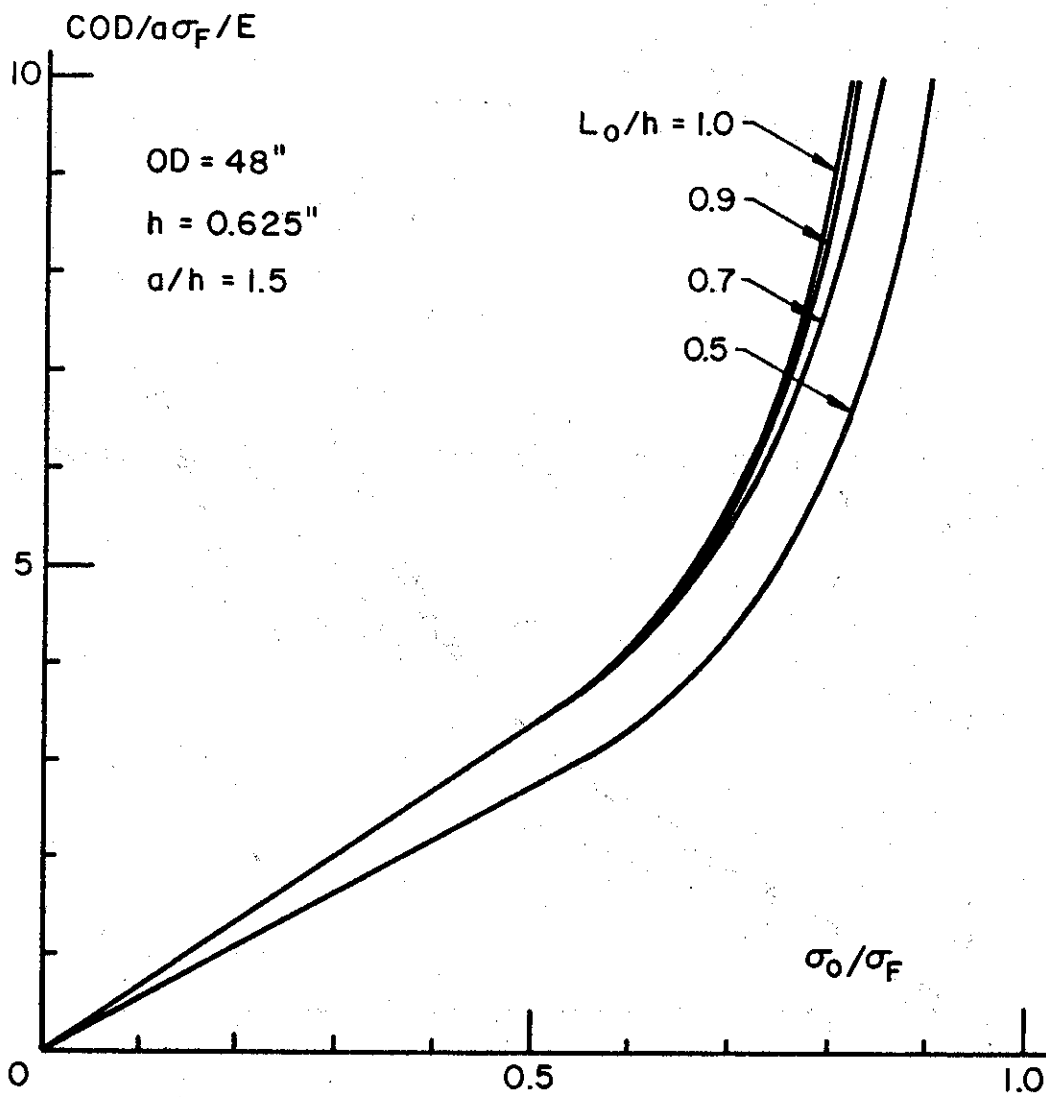


Figure H-13 COD vs. σ_0/σ_F for a 48 in. diameter pipe.

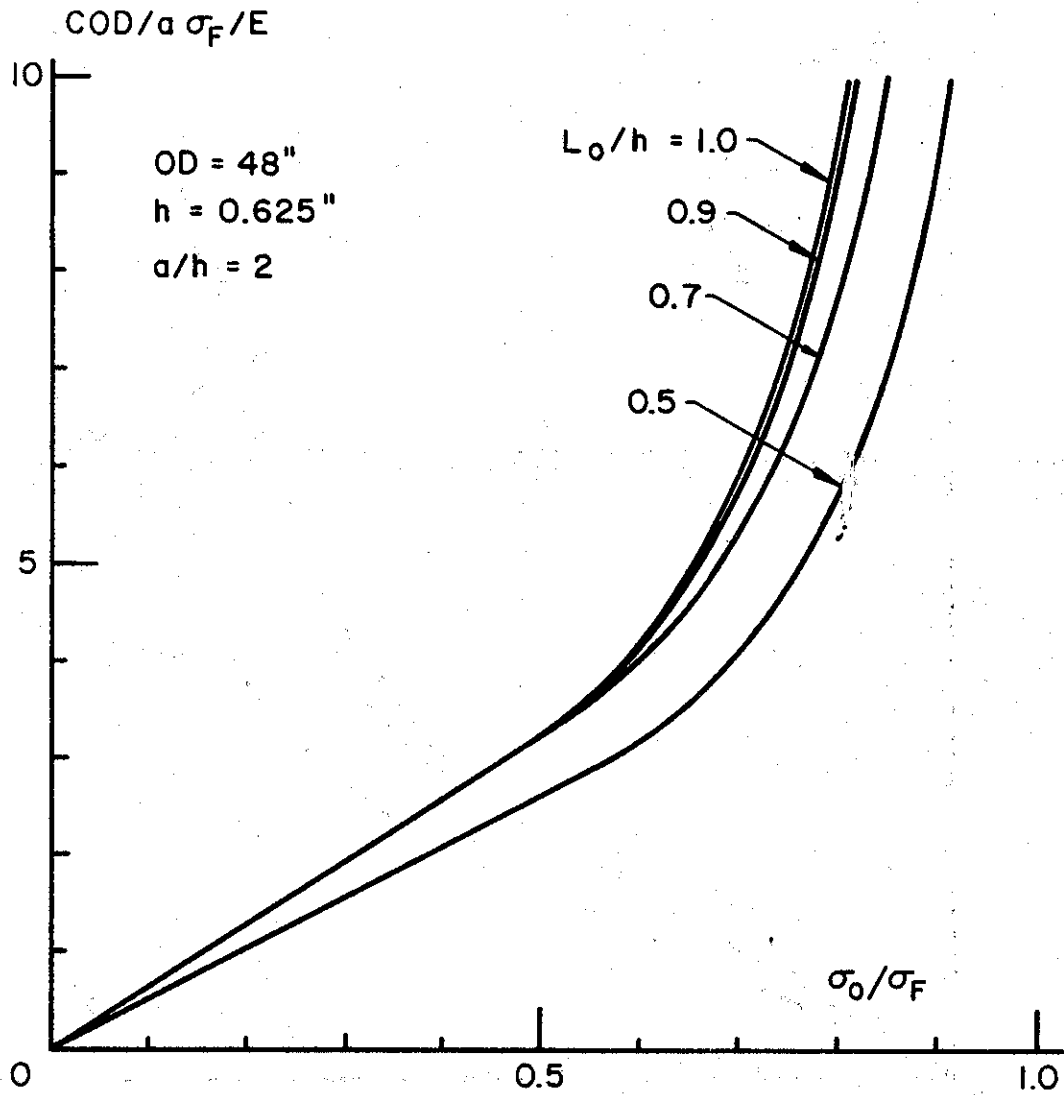


Figure H-14 COD vs. σ_0/σ_F for a 48 in. diameter pipe.

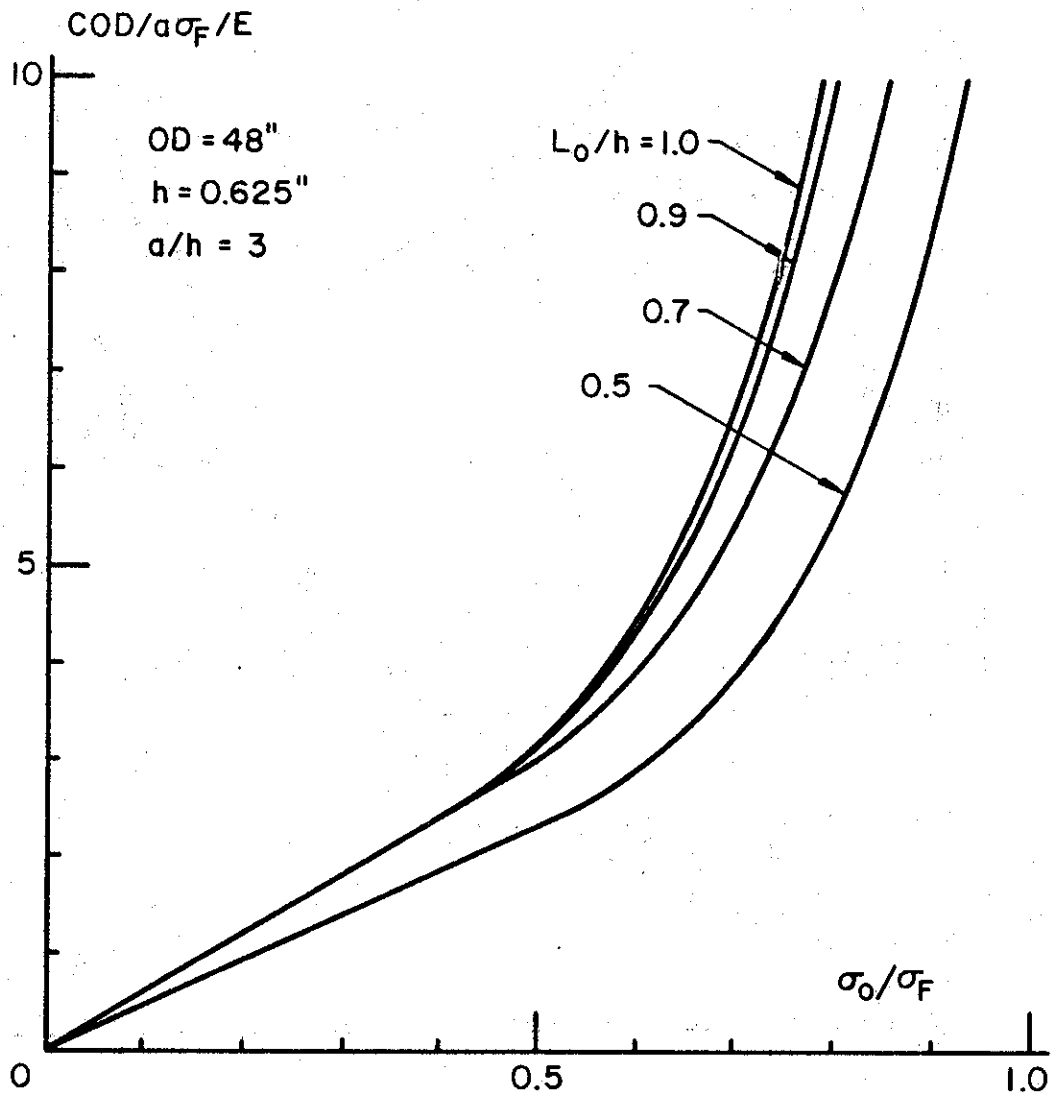


Figure H-15 COD vs. σ_0/σ_F for a 48 in. diameter pipe.

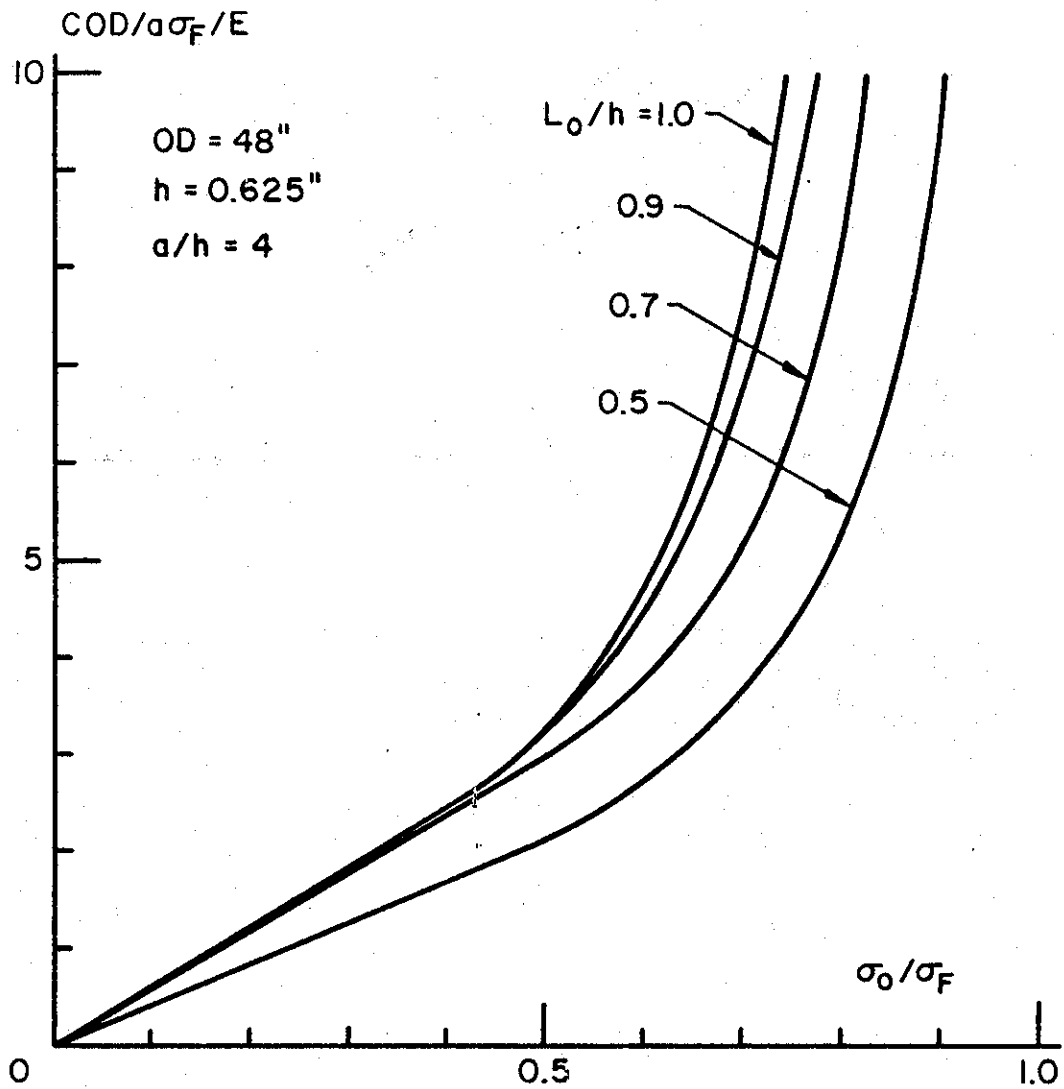


Figure H-16 COD vs. σ_0/σ_F for a 48 in. diameter pipe.

REQUEST FOR FEEDBACK TO The DOT Program Of University Research

This booklet is intended to serve as a reference source for transportation analysts, planners and operators. Your comments will be reviewed by the persons responsible for writing and publishing this material. Feedback is extremely important in improving the quality of research results, the transfer of research information, and the communication link between the researcher and the user.

- | YES | NO | |
|--------------------------|--------------------------|--|
| <input type="checkbox"/> | <input type="checkbox"/> | Did you find the report useful for your particular needs?
If so, how? |
| <input type="checkbox"/> | <input type="checkbox"/> | Did you find the research to be of high quality? |
| <input type="checkbox"/> | <input type="checkbox"/> | Were the results of the research communicated effectively
by this report? |
| <input type="checkbox"/> | <input type="checkbox"/> | Do you think this report will be valuable to workers in the
field of transportation represented by the subject area of
the research? |
| <input type="checkbox"/> | <input type="checkbox"/> | Are there one or more areas of the report which need
strengthening? Which areas? |
| <input type="checkbox"/> | <input type="checkbox"/> | Would you be interested in receiving further reports in this
area of research? If so, fill out form on other side. |

Please furnish in the space below any comments you may have concerning the report. We are particularly interested in further elaboration of the above questions.

COMMENTS

Cut Out Along This Line

Thank you for your cooperation. No postage necessary if mailed in the U.S.A.

RESEARCH INTEREST

PLEASE CHECK YOUR AREAS OF INTEREST. YOU WILL BE NOTIFIED AS NEW REPORTS ARE PUBLISHED.

TRANSPORTATION

- Air
- Highway
- Maritime & Ports
- Mass Transit
- Pipeline
- Rail

ECONOMIC REGULATION

- Air Carrier
- Motor Carrier
- Railroads

TRANSPORTATION STUDIES IN SPECIAL AREAS

- Advanced Technology
- Energy
- Environment
- Facilities & Terminals
- Hazardous Materials
- Safety
- Tunnelling
- Construction, Rehabilitation & Maintenance
- Efficiency, Productivity & Innovation
- Elderly, Handicapped & Disadvantaged
- Freight, Goods Movement & Commodity Flow
- Modeling - Demand, Supply & Traffic
- Rural Development, Planning & Policy
- Urban Development, Planning & Policy

OTHER (PLEASE LIST) _____

U.S. DEPARTMENT OF TRANSPORTATION
Research and Special Programs Administration
Washington, D.C. 20590



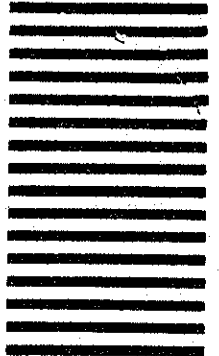
NO POSTAGE
NECESSARY
IF MAILED
IN THE
UNITED STATES

BUSINESS REPLY MAIL

FIRST CLASS PERMIT NO. G-126

POSTAGE WILL BE PAID BY ADDRESSEE

Dr. Lloyd J. Money, DMA-50
Director
Office of University Research
U.S. Department of Transportation
400 7th Street, S. W.
Washington, D. C. 20590



PLEASE LIST YOUR NAME AND ADDRESS.

NAME _____

TITLE _____

ORGANIZATION _____

STREET _____

CITY, STATE, ZIP CODE _____